

FUNCTIONALIZED POLYPEPTIDES AND THEIR COPOLYMERS: SYNTHESIS, PROPERTIES AND APPLICATIONS

**THESIS SUBMITTED TO JADAVPUR UNIVERSITY
FOR THE DEGREE OF
DOCTOR OF PHILOSOPHY (SCIENCE)**

2023

By

MD. ANAS



**SCHOOL OF CHEMICAL SCIENCES
INDIAN ASSOCIATION FOR THE CULTIVATION OF SCIENCE
JADAVPUR KOLKATA-700 032, INDIA**



Indian Association for the Cultivation of Science

2A & 2B Raja S. C. Mullick Road, Jadavpur, Kolkata 700032, INDIA

Dr. Tarun K. Mandal
Sr. Professor
School of Chemical Sciences

CERTIFICATE FROM THE SUPERVISOR

This is to certify that this thesis entitled "**FUNCTIONALIZED POLYPEPTIDES AND THEIR COPOLYMERS: SYNTHESIS, PROPERTIES AND APPLICATIONS**" submitted by **MD. ANAS**, who got his name registered on **6th September, 2018** for the award of **Ph.D. (Science) degree** (Index No.: **157/18/Chem./26**) of **Jadavpur University**, is absolutely based upon his own work under the supervision of **Prof. Tarun Kumar Mandal** and that neither this thesis nor any part of it has been submitted for either any degree/diploma or any other academic award anywhere before.

Tarun Kumar Mandal
(Dr. Tarun K. Mandal) 01.08.2023

Signature of the Supervisor

Date with official seal



Dr. Tarun K. Mandal

Senior Professor

School of Chemical Sciences

Indian Association for the Cultivation of Science

Jadavpur, Kolkata - 700 032

Dedicated To...
My Beloved Parents, Sister
and Raju

CONTENTS

Acknowledgement	i
List of Abbreviations	v
Abstract	ix

Chapter 1: Introduction

A Brief Illustration of The Synthetic Functionalized Polypeptides: Synthesis, Solution Properties and Applications

1.1. Introduction of Polypeptides	3
1.2. Synthesis of Polypeptides: ROP of NCA Route	8
1.2.1 ROP Initiated by Normal Amines.	11
1.2.2. ROP Initiated by Transition Metal Catalyst.	13
1.2.3. ROP Initiated by Silazane Derivatives.	15
1.2.4. ROP by Other Techniques.	17
1.3. Functionalization of Polypeptide	23
1.4. Polypeptide Architectures formed via ROP of NCA	28
1.5. Solution Properties of Functionalized Polypeptides	30
1.5.1. Stimuli-Responsive Functionalized Polypeptides	32
1.5.1.1. Thermo-Responsive Polypeptides.	32
1.5.1.2. pH-Responsive Polypeptides.	45
1.5.1.3. Photo-Responsive Polypeptides.	50
1.5.1.4. Redox-Responsive Polypeptides	54
1.5.1.5. Other Responsive Polypeptides	58
1.5.2. Self-Assembly of Functionalized Polypeptides	59
1.5.2.1. Micellar Self-Assembly	61
1.5.2.2. Vesicular Self-Assembly	68

1.5.2.3. Gelation	75
1.6. Applications of Functionalized Polypeptides	82
1.6.1. Control Release System	84
1.6.2. Tissue Engineering Scaffold	89
1.6.3. Antibacterial Applications	92
1.7. Objectives and Scope of the Present Research Work	95
1.8. References	98

Chapter 2: LCST Polypeptide

Thermoresponsive Amphiphilic Poly(L-Cysteine): Synthesis, Self-Assembly and Guest Encapsulation/Release

2.1. Introduction	151
2.2. Objectives and Scope of the Work	153
2.3. Experimental	155
2.3.1. Materials	155
2.3.2. Synthetic Procedure	155
2.3.2.1. Synthesis of Propargyl L-Cysteine (Cys-S-Pr)	155
2.3.2.2. Synthesis of Cys-S-Pr NCA	156
2.3.2.3. Synthesis of 2-Isopropyl-2-Oxazoline (<i>t</i> POx)	158
2.3.2.4. ROP of Cys-S-Pr NCA by HMDS	159
2.3.2.5. CROP of <i>t</i> POx and Successive Azide Termination	159
2.3.2.6. Synthesis of Graft Copolymer (PCys- <i>g</i> -P <i>t</i> POx)	161
2.3.3. Experimental Methods	163
2.3.3.1. Microwave Polymerization	163
2.3.3.2. Determination of T_{cp}	163
2.3.3.3. Determination of Critical Aggregation Concentration (CAC) in Water	163

2.3.3.4. Self-Aggregation of PCys- <i>g</i> -P'POx Copolymer	165
2.3.3.5. Dye Encapsulation Study	165
2.3.3.6. Drug Encapsulation Study	166
2.3.4. Characterization	167
2.4. Results and Discussion	169
2.4.1. Synthesis of PCys- <i>g</i> -P'POx copolymers	169
2.4.2. Thermoresponsive Properties of P'POx and PCys- <i>g</i> -P'POx	174
2.4.3. Self-Assembly of PCys- <i>g</i> -P'POx	177
2.4.4. Dye/Drug Encapsulation by Graft Copolymer	185
2.5. Conclusion	196
2.6. Appendix: Characterization and Other Experimental Data	197
2.7. References	204

Chapter 3: UCST Polypeptide

Synthesis and Anion-Induced Thermoresponsiveness of Cationic Poly(L-Cysteine) and Its Interaction with DNA

3.1. Introduction	219
3.2. Objective and Scope of the Work	222
3.3. Experimental	223
3.3.1. Materials	223
3.3.2. Synthetic Procedure	224
3.3.2.1. Synthesis of 2-Bromoethyl Acrylate (2-BrEt-Ac)	224
3.3.2.2. Synthesis of Bromo and Chloro Functionalized L-Cysteine	225
3.3.2.3. Synthesis of NCAs	230
3.3.2.4. ROP of Cys-Br/ Cys-Cl NCAs	231
3.3.2.5. Synthesis of Cationic Poly(L-cysteine) (P[Cys-	232

	$\text{PPh}_3]^+[\text{X}^-]$ (X = Br, Cl)	
3.3.3. Experimental Methods		234
3.3.3.1. Anion-Responsiveness of Aqueous P[Cys- $\text{PPh}_3]^+[\text{Br}^-]$ Solution		234
3.3.3.2. Determination of Cloud Point (T_{cp}) of Aqueous P[Cys $\text{PPh}_3]^+[\text{Br}^-]$ solution in the Presence of Added Anions		234
3.3.3.3. ctDNA-P[Cys- $\text{PPh}_3]^+[\text{Br}^-]$ Polyplex Formation: Spectroscopic/ Gel Electrophoresis Study and the Effect of Ionic-Strength		235
3.3.4. Characterization		237
3.4. Results and Discussion		240
3.4.1. Synthesis of PCys-Br and P[Cys- $\text{PPh}_3]^+[\text{Br}^-]$		240
3.4.2. Anion-Responsive Behavior of [PCys- $\text{PPh}_3]^+[\text{Br}^-]$		244
3.4.3. Thermoresponsiveness of [PCys- $\text{PPh}_3]^+[\text{Br}^-]$ in Water with Added Anions		249
3.4.4. Intercalation of [PCys- $\text{PPh}_3]^+[\text{Br}^-]$ with DNA		258
3.5. Conclusion		265
3.6. Appendix: Characterization and Other Experimental Data		267
3.7. References		274

Chapter 4: Crystalline Polypeptide

Alkyl Functionalized Thermoresponsive Semicrystalline Poly(L-Glutamate)s and Their Self-Assembly

4.1. Introduction	285
4.2. Objective and Scope of the Work	289
4.3. Experimental	290
4.3.1. Materials	290
4.3.2. Synthetic Procedure	291
4.3.2.1. Azidation of Alkyl Bromide (C_n -Br) ($n = 10, 12, 16, 20$)	291
4.3.2.2. Synthesis of γ -Propargyl-L-Glutamate (Glu-Pr)	292
4.3.2.3. Synthesis of N-Carboxyanhydride of Glu-Pr (Glu-Pr NCA)	295
4.3.2.4. Synthesis of Poly(γ -propargyl-L-glutamate) (PGlu-Pr)	296
4.3.2.5. Click Reaction Between the PGlu-Pr and Long-Chain-Alkyl Azides	297
4.3.2.6. Synthesis of Alkyl-L-Glutamates (Glu- C_n , $n = 10, 12, 16, 20$)	298
4.3.3. Experimental Methods	301
4.3.3.1. Cloud point (T_{cp}) Measurement of PGlu- C_n (s) in Non-Aqueous Solvents	301
4.3.3.2. Self-Aggregation Study of PGlu- C_n (s) ($n = 12, 16, 20$)	301
4.3.3.3. Dye Encapsulation Study	302
4.3.4. Characterization	302

4.4. Results and Discussion	306
4.4.1. Synthesis of PGlu-C_n(s) (n = 10, 12, 16, 20)	306
4.4.2. Thermoresponsive Property of PGlu-C_n(s) (n = 12, 16, 20)	314
4.4.3. Crystalline Properties of The Glu-C_n(s) and PGlu-C_n(s)	321
4.4.4. Self-Assembly of The PGlu-C_n(s) (n= 12, 16, 20)	331
4.4.5. Dye Encapsulation by PGlu-C_n vesicles	335
4.5. Conclusion	337
4.6. Appendix: Characterization and Other Experimental Data	338
4.7. References	345
Summary	353
List of Publications	357
Reprints of the First Page of the Published Papers	

Acknowledgement

“At times, our own light goes out and is rekindled by a spark from another person”

First and foremost, I would like to praise and thank Almighty God for giving me the ‘strength’ to complete this thesis. I would like to express my deepest gratitude to my supervisor, Prof. Tarun Kumar Mandal for his constant guidance and encouragement throughout my doctoral studies without which this thesis work would not have been possible. His educational perspective motivated me to learn more than I thought possible and pushed me to work hard and strive for excellence in my research career and beyond. I am indebted to him for enlightening my global perspective of scientific and professional view.

I would also like to thank my research advisory committee (RAC) members: Head of the Department of Chemistry (Prof. Subratanath Koner, Prof. Swapan Kumar Bhattacharya, and Prof. Chittaranjan Sinha), Jadavpur University and Prof. Sudip Malik, SAIS, IACS for assessing my research work and providing their scientific insights, suggestions, and encouragement.

I am thankful to the ex-directors (Prof. Santanu Bhattacharya, Prof. Tapas Chakraborty) and present director (Prof. Ranjan Sen) of Indian Association for Cultivation of Science (IACS), for offering me the research support during my Ph.D. at IACS. I gratefully acknowledge the funding agencies that have aided me in my research- DST India (Inspire Fellowship) and IACS. I take this opportunity to thank other professors of IACS that have always supported and guided me - Prof. Rajib Kumar Goswami, Prof. Joyram Guin, Prof. Pradyut Ghosh, and Prof. Abhishek Dey of my department at IACS (SCS), Prof. Prosenjit Sen (SBS), Prof. Suhrit Ghosh (SAIS), Prof. Arun Kumar Nandi (SMS). I have also received guidance from multiple professors of my alma mater, Jadavpur University - Prof. Umesh Chandra Halder (M.Sc. project

supervisor), Prof. Mahammad Ali, Prof. Rina Ghosh, Prof. Samaresh Bhattacharya, Prof. Arup Gayen, and numerous other professors that have always inspired me to do better as a chemist.

In my PhD journey, I have been fortunate to receive global exposure and to work with some of the best scientific minds in the field. And none of this would have been possible if not for the British Council and the Newton Bhabha Fellowship they awarded to me that enabled me to work with Dr. Mischa Zelzer, School of Pharmacy, University of Nottingham, UK, to whom I am forever grateful for hosting and guiding me.

The ease with which I was able to immediately ramp up in a foreign lab was only possible because of the strong working culture that has been imbibed in me owing to the people I have worked with in my own lab and IACS. A big and indispensable part of this learning curve are as well my lab seniors- Madhab da, Tanmoy da, Somdeb da, Yajnaseni di, and colleagues- Palash, Priyanka, Mahuya, Ambuz, Joy, and Sunetra. I also take this moment to apologize to my colleagues with whom I shared the lab space, for my occasional crankiness, any unpleasant circumstances created due to my need to be "Perfectionist" and habit of keeping things in their right place after use! I cannot miss to thank other young minds whom with I have worked like Debabrata, Amal, Suman, Nadira, Ritobroto, Pritha, Saumik, Ayntika, Pinki, Soumyadip.

IACS would not be so fun and interesting if not for other friends and acquaintances I made along the way. Thank you to each one of you - Raihan, Suja, Isha, Kalim, Anurag, Debayan, Paramita, Hayder da, Sahidul da, Aman da, Estak da, Rafikul da, Pulak da, Surojit da, Subhasis da, Prasenjit da and others I have interacted with along the way. I would also like to thank and recognize the help of the analytical staff of IACS like Sumit da, Champa di, Ashish da, Chanchal da, Gautam da and other non-teaching staffs.

My life's journey might be reaching a very important milestone as I complete my Ph.D., but it started way back in my school (Birbhum Zilla School aka BZS). So, any acknowledgement is incomplete without thanking my school and tuition teachers - Mujibar Sir, Ruhul Sir, Nema Sir, Late Pratyush Sir, Milan Sir, Manas Sir, Sujit Sir, Anis Sir, Meghnad Sir, Afghan da, and Moin da. I have made some lifelong bonds in my school life with Sarwar, Arzoo, Kanchan, and others. My brothers – thanks for all those sweet memories we have created in our school days. Special mention to my school senior Venkat da, who took me in his home, hosted me, and guided me at every step during my UK journey.

The next big turning point of my life were my 5 years at Jadavpur University, where I met some of brightest minds and made some of my best friends. Whether it was seniors like Baitan da, Arijit da, Subrata da, Sanhita di, Sampa di, Nayim da or juniors like Aftab, Shamim, Raunak, I have only received love and companionship. Who would have thought I would meet some of my best buddies –Trisha, Late Rajdeep, Writhabrata, Shantanu, Subarna, Deblina, Kaustuv, Souradeep, Supriya, Rapti, Souma, and Sumit at JU. Special thank you to Writhabrata, Shantanu, Subarna, and Deblina, for always having my back and for the countless memories we have gathered over the years through our fun outings, trips and just casually chilling over food and laughter.

A pivotal person in this journey is Late Rajdeep (Raju), my dearest friend. I have such fond memories of him and of our time spent together. Hostel life would not have been as fun for Writhabrata and I, without Raju, and our common love for sports. Kaustuv, Raju and I also share fun memories of playing card games together for hours and always studying together before our semester exams. I wish I could express in words how much I miss those days and how much I miss Raju. May his soul rest in peace wherever he is. May we meet again and grow our friendship even stronger.

After all is said and done, it is family that holds us together in the darkest as well as the brightest days. My family is no exception. I am nothing without my Abbu, Md. Year Ali, and Ma, Nasima Begum. While my father has been the '*teacher and guide, mentor and pride*' of my life, my loving mother has always been a source of comfort and selfless love. I owe them my everything for all their sacrifices. Apart from my parents, the most important person in my life is my elder sister, my Api, Nasrin Khatun. I am fortunate for having her in my life and for all the love I have received from her. Two relatively new members in my close family, but no less important, are my brother-in-law Dr. Mohosin Alam and my nephew Ridza (Bhontu). Mohosin da- thank you for always being a brother to me. Ridza is too young to read this, but the truth is, I had no idea I could love anyone as much as I love that little fellow. A few young members of my extended family deserve special mention as they all hold a place in my heart - Mariom, Tahir (Bhodu), Zubayir (Bheblu), Ashiq, Arish, Asira, Arash. This acknowledgement will not be complete without thanking a few others - Alisha, Aiman, Lamiya- thank you for being there. I also thank my other relatives for their love and unconditional support.

Last but not the least, I want to thank wholeheartedly my very own Grammarly, alarm clock, entertainment, bully, and favourite person rolled into one – my best friend, Trisha. I feel myself very much fortunate to have her who understands me like no one else even from the distant. Thank you for staying alongside me in my good, bad, and ugly days. And of course, a big thank for the help with correcting this thesis and for everything else.

Md. Anas

(MD. ANAS)

July 23

School of Chemical Sciences

Indian Association for the Cultivation of Science

Kolkata 700032

List of Abbreviations and Symbols

AA	α - Amino Acid
AMM	Activated monomer mechanism
AAMMA	Accelerated amine mechanism through monomer activation
ACN	Acetonitrile
AFM	Atomic force microscopy
AMM	Activated monomer mechanism
AMP	Antimicrobial peptide/polypeptide
ATRP	Atom transfer radical polymerization
Asp	Aspartic acid
BLG	γ -Benzyl-L-glutamate
CD	Circular dichroism
CAC	Critical aggregation concentration
CGC	Critical gelation concentration
CMC	Critical micellar concentration
CROP	Cationic ring opening polymerization
CuAAC	Copper(I)-catalyzed alkyne-azide cycloaddition
ctDNA	Calf thymus DNA
Cys	L-Cysteine
\mathcal{D}	Dispersity
D_h	Hydrodynamic diameter
DCM	Dichloromethane
DCTB	Trans-2-[3-(4-t-butyl-phenyl)-2-methyl-2-propenylidene]malononitrile
DEE	Diethyl ether
DHB	2,5-Dihydroxybenzoic acid
DIPEA	N,N-Diisopropylethylamine

DLS	Dynamic light scattering
DMF	N,N-Dimethylformamide
DMSO	Dimethyl sulfoxide
DNA	Deoxyribonucleic acid
DOX	Doxorubicin
DP	Degree of polymerization
DSC	Differential scanning calorimetry
EB	Eosin B
ECM	Extracellular matrix
EG	Ethylene glycol
ESI-MS	Electrospray ionization mass spectrometry
EtOAc	Ethyl acetate
EtOH	Ethanol
FESEM	Field emission scanning electron microscopy
FTIR	Fourier-transform infrared
Gly	L-Glycine
Glu	L-Glutamic acid
GPC	Gel permeation chromatography
ΔH_c	Enthalpy change of crystallization
ΔH_m	Enthalpy change of melting
HMDS	Hexamethyldisilazane
IL	Ionic liquid
iPOx	2-(isopropyl-2-oxazoline)
LCST	Lower critical solution temperature
Leu	L-Leucine
Lys	L-Lysine
MALDI-TOF	Matrix-assisted laser desorption/ionization time of-flight mass spectrometry
MeOH	Methanol

Micro DSC	Micro differential scanning calorimetry
M_n	Number average molecular weight
M_w	Weight average molecular weight
MW	Molecular weight
NAM	Normal amine mechanism
NCA	N-Carboxyanhydride
NHC	N-Heterocyclic carbene
NHS	N-hydroxysuccinimide
NIPAM	N-isopropylacrylamide
NMR	Nuclear magnetic resonance
NR	Nile red
OEG	Oligo(ethylene glycol)
PBLA	Poly(γ -benzyl-L-aspartate)
PBLG	Poly(γ -benzyl-L-glutamate)
PDI	Polydispersity index (M_w/M_n)
PEG	Poly(ethylene glycol)
PEGA	Poly(ethylene glycol) acrylate
PGA	Poly(glutamic acid)
Phe	L-Phenylalanine
PIL	Poly(ionic liquid)
PMMA	Poly(methyl methacrylate)
PNIPAM	Poly(N-isopropylacrylamide)
POM	Polarized optical microscope
Pox	Poly(2-oxazoline)
PPLG	Poly(γ -propargyl-L-glutamate)
PPM	Parts per million
PS	Polystyrene
PTyr	Poly(L-tyrosine)
PXRD	Powder X-ray diffraction

RNA	Ribonucleic acid
ROP	Ring opening polymerization
RT	Room temperature
SDS	Sodium dodecyl sulphate
SEC	Size exclusion chromatography
SPPS	Solid-phase peptide synthesis
%T	Percentage transmittance
T_c	Crystallization temperature
T_{cL}	LCST-type cloud point temperature
T_{cp}	Cloud point temperature
T_{cU}	UCST-type cloud point temperature
T_d	Decomposition temperature
T_g	Glass transition temperature
T_m	Melting temperature
TEA	Triethylamine
TEM	Transmission electron microscopy
TGA	Thermo gravimetric analysis
THF	Tetrahydrofuran
TMS	Trimethylsilyl
TPP	Triphenylphosphine
Tyr	L-Tyrosine
UCST	Upper critical solution temperature
WXRD	Wide-angle X-ray diffraction

Abstract

Synthetically prepared functionalized polypeptides are one of the most challenging areas for the polymer chemists to introduce specific functional groups or modifications of artificially designed/modified polypeptides for both fundamental understanding and technology development. Ring opening polymerization (ROP) of α -amino acid N-carboxyanhydride (NCA), is mostly used by the researchers for synthesis of long chain polypeptides. Subsequent post-functionalization enables the production of polypeptides with tailored properties such as improved stability, enhanced solubility, stimuli-responsiveness, good self-assembly property, or specific interactions with other biomolecules. This functionalization can be achieved through various chemical reactions, such as coupling reactions, click chemistry, or post-translational modifications. The specific functional groups introduced, or modifications done to the polypeptides can impart unique properties that are useful for specific applications in various fields, including biotechnology, biomedical research, material science, and drug delivery. Overall, synthetically prepared functionalized polypeptides offer a versatile platform for designing and engineering customized biomolecules with desired functionalities, opening up opportunities for numerous scientific and technological advancements.

The aim of this thesis is to synthesize, explore and study of the solution properties of differently modified polypeptides exhibiting diverse functionalities and self-assembled structures. The focus is on investigating the potential of these functionalized polypeptides to enhance therapeutic effectiveness, biocompatibility, and materialistic applications. This thesis is divided into four chapters based on the results obtained by the experiments conducted during the period of research.

Chapter 1 provides complete literature review on developments of functionalized polypeptide through the ROP of NCA and their application as

biomaterials. Different available methods of ROP using different initiators for the synthesis of functional polypeptide with different architectures have been discussed in detail. A brief emphasis also has been made on the stimuli-responsiveness of these functionalized polypeptides which includes different stimuli such as thermo, pH, photo, redox and others. This chapter also concentrates on the self-assembly behaviours of the synthetically prepared polypeptides to form different micro-/nano-structured aggregates in different solvents in a systematic way. Finally, in the last section of this chapter, the potential applicability of these functionalized responsive polypeptides as a biomaterial have been classified into three main category such as, drug/gene delivery application, tissue engineering and as antimicrobial agents.

Chapter 2 focuses on the development of amphiphilic graft-copolypeptides poly(cysteine)-*graft*-poly(2-isopropyl-2-oxazoline) (PCys-*g*-P'POx) that can self-assemble into vesicular nanostructures in different solvents, making them suitable for various biomedical applications. A click-grafting technique is adopted to develop water-soluble amphiphilic PCys-*g*-P'POx copolypeptides with hydrophobic polycysteine backbone and hydrophilic pendant poly(2-isopropyl-2-oxazoline) side chain. The process involves synthesizing propargylated polycysteine (PCys-S-Pr) and azide-end-functional poly(2-isopropyl-2-oxazoline) (P'POx-N₃) blocks through ROP and cationic ring-opening polymerization (CROP) techniques, respectively. These blocks are then grafted together via Cu-AAC click reaction to form PCys-*g*-P'POx. The grafting of the thermoresponsive P'POx block into polycysteine backbone makes the resulting graft copolypeptides PCys-*g*-P'POx thermoresponsive, exhibiting lower critical solution temperature (LCST)-type phase behaviour in water. The cloud point of the copolypeptide can be tuned by adjusting its composition and concentration.

Self-assembly of PCys-*g*-PPOx in aqueous and nonaqueous media, results in vesicular morphologies with different size distribution. These vesicles can encapsulate different types of dye/drugs with high efficiency. Those encapsulated dye/drug further can be released from the vesicular environment simply by heating or treating them with concentrated HCl. Overall, the integration of synthetic polypeptides with pseudopeptidic poly(2-oxazoline)s in the form of PCys-*g*-PPOx copolymers opens up new possibilities for their application in various biomedical fields.

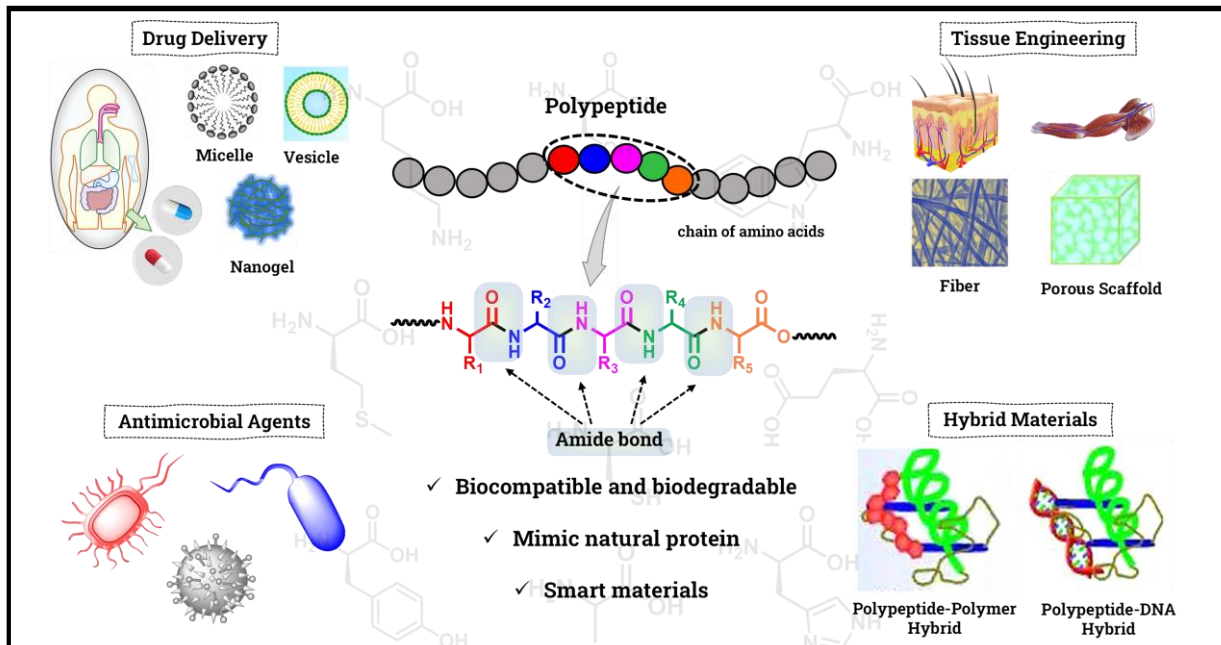
Chapter 3 presents the synthesis of a water-soluble cationic polypeptide derived from L-cysteine and explores its thermoresponsive behaviour in the presence of various anions, as well as its binding capacity with DNA. The process begins with the ROP of a newly designed bromo-functionalized L-cysteine NCA monomer, resulting in the formation of polycysteine with a pendant bromine (Br) atom. Subsequently, the Br atom is substituted with triphenylphosphine, yielding cationic polycysteine (P[Cys-PPh₃]⁺Br⁻). Aqueous solution, P[Cys-PPh₃]⁺Br⁻ demonstrates responsiveness to different anions from the Hofmeister series, including BF₄⁻, I⁻, ClO₄⁻, and SCN⁻. This response is evident through the transformation from the transparent solution to a cloudy suspension, caused by the formation of water-insoluble aggregates of cationic polypeptide and anions through anion-bridge interaction. Upon heating, the cloudy suspension turns transparent, and it reappears when cooled, exhibiting a thermoresponsive behaviour akin to an upper critical solution temperature (UCST). The cloud point of the UCST-type phase transition can be tuned by varying the molecular weight, and concentration of the polypeptides, as well as the nature and concentration of the added anions. Furthermore, the biocompatibility of the cationic polypeptide is validated by the MTT assay, which indicates low cytotoxicity against human cells. This characteristic highlights its potential for biomedical applications. The study also explores the polyplexation of cationic P[Cys-PPh₃]⁺Br⁻ with calf-thymus DNA (ctDNA) using

various techniques such as fluorescence spectroscopy, gel electrophoresis, and circular dichroism spectroscopy. Additionally, the influence of ionic strength on the polyplexation process is evaluated through fluorescence spectroscopy.

Chapter 4 primarily emphasize on the functionalization of poly(L-glutamate)s with long-chain alkyl groups and investigation of their semicrystalline and solution-phase behaviour, including thermoresponsiveness and self-aggregation. The study reveals the ROP of the as-synthesized γ -propargyl-L-glutamate NCA to produce poly(L-glutamate) (PGlu-Pr) with a pendant propargyl group. Next, the PGlu-Pr is subjected to Cu-AAC reaction with long-chain alkyl azides to yield alkyl-grafted poly(L-glutamate)s [PGlu-C_n(s), n= 10, 12, 16, 20]. In both the solution phase and the solid state, PGlu-Pr and PGlu-C_n(s) exhibit a helical secondary conformation. However, the extent of helicity decreases with an increase in the length of the alkyl chains. Interestingly, the control monomeric analogues, alkyl-grafted L-glutamates (Glu-C_n)s, form birefringent crystals due to the presence of the long alkyl chains, as observed by DSC and polarized optical microscopy. On the other hand, PGlu-C_n(s) with n \geq 12 display feeble crystallinity in their solid state. CHCl₃ and THF solutions of PGlu-C_n(s) demonstrate UCST-type thermoresponsive properties with a tunable cloud point with respect to the chain length of the pendant alkyl groups and solvent polarity, while Glu-C_n(s) do not exhibit such behaviour. Moreover, self-assembly of PGlu-C_n(s) in these solvents results in the formation of vesicular nanoaggregates, as confirmed by DLS and TEM. These nanoaggregates have the ability to encapsulate organic dye (Eosin B), as studied through fluorescence and confocal microscopy. Overall, this work showcases the successful functionalization of poly(L-glutamate)s with long-chain alkyl groups and explores the intriguing thermoresponsive, self-aggregation and crystalline behaviour of the resulting polypeptides.

Chapter 1: Introduction

A Brief Illustration of The Synthetic Functionalized Polypeptides: Synthesis, Solution Properties and Applications



1.1. Introduction to Polypeptides

Proteins and peptides are fundamental components of cells that regulate the important biological functions.¹ They can transport small molecules through organism (e.g., transport protein: Haemoglobin), help in the recognizing external biological substrates (e.g., antibody: T-cell receptor), act as catalysts (e.g., enzymes: Sucrase) and have advanced structural properties (e.g., elastin and collagen) in organisms. Proteins, which primarily act as the building block of the living system by giving structural support to the cells and tissues, are made up of same or different naturally occurring α -amino acids, chemically linked by the amide bonds. Amino acids are a special class of compounds containing an α -carbon that is covalently link to an amino (NH_2) group, a carboxyl group (COOH), and a variable side group (R). The amide/peptide bond is formed by the covalent linking an amino group to a carboxylic group of another amino acid while one molecule of water is removed (Figure 1.1).

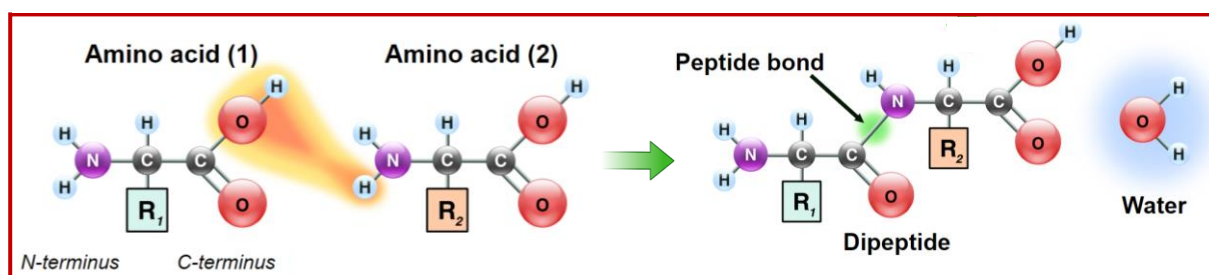


Figure 1.1. Peptide bond formation between two amino acids. (Image source: Wikimedia Commons)

Structurally, protein and peptide are very similar, being made up of chains of amino acids that are held together by peptide bonds. The basic differences between the proteins and peptides are the size and structure of amino acid chains. Conventionally, peptides are smaller than proteins consisting of 2 to 50 amino acids. Oligopeptides have 10 or fewer amino acids, whereas polypeptides consist of more than 10 amino acids. However, peptides consisting of more than 50 amino acid units are classified as proteins.

The DNA transcription and RNA translation are two biosynthetic processes that lead to the formation of monodisperse, length-specific and sequence-specific peptide/protein.² These proteins are mainly responsible for providing structural and mechanical support to cells, tissues, and organs, catalysing various biochemical reactions, and regulating the cell signalling, cell adhesion, and immune responses etc in the living systems. The primary structure of a protein refers to the linear sequence of amino acids that fold into complex hierarchical structures (Figure 1.2). The secondary structure is the arrangement of hydrogen bonds between adjacent amino acids of the peptide backbone, while the tertiary structure is the three-dimensional conformation that results

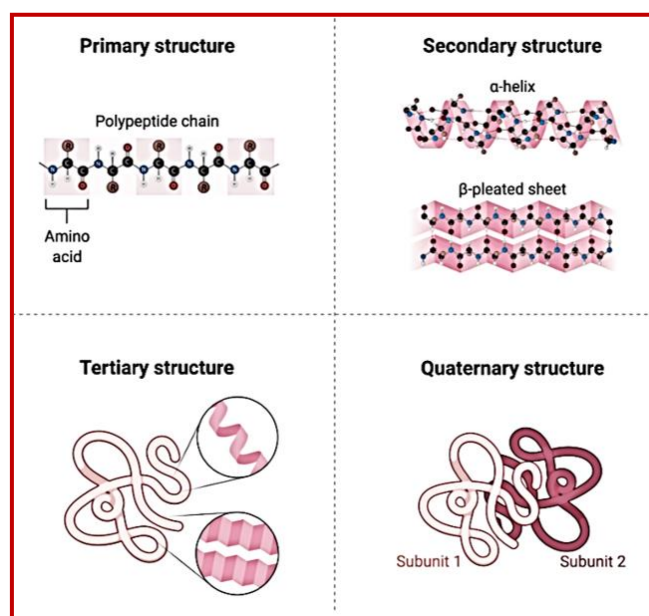


Figure 1.2. Different types of structures of protein. (Image source: Microbe Notes)

from interactions between side chains. On the other hand, quaternary structure of proteins relates to the arrangement of multiple polypeptide chains (subunits) held together by non-covalent bonds such as hydrogen bonds, ionic interactions, and hydrophobic interactions. The ability to form higher-order secondary structures such as α -helices and β -sheets or turns through inter or intra chain hydrogen bonding among the amide backbone of the proteins regulates their functionalities in the living systems. The order of the amino

acids in those proteins dictate their secondary structure. The different interactions present in protein molecules can lead to different stable secondary structures contribute to the overall three-dimensional conformation, the tertiary structure. This draw the attention of the scientists to synthesize protein mimicking molecules that can adopt these higher-ordered secondary structures. Synthetically prepared functionalized polypeptides, having same backbone as proteins, are excellent resources to mimic the natural protein (Figure 1.3).³⁻⁴

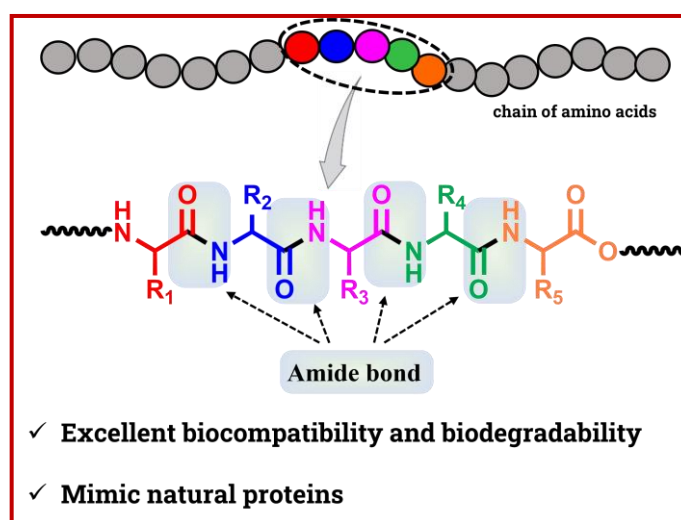


Figure 1.3. Primary structure of polypeptide.

They are also biodegradable and biocompatible with different functions and hence play a pivotal role in biology.⁵ Several research groups have developed different synthetic biodegradable systems such as polyesters⁶⁻⁷, poly(amino ester)s⁸, poly(organo phosphazenes)⁹, poly(amino acid) etc. Poly(amino acid)s/polypeptides are widely studied by various research groups due to their inherent biocompatibility and wide range of applications.³⁻⁵ Additionally, the natural availability of more than twenty monomeric amino acids and their artificial precursors allow customization of polymeric amino acids in numerous ways simply by conjugating or grafting different reactive or responsive segments into the main or side chain of the polypeptides.¹⁰ Polypeptide chains with reactive or responsive functionalities show prominent

responses to the changes of environments by external stimuli. It is worth mentioning that a small change in the environmental conditions can significantly change the properties such as solubility, nature of surface, permeability, and shape as well as mechanical, optical, electrical and chemical properties of these synthetic peptide-based materials.¹¹ Polypeptides with different functional groups respond specifically towards different stimuli such as temperature¹²⁻¹³, pH¹⁴⁻¹⁶, light¹⁷⁻¹⁸, redox reaction¹⁹⁻²⁰, enzyme²¹⁻²³, ionic strength²⁴⁻²⁵ etc. Furthermore, unlike conventional polymers, these synthetic polypeptides resembles their natural precursor (protein), adopting different stable secondary structures such as α -helix, β -sheet, random coil etc. in different solvents or in solid state.^{3,26} Synthetic polypeptides with such types of secondary structures can also regulate their properties like self-assembly, which in turn leads to novel supramolecular assemblies with potential biomedical and pharmacological applications.²⁷ These stimuli-responsive polypeptides are also belonging to the class of "smart polymer" with huge demand in biomedical areas due to their wide range of application in drug delivery, as therapeutic agent and as well as in tissue engineering.^{5,28-29}

In early days, synthesis of peptide was quite challenging to the researchers as it involved tedious synthesis process for protection and deprotection of amino acids and as well as their purifications. Since the pioneer discovery of 'solid phase peptide synthesis' (SPPS) by Robert Bruce Merrifield (Nobel prize, 1984), the synthesis of short chain sequential peptides of same or different amino acid residue became less complicated.³⁰ Merrifield's SPPS method involved the step-by-step attachment of the protected amino acids on solid resin backing (Figure 1.4). This method has the advantage that all reactions take place on the resin support, and therefore, the final peptide stays attached to the resin while the impurities and any extra reagents, which can be easily washed off. The peptide is then cleaved from the resin after the "global deprotection step", during which side chain functionalities are also

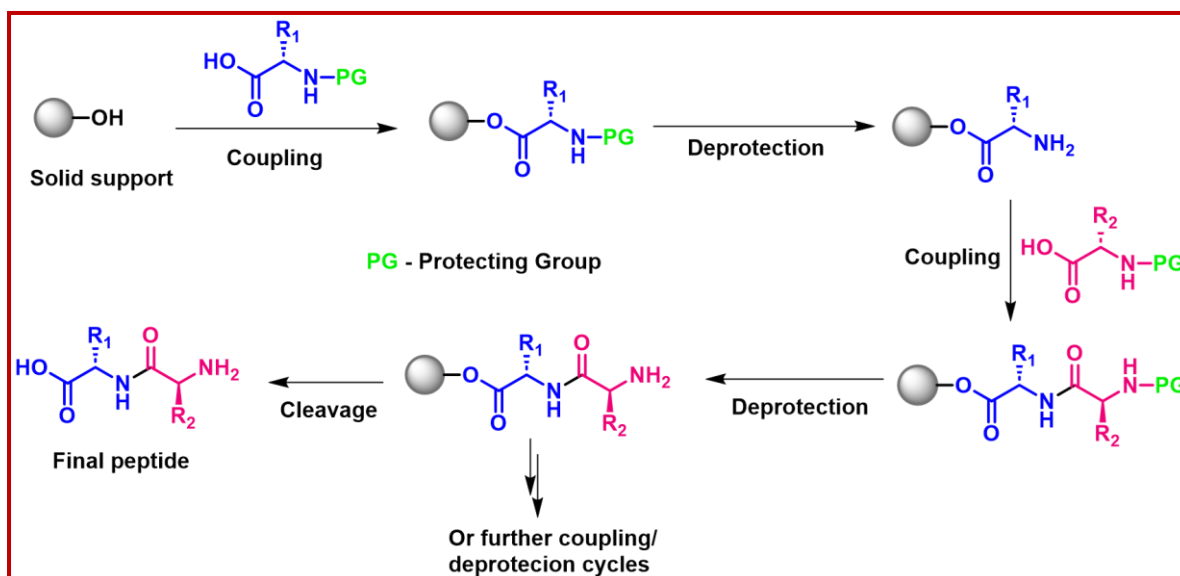
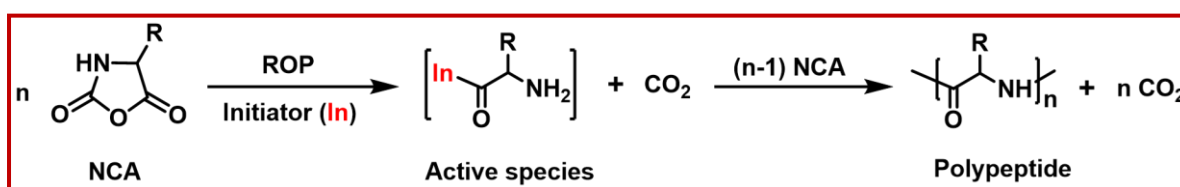


Figure 1.4. Simple schematic representation of the solid phase peptide synthesis (SPPS).

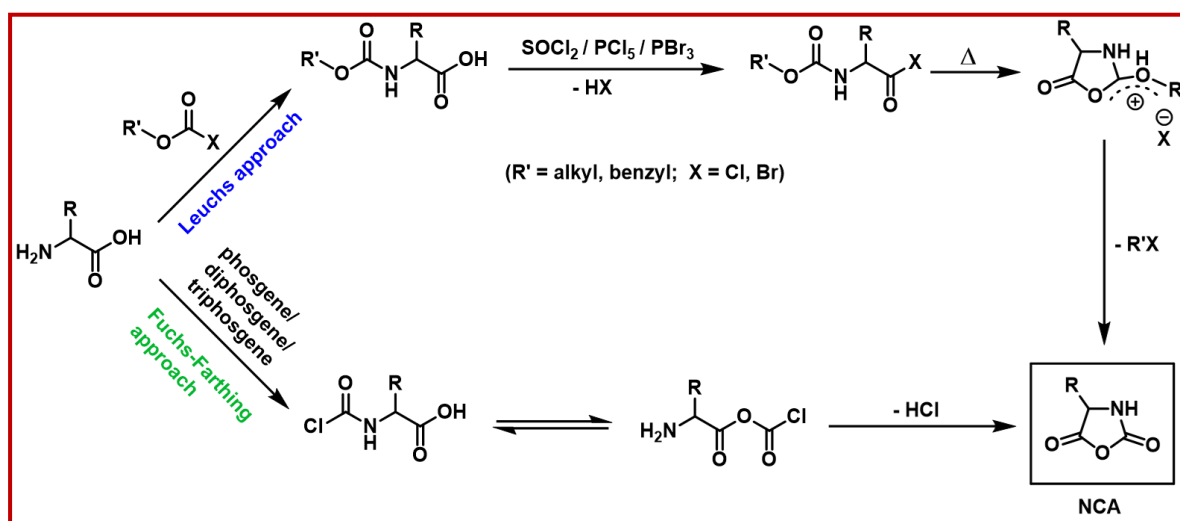
deprotected. Note that monodispersity, length-specificity and sequence-specificity of peptides (up to 50 residues) can be achieved by this method. However, this technique is limited in terms of its scalability and short peptide size. Very poor yield due to the incomplete deprotection and coupling steps and use of expensive chemicals make the conventional SPPS neither useful nor practical for preparation of large polypeptides (> 50 residues). The most economical and expedient process for synthesis of long polypeptide chains is the ring-opening polymerization (ROP) of α -amino acid N-carboxyanhydride (NCA) (Scheme 1.1).³¹⁻³² This method involves the use of simple reagents for preparing polypeptides of high molecular weights with good yield and in large scale with no detectable racemization at the chiral centres.



Scheme 1.1. Schematic representation of the ROP of NCA.

1.2. Synthesis of Polypeptides: ROP of NCA Route

In comparison to SPPS, the ROP of α -amino acid NCA, an economically fruitful and desirable method for synthesis of long chain polypeptides, is used more prevalently by the scientific community. In 1906, Hermann Leuchs first synthesized the α -amino acid NCA (also known as Leuchs' anhydride) involving the distillation of N-carbamoyl α -amino acids with thionyl chloride (SOCl_2) to produce NCA (Scheme 1.2).³³



Scheme 1.2. Synthetic approach of Leuchs method and Fuchs-Farthing method for synthesis of NCA.

It was also found that use of more reactive phosphorous pentachloride (PCl_5) and phosphorus tribromide (PBr_3) as halogenating agents substantially diminishes the reaction temperature and decomposition of the NCA monomers. But due to the limitations of unavoidable impurities, poor yield and mixture of racemic products of Leuchs method, the 'Fuchs-Farthing' method is adopted widely by the scientific community.³⁴⁻³⁵ In 'Fuchs-Farthing' method, NCAs are prepared by the direct phosgenation of the α -amino acids using phosgene gas at moderately elevated temperature and in the presence of inert atmosphere (Scheme 1.2). Dry solvents like THF, EtOAc, ACN, dioxane etc. have also been used for better yield of NCAs. To avoid the difficulties of handling toxic

phosgene gas in laboratory, varieties of its substitutes, notably diphosgene (trichloromethyl chloroformate), a liquid at room temperature and crystalline triphosgene (bis(trichloromethyl) carbonate) are used widely. Since then a huge number of NCAs have been synthesized for the preparation of high molecular weight (MW) polypeptides via ROP in good yield and at large scale with almost negligible amino acid racemization.^{29, 31-32} A huge number of functional/responsive polypeptides have been developed by the researchers in last few decades due to the availability of the large varieties of structurally different amino acids.^{13, 21}

The Fuchs-Farthing method is the simple and effective approach for the preparation of NCA. However, it has a major drawback in that it generates HCl as an unwanted by-product during the process. Thus, it is important to find efficient ways to remove this by-product in order to make the process more competent as HCl can impede the ongoing formation of the polypeptide chain at elevated temperature and lead to undesirable side-reactions results in lack of control over the polymerization process. To minimize the effect of HCl impurities in NCA, various techniques have been developed. The most common approach for purifying NCA after extraction from the reaction mixture is to recrystallize in inert atmosphere using dry solvents, which also resulted in the loss of the product. To overcome this challenge several HCl scavengers such as α -pinene, limonene or activated charcoal etc. has been used directly during the NCA synthesis.³⁶ Further in order to purify the NCA, different approaches such as i) rapid aqueous work up at low temperature and slight basic pH followed by thorough drying,³⁷ ii) flash chromatography under inert conditions³⁸ and iii) filtration over celite bed were reported to be effective. Among them filtration of NCA solutions in dichloromethane over a celite bed followed by its crystallization³⁹ was most advantageous over the other processes due to its applicability in the high scale purification of the synthesized NCA with lowest chloride content.

The synthesis of NCA using flow chemistry was recently investigated, and a wide variety of NCAs were synthesized with acid-sensitive groups such as silyl, tert-butyl ether, acetonide, trityl, Boc, etc. NCAs are obtained in less than one second, where sodium salts of amino acid containing N-methyl morpholine are rapidly mixed with triphosgene solution in ACN followed by a dilution with EtOAc.⁴⁰ In many cases, after evaporation of EtOAc isolated NCA does not require additional purification through recrystallization since it is highly pure.

Recently, a moisture-stable protocols for the synthesis of NCAs using propylene oxide or epichlorohydrin as HCl scavengers has been developed, which involved the mixing of amino acids with triphosgene in the presence of propylene oxide or epichlorohydrin in THF at ambient temperature.⁴¹ No external heating is required in this process as in-situ heat generation can perform the desired reaction. A straightforward workup procedure following crystallization under ambient conditions allowed the isolation of highly pure NCAs without using any anhydrous solvents. In particular, NCAs of unprotected functional amino acids such as L-glutamic acid, L-serine, and L-cysteine were synthesized for the first time using this approach without any protection-deprotection steps. Endo and co-workers developed an approach in which the NCA can be generated in-situ during ROP, in order to avoid dealing with by-products like HCl as well as the moisture sensitivity associated with NCA and the hazardous nature of phosgene.⁴²⁻⁴³ Their method entailed treating amino acids with non-toxic bis-aryl carbonates to produce N-aryl carbamates. These N-aryl carbamates of amino acids can function as precursors for NCA monomer via thermal intramolecular cyclization during polypeptide synthesis and were stable in ambient settings. Laconde and Martinez have developed a simple phosgene and halogen-free approach for the synthesis of NCA from Boc-protected α -amino acids using n-propanephosphonic acid anhydride (T3P).⁴⁴ The process is safe and easy-to-operate, and does not require any specific

equipment. As this method liberates nontoxic and easy to remove by-products, thus large quantity of pure NCAs with excellent yield can be prepared. In recent years, interest in these greener approaches of producing NCA without the use of harmful phosgene has greatly increased.

In recent decades, the development of precise and efficient methods for ROP of NCAs has been a challenge. The following topic will explain the advances made in NCA synthesis and discuss possible ways for ROP of NCAs in polymer synthesis. It will also look into the advancement of the synthetic methods for ROP of NCA that enabled researchers to develop novel materials through different ROP techniques.

1.2.1. ROP Initiated by Normal Amine

Classically, ROP of NCA involves the initiation by any nucleophiles (typically primary amines) or bases (most common being tertiary amines and alkoxide anions).³² The cyclic structure of NCA is kinetically favoured but not thermodynamically, hence when exposed to any such nucleophile, it attacks the carbonyl group of the NCA molecule to open the ring (Scheme 1.3). Release of one molecule of carbon dioxide (CO_2), results in an active species to react with the next NCA monomer which further propagates in the same way until termination to generated polypeptide. When nucleophiles with at least one proton source, like primary amine, alcohol etc. are used as initiator, ROP of NCA follows the 'normal amine' mechanism (NAM) (Scheme 1.3).^{32, 45} The nucleophilic attack on the carbonyl group of the NCA molecule initiates the reaction, resulting in an unstable carbamic acid, which further decarboxylates

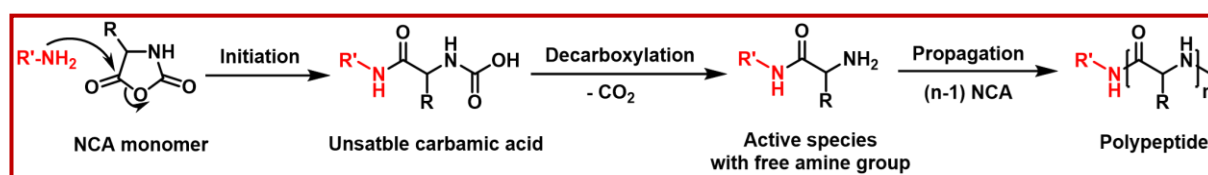
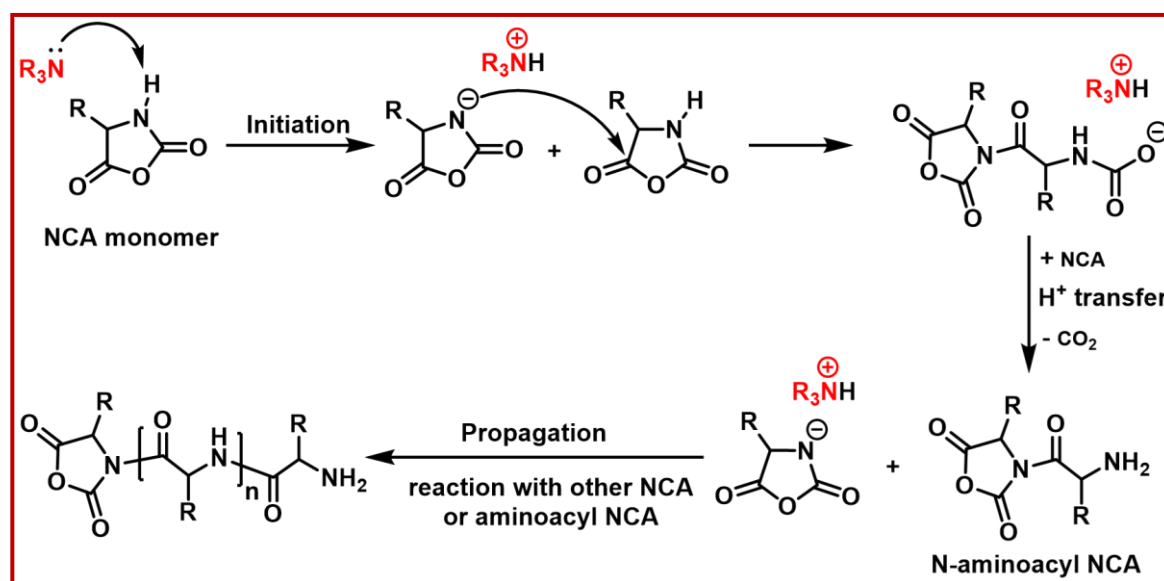


Figure 1.3. Synthetic pathway of normal amine mechanism (NAM) (Redrawn from ref. ⁴⁵)

to produce an active species with a free amine group to propagate the polymerization. High reactivities of the simple unhindered primary amines initiators such as n-hexylamine, n-butylamine, benzylamine etc. over the ω -amino groups of the propagating polypeptide chains, is the main reason for the relatively faster initiation than the propagation of the polymerization reaction, which subsequently resulted in the polypeptide with desired molecular weight and low \mathcal{D} . 'Activated monomer' mechanism (AMM) is also proposed when a strong basic and a less nucleophilic initiator, like tertiary amine or metal alkoxide etc., are used for ROP.^{32, 45} This mechanism consisted of the first deprotonation of the NCA molecule by effectively basic initiator, resulting in an anionic species, which further attacks another NCA molecule to promote the polymerization (Scheme 1.4). Although, AM mechanism is capable of producing



Scheme 1.4. Synthetic pathway of activated monomer mechanism (AAM) (Redrawn from ref. ⁴⁵)

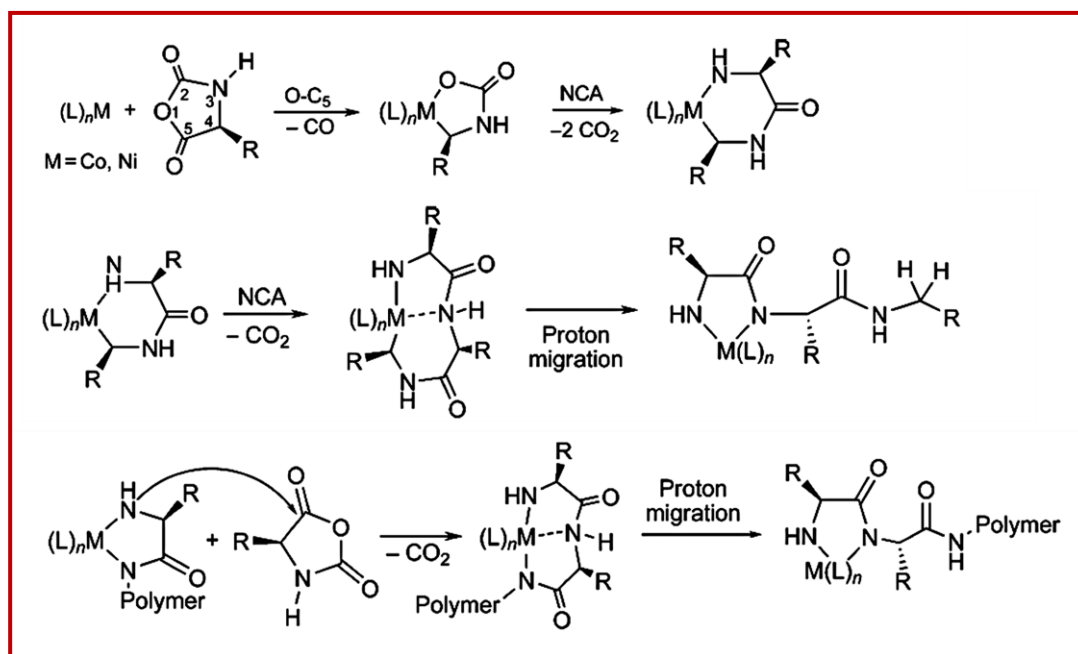
polypeptides with higher molecular weights, but \mathcal{D} s of the resulting polypeptides remain comparatively high due to relatively slow initiation than the propagation.⁴⁶ However, there are still some limitations of amine-initiated ROP of NCA. In ROP, using amines as initiators, control of chain-end functionality get prevented by the side reactions, resulted due to switching back and forth between the 'NAM' and 'AMM': a

propagation step for one mechanism is a side reaction for the other, and vice versa.⁴⁷⁻⁴⁹ These two methods may coexist and compete during polymerization depending on the extent of nucleophilicity or basicity of the initiator. More basic initiators, such as alkoxides or tertiary amines, tend to follow AMM and have weak control over the polymerization process. In contrast, primary amines or other initiators with more nucleophilicity followed NAM primarily, making them the most favoured initiators for ROP of NCA. Despite the fact that primary amines are stronger nucleophiles and follow the NAM pathway, they are still basic by nature and can, in some cases, follow the AMM pathway as a side reaction. These side reactions resulted in poor control over the growing polypeptide chain which eventually leads to the polypeptides with uncontrolled and broad molecular weight distributions.⁴⁶ Even though the majority of NCAs are crystalline substances, they frequently have minor amounts of impurities in terms of acids, acid chlorides, or isocyanates that can lead to the premature termination of the propagating polypeptide chain. Also, it has been reported that impurities such as water can act as catalysts for the side reactions or as chain transfers agent. These inherent problems of the conventional ROP of NCA using amines or alkoxides based initiators, makes it challenging for the researchers to developed different architecture, such as block copolypeptides and high molecular weight polypeptides.

1.2.2. ROP Initiated by Transition Metal Catalyst

It is challenging to synthesise functional polypeptides with precise architecture (e.g., block copolypeptides) and high molecular weight by the ROP of NCA using normal amine-based initiators since the discovery of the organometallic initiators. The use of transition metal complexes as active species to regulate ROP of NCA monomers to polypeptide chain ends has been proven to be a successful method for preventing side reactions. Deming invented highly efficient zero-valent nickel and cobalt initiators, such as bpyNi(COD) and $(\text{PMe}_3)_4\text{Co}$, which enable ROP of NCAs into high-molecular-weight polypeptides through activation of the NCAs in order to generate covalent propagating species.⁵⁰⁻⁵² After polymerization, the metal ions can be simply removed from

the polymers by conventional precipitation or dialysis of the samples' solution. Mechanistic studies revealed in the initiation step, both of these metals react with NCA monomers in the same way to create metalacyclic complexes through oxidative addition across the anhydride bonds of NCA (Scheme 1.5).



Scheme 1.5. Schematic representation of mechanism of NCA ROP by transition metal initiators. (Reproduced from ref.⁵¹⁻⁵²)

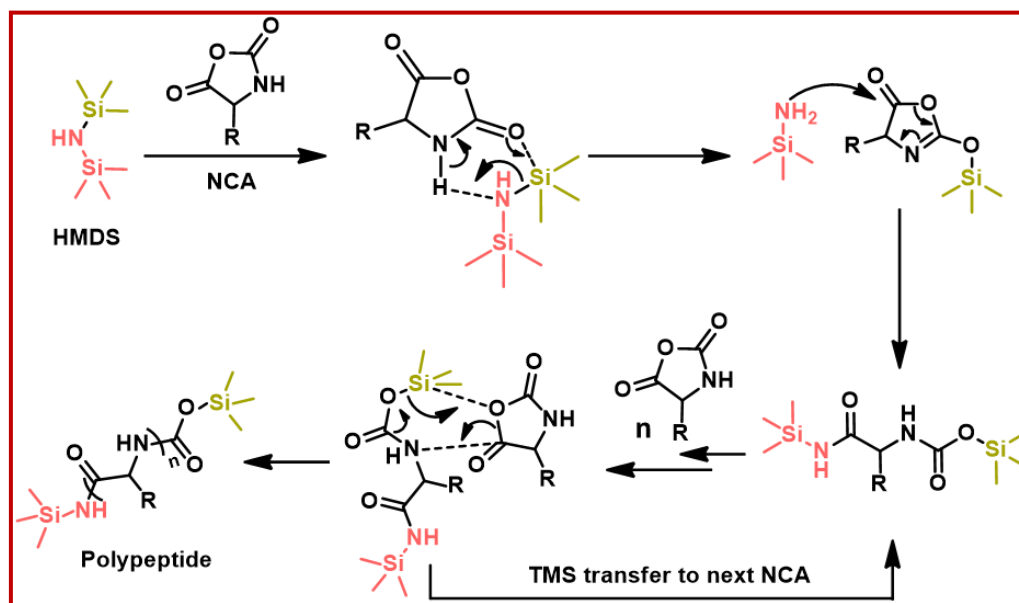
Following these oxidative-addition reactions, a second NCA monomer was added, resulting in a six-membered amido-alkyl metallacycles complex. When these intermediates react with more NCA monomers, it turns out that they further shrink to form five-membered amidate metallacycles. The transfer of an amide proton to the metal-bound carbon, which releases the chain end from the metal, is hypothesized to cause this ring shrinkage. In this approach, metal migrates along the growing polypeptide chain while being retained by chelation at the active chain end (in the form of a five-membered amido-alkyl metallacycle). This chelation by the transition metal is essential for achieving the livingness of the polymerization process. This method is thus very much fruitful in synthesizing (co)polypeptides with control molecular weights ($500 <$

$M_n < 500000$), low dispersity ($\mathcal{D} < 1.2$) and well-defined amino acid sequences and compositions. A wide range of NCAs with different enantiomeric configurations or as racemic mixture can be polymerized using this method in different solvents (DMF, THF, EtOAc, MeCN, dioxane etc.) and over a broad temperature range (10-100 °C). This approach has a significant disadvantage as it cannot be used with NCAs containing secondary amine, such as proline NCA, because it lacks the N-H moiety. To overcome this problem, Kramer et al. recently used the Ni-amidoamidate complex as an initiator for the ROP of proline NCA.⁵³ The inability of this approach to produce polypeptides with chain-end functionality at the C-terminus is solved by the invention of allyloxycarbonylaminoamides as a generic precursor to amido-amidate nickelacycle.⁵⁴ Although this process is excellent for synthesising well-defined polypeptides architecture with decent control over the molecular weight, however, it must be carried out in a glove box and under extremely strict inert conditions.

1.2.3. ROP Initiated by Silazane Derivatives

Amine initiated polymerization of NCA is vastly adopted by the scientific community due to its less chaotic procedure. Chen et al. is the first to report that hexamethyldisilazane (HMDS), an organosilicon based secondary amine compound, is more efficient as an initiator for ROP of NCA than the normal amines.⁵⁵ Unlike several aliphatic amines, HMDS initiated ROP can be completed overnight at ambient temperature with efficient monomer conversion and produce well-defined polypeptides with controlled chain lengths and low polydispersities in a high yield. Block copolymers were yielded when a second batch of monomer was added to matured chains. The unconventional characteristics of the N-trimethylsilyl (N-TMS) groups are thought to be the reason why chain growth in this system does not appear to exhibit any of the frequent side reactions (NAM/AAM) seen in amine-initiated

NCA polymerization. It has been suggested that the HMDS transfer a TMS group to the NCA before the silylamine is added to the resulting intermediate. This approach leads to the formation of a ring-opened monomer with an active TMS-carbamate end group (Scheme 1.6).

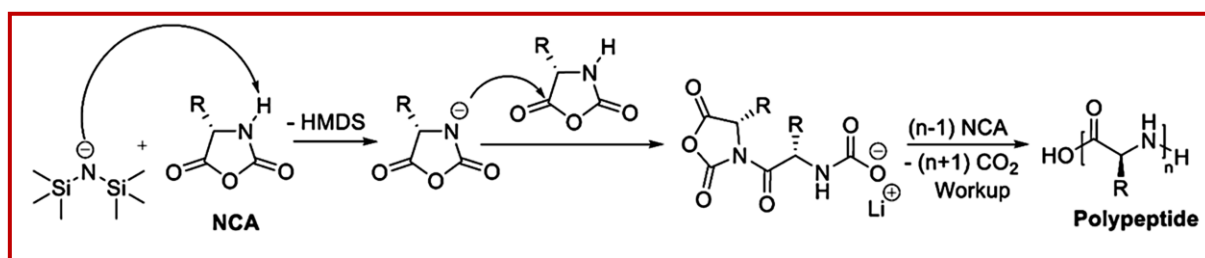


Scheme 1.6. Synthetic pathway of HMDS-initiated ROP of NCA. (Redrawn for the ref.⁵⁵)

Higher basicity than the normal aliphatic amines and presence of TMS group makes HMDS a potential candidate to initiate and propagate ROP of NCA in a diverse and controlled way than conventional NAM or AMM. This organosilicon based initiator offers a metal free technique for ROP of NCA to produce homo-or block copolypeptides with expected M_n s low D_s . Consequently, a variety of N-TMS based amines were developed for well-controlled ROP of NCA to synthesis polypeptides with enhanced end-group functionality.⁵⁶

Recently, Lithium hexamethyldisilazide (LiHMDS) initiated polymerization of NCA under anhydrous conditions has been reported by Runhui Liu and colleagues, producing exceptionally high molecular weight

polypeptides with narrow dispersities.⁵⁷ Although the polymerization process uses AMM (Scheme 1.7), it still results in narrowly dispersed polypeptides.



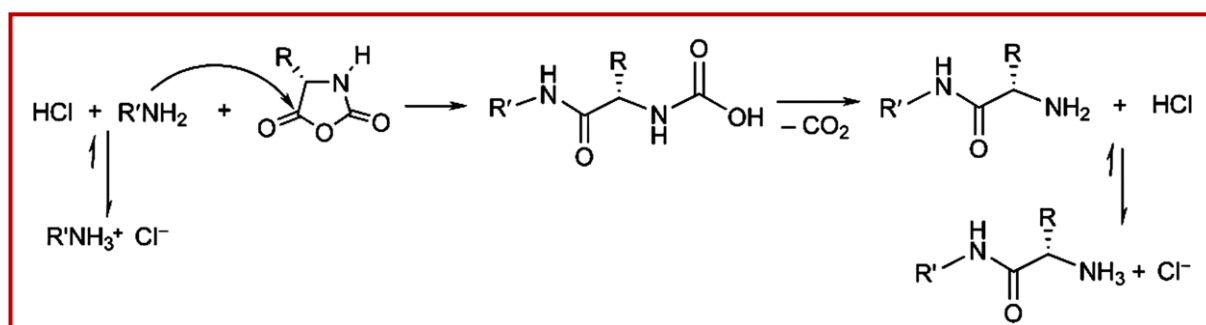
Scheme 1.7. Mechanism for NCA ROP initiated by LiHMDS. (Taken from ref ⁵⁷)

Migration of Li in the form of Li-carbamate along the growing polypeptide chain (Scheme 1.7), is responsible for the effectively faster polymerization. One of the most rapid methods for synthesizing linear polypeptides by ROP of NCA reported till date is the LiHMDS-initiated polymerization. Thanks to its superfast kinetics, this polymerization could take place in ambient conditions (in the open air) without hydrolysis of the NCA monomer. Additionally, the same group reported an even higher acceleration in polymerization utilizing potassium and sodium hexamethyldisilazides (KHMDS and NaHMDS), and this time the polymerization was much faster and followed a similar pathway (Scheme 1.7) via potassium or sodium carbamate intermediate.⁵⁸

1.2.4. ROP by Other Techniques

Over the past few years, there has been an increased focus on the development of novel initiators to control and accelerate the rate of polymerization (ROP) of NCA. Deming et al. first reported the living polymerization of NCA using transition metal (Fe, Ni, Co) catalysts as initiator to develop polypeptides with controllable molecular weight and low \mathcal{D} .^{50, 52} However, other living polymerization techniques have also been introduced by several research groups which include ammonium salt mediated initiation of ROP,⁵⁹ high

vacuum system,⁶⁰ low temperature method,⁶¹ nitrogen flow technique⁶² etc. Dimitrov and Schlaad developed an inventive method for controlling amine-initiated NCA polymerizations using amine hydrochloride salts as initiator.⁵⁹ AMM is impossible with the amine hydrochloride salt because it cannot behave as a base despite being less nucleophilic (scheme 1.8).

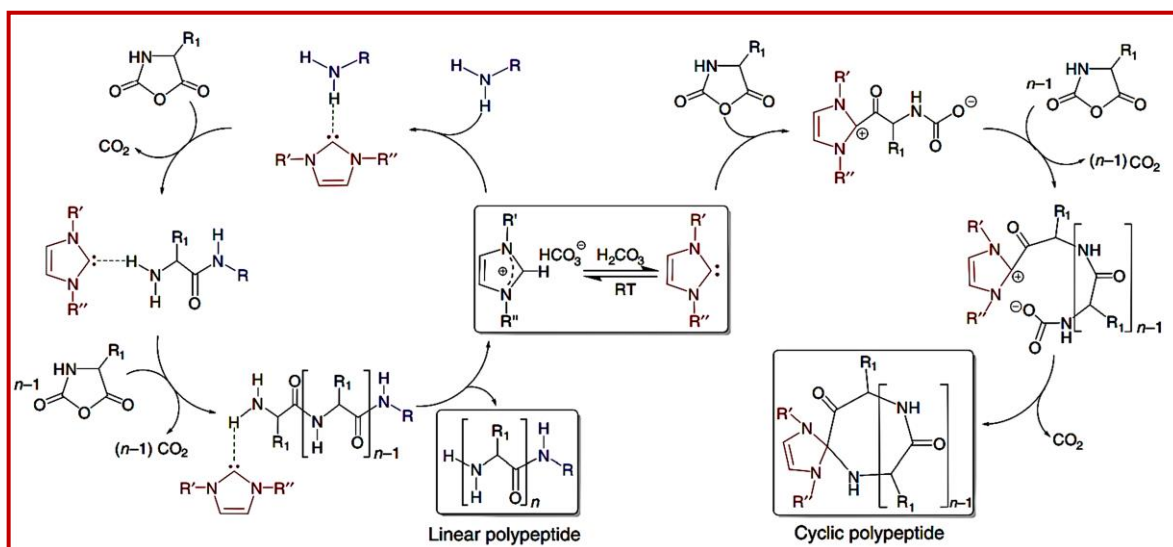


Scheme 1.8. Tentative mechanism of the ROP of NCA using amine hydrochloride salt. (Represented from ref.⁵⁹)

This method lacks complete polymerization due to sluggish reactivity of the initiators, and the polymerization can take up to several days. However, it is also found that the polymerization was accelerated and controlled as long as the ratio of primary amine hydrochloride to tertiary amine was maintained below 0.9 (upon decreasing further, it resulted in uncontrolled polymerization due to AMM by more tertiary amine).⁶³ This was done in an effort to improve the kinetics. Furthermore, Peng et al. first reported the NCA polymerization initiated by rare earth complexes to synthesize differently architected-polypeptides (homo, block and random) with controlled MWs and low \overline{D}_s .⁶⁴ Recently, Pahovnik and co-workers have also reported a method for the preparation of well-defined synthetic polypeptides by ROP of α -amino acid NCA, initiated by hydroxyl group.⁶⁵ They have smartly adopted a methodology where hydroxyl group in combination with an acid catalyst was used for the initiation and controlled ROP of NCA. Additionally, the reported methodology was also said to be fruitful for one-pot sequential polymerization of different

heterocyclic monomers and NCA. Very recently Grazon et al. have reported the first ever aqueous ROP of γ -benzyl-L-glutamate NCA using an α -amino-poly(ethylene oxide) macroinitiator.⁶⁶ Hadjichristidis and co-workers reported controlled-ROP of NCA using TRENs (triethylaminetriamine)s as an intriguing initiator that are the combination of tertiary and primary amine, which allowed ROP at a high speed compared to primary amines through a pathway coined as 'accelerated amine mechanism by monomer activation (AAMMA)'.⁶⁷⁻⁶⁸ Runhiu Liu and colleagues have developed a technique for ultrafast ROP of NCAs using tetraalkylammonium carboxylate initiator.⁶⁹ Carboxylates, a novel initiator for ROP of NCA, was found to initiate the process rapidly and without any additional catalysts. The polymerization was carried out using that initiator on crude NCAs in aqueous environments and open vessels at ambient conditions without requiring a glove box.

In addition to the different initiators mentioned earlier, a number of many different catalysts have been designed to control and expedite the ROP of NCA. The N-heterocyclic carbenes (NHCs) are an important class of compounds that have excellent Bronsted base properties and strong σ -donor characteristics. This makes them ideal for forming hydrogen bonding with amine initiators, which can be used to initiate ROP of NCA. People have studied the role of NHCs in polymerization processes and explore the potential applications of these compounds as catalysts or initiators.⁷⁰⁻⁷³ For example, NHCs have been employed by Lu and co-workers to accelerate the ROP of NCA initiated by HMDS.⁷² However, they (NHCs) have a major drawback as they are highly sensitive to moisture. Therefore, it is important to handle them strictly under inert conditions in order to ensure their safe use. The bicarbonate salts of NHCs have also been shown to be extremely air-stable and can act as precursors for NHCs.⁷⁴ When primary amines and NHC-bicarbonates were used as an initiator together, linear polypeptides were produced (Scheme 1.9) and in the absence of primary amine initiators, NHC alone has been found to trigger



Scheme 1.9. Mechanism of ROP of NCA catalyzed by NHC. (Taken from ref ⁷¹)

ROP of NCA and produce cyclic polypeptides.⁷¹ Recently, Tao et al. have pioneered living anionic ROP of NCA by tri-thiourea catalysts.⁷⁵ They have developed a very new and exceptional anion-binding catalytic framework composed of tripodal tri-thiourea with sodium thiophenolate which promotes anionic-ROP NCA precisely and selectively. Polypeptides produced by this technique are living and show narrow molecular weight distribution. The following two figures (Figures 1.5 and Figure 1.6) summarize most of the common methods for ROP of α -amino acid NCA mentioned in this section. They have been arranged according to their period of discovery.

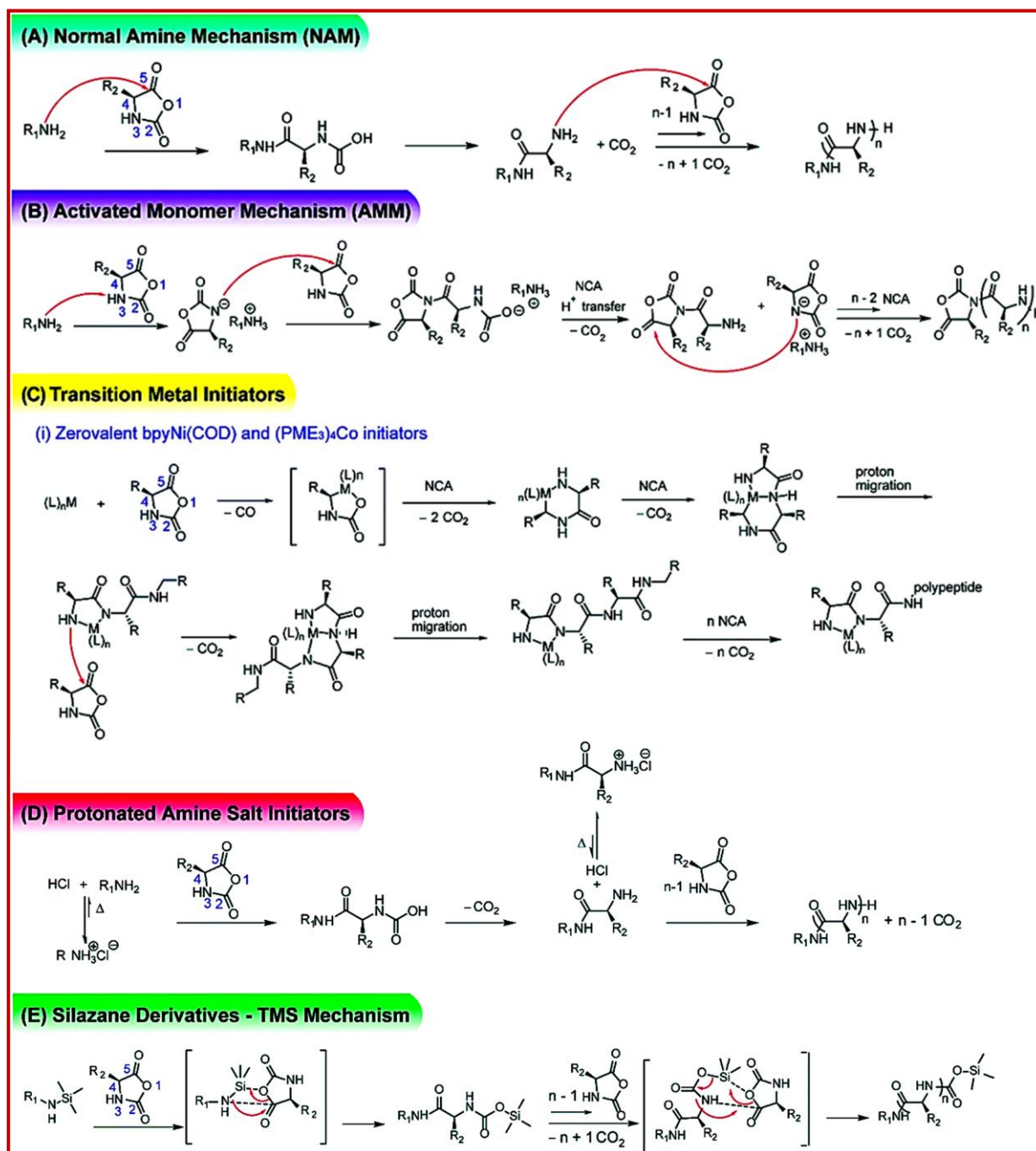


Figure 1.5. Early established methods of ring opening polymerization of α -amino acid NCAs and their mechanisms. (Represented from ref.³⁶)

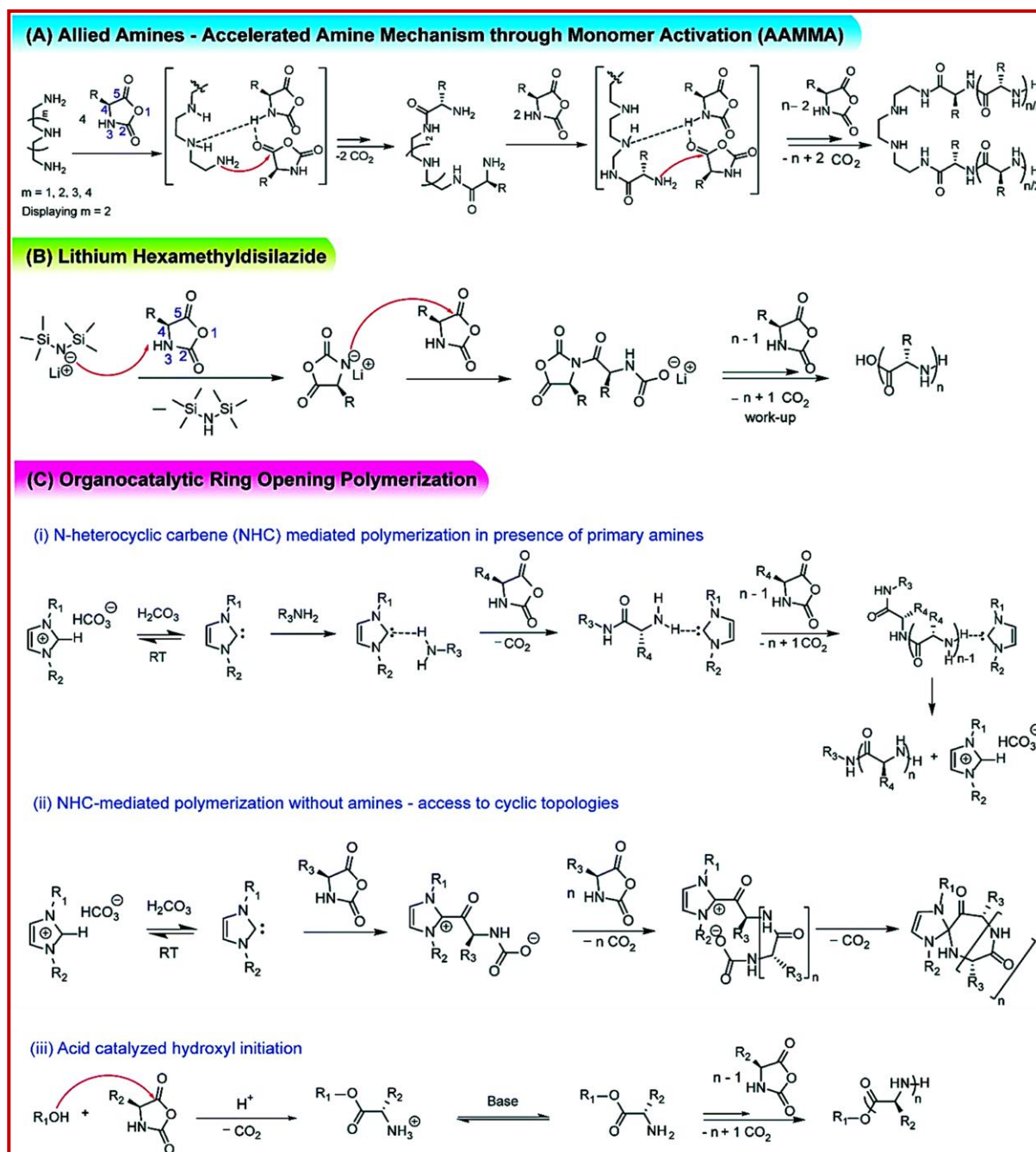


Figure 1.6. Some of the recently developed methods of ring opening polymerization of α -amino acid NCAs. (Represented from ref. ³⁶)

1.3. Functionalization of Polypeptides

For the last few decades, synthesis of novel NCAs along with the advancement of living or controlled ROP find itself as a ground-breaking revelation in the area of synthetic polypeptides. These structurally well-defined synthetic polypeptides with tunable functionality and stimuli-responsiveness can be achieved through following these two fundamental strategies: i) *pre-polymerization modification* (Figure 1.7A)- natural amino acids are chemically

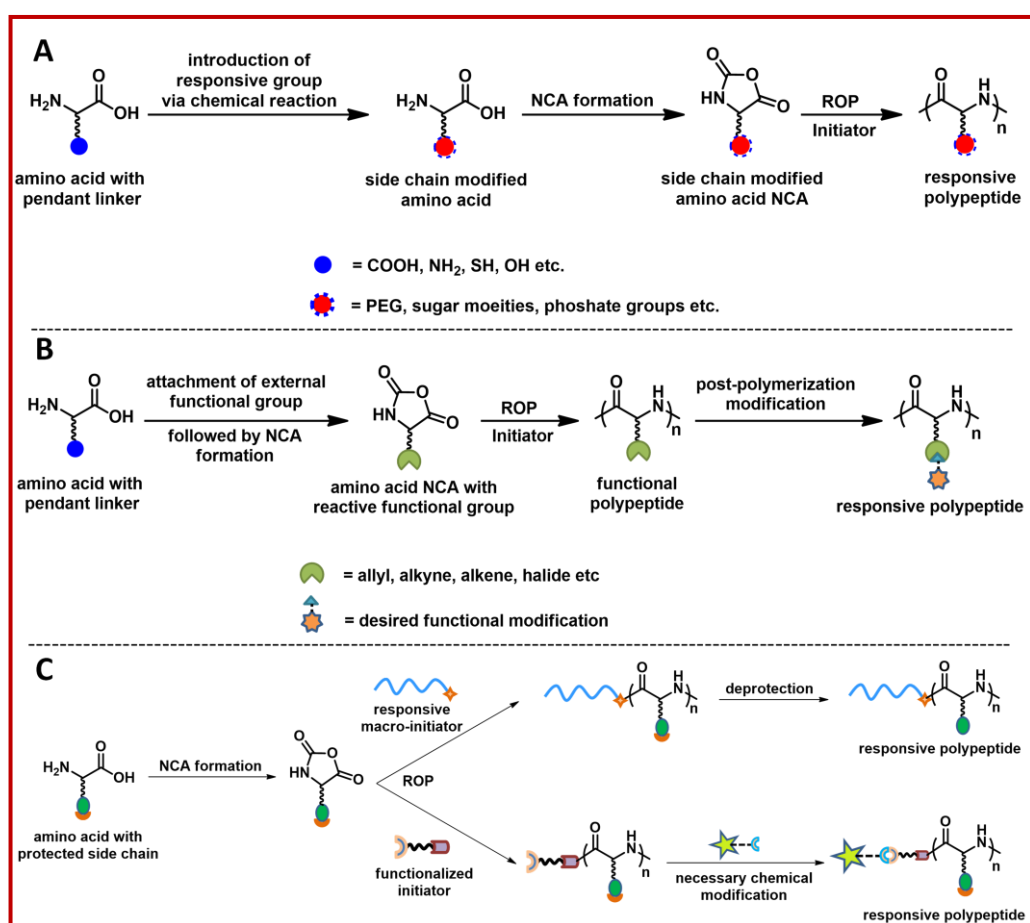


Figure 1.7. Schematic representation of different pathways for the synthesis of responsive polypeptide.

conjugated with responsive moieties or various functionalities through pendant linkers (carboxylic acid, thiol, amine, hydroxyl etc.) followed by NCA formation and subsequent ROP of that sidechain functionalized NCA directly resulted in mainly the stimuli-responsive polypeptides⁷⁶⁻⁸¹;

ii) *post-polymerization modification* (Figure 1.7B)- ROP of NCA, containing different reactive units like allyl, alkyne, alkene, azide, halide etc. followed by their post-polymerization modification through different chemical reactions such as Michael addition, click reaction, substitution reaction etc. to incorporate stimuli-responsiveness.⁸²⁻⁸⁶ Apart from these two strategies, use of differently functionalized or responsive initiators (macroinitiators) to carry out the ROP of NCA (Figure 1.7C) and further necessary modification at the chain-end leads to the formation of functional polypeptides with stimuli sensitivity also.^{18, 87-90} Figure 1.8 summaries some of the reported responsive polypeptides synthesized via side chain modified monomer/pre-polymerization modification strategy.

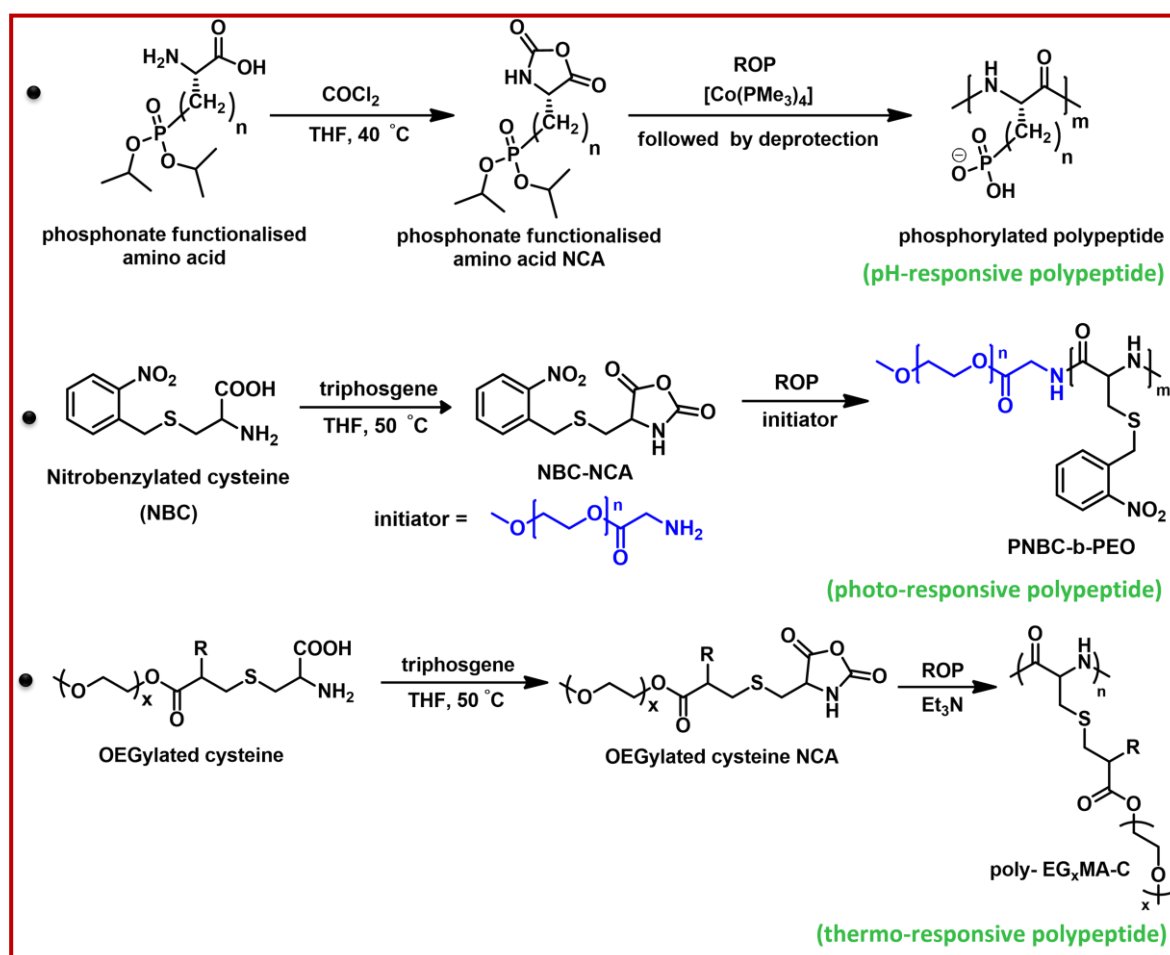


Figure 1.8. Responsive polypeptides, synthesized via 'side chain modified monomer' route. (Represented from the ref.^{79, 81, 91})

Figure 1.9 shows some of the reported functionalized polypeptides synthesized via post-polymerization approach. A few functionalized polypeptides have also been synthesized using the third approach mentioned above (Figure 1.10).

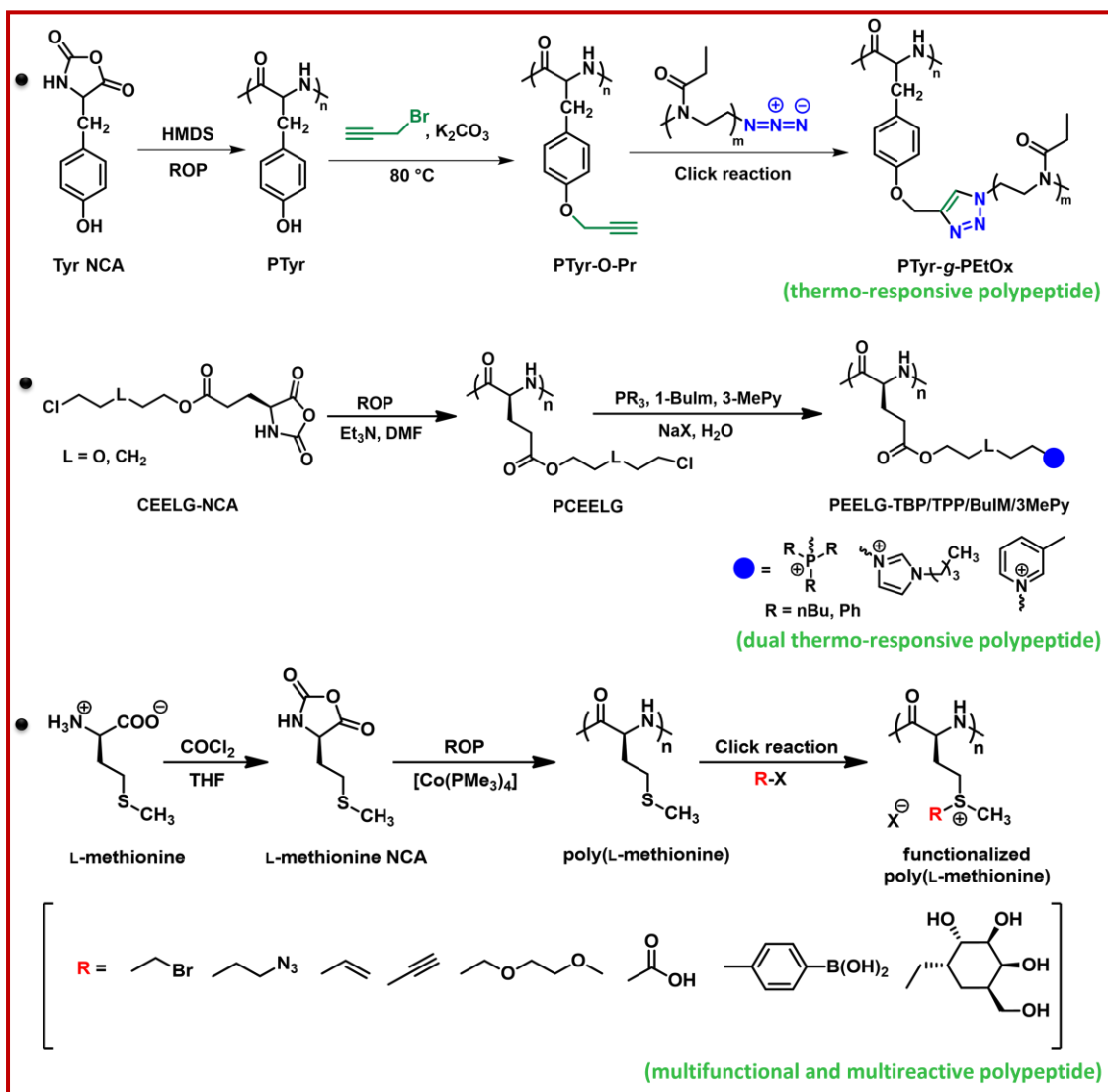


Figure 1.9. Responsive polypeptides, synthesized via 'post-polymerization modification' route. (Represented from the ref. ^{12, 92-93})

The first one is the direct polymerization of functional NCA, and it is simple enough to deliver 100% functionalized synthetic polypeptides exclusively with known chain-end. But sometimes in order to avoid side reaction during NCA

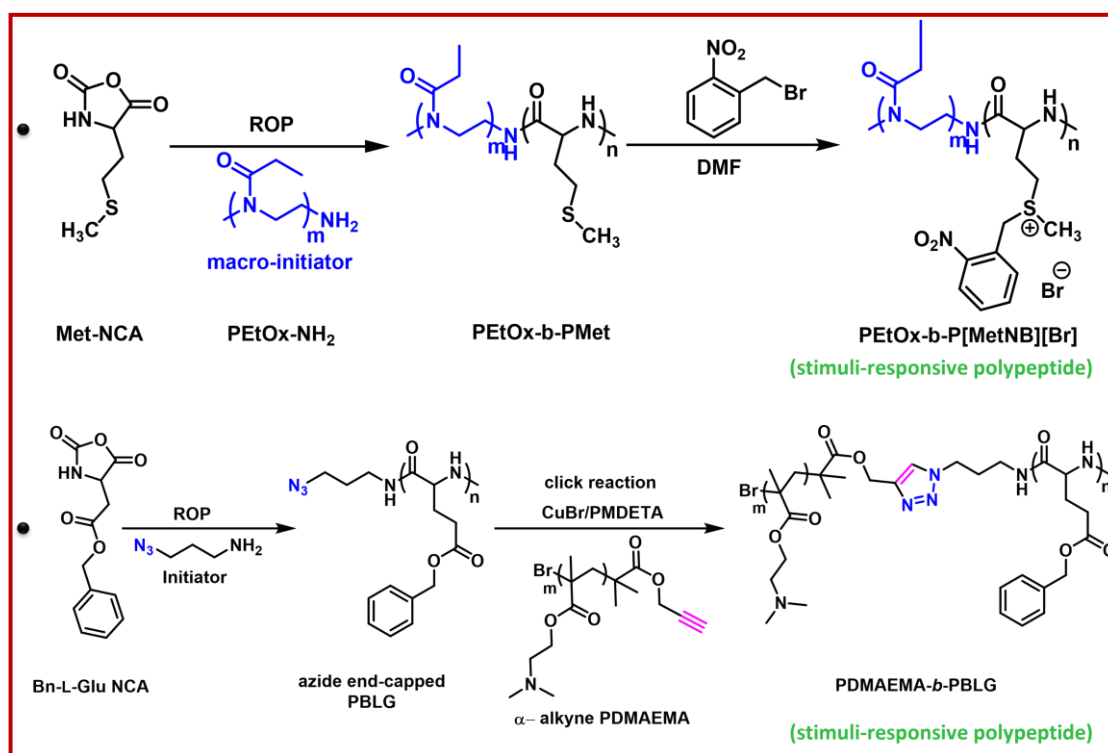


Figure 1.10. Responsive polypeptides synthesized using different responsive/functional initiators. (Represented from the ref. ^{17,87})

preparation, protection and deprotection of the externally conjugated functional groups, leads to the multistep NCA synthesis. However, the long and complex purification of functionalized NCA before final polymerization resulted in poor yield. On the other hand, post polymerization modification allows to synthesis divers responsive polypeptides from a single functionalized monomer. Responsive/functional groups those are not compatible with the chemical environment of the formation of NCA can be incorporated into the polymer chain by this strategy. But this strategy suffers from incomplete functionalization due to the steric factor of relatively bulk polypeptide precursors. Less selectivity and solubility of the polypeptide precursors also limits this process to apply several chemical modifications which are friendly enough with the small molecules. However, researchers have widely used click chemistry and chemical reactions as a tool to overcome the limitations of this post-polymerization strategy.⁹⁴ The Cu(I)-catalyzed azide-alkyne cycloaddition

(Cu-AAC) reaction has proven to be effective in synthesizing a variety of functionalized polypeptides through post-polymerization modification.^{12, 87, 95} This involved attaching an alkyne to one end of the polymer chain and an azide to the other end, which then reacted in the presence of a copper(I) catalyst to form a triazole ring. Additionally, the polymer can contain functional groups as side groups that originate from the monomer. For non-linear polymer architectures, e.g., star polymer can be synthesized using an amine initiator with difunctional alkyne functionality.⁹⁶ Recent efforts have focused on producing polypeptides with alkyne side groups through NCA ROP.^{85, 97-98} These alkyne side groups can react with azide-functionalized PEG chains to form a grafted polymer structure. Moreover, small functional molecules, such as carbohydrates, can be added to the polymer for specific targeting of cell membranes.^{26, 77, 99}

In addition to the introduction of alkyne or azide, functional polypeptides can also be obtained by incorporating different reactive functional groups (alkene, halide, thiols, thio- and selenoethers etc.) before polymerization.^{83, 92, 100-103} These functional polypeptides can undergo efficient post-polymerization modifications from reactive side groups by thiol-ene click reaction,¹⁰⁴ Michael addition,⁸⁴ olefin metathesis,⁸³ nucleophilic substitution,¹⁰⁵ and photo-cross-linking¹⁰⁶ etc.. Even functionalities such as carboxylic acid,¹⁰⁷ oligo(ethylene glycol) (OEG),⁸² and sugar⁸⁴ which may hinder the polymerization process, can also be conjugated onto polypeptide side chains with high efficiency.

Based on these well-devised synthetic strategies, polypeptides can be customised in different ways to serve the purpose of various biomedical applications. Incorporation of stimuli-responsive segments into the polypeptides also improve their applicability in different areas. Different types of stimuli-responsive polypeptides have been discussed in this thesis along with their self-assembly behaviour and biomedical applications.

1.4. Polypeptide Architectures formed via ROP of NCA

A diverse range of polypeptide architectures have been designed using the library of available amino acids, each possessing their unique characteristics and functionalities.^{32, 108} Copolypeptides are typically synthesized by dissolving NCA monomers simultaneously and then adding an initiator. However, the reactivity of amino acid NCAs may differ, leading to varied distributions of monomer residues, including alternating, random, or gradient-containing chains. Reactivity ratios of NCA monomers have been determined using various methods as reported elsewhere.¹⁰⁹⁻¹¹¹

Different block copolypeptides have also been prepared using living NCA ROP techniques as discussed earlier. The order of addition of NCAs is critical in the synthesis of block copolypeptides, with the more soluble polypeptide block typically prepared first. When a bifunctional initiator is used, sequential addition of the second monomer results in a triblock copolypeptide. A short library of synthetic block copolypeptides that are available in the literature has been presented in Table 1.1. While block copolymerization's of NCAs are highly versatile, as shown in Table 1.1, there are also some limitations. The number of species used for the first block is limited due to solubility considerations. However, the second block can have a less soluble composition, such as with leucine, alanine, and phenylalanine amino acid residues. Among the different available living polymerization methods, the catalytic polymerization using nickel and cobalt offered the greatest variability for NCAs and have the ability to produce the highest number of blocks during ROP (Table 1.1). Additionally, the high vacuum technique (HVT) has also shown to be successful for few cases (Table 1.1). In this technique, the removal of water and other impurities from the reaction vessel paved the pathways for successful synthesis of living polypeptides with well-defined architectures, as explored by Hadjichristidis and co-workers.⁶⁰

Table 1.1. Block copolypeptides prepared by ROP of different NCAs.

1 st block	2 nd block	3 rd block	4 th block	5 th block	Method	References
PBLG	PLeu				HV, Ni-Cat	50, 60
	PCys(Z)				Ni-Cat	112
	PAla				HV	113
PMeLG	PLeu				RT	114
PZLL	PLeu	PZLL	PLeu	PZLL	Co-Cat	115
	PCystine				Silazane	116
	PBLG				HV, Ni-Cat	50, 60
P(EG₂Lys)	PBLA				Ni-Cat	117
P(α-man Lys)	PZLL				Co-Cat	77
P_{TLL}	PLeu				0 °C	118
PArg(Z₂)	PLeu				Co-Cat	119
PBLT	PBLG				35 °C	120

HV: high vacuum method, Co- / Ni-Cat: catalytic cobalt- / nickel-mediated method. A temperature represents the polymerization reaction temperature.

ROP of NCA has been used in combination with post-functionalization or selective deprotection methods to prepare non-linear polypeptides.¹²¹⁻¹²⁴ For examples, non-linear polypeptides include dendritic-graft and branched copolypeptides which were synthesized via living NCA ROP using lysine NCA monomers with different protective groups.¹²⁵⁻¹²⁶ Dendritic-grafted polypeptides were prepared using a copolypeptide of N_ε-benzyloxycarbonyl-L-lysine (ZLL) and N_ε-tert-butyloxycarbonyl-L-lysine (^tBocLL), where the *t*-Boc groups were

selectively removed before polymerizing the grafts from the free amines.¹²⁵ Branched polypeptides were also prepared by end-group functionalization of a linear lysine block with N_α, N_ϵ -diFmoc-L-lys, which produced two primary amines upon selective deprotection with piperidine for initiating new polypeptide branches.¹²⁶ There are huge number of reported articles in the literature which deal with the synthesis of the block copolypeptides using different techniques (Table 1.1). On the other hand, synthesis of graft, branched or network type copolypeptides, comprising of different responsive polymeric segments in their side chains are very limited. Graft copolypeptides can be synthesized using either 'grafting from' or 'grafting to' techniques. On the other hand, one way to create covalently bonded polypeptide-based network is by using a difunctional monomer or a postpolymerization step.¹²⁷⁻¹³⁰ An intriguing option is to use a diNCA monomer made from L-cystine.^{116, 131} Cystine consists of two cysteine molecules connected by a sulfur-sulfur bond, and this bond can be reduced after polymerization to form thiols and break the crosslinking in the final material. Several methods can be used to form a network after polymerization, including the oxidation of free thiols or the use of 3,4-dihydroxyphenyl-L-alanine (DOPA),¹³² an amino acid that can be cross-linked through oxidation to form quinone side groups that can be linked through a radical process. To achieve these crosslinking reactions, a high concentration of reactive groups is required, which can be achieved through self-organized structures.

1.5. Solution-Properties of Functionalized Polypeptides

Synthetic functionalized polypeptides can possess interesting solution properties depending on the specific modifications and functional groups incorporated into their structures. Some notable solution properties are:

Solubility. Functionalized polypeptides can exhibit different solubility characteristics compared to their unmodified counterparts. Introduction of

hydrophilic groups, such as charged residues¹⁰⁷ or polyethylene glycol (PEG)¹³³ /other hydrophilic segments¹², can enhance water solubility and promote self-assembly.

Stability. Modifications in polypeptides can enhance their stability against chemical or enzymatic degradation. For example, incorporation of non-natural amino acids, such as D-amino acids, can improve resistance to proteolytic enzymes.¹³⁴ Additionally, functional groups like thiol or disulfide linkages can confer increased stability against reducing or oxidative environments.¹³⁵

Biocompatibility and Bioactivity. Functionalized polypeptides can be designed to exhibit improved biocompatibility, reducing adverse reactions and cytotoxicity, which promotes their specific bioactive properties, such as enzymatic activity or receptor-binding capabilities.^{94, 136-138} These modifications can enable tailored interactions with target molecules or biological systems, making them valuable in applications such as enzymatic catalysis, drug delivery, or tissue engineering.¹³⁹⁻¹⁴¹

Rheology. Functionalized polypeptides can exhibit unique rheological properties in solution. Depending on the specific modifications, they can form gels, display shear-thinning or shear-thickening behaviour, or exhibit viscoelasticity. These properties are crucial for applications involving injectable hydrogels, coatings, or 3D printing.¹⁴²⁻¹⁴⁴

Optical properties. Certain functionalized polypeptides can possess optical properties, such as fluorescence or light absorption, due to the presence of chromophores or conjugated groups. These properties enable their use in applications like imaging, biosensing, or optoelectronics.¹⁴⁵

It's important to note that the specific solution properties of functionalized polypeptides can be highly dependent on the nature, position, and density of the introduced functional groups, as well as external factors such as temperature, pH, redox, light etc. Tailoring these properties allows for the

development of innovative materials and applications in a wide range of fields, including biomedicine, materials science, and nanotechnology. The following topic describes a brief description of different stimuli-responsive polypeptides as well their self-assembly behaviour in various solvents, mostly in water.

1.5.1. Stimuli-Responsive Functionalized Polypeptides

Stimuli-responsive property refers to the characteristic of a material or system to alter its behaviour or properties in response to an external stimulus. This stimulus can take the form of temperature, light, pH, redox, electric, or magnetic fields, pressure, or specific chemicals (external ions, enzymes etc.). When subjected to these stimuli, the material undergoes reversible or irreversible changes, leading to modifications in its physical, chemical, or biological attributes. Stimuli-responsive materials, particularly "smart" polymers with both ionic and non-ionic characters, have gained significant attention due to their wide range of applications in drug delivery systems, sensor-based material fabrication, and more.¹⁴⁶⁻¹⁴⁸ Functionalized polypeptides can be designed to respond to specific stimuli by incorporating responsive moieties or functional groups into the polypeptide backbone or side chains.⁴⁶ These smart polypeptides containing the reactive functional groups that exhibit highly responsive behaviours to changes in external environments can result in significant changes in their properties such as solubility, surface nature, permeability, shape, as well as mechanical, optical, electrical, and chemical properties. Stimuli-responsive polypeptide materials find applications in various fields of biomedical applications, including drug delivery, tissue engineering, membrane, and adhesive etc.^{3, 5, 28-29}

1.5.1.1. Thermo-Responsive Polypeptides

Polymers that are sensitive to the external temperature are known to be thermoresponsive polymers. Among different stimuli, temperature is the most widely investigated and used stimulus because of its easy tuning from the

outside and successively monitoring of the different properties of the polymer sample, specially focused on their solution properties and morphologies of the adopted nanostructures (micelles, vesicles etc.) in solution. Typically, thermoresponsive polymers undergo a reversible phase transition (from soluble state to cloudy suspension or vice versa, which is sometimes termed as “coil-globule transition”) due to the abrupt change in their solvation behaviour at a critical temperature which includes lower critical solution temperature (LCST) and upper critical solution temperature (UCST) (Figure 1.11).

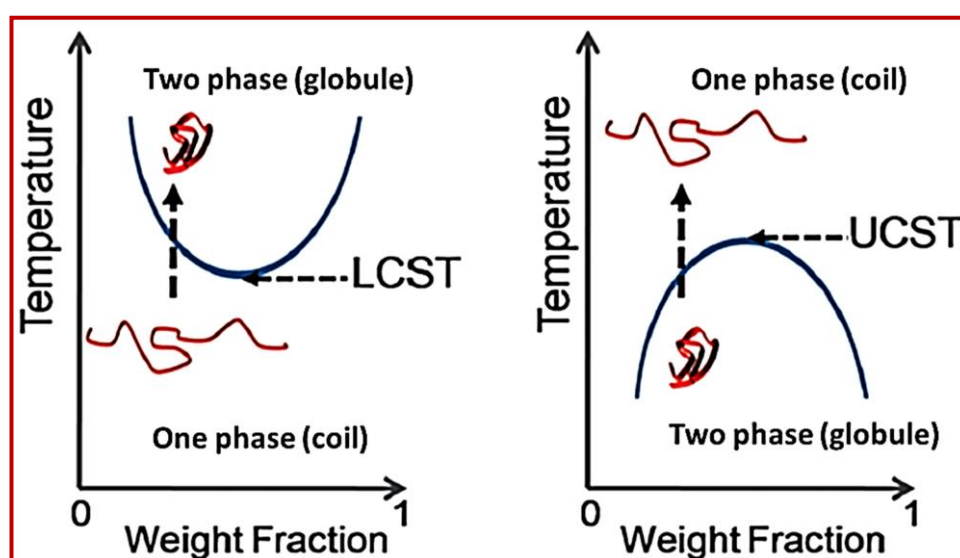


Figure 1.11. Schematic representation of the phase transition of LCST- and UCST-type thermoresponsiveness. (Taken from ref.¹⁴⁹)

In the former case, extensive hydrogen bonding interactions between the polymer chain and the solvent molecules (especially water) results in the solubilisation of the whole polymer restricting the inter-chain hydrophobic interactions among the neighbouring polymer chains. Upon heating disruption of these hydrogen bonding interactions increases the polymer-polymer hydrophobic interactions, resulting in an aggregation of enthalpically favoured polymer coil structure to an entropically favoured dense globular structure.¹⁵⁰ This process is reversible in nature as it goes back to clear solution on cooling

again. Most of the reported LCST polymers are non-ionic in nature and some of the common examples are poly(N-isopropyl acrylamide) (PNIPAM),¹⁵¹ poly(2-oxazoline)s (POxs),¹⁵² poly(N,N-dimethylaminoethyl methacrylate) (PDMAEMA),¹⁵³ poly(methacrylamide) (PMAAm),¹⁵⁴ etc. In contrast, there has been relatively less emphasis on UCST-type polymers, which exhibit a distinct behaviour of phase transition from insoluble to soluble states (globule-to-coil) upon heating, and vice versa upon cooling in a particular solvent. It is important to note that UCST-type phase transitions are driven by strong polymer-polymer and solvent-solvent interactions, rather than weak interactions between the polymer and solvent.¹⁵⁵ Additionally, in UCST-type polymers, the influence of the hydrophobic effect (entropic) is less significant. As a result, the behaviour of UCST-type polymers is often described as being driven by enthalpy, depending on either hydrogen bonding (HB-UCST polymers) or Coulomb interactions (C-UCST polymers). The thermoresponsiveness of different polymers is solely dependent on the proper hydrophilic-hydrophobic balance within the polymeric system. Biocompatible polymers with thermo-sensitivity are of great demand due to their vast applications as nanoreactors and as drug delivery systems. Thus, considering their applications, it is equally important to develop novel LCST- and UCST-polymers.

Poly(N-isopropylacrylamide) (PNIPAM) is a well-known thermoresponsive polymer that exhibits a LCST of approximately 32 °C, which is close to human body temperature.¹⁵⁶ The unique thermoresponsive property of PNIPAM has led to the exploration of various potential applications, such as cell adhesion,¹⁵⁷ drug delivery,¹⁵⁸ and cellular imaging¹⁵⁹ etc. However, studies have shown that PNIPAM-based materials are not biocompatible,¹⁶⁰ which limits their applications in certain biological contexts. To address the issue of protein adsorption and develop alternative materials to PNIPAM, researchers have turned to poly(ethylene glycol) (PEG) and oligo(ethylene glycol) (OEG)

based LCST-polymers, often referred to as OEGylated polymers.¹⁶¹⁻¹⁶² The introduction of OEG groups with specific lengths allows the polymers to exhibit a transition from a hydrophilic state to a hydrophobic state as the temperature increases or decreases. This thermoresponsive behaviour adds an additional dimension to their functionality and versatility for applications such as biomedical devices, drug delivery systems, and bioimaging.¹⁶³⁻¹⁶⁴

LCST Polypeptides: There are huge number of articles in the literature dealing with the thermoresponsive polypeptides as well as and their applications.^{8, 12, 17, 76, 81, 165-167} Thermoresponsive polypeptides demonstrating LCST, have been developed by different research groups.^{12, 76, 81, 168-169} LCST-type thermoresponsive polypeptide materials have been obtained by conjugating different hydrophilic side chains (mainly PNIAPM, OEG or PEG etc.), incorporated into hydrophobic polypeptide backbone either by pre-/post-polymerization modification or by using them as macro-initiator for NCA polymerization. For example, research group of Lecommandoux and others reported the synthesis of responsive polypeptides where they have incorporated temperature-responsive polymer segments like PDMAEMA, PNIPAM, etc. into the polypeptide backbone to obtain novel thermoresponsive polypeptides.⁸⁸⁻⁸⁹ Incorporation of PEG units into the side chain of polypeptide, results in thermoresponsive polypeptides with tunable LCSTs.¹⁷⁰⁻¹⁷³ Zhibo Li and co-workers have reported a series of thermoresponsive polypeptides synthesized by direct polymerization of PEGylated NCA monomers.^{19, 76, 81} Chen et al. have synthesized PEGylated poly-L-glutamate (poly-L-EG_xGlu) with tunable LCST-type phase transition in water (Figure 1.12). They have synthesized different NCAs with variable PEG chain length and it was found that the copolymerization of those NCAs at varied molar ratio was able to manipulate the LCST of the final copolypeptide. Depending upon the chain length of the PEG units, different poly(L-EG_xGlu)s and copolypeptides adopt different secondary structures which in turn control the thermoresponsive

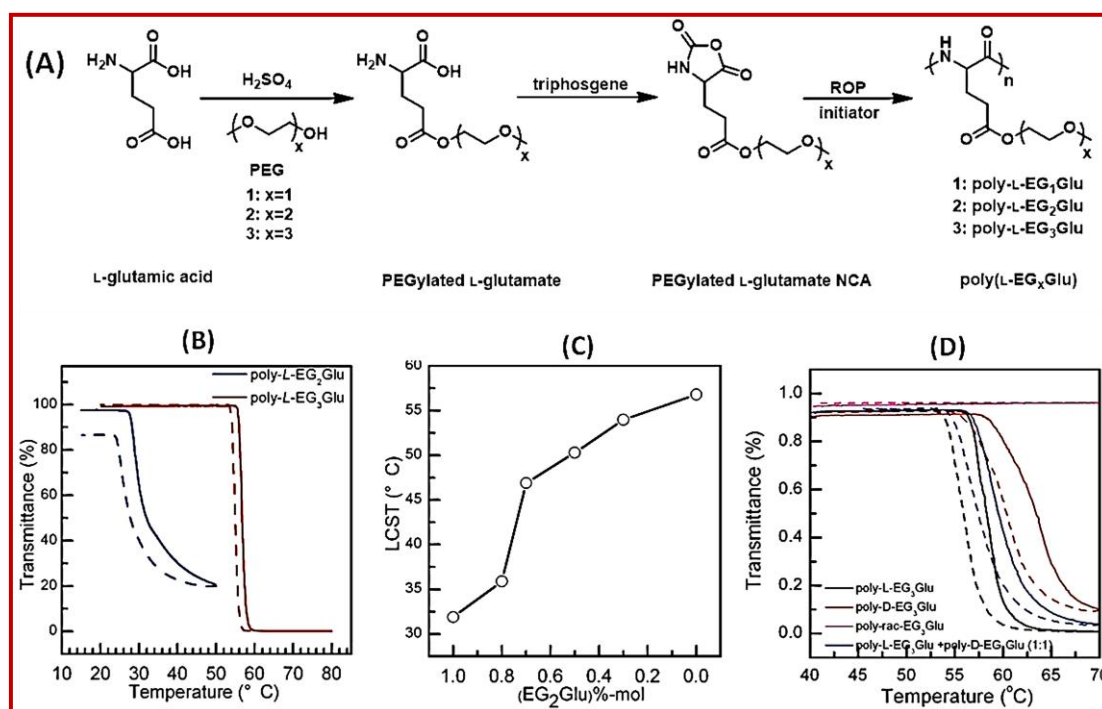


Figure 1.12. (A) Synthetic scheme for poly(L-EG_xGlu); (B) Transmittance vs. temperature plot of aqueous solution (2 mg/mL) of poly(L-EG_xGlu) with different PEG chain length; (C) LCST of poly(L-EG₂Glu-co-EG₃Glu) copolypeptides as a function of sample composition; (D) Transmittance vs. temperature plot of different poly(L-EG_xGlu) homo- and co-polypeptides. [Solid line: heating cycle; dashed line: cooling cycle] (Represented from the ref.⁷⁶)

properties of the homo/copolypeptides. Hydrogen bonding (inter/intra molecular) interaction of amide linkage in solution is thought to be responsible behind this secondary structure driven LCST behaviour of PEGylated polypeptides.⁷⁶ Xiaohui Fu from the same group reported the synthesis of a series of oligo(ethylene glycol) functionalized cysteine NCA monomer and their subsequent ROP resulting in OEGylated poly(L-cysteine) homopolypeptides.⁸¹ These functionalized polypeptides were soluble in multiple solvents other than water. It was also found that solubility in water of these polypeptides increases with the length of the OEG moiety, grafted in the side chain. LCST-type reversible phase transition was also noticed in water when the repeating unit

of OEG residue reside between 3 and 5. However, unlike the OEGylated polyglutamate, due to the presence of additional methylene group coming from the (me)acrylate, more ethylene glycol units are required for OEGylated polycysteine to be thermoresponsive.⁸¹ Yilong et al. have prepared thermosensitive hydrogels by ROP of L-glutamate NCA with varying alkyl chain length (methyl, ethyl, n-propyl, and n-butyl) using mPEG₄₅-NH₂ as a macroinitiator.¹⁷⁴ The resulting copolymers exhibited sol-gel transitions upon changing temperature. Interestingly, the polypeptides containing methyl and ethyl groups demonstrated considerably lower critical gelation temperatures (CGTs) compared to those incorporating n-propyl and butyl side groups.¹⁷⁴

These examples highlight the sensitivity of thermoresponsive behaviour to even slight structural variations in polypeptides, conjugated with OEG units. The delicate balance between hydrophilicity and hydrophobicity is necessary for displaying thermoresponsive properties, which can be disrupted by modifications that also affect the conformational stability of the polypeptide chain, causing the loss of thermoresponsive behaviour in certain OEG-conjugated polypeptides. For example, Deming reported the synthesis of OEGylated poly(L-lysine), which was a non-ionic helical polypeptide that didn't display thermoresponsive properties.¹⁷⁰ Similarly, poly(L-EG_xAsp) (x = 1, 2, 3), synthesized from OEGylated aspartic NCAs, didn't exhibit a LCST behaviour in water.¹⁷⁵

Indeed, there has been a growing interest in developing alternatives to PEGylation in the past decade. To address these issues, researchers have explored various PEG alternatives that can provide similar benefits. Some of these alternatives include, poly(N-vinylpyrrolidone),¹⁷⁶ poly(glycerol),¹⁷⁷ poly(zwitterions),¹⁷⁸ poly(carbonates),¹⁷⁹ poly(oxazolines),¹⁵² and poly(sacharrides)¹⁸⁰. In this context, poly(2-oxazoline)s (POxs) have been found to be an important alternative to PEG because of their biocompatibility, biodegradability, similar architecture to biomolecules, and ability to be

functionalized.¹⁵² Due to their structural resemblances, the POXs are referred to as pseudo-peptides. The most common method for producing POXs is living cationic ring-opening polymerization (CROP), which can be end-capped by any nucleophilic attack of hydroxyl,¹⁸¹ carboxylic acid,¹⁸² amine,¹⁸³ or azide¹² functional groups and then used in POXylation of the biomacromolecules.¹⁸⁴ The functionalized POXs can also be used as macroinitiators to create diblock copolymers.^{17, 185} By varying the 2-substituent of the monomer (oxazolines), a good control over the hydrophilic-hydrophobic balance of the resulting POXs can be achieved.^{181, 184} Thermoresponsive poly(2-oxazoline)s with LCST behaviour can be obtained by conjugating the hydrophilic tertiary amide bond of the polymer backbone with small hydrophobic side chains. Owing to these versatile properties and excellent biocompatibility of POXs, researchers have administered different post-polymerization approaches, such as 'grafting from' or 'grafting onto', to modify the synthetic polypeptides for developing novel biomaterials. For example, our group have reported the synthesis of a novel thermoresponsive graft copolypeptide PTyr-*g*-PEtOx with the help of 'click-grafting' strategy (Figure 1.13A), which showed LCST-type thermoresponsive behaviour in water.¹² The amphiphilic copolypeptide (PTyr-*g*-PEtOx) was composed of a hydrophobic polytyrosine backbone and a hydrophilic poly(2-ethyl-2-oxazoline) (PEtOx) pendant side chain. Incorporation of the inherently thermoresponsiveness PEtOx into the side chain of propargyl-functionalized poly(L-tyrosine) (PTyr) gave rise to the thermoresponsive PTyr-*g*-PEtOx copolypeptide with LCST-type phase behaviour in water (Figure 1.13B). Cloud point of the PTyr-*g*-PEtOx was tuned by varying the chain length of both the backbone and pendant side chain. It was found that with increase in the grafting density of the hydrophilic pendant PEtOx chain as well as the chain length of the hydrophobic polytyrosine backbone, cloud point (T_{cp}) of the PTyr-*g*-PEtOx decreases (Figure 1.13C). This decrease of T_{cp} ascribed to the overall increase in the hydrophobicity of the system after grafting.

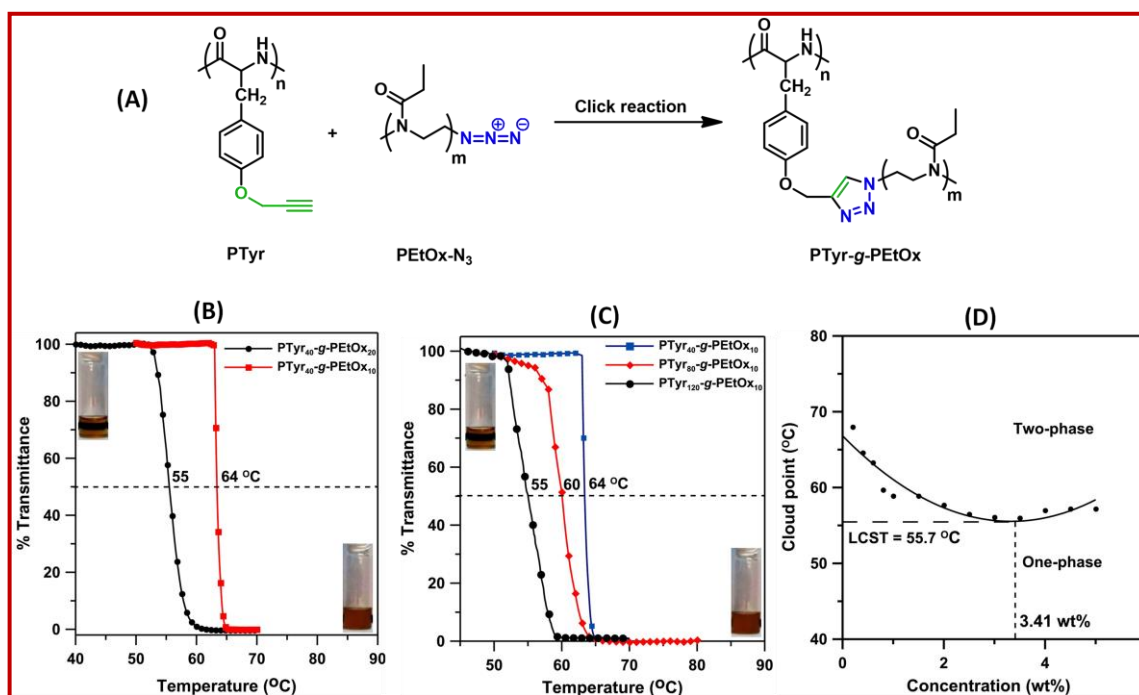


Figure 1.13. (A) Synthetic scheme for PTyr-*g*-PEtOx; Transmittance vs. temperature plots of PTyr-*g*-PEtOx with varying side chain length (B) and backbone chain length (C); (D) LCST of PTyr-*g*-PEtOx as a function of sample concentration. (Represented from the ref.¹²)

There are few other examples of synthesis of polypeptide-polyoxazoline conjugates, where amine-end-capped polyoxazoline(s) have been used for ROP of NCAs to prepare the block copolypeptides. Soliman et al. have reported the synthesis of poly(2-ethyl-2-oxazoline)-*b*-poly(benzyl L-glutamate) (pEox-*b*-pBLG), which self-assembled into micellar aggregates in water.¹⁸⁶ Similarly, Okada and co-workers have synthesized polyoxazoline-(glyco)peptide copolymers by ROP of sugar-substituted α -amino acid NCAs using polyoxazoline macroinitiators.¹⁸⁷ However, none of them have studied the thermoresponsiveness of the final copolypeptides. These are the very few examples of polypeptide-polyoxazoline conjugates that are available in the literature. Thus, it would be worthy of interest to synthesize novel polyoxazoline-polypeptide copolymers and investigate their solution properties.

UCST Polypeptides: Polymers with UCST-behaviour undergo insoluble to soluble phase transition in solution when the temperature is increased above a certain threshold. The UCST behaviour of polymers can be attributed to various factors, including the interplay between hydrophobic and hydrophilic interactions, chain conformational changes, and the nature of the solvent or the externally added materials.¹⁸⁸ These UCST polymers have potential applications in various fields, such as drug delivery systems, biomaterials, etc. where the ability to undergo a reversible phase transition in response to temperature changes is desirable.¹⁸⁹⁻¹⁹⁰ By manipulating the polymer composition and environmental conditions, researchers can tune the UCST behaviour of synthetic polymers to suit specific applications. However, unlike LCST-polypeptide, UCST-polypeptides are very less explored and can be both ionic and nonionic despite their importance similar to LCST-polypeptides. The research groups of Haoyu Tang have prepared a series of poly(L-glutamate) based functionalized polypeptides and investigated their UCST-type thermoresponsiveness by varying the polypeptide architecture, solvents and as well as the counter anions.^{13, 93, 166, 191-194}

For example, Tang and his co-workers have studied the solution behaviour of a newly synthesized series of ABA type triblock copolypeptide (PImBF₄-*b*-PPG-*b*-PImBF₄) consisting of polypropylene glycol (PPG) as the middle block and polyglutamate based terminal blocks containing 1-butylimidazolium fluoroborate (PImBF₄) as the pendant ionic groups (Figure 1.14A).¹³ In this case, the authors observed UCST-type phase behaviour of PImBF₄-*b*-PPG-*b*-PImBF₄ in water (Figures 1.14B-1.14C). The tuning of the phase transition temperature (T_{cp}) by adjusting the polymer concentration and also chain length of both of the PPG and PImBF₄ units has been demonstrated (Figure 1.14D). They have explained that the polymer block units of longer chain length present in a triblock copolymer were prone to generate larger self-assembled structures, which aggregated fast on lowering temperature

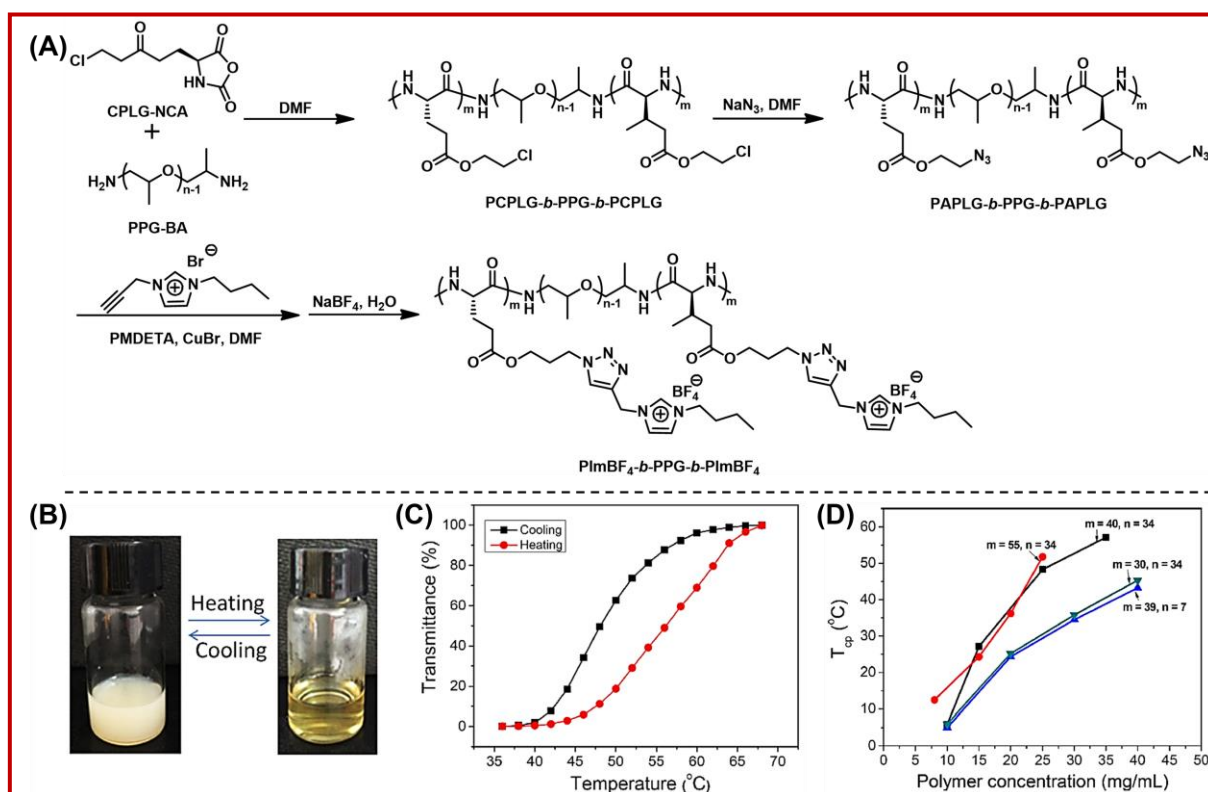


Figure 1.14. (A) Schematic pathways of $PImBF_4$ -*b*-PPG-*b*- $PImBF_4$; (B) photograph of the representative $P(ImBF_4)_{40}$ -*b*-PPG₃₄-*b*- $P(ImBF_4)_{40}$ sample solution (25 mg/mL in water) at different temperatures; (C) Plots of %T vs temperature ($\lambda=500$ nm) of $P(ImBF_4)_{40}$ -*b*-PPG₃₄-*b*- $P(ImBF_4)_{40}$ in water; (D) Plots of T_{cp} v polymer concentration for $PImBF_4$ -*b*-PPG-*b*- $PImBF_4$ with different polypeptide and PPG chain lengths. (Represented from ref.¹³)

compared to the triblock copolymers with shorter chain length, leading to a more prominent increase in T_{cp} . The same group have also prepared a similar type of poly(L-glutamate)-based water soluble homopolypeptides bearing 1-alkylimidazolium (methyl or n-butyl) group in their side-chain and with different counter anions (Cl^- , I^- , BF_4^-) via multistep process.¹⁹³ The resulting polypeptides showed thermoresponsive behaviour in different solvents (aqueous and non-aqueous), which can be effectively regulated by the polarity of the solvents, length of the alkyl groups attached with the imidazole ring, or the types of counter anions present. For example, polypeptide bearing more

hydrophobic butyl substituent and BF_4^- counter anion showed UCST-type phase behaviour in water, while the same showed LCST-type phase behaviour in acetone. T_{cps} were reported to be independent of the molecular weight of the polypeptide, but greatly affected by the externally added salts (NaCl , NaI , BaBF_4), suggesting the electrostatic interaction-driven thermoresponsiveness of the polypeptides. Externally added anions-induced UCST-type thermoresponsiveness in water of a L-methionine based cationic homo-/co-polypeptides ($\text{P}[\text{MetNB}][\text{Br}]$ / $\text{PEtOx-}b\text{-P}[\text{MetNB}][\text{Br}]$) were also reported by our group.¹⁷ They have proposed that the added anions (SCN^- , ClO_4^- , I^-) formed an anion-bridge interaction (Figure 1.15) with the neighbouring cationic polypeptide chains to cause hazy suspension at room temperature, which became clear on heating and vice-versa.

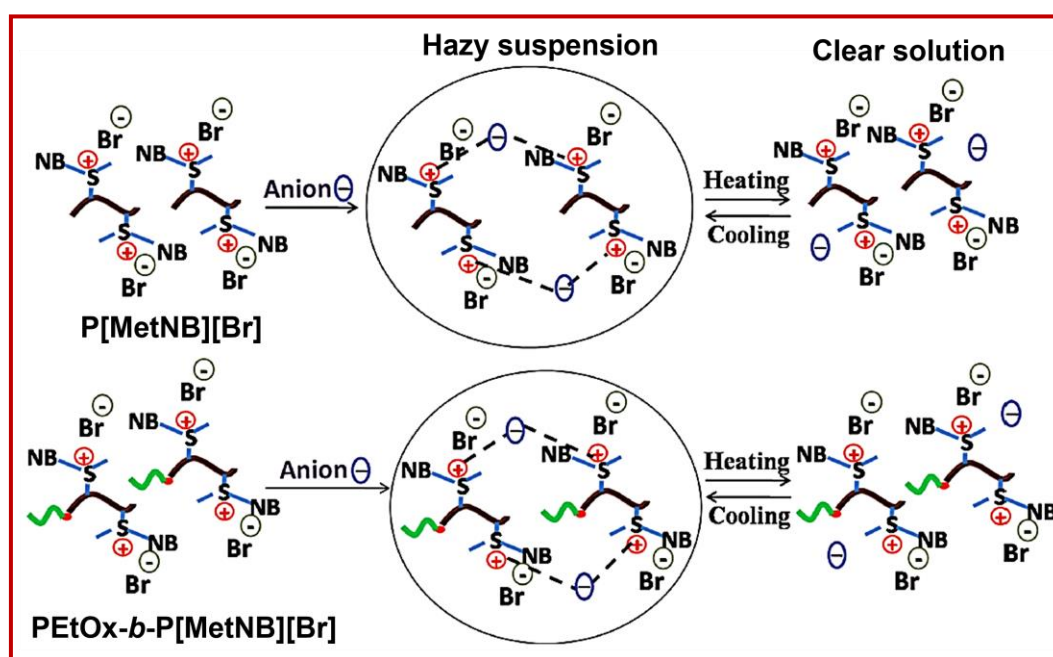


Figure 1.15. Probable mechanism of formation of the anion-bridge interaction between the cationic polypeptide and the added anions and the subsequent thermoresponsiveness in water. (Taken from the ref.¹⁷)

These interactions were a complex interplay affected not only by the size, polarizability, and concentration of the added ions, but also by the proper

hydrophobic/hydrophilic balance of the polypeptides, which eventually help to regulate the cloud point of the phase transition. They have observed that the anions with higher polarizability (SCN^-) required less in concentration to create higher extent of anion-bridging with more polypeptide chains through the electrostatic interactions. It is obvious that more energy is required to break this effectively strong interaction. Consequently, the T_{cp} of that anion containing solution also found to be higher compared to other anions with low polarizabilities. Although there are several reported examples of ion-induced UCST-behaviour of conventional polymers,¹⁹⁵⁻²⁰⁰ it is less likely for polypeptide-based systems. Thus, it would be interesting to explore such systems and study their thermoresponsiveness in the presence of externally added salts.

The effect of chirality on the UCST-phase behaviour of a polypeptide-based materials also have been studied by several groups. Kuroyanagi et al, have reported the UCST-type behaviour of poly(ornithine-*co*-citrulline) (POC) under physiological relevant conditions.²⁰¹ They have prepared POCs with homochiral or racemic backbones to explore the effect of the stereoregularity on thermoresponsiveness of the citrulline polypeptides (PLOC, PDLOC, and PDOC). Interestingly, the T_{cp} s of homochiral POCs were reported to be higher than those of racemic POCs. T_{cp} s of POC increased with increasing citrulline content and the molecular weight of the main chain. Similarly, Liu et al. synthesized chiral and racemic polypeptides (Figure 1.16A), each containing distinct side chains, which showed pH-dependent UCST-type phase transition in water (Figure 1.16B).²⁰² They have further investigated the influence of chirality of amino acid residues of the polypeptides on their UCST-phase transition. They have found that the chiral polypeptide exhibited a reversible and sharp UCST-type phase transition, whereas the racemic polypeptide did not undergo any such transition during heating or cooling (Figure 1.16B). It has been shown by the analysis using CD and $^1\text{H-NMR}$ spectra that the helical secondary structure of the chiral polypeptide was stabilized by the formation of

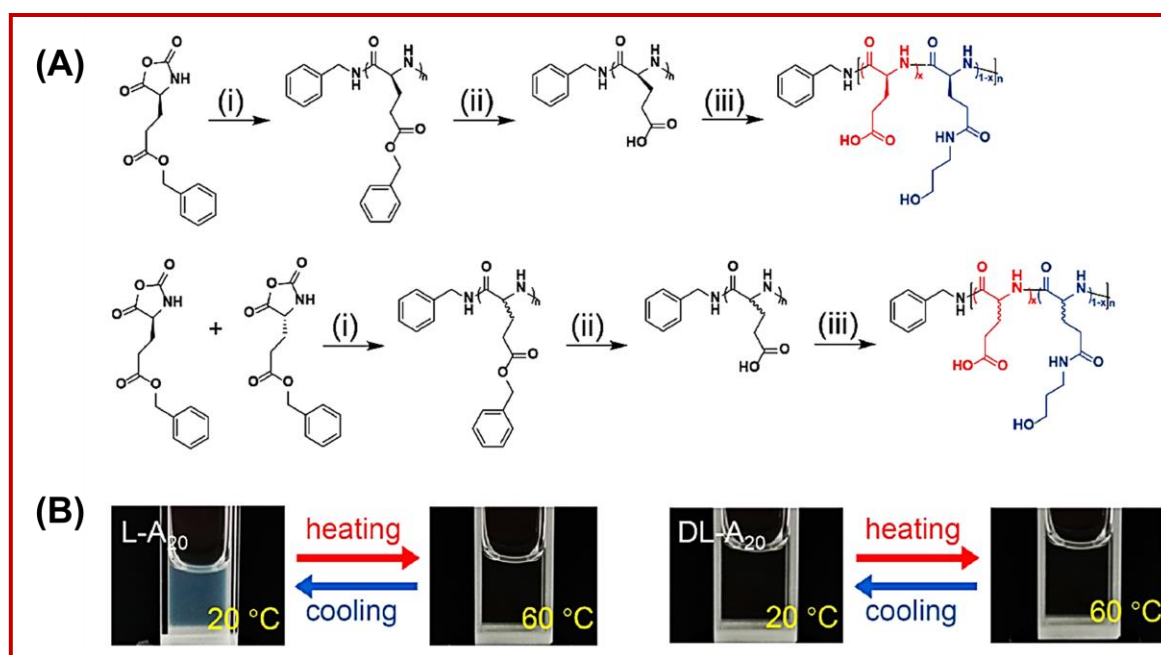


Figure 1.16. (A) Synthetic route of chiral and racemic polypeptides with different side chains; (B) Photograph of the UCST-type phase transition of chiral (left) and racemic (right) polypeptides in water at pH = 1. (Represented from ref.²⁰²)

intramolecular hydrogen bonds between homochiral amino acid residues. Additionally, the helical structure caused the side chains to protrude outward from each repeat unit, thereby increasing the availability of the side chains for intermolecular hydrogen bonds. Consequently, this led to the aggregation of polypeptides. It is worth noting that the adjustment of the content of hydroxyl- and hexyl-terminated side chains, the UCST behaviour of the polypeptides could be engineered to vary between 33.7 and 50.1 °C, as desired.

Thermoresponsive polypeptides that have been discussed above are all primarily in aqueous solution. There are also few reported examples of thermoresponsiveness of functionalized polypeptides in non-aqueous solvents, compared to those of reported in aqueous solution. UCST-type thermoresponsiveness of polypeptides and glycopeptides have been explored in water/alcohol mixtures that showed a tunable cloud point.²⁰³⁻²⁰⁵ Methanol is

one of the most studied non-aqueous solvents for the evaluation of the thermoresponsive behaviour of polymers in solution. For example, poly(γ -4-oligo(ethylene glycol) benzyl-L-glutamate)-random-(γ -benzyl-L-glutamate) containing an OEG (0.75 mol%) and a degree of polymerization (DP) of 3 prepared exhibited a UCST-type phase transition in methanol.²⁰⁶ UCST-type phase transition in MeOH was observed for the polypeptides bearing *p*-tolyl pendants and 3-methyl-1,2,3-triazolium linkages synthesized via N-alkylation of poly(γ -propyl-L glutamate)-*g*-(4-methylbenzene) and subsequent ion-exchange reactions.²⁰⁷ Functionalized poly(L-glutamate) containing 1-butyl, 1-hexyl, or 1-dodecyl side-chains, which were synthesized by CuAAC between poly(γ -4-(propargoxycarbonyl)benzyl-L-glutamate) and 1-azidoalkanes showed alkyl-side-chain- and the main-chain-length-dependent UCST-type phase transition in MeOH.²⁰³ Those polypeptides with a short main chain (DP = 41–44) have T_{CP} of 55, 50 and 54.7 °C when the pendants alkyl chain length was varied from 1-butyl to 1-hexyl, to 1-dodecyl, respectively.

1.5.1.2. pH-Responsive Polypeptides

Stimuli-responsive nanocarriers, such as liposomes, polymeric micelles/vesicles, polyplexes etc. play a crucial role in targeted drug delivery in biological systems.²⁰⁸ In this context, pH-responsive nanocarriers (for site-specific drugs) hold significant importance as they enable drug release at specific target sites by responding to the varying pH levels in different parts of the body.²⁰⁹⁻²¹⁰ This is particularly advantageous in addressing the limitations of conventional chemotherapy, which lacks specificity and often harms healthy cells. In normal physiological conditions, the extracellular pH is around 7.4. However, tumour cells exhibit a lower pH range of 5-6. By introducing a pH-responsive carrier molecule capable of specifically responding to acidic pH, drugs can be released precisely within the tumour environment, leading to targeted cytotoxicity against cancer cells. To achieve this, various polymeric materials have been designed with tailored pH-responsive properties, thereby

improving the efficacy of drug release rates in response to pH variations.²¹¹⁻²¹³ Polypeptides can be functionalized with pH-sensitive groups, such as acidic or basic residues or pH-responsive polymers. These functionalized polypeptides can undergo conformational changes, charge variations, or solubility transitions in response to pH changes in their environment.^{16, 169, 214-215} Due to their desirable attributes, including biodegradability, biocompatibility, stimuli-responsiveness, and the capacity to form micelles, vesicles etc. functionalized polypeptides have emerged as highly promising candidates for synthesizing carrier molecules in biological systems.²¹⁶ In recent times, there has been a significant emphasis on developing pH-responsive polypeptides for drug delivery systems.²¹⁷ The most extensively studied systems involving acidic or basic amino acids residue are consisting of poly(L-glutamic acid) (PLGA)²¹⁸⁻²²¹ and poly(L-lysine) (PLL)²²²⁻²²⁴. PLGA, a linear homopolymer, dissolved in water as an anionic form and adopts an extended random coil structure. It has been observed that below pH 4.3, it became neutral and underwent a helix-to-coil transition, resulting in precipitation (Figure 1.17A).²²⁵ Similarly, PLL, with a pKa of approximately 10.53, also exhibited pH-dependent transitions from helical to coil conformations (Figure 1.17A). Numerous studies have showcased the functional utility of PLGA and PLL by harnessing their helix-to-coil conformational changes. These conformational switches have been utilized as the basis for various functional applications.²²⁵⁻²²⁶ In another approach, hydrogels were developed by crosslinking PLGA with PEG and encapsulating a model protein, lysozyme (Figure 1.17B).²⁵ These hydrogels exhibited pH-responsive swelling and de-swelling behaviour, remarkably within the pH range of 4 to 6, where PLGA became gradually ionized. Significantly, this process was exhibited to be fully revocable. The hydrogels showed rapid contractions in response to pH and ionic concentration changes, providing a means to accelerate the release of therapeutics, including large biomacromolecules like proteins.

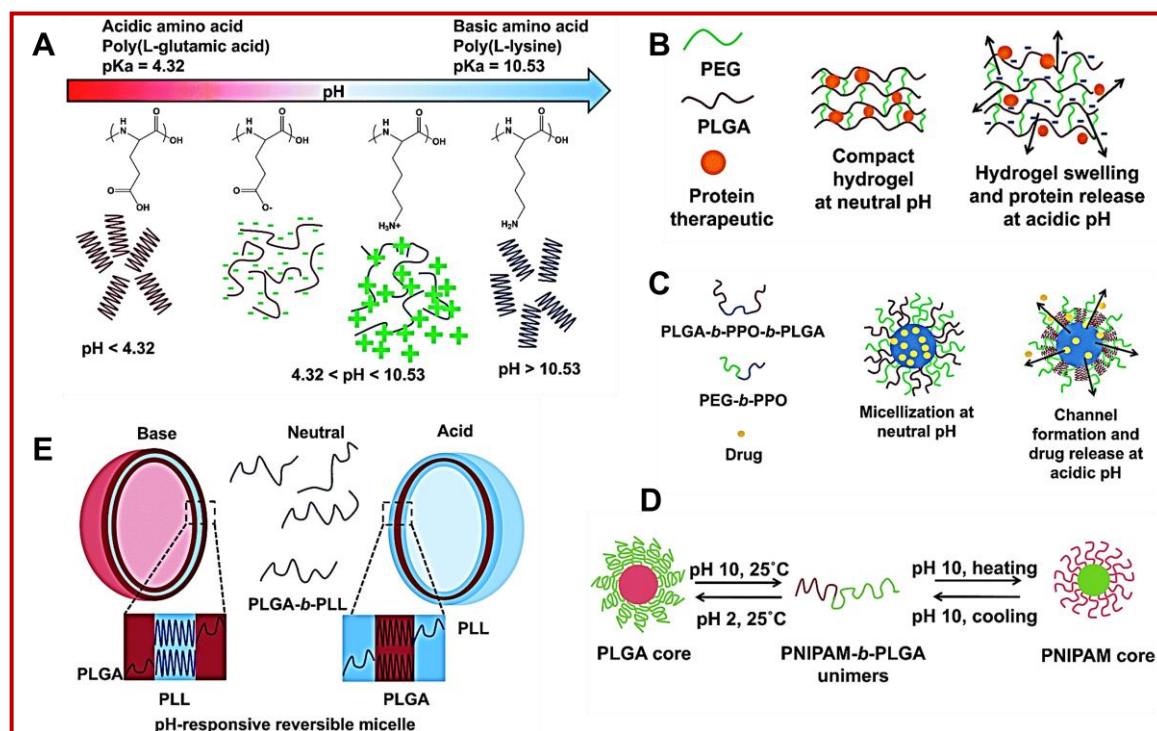


Figure 1.17. pH-responsive polypeptide-based systems. (A) Helix-to-coil conformational changes; (B) PEG cross-linked PLGA hydrogels; (C) Mixture of PPO-flanked PLGA polymers and PEG-*b*-PPO for micellar pH-induced channel formation and triggered drug release; (D) Dual pH and thermal-responsive system (PNIPAM-*b*-PLGA) for reversible properties. (E) Helix-to-coil conformational changes of self-assembled reversible vesicles formed by PLGA-*b*-PLL. (Represented from ref.²¹⁶)

Amphiphilic block copolymers possess the ability to self-assemble into various nanoaggregates, such as micelles, vesicles etc. to be used in various biomedical fields. One of such example is the combination of polypropylene oxide (PPO) flanked by PLGA on both sides (PLGA-*b*-PPO-*b*-PLGA) with PEG-*b*-PPO to form hybrid micelles (Figure 1.17C).²²⁷⁻²²⁹ In these hybrid micelles, corona region is consisted of a mixture of PLGA and PEG chains, while the hydrophobic PPO segment is resided in the core. When the environmental pH changed, PLGA underwent a pH-dependent conformational shift from water-soluble coils to water-insoluble α -helices. This resulted in microphase

separation within the micelle corona, leading to the formation of PEG channels. These channels served as pathways connecting the inner core to the exterior, facilitating the diffusion of drugs, and enabling accelerated drug release. Furthermore, the development of thermo- and pH-responsive micelles bearing polyelectrolytes has been achieved by incorporating hydrophilic thermosensitive building blocks such as PNIPAM as macroinitiators in NCA polymerizations (Figure 1.17D).²³⁰⁻²³² These dual-responsive micelles exhibit the ability to undergo sequential switching of corona and core structures in response to changes in pH and temperature. Additionally, the preparation of vesicles using pH-responsive amphiphilic block polypeptides has received significant attention.²³³ These vesicles, derived from amphiphilic block (co)polypeptides, exhibit pH-dependent behaviour, allowing controlled release of encapsulated substances (Figure 1.17E).²³⁴ In this context, Lecommandoux et al. have demonstrated the pH-dependent vesicular self-assembly of a block copolypeptide comprising of L-glutamic acid and L-lysine residue (poly(L-glutamic acid)₁₅-*b*-poly(L-lysine)₁₅) in water (Figure 1.18).¹⁶ When both amino acid residues carry charges near neutral pH ($5 < \text{pH} < 9$), the polypeptide remains soluble in water. However, under acidic conditions ($\text{pH} < 4$), the poly(L-lysine) segment retains its coiled conformation while the poly(L-glutamic acid) block becomes neutralized and adopts an α -helical structure. This conformational change triggers the formation of vesicles, where the insoluble poly(L-glutamic acid) serves as the membrane layer and the poly(L-lysine) block forms the corona. Conversely, at alkaline pH ($\text{pH} > 10$), poly(L-glutamic acid) assumes a coiled conformation while poly(L-lysine) becomes α -helical and insoluble, resulting in vesicles with poly(L-glutamic acid) as the corona and poly(L-lysine) as the membrane. A pH-responsive vesicle was developed by Deming's group using poly(N ϵ -2-[2-(2-methoxyethoxy) ethoxy] acetyl-L-lysine)₁₆₀-*b*-poly(L-leucine_{0.3}-*co*-L-lysine_{0.7})₄₀, denoted as K^P₁₆₀(L_{0.3}/K_{0.7})₄₀.²³⁵ The study demonstrated the formation of pH-responsive vesicles composed of a

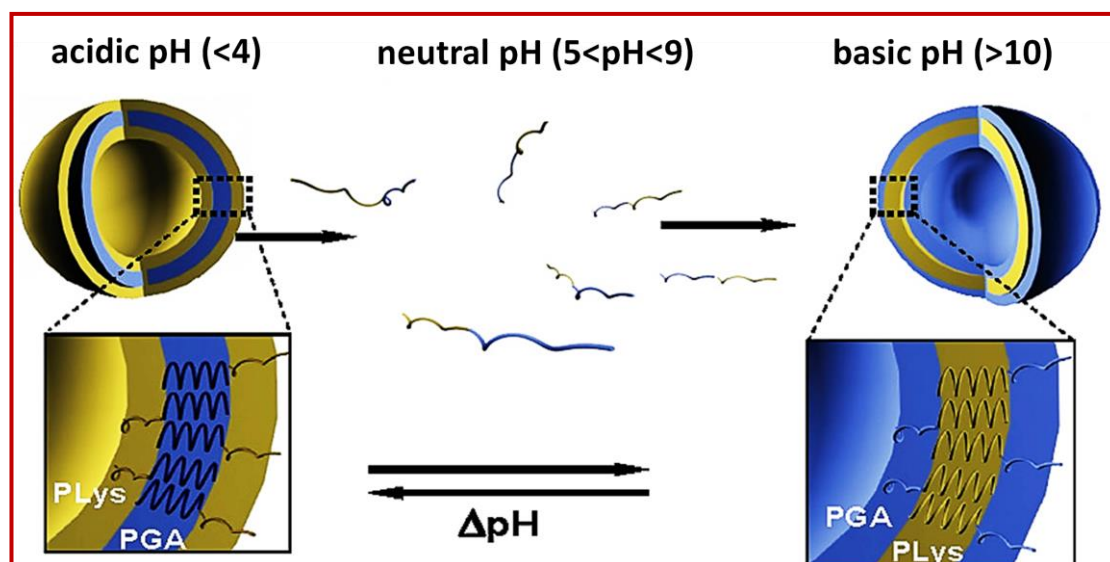


Figure 1.18. Schematic representation of the pH-dependent vesicular self-assembly of poly(L-glutamic acid)₁₅-*b*-poly(L-lysine)₁₅ in water. (Taken from ref.¹⁶)

hydrophobic P(L_{0.3}/K_{0.7})₄₀ layer and hydrophilic K^P₁₆₀ inner and outer shells in the presence of Fura-2 dye at pH 10.6. Upon decreasing the pH of the medium, the vesicle membranes were rapidly disrupted, leading to the release of the encapsulated Fura-2 dye.

Furthermore, pH-responsive vesicles were prepared using various block copolypeptides, such as poly(L-lysine)-*b*-poly(g-benzyl-L-glutamate)-*b*-poly(L-lysine),²³⁶ poly(L-lysine)-*b*-poly(L-phenylalanine),²³⁷ poly(L-lysine)-*b*-poly(L-glycine),²³⁸ and poly(L-glutamic acid)-*b*-poly(L-phenylalanine)²²⁰. The concept of pH-responsive poly(glutamic acid) has also been employed in the development of pH-responsive polypeptide core-shell nanoparticles.²³⁹⁻²⁴⁰ In order to enhance the targeting efficiency of solid tumours, which often have a lower extracellular pH compared to normal tissues, Bae and colleagues explored the use of poly(histidine) (polyHis) to design smart pH-sensitive tumour-targeted nanocarriers, such as micelles and nanogels.²⁴¹

In a recent study, Hammond and colleagues employed a post-modification approach to synthesize novel pH-responsive polypeptides.²¹⁵ They employed the click reaction between poly(g-propargyl-L-glutamate) and various amino azides (primary amine, secondary amine, dimethylethanamine, dimethylpropanamine, diethylamine, and diisopropylamine). This approach led to the development of a diverse library of pH-responsive polypeptides. They further discovered that all of these amine-functionalized polypeptides exhibited robust buffering capacity within the typical pH range found in extracellular tissues (5.0–7.35), which is crucial for maintaining the stability and functionality of the polypeptides under physiological conditions. To demonstrate the potential applications of these pH-responsive polypeptides in systemic drug and gene delivery, experiments involving reversible micellization with polypeptide block copolymers were conducted, which successfully encapsulated nucleic acids in different pH environments.

1.5.1.3. Photo-Responsive Polypeptides

Photo-responsive polypeptides have also garnered significant interest due to their ability to enable remote control of drug release in a spatially and temporally controlled manner using light. Although, the research on photo-responsive polypeptides is relatively limited compared to other stimuli-responsive systems, there have been notable advancements in this field.²⁴²⁻²⁴³ Several moieties have been incorporated into polypeptides to create photo-responsive systems, which includes azobenzene derivatives, coumarin, 2-nitrobenzyl, cinnamyl, spiropyran, and diazonaphthoquinone compounds.²⁴⁴⁻²⁴⁶ These photoresponsive molecules can induce conformational changes, reversible isomerization, dimerization, or even phase transitions upon exposure to light of the appropriate wavelength, thus providing control over the properties and behaviour of the polypeptides.²⁴⁷⁻²⁴⁹ To generate photoactive materials, various synthetic approaches have been employed to incorporate photochromic molecules into polypeptides. These approaches include i) using

photo-responsive species as initiators of NCA polymerization,²⁵⁰ ii) introducing photochromic moieties into the side chain of polypeptides through post-modification,²⁴⁴ or iii) synthesizing new NCA monomers with light-responsive groups in the side chain²⁵¹. Each approach offers unique advantages and allows for the design and synthesis of tailored photo-responsive polypeptides. The ability to achieve precise control over the photo-responsive properties of these compounds opens up opportunities for applications in fields such as drug delivery, bioimaging, and tissue engineering, where spatial and temporal control of biological processes is desired.²⁵²

The literature extensively describes the photochromic behaviour of various photoresponsive polypeptides that incorporate azobenzene and spiropyran groups into the side chains of different polypeptide backbones such as poly(L-phenylalanine), poly(L-aspartate), poly(L-glutamate), poly(L-lysine), poly(L-ornithine), and other poly(L-lysine) analogues.²⁵³⁻²⁵⁸ These light-responsive polypeptides undergo conformational and structural changes on irradiating at specific wavelength, resulting in variations in their physical and chemical properties. Examples include transitions between random coil and α -helix conformations, photo-triggered aggregation-disaggregation processes, and reversible changes in viscosity and solubility.²⁴⁸⁻²⁴⁹ In a recent study, Mezzenga and colleagues designed amphiphilic polypeptide block copolymers that incorporated spiropyran (SP) into the side chain of poly(L-glutamic acid).²⁴⁴ PEG-*b*-PLGA modified with SP side chains demonstrated complete reversible aggregation-dissolution-aggregation micellar transition in response to UV exposure in water (Figure 1.19). Initially, before exposure to UV irradiation, the polypeptide block exhibited hydrophobic characteristics, forming a micellar structure resembling a flower like morphology in aqueous solution. However, upon UV irradiation ($\lambda = 350$ nm), the entire block become water soluble due to the presence of a phenolic OH group, leading to the dissolution of the micelle.

This property holds potential for applications in photo-triggered controlled drug release processes or light-controlled biomedical applications.

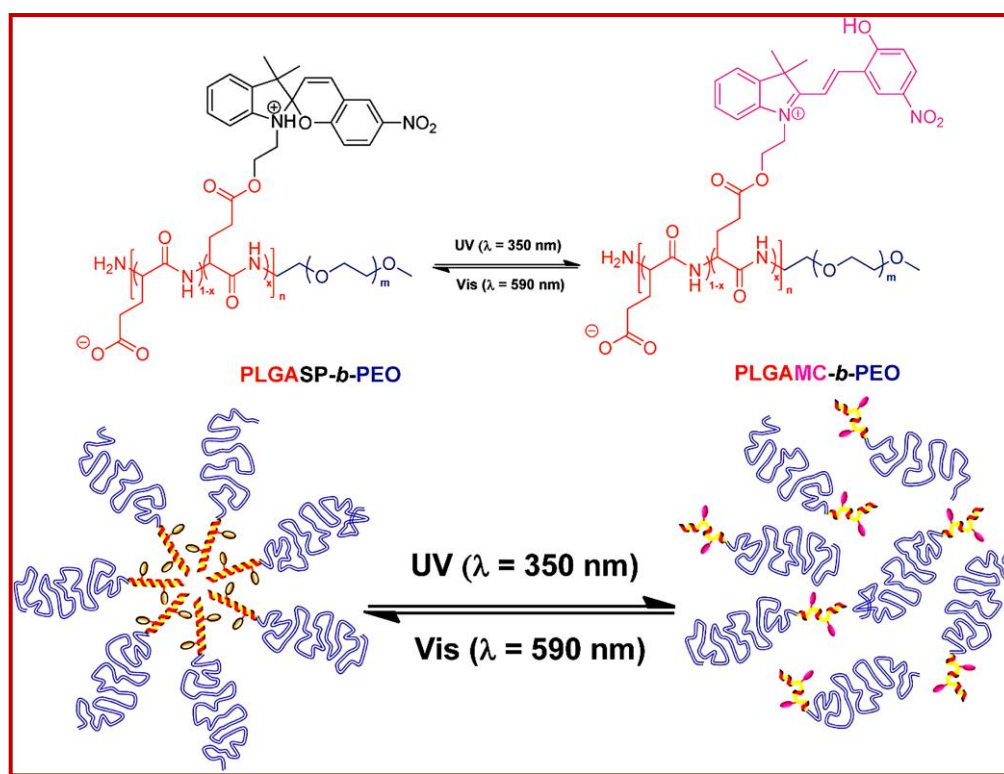
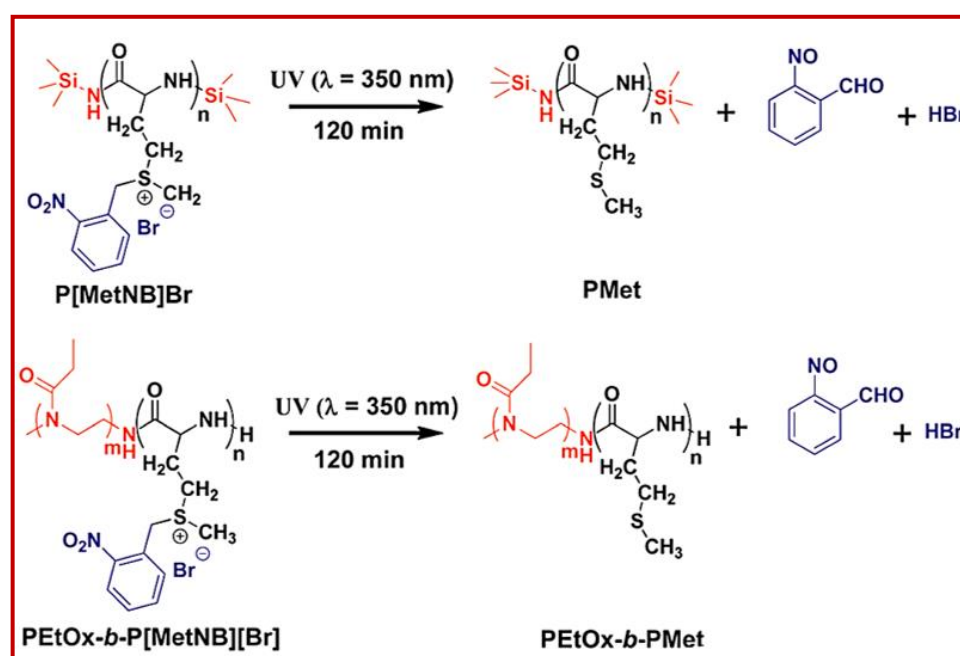


Figure 1.19. Schematic representation of the photoresponsive micellization/dissolution process for the SP functionalized PLGA-*b*-PEO block copolymer in water. (Represented from ref.²⁴⁴)

Novel photoresponsive crosslinked gels were reported by Yamamoto et al., where coumarin-containing polypeptides underwent cycloaddition reactions between coumarin moieties in the side chains upon irradiation.²⁵⁹⁻²⁶¹ More recently, photocleavable moieties such as 2-nitrobenzyl groups were introduced to prepare light-sensitive polypeptide that could trigger drug release from the self-assembly of amphiphilic polypeptides, such as micelles, upon light irradiation ($\lambda = 365 \text{ nm}$).¹⁸ The removal of the photocleavable groups disrupts the self-assembly of amphiphilic polypeptide in aqueous solutions. Our group has also demonstrated the synthesis of multi-stimuli-responsive

positively charged functionalized polymethionine (P[MetNB][Br]) and its block copolymer of pseudopeptidic poly(2-ethyl-2-oxazoline) (PEtOx-*b*-P[MetNB][Br]) via ROP and post-functionalization with nitrobenzyl bromide.¹⁷ The sulfonium cation was linked to the nitrobenzyl moiety, and its photodissociation resulted in the transformation of cationic functional polypeptides into neutral polypeptides (Scheme 1.10). Conversely, these cationic polypeptides exhibited the ability to electrostatically bind with negatively charged ctDNA, forming polyplexes. The photodissociation characteristics of the functional polypeptides were then effectively employed to investigate the release of bound ctDNA.



Scheme 1.10. Photodegradation of P[MetNB][Br] and PEtOx-*b*-P[MetNB][Br] in water. (Represented from ref.¹⁷)

For *in-vivo* applications, light-responsive systems need to utilize a light source capable of deep tissue penetration without causing harm to cells. The previously mentioned systems, which rely on UV and visible light, may not be suitable for *in-vivo* use. However, among various photo-responsive polypeptides, those responsive to near-infrared (NIR) light are particularly

appealing due to their ability to penetrate deeper into tissues with minimal harm compared to UV or visible light. Recently, a NIR light-responsive polypeptide was synthesized by incorporating 6-bromo-7-hydroxycoumarin-4-ylmethyl groups into PEG-poly(L-glutamic acid).²⁴⁵ This copolypeptide forms micelles that can be disrupted by the NIR-induced cleavage of the coumarin groups, resulting in a shifted hydrophilic/hydrophobic balance.

1.5.1.4. Redox-Responsive Polypeptides

The design and synthesis of redox (reduction–oxidation) responsive polypeptides is also another key area of research due to their promising potential in drug and gene delivery, particularly in the field of cancer therapy. Among the extensively studied redox-responsive groups, those based on thiol chemistry have shown great promise, including the disulfide bond (in the main chain, at the side chain, or in the cross-linker) and the thioether group.²⁶²⁻²⁶³ The thioether group can be oxidized to sulfoxide and sulfone, while the disulfide bond can undergo reversible reduction to form the thiol group in the presence of dithiothreitol (DTT) or glutathione (GSH).²⁶⁴ Disulfide linkages offer adequate stability while exhibiting a fast ‘reductive-disruption’ kinetics.²⁶⁵ This property is particularly advantageous considering the well-established reductive environment present inside cells offered by GSH, compared to the extracellular environment.²⁶⁶ Therefore, the exceptional stability exhibited under extracellular physiological conditions, combined with their selective disulfide cleavage, makes these redox-responsive polypeptides as promising candidates for the advancement of sophisticated delivery systems. These systems have the potential to encompass a wide range of therapeutic cargoes, such as DNA, siRNA, proteins, anti-cancer drugs, and more.²⁶⁷

Taking advantage of this characteristic, several redox-responsive polypeptides containing disulfide bonds have been synthesized. Two synthetic approaches have been employed for the synthesis of disulfide bond-containing

polypeptides: i) utilizing a disulfide-containing PEG as a macroinitiator or ii) incorporating poly(L-cystine) as a component by ROP of respective NCA. For instance, Kataoka and colleagues developed innovative redox-sensitive polypeptides, namely PEG-SS-poly[[N-(2-aminoethyl)-2-aminoethyl]- α , β -aspartamide] and PEG-SS-poly(α , β -aspartic acid), by employing a disulfide-linked PEG as a macroinitiator for NCA polymerization.²⁶⁸ These materials exhibited significantly enhanced transfection efficiency against cultured cells. Furthermore, it was demonstrated that the reduction of disulfide bonds induced morphological transitions in the self-assembly of the block copolymers in solution, showcasing their versatile capabilities.²⁶⁹

In recent studies, redox-sensitive nanocarriers (micelles) for drug delivery have been developed using PEG-SS-poly(ϵ -benzyloxycarbonyl-L-lysine),²⁷⁰ PEG-SS-poly(γ -benzyl-L-glutamate),²⁷¹ PEG-SS-poly(phenylalanine),²⁷² and PEG-SS-poly(rac-leucine)²⁷³. These nanocarriers were designed with disulfide-linked PEG, and upon reduction by GSH or DTT, the disulfide cleavage triggered a rearrangement of the micellar structure, leading to the rapid release of the encapsulated doxorubicin (DOX), a commonly used anti-cancer drug. This controlled release mechanism offers potential benefits for drug delivery applications.

ROP of L-cysteine or L-cystine NCAs also allowed the incorporation of disulfide bonds into a polypeptide chain, enhancing the responsiveness of the polypeptides to redox. A novel approach was employed to synthesize a PEGylated disulfide core crosslinked polypeptide nanogel, utilizing disulfide-linked cysteine NCA as both a bifunctional monomer and a crosslinker in combination with γ -benzyl-L-glutamate NCA.²⁷⁴ This nanogel system aimed to address the solubility issues of Indometacin, a model drug commonly used for pain relief, fever reduction, and inflammation management. By incorporating the drug into the hydrophobic core, the nanogel exhibited a sustained drug release profile when subjected to physiological conditions. Notably, the

introduction of GSH triggered a redox-responsive drug delivery mechanism, leading to nearly 100% drug release within 200 hours.

Recently, redox-sensitive *core crosslinked star* (CCS) polypeptide was formed using L-cystine NCA as a crosslinker. Qiao et al. introduce a novel difunctional monomer of L-cystine NCA to prepare CCS polypeptides using the "arm-first approach," (Figure 1.20).¹³¹ The core of the CCS polypeptide consisted of poly(L-cystine) and the arms were composed of poly(L-lysine) or poly(L-glutamic acid). Notably, the disulfide bonds present in the core of the CCS polypeptides could be easily cleaved using an excess of dithiothreitol (DTT).

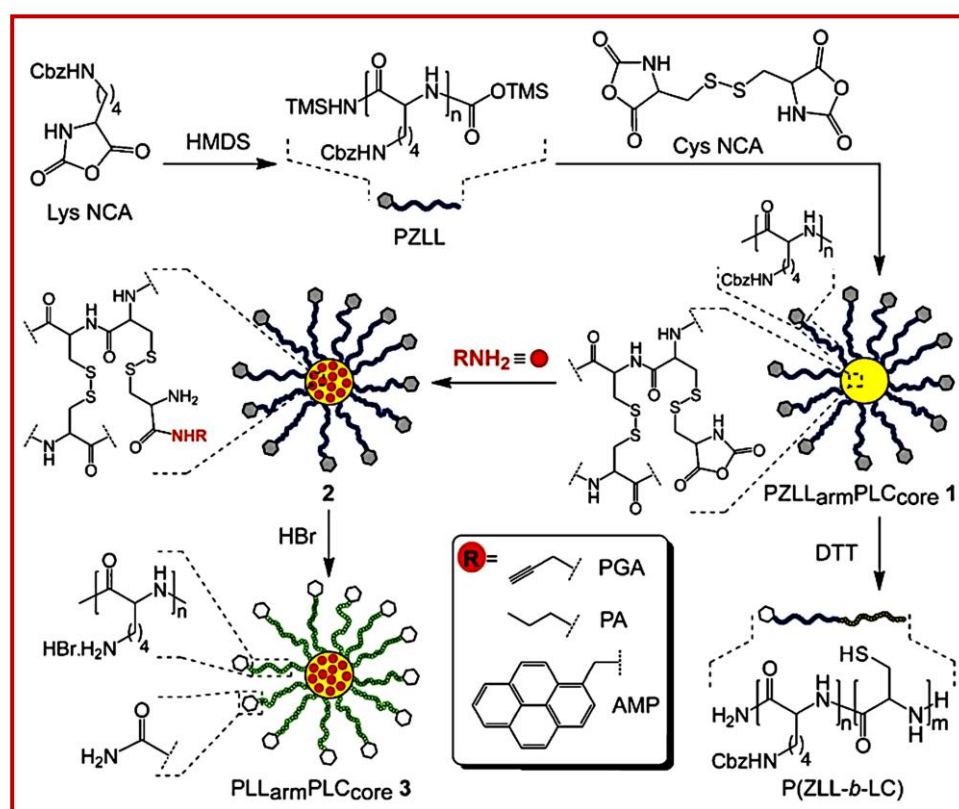


Figure 1.20. Synthetic scheme for different amino acids based 'core crosslinked star' (CCS) polypeptide using arm-first approach and its subsequent redox responsiveness. (Represented from ref.¹³¹)

Contrary to the reduction-responsive disulfide bond, an oxidation-responsive polypeptide have been constructed by Deming and Kramer, which was capable of undergoing a conformational switch under different oxidation conditions.²⁶ They have synthesized glycosylated L-cysteine (glycol-C) monomer by coupling with alkene-terminated C-linked glycosides of D-galactose or D-glucose to L-cysteine with the help of thiol-ene 'Click' chemistry. NCA formation followed by ROP produced the respective glycopolypeptide having thioether group in its side chain. The oxidation of the thioether bond to form a more polar sulfone group triggered a conformational transition in these glycopolypeptides from an α -helix to a random coil structure, while retaining their solubility in water. Interestingly, for a similar glycopolypeptide, based on L-homocysteine, it remained in an α -helix conformation even upon oxidation to sulfone. Although the oxidation of the thioether group to sulfone is an irreversible process, partially oxidized thioether to the sulfoxide group can be reversibly reduced in the presence of appropriate reducing agents or reductase enzymes. Deming et al. designed an enzyme-responsive copolypeptide by incorporating oxidizable methionine units into a hydrophobic copolypeptide, poly(L-methionine)₆₅-*b*-poly(L-leucine_{0.5}-stat-L-phenylalanine_{0.5})₂₀ ($M_{65}(L_{0.5}/F_{0.5})_{20}$).²³ It was shown that the poly(L-methionine) block underwent a conformational transition from an α -helix to a random coil (Figure 1.21)

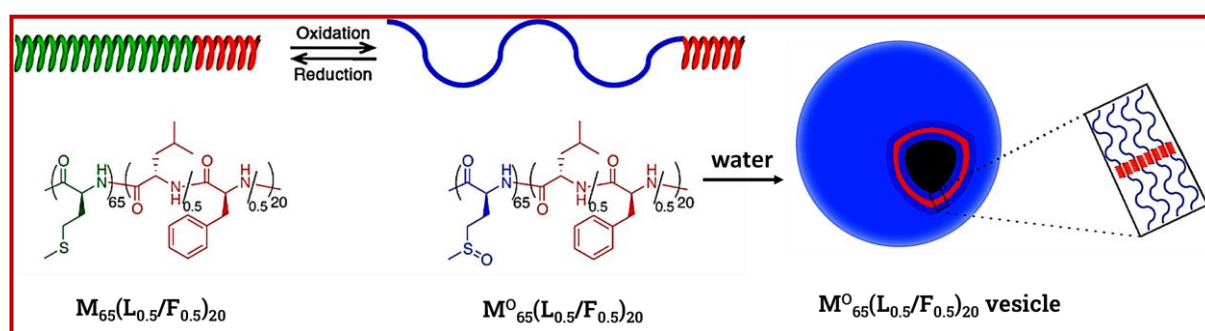


Figure 1.21. Schematic diagram showing structure, redox properties, and proposed self-assembly of $M_{65}^O(L_{0.5}/F_{0.5})_{20}$ copolypeptides into vesicles. (Represented from ref.²³)

on mild oxidation, which was accompanied by increase in the hydrophilicity. Consequently, the resulting amphiphilic copolyptide, $(M_{65}^0(L_{0.5}/F_{0.5})_{20})$ was shown to exhibit vesicular self-assembly in aqueous media, to be used in drug encapsulation. In the presence DTT and methionine sulfoxide reductase (MSR) enzyme, the vesicles could be disrupted, leading to the release of the encapsulated drug. This disruption occurred due to the reduction of methionine sulfoxide back to methionine, allowing for the redox-triggered release of the drug.

1.5.1.5. Other Responsive Polypeptides (Miscellaneous)

Glucose-responsive materials have been widely explored in controlled delivery of insulin because insulin should be released at a high blood glucose level.²⁷⁵ Glucose-responsiveness has been introduced into a functional polypeptide by conjugating phenylboronic acid (PBA) moiety into the side chain using carbodiimide chemistry.²⁷⁶⁻²⁷⁸ Adenosine triphosphate (ATP), a primary source of energy produced by glucose metabolism in cells, can also facilitate the release of cargo molecules in the cytoplasm using ATP-responsive delivery carriers. ATP-responsive polypeptide has been developed by attaching PBA derivatives into the side chain of a polypeptide through post-polymerization modifications.²⁷⁹⁻²⁸⁰

Enzyme-responsive materials or enzymatically degradable materials are a class of biomaterials that possess specific sequences susceptible to enzymatic cleavage. Enzyme-responsive polypeptides have gained significant attention in the field of drug delivery and tissue engineering as these polypeptides can undergo controlled degradation or triggered release of encapsulated substances in response to the specific enzymes.^{221, 281}

Metal-responsive poly(γ -benzyl-L-glutamate) was synthesized by initiating NCA ROP using aminobenzo-15-crown-5 to produce a benzo-15-crown-5 capped poly(L-glutamate). This terminal crown ether enabled the

polypeptide to exhibit a responsiveness towards potassium ions (K^+) forming a sandwich-complex in 1,2-dichloroethane.²⁸²⁻²⁸³

Magnetic-responsive polypeptide-based hybrid materials have been recently developed for a wide range of applications including separation and purification of biochemical products, magnetic resonance imaging contrast agents, targeted drug delivery labelling, enzyme immobilization, and hyperthermia treatment for cancers etc.²⁸⁴⁻²⁸⁶ Surface-initiated polymerisation of alanine NCA from the amine functionalized Fe_3O_4 , resulted in polypeptide brush-magnetic microspheres.²⁸⁷

Deming and co-workers have synthesized chemical-responsive polypeptides, notably, poly(methionine) and poly(homocysteine) derivatives, exhibiting reversible alkylation, leading to the formation of polysulfonium with nearly quantitative yield.²⁸⁸

1.5.2. Self-Assembly of Functionalized Polypeptides

Functionalized peptides/polypeptides can self-assemble into ordered structures in solution, driven by a variety of interactions, such as hydrogen bonding, hydrophobic interactions, electrostatic interactions, and π - π stacking.²⁸⁹ The self-assembly behaviour of these materials can be influenced by factors such as the amino acid sequence, chain length, concentration, pH, temperature, and the presence of specific functional groups.²⁹⁰ Self-assembly of polypeptides can lead to the formation of various nanostructures, including micelles, vesicles, fibers, nanogels or hydrogels.²⁹¹⁻²⁹³ By incorporating hydrophobic or amphiphilic segments into the polypeptide chain, the self-assembly behaviour can be precisely controlled.²⁹⁴⁻²⁹⁷ Due to their excellent biocompatibility and biodegradability, polypeptide copolymers and their assemblies find important applications in bio-related fields, such as drug delivery, biomaterials, nanotechnology, and biotechnology and tissue engineering etc.

The self-aggregation of the polypeptides is very complex phenomenon which depends on the various factors, primarily the proper hydrophilic-hydrophobic balance within the polymeric system. However, majority of the self-assembled polypeptides have been studied in aqueous solution. Generally, the self-aggregation process involves the following steps:

Critical concentration: The limiting concentration of the polypeptides above which this aggregates formation occurs is known as 'critical aggregation concentration' (CAC). For micelles, it is known as critical micelle concentration (CMC).

Hydrophobic collapse: In an aqueous solution, the hydrophobic regions of polypeptide chains tend to avoid contact with water. As the concentration of polypeptides increases, these hydrophobic regions come into closer proximity, leading to a hydrophobic collapse.

Aggregates nucleation: Once the hydrophobic regions collapse, the polypeptides can start forming small aggregates or nuclei. These nuclei act as templates for further aggregation.

Aggregates growth: The nuclei grow by the addition of more polypeptide chains, driven by hydrophobic/hydrophilic interactions. The hydrophilic regions of the polypeptides face the surrounding water, while the hydrophobic regions are sequestered within the core of the growing aggregates.

Aggregates stabilization: The resulting aggregates are stabilized by a balance of hydrophobic interactions and interactions between the hydrophilic regions of the polypeptides and water molecules.

Depending on these factors, polypeptides may adopt numerous morphological structures in different solutions. However, this topic covers only three basic self-assembled nanostructures (micelle, vesicle, hydrogel/nanogel) formed by different synthetic functionalized polypeptides.

1.5.2.1. Micellar Self-Assembly

Micelles are spherical structures formed when amphiphilic molecules, such as polypeptides, organize themselves in a way that their hydrophilic regions are exposed to the surrounding aqueous environment, forming the shell/corona while their hydrophobic regions are shielded within the interior of the micelle, also called as core (Figure 1.22).

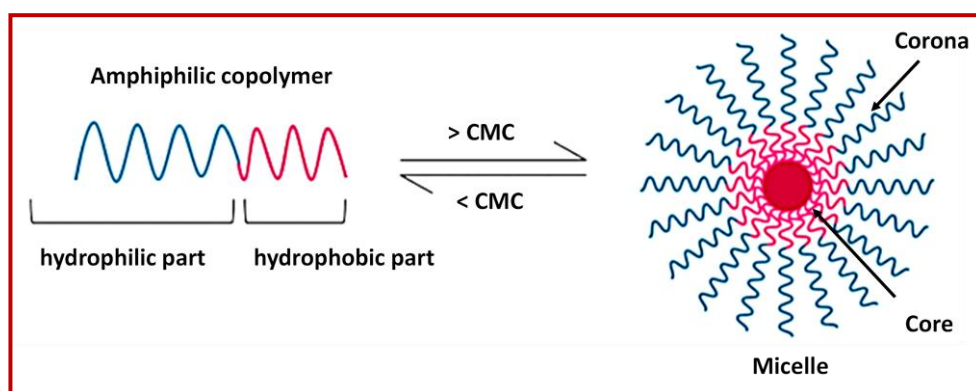
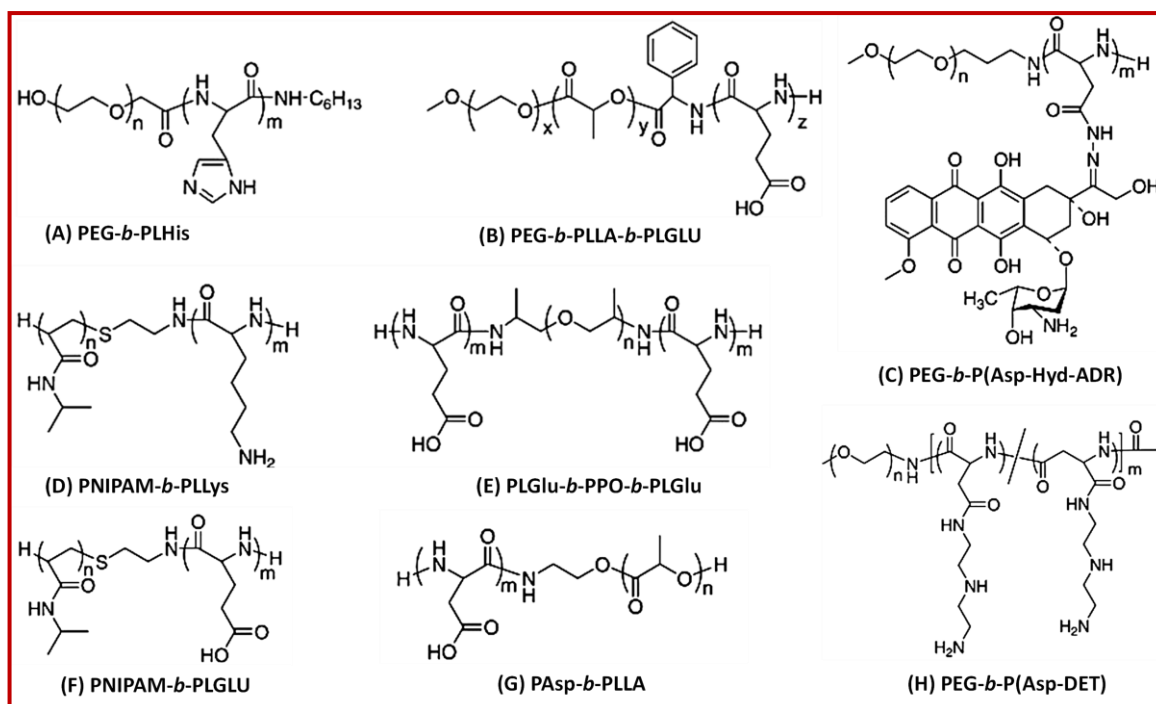


Figure 1.22. Simple schematic representation of formation of micelle by amphiphilic block copolymer. (Taken from ref.²⁹⁸)

Depending on the chemical nature, certain polypeptides form the core of a micelle and there are certain corona forming polypeptides. There are a huge number of scientific articles in the literature describing the micellar self-assembly of functionalized block copolypeptides (Scheme 1.11). Indeed, micelles based on stimuli-sensitive functionalized polypeptides have gained significant attention as drug delivery systems in nanomedicine, particularly for cancer therapy.²⁹⁹⁻³⁰⁰ These micelles offer several advantages, including their ability to load hydrophobic drugs in their hydrophobic cores and the hydrophilic shells surrounding the micelles contribute to their stability and biocompatibility in the circulation system *in-vivo*. This loading capability is beneficial for delivering drugs that have poor water solubility, as it allows for their effective delivery through controlled release.



Scheme 1.11. Chemical structures of some representative polypeptide-based block copolymers that form stimuli-sensitive micelles (A-H)^{230-231, 301-306}

The presence of the hydrophilic shell helps to prevent opsonization and recognition by the immune system, thereby extending the circulation time of the micelles and enhancing their accumulation in tumour sites through the enhanced permeation and retention (EPR) effect.³⁰⁷ This effect takes the advantage of the leaky vasculature and impaired lymphatic drainage commonly found in tumour tissues, allowing the micelles to passively accumulate at the tumour site.

Moreover, micelles based on stimuli-sensitive synthetic polypeptides exhibit stimuli-responsive self-assembly behaviours and conformation transitions. This means that these micelles can respond to specific triggers, such as changes in pH, temperature, or enzyme activity, by undergoing structural changes. Such stimuli-responsiveness can be harnessed to achieve controlled drug release at the target site, improving the therapeutic efficacy while minimizing off-target effects.

In addition to their stimuli-responsive properties, micelles based on synthetic polypeptides offer good biocompatibility and biodegradability. These characteristics are important for minimizing toxicity and ensuring the safe elimination of the micelles from the body after drug delivery. Overall, the combination of stimuli-responsive self-assembly behaviours, biocompatibility, and biodegradability make manometer-sized polymeric micelles based on stimuli-sensitive synthetic polypeptides promising drug delivery systems for cancer therapy in the field of nanomedicine.

Savin et al. have synthesized an pH-responsive amphiphilic block copolypeptide consisting of two different blocks, poly(butadiene)-*b*-poly(L-lysine) (PB-*b*-PLL) (Figure 1.23A), which underwent micellar self-assembly in water.³⁰⁸ The hydrophobic PB block formed the core of the micelle while the hydrophilic PLL block formed the shell. These block copolymers formed differently-shaped aggregates, either rod-like micelles (Figure 1.23B) or spherical micelles (Figure 1.23C) at high pH depending on the composition of the blocks. It was also found that on decreasing the pH of the solution, the PLL-based corona shell became positively charged and electrostatic repulsion

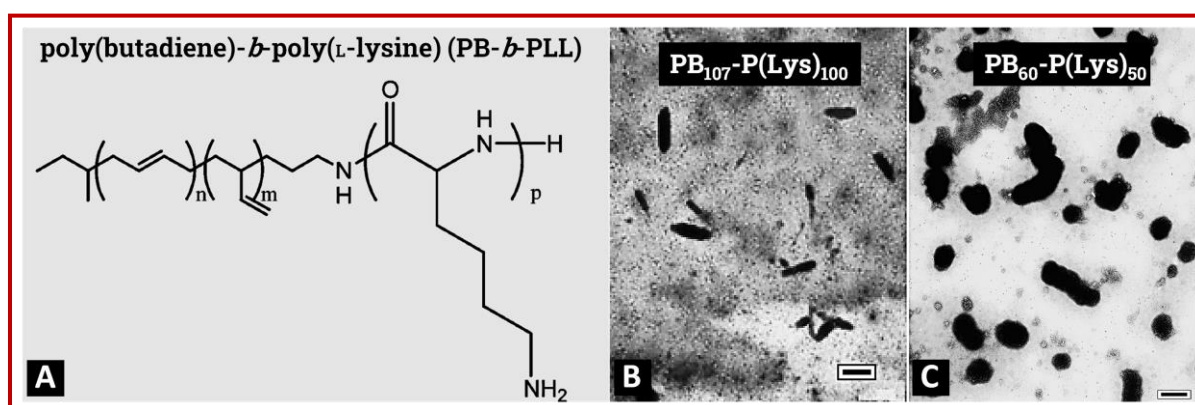


Figure 1.23. (A) Chemical structure of the PB-*b*-PLL block copolypeptide; (B) Rod-like micelles and (C) spherical micelles formed in water by PB-*b*-PLL block copolypeptides having different block composition. (Represented from ref.³⁰⁸)

between the corona resulted in the swelling of the micelles and swell due to charge-charge repulsions between corona chains accompanied by a helix to coil conformational transition of the polypeptide blocks.

Shiyong Liu et al. have reported the formation of a pH- and thermo-responsive 'schizophrenic' micelle by the self-assembly of double hydrophilic diblock copolymer, poly(*N*-isopropylacrylamide)-*b*-poly(glutamic acid) (PNIPAM-*b*-PLGA) in water.²³² At alkaline pH and higher solution temperature, the block copolymer self-assembled in such a way that the PNIPAM-block formed the core while the PLGA-block formed the corona (Figure 1.24).

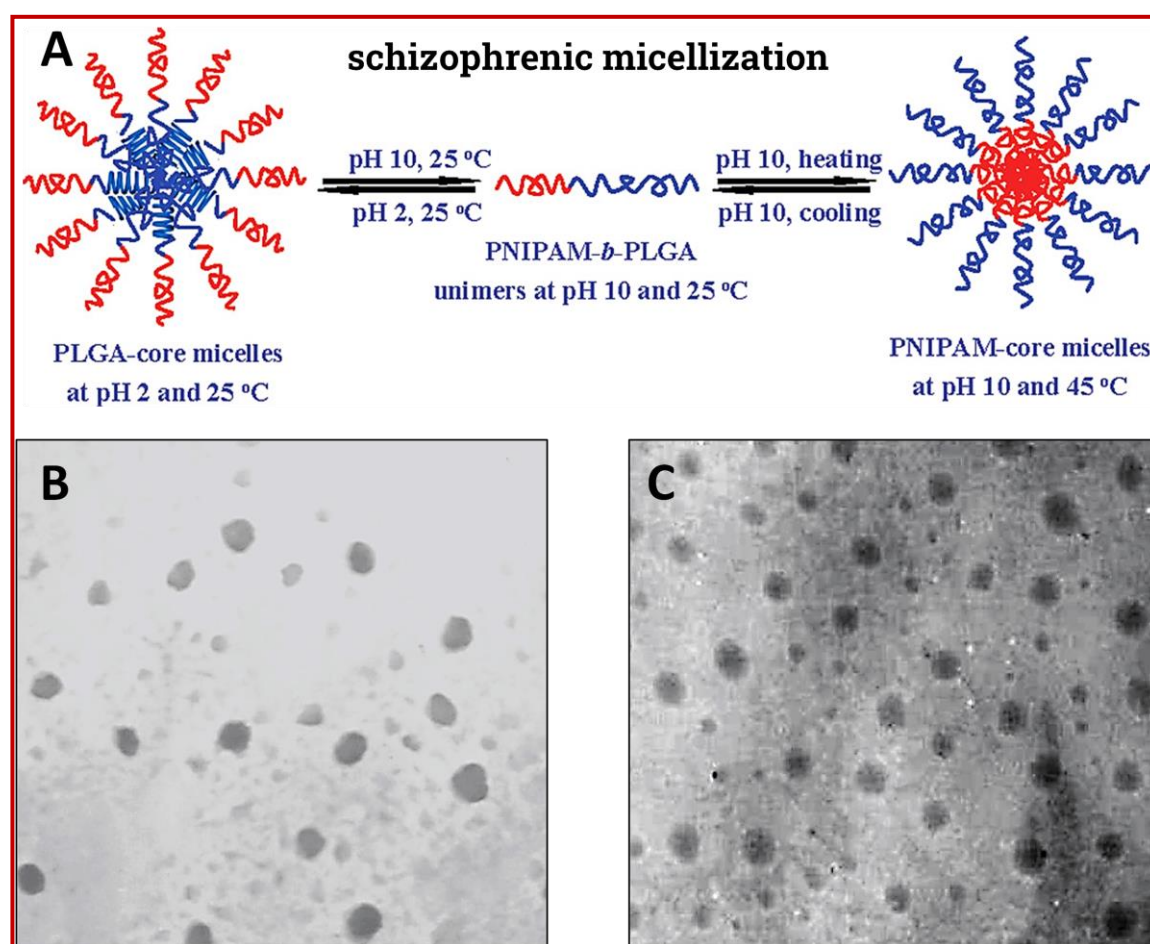


Figure 1.24. (A) Scheme for thermo- and pH-responsive schizophrenic' micellization of PNIPAM₆₅-*b*-PLGA₁₁₀ in water; TEM image of PNIPAM₆₅-*b*-PLGA₁₁₀ (B) at pH 2 and 25 °C and (C) at pH 10 and 45 °C. (Represented from ref.²³²)

Reverse phenomenon was observed at acidic pH and ambient temperature, i.e., PLGA-block formed the core and corona was formed by the PNIPAM-block. During 'schizophrenic' micellization of PNIPAM₆₅-*b*-PLGA₁₁₀ at different condition, a conformational change of the PLGA block was also observed with coil-to-helix transition. In recent studies, conducted by independent research groups led by Klok, Schlaad, and Lecommandoux, a significant attention has been given to exploring synthetic polymer-polypeptide block copolymers.³⁰⁹⁻³¹¹ Their investigations have focused on modifying the hydrophobic blocks and amino acids within the polypeptide segments, resulting in the development of pH-responsive micelles. However, the development of rod-like micelles derived from polypeptide-based block copolymers that exhibited pH-responsiveness has remained a challenging pursuit. Typically, as per their report, when the weight fraction of the hydrophilic block approached to 0.55 in a neutral amphiphilic block copolymer, the formation of cylindrical micelles has been observed.³¹²⁻³¹⁴

Like the block copolypeptides, polypeptide-based graft copolymer also transformed into micellar aggregates through self-assembly in various solvents. For example, thermoresponsive poly(EtOx) grafted poly(L-tyrosine)s (PTyr-*g*-PEtOx)s were synthesized by our group by varying the chain length of both the main polypeptide backbone as well as the pendant PEtOx segments.¹² The resultant amphiphilic graft copolypeptides underwent micellar self-assembly in both aqueous and non-aqueous (DCM) solvents. In water the hydrophobic polypeptide block constructs the core of the micelle and pendant hydrophilic PEtOx block formed the corona. These micelles were very stable and didn't get ruptured even at elevated solution temperature. The DLS study (Figure 1.25A) of the PTyr-*g*-PEtOx copolypeptides showed the presence of both small and large particles simultaneously. TEM analysis also confirmed this observation (Figures 1.25B-1.25C). The authors postulated that the small particles were unit micelles formed by the primary aggregation of the

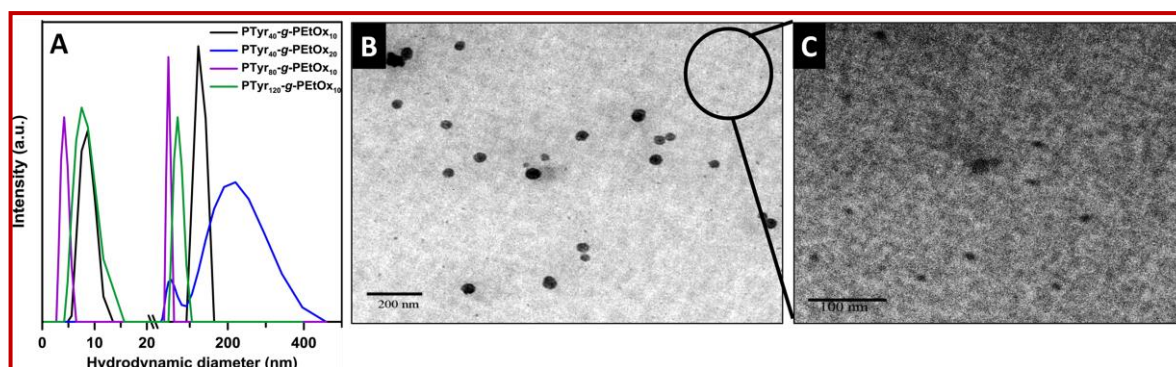


Figure 1.25. (A) DLS plot of different PTyr-*g*-PEtOx copolypeptides in water; TEM images of PTyr-*g*-PEtOx in water below cloud point showing compound micelles (B) and unit micelles (C). (Represented from ref.¹²)

copolypeptide. However, the particles of higher diameter were assigned to the formation of compound micelles formed by the secondary aggregation of unit micelles through non-covalent interactions (hydrophobic interaction) among the pseudopeptidic PEtOx blocks present in the coronas. This process of primary and secondary aggregation remained in an equilibrium and as a result both small- and large-sized particles were always present in the medium even after ageing for several days. However, temperature dependent DLS study of a representative graft copolypeptide (PTyr₄₀-*g*-PEtOx₁₀) showed that with increase in the solution temperature, small-sized particles vanished, and the size of the larger particles increased, which also suggested the secondary aggregation of the unit micelles to effectively large composite micelles. These micelles was observed to be capable of encapsulating hydrophobic dye molecules into their core through hydrophobic interactions and can retain it at high temperature also without any leaching of the dye molecules.

Our group have also reported the synthesis of polymer-polypeptide conjugate (PMMA-*b*-PTyr) by combing atom transfer radical polymerization (ATRP) and ROP and their successive self-assembly in DMF.⁹⁰ They predicted that the hybrid micro/nanospheres observed were actually composite micelles,

which formed through the aggregation of individual micelles consisting of PMMA-*b*-PTyr conjugate molecules (Figure 1.26). This aggregation was driven by the contrasting polarities of the PMMA and PTyr blocks, resulting in varying solubilities in DMF. The larger spheres were believed to be composite micelles comprised of the initially formed unit micelles from the PMMA-*b*-PTyr block copolymer. Over time, the hydrodynamic diameter of these composite micelles increased, a finding supported by DLS measurements. The formation of such composite structures was attributed to additional secondary interactions among the shell peptide of unit micelles, facilitated by H-bonding between the amide groups present in the polypeptide chains.

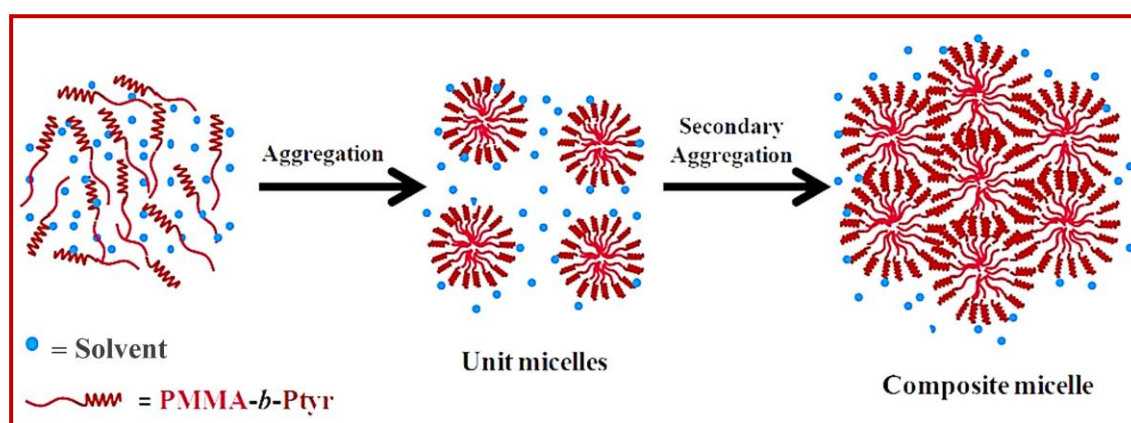


Figure 1.26. Proposed schematic representation of the formation of composite micelle formed due to secondary aggregation. (Taken from ref.⁹⁰)

Presence of both the small and large aggregates basically implies some sort of equilibrium between aggregates formation. This equilibrium is not stable thermodynamic equilibrium rather may be metastable kinetic equilibrium. This mechanism is quite similar to a phenomenon called '*Ostwald ripening*', which usually occurred in liquid sol, where small particles dissolve and redeposit onto larger particles while increasing its size.³¹⁵ The mechanism of composite/compound micelle formation through secondary aggregation of primary unit micelles in pseudopeptide-polymer or peptide-polymer conjugates has been extensively reported and established by our group.³¹⁶⁻³¹⁸

1.5.2.2. Vesicular Self-Assembly

Polymer vesicles, also known as polymersomes, are spherical nanometer-sized or micrometer-sized hollow self-assembled structures of amphiphilic polymers in solution. Similar to liposomes, vesicles are formed from phospholipids, polymer vesicles have a hydrophilic outer shell and a hydrophobic inner core (Figure 1.27). Polymersomes are primarily characterized by the presence of an amphiphilic block copolymer, which constitutes the bilayer structure of the vesicle (Figure 1.27). By carefully adjusting parameters such as degrees of polymerization (DP), composition, and the ratio between the hydrophilic and hydrophobic blocks, the specific vesicle

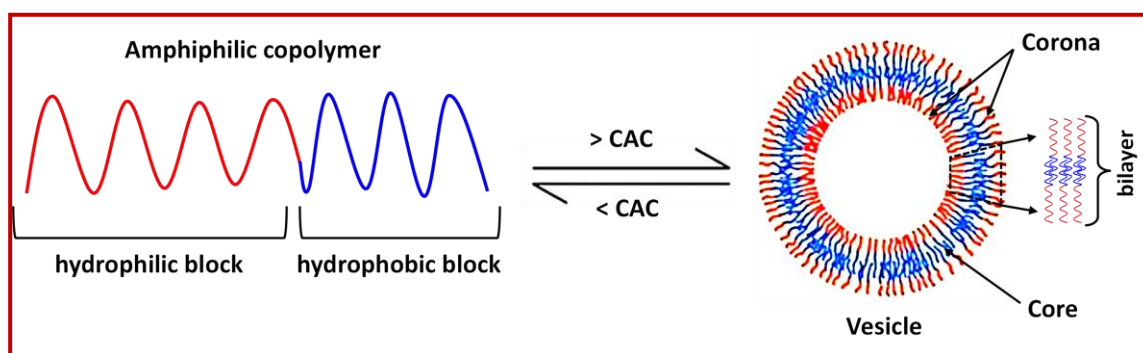
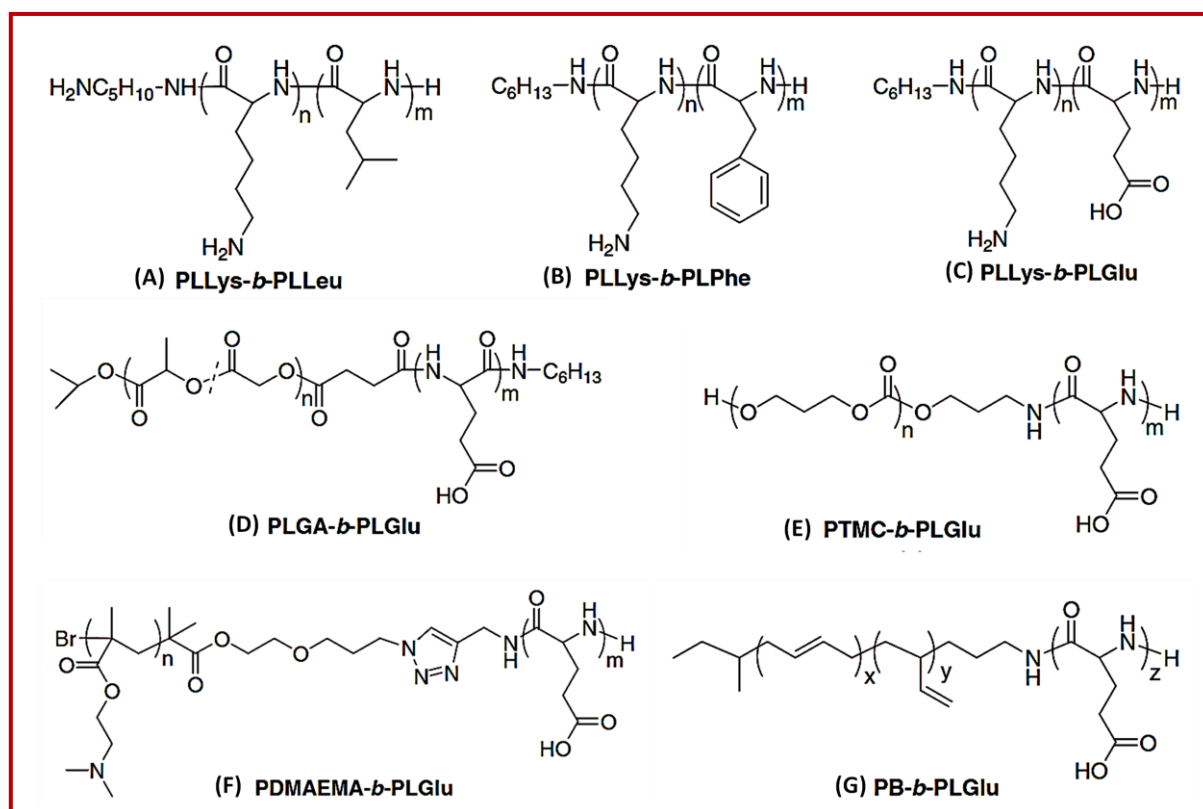


Figure 1.27. Simple schematic representation of formation of vesicle through bilayer formation.

morphology can be precisely attained.³¹⁹ In general, amphiphilic block copolymers with the hydrophilic to hydrophobic ratios more than 1:1 form micelle through self-assembly, and when the ratio is less than 1:2, preferably forms vesicle.³²⁰ Unlike micelles, which have a solid hydrophobic core, polymer vesicles possess semipermeable membranes that enable them to encapsulate hydrophilic moieties from solutions into their interior hydrophilic pool. Furthermore, in addition to their capacity for hydrophilic encapsulation, polymer vesicles also have the ability to load hydrophobic drugs within their hydrophobic membrane domains. This unique feature makes them highly

suitable for delivering both hydrophilic and hydrophobic drugs and bioactive molecules. Moreover, high chemical stability and easy tuning of the physical properties of the polymer vesicles such as size, membrane thickness, permeability etc. by modifying the composition and structure of the block segments, allow for prolonged storage and better control over drug release in biomedical applications. Additionally, the surface of polymer vesicles can be modified with targeting ligands or antibodies to selectively deliver drugs to specific cells or tissues. Research is ongoing to further improve the properties and functionalities of polymer vesicles. Advances in polymer synthesis and self-assembly techniques have led to the development of more sophisticated vesicles with enhanced stability, capability of controlled release profiles, and stimuli-responsive behaviour (Scheme 1.12).



Scheme 1.12. Chemical structures of some representative polypeptide-based block copolymers that form stimuli-sensitive vesicles (A-G).^{16, 87-88, 321-325}

Deming and co-workers have synthesized a series of amphiphilic diblock copolypeptides with appropriate composition and chain length.^{50, 129, 235} These copolypeptides led to the formation of large-sized vesicles ranging from 1-25 μm . Interestingly, it was observed that the morphology of these assemblies was highly influenced by two key factors: the hydrophobic block content and the overall chain length of the copolymer. For example, a pH-sensitive diblock copolypeptide, denoted as $\text{P}((\text{EO}_2)\text{LL})_{160}\text{-}b\text{-P}(\text{LLeu}_{0.3}\text{-}co\text{-LLys}_{0.7})_{40}$ [$\text{KP}_{160}(\text{L}_{0.3}/\text{K}_{0.7})_{40}$], was synthesized.²³⁵ This copolypeptide was designed by incorporating Llys residues into the hydrophobic PLLeu block. At a high pH 10.6, the diblock copolymer self-assembled into stable vesicles (Figure 1.28). These vesicles exhibited a hydrophobic $\text{P}(\text{LLeu}_{0.3}\text{-}co\text{-LLys}_{0.7})_{40}$ layer and hydrophilic $\text{P}((\text{EO}_2)\text{LL})_{160}$ inner and outer shells. Importantly, during the self-assembly process, hydrophilic Fura-2 dye was encapsulated within the vesicles.

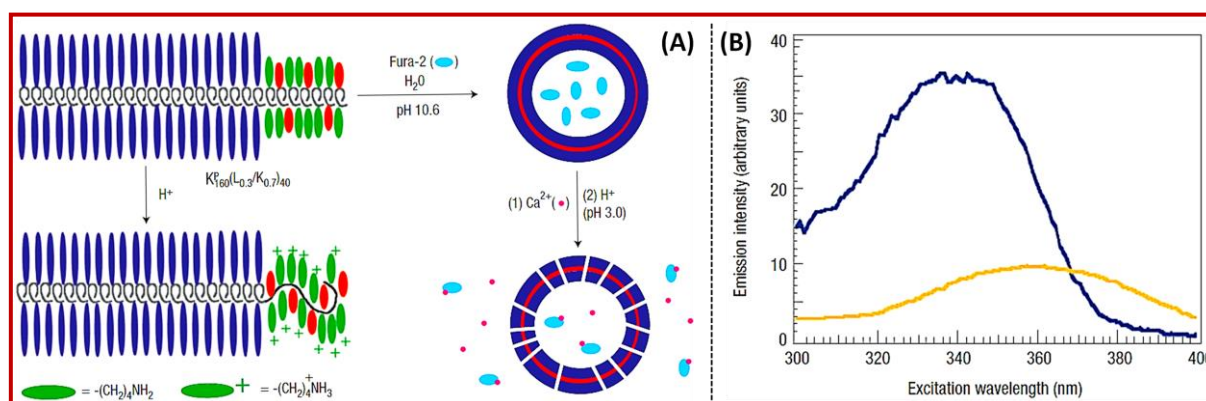


Figure 1.28. (A) Schematic representation of vesicular self-assembly of $\text{KP}_{160}(\text{L}_{0.3}/\text{K}_{0.7})_{40}$ and its change in conformation with pH, and release of encapsulated Fura-2 dye on pH change; (B) Fluorescence emission of Fura-2 dye (50 mM) entrapped in vesicles of $\text{KP}_{160}(\text{L}_{0.3}/\text{K}_{0.7})_{40}$ in the presence of external calcium (5.0 mM) at pH 10.6 and at pH 3.0. (Taken from ref.²³⁵)

When the pH was decreased by adding an acid, the vesicle membranes underwent rapid disruption. Consequently, the encapsulated dye was released

from the vesicles. This pH-triggered disruption of the vesicle membranes allowed for the controlled release of the dye. Deming et al. have also synthesized a block copolypeptides, P(Lys)₆₀-*b*-P(Leu)₂₀, forming large vesicles, driven by the preference of helical PLeu blocks to pack side-by-side along their long axes, resulting in a flat membrane structure (Figure 1.29).³²¹

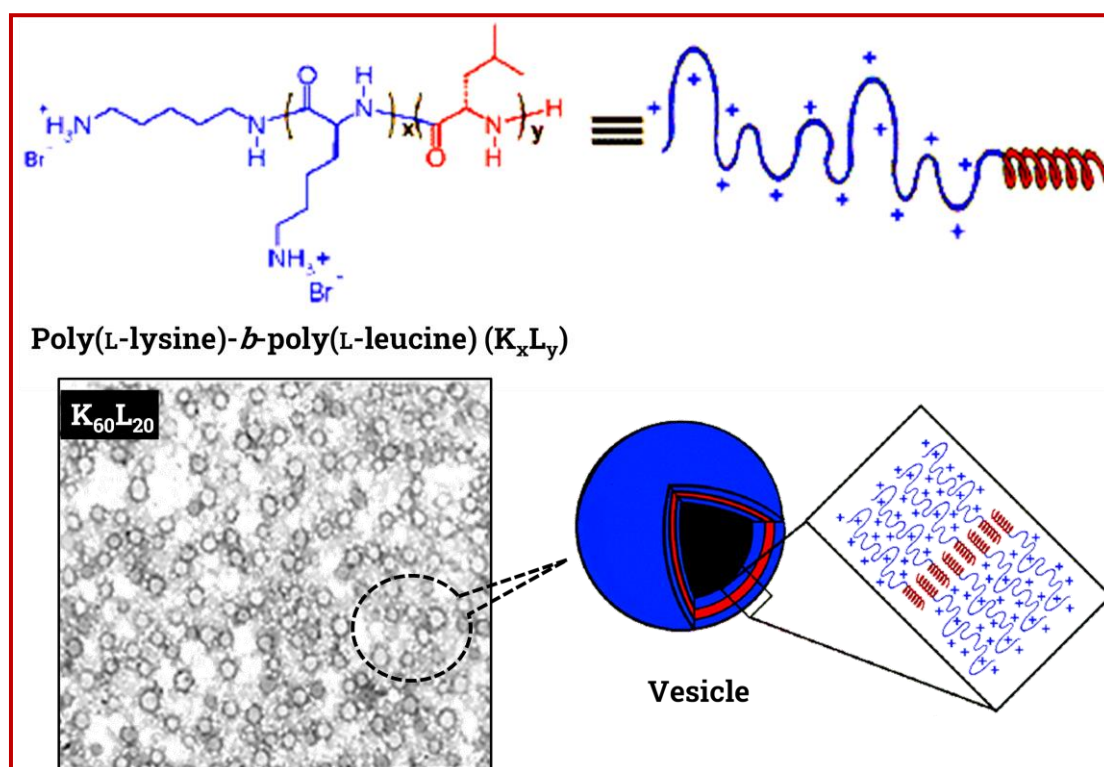


Figure 1.29. Schematic representation for proposed vesicular self-assembly of $K_{60}L_{20}$ and its TEM image. (Taken from ref.³²¹)

These vesicles demonstrated remarkable stability, as no visible changes or disruptions were observed even after three months at room temperature or when exposed to 80°C for 30 minutes. The vesicles efficiently encapsulated Texas Red labelled dextran (3000 Da) and exhibited minimal leakage, maintaining the encapsulated cargo for at least five days. However, it was observed that due to the coil-like structure of the polyelectrolyte blocks and the repulsion between the PLys chains, the vesicle membrane displayed enhanced flexibility and compliance. As a result, the vesicles formed from P(Lys)₆₀-*b*-

P(Leu)₂₀ copolypeptides (Figure 1.29) could be extruded through polycarbonate membranes, allowing for control over their diameter. On the other hand, the vesicles were sensitive to salt concentration. At low salt concentrations (NaCl, 100 mM), they tended to aggregate and clump together. Conversely, it was observed that at high salt concentrations (NaCl, 500 mM), the vesicles precipitated as flat sheets due to the charge screening effect induced by the salt ions.

Lecommandoux and colleagues discovered pH and temperature-responsive polypeptide-based vesicles using double hydrophilic block copolymers, (PDMAEMA-*b*-PGA)s.⁸⁸ At the isoelectric points, PDMAEMA₈₅-*b*-PGA₁₈₆ and PDMAEMA₈₅-*b*-PGA₇₇ self-assembled into vesicles in water at 25 °C, stabilized by electrostatic interactions between charged groups (Figure 1.30). PDMAEMA₈₅-*b*-PGA₁₈₆ formed vesicles with negatively charged PGA membrane, while PDMAEMA₈₅-*b*-PGA₇₇ formed vesicles with protonated amino groups as the outer layer. At pH 11 and elevated temperature, thermoresponsive PDMAEMA segments became hydrophobic, forming the core of the self-assemblies, and PGA stabilized the structure. PDMAEMA₈₅-*b*-PGA₇₇ and PDMAEMA₈₅-*b*-PGA₃₇ formed vesicles, while PDMAEMA₈₅-*b*-PGA₁₈₇ was reported to form micelles due to its high hydrophilic fraction. Lowering the pH at room temperature was expected to induce helical conformation in the PGA membrane.

Jin Huang et al. have employed the sequential ROP of benzyl-L-glutamate and propargylglycine (PG) NCA to obtain amphiphilic polypeptide block copolymers with varying block length ratios.³²⁶ The poly(PG) block was further glycosylated through a click reaction using azide-functionalized galactose. These copolymers, specifically PBLG-*b*-poly(galactosylated propargylglycine) (PBLG-*b*-PGG), were considered as potential candidates for producing glycopeptidic vesicles with galactose residues on the polymersome surface, allowing for lectin binding (Figure 1.31).

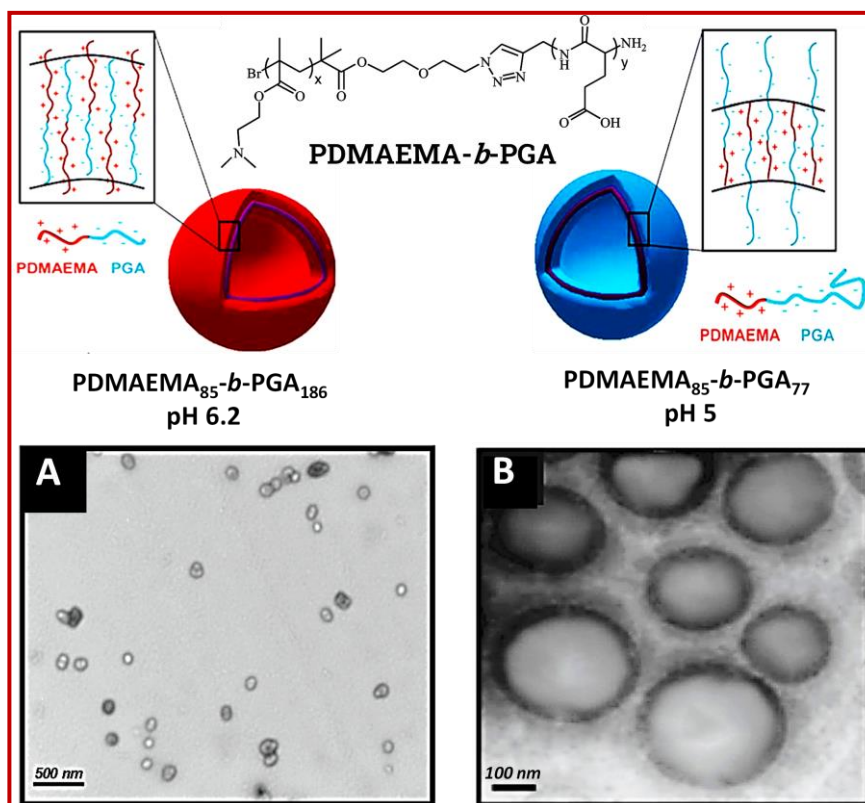


Figure 1.30. (A) Schematic representation of electrostatic vesicles formed by PDMAEMA₈₅-*b*-PGA₁₈₆ at pH 6.2; (B) Schematic representation of electrostatic vesicles formed by PDMAEMA₈₅-*b*-PGA₇₇ at pH 4–6; (C) Schematic illustration of different morphologies of PDMAEMA-*b*-PGA under different conditions. (Represented from ref.⁸⁸)

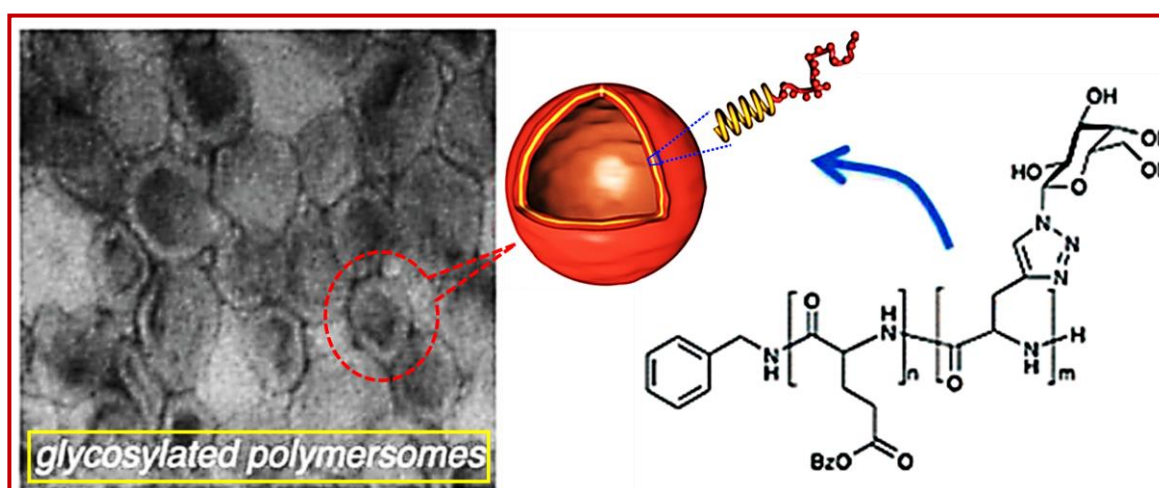


Figure 1.31. Chemical structure of the PBLG-*b*-PGG copolypeptide and TEM image of the vesicles formed by the PBLG₂₀-*b*-PGG₂₅. (Taken from ref.³²⁶)

The morphological nature of the formed structures, ranging from wormlike micelles to polymersomes, could be controlled by adjusting the composition of the block copolymers and employing specific self-assembly protocols. The nanoprecipitation method, involving the addition of a nonsolvent for the hydrophobic segment, was utilized to self-assemble all the block copolymers. In the case of PBLG₂₀-*b*-PGG₃₂, a combination of spherical micelles and vesicles was observed, indicating that the upper limit of the hydrophilic weight ratio had been reached for polymersome formation with these diblock copolymers. Vesicles composed of PBLG₂₀-*b*-PGG₁₈ exhibited significant aggregation in solution, as confirmed by TEM, atomic force microscopy (AFM), and DLS measurements. Conversely, vesicles formed from the copolymer PBLG₂₀-*b*-PGG₂₅ displayed greater stability. The bioactivity of the glycopeptide polymersomes generated from the PBLG₂₀-*b*-PGG₂₅ copolymer was evaluated through carbohydrate-lectin binding experiments, demonstrating that the carbohydrate groups on the surface of the polymersomes were capable of interacting with the intended biological target molecules.

Vesicles forming block copolypeptides with other hydrophobic polypeptide segments have also been synthesized and explored. Jing et al. successfully synthesized a series of PLLys-*b*-poly(L-phenylalanine) (PLLys-*b*-PLPhe) through sequential ROP of ZLL-NCA and L-phenylalanine NCA (LPhe-NCA) using n-hexylamine as an initiator followed by ε-benzyloxycarbonyl group deprotection.³²² Interestingly, the diblock copolypeptides with shorter PLPhe blocks demonstrated water solubility and spontaneously formed large vesicles. The formation of these vesicles was confirmed through AFM. The central part of the vesicles exhibited a lower height compared to the peripheral part, attributable to the collapse of the hollow vesicles. Confocal laser scanning microscopy (CLSM) examination demonstrated the encapsulation of a hydrophilic dye, Rhodamine B, within the interior aqueous compartments of the vesicles.

1.5.2.3. Gelation

Hydrogels are three-dimensional networks of hydrophilic or amphiphilic polymers, formed through chemical or physical crosslinking. Stimuli-responsive macroscopic hydrogels undergo volume phase transitions or sol-gel phase transitions in response to changes in environmental conditions (Figure 1.32).³²⁷⁻³²⁸ Chemically crosslinked hydrogels form permanent polymer networks and exhibit volume phase transitions under environmental stimuli, while physically crosslinked hydrogels typically consist of reversible networks

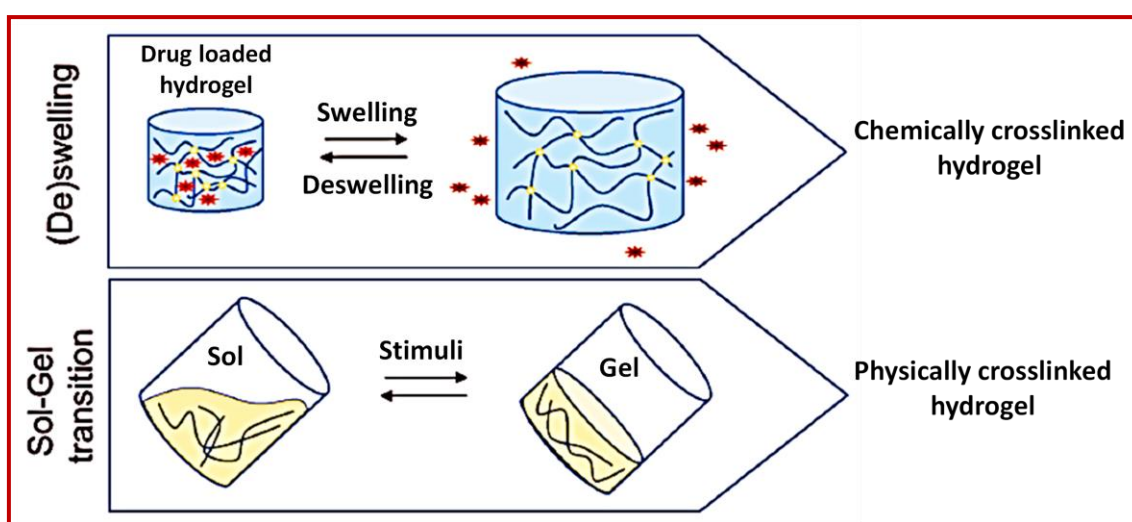


Figure 1.32. Schematic representation of the stimuli-responsiveness of differently functionalized hydrogels. (Taken from ref.³²⁹)

that can transition back and forth between a crosslinked gel state and an uncross-linked sol state upon exposure to external stimuli.³²⁸ Consequently, covalently crosslinked hydrogels that experience volume phase transitions in response to environmental stimuli have been designed for controlled drug delivery, leveraging stimuli-induced swelling and deswelling transitions. On the other hand, physically crosslinked hydrogels that can be formed in situ, such as thermo-gelling hydrogels, have been developed for localized drug delivery.³²⁸ Recently, chemically crosslinked hydrogels and in situ gelling

hydrogels based on polypeptides have been prepared and assessed for diverse drug delivery applications.^{293, 330-333}

A series of pH-responsive hydrogels based on PLGlu were synthesized by Yang et al., utilizing diamino-capped PEG as a crosslinker.²⁵ The hydrogels demonstrated a sharp increase in equilibrium swelling ratio as the pH was increased from 4 to 6 due to the gradual ionization of carboxylic groups within the hydrogel network, accompanied by a secondary conformational transition. However, at higher pH, an increase in ionic strength resulted in a decrease in swelling ratio due to the charge screening effect of salt. Following this investigation, the same research group have also prepared PLGlu-based hydrogels through photopolymerization of PEG-methacrylate substituted PLGlu with PEG dimethacrylate (PEG-DA) crosslinker.³³⁰ Thermo- and pH-responsive hydrogels based on poly(L-glutamic acid) (PLGlu) and poly(N-isopropylacrylamide-co-hydroxyethyl methacrylate) (poly(NIPAM-co-HEMA)) of (PLGlu) have been successfully synthesized by Chen et al.³³² The hybrid hydrogels were prepared by coupling PLGlu with poly(NIPAM-co-HEMA) using 1-ethyl-3-(3-dimethylaminopropyl) carbodiimide hydrochloride (EDC·HCl) as a coupling agent. The swelling behaviour of the as synthesized hybrid hydrogels was found to be dependent on both pH and the composition of the hydrogel. Increasing the PLGlu content resulted in an enhanced swelling ratio, larger pore size, and increased enzymatic degradation rate at pH 7.4. Furthermore, all the hydrogels exhibited rapid swelling-deswelling transitions when the pH was varied from 7.0 to 4.0 at 37 °C, indicating their potential applications in oral drug delivery. Although, a sharp temperature-induced phase transitions were observed for the hydrogels, the effect of temperature on the swelling capacity of the hydrogels was found to be less compared to the pH, due to the greater hydrophilicity and electrostatic repulsion of the PLGLU segments at elevated pH. These hydrogels were loaded with a model protein, lysozyme by swelling-diffusion, and subsequent release was monitored by pH. In recent studies

conducted by the same research group, novel pH- and temperature-sensitive hybrid hydrogels were developed by combining poly(L-glutamic acid) (PLGlu) with a naturally derived polysaccharide, hydroxypropylcellulose (HPC).³³⁴⁻³³⁵ The synthesis of PLGlu/HPC hybrid hydrogels involved the free-radical copolymerization of HEMA-modified PLGlu (PLGlu-*g*-HEMA) and acrylate-substituted HPC. The incorporation of HPC, which exhibits a LCST type thermoresponsiveness at around 41 °C, enabled the hybrid hydrogels to display pH- and temperature-dependent swelling behaviours. Specifically, at a temperature of 37 °C, the swelling ratio of the hydrogels exhibited a significant increase as the pH was raised from 4.0 to 6.8. Conversely, at pH 6.8, the swelling ratio gradually decreased with increasing temperature from 25 °C to 48 °C. The swelling ratio of the hydrogels could also be regulated by varying the composition of the different component of the copolypeptides at different pH level.

Amphiphilic functionalized polypeptide with hydrophilic and hydrophobic side groups can exhibit gelation phenomena triggered by changes in temperature. Yasushi et al. synthesized poly(α/β -aspartamide) (PAspAm) derivatives by aminolysis of polysuccinimide (PSI) using dodecylamine and amino alcohols.³³⁶⁻³³⁷ These PAspAm derivatives underwent sol-gel transitions in PBS, influenced by graft composition, side chain length, polymer concentration, and additives. Kim et al. developed thermo- and pH-sensitive PAspAm derivatives through aminolysis of PSI using N-alkylamines and N-isopropylethylenediamine.³³⁸⁻³³⁹ The copolymers showed pH-dependent thermoresponsiveness, and their phase transition temperature depended on alkyl chain length and graft composition. A concentrated solution of that copolymer in PBS exhibited temperature-induced sol-gel transitions *in-vitro* and *in-vivo*.

In-situ forming hydrogels are injectable and can be developed through the formation of physical crosslinking in response to environmental stimuli.³²⁸

³⁴⁰⁻³⁴¹ Alternatively, they can be also formed through in-situ chemical reactions, such as Michael addition reactions,³⁴² enzyme-catalyzed reactions,³⁴³⁻³⁴⁴ or Schiff base reaction.³⁴⁵ In comparison to stable crosslinked polymer networks formed by covalent bonds, in-situ forming hydrogels with physical crosslinking exhibit reversible networks formation with respect to external stimuli. For instance, Deming et al. have developed a series of in-situ forming hydrogels using diblock copolypeptides consisting of a charged block (PLLys or PLGlu) and a hydrophobic block (PLLeu or PLVal).¹²⁹⁻¹³⁰ These diblock copolypeptides formed rigid hydrogels at very low polymer concentrations (0.25-2.0 wt%). The gelation at low concentrations was primarily attributed to the presence of the charged block, as the gel formation was not affected by the substitution of the positively charged PLLys block with the negatively charged PLGlu block. However, the addition of salt resulted in weaker hydrogels due to charge screening effects. Furthermore, the ordered secondary structures, such as α -helix and β -sheet, in the hydrophobic block promoted gel formation. The strength of the hydrogels could be adjusted by modifying the composition and concentration of the polypeptides. These physically crosslinked polypeptide hydrogels demonstrated the ability to undergo deformation, thinning under stress, and were suitable for injection through small-bore cannulae.³⁴⁶

In situ thermo-gelling hydrogels have gained significant attention and widely investigated in situ forming systems.^{328, 340-341} Recently, polypeptide-based thermo-gelling systems have also been reported. Jeong et al. successfully synthesized a diblock copolymer, PEG-*b*-poly(L-alanine) (PEG-*b*-PLAla) through ROP of L-alanine NCA mPEG-NH₂ as a macro-initiator.³⁴⁷ Aqueous solutions of PEG-*b*-PLAla exhibited sol-to-gel transitions upon increasing temperature, at a polymer concentration ranging from 6% to 12% (wt%). The sol-gel transition temperatures varied between 20°C and 40°C, depending on the polymer concentration. These findings highlight the potential of these materials for in situ forming drug delivery systems.

Hydrogel nanoparticles/nanogels are polymeric networks of swollen nanometer-sized structures (crosslinked nanoparticles or micelles) formed by self-assembly of hydrophilic or amphiphilic polymers, which offer distinct advantages such as enhanced stability, high drug loading capacity, and the ability to react to external stimuli.³⁴⁸⁻³⁵⁰ Nanogels can exist as complete polymeric networks or possess a core-shell structure with a hydrogel core or shell (Figure 1.33). These nanocarriers can encapsulate drugs, and their subsequent site-specific release can be triggered by environmental stimuli such as temperature, pH, redox etc. Over the past decade, polypeptide-based stimuli-responsive nanogels attracted significant attention due to their intelligent swelling and deswelling transitions in specific solvent, as well as improved biocompatibility.³⁵¹⁻³⁵³

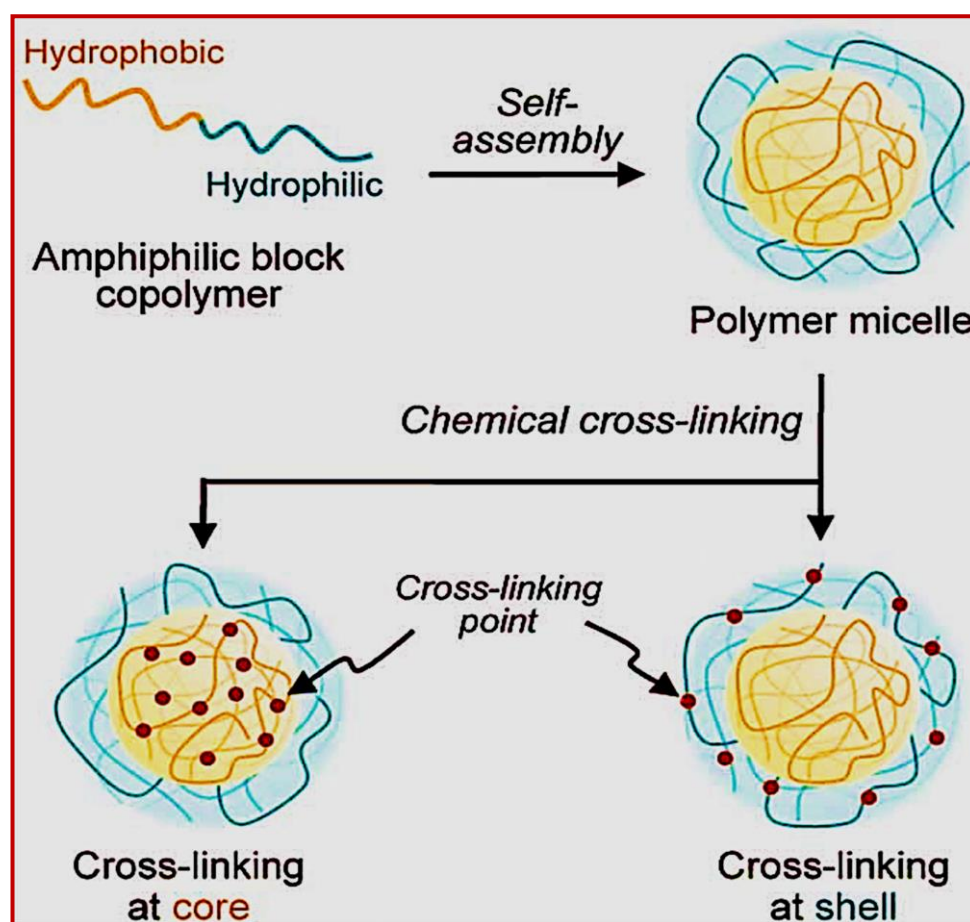


Figure 1.33. Preparation of nanogels by cross-linking of amphiphilic block copolymer at core or shell of the polymer micelles in water. (Taken from ref.³⁵⁴)

Reversible shell crosslinked micelles were synthesized using a series of poly(L-cysteine)-*b*-PLLA diblock copolymers (PLCys-*b*-PLLA).³⁵⁵ The synthesis involved the ROP of β -benzyloxycarbonyl-L-cysteine NCA (ZLC-NCA) using amino-terminated PLLA as a macro-initiator. Subsequently, the benzyloxycarbonyl groups were deprotected using HBr. Initially, micelles with a PLLA core and a PLCys shell were formed in the presence of DTT. These micelles were then transformed into shell crosslinked micelles containing disulfide bonds by removing DTT and allowing aerial oxidation to occur. Kataoka et al., have developed reversible-core crosslinked micelles with disulfide bonds.³⁵⁶ These micelles were prepared by mixing thiolated PEG-*b*-PLLys and PAsp, followed by crosslinking of the micellar core through aerial oxidation. The crosslinking process involved the formation of disulfide bonds. This approach resulted in the formation of core-crosslinked polyion complex (PIC) micelles.

Nanometer-sized polypeptide networks (nanogels) are capable of undergoing swelling-deswelling transitions in response to changes in pH. Such pH-responsive gel has gained significant interest as potential drug delivery systems. To create these nanogels, PEG-*b*-PAsp (polyethylene glycol-*b*-polyaspartic acid) was synthesized through the crosslinking of PAsp blocks using 1,6-hexanediamine as a crosslinker and N,N'-diisopropylcarbodiimide (DIC) as a coupling agent.³⁴⁸ This process resulted in the formation of a core-shell structure, with a crosslinked PAsp hydrogel core surrounded by a PEG shell. The pH-dependent behaviour of these nanogels was observed. It was observed that, when the pH increased from 4 to 9, the size of the nanogels underwent a significant change, expanding from below 20 nm to over 40 nm. This transition was attributed to the swelling of the polypeptide core, caused by the gradual ionization of the Asp residues when the pH exceeded their pKa value of approximately 3.9. These pH-sensitive nanogels hold promise for precise and controlled drug release triggered by variations in pH levels.

Doxorubicin-loaded nanogels were prepared by combining Dox with the nanogels in deionized water. Remarkably, a relatively high drug loading capacity of 26.6 wt% was achieved, mainly attributed to the electrostatic interactions between oppositely charged Asp residues and Dox. The incorporation of the drug did not significantly affect the particle size of the nanogels. Upon investigation, it was observed that Dox was rapidly released from the nanogels at both pH 5.0 and 7.4. Interestingly, the drug release profile showed a slightly faster release rate at pH 5.0 compared to pH 7.4. Notably, at pH 7.4, the nanogels were found to be in a swollen state, which potentially facilitated the diffusion of the drug within the system. This finding highlights the potential of the nanogels for efficient drug delivery and release under physiological conditions.

Photocrosslinking, an alternative method for in-situ crosslinking, offers controllable crosslinking without the need for photo-initiators. Chen et al. developed pH-responsive polypeptide nanogels using photocrosslinkable PEG-*b*-poly(LGlu-*co*- γ -cinnamyl L-glutamate) (PEG-*b*-P(LGlu-*co*-CLG)) diblock copolymers.³⁵⁷ These copolymers were synthesized by grafting cinnamyl alcohol to LGlu residues after ROP of BLG-NCA, using mPEG-NH₂ initiator. PEG-*b*-P(LGlu-*co*-CLG) self-assembled into nanoparticles via hydrophobic interactions between CLG segments in an aqueous solution. Upon UV irradiation at 254 nm, the pendant cinnamyl groups underwent dimerization, leading to in situ crosslinking of the polypeptide segments and the formation of nanogels. The size of the nanogels, with hydrodynamic radii ranging from 80–135 nm at pH 7.4, depending on the length of the polypeptide block and the degree of cinnamyl group substitution. A model drug, rifampicin, was incorporated into the PEG-*b*-P(LGlu-*co*-CLG) nanogels, by mixing with an aqueous solution of the drug followed by in-situ photocrosslinking. The drug-loaded nanogels exhibited pH-dependent release profiles *in-vitro*, with faster

drug release observed at pH 7.4 and minimal release at pH 4.0, attributed to nanogel swelling at higher pH levels.

Overall, polypeptide-based hydrogels/nanogels are versatile soft materials with unique properties that make them valuable for a wide range of applications in the fields of biomedical engineering, drug delivery, wound healing, tissue engineering, and biosensing in biotechnology, medicine, and other scientific fields.

1.6. Applications of Functionalized Polypeptides

The advancements in synthetic polypeptides have opened up new possibilities for a wide range of polypeptide architectures. Thanks to the different impressive ROP techniques, now any type of polypeptide material (block and random copolypeptides of controlled dimensions including molecular weight, sequence, composition, and molecular weight distribution) can easily be developed according to specific requirements.¹⁰ A significant advantage lies in the production of NCA monomers with a diverse range of functional group handles. Currently, there are approximately 200 known NCA monomers, with the potential for further expansion to meet specific needs. This remarkable diversity greatly enhances the applications of polypeptides compared to natural proteins, which are limited to 20 natural amino acids.

Polypeptides possess desirable characteristics such as amphiphilicity as well as biocompatibility, biodegradability, and the ability to mimic proteins by forming various secondary structures. As a result, they have become strong candidates in a wide range of applications, including drug or gene delivery,³⁵⁸⁻³⁶⁵ tissue engineering,^{129-130, 293} antimicrobial agents,³⁶⁶⁻³⁶⁹ antifouling coatings,³⁷⁰⁻³⁷² and more. Moreover, enormous effort have been given to develop responsive polypeptide adhesives for use as surgical sealants, and immunomodulating polypeptides for treatment of autoimmune disorders.^{5, 36}

Polypeptide adhesives as surgical sealants: Polypeptides have shown great potential as adhesive materials for manufacturing of surgical applications. These adhesive polypeptides can be designed to have excellent biocompatibility, strong adhesive properties, and controllable degradation rates. They can be used as surgical sealants to promote wound healing and prevent fluid leakage or as tissue adhesives for various surgical procedures.³⁷³⁻³⁷⁵

Immunomodulating polypeptides for treatment of autoimmune disorders: Polypeptides can be designed to modulate the immune response and hold promise for the treatment of autoimmune disorders. By selectively targeting immune cells or regulating immune signalling pathways, immunomodulating polypeptides can help restore immune balance and alleviate symptoms associated with autoimmune diseases.³⁷⁶⁻³⁷⁷

Among these applications, this section will briefly focus on the functionalized polypeptides which have been used as control release systems, tissue engineering scaffold and antimicrobial/antibacterial agents (Figure 1.34).

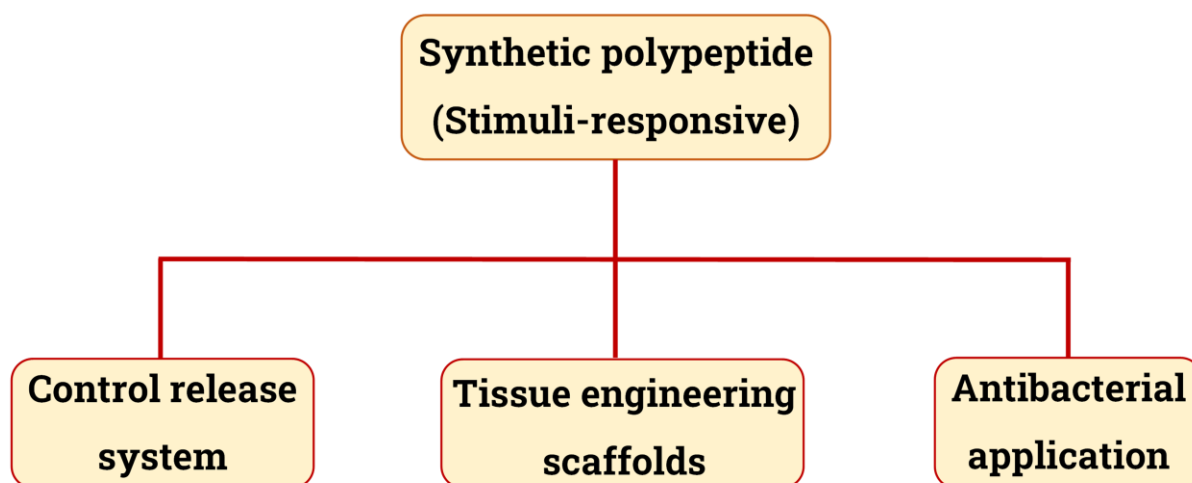


Figure 1.34. Schematic representation of different applications of functionalized polypeptides.

1.6.1. Control Release Systems

A control release system refers to a technology or mechanism designed to deliver a substance or drug or gene in a controlled manner over an extended period of time. It allows for the sustained release of the substance, ensuring a consistent and controlled dosage over a specified duration. Control release systems are widely used in various fields, including pharmaceuticals, agriculture, and consumer products. In the pharmaceutical industry, control release systems are commonly employed to enhance the therapeutic efficacy of drugs. They are particularly useful for medications that require a sustained and controlled release to achieve the desired therapeutic effect or to minimize side effects. These systems can be designed to release drugs at a specific rate, maintain therapeutic levels in the body, or target specific sites within the body.

Drug-delivery: Synthetic polypeptides are one of the most used biomaterials for therapeutic delivery purposes due to their inherent biocompatibility and biodegradability.⁵ Recent advancements in polypeptide synthesis have led to the development of various amphiphilic architectures, including linear polypeptides, brush polypeptides, and star polypeptides, which can self-assemble into different nanostructures such as vesicles, micelles, and gels.³⁷⁸ The self-assembly behaviour of polypeptides with different secondary structures, along with encapsulated or conjugated drug molecules, significantly influences their performance as nano carriers.³⁷⁹ An illustrative example highlighting the impact of polypeptide secondary structure in drug delivery applications is a study conducted by Kataoka and colleagues. They demonstrated that polymeric micelles loaded with cisplatin, composed of bundled α -helices formed by PEG-*b*-poly(L-glutamate) or PEG-*b*-poly(D-glutamate), exhibited higher micelle yield, prolonged release profile, and extended circulation in plasma compared to micelles composed of racemic PEG-*b*-poly(DL-glutamate).³⁸⁰ However, in certain cases, the ordered secondary structures adopted by polypeptides can hinder co-assembly or drug

encapsulation in polypeptide-based nanocarriers. Semple et al. reported an example where micelles formed by racemic PEG-*b*-poly(DL-glutamate) demonstrated better loading of irinotecan compared to helical PEG-*b*-poly(L-glutamate).³⁵⁹ In addition to the secondary structure of polypeptides, the functional groups present on the side chains of amino acids play a crucial role in drug encapsulation within polypeptide-based nano carriers. An exceptional study by Zhiyuan Zhong and colleagues showcased the ultra-high loading (63 wt%) of the anticancer drug doxorubicin in PEG-*b*-polytyrosine, attributed to enhanced π - π stacking interactions between aromatic tyrosine residues and the drug molecule.³⁶⁰

In recent years, there has been a significant focus on the development of targeted and/or stimuli-responsive nanocarriers in the field of drug delivery. These nanocarriers offer improved potential for triggered drug release at the desired site and enhanced therapeutic effects. Polypeptide-based pH-responsive micelles and polymersomes have been extensively studied for drug delivery applications.³⁸¹⁻³⁸⁶ For example, Chen et al. developed PEG-*b*-PLeu-*b*-PLGlu linear copolypeptides that formed stable aggregates at physiological pH (7.4) but were de-assembled at the endolysosomal pH (5).³⁸⁴ This pH-dependent conformational change allowed the encapsulation and *in-vitro* release of doxorubicin (Dox), a water-soluble anti-cancer drug, by these self-assembled nanocarriers.

Polypeptide based vesicles offer additional advantages due to their distinct hydrophilic and hydrophobic regions. Iatrou et al. demonstrated the formation of polymersomes by PEG-*b*-PBLG-*b*-PLLys linear copolypeptide, where water-soluble drugs like Dox-HCl could be loaded into the interior aqueous pool of the vesicle and hydrophobic drugs like paclitaxel could be loaded into the hydrophobic layer.³⁸⁵ Moreover, Chen et al. showcased the dual loading of hydrophilic (Dox. HCl) and hydrophobic (Gefitinib) drugs within the

same polymersomes for the co-delivery of two chemotherapeutics both *in-vitro* and *in-vivo* (Figure 1.35).³⁸⁷

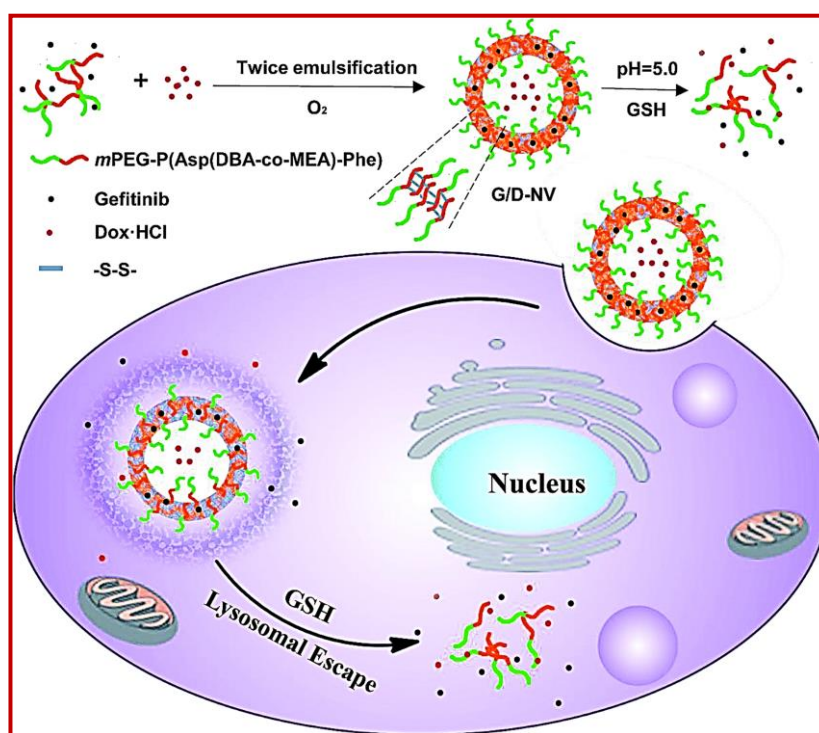


Figure 1.35. Schematic representation of encapsulation of both hydrophilic (Dox) and hydrophobic (Gefitinib) drugs by polypeptide vesicles and their subsequent release. (Taken from ref.³⁸⁷)

Gene-therapy: The therapy involves the delivery of DNA or RNA molecules such as plasmid DNA (pDNA), messenger RNA (mRNA), small interfering RNA (siRNA), and microRNA (miRNA) etc., into specific cells to modify gene expression for the treatment of various pathological conditions, including cancer, infectious diseases, and immunodeficiency. Successful nucleic acid-based therapy relies on the efficient and safe transfer of DNA or RNA into targeted cells, requiring the development of delivery vectors that are both effective and biocompatible.³⁸⁸⁻³⁹⁰ The first option involves the use of viral vectors, which are highly efficient but raise safety concerns, have low loading capacity, and face challenges in scaling up the production process.³⁹¹ As an

alternative approach, non-viral vectors can be utilized for gene therapy due to their biocompatibility and minimal risk of causing mutations.³⁹² One common strategy for designing non-viral gene delivery vectors (e.g., polymers) is to form an electrostatic complex between the positively charged functional groups of the cationic vector and the negatively charged phosphate groups of the genetic materials (polyplex formation) (Figure 1.36).^{17, 389, 393}

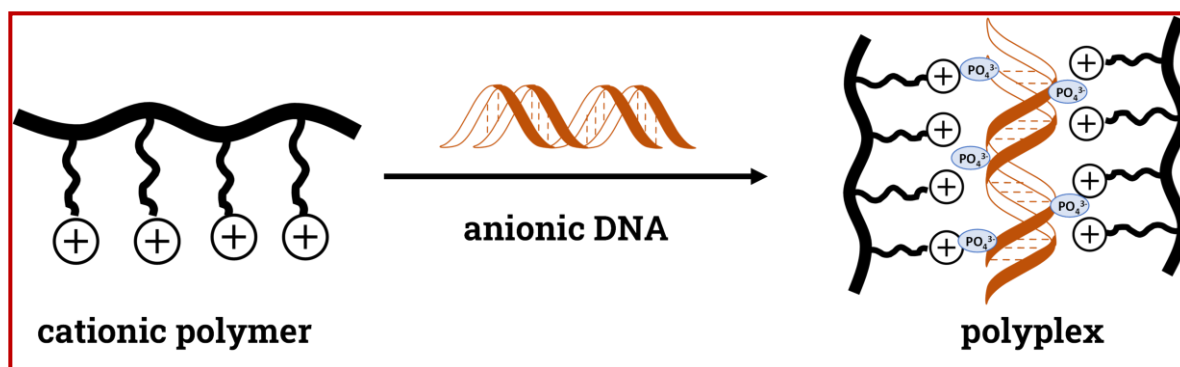


Figure 1.36. Schematic representation of polyplex formation between positively charged vector (polymer) and negatively charged DNA.

Significant advancements have been made in recent decades regarding the design and synthesis of biodegradable polymeric cationic non-viral gene delivery vectors that exhibit low cytotoxicity. Polypeptides have emerged as promising gene delivery carriers due to their biocompatibility, biodegradability, well-defined structure, and responsive properties. Among the various polypeptide architectures obtained through NCA ROP, block copolymers, homopolymers, and a few star-shaped polypeptide structures have been predominantly employed for delivering nucleic acids. For example, Johnson et al. conducted a study where they have synthesized a library of biocompatible block copolymers consisting of poly(2-hydroxyethyl methacrylate)₄₀/(PHEMA)₄₀ and poly(L-lysine)_n/(PLLys)_n blocks (PHEMA-*b*-PLLys) to use as gene (pDNA) delivery vectors with enhanced transfection efficacy and minimal cytotoxicity.³⁹⁴ The biodegradable poly(L-lysine) possessed pDNA binding

ability, while the biocompatible PHEMA ensured compatibility. Furthermore, Qiao et al. have synthesized PEG-functionalized 16- and 32-arm star copolypeptides containing PAMAM dendritic cores and poly(lysine) arms. These biocompatible star polypeptides have the ability to form polyplex with siRNA and hence can be used as potential carriers for siRNA delivery.³⁹⁵ Kostadinova et al. have developed a series of thermoresponsive copolypeptides vectors for gene-delivery using a combination of free radical copolymerization and ROP of NCA.³⁹⁶ These vectors [poly(2-hydroxyethyl methacrylate)-*b*-poly(*N*-isopropylacrylamide)-*b*-PLLys] exhibited a strong binding capability with DNA, leading to the condensation of DNA and the formation of well-defined polyplexes. In another study, Zhang et al. have designed and synthesized various cationic, α -helical polypeptides with guanidine and amine side groups to investigate how the structure and functionality of these polypeptides influenced the efficiency of delivering pDNA in two different mammalian cell lines, namely HeLa and COS-7.³⁹⁷

In a recent study, Dang et al. introduced a novel spherical, multivalent, helical guanidine-rich polypeptide designed for siRNA delivery.³⁹⁸ The researchers utilized ROP followed by click reaction to develop the final spherical dendrimer-polypeptide (DPP) with a hydrophobic internal cavity, which was loaded with a photothermal reagent called ICG. Additionally, siRNA targeting PKM2 (siPKM2) was condensed with the DPP via electrostatic interactions, resulting in the formation of DPP-siPKM2 complexes (referred to as D-I/P NCs). Additionally, to improve the stability of the nanoparticle and to promote efficient circulation within the bloodstream, the final nanoparticle structure was further coated with human serum albumin (HSA) (Figure 1.37). The developed polypeptide-based delivery system holds promise for enhancing the efficacy of photothermal ablation and inhibiting tumour metabolism.

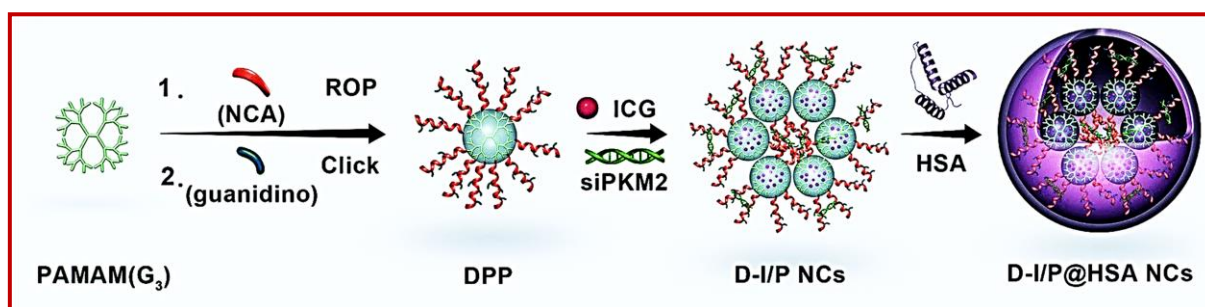


Figure 1.37. Schematic representation of DPP synthesis, ICG loading, siPKM2 complexation, and interaction with HAS to produce final stable D-I/P@HSA NCs. (Taken from ref.³⁹⁸)

In another intriguing study, researchers designed and synthesized a library of cationic α -helical polypeptides with membrane-penetrating capabilities to enhance the delivery of DNA and siRNA by using the similar methodology of click-grafting approach. Typically, poly(γ -propargyl-L-glutamate) was clicked with guanidinium groups and various aromatic groups using the Cu-AAC reaction. The aromatic functionalization of the polypeptide chains effectively improved the efficiency of siRNA delivery.³⁹⁹

1.6.2. Tissue Engineering Scaffold

Polypeptide hydrogels have emerged as promising materials in the field of tissue engineering. Their unique properties, such as biocompatibility, biofunctionality, and the ability to undergo environmentally-triggered changes in vivo, make them well-suited for various tissue engineering applications. Efforts have been focused on developing polypeptide hydrogels that can mimic the extracellular matrix (ECM) and provide a supportive environment for tissue regeneration.⁴⁰⁰⁻⁴⁰² These hydrogels can be engineered with specific properties to promote cell adhesion, proliferation, and differentiation, making them promising materials for tissue engineering applications.

In tissue engineering, it is crucial for cells to adhere to the scaffold material to establish a stable and functional tissue construct. By promoting cell adhesion, the scaffold provides a favourable environment for cells to attach and interact with the surrounding matrix. Cell proliferation, on the other hand, refers to the process of cell division and replication. It is necessary for tissue regeneration and growth within the scaffold. The scaffold should support the proliferation of cells, allowing them to multiply and populate the tissue-engineered construct.⁴⁰¹ By designing polypeptides with specific amino acids, it is possible to create synthetic materials that are tailored to promote cell adhesion and proliferation. Certain amino acids have been identified to have favourable properties for cell attachment and growth. By incorporating these amino acids into the synthetic polypeptides, the scaffold can provide an environment that is conducive to cell adhesion and proliferation.⁴⁰⁰

Cell adhesion can be facilitated by introducing polypeptide segments containing ionic side chains, such as PLLys (cationic) and PLGlu (anionic), without the need for side chain modifications. Qiao group demonstrated the utilization of ionic polypeptide side chains in scaffolds through the synthesis of P(LLys-*co*-LGlu)-based cryogels, which effectively guided cell adhesion and proliferation without requiring additional modifications (Figure 1.38).⁴⁰³ However, it is still possible to pursue further chemical modifications to precisely control cellular behaviours, such as cell adhesion, in scaffold materials. One such modification involves the incorporation of RGD, a peptide sequence known for its cell adhesion signalling properties.⁴⁰⁴ For instance, in their study, Ahrens et al. utilized a PLGlu-based scaffold where each glutamic acid side chain underwent specific modifications, resulting in three different side chain groups: an inert PEG chain, a maleimide group, and a norbornene group.⁴⁰⁵ The hydrogel was crosslinked through thiol–ene reactions between a 4-arm PEG-thiol and the maleimide and norbornene side chains. These modified scaffolds demonstrated a significant four-fold increase in the

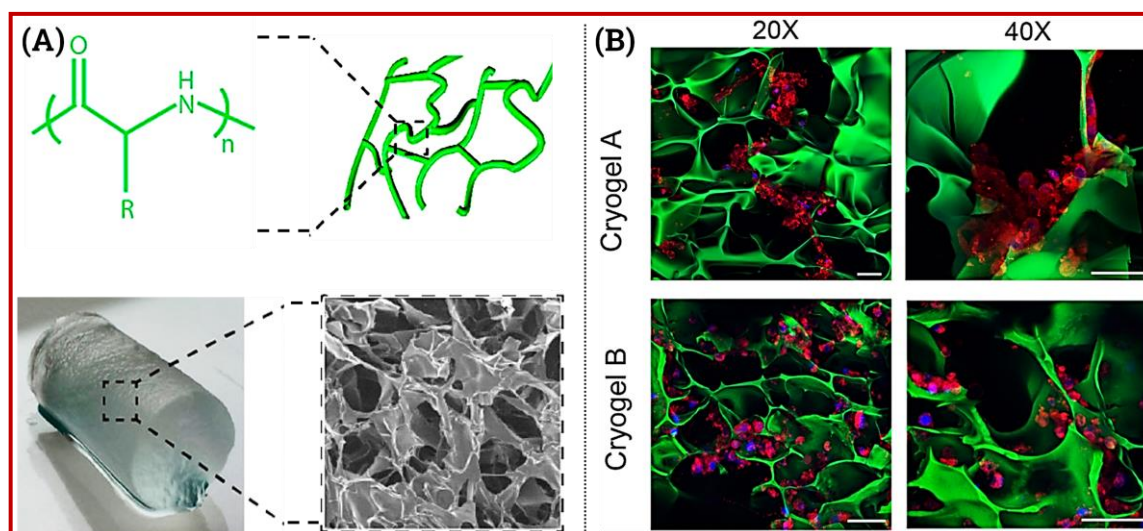


Figure 1.38. (A) Schematic diagram, photograph, and SEM image of the polypeptide gel; (B) CLSM images of the polypeptide gels colonized with NIH-3T3 cells obtained using different objective lens. (Represented from ref.⁴⁰³)

adhesion of human mesenchymal stem cells compared to a purely PEG-based control that also included RGD. The scaffolds incorporating the aforementioned modifications demonstrated a substantial four-fold enhancement in the adhesion of human mesenchymal stem cells when compared to a purely PEG-based control that also contained RGD.

The biocompatibility and biofunctionality of polypeptides have made them highly suitable for the development of injectable hydrogels for tissue engineering. One notable characteristic of these polypeptide-based hydrogel is their ability to undergo environmentally triggered changes *in vivo*. Among the various polypeptide thermogels (hydrogels which undergo thermally-triggered crosslinking) reported, poly(L-alanine) blocks have been extensively studied as thermally sensitive blocks.⁴⁰⁶⁻⁴⁰⁸ Studies consistently demonstrate that these hydrogels can undergo a sol-gel transition *in-vivo* under favourable physiological conditions. Notably, hydrogels containing L-alanine blocks have shown minimal production of inflammatory markers in the subcutaneous tissue surrounding the injection site.

1.6.3. Antibacterial Applications

Antimicrobial polypeptides have emerged as promising agents for combating infectious diseases, however, they remain relatively underutilized in this field. These polypeptides possess several desirable characteristics for antimicrobial applications. Firstly, their synthesis can be achieved rapidly. Additionally, their secondary structures can be modulated to enhance selectivity. Most importantly, polypeptides exert a non-specific mode of action against bacteria, making them effective against a wide range of bacterial strains. They offer a potential alternative to traditional antibiotics and can help address the growing issue of antimicrobial resistance.^{366, 409-410}

Amphiphilic polypeptides, which consist of hydrophobic and cationic amino acids residue, engage in electrostatic interactions with bacterial membranes which are negatively charged phospholipids. This interaction leads to the disruption of the bacterial cell-membrane, ultimately resulting in the eradication of the bacteria. This mode of action is considered a favourable alternative to the highly specific targeted approach of antibiotics, as it is less prone to antibacterial resistance.⁴¹¹ In the past couple of decades, a wide range of antibacterial agents has been developed using different architectures such as linear,³⁶⁶⁻³⁶⁷ graft,⁴¹²⁻⁴¹³ star-shaped,³⁶⁸⁻³⁶⁹ cyclic and hyperbranched,⁴¹⁴⁻⁴¹⁵ etc. and with diverse secondary structures. Among these different architected-polypeptides, copolypeptides comprising of lysine and arginine based cationic building blocks are widely studied, while alanine, leucine, phenylalanine, and valine are extensively studied as hydrophobic residues for these antibacterial polypeptides.⁴¹⁶⁻⁴¹⁷ Both block-copolymer and random copolymer architectures have been employed for various antimicrobial applications.

It has been observed that the secondary structures of polypeptides play a crucial role in modulating their antibacterial activity.³⁷⁹ Specifically, it has been found that polypeptides with ordered secondary structures, such as α -helix,

tend to exhibit enhanced antimicrobial properties compared to random coil structures. In 2015, Cheng et al. introduced a novel class of antimicrobial polypeptides known as radially amphiphilic (RA) polypeptides, obtained by ROP of corresponding NCA followed by successive cationization using 1-benzimidazole (Figure 1.39).⁴¹⁸

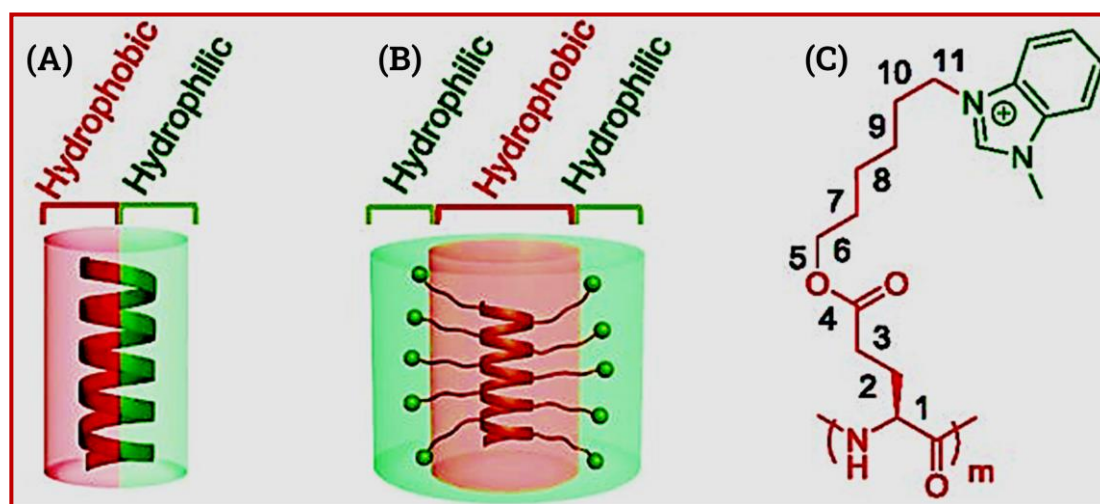


Figure 1.39. Schematic representation of antimicrobial peptides and polypeptides with (A) facial amphiphilicity or (B) radial amphiphilicity. (C) Chemical structure of RA polypeptide. (Taken from ref.⁴¹⁸)

These cationic polypeptides were designed to adopt a stable α -helical conformation, and this helicity was achieved through meticulous molecular design, ensuring that 11 σ bonds separated the backbone from the charged moiety (Figure 1.39C). The resulting α -helical polypeptides exhibited antimicrobial activity against both Gram-positive and Gram-negative bacteria and demonstrated stability in serum and plasma environments. Interestingly, the stereochemistry of the amino acid building blocks played a crucial role in the antibacterial efficacy. Polypeptides composed of a combination of D and L amino acid residues were unable to form stable α -helix and exhibited reduced antimicrobial activity compared to their all-L counterparts. It was also found that degree of polymerization also affects the antimicrobial activity.

Chen et al. significantly investigated the effect of both architecture and amphiphilic tuning in antimicrobial activity of polypeptides.³⁶⁸ They have developed a library of star-shaped PLLys-based polypeptides and examined the impact of different functional groups on their amphiphilicity. Notably, the incorporation of the indole functional group was found to be particularly effective in tuning the amphiphilicity of the hydrophilic stars. These modified materials exhibited enhanced antibacterial activity against various Gram-negative bacteria. In a recent study conducted by Kim et al., the importance of architectural design in achieving potent antibacterial activity was further highlighted.⁴¹⁴ The researchers have developed copolypeptides of different architectural designs, including linear, hinged, star, and cyclic structures. The antibacterial activity of these copolymers was tested against *B. subtilis*, and *E. coli* and the results showed that among the copolypeptides, the star-shaped polypeptides exhibited the most potent antibacterial activities. Some researchers have explored self-assembled polypeptide nanostructures as a means to enhance antibacterial properties. Du's research group specifically designed self-assembled polypeptide with PLLys and PLPhe blocks aiming to utilize electrostatic interactions with the bacterial cell wall and promote insertion into the lipophilic domains of the membranes.⁴¹⁹⁻⁴²⁰

Polypeptide based hydrogel also found to be effective towards different pathogens. For example, Bevilacqua et al. have synthesized amphiphilic diblock copolypeptide (PLLys₁₀₀-*b*-LLeu₄₀) which formed stable-hydrogels at certain concentration.⁴²¹ These amphiphilic hydrogels showed extensive antimicrobial activity against *S. aureus* and *P. aeruginosa*. Qiao and colleagues presented another antibacterial cryogel example.⁴²² They have synthesized macroporous gels comprising of two polypeptide blocks, PLLys-*b*-DLVal, crosslinked by glutaraldehyde (GA) with varying pore sizes. These cryogels have the ability to trap and kill *E. Coli* colony.

1.7. Objectives and Scope of the Present Research Work

Stimuli-responsive functionalized polypeptides are 'smart-materials' that consist of polypeptide chains modified with specific functional groups or motifs, allowing them to respond to external stimuli. The responsiveness of these polypeptides is achieved through the incorporation of stimuli-responsive moieties into the polypeptide backbone as end groups or by attaching them as pendant groups. Some of the common stimuli include temperature, pH, light, enzymes, electric fields, magnetic field, etc. The specific type of stimulus determines the nature of the response, such as conformational changes, solubility changes, or release of encapsulated cargo. Stimuli-responsive functionalized polypeptides offer a wide range of applications in areas such as drug delivery, tissue engineering, biosensing, and as smart materials. The ability to precisely tailor their properties in response to specific stimuli makes them valuable tools for developing advanced biomaterials.

This objective of this thesis focuses on designing, synthesizing, and characterizing functionalized polypeptides with diverse architectures and functionalities. The goal is to explore their potential in various important areas. Firstly, the study aims to investigate how these polypeptides can respond effectively to temperature and other stimuli. By incorporating specific chemical moieties or structural motifs, we aim to engineer polypeptides that exhibit remarkable responsiveness and self-assembly in different solvents. This self-assembled responsive polypeptide can be utilized for controlled release of therapeutic agents and targeted drug delivery, enhancing therapeutic efficacy.

Thermoresponsive polypeptides, exhibiting LCST type-phase transition are the most-widely studied systems among the scientific communities. Below the LCST, the polymer is soluble, but above the LCST, it undergoes a phase transition and becomes insoluble, leading to the formation of functionalized polypeptide gels or aggregates. These aggregates are useful as drug delivery systems that can release drugs in response to temperature changes. To

synthesize a thermoresponsiveness polypeptide-based drug delivery system, propargyl functionalized polycysteine is developed followed by successive click reaction with azide-end-capped poly(2-isopropyl-2-oxazoline) via grafting-onto technique. The resultant amphiphilic graft copolypeptides show LCST-type behaviour in water with tunable cloud point. These amphiphilic graft copolypeptide self-assemble into vesicular aggregates in both polar and nonpolar solvents, which are capable of encapsulating both hydrophilic and hydrophobic guest molecules. Furthermore, those encapsulated guest molecule can be released from the vesicles by treating them with conc. HCl or temperature.

In comparison to LCST-type polypeptide, UCST-type thermoresponsive polypeptides are effectively less reported in the literature. As discussed earlier in this chapter, ionic polypeptides showing UCST-type thermoresponsiveness in the presence of the externally added materials are very interesting to study, because of their applicability in drug/gene delivery and most of them are either ammonium or sulphonium-based materials. There are handful of reports of the phosphonium-based polypeptide materials. To address this issue, L-cysteine based cationic polypeptide is synthesized by ROP of NCA of the corresponding bromo-functionalized L-cysteine monomer, followed by cationization using triphenylphosphine to yield a cationic polycysteine with pendant phosphonium ions. The water-soluble cationic polypeptides show UCST-type thermoresponsiveness in the presence of externally added chaotropic anions. The cloud point of the phase transition can be modulated with respect to concentration of the polypeptide as well as the polarizability and concentration of the added anions. Furthermore, the cationic polypeptide is found to be potent for polyplex formation with DNA through electrostatic interaction, which is dependent on the ionic strength of the solution.

Research on the thermoresponsive polypeptide has increased tremendously over last two decades. In order to use those thermoresponsive

polypeptide-based system as functional biomaterials, researchers have functionalized those polypeptides in such a way that it should easily be soluble in water. However, functionalized polypeptides showing thermoresponsiveness in non-aqueous solvents are also interesting to explore. Till now there is very little effort has been made to develop functionalized polypeptide which exhibit thermoresponsiveness in single organic solvent or cosolvent mixture. To explore further, propargyl functionalized poly(L-glutamate) was clicked with long chain alkyl groups with varying chain length, to produce a water insoluble material showing UCST-type thermoresponsiveness in non-aqueous solvents. The cloud point of the phase transition is tunable with respect to the alkyl chain length as well as the polarity of the solvents. Owing to the presence of long alkyl chain in the side chain alkyl-PGlu(s) shows crystalline arrangements, which is thoroughly investigated in comparison to their respective monomeric segments. Self-assembly of these alkyl-functionalized PGlu in organic solvents leads to the formation of vesicles with different diameters, which is used to encapsulate hydrophilic guest molecules.

1.8. References

1. Whitford, D., *Proteins: Structure and Function*; John Wiley & Sons, 2005.
2. Lucas-Lenard, J.; Lipmann, F., Protein Biosynthesis. *Annu. Rev. Biochem.* **1971**, *40*, 409-448.
3. Lu, H.; Wang, J.; Song, Z.; Yin, L.; Zhang, Y.; Tang, H.; Tu, C.; Lin, Y.; Cheng, J., Recent Advances in Amino Acid N-Carboxyanhydrides and Synthetic Polypeptides: Chemistry, Self-Assembly and Biological Applications. *Chem. Commun.* **2014**, *50*, 139-155.
4. Rad-Malekshahi, M.; Lempsink, L.; Amidi, M.; Hennink, W. E.; Mastrobattista, E., Biomedical Applications of Self-Assembling Peptides. *Bioconjugate Chem.* **2016**, *27*, 3-18.
5. Deming, T. J., Synthetic Polypeptides for Biomedical Applications. *Prog. Polym. Sci.* **2007**, *32*, 858-875.
6. Ajiro, H.; Takahashi, Y.; Akashi, M., Thermosensitive Biodegradable Homopolymer of Trimethylene Carbonate Derivative at Body Temperature. *Macromolecules* **2012**, *45*, 2668-2674.
7. Zhang, L.-J.; Dong, B.-T.; Du, F.-S.; Li, Z.-C., Degradable Thermoresponsive Polyesters by Atom Transfer Radical Polyaddition and Click Chemistry. *Macromolecules* **2012**, *45*, 8580-8587.
8. Wu, D.-C.; Liu, Y.; He, C.-B., Thermal- and Ph-Responsive Degradable Polymers. *Macromolecules* **2008**, *41*, 18-20.
9. Lee, S. B.; Song, S.-C.; Jin, J.-I.; Sohn, Y. S., A New Class of Biodegradable Thermosensitive Polymers. 2. Hydrolytic Properties and Salt Effect on the Lower Critical Solution Temperature of Poly(Organophosphazenes) with Methoxypoly(Ethylene Glycol) and Amino Acid Esters as Side Groups. *Macromolecules* **1999**, *32*, 7820-7827.

10. Deming, T. J., Synthesis of Side-Chain Modified Polypeptides. *Chem. Rev.* **2016**, *116*, 786-808.
11. Meng, H.; Li, G., A Review of Stimuli-Responsive Shape Memory Polymer Composites. *Polymer* **2013**, *54*, 2199-2221.
12. Bose, A.; Jana, S.; Saha, A.; Mandal, T. K., Amphiphilic Polypeptide-Polyoxazoline Graft Copolymer Conjugate with Tunable Thermoresponsiveness: Synthesis and Self-Assembly into Various Micellar Structures in Aqueous and Nonaqueous Media. *Polymer* **2017**, *110*, 12-24.
13. Zheng, Z.; Zhang, L.; Ling, Y.; Tang, H., Triblock Copolymers Containing Ucst Polypeptide and Poly(Propylene Glycol): Synthesis, Thermoresponsive Properties, and Modification of Pva Hydrogel. *Eur. Polym. J.* **2019**, *115*, 244-250.
14. Chen, L.; Chen, T.; Fang, W.; Wen, Y.; Lin, S.; Lin, J.; Cai, C., Synthesis and Ph-Responsive "Schizophrenic" Aggregation of a Linear-Dendron-Like Polyampholyte Based on Oppositely Charged Polypeptides. *Biomacromolecules* **2013**, *14*, 4320-4330.
15. Krannig, K.-S.; Schlaad, H., Ph-Responsive Bioactive Glycopolypeptides with Enhanced Helicity and Solubility in Aqueous Solution. *J. Am. Chem. Soc.* **2012**, *134*, 18542-18545.
16. Rodríguez-Hernández, J.; Lecommandoux, S., Reversible inside-out Micellization of Ph-Responsive and Water-Soluble Vesicles Based on Polypeptide Diblock Copolymers. *J. Am. Chem. Soc.* **2005**, *127*, 2026-2027.
17. Jana, S.; Biswas, Y.; Mandal, T. K., Methionine-Based Cationic Polypeptide/Polypeptide Block Copolymer with Triple-Stimuli Responsiveness: DNA Polyplexation and Phototriggered Release. *Polym. Chem.* **2018**, *9*, 1869-1884.
18. Liu, G.; Dong, C.-M., Photoresponsive Poly(S-(O-Nitrobenzyl)-L-Cysteine)-B-Peo from a L-Cysteine N-Carboxyanhydride Monomer: Synthesis, Self-

- Assembly, and Phototriggered Drug Release. *Biomacromolecules* **2012**, *13*, 1573-1583.
19. Fu, X.; Ma, Y.; Shen, Y.; Fu, W.; Li, Z., Oxidation-Responsive Oegylated Poly-L-Cysteine and Solution Properties Studies. *Biomacromolecules* **2014**, *15*, 1055-1061.
 20. Kramer, J. R.; Deming, T. J., Multimodal Switching of Conformation and Solubility in Homocysteine Derived Polypeptides. *J. Am. Chem. Soc.* **2014**, *136*, 5547-5550.
 21. Carlini, A. S.; Gaetani, R.; Braden, R. L.; Luo, C.; Christman, K. L.; Gianneschi, N. C., Enzyme-Responsive Progelator Cyclic Peptides for Minimally Invasive Delivery to the Heart Post-Myocardial Infarction. *Nat. Commun.* **2019**, *10*, 1735.
 22. Fan, J.; Li, R.; Wang, H.; He, X.; Nguyen, T. P.; Letteri, R. A.; Zou, J.; Wooley, K. L., Multi-Responsive Polypeptide Hydrogels Derived from N-Carboxyanhydride Terpolymerizations for Delivery of Nonsteroidal Anti-Inflammatory Drugs. *Org. Biomol. Chem.* **2017**, *15*, 5145-5154.
 23. Rodriguez, A. R.; Kramer, J. R.; Deming, T. J., Enzyme-Triggered Cargo Release from Methionine Sulfoxide Containing Copolypeptide Vesicles. *Biomacromolecules* **2013**, *14*, 3610-3614.
 24. Ma, G.; Lin, W.; Yuan, Z.; Wu, J.; Qian, H.; Xu, L.; Chen, S., Development of Ionic Strength/Ph/Enzyme Triple-Responsive Zwitterionic Hydrogel of the Mixed L-Glutamic Acid and L-Lysine Polypeptide for Site-Specific Drug Delivery. *J. Mater. Chem. B* **2017**, *5*, 935-943.
 25. Markland, P.; Zhang, Y.; Amidon, G. L.; Yang, V. C., A Ph- and Ionic Strength-Responsive Polypeptide Hydrogel: Synthesis, Characterization, and Preliminary Protein Release Studies. *J. Biomed. Mater. Res.* **1999**, *47*, 595-602.
 26. Kramer, J. R.; Deming, T. J., Glycopolypeptides with a Redox-Triggered Helix-to-Coil Transition. *J. Am. Chem. Soc.* **2012**, *134*, 4112-4115.

27. Duncan, R., The Dawning Era of Polymer Therapeutics. *Nat. Rev. Drug Discov.* **2003**, *2*, 347-360.
28. Lee, D.; Rejinold, N. S.; Jeong, S. D.; Kim, Y.-C., Stimuli-Responsive Polypeptides for Biomedical Applications. *Polymers* **2018**, *10*, 830.
29. Song, Z.; Han, Z.; Lv, S.; Chen, C.; Chen, L.; Yin, L.; Cheng, J., Synthetic Polypeptides: From Polymer Design to Supramolecular Assembly and Biomedical Application. *Chem. Soc. Rev.* **2017**, *46*, 6570-6599.
30. Merrifield, R. B., Solid Phase Peptide Synthesis. I. The Synthesis of a Tetrapeptide. *J. Am. Chem. Soc.* **1963**, *85*, 2149-2154.
31. Cheng, J.; Deming, T. J., Synthesis of Polypeptides by Ring-Opening Polymerization of α -Amino Acid N-Carboxyanhydrides. In *Peptide-Based Materials*, Deming, T., Ed. Springer Berlin Heidelberg: Berlin, Heidelberg, 2012; pp 1-26.
32. Hadjichristidis, N.; Iatrou, H.; Pitsikalis, M.; Sakellariou, G., Synthesis of Well-Defined Polypeptide-Based Materials Via the Ring-Opening Polymerization of α -Amino Acid N-Carboxyanhydrides. *Chem. Rev.* **2009**, *109*, 5528-5578.
33. Leuchs, H., Ueber Die Glycin-Carbonsäure. *Berichte der deutschen chemischen Gesellschaft* **1906**, *39*, 857-861.
34. Farthing, A. C.; Reynolds, R. J. W., Anhydro-N-Carboxy-Dl-B-Phenylalanine. *Nature* **1950**, *165*, 647-647.
35. Coleman, D.; Farthing, A. C., Synthetic Polypeptides. Part II. Properties of Oxazolid-2 : 5-Diones and an Initial Study of the Preparation of Polypeptides There-From. *J. Chem. Soc.* **1950**, 3218-3222.
36. Rasines Mazo, A.; Allison-Logan, S.; Karimi, F.; Chan, N. J.-A.; Qiu, W.; Duan, W.; O'Brien-Simpson, N. M.; Qiao, G. G., Ring Opening Polymerization of α -Amino Acids: Advances in Synthesis, Architecture and Applications of Polypeptides and Their Hybrids. *Chem. Soc. Rev.* **2020**, *49*, 4737-4834.

37. Poché, D. S.; Moore, M. J.; Bowles, J. L., An Unconventional Method for Purifying the N-Carboxyanhydride Derivatives of Γ -Alkyl-L-Glutamates. *Synth. Commun.* **1999**, *29*, 843-854.
38. Kramer, J. R.; Deming, T. J., General Method for Purification of α -Amino Acid-N-Carboxyanhydrides Using Flash Chromatography. *Biomacromolecules* **2010**, *11*, 3668-3672.
39. Semple, J. E.; Sullivan, B.; Sill, K. N., Large-Scale Synthesis of α -Amino Acid-N-Carboxyanhydrides. *Synth. Commun.* **2017**, *47*, 53-61.
40. Otake, Y.; Nakamura, H.; Fuse, S., Rapid and Mild Synthesis of Amino Acid N-Carboxy Anhydrides: Basic-to-Acidic Flash Switching in a Microflow Reactor. *Angew. Chem. Int. Ed.* **2018**, *57*, 11389-11393.
41. Tian, Z.-Y.; Zhang, Z.; Wang, S.; Lu, H., A Moisture-Tolerant Route to Unprotected A/B-Amino Acid N-Carboxyanhydrides and Facile Synthesis of Hyperbranched Polypeptides. *Nat. Commun.* **2021**, *12*, 5810.
42. Yamada, S.; Sudo, A.; Goto, M.; Endo, T., Phosgene-Free Synthesis of Polypeptides Using Activated Urethane Derivatives of α -Amino Acids: An Efficient Synthetic Approach to Hydrophilic Polypeptides. *RSC Adv.* **2014**, *4*, 29890-29896.
43. Kamei, Y.; Sudo, A.; Nishida, H.; Kikukawa, K.; Endo, T., Synthesis of Polypeptides from Activated Urethane Derivatives of α -Amino Acids. *J. Polym. Sci. A Polym. Chem.* **2008**, *46*, 2525-2535.
44. Laconde, G.; Amblard, M.; Martinez, J., Synthesis of α -Amino Acid N-Carboxyanhydrides. *Org. Lett.* **2021**, *23*, 6412-6416.
45. Deming, T. J., Polypeptide and Polypeptide Hybrid Copolymer Synthesis Via Nca Polymerization. In *Peptide Hybrid Polymers*, Klok, H.-A.; Schlaad, H., Eds. Springer Berlin Heidelberg: Berlin, Heidelberg, 2006; pp 1-18.
46. Deng, C.; Wu, J.; Cheng, R.; Meng, F.; Klok, H.-A.; Zhong, Z., Functional Polypeptide and Hybrid Materials: Precision Synthesis Via α -Amino Acid

- N-Carboxyanhydride Polymerization and Emerging Biomedical Applications. *Prog. Polym. Sci.* **2014**, *39*, 330-364.
47. Habraken, G. J. M.; Peeters, M.; Dietz, C. H. J. T.; Koning, C. E.; Heise, A., How Controlled and Versatile Is N-Carboxy Anhydride (Nca) Polymerization at 0 °C? Effect of Temperature on Homo-, Block- and Graft (Co)Polymerization. *Polym. Chem.* **2010**, *1*, 514-524.
 48. Kricheldorf, H. R.; v. Lossow, C.; Schwarz, G., Primary Amine and Solvent-Induced Polymerizations of L- or D,L-Phenylalanine N-Carboxyanhydride. *Macromol. Chem. Phys.* **2005**, *206*, 282-290.
 49. Kricheldorf, H. R.; von Lossow, C.; Schwarz, G., Cyclic Polypeptides by Solvent-Induced Polymerizations of α -Amino Acid N-Carboxyanhydrides. *Macromolecules* **2005**, *38*, 5513-5518.
 50. Deming, T. J., Facile Synthesis of Block Copolypeptides of Defined Architecture. *Nature* **1997**, *390*, 386-389.
 51. Deming, T. J., Amino Acid Derived Nickelacycles: Intermediates in Nickel-Mediated Polypeptide Synthesis. *J. Am. Chem. Soc.* **1998**, *120*, 4240-4241.
 52. Deming, T. J., Cobalt and Iron Initiators for the Controlled Polymerization of α -Amino Acid-N-Carboxyanhydrides. *Macromolecules* **1999**, *32*, 4500-4502.
 53. Detwiler, R. E.; Schlirf, A. E.; Kramer, J. R., Rethinking Transition Metal Catalyzed N-Carboxyanhydride Polymerization: Polymerization of Pro and Acopro N-Carboxyanhydrides. *J. Am. Chem. Soc.* **2021**, *143*, 11482-11489.
 54. Curtin, S. A.; Deming, T. J., Initiators for End-Group Functionalized Polypeptides Via Tandem Addition Reactions. *J. Am. Chem. Soc.* **1999**, *121*, 7427-7428.

55. Lu, H.; Cheng, J., Hexamethyldisilazane-Mediated Controlled Polymerization of α -Amino Acid N-Carboxyanhydrides. *J. Am. Chem. Soc.* **2007**, *129*, 14114-14115.
56. Lu, H.; Cheng, J., N-Trimethylsilyl Amines for Controlled Ring-Opening Polymerization of Amino Acid N-Carboxyanhydrides and Facile End Group Functionalization of Polypeptides. *J. Am. Chem. Soc.* **2008**, *130*, 12562-12563.
57. Wu, Y.; Zhang, D.; Ma, P.; Zhou, R.; Hua, L.; Liu, R., Lithium Hexamethyldisilazide Initiated Superfast Ring Opening Polymerization of Alpha-Amino Acid N-Carboxyanhydrides. *Nat. Commun.* **2018**, *9*, 5297.
58. Wu, Y.-M.; Zhang, W.-W.; Zhou, R.-Y.; Chen, Q.; Xie, C.-Y.; Xiang, H.-X.; Sun, B.; Zhu, M.-F.; Liu, R.-H., Facile Synthesis of High Molecular Weight Polypeptides Via Fast and Moisture Insensitive Polymerization of α -Amino Acid N-Carboxyanhydrides. *Chin. J. Polym. Sci.* **2020**, *38*, 1131-1140.
59. Dimitrov, I.; Schlaad, H., Synthesis of Nearly Monodisperse Polystyrene-Polypeptide Block Copolymers Via Polymerisation of N-Carboxyanhydrides. *Chem. Commun.* **2003**, 2944-2945.
60. Aliferis, T.; Iatrou, H.; Hadjichristidis, N., Living Polypeptides. *Biomacromolecules* **2004**, *5*, 1653-1656.
61. Vayaboury, W.; Giani, O.; Cottet, H.; Deratani, A.; Schué, F., Living Polymerization of α -Amino Acid N-Carboxyanhydrides (Nca) Upon Decreasing the Reaction Temperature. *Macromol. Rapid Commun.* **2004**, *25*, 1221-1224.
62. Zou, J.; Fan, J.; He, X.; Zhang, S.; Wang, H.; Wooley, K. L., A Facile Glovebox-Free Strategy to Significantly Accelerate the Syntheses of Well-Defined Polypeptides by N-Carboxyanhydride (Nca) Ring-Opening Polymerizations. *Macromolecules* **2013**, *46*, 4223-4226.

63. Vacogne, C. D.; Schlaad, H., Primary Ammonium/Tertiary Amine-Mediated Controlled Ring Opening Polymerisation of Amino Acid N-Carboxyanhydrides. *Chem. Commun.* **2015**, *51*, 15645-15648.
64. Peng, H.; Ling, J.; Shen, Z., Ring Opening Polymerization of α -Amino Acid N-Carboxyanhydrides Catalyzed by Rare Earth Catalysts: Polymerization Characteristics and Mechanism. *J. Polym. Sci. Part A: Polym. Chem.* **2012**, *50*, 1076-1085.
65. Gradišar, Š.; Žagar, E.; Pahovnik, D., Ring-Opening Polymerization of N-Carboxyanhydrides Initiated by a Hydroxyl Group. *ACS Macro Lett.* **2017**, *6*, 637-640.
66. Gazon, C.; Salas-Ambrosio, P.; Ibarboure, E.; Buol, A.; Garanger, E.; Grinstaff, M. W.; Lecommandoux, S.; Bonduelle, C., Aqueous Ring-Opening Polymerization-Induced Self-Assembly (Ropisa) of N-Carboxyanhydrides. *Angew. Chem. Int. Ed.* **2020**, *59*, 622-626.
67. Zhao, W.; Gnanou, Y.; Hadjichristidis, N., From Competition to Cooperation: A Highly Efficient Strategy Towards Well-Defined (Co)Polypeptides. *Chem. Commun.* **2015**, *51*, 3663-3666.
68. Zhao, W.; Gnanou, Y.; Hadjichristidis, N., Fast and Living Ring-Opening Polymerization of α -Amino Acid N-Carboxyanhydrides Triggered by an "Alliance" of Primary and Secondary Amines at Room Temperature. *Biomacromolecules* **2015**, *16*, 1352-1357.
69. Wu, Y., et al., Superfast and Water-Insensitive Polymerization on α -Amino Acid N-Carboxyanhydrides to Prepare Polypeptides Using Tetraalkylammonium Carboxylate as the Initiator. *Angew. Chem.* **2021**, *133*, 26267-26275.
70. Li, K.; Li, Z.; Shen, Y.; Fu, X.; Chen, C.; Li, Z., Organobase 1,1,3,3-Tetramethyl Guanidine Catalyzed Rapid Ring-Opening Polymerization of α -Amino Acid N-Carboxyanhydrides Adaptive to Amine, Alcohol and Carboxyl Acid Initiators. *Polym. Chem.* **2022**, *13*, 586-591.

71. Zhang, Y.; Liu, R.; Jin, H.; Song, W.; Augustine, R.; Kim, I., Straightforward Access to Linear and Cyclic Polypeptides. *Commun. Chem.* **2018**, *1*, 40.
72. Sun, Y.; Hou, Y.; Zhou, X.; Yuan, J.; Wang, J.; Lu, H., Controlled Synthesis and Enzyme-Induced Hydrogelation of Poly(L-Phosphotyrosine)S Via Ring-Opening Polymerization of α -Amino Acid N-Carboxyanhydride. *ACS Macro Lett.* **2015**, *4*, 1000-1003.
73. Chan, B. A.; Xuan, S.; Horton, M.; Zhang, D., 1,1,3,3-Tetramethylguanidine-Promoted Ring-Opening Polymerization of N-Butyl N-Carboxyanhydride Using Alcohol Initiators. *Macromolecules* **2016**, *49*, 2002-2012.
74. Fèvre, M.; Pinaud, J.; Leteneur, A.; Gnanou, Y.; Vignolle, J.; Taton, D.; Miqueu, K.; Sotiropoulos, J.-M., Imidazol(in)ium Hydrogen Carbonates as a Genuine Source of N-Heterocyclic Carbenes (Nhcs): Applications to the Facile Preparation of Nhc Metal Complexes and to Nhc-Organocatalyzed Molecular and Macromolecular Syntheses. *J. Am. Chem. Soc.* **2012**, *134*, 6776-6784.
75. Lv, W.; Wang, Y.; Li, M.; Wang, X.; Tao, Y., Precision Synthesis of Polypeptides Via Living Anionic Ring-Opening Polymerization of N-Carboxyanhydrides by Tri-Thiourea Catalysts. *J. Am. Chem. Soc.* **2022**, *144*, 23622-23632.
76. Chen, C.; Wang, Z.; Li, Z., Thermoresponsive Polypeptides from Pegylated Poly-L-Glutamates. *Biomacromolecules* **2011**, *12*, 2859-2863.
77. Kramer, J. R.; Deming, T. J., Glycopolypeptides Via Living Polymerization of Glycosylated-L-Lysine N-Carboxyanhydrides. *J. Am. Chem. Soc.* **2010**, *132*, 15068-15071.
78. Das, S.; Kar, M.; Gupta, S. S., Synthesis of End-Functionalized Phosphate and Phosphonate-Polypeptides by Ring-Opening Polymerization of Their Corresponding N-Carboxyanhydride. *Polym. Chem.* **2013**, *4*, 4087-4091.

79. Yakovlev, I.; Deming, T. J., Analogues of Poly(L-Phosphoserine) Via Living Polymerization of Phosphonate-Containing N-Carboxyanhydride Monomers. *ACS Macro Lett.* **2014**, *3*, 378-381.
80. Yin, L.; Tang, H.; Kim, K. H.; Zheng, N.; Song, Z.; Gabrielson, N. P.; Lu, H.; Cheng, J., Light-Responsive Helical Polypeptides Capable of Reducing Toxicity and Unpacking DNA: Toward Nonviral Gene Delivery. *Angew. Chem. Int. Ed.* **2013**, *52*, 9182-9186.
81. Fu, X.; Shen, Y.; Fu, W.; Li, Z., Thermo-responsive Oligo(Ethylene Glycol) Functionalized Poly-L-Cysteine. *Macromolecules* **2013**, *46*, 3753-3760.
82. Sun, J.; Schlaad, H., Thiol-Ene Clickable Polypeptides. *Macromolecules* **2010**, *43*, 4445-4448.
83. Lu, H.; Bai, Y.; Wang, J.; Gabrielson, N. P.; Wang, F.; Lin, Y.; Cheng, J., Ring-Opening Polymerization of Γ -(4-Vinylbenzyl)-L-Glutamate N-Carboxyanhydride for the Synthesis of Functional Polypeptides. *Macromolecules* **2011**, *44*, 6237-6240.
84. Zhou, J.; Chen, P.; Deng, C.; Meng, F.; Cheng, R.; Zhong, Z., A Simple and Versatile Synthetic Strategy to Functional Polypeptides Via Vinyl Sulfone-Substituted L-Cysteine N-Carboxyanhydride. *Macromolecules* **2013**, *46*, 6723-6730.
85. Engler, A. C.; Lee, H.-i.; Hammond, P. T., Highly Efficient "Grafting onto" a Polypeptide Backbone Using Click Chemistry. *Angew. Chem. Int. Ed.* **2009**, *48*, 9334-9338.
86. Rhodes, A. J.; Deming, T. J., Soluble, Clickable Polypeptides from Azide-Containing N-Carboxyanhydride Monomers. *ACS Macro Lett.* **2013**, *2*, 351-354.
87. Agut, W.; Taton, D.; Lecommandoux, S., A Versatile Synthetic Approach to Polypeptide Based Rod-Coil Block Copolymers by Click Chemistry. *Macromolecules* **2007**, *40*, 5653-5661.

88. Agut, W.; Brûlet, A.; Schatz, C.; Taton, D.; Lecommandoux, S., Ph and Temperature Responsive Polymeric Micelles and Polymersomes by Self-Assembly of Poly[2-(Dimethylamino)Ethyl Methacrylate]-B-Poly(Glutamic Acid) Double Hydrophilic Block Copolymers. *Langmuir* **2010**, *26*, 10546-10554.
89. Li, J.; Wang, T.; Wu, D.; Zhang, X.; Yan, J.; Du, S.; Guo, Y.; Wang, J.; Zhang, A., Stimuli-Responsive Zwitterionic Block Copolypeptides: Poly(N-Isopropylacrylamide)-Block-Poly(Lysine-Co-Glutamic Acid). *Biomacromolecules* **2008**, *9*, 2670-2676.
90. Saha, A.; Paira, T. K.; Biswas, M.; Jana, S.; Banerjee, S.; Mandal, T. K., Combined Atom-Transfer Radical Polymerization and Ring-Opening Polymerization to Design Polymer–Polypeptide Copolymer Conjugates toward Self-Aggregated Hybrid Micro/Nanospheres for Dye Encapsulation. *J. Polym. Sci. Part A: Polym. Chem.* **2015**, *53*, 2313-2319.
91. Ji, S.; Xu, L.; Fu, X.; Sun, J.; Li, Z., Light- and Metal Ion-Induced Self-Assembly and Reassembly Based on Block Copolymers Containing a Photoresponsive Polypeptide Segment. *Macromolecules* **2019**, *52*, 4686-4693.
92. Kramer, J. R.; Deming, T. J., Preparation of Multifunctional and Multireactive Polypeptides Via Methionine Alkylation. *Biomacromolecules* **2012**, *13*, 1719-1723.
93. Li, M.; He, X.; Ling, Y.; Tang, H., Dual Thermoresponsive Homopolypeptide with Lcst-Type Linkages and Ucst-Type Pendants: Synthesis, Characterization, and Thermoresponsive Properties. *Polymer* **2017**, *132*, 264-272.
94. Song, Z.; Tan, Z.; Cheng, J., Recent Advances and Future Perspectives of Synthetic Polypeptides from N-Carboxyanhydrides. *Macromolecules* **2019**, *52*, 8521-8539.

95. Zhao, X.; Poon, Z.; Engler, A. C.; Bonner, D. K.; Hammond, P. T., Enhanced Stability of Polymeric Micelles Based on Postfunctionalized Poly(Ethylene Glycol)-B-Poly(Γ -Propargyl L-Glutamate): The Substituent Effect. *Biomacromolecules* **2012**, *13*, 1315-1322.
96. Rao, J.; Zhang, Y.; Zhang, J.; Liu, S., Facile Preparation of Well-Defined Ab₂ Y-Shaped Miktoarm Star Polypeptide Copolymer Via the Combination of Ring-Opening Polymerization and Click Chemistry. *Biomacromolecules* **2008**, *9*, 2586-2593.
97. Tang, H.; Zhang, D., General Route toward Side-Chain-Functionalized α -Helical Polypeptides. *Biomacromolecules* **2010**, *11*, 1585-1592.
98. Huang, J.; Habraken, G.; Audouin, F.; Heise, A., Hydrolytically Stable Bioactive Synthetic Glycopeptide Homo- and Copolymers by Combination of Nca Polymerization and Click Reaction. *Macromolecules* **2010**, *43*, 6050-6057.
99. Kramer, J. R.; Deming, T. J., Recent Advances in Glycopolypeptide Synthesis. *Polym. Chem.* **2014**, *5*, 671-682.
100. Liu, Y.; Chen, P.; Li, Z., Molecular Bottlebrushes with Polypeptide Backbone Prepared Via Ring-Opening Polymerization of Nca and Atrp. *Macromol. Rapid Commun.* **2012**, *33*, 287-295.
101. Habraken, G. J. M.; Koning, C. E.; Heuts, J. P. A.; Heise, A., Thiol Chemistry on Well-Defined Synthetic Polypeptides. *Chem. Commun.* **2009**, 3612-3614.
102. Gharakhanian, E. G.; Deming, T. J., Versatile Synthesis of Stable, Functional Polypeptides Via Reaction with Epoxides. *Biomacromolecules* **2015**, *16*, 1802-1806.
103. Wu, G.; Ge, C.; Liu, X.; Wang, S.; Wang, L.; Yin, L.; Lu, H., Synthesis of Water Soluble and Multi-Responsive Selenopolypeptides Via Ring-Opening Polymerization of N-Carboxyanhydrides. *Chem. Commun.* **2019**, *55*, 7860-7863.

104. Yuan, J.; Zhang, Y.; Sun, Y.; Cai, Z.; Yang, L.; Lu, H., Salt- and Ph-Triggered Helix–Coil Transition of Ionic Polypeptides under Physiology Conditions. *Biomacromolecules* **2018**, *19*, 2089-2097.
105. Song, Z.; Zheng, N.; Ba, X.; Yin, L.; Zhang, R.; Ma, L.; Cheng, J., Polypeptides with Quaternary Phosphonium Side Chains: Synthesis, Characterization, and Cell-Penetrating Properties. *Biomacromolecules* **2014**, *15*, 1491-1497.
106. Yan, L.; Yang, L.; He, H.; Hu, X.; Xie, Z.; Huang, Y.; Jing, X., Photo-Cross-Linked Mpeg-Poly(Γ -Cinnamyl-L-Glutamate) Micelles as Stable Drug Carriers. *Polym. Chem.* **2012**, *3*, 1300-1307.
107. Zhang, Y.; Lu, H.; Lin, Y.; Cheng, J., Water-Soluble Polypeptides with Elongated, Charged Side Chains Adopt Ultrastable Helical Conformations. *Macromolecules* **2011**, *44*, 6641-6644.
108. Kricheldorf, H. R., Polypeptides and 100 Years of Chemistry of α -Amino Acid N-Carboxyanhydrides. *Angew. Chem. Int. Ed.* **2006**, *45*, 5752-5784.
109. Nylund, R. E.; Miller, W. G. J. J. o. t. A. C. S., Synthesis and Potentiometric Titration of Random Copolymers of L-Leucine and L-Glutamic Acid1a, B. *J. Am. Chem. Soc.* **1965**, *87*, 3537-3542.
110. Wamsley, A.; Jasti, B.; Phiasivongsa, P.; Li, X., Synthesis of Random Terpolymers and Determination of Reactivity Ratios of N-Carboxyanhydrides of Leucine, B-Benzyl Aspartate, and Valine. *J. Polym. Sci. A Polym. Chem.* **2004**, *42*, 317-325.
111. Kricheldorf, H. R., ¹⁵n Nmr Spectroscopy, 13. Copolymerization of Glycine-N-Carboxyanhydride and B-Alanine-N-Carboxyanhydride. *Makromol. Chem.* **1979**, *180*, 147-159.
112. Cha, J. N.; Stucky, G. D.; Morse, D. E.; Deming, T. J., Biomimetic Synthesis of Ordered Silica Structures Mediated by Block Copolypeptides. *Nature* **2000**, *403*, 289-292.
113. Gitsas, A.; Floudas, G.; Mondeshki, M.; Spiess, H. W.; Aliferis, T.; Iatrou, H.; Hadjichristidis, N., Control of Peptide Secondary Structure and Dynamics

- in Poly(Γ -Benzyl-L-Glutamate)-B-Polyalanine Peptides. *Macromolecules* **2008**, *41*, 8072-8080.
114. Goury, V.; Jhurry, D.; Bhaw-Luximon, A.; Novak, B. M.; Belleney, J., Synthesis and Characterization of Random and Block Copolypeptides Derived from Γ -Methylglutamate and Leucine N-Carboxyanhydrides. *Biomacromolecules* **2005**, *6*, 1987-1991.
115. Li, Z.; Deming, T. J., Tunable Hydrogel Morphology Via Self-Assembly of Amphiphilic Pentablock Copolypeptides. *Soft Matter* **2010**, *6*, 2546-2551.
116. Sulistio, A.; Blencowe, A.; Widjaya, A.; Zhang, X.; Qiao, G., Development of Functional Amino Acid-Based Star Polymers. *Polym. Chem.* **2012**, *3*, 224-234.
117. Euliss, L. E.; Grancharov, S. G.; O'Brien, S.; Deming, T. J.; Stucky, G. D.; Murray, C. B.; Held, G. A., Cooperative Assembly of Magnetic Nanoparticles and Block Copolypeptides in Aqueous Media. *Nano Lett.* **2003**, *3*, 1489-1493.
118. Vayaboury, W.; Giani, O.; Cottet, H.; Bonaric, S.; Schué, F., Mechanistic Study of α -Amino Acid N-Carboxyanhydride (Nca) Polymerization by Capillary Electrophoresis. *Macromol. Chem. Phys.* **2008**, *209*, 1628-1637.
119. Holowka, E. P.; Sun, V. Z.; Kamei, D. T.; Deming, T. J., Polyarginine Segments in Block Copolypeptides Drive Both Vesicular Assembly and Intracellular Delivery. *Nature Mater.* **2007**, *6*, 52-57.
120. Gibson, M. I.; Cameron, N. R., Experimentally Facile Controlled Polymerization of N-Carboxyanhydrides (Ncas), Including O-Benzyl-L-Threonine Nca. *J. Polym. Sci. A Polym. Chem.* **2009**, *47*, 2882-2891.
121. Ding, J.; Xiao, C.; Zhuang, X.; He, C.; Chen, X., Direct Formation of Cationic Polypeptide Vesicle as Potential Carrier for Drug and Gene. *Mater. Lett.* **2012**, *73*, 17-20.

122. Ding, J.; Xiao, C.; He, C.; Li, M.; Li, D.; Zhuang, X.; Chen, X., Facile Preparation of a Cationic Poly (Amino Acid) Vesicle for Potential Drug and Gene Co-Delivery. *Nanotechnology* **2011**, *22*, 494012.
123. Huang, Y.-C.; Arham, M.; Jan, J.-S., Alkyl Chain Grafted Poly(L-Lysine): Self-Assembly and Biomedical Application as Carriers. *Soft Matter* **2011**, *7*, 3975-3983.
124. Zhu, L.; Zhao, L.; Qu, X.; Yang, Z., Ph-Sensitive Polymeric Vesicles from Coassembly of Amphiphilic Cholate Grafted Poly(L-Lysine) and Acid-Cleavable Polymer-Drug Conjugate. *Langmuir* **2012**, *28*, 11988-11996.
125. Klok, H.-A.; Rodríguez-Hernández, J., Dendritic-Graft Polypeptides. *Macromolecules* **2002**, *35*, 8718-8723.
126. Rodríguez-Hernández, J.; Gatti, M.; Klok, H.-A., Highly Branched Poly(L-Lysine). *Biomacromolecules* **2003**, *4*, 249-258.
127. Lee, H. J.; Bae, Y., Cross-Linked Nanoassemblies from Poly(Ethylene Glycol)-Poly(Aspartate) Block Copolymers as Stable Supramolecular Templates for Particulate Drug Delivery. *Biomacromolecules* **2011**, *12*, 2686-2696.
128. Zhao, C.; He, P.; Xiao, C.; Gao, X.; Zhuang, X.; Chen, X., Synthesis of Temperature and Ph-Responsive Crosslinked Micelles from Polypeptide-Based Graft Copolymer. *J. Colloid Interface Sci.* **2011**, *359*, 436-442.
129. Nowak, A. P.; Breedveld, V.; Pakstis, L.; Ozbas, B.; Pine, D. J.; Pochan, D.; Deming, T. J., Rapidly Recovering Hydrogel Scaffolds from Self-Assembling Diblock Copolypeptide Amphiphiles. *Nature* **2002**, *417*, 424-428.
130. Deming, T. J., Polypeptide Hydrogels Via a Unique Assembly Mechanism. *Soft Matter* **2005**, *1*, 28-35.
131. Sulistio, A.; Widjaya, A.; Blencowe, A.; Zhang, X.; Qiao, G., Star Polymers Composed Entirely of Amino Acid Building Blocks: A Route Towards

- Stereospecific, Biodegradable and Hierarchically Functionalized Stars. *Chem. Commun.* **2011**, *47*, 1151-1153.
132. Yu, M.; Deming, T., Synthetic Polypeptide Mimics of Marine Adhesives. *Macromolecules* **1998**, *31*, 4739-4745.
133. Zalipsky, S.; Lee, C., Use of Functionalized Poly(Ethylene Glycol)S for Modification of Polypeptides. In *Poly(Ethylene Glycol) Chemistry: Biotechnical and Biomedical Applications*, Harris, J. M., Ed. Springer US: Boston, MA, 1992; pp 347-370.
134. Lu, J.; Xu, H.; Xia, J.; Ma, J.; Xu, J.; Li, Y.; Feng, J., D- and Unnatural Amino Acid Substituted Antimicrobial Peptides with Improved Proteolytic Resistance and Their Proteolytic Degradation Characteristics. *Frontiers in microbiology* **2020**, *11*, 563030.
135. Ulrich, K.; Jakob, U., The Role of Thiols in Antioxidant Systems. *Free. Radic. Biol. Med.* **2019**, *140*, 14-27.
136. Yu, A.; Gentle, I. R.; Lu, G. Q., Biocompatible Polypeptide Microcapsules Via Templating Mesoporous Silica Spheres. *J. Colloid Interface Sci.* **2009**, *333*, 341-345.
137. Ding, J.; Chen, J.; Li, D.; Xiao, C.; Zhang, J.; He, C.; Zhuang, X.; Chen, X., Biocompatible Reduction-Responsive Polypeptide Micelles as Nanocarriers for Enhanced Chemotherapy Efficacy in Vitro. *J. Mater. Chem. B* **2013**, *1*, 69-81.
138. Watanabe, H.; Takehana, K.; Date, M.; Shinozaki, T.; Raz, A., Tumor Cell Autocrine Motility Factor Is the Neuroleukin/Phosphohexose Isomerase Polypeptide¹. *Cancer Res* **1996**, *56*, 2960-2963.
139. Deng, J.; Gao, N.; Wang, Y.; Yi, H.; Fang, S.; Ma, Y.; Cai, L., Self-Assembled Cationic Micelles Based on Peg-Pll-Plleu Hybrid Polypeptides as Highly Effective Gene Vectors. *Biomacromolecules* **2012**, *13*, 3795-3804.

140. Wang, X.; Song, Z.; Wei, S.; Ji, G.; Zheng, X.; Fu, Z.; Cheng, J., Polypeptide-Based Drug Delivery Systems for Programmed Release. *Biomaterials* **2021**, *275*, 120913.
141. Song, Y.; Ding, Y.; Dong, C.-M., Stimuli-Responsive Polypeptide Nanoassemblies: Recent Progress and Applications in Cancer Nanomedicine. *Wiley Interdiscip. Rev. Nanomed. Nanobiotechnol.* **2022**, *14*, e1742.
142. Xu, Q.; Zhang, Z.; Xiao, C.; He, C.; Chen, X., Injectable Polypeptide Hydrogel as Biomimetic Scaffolds with Tunable Bioactivity and Controllable Cell Adhesion. *Biomacromolecules* **2017**, *18*, 1411-1418.
143. Zhou, X.; Li, Z., Advances and Biomedical Applications of Polypeptide Hydrogels Derived from α -Amino Acid N-Carboxyanhydride (Nca) Polymerizations. *Adv. Healthcare Mater.* **2018**, *7*, 1800020.
144. Murphy, R. D.; Kimmins, S.; Hibbitts, A. J.; Heise, A., 3d-Extrusion Printing of Stable Constructs Composed of Photoresponsive Polypeptide Hydrogels. *Polym. Chem.* **2019**, *10*, 4675-4682.
145. Benavides, I.; Raftery, E. D.; Bell, A. G.; Evans, D.; Scott, W. A.; Houk, K. N.; Deming, T. J., Poly(Dehydroalanine): Synthesis, Properties, and Functional Diversification of a Fluorescent Polypeptide. *J. Am. Chem. Soc.* **2022**, *144*, 4214-4223.
146. Wei, M.; Gao, Y.; Li, X.; Serpe, M. J., Stimuli-Responsive Polymers and Their Applications. *Polym. Chem.* **2017**, *8*, 127-143.
147. Zhang, Y.; Uthaman, S.; Song, W.; Eom, K. H.; Jeon, S. H.; Huh, K. M.; Babu, A.; Park, I.-K.; Kim, I., Multistimuli-Responsive Polymeric Vesicles for Accelerated Drug Release in Chemo-Photothermal Therapy. *ACS Biomater. Sci. Eng.* **2020**, *6*, 5012-5023.
148. Zhang, A.; Jung, K.; Li, A.; Liu, J.; Boyer, C., Recent Advances in Stimuli-Responsive Polymer Systems for Remotely Controlled Drug Release. *Prog. Polym. Sci.* **2019**, *99*, 101164.

149. Gibson, M. I.; O'Reilly, R. K., To Aggregate, or Not to Aggregate? Considerations in the Design and Application of Polymeric Thermally-Responsive Nanoparticles. *Chem. Soc. Rev.* **2013**, *42*, 7204-7213.
150. Hocine, S.; Li, M.-H., Thermoresponsive Self-Assembled Polymer Colloids in Water. *Soft Matter* **2013**, *9*, 5839-5861.
151. Pelton, R., Poly(N-Isopropylacrylamide) (Pnipam) Is Never Hydrophobic. *J. Colloid Interface Sci.* **2010**, *348*, 673-674.
152. Jana, S.; Uchman, M., Poly(2-Oxazoline)-Based Stimulus-Responsive (Co)Polymers: An Overview of Their Design, Solution Properties, Surface-Chemistries and Applications. *Prog. Polym. Sci.* **2020**, *106*, 101252.
153. Banerjee, P.; Kar, M.; Dinda, P.; Mandal, T. K., Ionic Liquid-Based Unconventional Photoinitiators for Aqueous Polymerization. *Eur. Polym. J.* **2022**, *162*, 110870.
154. Lerch, A.; Käfer, F.; Prévost, S.; Agarwal, S.; Karg, M., Structural Insights into Polymethacrylamide-Based Lcst Polymers in Solution: A Small-Angle Neutron Scattering Study. *Macromolecules* **2021**, *54*, 7632-7641.
155. Seuring, J.; Agarwal, S., Polymers with Upper Critical Solution Temperature in Aqueous Solution. *Macromol. Rapid Commun.* **2012**, *33*, 1898-1920.
156. Halperin, A.; Kröger, M.; Winnik, F. M., Poly(N-Isopropylacrylamide) Phase Diagrams: Fifty Years of Research. *Angew. Chem. Int. Ed.* **2015**, *54*, 15342-15367.
157. Hentschel, J.; Bleek, K.; Ernst, O.; Lutz, J.-F.; Börner, H. G., Easy Access to Bioactive Peptide-Polymer Conjugates Via Raft. *Macromolecules* **2008**, *41*, 1073-1075.
158. Luo, L.-J.; Lai, J.-Y., Epigallocatechin Gallate-Loaded Gelatin-G-Poly(N-Isopropylacrylamide) as a New Ophthalmic Pharmaceutical Formulation for Topical Use in the Treatment of Dry Eye Syndrome. *Sci. Rep.* **2017**, *7*, 9380.

159. Tang, F.; Ma, N.; Wang, X.; He, F.; Li, L., Hybrid Conjugated Polymer-Ag@PnIPam Fluorescent Nanoparticles with Metal-Enhanced Fluorescence. *J. Mater. Chem.* **2011**, *21*, 16943-16948.
160. Wu, J.-Y.; Liu, S.-Q.; Heng, P. W.-S.; Yang, Y.-Y., Evaluating Proteins Release from, and Their Interactions with, Thermosensitive Poly (N-Isopropylacrylamide) Hydrogels. *J. Control. Release* **2005**, *102*, 361-372.
161. Ma, H.; Hyun, J.; Stiller, P.; Chilkoti, A., "Non-Fouling" Oligo(Ethylene Glycol)- Functionalized Polymer Brushes Synthesized by Surface-Initiated Atom Transfer Radical Polymerization. *Adv. Mater.* **2004**, *16*, 338-341.
162. Ionov, L.; Synytska, A.; Kaul, E.; Diez, S., Protein-Resistant Polymer Coatings Based on Surface-Adsorbed Poly(Aminoethyl Methacrylate)/Poly(Ethylene Glycol) Copolymers. *Biomacromolecules* **2010**, *11*, 233-237.
163. Lutz, J.-F., Thermo-Switchable Materials Prepared Using the Oegma-Platform. *Adv. Mater.* **2011**, *23*, 2237-2243.
164. Chua, G. B. H.; Roth, P. J.; Duong, H. T. T.; Davis, T. P.; Lowe, A. B., Synthesis and Thermoresponsive Solution Properties of Poly[Oligo(Ethylene Glycol) (Meth)Acrylamide]S: Biocompatible Peg Analogues. *Macromolecules* **2012**, *45*, 1362-1374.
165. He, X.; Zhou, R.; Ge, C.; Ling, Y.; Luan, S.; Tang, H., Oegylated Polypeptide Bearing Y-Shaped Pendants with a Lcst Close to Body Temperature: Synthesis and Thermoresponsive Properties. *Eur. Polym. J.* **2019**, *112*, 547-554.
166. Zhao, L.; Wang, X.; Sun, L.; Zhou, R.; Zhang, X.; Zhang, L.; Zheng, Z.; Ling, Y.; Luan, S.; Tang, H., Synthesis and Ucst-Type Thermoresponsive Properties of Polypeptide Based Single-Chain Nanoparticles. *Polym. Chem.* **2019**, *10*, 5206-5214.

167. Kapetanakis, A.; Heise, A., Thermoresponsive Glycopolypeptides with Temperature Controlled Selective Lectin Binding Properties. *Eur. Polym. J.* **2015**, *69*, 483-489.
168. Chopko, C. M.; Lowden, E. L.; Engler, A. C.; Griffith, L. G.; Hammond, P. T., Dual Responsiveness of a Tunable Thermosensitive Polypeptide. *ACS Macro Lett.* **2012**, *1*, 727-731.
169. Xiao, C.; Cheng, Y.; Zhang, Y.; Ding, J.; He, C.; Zhuang, X.; Chen, X., Side Chain Impacts on Ph- and Thermo-Responsiveness of Tertiary Amine Functionalized Polypeptides. *J. Polym. Sci. Part A: Polym. Chem.* **2014**, *52*, 671-679.
170. Yu, M.; Nowak, A. P.; Deming, T. J.; Pochan, D. J., Methylated Mono- and Diethyleneglycol Functionalized Polylysines: Nonionic, α -Helical, Water-Soluble Polypeptides. *J. Am. Chem. Soc.* **1999**, *121*, 12210-12211.
171. Wang, J.; Gibson, M. I.; Barbey, R.; Xiao, S.-J.; Klok, H.-A., Nonfouling Polypeptide Brushes Via Surface-Initiated Polymerization of N ϵ -Oligo(Ethylene Glycol)Succinate-L-Lysine N-Carboxyanhydride. *Macromol. Rapid Commun.* **2009**, *30*, 845-850.
172. Hwang, J.; Deming, T. J., Methylated Mono- and Di(Ethylene Glycol)-Functionalized β -Sheet Forming Polypeptides. *Biomacromolecules* **2001**, *2*, 17-21.
173. Ma, Y.; Fu, X.; Shen, Y.; Fu, W.; Li, Z., Irreversible Low Critical Solution Temperature Behaviors of Thermal-Responsive Oegylated Poly(L-Cysteine) Containing Disulfide Bonds. *Macromolecules* **2014**, *47*, 4684-4689.
174. Cheng, Y.; He, C.; Xiao, C.; Ding, J.; Zhuang, X.; Huang, Y.; Chen, X., Decisive Role of Hydrophobic Side Groups of Polypeptides in Thermosensitive Gelation. *Biomacromolecules* **2012**, *13*, 2053-2059.

175. Zhang, S.; Li, Z., Stimuli-Responsive Polypeptide Materials Prepared by Ring-Opening Polymerization of α -Amino Acid N-Carboxyanhydrides. *J. Polym. Sci. B Polym. Phys.* **2013**, *51*, 546-555.
176. Zelikin, A. N.; Such, G. K.; Postma, A.; Caruso, F., Poly(Vinylpyrrolidone) for Bioconjugation and Surface Ligand Immobilization. *Biomacromolecules* **2007**, *8*, 2950-2953.
177. Imran ul-haq, M.; Lai, B. F. L.; Chapanian, R.; Kizhakkedathu, J. N., Influence of Architecture of High Molecular Weight Linear and Branched Polyglycerols on Their Biocompatibility and Biodistribution. *Biomaterials* **2012**, *33*, 9135-9147.
178. Lewis, A.; Tang, Y.; Brocchini, S.; Choi, J.-w.; Godwin, A., Poly(2-Methacryloyloxyethyl Phosphorylcholine) for Protein Conjugation. *Bioconju. Chem.* **2008**, *19*, 2144-2155.
179. Engler, A. C.; Ke, X.; Gao, S.; Chan, J. M. W.; Coady, D. J.; Ono, R. J.; Lubbers, R.; Nelson, A.; Yang, Y. Y.; Hedrick, J. L., Hydrophilic Polycarbonates: Promising Degradable Alternatives to Poly(Ethylene Glycol)-Based Stealth Materials. *Macromolecules* **2015**, *48*, 1673-1678.
180. Lee, S.; Saito, K.; Lee, H.-R.; Lee, M. J.; Shibasaki, Y.; Oishi, Y.; Kim, B.-S., Hyperbranched Double Hydrophilic Block Copolymer Micelles of Poly(Ethylene Oxide) and Polyglycerol for Ph-Responsive Drug Delivery. *Biomacromolecules* **2012**, *13*, 1190-1196.
181. Weber, C.; Becer, R. C.; Baumgaertel, A.; Hoogenboom, R.; Schubert, U. S., Preparation of Methacrylate End-Functionalized Poly(2-Ethyl-2-Oxazoline) Macromonomers. *Des. Monomers Polym.* **2009**, *12*, 149-165.
182. Zarka, M. T.; Nuyken, O.; Weberskirch, R., Polymer-Bound, Amphiphilic Hoveyda-Grubbs-Type Catalyst for Ring-Closing Metathesis in Water. *Macromol. Rapid Commun.* **2004**, *25*, 858-862.

183. Gaertner, F. C.; Luxenhofer, R.; Blechert, B.; Jordan, R.; Essler, M., Synthesis, Biodistribution and Excretion of Radiolabeled Poly(2-Alkyl-2-Oxazoline)S. *J. Control. Release* **2007**, *119*, 291-300.
184. Lava, K.; Verbraeken, B.; Hoogenboom, R., Poly(2-Oxazoline)S and Click Chemistry: A Versatile Toolbox toward Multi-Functional Polymers. *Eur. Polym. J.* **2015**, *65*, 98-111.
185. Krieg, A.; Weber, C.; Hoogenboom, R.; Becer, C. R.; Schubert, U. S., Block Copolymers of Poly(2-Oxazoline)S and Poly(Meth)Acrylates: A Crossover between Cationic Ring-Opening Polymerization (Crop) and Reversible Addition–Fragmentation Chain Transfer (Raft). *ACS Macro Lett.* **2012**, *1*, 776-779.
186. Salmanpour, M.; Tamaddon, A.; Yousefi, G.; Mohammadi-Samani, S., "Grafting-from" Synthesis and Characterization of Poly (2-Ethyl-2-Oxazoline)-B-Poly (Benzyl L-Glutamate) Micellar Nanoparticles for Potential Biomedical Applications. *BioImpacts* **2017**, *7*, 155-166.
187. Tsutsumiuchi, K.; Aoi, K.; Okada, M., Synthesis of Polyoxazoline–(Glyco)Peptide Block Copolymers by Ring-Opening Polymerization of (Sugar-Substituted) A-Amino Acid N-Carboxyanhydrides with Polyoxazoline Macroinitiators. *Macromolecules* **1997**, *30*, 4013-4017.
188. Niskanen, J.; Tenhu, H., How to Manipulate the Upper Critical Solution Temperature (Ucst)? *Polym. Chem.* **2017**, *8*, 220-232.
189. Lin, Y.-C.; Fang, T.-Y.; Kao, H.-Y.; Tseng, W.-C., Nanoassembly of Ucst Polypeptide for Nir-Modulated Drug Release. *Biochem. Eng. J.* **2021**, *176*, 108194.
190. Xue, X.; Thiagarajan, L.; Dixon, J. E.; Saunders, B. R.; Shakesheff, K. M.; Alexander, C., Post-Modified Polypeptides with Ucst-Type Behavior for Control of Cell Attachment in Physiological Conditions. *Materials* **2018**, *11*, 95.

191. Ge, C.; Liu, S.; Liang, C.; Ling, Y.; Tang, H., Synthesis and Ucst-Type Phase Behavior of A-Helical Polypeptides with Y-Shaped and Imidazolium Pendants. *Polym. Chem.* **2016**, *7*, 5978-5987.
192. Ge, C.; Zhao, L.; Ling, Y.; Tang, H., Thermo and Ph Dual Responsive Polypeptides Derived from “Clickable” Poly(Γ -3-Methylthiopropyl-L-Glutamate). *Polym. Chem.* **2017**, *8*, 1895-1905.
193. Deng, Y.; Xu, Y.; Wang, X.; Yuan, Q.; Ling, Y.; Tang, H., Water-Soluble Thermoresponsive A-Helical Polypeptide with an Upper Critical Solution Temperature: Synthesis, Characterization, and Thermoresponsive Phase Transition Behaviors. *Macromol. Rapid Commun.* **2015**, *36*, 453-458.
194. Wu, Y.; Wang, X.; Ling, Y.; Tang, H., Preparation and Thermoresponsive Properties of Helical Polypeptides Bearing Pyridinium Salts. *RSC Adv.* **2015**, *5*, 40772-40778.
195. Kar, M.; Anas, M.; Singh, A.; Basak, A.; Sen, P.; Mandal, T. K., Ion-/Thermo-Responsive Fluorescent Perylene-Poly(Ionic Liquid) Conjugates: One-Pot Microwave Synthesis, Self-Aggregation and Biological Applications. *Eur. Polym. J.* **2022**, *179*, 111561.
196. Banerjee, P.; Jana, S.; Mandal, T. K., Coulomb Interaction-Driven Ucst in Poly(Ionic Liquid) Random Copolymers. *Eur. Polym. J.* **2020**, *133*, 109747.
197. Jana, S.; Biswas, Y.; Anas, M.; Saha, A.; Mandal, T. K., Poly[Oligo(2-Ethyl-2-Oxazoline)Acrylate]-Based Poly(Ionic Liquid) Random Copolymers with Coexistent and Tunable Lower Critical Solution Temperature- and Upper Critical Solution Temperature-Type Phase Transitions. *Langmuir* **2018**, *34*, 12653-12663.
198. Biswas, Y.; Mandal, T. K., Structural Variation in Homopolymers Bearing Zwitterionic and Ionic Liquid Pendants for Achieving Tunable Multi-Stimuli Responsiveness and Hierarchical Nanoaggregates. *Macromolecules* **2017**, *50*, 9807-9820.

199. Maji, T.; Banerjee, S.; Bose, A.; Mandal, T. K., A Stimuli-Responsive Methionine-Based Zwitterionic Methacryloyl Sulfonium Sulfonate Monomer and the Corresponding Antifouling Polymer with Tunable Thermosensitivity. *Polym. Chem.* **2017**, *8*, 3164-3176.
200. Biswas, Y.; Maji, T.; Dule, M.; Mandal, T. K., Tunable Doubly Responsive Ucst-Type Phosphonium Poly(Ionic Liquid): A Thermosensitive Dispersant for Carbon Nanotubes. *Polym. Chem.* **2016**, *7*, 867-877.
201. Kuroyanagi, S.; Shimada, N.; Fujii, S.; Furuta, T.; Harada, A.; Sakurai, K.; Maruyama, A., Highly Ordered Polypeptide with Ucst Phase Separation Behavior. *J. Am. Chem. Soc.* **2019**, *141*, 1261-1268.
202. Liu, Y.; Zhao, C.; Chen, C., Chirality-Governed Ucst Behavior in Polypeptides. *Macromolecules* **2022**, *55*, 3801-3810.
203. Liu, W.; Zhu, M.; Xiao, J.; Ling, Y.; Tang, H., Synthesis and Ucst-Type Phase Behavior of Polypeptide with Alkyl Side-Chains in Alcohol or Ethanol/Water Solvent Mixtures. *J. Polym. Sci. Part A: Polym. Chem.* **2016**, *54*, 3425-3435.
204. Li, M.; Wang, X.; Xu, Y.; Ling, Y.; Tang, H., Preparation of Glycopolypeptides Bearing Mannose Moieties and Biphenyl Pendants and Their Upper-Critical-Solution-Temperature-Type Thermoresponsive Properties in Alcohol/Water Solvent Mixtures. *Polym. Int.* **2016**, *65*, 1493-1500.
205. Ge, C.; Liu, W.; Ling, Y.; Tang, H., Synthesis and Thermoresponsive Properties of Oegylated Polypeptide with a Lcst at Body Temperature in Water and with a Ucst in Alcohol or Ethanol/Water Solvent Mixture. *J. Polym. Sci. Part A: Polym. Chem.* **2018**, *56*, 163-173.
206. Zhu, M.; Liu, W.; Xiao, J.; Ling, Y.; Tang, H., Synthesis and Ucst-Type Phase Behaviors of Oegylated Random Copolypeptides in Alcoholic Solvents. *J. Polym. Sci. Part A: Polym. Chem.* **2016**, *54*, 3444-3453.

207. Li, M.; Xu, Y.; Liu, T.; Li, Y.; Ling, Y.; Tang, H., Preparation and Thermo-responsive Properties of Ucst-Type Polypeptide Bearing P-Tolyl Pendants and 3-Methyl-1,2,3-Triazolium Linkages in Methanol or Ethanol/Water Solvent Mixtures. *Macromol. Chem. Phys.* **2017**, *218*, 1700006.
208. Muthu, M. S.; Rajesh, C. V.; Mishra, A.; Singh, S., Stimulus-Responsive Targeted Nanomicelles for Effective Cancer Therapy. *Nanomed.* **2009**, *4*, 657-667.
209. Gao, W.; Chan, J. M.; Farokhzad, O. C., Ph-Responsive Nanoparticles for Drug Delivery. *Mol. Pharmaceutics* **2010**, *7*, 1913-1920.
210. Felber, A. E.; Dufresne, M.-H.; Leroux, J.-C., Ph-Sensitive Vesicles, Polymeric Micelles, and Nanospheres Prepared with Polycarboxylates. *Adv. Drug Deliv. Rev.* **2012**, *64*, 979-992.
211. Palanikumar, L.; Al-Hosani, S.; Kalmouni, M.; Nguyen, V. P.; Ali, L.; Pasricha, R.; Barrera, F. N.; Magzoub, M., Ph-Responsive High Stability Polymeric Nanoparticles for Targeted Delivery of Anticancer Therapeutics. *Commun. Biol.* **2020**, *3*, 95.
212. Deirram, N.; Zhang, C.; Kermaniyan, S. S.; Johnston, A. P. R.; Such, G. K., Ph-Responsive Polymer Nanoparticles for Drug Delivery. *Macromol. Rapid Commun.* **2019**, *40*, 1800917.
213. Schmaljohann, D., Thermo- and Ph-Responsive Polymers in Drug Delivery. *Adv. Drug Deliv. Rev.* **2006**, *58*, 1655-1670.
214. Gao, H.; Li, G.; Hu, Z.; Xiao, Z.; Liang, G.; Wu, Q., Synthesis of Amphiphilic Polyethylene-B-Poly(L-Glutamate) Block Copolymers with Vastly Different Solubilities and Their Stimuli-Responsive Polymeric Micelles in Aqueous Solution. *Polymer* **2014**, *55*, 4593-4600.
215. Engler, A. C.; Bonner, D. K.; Buss, H. G.; Cheung, E. Y.; Hammond, P. T., The Synthetic Tuning of Clickable Ph Responsive Cationic Polypeptides and Block Copolypeptides. *Soft Matter* **2011**, *7*, 5627-5637.

216. Wong, S.; Shim, M. S.; Kwon, Y. J., Synthetically Designed Peptide-Based Biomaterials with Stimuli-Responsive and Membrane-Active Properties for Biomedical Applications. *J. Mater. Chem. B* **2014**, *2*, 595-615.
217. Augustine, R.; Kalva, N.; Kim, H. A.; Zhang, Y.; Kim, I., Ph-Responsive Polypeptide-Based Smart Nano-Carriers for Theranostic Applications. *Molecules* **2019**, *24*, 2961.
218. Tian, H.; Chen, X.; Lin, H.; Deng, C.; Zhang, P.; Wei, Y.; Jing, X., Micellization and Reversible Ph-Sensitive Phase Transfer of the Hyperbranched Multiarm Pei-Pblg Copolymer. *Chem. -Euro. J.* **2006**, *12*, 4305-4312.
219. Huang, H.; Li, J.; Liao, L.; Li, J.; Wu, L.; Dong, C.; Lai, P.; Liu, D., Poly(L-Glutamic Acid)-Based Star-Block Copolymers as Ph-Responsive Nanocarriers for Cationic Drugs. *Eur. Polym. J.* **2012**, *48*, 696-704.
220. Kim, M. S.; Dayananda, K.; Choi, E. K.; Park, H. J.; Kim, J. S.; Lee, D. S., Synthesis and Characterization of Poly(L-Glutamic Acid)-Block-Poly(L-Phenylalanine). *Polymer* **2009**, *50*, 2252-2257.
221. Byrne, M.; Thornton, P. D.; Cryan, S.-A.; Heise, A., Star Polypeptides by Nca Polymerisation from Dendritic Initiators: Synthesis and Enzyme Controlled Payload Release. *Polym. Chem.* **2012**, *3*, 2825-2831.
222. Li, Y.-Y.; Hua, S.-H.; Xiao, W.; Wang, H.-Y.; Luo, X.-H.; Li, C.; Cheng, S.-X.; Zhang, X.-Z.; Zhuo, R.-X., Dual-Vectors of Anti-Cancer Drugs and Genes Based on Ph-Sensitive Micelles Self-Assembled from Hybrid Polypeptide Copolymers. *J. Mater. Chem.* **2011**, *21*, 3100-3106.
223. Lu, C.; Jiang, L.; Xu, W.; Yu, F.; Xia, W.; Pan, M.; Zhou, W.; Pan, X.; Wu, C.; Liu, D., Poly(Ethylene Glycol) Crosslinked Multi-Armed Poly(E-Benzylloxycarbonyl-L-Lysine)S as Super-Amphiphiles: Synthesis, Self-Assembly, and Evaluation as Efficient Delivery Systems for Poorly Water-Soluble Drugs. *Colloids. Surf. B.* **2019**, *182*, 110384.

224. Wang, C.; Kang, Y.; Liu, K.; Li, Z.; Wang, Z.; Zhang, X., Ph and Enzymatic Double-Stimuli Responsive Multi-Compartment Micelles from Supra-Amphiphilic Polymers. *Polym. Chem.* **2012**, *3*, 3056-3059.
225. Ito, Y.; Park, Y. S.; Imanishi, Y., Nanometer-Sized Channel Gating by a Self-Assembled Polypeptide Brush. *Langmuir* **2000**, *16*, 5376-5381.
226. Osada, Y.; Honda, K.; Ohta, M., Control of Water Permeability by Mechanochemical Contraction of Poly(Methacrylic Acid)-Grafted Membranes. *J. Membr. Sci.* **1986**, *27*, 327-338.
227. Lin, J.; Zhu, J.; Chen, T.; Lin, S.; Cai, C.; Zhang, L.; Zhuang, Y.; Wang, X.-S., Drug Releasing Behavior of Hybrid Micelles Containing Polypeptide Triblock Copolymer. *Biomaterials* **2009**, *30*, 108-117.
228. Cai, C.; Zhang, L.; Lin, J.; Wang, L., Self-Assembly Behavior of Ph- and Thermosensitive Amphiphilic Triblock Copolymers in Solution: Experimental Studies and Self-Consistent Field Theory Simulations. *J. Phys. Chem. B* **2008**, *112*, 12666-12673.
229. Ray, J. G.; Naik, S. S.; Hoff, E. A.; Johnson, A. J.; Ly, J. T.; Easterling, C. P.; Patton, D. L.; Savin, D. A., Stimuli-Responsive Peptide-Based ABA-Triblock Copolymers: Unique Morphology Transitions with Ph. *Macromol. Rapid Commun.* **2012**, *33*, 819-826.
230. He, C.; Zhao, C.; Chen, X.; Guo, Z.; Zhuang, X.; Jing, X., Novel Ph- and Temperature-Responsive Block Copolymers with Tunable Ph-Responsive Range. *Macromol. Rapid Commun.* **2008**, *29*, 490-497.
231. Zhang, X.; Li, J.; Li, W.; Zhang, A., Synthesis and Characterization of Thermo- and Ph-Responsive Double-Hydrophilic Diblock Copolypeptides. *Biomacromolecules* **2007**, *8*, 3557-3567.
232. Rao, J.; Luo, Z.; Ge, Z.; Liu, H.; Liu, S., "Schizophrenic" Micellization Associated with Coil-to-Helix Transitions Based on Polypeptide Hybrid Double Hydrophilic Rod-Coil Diblock Copolymer. *Biomacromolecules* **2007**, *8*, 3871-3878.

233. Carlsen, A.; Lecommandoux, S., Self-Assembly of Polypeptide-Based Block Copolymer Amphiphiles. *Curr. Opin. Colloid Interface Sci.* **2009**, *14*, 329-339.
234. Chécot, F.; Rodríguez-Hernández, J.; Gnanou, Y.; Lecommandoux, S., Ph-Responsive Micelles and Vesicles Nanocapsules Based on Polypeptide Diblock Copolymers. *Biomol. Eng.* **2007**, *24*, 81-85.
235. Bellomo, E. G.; Wyrsta, M. D.; Pakstis, L.; Pochan, D. J.; Deming, T. J., Stimuli-Responsive Polypeptide Vesicles by Conformation-Specific Assembly. *Nature Mater.* **2004**, *3*, 244-248.
236. Iatrou, H.; Frielinghaus, H.; Hanski, S.; Ferderigos, N.; Ruokolainen, J.; Ikkala, O.; Richter, D.; Mays, J.; Hadjichristidis, N., Architecturally Induced Multiresponsive Vesicles from Well-Defined Polypeptides. Formation of Gene Vehicles. *Biomacromolecules* **2007**, *8*, 2173-2181.
237. Sun, J.; Huang, Y.; Shi, Q.; Chen, X.; Jing, X., Oxygen Carrier Based on Hemoglobin/Poly(L-Lysine)-Block-Poly(L-Phenylalanine) Vesicles. *Langmuir* **2009**, *25*, 13726-13729.
238. Gaspard, J.; Silas, J. A.; Shantz, D. F.; Jan, J.-S., Supramolecular Assembly of Lysine-B-Glycine Block Copolypeptides at Different Solution Conditions. *Supramol. Chem.* **2010**, *22*, 178-185.
239. Knoop, R. J. I.; de Geus, M.; Habraken, G. J. M.; Koning, C. E.; Menzel, H.; Heise, A., Stimuli Responsive Peptide Conjugated Polymer Nanoparticles. *Macromolecules* **2010**, *43*, 4126-4132.
240. Borase, T.; Iacono, M.; Ali, S. I.; Thornton, P. D.; Heise, A., Polypeptide Core-Shell Silica Nanoparticles with High Grafting Density by N-Carboxyanhydride (Nca) Ring Opening Polymerization as Responsive Materials and for Bioconjugation. *Polym. Chem.* **2012**, *3*, 1267-1275.
241. Lee, E. S.; Gao, Z.; Bae, Y. H., Recent Progress in Tumor Ph Targeting Nanotechnology. *J. Control. Release* **2008**, *132*, 164-170.

242. Burnworth, M.; Tang, L.; Kumpfer, J. R.; Duncan, A. J.; Beyer, F. L.; Fiore, G. L.; Rowan, S. J.; Weder, C., Optically Healable Supramolecular Polymers. *Nature* **2011**, *472*, 334-337.
243. Fomina, N.; Sankaranarayanan, J.; Almutairi, A., Photochemical Mechanisms of Light-Triggered Release from Nanocarriers. *Adv. Drug Deliv. Rev.* **2012**, *64*, 1005-1020.
244. Kotharangannagari, V. K.; Sánchez-Ferrer, A.; Ruokolainen, J.; Mezzenga, R., Photoresponsive Reversible Aggregation and Dissolution of Rod-Coil Polypeptide Diblock Copolymers. *Macromolecules* **2011**, *44*, 4569-4573.
245. Kumar, S.; Allard, J.-F.; Morris, D.; Dory, Y. L.; Lepage, M.; Zhao, Y., Near-Infrared Light Sensitive Polypeptide Block Copolymer Micelles for Drug Delivery. *J. Mater. Chem.* **2012**, *22*, 7252-7257.
246. Yan, B.; Boyer, J.-C.; Branda, N. R.; Zhao, Y., Near-Infrared Light-Triggered Dissociation of Block Copolymer Micelles Using Upconverting Nanoparticles. *J. Am. Chem. Soc.* **2011**, *133*, 19714-19717.
247. Lowe, A. B.; McCormick, C. L., Stimuli Responsive Water-Soluble and Amphiphilic (Co)Polymers. In *Stimuli-Responsive Water Soluble and Amphiphilic Polymers*, American Chemical Society: 2000; Vol. 780, pp 1-13.
248. Pieroni, O.; Fissi, A.; Angelini, N.; Lenci, F., Photoresponsive Polypeptides. *Acc. Chem. Res.* **2001**, *34*, 9-17.
249. Pieroni, O.; Fissi, A.; Ciardelli, F., Photochromic Poly(A-Amino Acid)S: Photomodulation of Molecular and Supramolecular Structure. *React. Funct. Polym.* **1995**, *26*, 185-199.
250. Williams, A. J.; Gupta, V. K., Incorporation of a Photochromic Hinge in a Rodlike Polypeptide and Its Influence on Dielectric and Optical Properties. *J. Polym. Sci. B Polym. Phys.* **2001**, *39*, 2759-2773.
251. Hernández, J. R.; Klok, H.-A., Synthesis and Ring-Opening (Co)Polymerization of L-Lysine N-Carboxyanhydrides Containing Labile

- Side-Chain Protective Groups. *J. Polym. Sci. A Polym. Chem.* **2003**, *41*, 1167-1187.
252. Liu, G.; Liu, W.; Dong, C.-M., Uv- and Nir-Responsive Polymeric Nanomedicines for on-Demand Drug Delivery. *Polym. Chem.* **2013**, *4*, 3431-3443.
253. Goodman, M.; Falxa, M. L., Conformational Aspects of Polypeptide Structure. Xxiii. Photoisomerization of Azoaromatic Polypeptides. *J. Am. Chem. Soc.* **1967**, *89*, 3863-3867.
254. Ueno, A.; Adachi, K.; Nakamura, J.; Osa, T., Photoinduced Conformational Changes of Azoaromatic Polyaspartates Containing Octadecyl Side Chains. *J. Polym. Sci. A Polym. Chem.* **1990**, *28*, 1161-1170.
255. Menzel, H.; Hallensleben, M.; Schmidt, A.; Knoll, W.; Fischer, T.; Stumpe, Langmuir-Blodgett Films of Photochromic Polyglutamates. 4. Spectroscopic and Structural Studies on Langmuir-Blodgett Films of Copolyglutamates Bearing Azobenzene Moieties and Long Alkyl Chains. *Macromolecules* **1993**, *26*, 3644-3649.
256. Pieroni, O.; Fissi, A.; Viegi, A.; Fabbri, D.; Ciardelli, F., Modulation of Chain Conformation of Spiropyran-Containing Poly (L-Lysine) by Combined Action of Visible Light and Solvent. *J. Am. Chem. Soc.* **1992**, *114*, 2734-2736.
257. Yamamoto, H.; Nishida, A.; Takimoto, T.; Nagai, A., Photoresponsive Peptide and Polypeptide Systems. Viii. Synthesis and Reversible Photochromism of Azo Aromatic Poly(L-Ornithine). *J. Polym. Sci. A Polym. Chem.* **1990**, *28*, 67-74.
258. Yamamoto, H.; Nishida, A.; Kawaura, T., Photoresponsive Peptide and Polypeptide Systems: 10. Synthesis and Reversible Photochromism of Azo Aromatic Poly(L-A,B-Diaminopropionic Acid). *Int. J. Biol. Macromol.* **1990**, *12*, 257-262.

259. Yamamoto, H.; Kitsuki, T.; Nishida, A.; Asada, K.; Ohkawa, K., Photoresponsive Peptide and Polypeptide Systems. 13. Photoinduced Cross-Linked Gel and Biodegradation Properties of Copoly(L-Lysine) Containing E-7-Coumaryloxyacetyl-L-Lysine Residues. *Macromolecules* **1999**, *32*, 1055-1061.
260. Ohkawa, K.; Shoumura, K.; Yamada, M.; Nishida, A.; Shirai, H.; Yamamoto, H., Photoresponsive Peptide and Polypeptide Systems, 14. Biodegradation of Photocrosslinkable Copolypeptide Hydrogels Containing L-Ornithine and Δ -7-Coumaryloxyacetyl-L-Ornithine Residues. *Macromol. Biosci.* **2001**, *1*, 149-156.
261. Ohkawa, K.; Shoumura, K.; Shirakabe, Y.; Yamamoto, H., Photoresponsive Peptide and Polypeptide Systems 15*: Synthesis of Photo-Crosslinkable Poly(Amino Acid)S by Watery Process and Its Application as a Reinforcement for Polyion Complex Fibers. *J. Mater. Sci.* **2003**, *38*, 3191-3197.
262. Meng, F.; Hennink, W. E.; Zhong, Z., Reduction-Sensitive Polymers and Bioconjugates for Biomedical Applications. *Biomaterials* **2009**, *30*, 2180-2198.
263. Yamada, S.; Ikkyu, K.; Iso, K.; Goto, M.; Endo, T., Facile Synthesis of Polymethionine Oxides through Polycondensation of Activated Urethane Derivative of α -Amino Acid and Their Application to Antifouling Polymer against Proteins and Cells. *Polym. Chem.* **2015**, *6*, 1838-1845.
264. Raina, S.; Missiakas, D., Making and Breaking Disulfide Bonds. *Annu. Rev. Microbiol.* **1997**, *51*, 179-202.
265. Gilbert, H. F., Thiol/Disulfide Exchange Equilibria and Disulfidebond Stability. In *Methods Enzymol.*, Academic Press: 1995; Vol. 251, pp 8-28.
266. Wu, G.; Fang, Y.-Z.; Yang, S.; Lupton, J. R.; Turner, N. D., Glutathione Metabolism and Its Implications for Health. *J. Nutr.* **2004**, *134*, 489-492.

267. Kim, T.-i.; Kim, S. W., Bioreducible Polymers for Gene Delivery. *React. Funct. Polym.* **2011**, *71*, 344-349.
268. Takae, S.; Miyata, K.; Oba, M.; Ishii, T.; Nishiyama, N.; Itaka, K.; Yamasaki, Y.; Koyama, H.; Kataoka, K., Peg-Detachable Polyplex Micelles Based on Disulfide-Linked Block Cationomers as Bioresponsive Nonviral Gene Vectors. *J. Am. Chem. Soc.* **2008**, *130*, 6001-6009.
269. Dong, W.-F.; Kishimura, A.; Anraku, Y.; Chuanoi, S.; Kataoka, K., Monodispersed Polymeric Nanocapsules: Spontaneous Evolution and Morphology Transition from Reducible Hetero-Peg Picmicelles by Controlled Degradation. *J. Am. Chem. Soc.* **2009**, *131*, 3804-3805.
270. Wen, H.-Y.; Dong, H.-Q.; Xie, W.-j.; Li, Y.-Y.; Wang, K.; Pauletti, G. M.; Shi, D.-L., Rapidly Disassembling Nanomicelles with Disulfide-Linked Peg Shells for Glutathione-Mediated Intracellular Drug Delivery. *Chem. Commun.* **2011**, *47*, 3550-3552.
271. Thambi, T.; Yoon, H. Y.; Kim, K.; Kwon, I. C.; Yoo, C. K.; Park, J. H., Bioreducible Block Copolymers Based on Poly(Ethylene Glycol) and Poly(Γ -Benzyl L-Glutamate) for Intracellular Delivery of Camptothecin. *Bioconjugate Chem.* **2011**, *22*, 1924-1931.
272. Waku, T.; Matsumoto, M.; Matsusaki, M.; Akashi, M., Complete Surface Control of Peptide Nanospheres with Detachable and Attachable Polymer Brush Layers. *Chem. Commun.* **2010**, *46*, 7025-7027.
273. Ren, T.-B.; Xia, W.-J.; Dong, H.-Q.; Li, Y.-Y., Sheddable Micelles Based on Disulfide-Linked Hybrid Peg-Polypeptide Copolymer for Intracellular Drug Delivery. *Polymer* **2011**, *52*, 3580-3586.
274. Xing, T.; Lai, B.; Ye, X.; Yan, L., Disulfide Core Cross-Linked Pegylated Polypeptide Nanogel Prepared by a One-Step Ring Opening Copolymerization of N-Carboxyanhydrides for Drug Delivery. *Macromol. Biosci.* **2011**, *11*, 962-969.

275. Matsumoto, A., et al., Synthetic “Smart Gel” Provides Glucose-Responsive Insulin Delivery in Diabetic Mice. *Sci. Adv.* **2017**, *3*, eaaq0723.
276. Lee, D.; Choe, K.; Jeong, Y.; Yoo, J.; Lee, S. M.; Park, J.-H.; Kim, P.; Kim, Y.-C., Establishment of a Controlled Insulin Delivery System Using a Glucose-Responsive Double-Layered Nanogel. *RSC Adv.* **2015**, *5*, 14482-14491.
277. Lee, D.; Choe, K.; Jeong, Y.; Yoo, J.; Lee, S. M.; Park, J.-H.; Kim, P.; Kim, Y.-C., Establishment of a Controlled Insulin Delivery System Using a Glucose-Responsive Double-Layered Nanogel. *RSC Adv.* **2015**, *5*, 14482-14491.
278. Liu, G.; Ma, R.; Ren, J.; Li, Z.; Zhang, H.; Zhang, Z.; An, Y.; Shi, L., A Glucose-Responsive Complex Polymeric Micelle Enabling Repeated on–Off Release and Insulin Protection. *Soft Matter* **2013**, *9*, 1636-1644.
279. Naito, M.; Yoshinaga, N.; Ishii, T.; Matsumoto, A.; Miyahara, Y.; Miyata, K.; Kataoka, K., Enhanced Intracellular Delivery of Sirna by Controlling Atp-Responsivity of Phenylboronic Acid-Functionalized Polyion Complex Micelles. *Macromol. Biosci.* **2018**, *18*, 1700357.
280. Yoshinaga, N.; Ishii, T.; Naito, M.; Endo, T.; Uchida, S.; Cabral, H.; Osada, K.; Kataoka, K., Polyplex Micelles with Phenylboronate/Gluconamide Cross-Linking in the Core Exerting Promoted Gene Transfection through Spatiotemporal Responsivity to Intracellular Ph and Atp Concentration. *J. Am. Chem. Soc.* **2017**, *139*, 18567-18575.
281. Shen, Y.; Fu, X.; Fu, W.; Li, Z., Biodegradable Stimuli-Responsive Polypeptide Materials Prepared by Ring Opening Polymerization. *Chem. Soc. Rev.* **2015**, *44*, 612-622.
282. Minoura, N., Control of Helix–Helix Association Induced by Alkali Metal Ions in A-Helical Polypeptide Having a Terminal Crown Ether. *J. Chem. Soc., Chem. Commun.* **1993**, 196-197.

283. Minoura, N.; Higuchi, M.; Kinoshita, T., Stimuli-Responsive Formation of Helical Polypeptide Rod Assemblies. *Mater. Sci. Eng.* **1997**, *4*, 249-254.
284. Mornet, S.; Vasseur, S.; Grasset, F.; Duguet, E., Magnetic Nanoparticle Design for Medical Diagnosis and Therapy. *J. Mater. Chem.* **2004**, *14*, 2161-2175.
285. Bae, S.; Lee, S. W.; Takemura, Y., Applications of NiFe₂O₄ Nanoparticles for a Hyperthermia Agent in Biomedicine. *Appl. Phys. Lett.* **2006**, *89*.
286. Jun, Y.-w., et al., Nanoscale Size Effect of Magnetic Nanocrystals and Their Utilization for Cancer Diagnosis Via Magnetic Resonance Imaging. *J. Am. Chem. Soc.* **2005**, *127*, 5732-5733.
287. Xu, Z.; Feng, Y.; Liu, X.; Guan, M.; Zhao, C.; Zhang, H., Synthesis and Characterization of Fe₃O₄@SiO₂@Poly-L-Alanine, Peptide Brush–Magnetic Microspheres through Nca Chemistry for Drug Delivery and Enrichment of Bsa. *Colloids Surf., B*, **2010**, *81*, 503-507.
288. Kramer, J. R.; Deming, T. J., Reversible Chemoselective Tagging and Functionalization of Methionine Containing Peptides. *Chem. Commun.* **2013**, *49*, 5144-5146.
289. Wang, J.; Liu, K.; Xing, R.; Yan, X., Peptide Self-Assembly: Thermodynamics and Kinetics. *Chem. Soc. Rev.* **2016**, *45*, 5589-5604.
290. Li, T.; Lu, X.-M.; Zhang, M.-R.; Hu, K.; Li, Z., Peptide-Based Nanomaterials: Self-Assembly, Properties and Applications. *Bioact. Mater.* **2022**, *11*, 268-282.
291. Cai, C.; Wang, L.; Lin, J., Self-Assembly of Polypeptide-Based Copolymers into Diverse Aggregates. *Chem. Commun.* **2011**, *47*, 11189-11203.
292. Lu, H.; Wang, J.; Song, Z.; Yin, L.; Zhang, Y.; Tang, H.; Tu, C.; Lin, Y.; Cheng, J., Recent Advances in Amino Acid N-Carboxyanhydrides and Synthetic Polypeptides: Chemistry, Self-Assembly and Biological Applications. *Chem. Commun.* **2014**, *50*, 139-155.

293. Zhang, Y.-N.; Avery, R. K.; Vallmajo-Martin, Q.; Assmann, A.; Vegh, A.; Memic, A.; Olsen, B. D.; Annabi, N.; Khademhosseini, A., A Highly Elastic and Rapidly Crosslinkable Elastin-Like Polypeptide-Based Hydrogel for Biomedical Applications. *Adv. Funct. Mater.* **2015**, *25*, 4814-4826.
294. Chécot, F.; Lecommandoux, S.; Gnanou, Y.; Klok, H.-A., Water-Soluble Stimuli-Responsive Vesicles from Peptide-Based Diblock Copolymers. *Angew. Chem. Int. Ed.* **2002**, *41*, 1339-1343.
295. Chécot, F.; Rodríguez-Hernández, J.; Gnanou, Y.; Lecommandoux, S., Responsive Micelles and Vesicles Based on Polypeptide Diblock Copolymers. *Polym. Adv. Technol.* **2006**, *17*, 782-785.
296. Chécot, F.; Brûlet, A.; Oberdisse, J.; Gnanou, Y.; Mondain-Monval, O.; Lecommandoux, S., Structure of Polypeptide-Based Diblock Copolymers in Solution: Stimuli-Responsive Vesicles and Micelles. *Langmuir* **2005**, *21*, 4308-4315.
297. Dong, C.-M.; Sun, X.-L.; Faucher, K. M.; Apkarian, R. P.; Chaikof, E. L., Synthesis and Characterization of Glycopolymer-Polypeptide Triblock Copolymers. *Biomacromolecules* **2004**, *5*, 224-231.
298. Ghezzi, M.; Pescina, S.; Padula, C.; Santi, P.; Del Favero, E.; Cantù, L.; Nicoli, S., Polymeric Micelles in Drug Delivery: An Insight of the Techniques for Their Characterization and Assessment in Biorelevant Conditions. *J. Control. Release* **2021**, *332*, 312-336.
299. Wang, Y.; Brown, P.; Xia, Y., Swarming Towards the Target. *Nature Mater.* **2011**, *10*, 482-483.
300. Xia, Y., Nanomaterials at Work in Biomedical Research. *Nature Mater.* **2008**, *7*, 758-760.
301. Gil, E. S.; Hudson, S. M., Stimuli-Responsive Polymers and Their Bioconjugates. *Prog. Polym. Sci.* **2004**, *29*, 1173-1222.

302. Deng, C.; Rong, G.; Tian, H.; Tang, Z.; Chen, X.; Jing, X., Synthesis and Characterization of Poly(Ethylene Glycol)-B-Poly (L-Lactide)-B-Poly(L-Glutamic Acid) Triblock Copolymer. *Polymer* **2005**, *46*, 653-659.
303. Lee, E. S.; Shin, H. J.; Na, K.; Bae, Y. H., Poly(L-Histidine)-Peg Block Copolymer Micelles and Ph-Induced Destabilization. *J. Control. Release* **2003**, *90*, 363-374.
304. Bae, Y.; Fukushima, S.; Harada, A.; Kataoka, K., Design of Environment-Sensitive Supramolecular Assemblies for Intracellular Drug Delivery: Polymeric Micelles That Are Responsive to Intracellular Ph Change. *Angew. Chem. Int. Ed.* **2003**, *42*, 4640-4643.
305. Kanayama, N.; Fukushima, S.; Nishiyama, N.; Itaka, K.; Jang, W.-D.; Miyata, K.; Yamasaki, Y.; Chung, U.-i.; Kataoka, K., A Peg-Based Biocompatible Block Copolymer with High Buffering Capacity for the Construction of Polyplex Micelles Showing Efficient Gene Transfer toward Primary Cells. *Chem. Med. Chem.* **2006**, *1*, 439-444.
306. Deng, L.; Shi, K.; Zhang, Y.; Wang, H.; Zeng, J.; Guo, X.; Du, Z.; Zhang, B., Synthesis of Well-Defined Poly(N-Isopropylacrylamide)-B-Poly(L-Glutamic Acid) by a Versatile Approach and Micellization. *J. Colloid Interface Sci.* **2008**, *323*, 169-175.
307. Danhier, F.; Feron, O.; Préat, V., To Exploit the Tumor Microenvironment: Passive and Active Tumor Targeting of Nanocarriers for Anti-Cancer Drug Delivery. *J. Control. Release* **2010**, *148*, 135-146.
308. Gebhardt, K. E.; Ahn, S.; Venkatachalam, G.; Savin, D. A., Rod-Sphere Transition in Polybutadiene-Poly(L-Lysine) Block Copolymer Assemblies. *Langmuir* **2007**, *23*, 2851-2856.
309. Babin, J.; Rodriguez-Hernandez, J.; Lecommandoux, S.; Klok, H.-A.; Achard, M.-F., Self-Assembled Nanostructures from Peptide-Synthetic Hybrid Block Copolymers: Complex, Stimuli-Responsive Rod-Coil Architectures. *Faraday Discuss.* **2005**, *128*, 179-192.

310. Lecommandoux, S.; Achard, M.-F.; Langenwalter, J. F.; Klok, H.-A., Self-Assembly of Rod-Coil Diblock Oligomers Based on A-Helical Peptides. *Macromolecules* **2001**, *34*, 9100-9111.
311. Schlaad, H., Solution Properties of Polypeptide-Based Copolymers. In *Adv. Polym. Sci.*, Klok, H.-A.; Schlaad, H., Eds. Springer Berlin Heidelberg: Berlin, Heidelberg, 2006; pp 53-73.
312. Jain, S.; Bates, F. S., On the Origins of Morphological Complexity in Block Copolymer Surfactants. *Science* **2003**, *300*, 460-464.
313. Zhulina, E. B.; Adam, M.; LaRue, I.; Sheiko, S. S.; Rubinstein, M., Diblock Copolymer Micelles in a Dilute Solution. *Macromolecules* **2005**, *38*, 5330-5351.
314. Gohy, J.-F., Block Copolymer Micelles. In *Adv. Polym. Sci.*, 2005; pp 65-136.
315. Voorhees, P. W., The Theory of Ostwald Ripening. *J. Stat. Phys.* **1985**, *38*, 231-252.
316. Jana, S.; Saha, A.; Paira, T. K.; Mandal, T. K., Synthesis and Self-Aggregation of Poly(2-Ethyl-2-Oxazoline)-Based Photocleavable Block Copolymer: Micelle, Compound Micelle, Reverse Micelle, and Dye Encapsulation/Release. *J. Phys. Chem. B* **2016**, *120*, 813-824.
317. Dule, M.; Biswas, M.; Paira, T. K.; Mandal, T. K., Hierarchical Nanostructures of Tunable Shapes through Self-Aggregation of Poss End-Functional Polymer and Poly(Ionic Liquid) Hybrids. *Polymer* **2015**, *77*, 32-41.
318. Saha, A.; Jana, S.; Mandal, T. K., Peptide-Poly(Tert-Butyl Methacrylate) Conjugate into Composite Micelles in Organic Solvents Versus Peptide-Poly(Methacrylic Acid) Conjugate into Spherical and Worm-Like Micelles in Water: Synthesis and Self-Assembly. *J. Polym. Sci. Part A: Polym. Chem.* **2016**, *54*, 3019-3031.

319. Lefley, J.; Waldron, C.; Becer, C. R., Macromolecular Design and Preparation of Polymersomes. *Polym. Chem.* **2020**, *11*, 7124-7136.
320. Du, J.; O'Reilly, R. K., Advances and Challenges in Smart and Functional Polymer Vesicles. *Soft Matter* **2009**, *5*, 3544-3561.
321. Holowka, E. P.; Pochan, D. J.; Deming, T. J., Charged Polypeptide Vesicles with Controllable Diameter. *J. Am. Chem. Soc.* **2005**, *127*, 12423-12428.
322. Sun, J.; Chen, X.; Deng, C.; Yu, H.; Xie, Z.; Jing, X., Direct Formation of Giant Vesicles from Synthetic Polypeptides. *Langmuir* **2007**, *23*, 8308-8315.
323. Yang, Y.; Cai, J.; Zhuang, X.; Guo, Z.; Jing, X.; Chen, X., Ph-Dependent Self-Assembly of Amphiphilic Poly(L-Glutamic Acid)-Block-Poly(Lactic-Co-Glycolic Acid) Copolymers. *Polymer* **2010**, *51*, 2676-2682.
324. Sanson, C.; Schatz, C.; Le Meins, J.-F.; Brûlet, A.; Soum, A.; Lecommandoux, S., Biocompatible and Biodegradable Poly(Trimethylene Carbonate)-B-Poly(L-Glutamic Acid) Polymersomes: Size Control and Stability. *Langmuir* **2010**, *26*, 2751-2760.
325. Kukula, H.; Schlaad, H.; Antonietti, M.; Förster, S., The Formation of Polymer Vesicles or "Peptosomes" by Polybutadiene-Block-Poly(L-Glutamate)S in Dilute Aqueous Solution. *J. Am. Chem. Soc.* **2002**, *124*, 1658-1663.
326. Huang, J.; Bonduelle, C.; Thévenot, J.; Lecommandoux, S.; Heise, A., Biologically Active Polymersomes from Amphiphilic Glycopeptides. *J. Am. Chem. Soc.* **2012**, *134*, 119-122.
327. Qiu, Y.; Park, K., Environment-Sensitive Hydrogels for Drug Delivery. *Adv. Drug Deliv. Rev.* **2001**, *53*, 321-339.
328. He, C.; Kim, S. W.; Lee, D. S., In Situ Gelling Stimuli-Sensitive Block Copolymer Hydrogels for Drug Delivery. *J. Control. Release* **2008**, *127*, 189-207.

329. Altomare, L.; Bonetti, L.; Campiglio, C. E.; De Nardo, L.; Draghi, L.; Tana, F.; Farè, S., Biopolymer-Based Strategies in the Design of Smart Medical Devices and Artificial Organs. *Int. J. Artif. Organs* **2018**, *41*, 337-359.
330. Yang, Z.; Zhang, Y.; Markland, P.; Yang, V. C., Poly(Glutamic Acid) Poly(Ethylene Glycol) Hydrogels Prepared by Photoinduced Polymerization: Synthesis, Characterization, and Preliminary Release Studies of Protein Drugs. *J. Biomed. Mater. Res.* **2002**, *62*, 14-21.
331. Chang, C. J.; Swift, G., Poly(Aspartic Acid) Hydrogel. *J. Macromol. Sci. A* **1999**, *36*, 963-970.
332. Zhao, C.; Zhuang, X.; He, P.; Xiao, C.; He, C.; Sun, J.; Chen, X.; Jing, X., Synthesis of Biodegradable Thermo- and Ph-Responsive Hydrogels for Controlled Drug Release. *Polymer* **2009**, *50*, 4308-4316.
333. Chen, Y.; Pang, X.-H.; Dong, C.-M., Dual Stimuli-Responsive Supramolecular Polypeptide-Based Hydrogel and Reverse Micellar Hydrogel Mediated by Host-Guest Chemistry. *Adv. Funct. Mater.* **2010**, *20*, 579-586.
334. Zhang, Z.; Chen, L.; Deng, M.; Bai, Y.; Chen, X.; Jing, X., Biodegradable Thermo- and Ph-Responsive Hydrogels for Oral Drug Delivery. *J. Polym. Sci. A Polym. Chem.* **2011**, *49*, 2941-2951.
335. Zhang, Z.; Chen, L.; Zhao, C.; Bai, Y.; Deng, M.; Shan, H.; Zhuang, X.; Chen, X.; Jing, X., Thermo- and Ph-Responsive Hpc-G-Aa/Aa Hydrogels for Controlled Drug Delivery Applications. *Polymer* **2011**, *52*, 676-682.
336. Takeuchi, Y.; Uyama, H.; Tomoshige, N.; Watanabe, E.; Tachibana, Y.; Kobayashi, S., Injectable Thermoreversible Hydrogels Based on Amphiphilic Poly(Amino Acid)s. *J. Polym. Sci. A Polym. Chem.* **2006**, *44*, 671-675.
337. Takeuchi, Y.; Tsujimoto, T.; Uyama, H., Thermogelation of Amphiphilic Poly(Asparagine) Derivatives. *Polym. Adv. Technol.* **2011**, *22*, 620-626.

338. Moon, J. R.; Park, Y. H.; Kim, J.-H., Synthesis and Characterization of Novel Thermo- and Ph-Responsive Copolymers Based on Amphiphilic Polyaspartamides. *J. Appl. Polym. Sci.* **2009**, *111*, 998-1004.
339. Moon, J. R.; Jeon, Y. S.; Chung, D. J.; Kim, D.; Kim, J.-H., In Situ Gelling and Drug Release Behavior from Novel Temperature-Sensitive Polyaspartamides. *Macromol. Res.* **2011**, *19*, 515-518.
340. Jeong, B.; Kim, S. W.; Bae, Y. H., Thermosensitive Sol–Gel Reversible Hydrogels. *Adv. Drug Deliv. Rev.* **2012**, *64*, 154-162.
341. Yu, L.; Ding, J., Injectable Hydrogels as Unique Biomedical Materials. *Chem. Soc. Rev.* **2008**, *37*, 1473-1481.
342. Burdick, J. A.; Prestwich, G. D., Hyaluronic Acid Hydrogels for Biomedical Applications. *Adv. Mater.* **2011**, *23*, H41-H56.
343. Jin, R.; Moreira Teixeira, L. S.; Dijkstra, P. J.; van Blitterswijk, C. A.; Karperien, M.; Feijen, J., Enzymatically-Crosslinked Injectable Hydrogels Based on Biomimetic Dextran–Hyaluronic Acid Conjugates for Cartilage Tissue Engineering. *Biomaterials* **2010**, *31*, 3103-3113.
344. Sakai, S.; Yamada, Y.; Zenke, T.; Kawakami, K., Novel Chitosan Derivative Soluble at Neutral Ph and in-Situ Gellable Via Peroxidase-Catalyzed Enzymatic Reaction. *J. Mater. Chem.* **2009**, *19*, 230-235.
345. Balakrishnan, B.; Jayakrishnan, A., Self-Cross-Linking Biopolymers as Injectable in Situ Forming Biodegradable Scaffolds. *Biomaterials* **2005**, *26*, 3941-3951.
346. Yang, C.-Y.; Song, B.; Ao, Y.; Nowak, A. P.; Abelowitz, R. B.; Korsak, R. A.; Havton, L. A.; Deming, T. J.; Sofroniew, M. V., Biocompatibility of Amphiphilic Diblock Copolypeptide Hydrogels in the Central Nervous System. *Biomaterials* **2009**, *30*, 2881-2898.
347. Choi, Y. Y.; Joo, M. K.; Sohn, Y. S.; Jeong, B., Significance of Secondary Structure in Nanostructure Formation and Thermosensitivity of Polypeptide Block Copolymers. *Soft Matter* **2008**, *4*, 2383-2387.

348. Kabanov, A. V.; Vinogradov, S. V., Nanogels as Pharmaceutical Carriers: Finite Networks of Infinite Capabilities. *Angew. Chem. Int. Ed.* **2009**, *48*, 5418-5429.
349. Smith, M. H.; Lyon, L. A., Multifunctional Nanogels for Sirna Delivery. *Acc. Chem. Res.* **2012**, *45*, 985-993.
350. Hendrickson, G. R.; Smith, M. H.; South, A. B.; Lyon, L. A., Design of Multiresponsive Hydrogel Particles and Assemblies. *Adv. Funct. Mater.* **2010**, *20*, 1697-1712.
351. Jiang, Z.; Chen, J.; Cui, L.; Zhuang, X.; Ding, J.; Chen, X., Advances in Stimuli-Responsive Polypeptide Nanogels. *Small Methods* **2018**, *2*, 1700307.
352. Wang, J.; Xu, W.; Zhang, N.; Yang, C.; Xu, H.; Wang, Z.; Li, B.; Ding, J.; Chen, X., X-Ray-Responsive Polypeptide Nanogel for Concurrent Chemoradiotherapy. *J. Control. Release* **2021**, *332*, 1-9.
353. Ding, J.; Xu, W.; Zhang, Y.; Sun, D.; Xiao, C.; Liu, D.; Zhu, X.; Chen, X., Self-Reinforced Endocytoses of Smart Polypeptide Nanogels for "on-Demand" Drug Delivery. *J. Control. Release* **2013**, *172*, 444-455.
354. Sasaki, Y.; Akiyoshi, K., Nanogel Engineering for New Nanobiomaterials: From Chaperoning Engineering to Biomedical Applications. *Chem. Record* **2010**, *10*, 366-376.
355. Sun, J.; Chen, X.; Lu, T.; Liu, S.; Tian, H.; Guo, Z.; Jing, X., Formation of Reversible Shell Cross-Linked Micelles from the Biodegradable Amphiphilic Diblock Copolymer Poly(L-Cysteine)-Block-Poly(L-Lactide). *Langmuir* **2008**, *24*, 10099-10106.
356. Kakizawa, Y.; Harada, A.; Kataoka, K., Environment-Sensitive Stabilization of Core-Shell Structured Polyion Complex Micelle by Reversible Cross-Linking of the Core through Disulfide Bond. *J. Am. Chem. Soc.* **1999**, *121*, 11247-11248.

357. Ding, J.; Zhuang, X.; Xiao, C.; Cheng, Y.; Zhao, L.; He, C.; Tang, Z.; Chen, X., Preparation of Photo-Cross-Linked Ph-Responsive Polypeptide Nanogels as Potential Carriers for Controlled Drug Delivery. *J. Mater. Chem.* **2011**, *21*, 11383-11391.
358. Xu, H.; Yao, Q.; Cai, C.; Gou, J.; Zhang, Y.; Zhong, H.; Tang, X., Amphiphilic Poly(Amino Acid) Based Micelles Applied to Drug Delivery: The in Vitro and in Vivo Challenges and the Corresponding Potential Strategies. *J. Control. Release* **2015**, *199*, 84-97.
359. Sill, K. N.; Sullivan, B.; Carie, A.; Semple, J. E., Synthesis and Characterization of Micelle-Forming Peg-Poly(Amino Acid) Copolymers with Iron-Hydroxamate Cross-Linkable Blocks for Encapsulation and Release of Hydrophobic Drugs. *Biomacromolecules* **2017**, *18*, 1874-1884.
360. Gu, X.; Qiu, M.; Sun, H.; Zhang, J.; Cheng, L.; Deng, C.; Zhong, Z., Polytyrosine Nanoparticles Enable Ultra-High Loading of Doxorubicin and Rapid Enzyme-Responsive Drug Release. *Biomater. Sci.* **2018**, *6*, 1526-1534.
361. Yi, H.; Liu, P.; Sheng, N.; Gong, P.; Ma, Y.; Cai, L., In Situ Crosslinked Smart Polypeptide Nanoparticles for Multistage Responsive Tumor-Targeted Drug Delivery. *Nanoscale* **2016**, *8*, 5985-5995.
362. Shirbin, S. J.; Ladewig, K.; Fu, Q.; Klimak, M.; Zhang, X.; Duan, W.; Qiao, G. G., Cisplatin-Induced Formation of Biocompatible and Biodegradable Polypeptide-Based Vesicles for Targeted Anticancer Drug Delivery. *Biomacromolecules* **2015**, *16*, 2463-2474.
363. Ahmed, M., Peptides, Polypeptides and Peptide-Polymer Hybrids as Nucleic Acid Carriers. *Biomater. Sci.* **2017**, *5*, 2188-2211.
364. Walsh, D. P.; Raftery, R. M.; Castaño, I. M.; Murphy, R.; Cavanagh, B.; Heise, A.; O'Brien, F. J.; Cryan, S.-A., Transfection of Autologous Host Cells in Vivo Using Gene Activated Collagen Scaffolds Incorporating Star-Polypeptides. *J. Control. Release* **2019**, *304*, 191-203.

365. Chen, B.; Yu, L.; Li, Z.; Wu, C., Design of Free Triblock Polylysine-B-Polyleucine-B-Polylysine Chains for Gene Delivery. *Biomacromolecules* **2018**, *19*, 1347-1357.
366. Wyrsta, M. D.; Cogen, A. L.; Deming, T. J., A Parallel Synthetic Approach for the Analysis of Membrane Interactive Copolypeptides. *J. Am. Chem. Soc.* **2001**, *123*, 12919-12920.
367. Zhou, C.; Qi, X.; Li, P.; Chen, W. N.; Mouad, L.; Chang, M. W.; Leong, S. S. J.; Chan-Park, M. B., High Potency and Broad-Spectrum Antimicrobial Peptides Synthesized Via Ring-Opening Polymerization of α -Aminoacid-N-Carboxyanhydrides. *Biomacromolecules* **2010**, *11*, 60-67.
368. Chen, Y.-F.; Lai, Y.-D.; Chang, C.-H.; Tsai, Y.-C.; Tang, C.-C.; Jan, J.-S., Star-Shaped Polypeptides Exhibit Potent Antibacterial Activities. *Nanoscale* **2019**, *11*, 11696-11708.
369. Pranantyo, D.; Xu, L. Q.; Hou, Z.; Kang, E.-T.; Chan-Park, M. B., Increasing Bacterial Affinity and Cytocompatibility with Four-Arm Star Glycopolymers and Antimicrobial α -Polylysine. *Polym. Chem.* **2017**, *8*, 3364-3373.
370. Zhang, C.; Lu, J.; Hou, Y.; Xiong, W.; Sheng, K.; Lu, H., Investigation on the Linker Length of Synthetic Zwitterionic Polypeptides for Improved Nonfouling Surfaces. *ACS Appl. Mater. Interfaces* **2018**, *10*, 17463-17470.
371. Yoo, J.; Birke, A.; Kim, J.; Jang, Y.; Song, S. Y.; Ryu, S.; Kim, B.-S.; Kim, B.-G.; Barz, M.; Char, K., Cooperative Catechol-Functionalized Polypept(O)ide Brushes and Ag Nanoparticles for Combination of Protein Resistance and Antimicrobial Activity on Metal Oxide Surfaces. *Biomacromolecules* **2018**, *19*, 1602-1613.
372. Zhang, C.; Yuan, J.; Lu, J.; Hou, Y.; Xiong, W.; Lu, H., From Neutral to Zwitterionic Poly(α -Amino Acid) Nonfouling Surfaces: Effects of Helical Conformation and Anchoring Orientation. *Biomaterials* **2018**, *178*, 728-737.

373. Yamamoto, H.; Hayakawa, T., Improved Synthetic Method and Conformation Studies of Polymers and Copolymers of L-B-3,4-Dihydroxyphenyl-A-Alanine with L-Glutamic Acid. *Polymer* **1978**, *19*, 1115-1117.
374. Yamamoto, H.; Nagai, A.; Okada, T.; Nishida, A., Synthesis and Adhesive Studies of Barnacle Model Proteins. *Mar. Chem.* **1989**, *26*, 331-338.
375. Yu, M.; Deming, T. J., Synthetic Polypeptide Mimics of Marine Adhesives. *Macromolecules* **1998**, *31*, 4739-4745.
376. Bornstein, M. B.; Miller, A. I.; Teitelbaum, D.; Arnon, R.; Sela, M., Multiple Sclerosis: Trial of a Synthetic Polypeptide. *Ann. Neurol.* **1982**, *11*, 317-319.
377. Fridkis-Hareli, M.; Rosloniec, E. F.; Fugger, L.; Strominger, J. L., Synthetic Amino Acid Copolymers That Bind to Hla-Dr Proteins and Inhibit Type Ii Collagen-Reactive T Cell Clones. *Proc. Natl. Acad. Sci.* **1998**, *95*, 12528-12531.
378. Deming, T. J., Synthesis and Self-Assembly of Well-Defined Block Copolypeptides Via Controlled Nca Polymerization. In *Advances in Polymer Science*, Percec, V., Ed. Springer International Publishing: Cham, 2013; Vol. 262, pp 1-37.
379. Song, Z.; Fu, H.; Wang, R.; Pacheco, L. A.; Wang, X.; Lin, Y.; Cheng, J., Secondary Structures in Synthetic Polypeptides from N-Carboxyanhydrides: Design, Modulation, Association, and Material Applications. *Chem. Soc. Rev.* **2018**, *47*, 7401-7425.
380. Mochida, Y.; Cabral, H.; Miura, Y.; Albertini, F.; Fukushima, S.; Osada, K.; Nishiyama, N.; Kataoka, K., Bundled Assembly of Helical Nanostructures in Polymeric Micelles Loaded with Platinum Drugs Enhancing Therapeutic Efficiency against Pancreatic Tumor. *ACS Nano* **2014**, *8*, 6724-6738.

381. Chen, B.-Y.; Huang, Y.-F.; Huang, Y.-C.; Wen, T.-C.; Jan, J.-S., Alkyl Chain-Grafted Poly(L-Lysine) Vesicles with Tunable Molecular Assembly and Membrane Permeability. *ACS Macro Lett.* **2014**, *3*, 220-223.
382. Johnson, R. P.; Uthaman, S.; John, J. V.; Lee, H. R.; Lee, S. J.; Park, H.; Park, I.-K.; Suh, H.; Kim, I., Poly(Pega)-B-Poly(L-Lysine)-B-Poly(L-Histidine) Hybrid Vesicles for Tumoral Ph-Triggered Intracellular Delivery of Doxorubicin Hydrochloride. *ACS Appl. Mater. Interfaces* **2015**, *7*, 21770-21779.
383. Lee, E. S.; Kim, J. H.; Sim, T.; Youn, Y. S.; Lee, B.-J.; Oh, Y. T.; Oh, K. T., A Feasibility Study of a Ph Sensitive Nanomedicine Using Doxorubicin Loaded Poly(Aspartic Acid-Graft-Imidazole)-Block-Poly(Ethylene Glycol) Micelles. *J. Mater. Chem. B* **2014**, *2*, 1152-1159.
384. Chen, P.; Qiu, M.; Deng, C.; Meng, F.; Zhang, J.; Cheng, R.; Zhong, Z., Ph-Responsive Chimaeric Pepsomes Based on Asymmetric Poly(Ethylene Glycol)-B-Poly(L-Leucine)-B-Poly(L-Glutamic Acid) Triblock Copolymer for Efficient Loading and Active Intracellular Delivery of Doxorubicin Hydrochloride. *Biomacromolecules* **2015**, *16*, 1322-1330.
385. Iatrou, H.; Dimas, K.; Gkikas, M.; Tsimblouli, C.; Sofianopoulou, S., Polymersomes from Polypeptide Containing Triblock Co- and Terpolymers for Drug Delivery against Pancreatic Cancer: Asymmetry of the External Hydrophilic Blocks. *Macromol. Biosci.* **2014**, *14*, 1222-1238.
386. Qiu, R.; Qian, F.; Wang, X.; Li, H.; Wang, L., Targeted Delivery of 20(S)-Ginsenoside Rg3-Based Polypeptide Nanoparticles to Treat Colon Cancer. *Biomed. Microdevices* **2019**, *21*, 18.
387. Chen, Y.; Li, X.; Xiao, H.; Xiao, J.; Li, B.; Chen, X.; Wang, Y.; Cheng, D.; Shuai, X., Reduction and Ph Dual-Sensitive Nanovesicles Co-Delivering Doxorubicin and Gefitinib for Effective Tumor Therapy. *RSC Adv.* **2018**, *8*, 2082-2091.

388. Yin, H.; Kanasty, R. L.; Eltoukhy, A. A.; Vegas, A. J.; Dorkin, J. R.; Anderson, D. G., Non-Viral Vectors for Gene-Based Therapy. *Nat. Rev. Genet.* **2014**, *15*, 541-555.
389. Chen, J.; Guan, X.; Hu, Y.; Tian, H.; Chen, X., Peptide-Based and Polypeptide-Based Gene Delivery Systems. In *Top. Curr. Chem.*, Cheng, Y., Ed. Springer International Publishing: Cham, 2018; pp 85-112.
390. Pack, D. W.; Hoffman, A. S.; Pun, S.; Stayton, P. S., Design and Development of Polymers for Gene Delivery. *Nat. Rev. Drug Discov.* **2005**, *4*, 581-593.
391. Thomas, C. E.; Ehrhardt, A.; Kay, M. A., Progress and Problems with the Use of Viral Vectors for Gene Therapy. *Nat. Rev. Genet.* **2003**, *4*, 346-358.
392. Mintzer, M. A.; Simanek, E. E., Nonviral Vectors for Gene Delivery. *Chem. Rev.* **2009**, *109*, 259-302.
393. Byrne, M.; Murphy, R.; Kapetanakis, A.; Ramsey, J.; Cryan, S.-A.; Heise, A., Star-Shaped Polypeptides: Synthesis and Opportunities for Delivery of Therapeutics. *Macromol. Rapid Commun.* **2015**, *36*, 1862-1876.
394. Johnson, R. P.; Uthaman, S.; John, J. V.; Heo, M. S.; Park, I. K.; Suh, H.; Kim, I., Poly(2-Hydroxyethyl Methacrylate)-B-Poly(L-Lysine) Cationic Hybrid Materials for Non-Viral Gene Delivery in Nih 3t3 Mouse Embryonic Fibroblasts. *Macromol. Biosci.* **2014**, *14*, 1239-1248.
395. Lam, S. J.; Sulistio, A.; Ladewig, K.; Wong, E. H. H.; Blencowe, A.; Qiao, G. G., Peptide-Based Star Polymers as Potential Sirna Carriers. *Aust. J. Chem.* **2014**, *67*, 592-597.
396. Veleva-Kostadinova, E.; Dimitrov, I.; Toncheva-Moncheva, N.; Novakov, C.; Momekova, D.; Rangelov, S., Nanoparticulate Polyelectrolyte Complexes of Thermally Sensitive Poly(L-Lysine)-Based Copolymers and DNA. *Eur. Polym. J.* **2018**, *102*, 219-230.

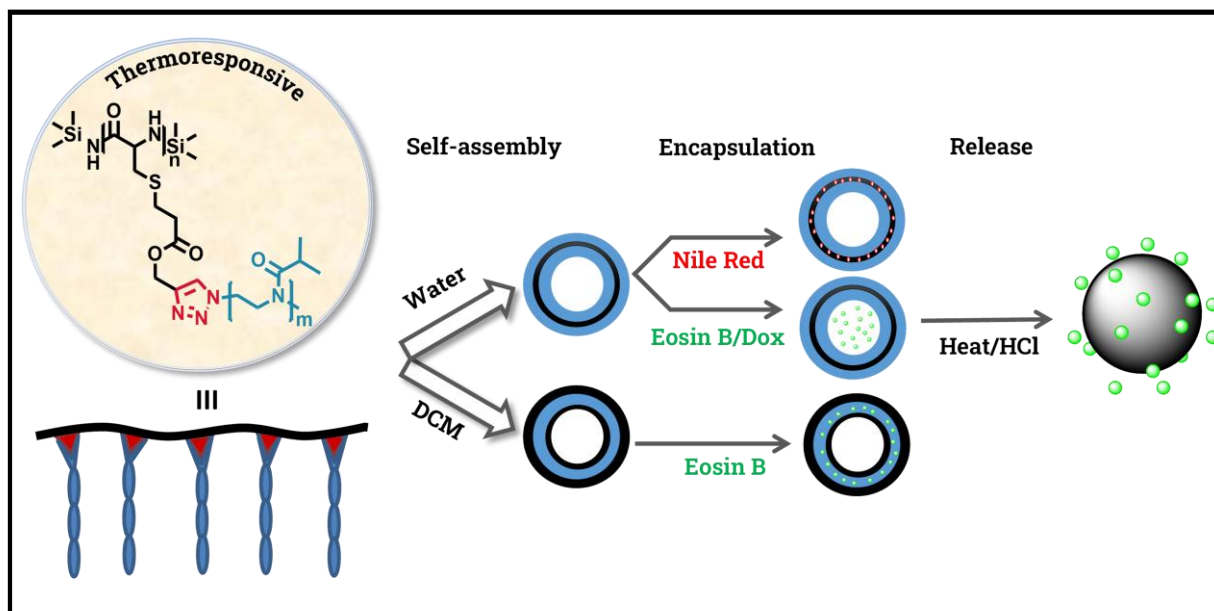
397. Zhang, R.; Zheng, N.; Song, Z.; Yin, L.; Cheng, J., The Effect of Side-Chain Functionality and Hydrophobicity on the Gene Delivery Capabilities of Cationic Helical Polypeptides. *Biomaterials* **2014**, *35*, 3443-3454.
398. Dang, J.; Ye, H.; Li, Y.; Liang, Q.; Li, X.; Yin, L., Multivalency-Assisted Membrane-Penetrating Sirna Delivery Sensitizes Photothermal Ablation Via Inhibition of Tumor Glycolysis Metabolism. *Biomaterials* **2019**, *223*, 119463.
399. Li, F.; Li, Y.; Zhou, Z.; Lv, S.; Deng, Q.; Xu, X.; Yin, L., Engineering the Aromaticity of Cationic Helical Polypeptides toward "Self-Activated" DNA/Sirna Delivery. *ACS Appl. Mater. Interfaces* **2017**, *9*, 23586-23601.
400. Huang, J.; Heise, A., Stimuli Responsive Synthetic Polypeptides Derived from N-Carboxyanhydride (Nca) Polymerisation. *Chem. Soc. Rev.* **2013**, *42*, 7373-7390.
401. Rosso, F.; Giordano, A.; Barbarisi, M.; Barbarisi, A., From Cell-Ecm Interactions to Tissue Engineering. *J. Cell. Physiol.* **2004**, *199*, 174-180.
402. O'Brien, F. J., Biomaterials & Scaffolds for Tissue Engineering. *Mater. Today* **2011**, *14*, 88-95.
403. Shirbin, S. J.; Karimi, F.; Chan, N. J.-A.; Heath, D. E.; Qiao, G. G., Macroporous Hydrogels Composed Entirely of Synthetic Polypeptides: Biocompatible and Enzyme Biodegradable 3d Cellular Scaffolds. *Biomacromolecules* **2016**, *17*, 2981-2991.
404. Jeschke, B.; Meyer, J.; Jonczyk, A.; Kessler, H.; Adamietz, P.; Meenen, N. M.; Kantlehner, M.; Goepfert, C.; Nies, B., Rgd-Peptides for Tissue Engineering of Articular Cartilage. *Biomaterials* **2002**, *23*, 3455-3463.
405. Ahrens, C. C.; Welch, M. E.; Griffith, L. G.; Hammond, P. T., Uncharged Helical Modular Polypeptide Hydrogels for Cellular Scaffolds. *Biomacromolecules* **2015**, *16*, 3774-3783.

406. Shinde, U. P.; Moon, H. J.; Ko, D. Y.; Jung, B. K.; Jeong, B., Control of Rhgh Release Profile from Peg–Paf Thermogel. *Biomacromolecules* **2015**, *16*, 1461-1469.
407. Park, M. H.; Moon, H. J.; Park, J. H.; Shinde, U. P.; Ko, D. Y.; Jeong, B., Peg-Poly(L-Alanine) Thermogel as a 3d Scaffold of Bone-Marrow-Derived Mesenchymal Stem Cells. *Macromol. Biosci.* **2015**, *15*, 464-472.
408. Wang, Y.; Jiang, Z.; Xu, W.; Yang, Y.; Zhuang, X.; Ding, J.; Chen, X., Chiral Polypeptide Thermogels Induce Controlled Inflammatory Response as Potential Immunoadjuvants. *ACS Appl. Mater. Interfaces* **2019**, *11*, 8725-8730.
409. Hancock, R. E. W.; Lehrer, R., Cationic Peptides: A New Source of Antibiotics. *Trends Biotechnol.* **1998**, *16*, 82-88.
410. Ghadiri, M. R.; Granja, J. R.; Milligan, R. A.; McRee, D. E.; Khazanovich, N., Self-Assembling Organic Nanotubes Based on a Cyclic Peptide Architecture. *Nature* **1993**, *366*, 324-327.
411. Walsh, C., *Antibiotics: Actions, Origins, Resistance*, American Society for Microbiology (ASM), 2003.
412. Li, P.; Zhou, C.; Rayatpisheh, S.; Ye, K.; Poon, Y. F.; Hammond, P. T.; Duan, H.; Chan-Park, M. B., Cationic Peptidopolysaccharides Show Excellent Broad-Spectrum Antimicrobial Activities and High Selectivity. *Adv. Mater.* **2012**, *24*, 4130-4137.
413. Nakamura, R.; Aoi, K.; Okada, M., Controlled Synthesis of a Chitosan-Based Graft Copolymer Having Polysarcosine Side Chains Using the Nca Method with a Carboxylic Acid Additive. *Macromol. Rapid Commun.* **2006**, *27*, 1725-1732.
414. Zhang, Y.; Song, W.; Li, S.; Kim, D.-K.; Kim, J. H.; Kim, J. R.; Kim, I., Facile and Scalable Synthesis of Topologically Nanoengineered Polypeptides with Excellent Antimicrobial Activities. *Chem. Commun.* **2020**, *56*, 356-359.

415. Gao, J.; Wang, M.; Wang, F.; Du, J., Synthesis and Mechanism Insight of a Peptide-Grafted Hyperbranched Polymer Nanosheet with Weak Positive Charges but Excellent Intrinsically Antibacterial Efficacy. *Biomacromolecules* **2016**, *17*, 2080-2086.
416. Lam, S. J., et al., Combating Multidrug-Resistant Gram-Negative Bacteria with Structurally Nanoengineered Antimicrobial Peptide Polymers. *Nat. Microbiol.* **2016**, *1*, 16162.
417. Kimmins, S. D., et al., Antimicrobial and Degradable Triazolinedione (Tad) Crosslinked Polypeptide Hydrogels. *J. Mater. Chem. B* **2021**, *9*, 5456-5464.
418. Xiong, M., et al., Helical Antimicrobial Polypeptides with Radial Amphiphilicity. *Proc. Natl. Acad. Sci.* **2015**, *112*, 13155-13160.
419. Zhou, C.; Wang, M.; Zou, K.; Chen, J.; Zhu, Y.; Du, J., Antibacterial Polypeptide-Grafted Chitosan-Based Nanocapsules as an "Armed" Carrier of Anticancer and Antiepileptic Drugs. *ACS Macro Lett.* **2013**, *2*, 1021-1025.
420. Wang, M.; Zhou, C.; Chen, J.; Xiao, Y.; Du, J., Multifunctional Biocompatible and Biodegradable Folic Acid Conjugated Poly(E-Caprolactone)-Polypeptide Copolymer Vesicles with Excellent Antibacterial Activities. *Bioconjugate Chem.* **2015**, *26*, 725-734.
421. Bevilacqua, M. P.; Huang, D. J.; Wall, B. D.; Lane, S. J.; Edwards III, C. K.; Hanson, J. A.; Benitez, D.; Solomkin, J. S.; Deming, T. J., Amino Acid Block Copolymers with Broad Antimicrobial Activity and Barrier Properties. *Macromol. Biosci.* **2017**, *17*, 1600492.
422. Shirbin, S. J.; Lam, S. J.; Chan, N. J.-A.; Ozmen, M. M.; Fu, Q.; O'Brien-Simpson, N.; Reynolds, E. C.; Qiao, G. G., Polypeptide-Based Macroporous Cryogels with Inherent Antimicrobial Properties: The Importance of a Macroporous Structure. *ACS Macro Lett.* **2016**, *5*, 552-557.

Chapter 2: LCST Polypeptide

Thermoresponsive Amphiphilic Poly(L-Cysteine): Synthesis, Self-Assembly and Guest Encapsulation/Release



2.1. Introduction

Polypeptides, with identical or diverse sequences of amino acids, play crucial roles in a wide range of biological functionalities.¹⁻³ However, the limited solubility of synthetic polypeptides, particularly in water and other solvents, has prompted numerous research groups to focus on enhancing their solubility. One effective approach to achieving water solubilization of polypeptides is through functionalization with hydrophilic polymers. These modified polypeptides possess remarkable biodegradability and biocompatibility, making them highly valuable in various biomedical applications such as tissue engineering, bio-inspired materials, and controlled release systems.⁴⁻⁷ While polypeptides composed of a single amino acid may not fully satisfy the requirements of diverse biomedical applications,⁸⁻⁹ there is a growing demand for polypeptide-polymer conjugates and copolypeptides in the field of biomedicine.¹⁰⁻¹¹ These conjugates exhibit improved mechanical properties due to the incorporation of synthetic polymeric components.¹²⁻¹⁴ Moreover, amphiphilic polypeptide-based conjugates, coupled with responsive polymeric constituents, readily form nanoaggregates (e.g., micelles, vesicles). These nanoaggregates are highly valuable for the development of sustainable drug and gene carriers in solution, thanks to their responsiveness to factors such as pH, light, ionic strength, or redox systems.¹⁵⁻¹⁸ Functionalizing polypeptides with poly(ethylene glycol) (PEG) or other polymers enhances their enzymatic and chemical stabilities, which is a critical requirement in numerous applications, including tissue engineering and delivery vehicles.¹⁹⁻²⁰

To date, various pathways have been employed, often involving controlled polymerization techniques, to synthesize conjugates, block/graft copolypeptides, and other related structures.²¹⁻²⁴ For instance, Ahrens et al. utilized a "click" reaction to synthesize a poly(L-glutamic acid)-based hydrogel for potential use as an extracellular matrix.²⁵ Guo et al. achieved the synthesis of a copolymer conjugate consisting of poly(γ -benzyl-L-glutamate) and

polytetrahydrofuran through controlled termination of living polytetrahydrofuran chains with functional -NH- groups along the poly(γ -benzyl-L-glutamate) backbone.²⁶ Incorporating thermoresponsive properties into amphiphilic polypeptide conjugates and block/graft copolymers has expanded their potential as delivery agents.²⁷⁻²⁹ Consequently, numerous studies have focused on developing thermoresponsive polymeric materials of this kind.³⁰⁻³³

However, it is worth noting that thermoresponsive, polypeptide-based block/graft conjugates have been relatively less explored, despite their greater biocompatibility compared to nonpeptide-based materials. There have been a few endeavours to synthesize water-soluble polypeptide conjugates/copolymers with LCST or UCST behaviour, which exhibit changes in solubility in response to temperature variations.^{27, 31, 33-37} Deng et al. reported the synthesis of α -helical poly(L-glutamic acid) functionalized with oligo(ethylene glycol) (OEG) and 1-butylimidazolium groups as side chains, demonstrating LCST and UCST behaviour in water.³⁸ The intriguing thermoresponsive characteristics of these materials make them promising candidate for the development of amphiphilic polypeptide-polymer conjugate nanostructures, such as micelles, vesicles, and hydrogels, for controlled drug delivery applications.³⁹ The thermoresponsive behaviour of graft conjugates can also be modulated by adjusting the length and composition of the pendant polymer/polypeptide block, as well as the length of the backbone.^{21, 27}

Hence, there exists significant potential for the development of novel polypeptide-based graft/block copolymers/conjugates that can be tailored to exhibit desired thermoresponsive and self-assembly properties through modifications in the chemical composition, lengths, and side chains of the backbone. While amphiphilic graft copolymers composed of two synthetic polymer blocks have been extensively investigated by various research

groups,⁴⁰⁻⁴³ there is limited literature available on polypeptide/peptide-based graft copolymers.^{27, 44}

Extensive research conducted by various groups has demonstrated the formation of self-assembled vesicles using block/graft copolymers with different polymer blocks.⁴⁵⁻⁴⁸ Moreover, the solution self-assembly of amphiphilic copolymers into nanostructures can be easily controlled by adjusting the graft/block length and graft densities in graft copolymers.^{27, 49} Thermoresponsive copolymer vesicles are particularly advantageous for their potential applications in controlled drug delivery. However, the literature on self-assembled vesicles from such copolymers remains limited. Furthermore, there is a scarcity of scientific reports specifically focusing on the synthesis of polypeptide-based graft copolymers and the detailed investigation of their self-assembly into various nanostructures in solution.⁵⁰⁻⁵² Particularly, the formation of vesicular structures and the encapsulation of guest molecules within these polypeptide-based systems are rarely reported.

2.2. Objective and Scope

Synthetic polypeptides possess excellent self-assembling properties and are biologically active materials. However, their hydrophobic nature limits their applicability in biomedical fields. On the other hand, pseudopeptidic poly(2-oxazoline)s are bio-inspired polymers with good solubility in water. Therefore, it would be nice to design diverse amphiphilic polypeptide-based graft copolymers with varying graft lengths and explore their self-assembly behaviour in solution. Additionally, the introduction of a thermoresponsive polymer block through grafting would lead to the development of even more intriguing materials for further study. Notably, graft conjugates incorporating polycysteine (PCys) and poly(2-isopropyl-2-oxazoline) (P²POx) have not been reported thus far. Therefore, the aim of this research work is to combine these two components and create amphiphilic copolypeptides that have a strong

tendency to self-assemble into vesicular nanostructures. These vesicles hold great promise for a wide range of potential applications.

This report presents a convenient synthesis method for water-soluble amphiphilic polycysteine-*graft*-poly(2-isopropyl-2-oxazoline) (PCys-*g*-PⁱPOx) graft copolymers with varying graft lengths using click chemistry. The PCys and PⁱPOx blocks were synthesized through ROP of corresponding NCA and cationic ring-opening polymerization (CROP) of 2-isopropyl-2-oxazoline (POx), respectively. PⁱPOx homopolymer exhibits a tunable LCST behaviour in aqueous solutions.⁵³ Intriguingly, the LCST phase behaviour of PCys-*g*-PiPOx copolymers can be easily controlled by adjusting the concentration and the length of the PCys and pendent PiPOx chains. In contrast to typical micelle formation observed in similar graft conjugates, these amphiphilic PCys-*g*-PiPOx molecules self-assemble into vesicles both in aqueous and nonaqueous (DCM) media.⁵⁴⁻⁵⁷ Moreover, these PCys-*g*-PiPOx vesicles efficiently encapsulate hydrophilic guest molecules (such as Eosin B) from both aqueous and nonaqueous media, as well as hydrophobic guest molecules (like Nile Red) from water. The encapsulation and release efficiency of the drug Doxorubicin by these vesicles are evaluated using spectroscopic and microscopic techniques.

While previous literature reports the formation of copolymer vesicles and demonstrates guest molecule encapsulation, and most studies focus on either aqueous or nonaqueous media.⁵⁸⁻⁵⁹ The thermoresponsive nature of these copolymers offers an additional advantage, as the formed vesicles exhibit responsiveness and can be employed for sustained delivery. A proposed mechanism is provided to explain the formation of these unusual vesicular aggregates and the mode of guest molecule encapsulation.

2.3. Experimental

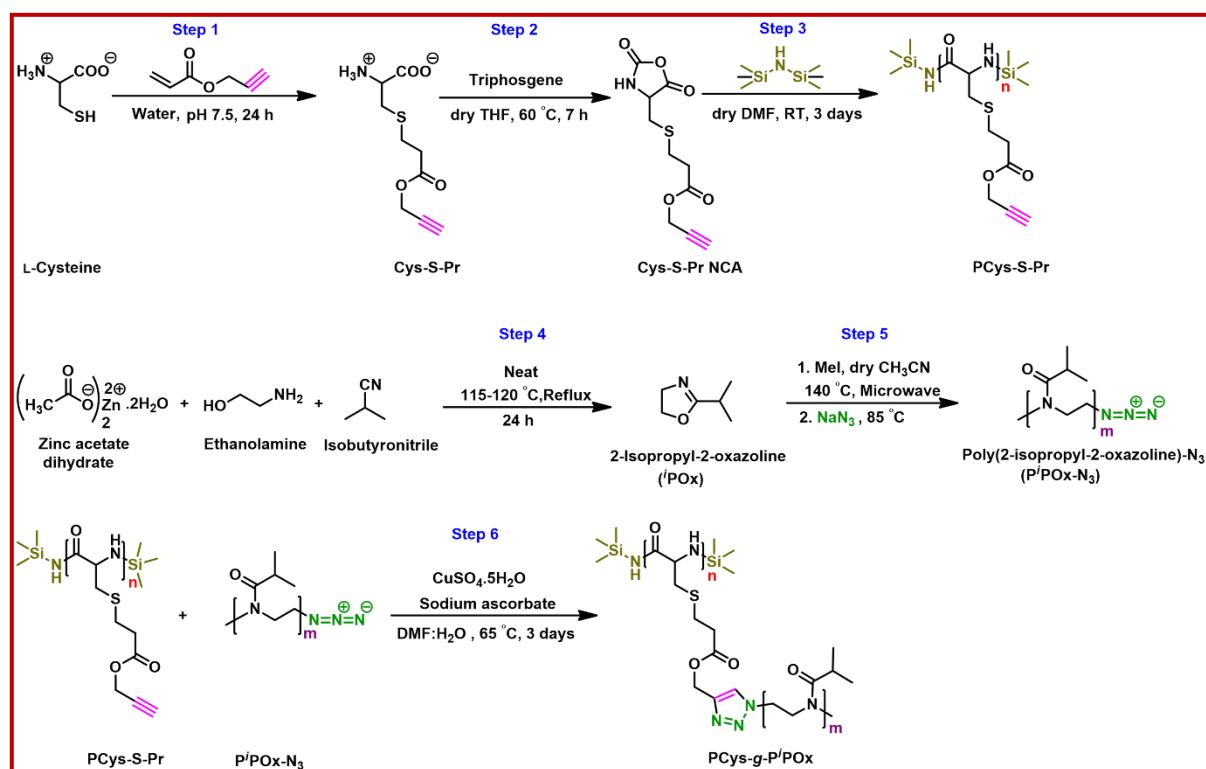
2.3.1. Materials

L-Cysteine (SRL, India), propargyl acrylate (98%; Aldrich), 1,1,1,3,3,3-hexamethyl disilazane (HMDS) (99.9%; Aldrich), triphosgene (>98%; TCI), isobutyronitrile (TCI), Doxorubicin hydrochloride (TCI) and methyl iodide (MeI) (Spectrochem, India) were used as received from the respective companies. Ethanol amine, sodium hydroxide, zinc acetate (dihydrate), sodium ascorbate, copper sulphate (pentahydrate), acetone, ethyl acetate, tetrahydrofuran (THF), N, N-dimethylformamide (DMF), hexane, acetonitrile were purchased from Merck. NaN₃ (Aldrich) was recrystallized from hot water before use. DMF and acetonitrile were distilled over calcium hydride under reduce pressure and kept over molecular sieve (Linde 4Å) before use. THF was distilled over metallic sodium prior to use. Acetone, ethyl acetate and hexane were used after distillation. All the aqueous solutions were prepared using Milli-Q water.

2.3.2. Synthetic Procedure

2.3.2.1. Synthesis of Propargyl L-Cysteine (Cys-S-Pr)

Cys-S-Pr was synthesized using the Michael reaction between L-cysteine and propargyl acrylate, following a modified version of a previously reported procedure (Scheme 2.1).²¹ In the synthesis, 2.0 g (16.5 mmol) of L-cysteine was dissolved in 25 mL of water, and the pH of the solution was adjusted to 7.5 by adding 0.1 N NaOH solution. The solution was stirred continuously for 30 minutes. Then, a solution of propargyl acrylate in acetone (2.7 g; 24.75 mmol/5 mL) was added dropwise to the basic solution over a period of 45 minutes at 25 °C with stirring. The reaction mixture was left to stir at room temperature for 24 hours. Afterward, the solution was neutralized with 0.5 N HCl, and the acetone was removed by evaporation using a rotary evaporator. The resulting aqueous solution was washed three times with ethyl acetate to eliminate any excess



Scheme 2.1. Synthetic pathways for PCys-*g*-P'POx graft copolymer.

propargyl acrylate. The product obtained was an off-white amorphous solid, which was further purified by lyophilization, yielding 91% of the desired product.

Characterization data: (Cys-S-Pr): FTIR (Figure 2.1), ESI-MS (Figure A2.1), ^1H -/ ^{13}C -NMR (Figure 2.2A and A2.2).

2.3.2.2. Synthesis of Cys-S-Pr NCA

Cys-S-Pr NCA was synthesized by modifying a previously reported procedure (Scheme 2.1).²⁷ In the synthesis, Cys-S-Pr (1.5 g; 6.48 mmol) and a small amount of charcoal were placed in a 100 mL double-necked round-bottom flask equipped with a bulb condenser and a rubber septum. The flask was heated under reduced pressure to remove any moisture, and then it was purged with nitrogen gas. Next, 10 mL of dry THF was added to the flask using a glass

syringe, resulting in a turbid suspension. A solution of triphosgene in THF (961.4 mg; 3.24 mmol/2 mL)

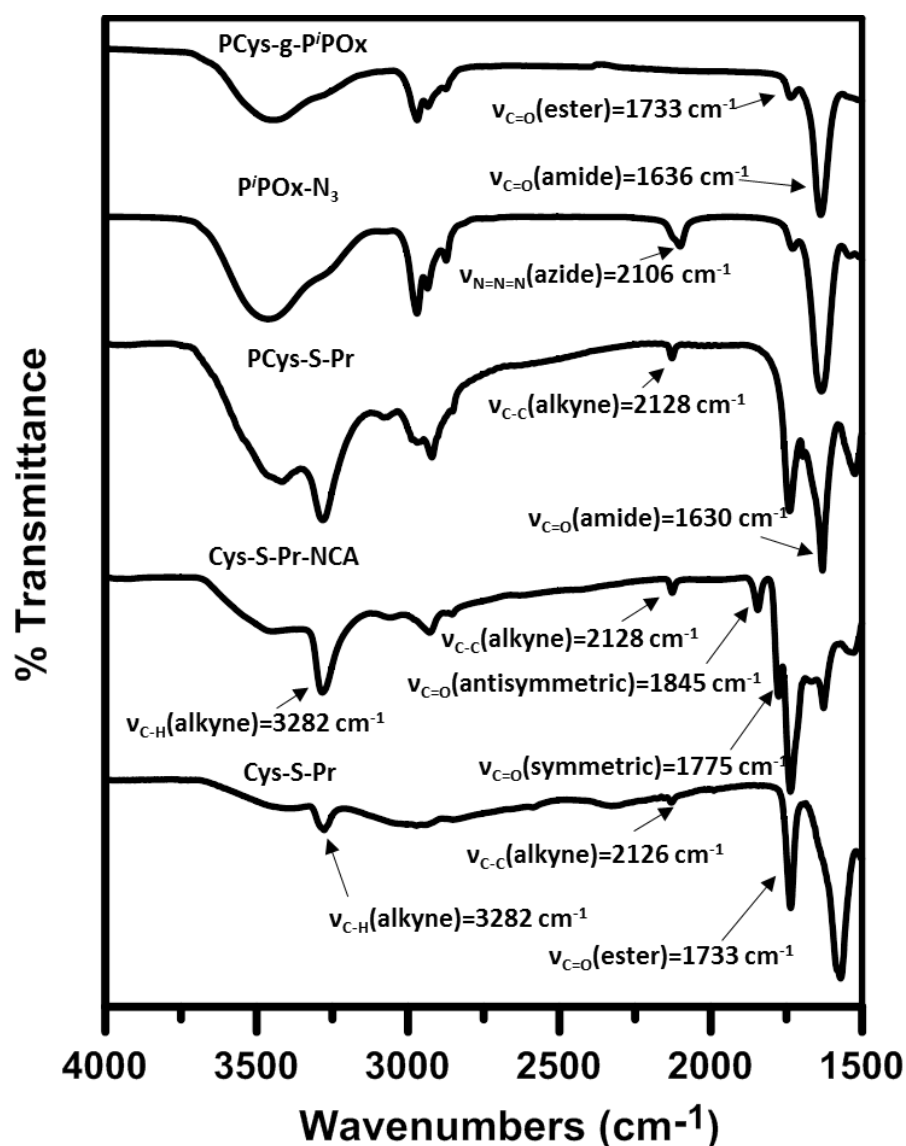


Figure 2.1. FT-IR spectra of all the compounds.

was added dropwise to the suspension. The reaction mixture was refluxed at 60 °C for 7 hours. After completion of the reaction, the brown-coloured solution containing the product was collected by centrifugation. The volume of the solution was reduced using a rotary evaporator. Subsequently, the brown sticky product was isolated by fractional precipitation from a concentrated THF

solution using cold hexane. Finally, the product was dried in a vacuum oven at 60 °C, resulting in a yield of 75.5%.

Characterization data: (Cys-S-Pr NCA): FTIR (Figure 2.1), MALDI-TOF-MS (Figure A2.3) and $^1\text{H}/^{13}\text{C}$ -NMR spectra (Figure 2.2B and A2.4).

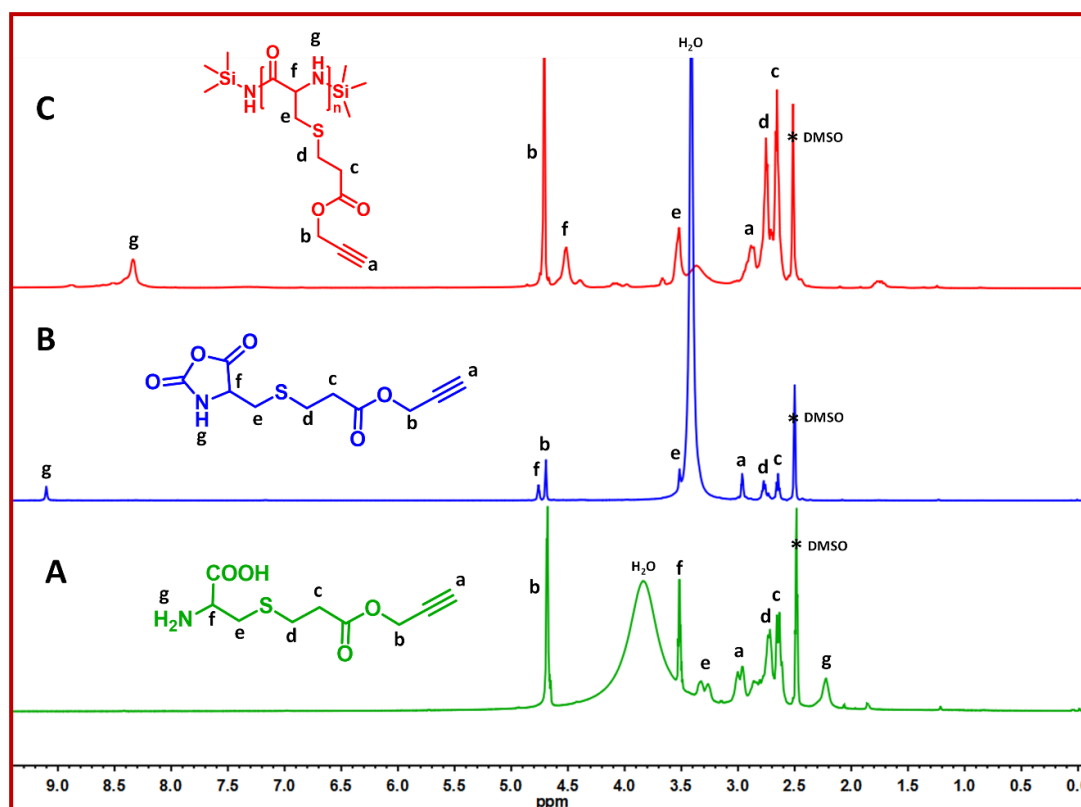


Figure 2.2. ^1H -NMR spectra of Cys-S-Pr (A), Cys-S-Pr NCA (B), PCys-S-Pr (C2) (C) in DMSO-d_6 .

2.3.2.3. Synthesis of 2-Isopropyl-2-oxazoline (^iPOx)

The ^iPOx monomer was synthesized by following the earlier reported protocol (Scheme 2.1).⁶⁰ At first zinc acetate dihydrate (2.86 g; 13.02 mmol) and isobutyronitrile (39 mL, 434.1 mmol) were taken in a 50 mL RB flask and heated at 120 °C for few minutes. Ethanolamine (31.5 mL; 520.9 mmol) was then added dropwise while refluxing the mixture at that temperature for 24 h. After that the whole solution was washed 3 times with water and 2 times with DCM and

finally distilled under reduced pressure to collect a colorless pure liquid product with almost 60% yield.

Characterization data: ESI-MS (Figure A2.5), ^1H -NMR (Figure A2.6) and ^{13}C -NMR (Figure A2.7).

2.3.2.4. ROP of Cys-S-Pr NCA by HMDS

The ring-opening polymerization (ROP) of Cys-S-Pr NCA was carried out at room temperature using HMDS as an initiator, following Scheme 2.1.²⁷ In the procedure, the as-synthesized Cys-S-Pr NCA (1.0 g; 3.88 mmol) was dissolved in dry DMF (3.0 mL) in a 25 mL round-bottom flask under a nitrogen atmosphere. Moisture and oxygen traces were eliminated from the mixture using the rapid freeze-pump-thaw technique. A DMF solution of HMDS (41 μL ; 0.194 mmol/0.5 mL) was added dropwise using a syringe, and the mixture was magnetically stirred for 72 h. The initial molar ratio of monomer to initiator ($[\text{M}]_0/[\text{I}]_0$) was maintained at 20:1. Finally, the functionalized polypeptide was isolated by precipitating it in excess cold diethyl ether. The precipitate was washed multiple times and then dried in a vacuum oven at 60 $^\circ\text{C}$ overnight. A pale brown solid was obtained with a yield of 85%. This functionalized polypeptide was designated as C1 according to Table 2.1. Another sample (C2) was prepared by varying the initial feed ratio of monomer to initiator, as indicated in Table 2.1.

Characterization data: FTIR (Figure A2.1), MALDI-TOF-MS (C1) (Figure 2.7), ^1H - ^{13}C -NMR spectra of C2 (Figures 2.2 and A2.8) and C1 (Figures 2.3 and A2.9).

2.3.2.5. CROP of ^iPOX and Successive Azide Termination

For the CROP of ^iPOx , the following procedure was employed. Initially, ^iPOx (0.95 g; 8.395 mmol) was dissolved in dry CH_3CN (2.5 mL) in a G-10 glass reactor vial under a nitrogen gas atmosphere. MeI (26.3 μL ; 0.42 mmol) was added to the vial, and the reaction mixture was transferred to a research-grade

microwave reactor. The reaction was carried out at 140 °C for 5 minutes. Upon completion, the vial

Table 2.1. Molecular characterization data for different polymers/copolymers.

Sample name	$[M]_0/[I]_0$	M_n (Theo) (Da)	M_n (SEC) (Da)	Dispersity (\mathcal{D})
^a C1	20	4200	1700	1.57
^a C2	40	8500	3200	1.43
^b P1	20	2200	2900	1.05
^b P2	30	3400	4200	1.08
^c G1 (C1-<i>g</i>-P1)	-	49000	25400	1.19
^c G2 (C1-<i>g</i>-P2)	-	72000	35400	1.29
^c G3 (C2-<i>g</i>-P1)	-	98000	47600	1.24

^a Condition for ROP of Cys-S-Pr NCA: Solvent = DMF, Initiator = HMDS, Temperature = 30 °C

^b Condition for CROP of ¹POx: Solvent = CH₃CN, Initiator = MeI, Quencher: NaN₃

^c Condition for click reaction: Solvent = DMF: H₂O (4:1) and Temperature = 65 °C

was allowed to cool to room temperature and removed from the reactor. The cooled reaction mixture was then treated with excess NaN₃ and returned to the microwave reactor. The reaction continued at 85 °C for 90 minutes. Subsequently, the reaction mixture was cooled to room temperature, and the unreacted NaN₃ was removed by centrifugation. The resulting product, a yellow powdery solid, was isolated by precipitation from a CH₃CN solution using cold diethyl ether. Finally, the solid was dried in a vacuum oven at 45 °C. This product was designated as P1 (Table 2.1). Another sample (P2) was prepared by varying the initial feed ratio of monomer to initiator (Table 2.1).

Characterization data: FT-IR (Figure 2.1), $^1\text{H}/^{13}\text{C}$ -NMR of P1 (Figures 2.3 and A2.10) and ^1H -NMR of P2 (Figures A2.14), MALDI-TOF-MS of P1 and P2 (Figure 2.4).

2.3.2.6. Synthesis of Graft Copolypeptides (PCys-*g*-PiPOx) via Click Reaction

Polycysteine-*g*-poly(2-isopropyl-2-oxazoline) (PCys-*g*-PⁱPox) was synthesized using the copper (I) catalyzed alkyne-azide "click" reaction between PCys-S-Pr and PⁱPOx-N₃, as shown in Scheme 2.1. In a typical reaction, solid C1 (40.0 mg)

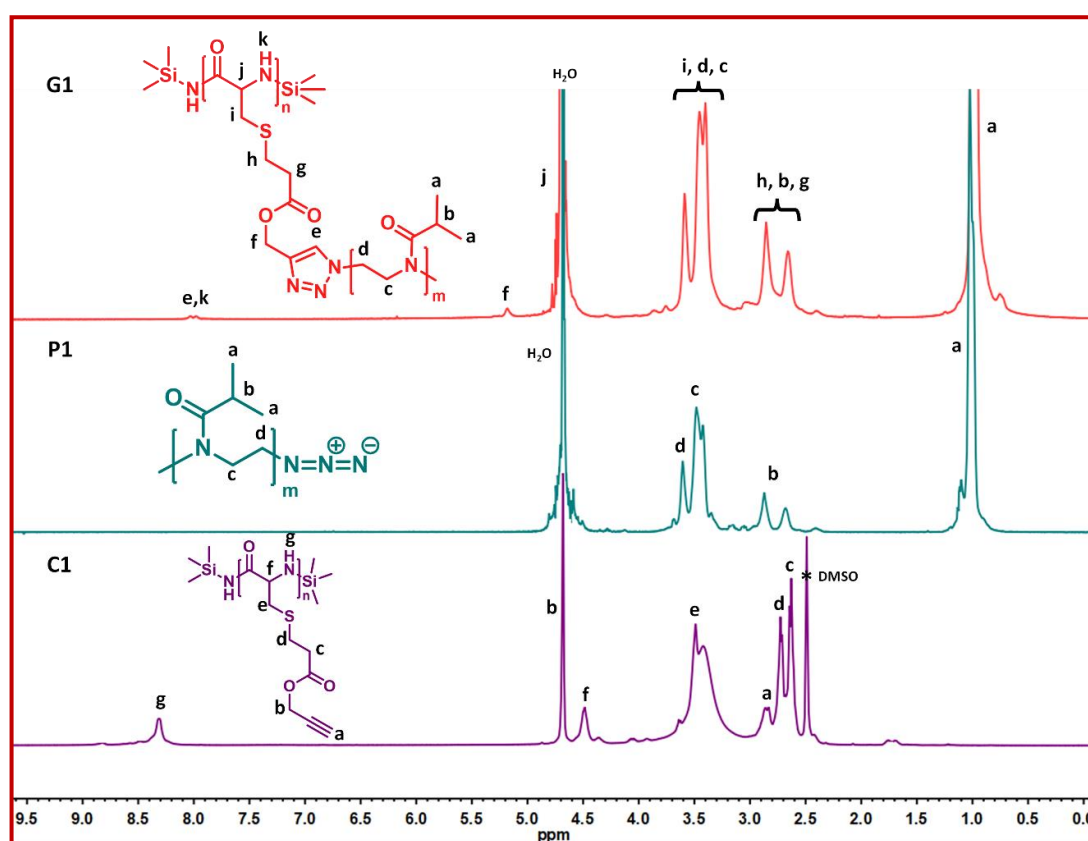


Figure 2.3. ^1H -NMR spectra of C1 in DMSO- d_6 , P1 and G1 in D_2O .

and excess P1 (500.0 mg) were taken in a 25 mL long-necked RB flask and dissolved in a mixture of DMF and water (4:1 v/v) while purging with N_2 gas for 45 min. Separately, $\text{CuSO}_4 \cdot 5\text{H}_2\text{O}$ (3.99 mg; 0.016 mmol) and sodium ascorbate (4.752 mg; 0.024 mmol) were dissolved in 100 μL of water, and these solutions were added consecutively to the reaction mixture while continuously purging

with N_2 gas. The reaction mixture was then placed in an oil bath and stirred at $65\text{ }^\circ\text{C}$ for 36 h. After completion, the water was evaporated from the DMF/water mixture, and the final product in DMF was isolated by precipitating it in excess diethyl ether. The resulting dark brown sticky material was dried in a vacuum oven overnight at $60\text{ }^\circ\text{C}$. To purify the product, dialysis against water was

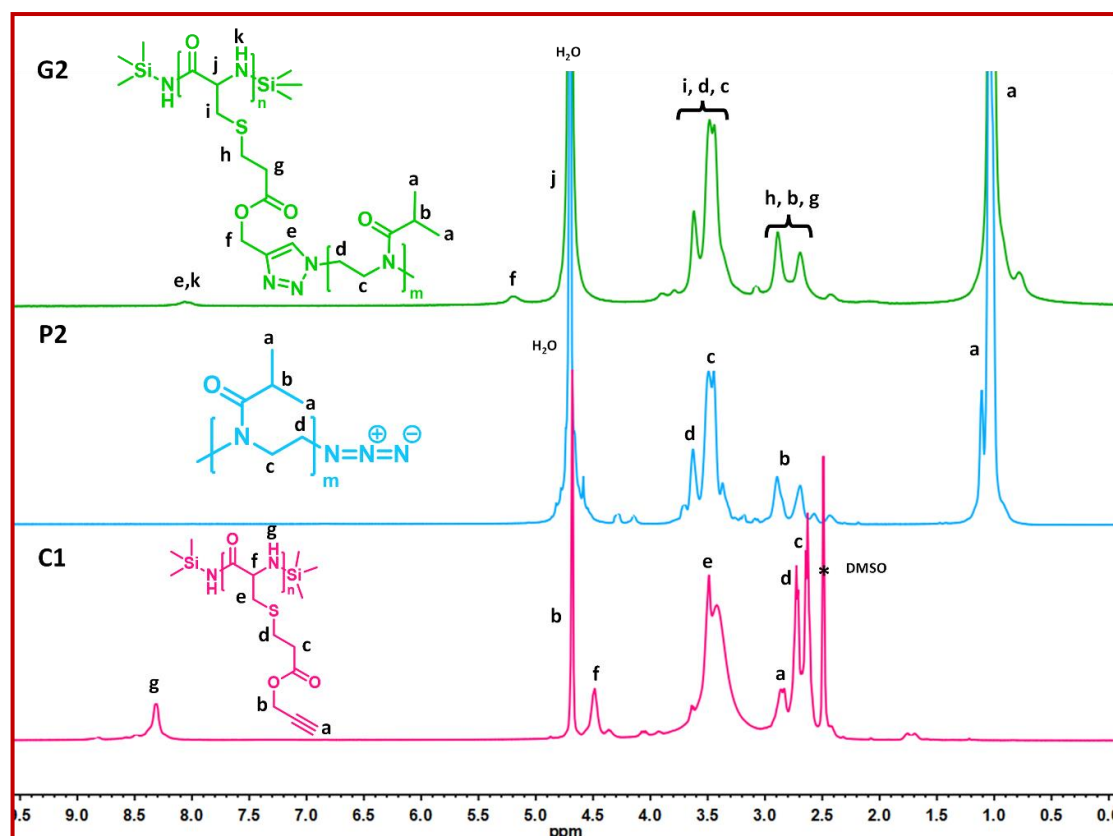


Figure 2.4. ^1H -NMR spectra of C1 in DMSO-d_6 , P2 and G2 in D_2O .

performed using a dialysis tubing with a molecular weight cutoff (MWCO) of 3500. Finally, the white product (PCys-*g*-PPOx, designated as G1) was obtained by lyophilization with a yield of 100%. Graft copolymer, G2 and G3 were also synthesized by the click reaction of C1 with P2 and C2 with P1 respectively. (Table 2.1).

Characterization data: ^1H -NMR of G1 (Figure 2.3), G2 (Figure 2.4) and G3 (Figure 2.6)

2.3.3. Experimental Methods

2.3.3.1. Microwave Polymerization

Microwave-assisted CROP of POx was performed using MeI as the initiator in an Anton Paar research grade Microwave Reactor (Model: Monowave 300). G-10 glass vial was used for the reaction in dry ACN.

2.3.3.2. Determination of T_{cp}

The lower critical solution temperature (LCST)-type cloud point (T_{cp}) of aqueous graft copolymer solution was determined by measuring the % transmittance at different temperatures at a fixed wavelength ($\lambda = 500 \text{ nm}$) in a Cary 60 UV-vis spectrometer (Agilent) equipped with single cell Peltier accessory (Agilent). For measurement, 1.0 mL of each polymer solution was taken in 1 mL of quartz cuvette and the % transmittance was recorded in the temperature ranges from 25-90 °C with a heating/cooling rate of 3 °C/min. T_{cp} is the temperature at which the transmittance of copolymer solution reaches to 50% of its original value.

2.3.3.3. Determination of Critical Aggregation Concentration (CAC) in water

Pyrene was used as the polarity probe for determination of CAC. Pyrene is a well-known dye to investigate the polarity changes in the microenvironment (micelle or vesicle) from polarity changes in the macroenvironment (bulk solvent) A characteristic property of pyrene, which indicates the polarity of the environment in which it is solubilized, is the ratio of its fluorescence peaks at $\lambda = 372 \text{ nm}$ for the 0-0 band (I_1) and at $\lambda = 383 \text{ nm}$ corresponds to the third principal vibronic band (I_3) in water, which are very much sensitive to polarity of the medium. For this a series of polymer sample (G2) solutions in water was prepared of concentration ranging from 1 mg/mL to $1 \times 10^{-2} \text{ mg/mL}$. A stock solution of pyrene of 10^{-4} (M) in acetone was prepared and 20 μL of that solution was transferred into 9 separate glass vials. After evaporating the acetone, 2mL of each polymer solution was added into those vials separately and sonicated

for 10 minutes and kept overnight undisturbed. The final concentration of pyrene was kept constant at 10^{-6} (M) for each solution. Fluorescence emission intensity was measured by exciting those solutions at $\lambda = 334$ nm and keeping the slit width at 5 nm. After normalizing the intensity at $\lambda = 372$ nm, the ratio of I_{383} and I_{372} (I_3/I_1) was plotted against the logarithm of the concentration (mg/mL) of different polymer solutions. The plot of intensity ratio (I_3/I_1) against the log of polymer concentration (mg/mL) showed a slow increase of the I_3/I_1 value with concentration followed by a sudden jump. The CAC was obtained from the interception point of two straight lines and was found to be 0.22 mg/mL (inset of Figure 2.5).

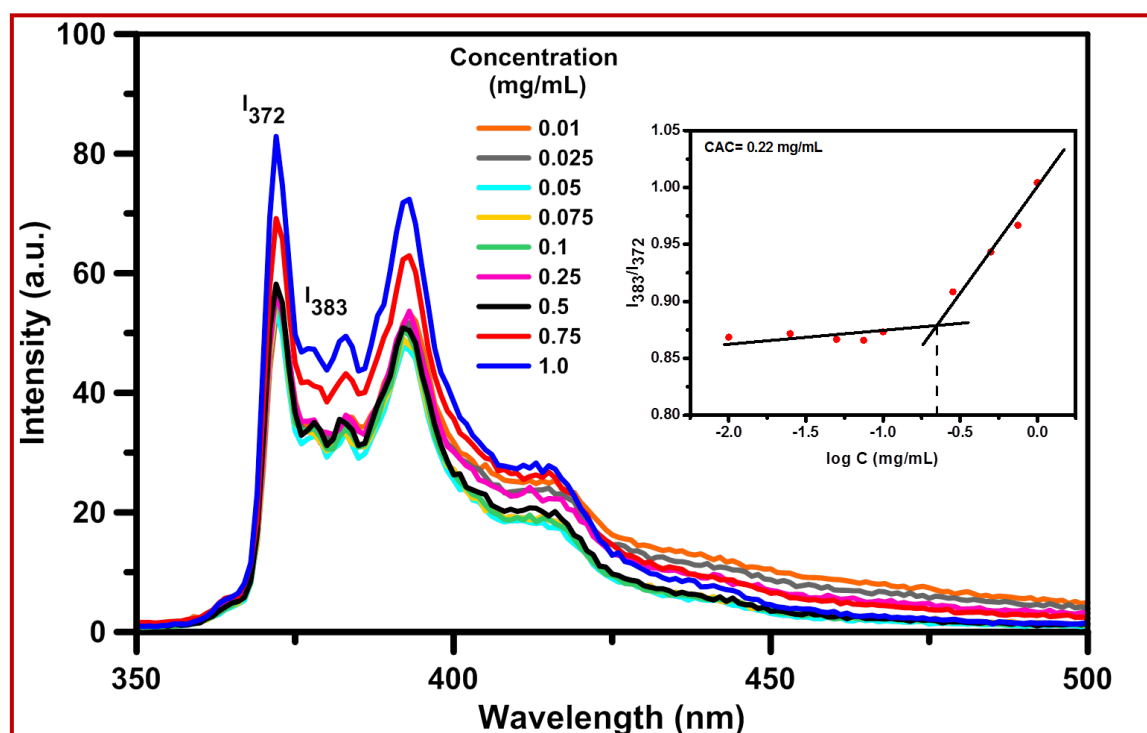


Figure 2.5. Emission spectra of pyrene ($\lambda_{ex} = 334$ nm) in the presence of aqueous G2 of varying concentration. Inset represented the plot of fluorescence vibronic intensities ratio (I_3/I_1) as a function of the G2 concentration as measured from emission spectra.

2.3.3.4. Self- Aggregation of PCys-*g*-P'POx Graft Copolymer

The self-aggregation of copolymer in water and DCM was studied by dynamic light scattering (DLS), field-emission scanning electron microscopy (FESEM), transmittance electron microscopy (TEM), and cryogenic transmission electron microscopy (Cryo-TEM). Typically, aqueous G1-G3 (0.5 mg/mL) and G3 (2.0 and 5.0 mg/mL) (above CAC) solutions were prepared using milli-Q water and were filtered through 0.22 μm membrane filter. The filtered solutions were kept undisturbed and were examined by DLS at different time intervals. A 1.0 mg/mL of DCM solution of the representative G2 sample was also kept undisturbed for different times for its self-assembly. The above mentioned self-assembled PCys-*g*-P'POx(s) copolymer solutions were drop cast on carbon coated Cu grid and thin glass slide respectively and dried at room temperature for examination via TEM, Cryo-TEM and FESEM. The self-assembled G2 solution was first heated above its cloud point to allow phase separation and was cast immediately on a clean, thin glass slide kept at 90 °C on a hot-plate and quenched to room temperature for FESEM analysis. To get the TEM image from DCM, 0.1 wt% DCM solution of G2 was filtered and drop cast on a Cu grid and dried at room temperature.

2.3.3.5. Dye Encapsulation Study

It was expected that the as-synthesized vesicles with hydrophobic shell and hydrophilic interior can encapsulate both hydrophobic and hydrophilic dye respectively in water. Nile Red (NR) was chosen as hydrophobic dye for its encapsulation into the shell of the vesicle. For this, at first, 300 μL of 1.0×10^{-3} M of NR solution in acetone was taken into a glass vial and was evaporated to dryness. An aqueous G2 solution (0.2 wt%) was added into it to make the final concentration of NR 1.5×10^{-4} M. This solution and a control solution without any copolymer were sonicated for 15 min and kept them overnight at stirring condition. The extent of dye encapsulation by those vesicles after

centrifugation and membrane filtration (pore size = 0.22 μm) was monitored by fluorescence spectroscopy in comparison to that of control solution.

For encapsulation in the interior of the vesicle, hydrophilic Eosin B (EB) dye (1.1×10^{-4} M) solution was added to an aqueous 0.2 wt% G2 solution. The solution was then dialyzed against water using a dialysis tubing of 3500 MWCO for four days. Note that there was no vesicle leaching through the dialysis membrane. The encapsulation of EB in the interior of vesicles was monitored via fluorescence spectroscopy. The emission of a control solution of EB without copolymer was also acquired for comparison.

To check the encapsulation of hydrophilic EB, 0.2 wt% G1 solution in DCM was mixed with EB at a final concentration of 1.5×10^{-4} M. Another solution of EB in DCM (1.0×10^{-4} M) was prepared without any copolymer. Each solution was sonicated for 15 min and kept overnight under stirring. Both the solution was then centrifuged and filtered through 0.45 μm pore size filter membrane to discard the free dye molecules and were examined via absorption and fluorescence spectroscopy.

2.3.3.6. Drug Encapsulation Study

An anticancer drug, Doxorubicin hydrochloride (1 mg) and 6 mg of G2 polymer sample were dissolved in 1 mL of water taken in glass vial and was stirred for 24 h. The resulting solution was then dialyzed (membrane of 3500 MWCO) against water to eliminate the unencapsulated drug. Dialysis was continued until there was no detectable absorbance of free Dox in bulk water. A calibration curve was constructed by acquiring the absorbance of Dox at $\lambda = 485$ nm (Figure A2.11). The amount of Dox encapsulated in the G2 vesicles was then estimated from the calibration curve. For release study, Dox-loaded vesicles were treated with concentrated HCl and phosphate buffer solution of different pH. Dox-encapsulated vesicles were also subjected to temperature change for its triggered release.

2.3.4. Characterization

FTIR spectra of all the samples were recorded either from KBr pellet or by casting film using Perkin Elmer Spectrum 400 spectrometer.

ESI-MS spectrum of Cys-S-Pr was recorded from its solution in MeOH:H₂O (1:1 v/v) by a QTOF Micro YA263 Mass spectrometer from Waters.

Molecular weights as well as end group analysis of Cys-S-Pr NCA, P¹POx-N₃(s) and PCys-S-Pr (C1) were performed by a Bruker MALDI-TOF-MS instrument using 2,5-dihydroxybenzoic acid (DHB) as matrix and NaI salt to enhance ionization.

Bruker DPX 500 MHz spectrometer was used to acquire the ¹H-NMR spectra of Cys-S-Pr, Cys-S-Pr NCA and PCys-S-Pr(s) in DMSO-d₆. The spectra of ¹POx and P¹POx-N₃(s)/PCys-*g*-P¹POx(s) were acquired from CDCl₃ and D₂O respectively. ¹³C-NMR spectra of different samples were obtained from suitable solvents using a 300 MHz spectrometer.

UV-vis absorption spectra of dye/dye-loaded vesicles were acquired using a Cary 60 spectrophotometer (Agilent Technologies). For turbidity study, the % transmittance of the copolymer solution/suspension was measured by the same instrument, but it was equipped with a Peltier temperature controller.

Emission spectra of dye-/drug-encapsulated vesicles were recorded from FluoroMax-3 spectrophotometer of Horiba Jobin Yvon.

Molecular characterizations were performed by size exclusion chromatography (SEC) technique using a Waters 1515 isocratic HPLC pump connected to an Agilent Polar Gel-M (Mn ~ 500 kDa) column at 50 °C and a Waters 2414 refractive index detector at 40 °C. DMF containing 30 mM LiBr was used as the eluent with 1 mL/min flow rate and narrow PMMA standards were used to calibrate the column. Waters Empower software was used for molecular weight analysis.

Hydrodynamic diameters (D_h s) of all the filtered solutions of PCys-*g*-P'POx(s) in water and DCM were measured from a DLS instrument (Malvern Zetasizer NANO ZS 90, Model: 3690) at 25 °C. Equilibration time and angle of detection were set to 2 min and 173° (Backscatter, NIBS default) respectively. Each data point was obtained by scanning the sample solution 15 times in a single run at a certain time. The intensity-weighted distribution data obtained from the DLS instrument was finally plotted to obtain D_h .

The morphology of aggregated G2 in water (0.5 mg/mL) was examined by acquiring the images from the cast samples using a JEOL JSM-6700F FESEM operated at an accelerating voltage of 2 kV. G2 copolymer aggregates were also imaged from the drop-cast sample from its suspension above its cloud point.

Sample solutions (0.5 mg/mL) were drop-cast onto carbon-coated copper grids and let the samples dried for two days. TEM images were taken by placing the grids under JEOL JEM-1400 Plus electron microscope working at an accelerating voltage of 100 kV. For Cryo-TEM measurements, aggregates' solutions of G3 (0.5 mg/mL) were drop-cast onto carbon-coated Cu grids followed by immediate vitrification of the grids by placing it inside the GATAN cryo-plunger. Afterward, TEM images of the aggregates were taken by placing the vitrified Cu grids under JEOL JEM-2100 PLUS microscope operated at an accelerating voltage of 120 kV.

Confocal microscopic images of dye-/drug-encapsulated vesicles were obtained by using LSM 880 (Carl Zeiss) instrument from drop-cast and dried samples.

Circular dichroism (CD) spectra of neat polypeptides and polypeptide-polyoxazoline conjugate were recorded in DMF using a Jasco J-815 CD spectropolarimeter. A quartz cuvette of 1 mm path length was used for this experiment.

2.4. Result and Discussion

2.4.1. Synthesis of PCys-*g*-P^lPOx copolymer

The synthesis of PCys-*g*-P^lPOx involved a series of sequential reactions (Scheme 2.1) The procedure consisted of the following steps: 1) Preparation of propargylated L-cysteine (Cys-S-Pr) through a thio-Michael addition reaction. 2) Formation of propargylated L-cysteine NCA (Cys-S-Pr NCA) using triphosgene. 3) ROP of Cys-S-Pr NCA using HMDS initiator to yield PCys-S-Pr. 4) Synthesis of the isopropyl oxazoline (POx) monomer. 5) Microwave-assisted controlled ROP of POx, followed by end functionalization with azide to obtain P^lPOx-N₃. 6) Grafting of P^lPOx-N₃ onto PCys-S-Pr through a click reaction to produce PCys-*g*-P^lPOx. It should be noted that while P^lPOx-N₃ was soluble in water, PCys-S-Pr was not. However, the resulting copolymer, PCys-*g*-P^lPOx, exhibited water-solubility. This indicated the formation of an amphiphilic copolymer comprising a hydrophobic PCys backbone and pendant hydrophilic P^lPOx blocks. Furthermore, both P^lPOx-N₃ and PCys-*g*-P^lPOx were soluble in dichloromethane (DCM).

The FTIR spectra exhibited bands at 2128 and 2106 cm⁻¹, which can be attributed to the terminal alkyne and azide groups present in PCys-S-Pr and P^lPOx-N₃, respectively (Figure 2.1). However, these bands were not observed in the FTIR spectrum of the conjugate, PCys-*g*-P^lPOx, indicating complete grafting between these two blocks. In the representative sample, G3, the ¹H-NMR signals at δ 8.03 and 5.18 ppm corresponded to protons originating from the triazole ring and the PCys block, respectively (Figure 2.6). The absence of a signal at δ 2.82 ppm, which corresponds to the terminal alkyne proton, further confirmed the formation of copolymers with a graft density of near 100%.

The MALDI-TOF-MS spectrum of C1 exhibited a series of peaks with a mass difference of $m/z = 213$ Da, which precisely corresponded to the molecular weight of the Cys-S-Pr monomeric unit (Figure 2.7). Figure 2.7 also showed that the peak at $m/z = 2566$ could be attributed to the combined molar masses of two

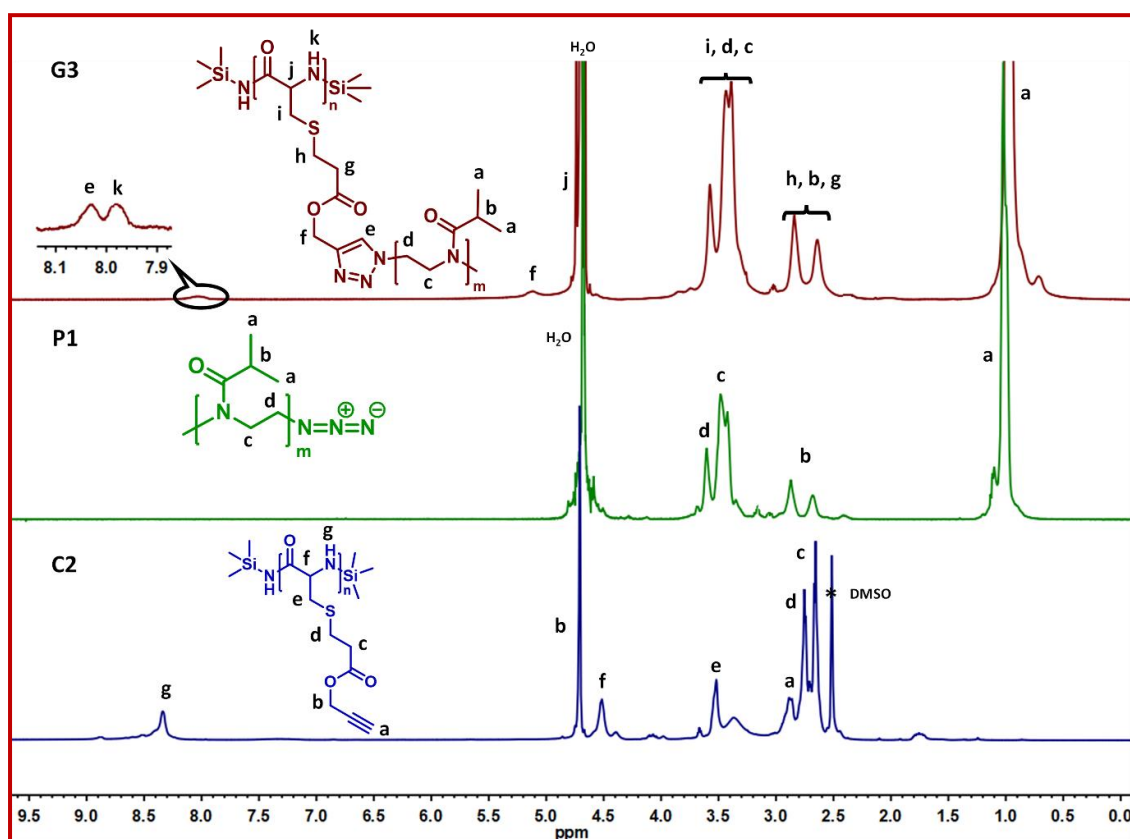


Figure 2.6. ^1H -NMR spectra of C2 in DMSO-d_6 , P1 and G3 in D_2O .

end groups (aminotrimethyl silane and trimethyl silane), 11 units of Cys-S-Pr, as well as Na^+ and K^+ ions formed during ionization. This observation confirmed that the ROP process was indeed initiated using the HMDS initiator.

The MALD-TOF-MS spectrum of $\text{P}^i\text{POx-N}_3(\text{s})$ also displayed a series of peaks with a separation of 113 (m/z) Da, corresponding to the molar mass of the ^iPOx repeating unit (Figure 2.7). In this case, the m/z value of a prominent peak at 1662/3002 for both P1 and P2 could be correlated with the sum of masses corresponding to 14/26 $i\text{POx}$ units, terminal methyl, and terminal azide groups, along with the mass of Na^+ ion for P1 and Li^+ ion for P2, respectively. These findings strongly suggested that the methyl and azide groups were located at the two distinct ends of the P^iPOx chain.

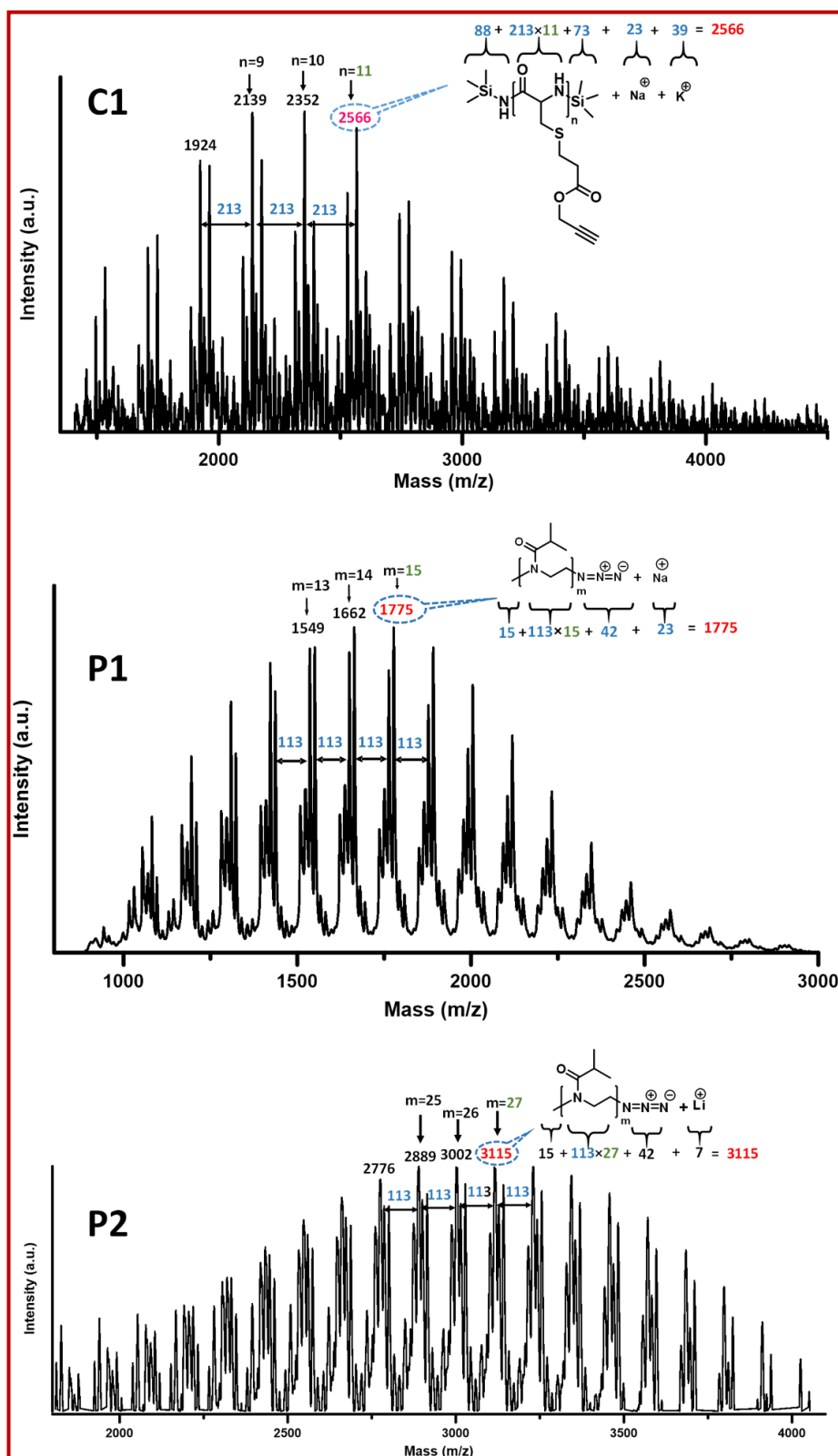


Figure 2.7. MALDI-TOF-MS spectra of C1 (top), P1 (middle) and P2 (bottom).

The size exclusion chromatography (SEC) traces of all the samples exhibited a unimodal nature (Figure 2.8). In each copolymer, there was a noticeable shift in the chromatogram of P'POx towards higher molecular weights, indicating grafting with the PCys chain. The unimodal nature of the SEC traces for the

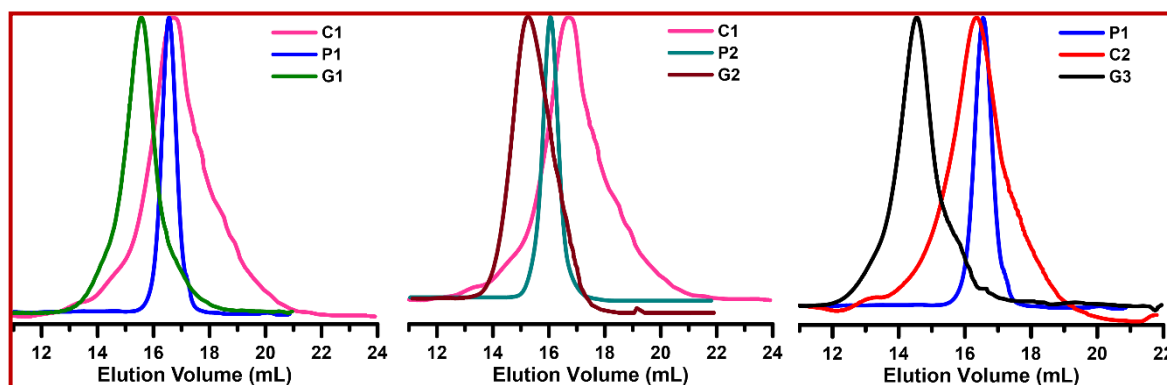


Figure 2.8. SEC chromatographs of all the polymer/copolymer samples.

copolymers (G1, G2, and G3) clearly indicated the complete grafting of the P'POx block. The obtained \bar{M}_n values for the polycysteines (C1 and C2) and polyoxazolines (P1 and P2) (Table 2.1) were found to be narrow, suggesting the controlled nature of their formation through ROP and CROP techniques, respectively. It is worth noting that the experimental number-average molecular weights (M_n) did not closely match the theoretical M_n values (Table 2.1). The exact reason for these discrepancies is currently unknown. However, it can be speculated that the differences in chemical structures between the synthesized polymers and the PMMA standards used in SEC measurements may be responsible for these discrepancies.

The CD spectra of neat PCys-S-Pr(s) (C1 and C2) obtained from DMF displayed negative CD ellipticity bands around ~ 215 nm, as shown in Figure 2.9A. These bands indicated the presence of a β -sheet-like secondary structure in the PCys samples. Similar CD spectra with β -sheet-like secondary structures

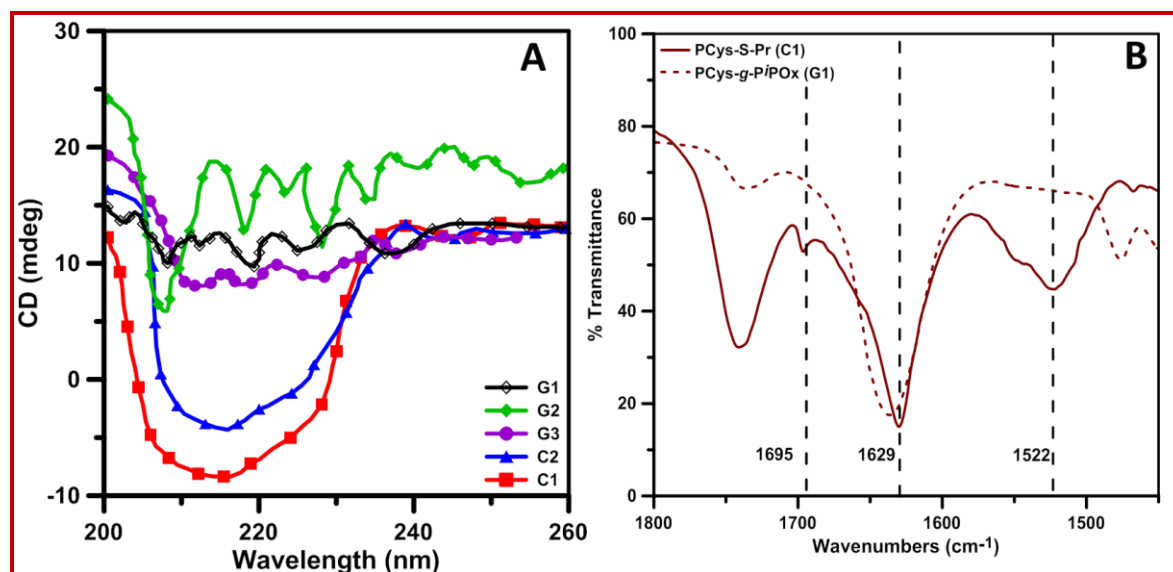


Figure 2.9. CD spectra of different synthesized compounds in DMF (A) and FTIR spectra showing band positions of different amide regions (B)

have been reported by various research groups for proteins and polypeptides.²¹ Generally, polycysteine exhibits a tendency to adopt a β -sheet-like secondary structure,⁶²⁻⁶³ which aligns with our experimental data. When PCys was chemically linked with the P'POx block, the resulting graft copolymers did not exhibit any characteristic peaks corresponding to such secondary structures in the CD spectra. It becomes challenging to identify such bands for the graft copolymers, and this may be attributed to the conformational changes that occur upon grafting the P'POx blocks onto the PCys backbone. This assumption is supported by the FTIR spectra of solid PCys and PCys-*g*-P'POx (Figure 2.9B). In the FTIR spectra, the amide-I (1600-1700 cm^{-1}) and amide-II (1500-1600 cm^{-1}) bands of polypeptides arise from the stretching vibration of the C=O bond and the bending vibration of the N-H bond, respectively. These two bands are primarily associated with the backbone conformation of polypeptides.⁶⁴⁻⁶⁵ Polypeptides adopting β -sheet-like secondary structures typically exhibit two bands near 1630 cm^{-1} (strong) and 1685 cm^{-1} (weak) in the amide-I region, along with a strong band around 1525-1530 cm^{-1} in the amide-II region.⁶⁶ The

spectrum of the representative sample, C1 (Figure 2.5B), clearly displayed the presence of all these characteristic bands of PCys, although the exact positions of the bands did not precisely match the reported values. In the case of the graft copolymers (G1), the absence of the conformationally sensitive amide-II band strongly suggests the disappearance of any kind of secondary structure after grafting.

2.4.2. Thermoresponsive Properties of P'POx and PCys-*g*-P'POx

Poly(2-alkyl-2-oxazoline)s, such as P'POx, exhibit temperature-dependent phase behavior in aqueous solutions known as lower critical solution temperature (LCST) transition.^{53, 67} This phase behavior is dependent on the alkyl chain length and molecular weight of the polymer. Low-molecular-weight P'POx with shorter alkyl chain lengths display a higher cloud point temperature (T_{cp}) compared to high-molecular-weight P'POx. This is because the shorter hydrophilic chains are more readily hydrated than the longer hydrophilic chains, while the hydration of the relatively hydrophobic chain is less affected by chain length.

In this study, the turbidity measurement data demonstrated that the as-synthesized P1 ($M_n = 2861$) had a higher T_{cp} (49.2°C) compared to P2 ($M_n = 4200$) (44.6°C), as shown in Figure 2.10A. As previously mentioned, the PCys-*g*-P'POx copolymers synthesized in this study were soluble in water, forming transparent solutions at room temperature. However, upon heating, these solutions became turbid and reverted to transparency upon cooling, indicating an LCST-type phase transition (Figure 2.10B). These transitions were reversible, as evidenced by the nearly identical turbidity curves during heating and cooling with negligible hysteresis observed (Figure 2.10). Furthermore, the transitions exhibited sharp changes in %transmittance from 100 to almost 0 as the solution temperature increased. The T_{cp} values for G1, G2, and G3 were found to be 45, 41, and 36 °C, respectively (Figure 2.10B). These results indicated that

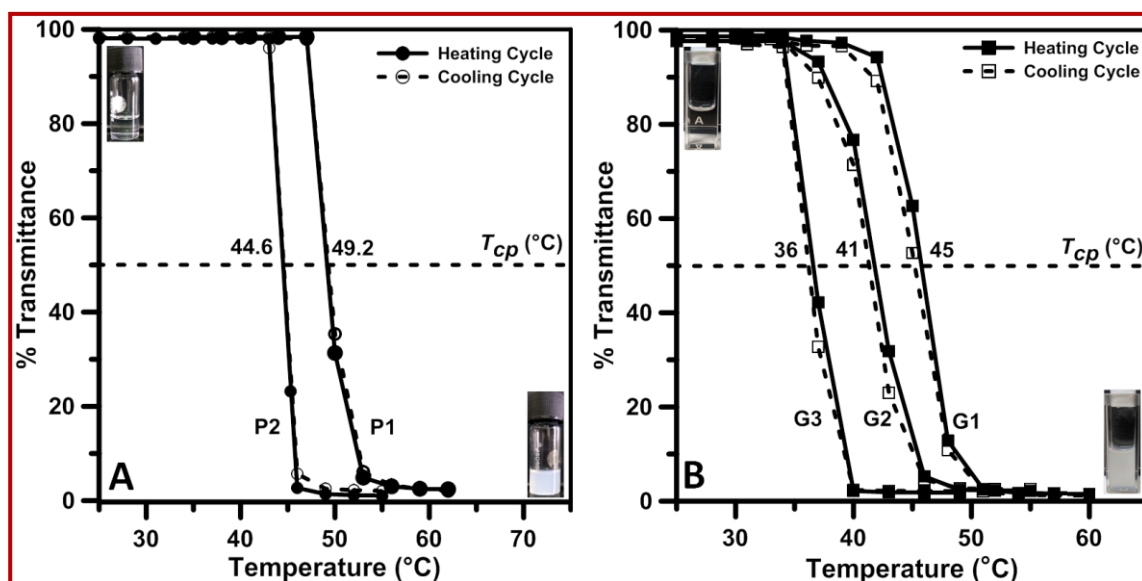


Figure 2.10. Turbidity curves of aqueous P1-P2 (A) and G1-G2-G3 (B) solutions (0.2 wt%) (at $\lambda = 500$ nm). The inset showed the snapshots of the transparent solution (top left) and cloudy suspension (bottom right) respectively of P1 (A) and G1 (B) at a temperature below and above the cloud point.

the T_{cp} value decreased as the chain length of the pendent P'POx block and the PCys backbone increased. The inherent thermosensitivity of the P'POx block contributed to the thermoresponsiveness of the resulting graft copolymer. However, due to the presence of the hydrophobic PCys block, the hydrophilic-hydrophobic balance of the copolymer changed, resulting in a decrease in its T_{cp} value compared to that of the neat P'POx homopolymer. The T_{cp} value for G3 further decreased due to the overall increase in the hydrophobicity of the graft copolymer resulting from the increased chain length of the hydrophobic PCys backbone.

To investigate the temperature-dependent phase behavior of a representative G2 sample, we determined the T_{cp} values at different concentrations in aqueous solutions (Figure 2.11A). The plot of T_{cp} against concentration exhibited a U-shaped curve with a minimum, revealing the actual LCST of G2 to be 29.2 °C at a concentration of 0.93 wt% (Figure 2.11B).

Initially, as the concentration increased, T_{cp} decreased due to enhanced polymer-polymer intermolecular interactions, promoting the aggregation of polymer molecules, and surpassing the polymer-solvent interactions. However, beyond a critical point, the polymer-solvent interactions began to dominate over the polymer-

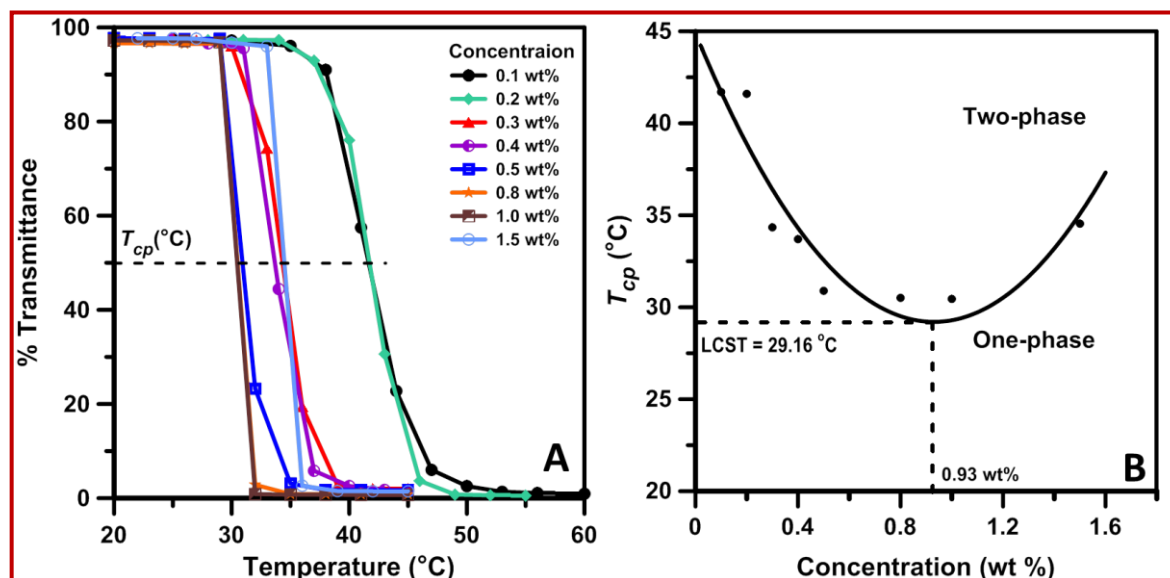


Figure 2.11. Turbidity curves (measured at $\lambda = 500$ nm) of aqueous G2 solution at different concentrations (A) and LCST-type phase diagram of binary mixture of G2 and H_2O (B).

polymer interactions, leading to an increase in T_{cp} value.⁶⁸⁻⁶⁹ Consequently, the variation of T_{cp} values with polymer concentration displayed a U-shaped concave curve. In the case of G2, the plot of T_{cp} versus concentration also exhibited a U-shaped curve, and the actual LCST of the copolymer in water was determined to be 29.2 $^{\circ}\text{C}$ at its minimum concentration of 0.93 wt%. This U-shaped binodal curve is commonly observed in conventional LCST polymers.⁷⁰

The reversible aggregation and disaggregation could be modulated several cycles for all two graft copolymers, which basically implied the consistency of LCST behavior and the thermal stabilities of these as-synthesized graft copolymers (Figure A2.12).

2.4.3. Self-Assembly of PCys-*g*-P'POx

The amphiphilic nature of the PCys-*g*-P'POx copolymer, which consists of a hydrophobic PCys backbone and hydrophilic pendent P'POx blocks, enables self-assembly into various nanostructured aggregates in both aqueous and non-aqueous solvents. To investigate the self-assembly behaviour, we determined the critical aggregation concentration (CAC) of a representative G2 sample in water using pyrene as a probe (vide 'Experimental Methods' and Figure 2.5 for details). The CAC was found to be 0.22 mg/mL. The formation of aggregates above the copolymer's CAC was further confirmed using dynamic light scattering (DLS), which revealed the presence of both small- and large-sized particles (Figure 2.12). Initially, the population of small-sized particles was

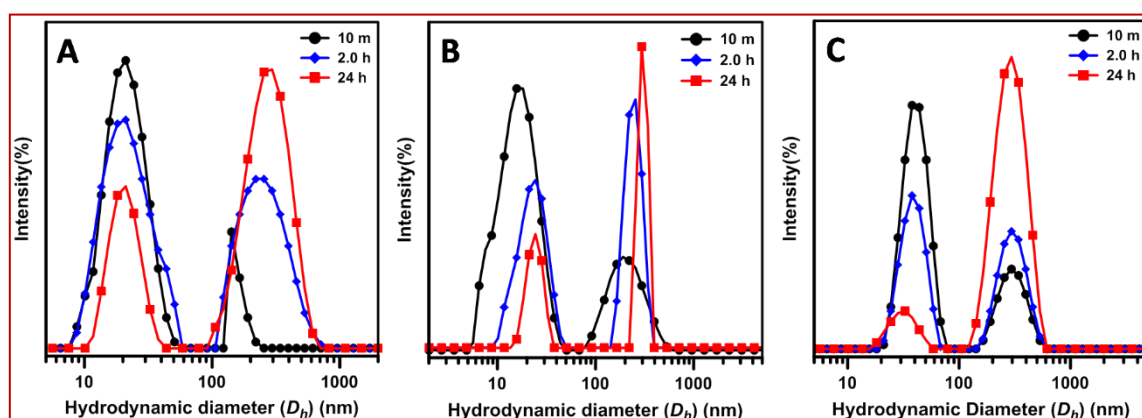


Figure 2.12. DLS curves of G1 (A), G2 (B) and G3 (C) at a concentration of 0.5 mg/mL in water.

higher than that of large-sized particles. However, over time, we observed a decreasing trend in the population of small-sized particles and an increasing trend in the population of large-sized particles. After 24 hours of assembly, G1, G2, and G3 formed small-sized aggregates with hydrodynamic diameters (D_h s) of 20, 25, and 30 nm, respectively, as well as large-sized aggregates with D_h s of 330, 350, and 300 nm, respectively (Figure 2.12). These results suggest the self-

assembly of copolymer molecules into nano-sized aggregates, followed by secondary aggregation leading to the formation of larger-sized aggregates over time. To further investigate the self-assembly behaviour, the particle size distributions of a representative sample G3 were examined at higher concentrations (2.0 and 5.0 mg/mL) in aqueous medium. At different time intervals, the intensity-weighted distribution of G3 at 2.0 mg/mL exhibited a similar distribution to that of G3 at 0.5 mg/mL concentration (Figure 2.12C and Figure 2.13A). However, at a relatively high sample concentration of 5.0 mg/mL, the intensity-weighted distribution showed the formation of only larger particles with diameters ranging from 200-350 nm at different time intervals, without any smaller particles (Figure 2.13B).

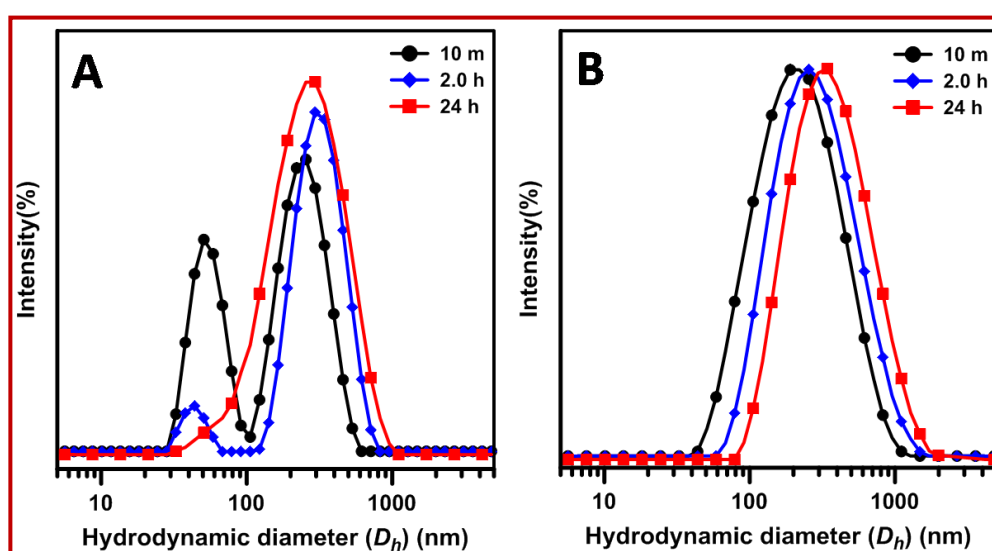


Figure 2.13. Time dependent intensity-weighted particle size distributions of G3 in water at a concentration of 2.0 (A) and 5.0 (B) mg/mL, as obtained from DLS.

The higher concentration of G3 resulted in a relatively higher number of particles compared to the concentrations of 0.5 and 2.0 mg/mL. It is important to note that the scattering intensity is proportional to the radius of the particle. Therefore, the larger G3 particles would exhibit significantly higher scattering intensity compared to the smaller particles. Consequently, only the large-sized

particles with higher scattering intensity would dominate the scattering signal, while the signature of the small-sized particles with lower scattering intensity would not be detected. Preliminary examination of a representative G2 sample in water beyond its CAC by FESEM resembled with DLS data of the formation of small- and large-sized spherical aggregates with average diameters of 20 nm and 230 nm respectively (Figure 2.14).

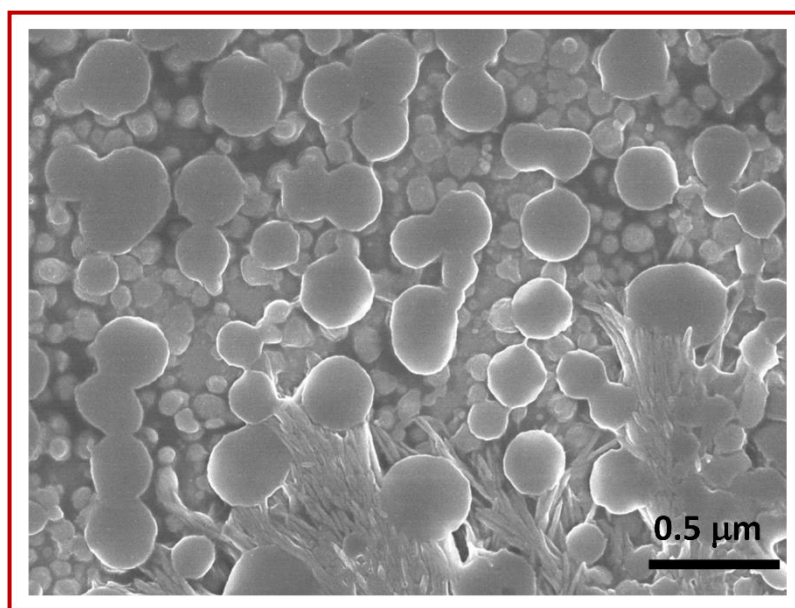


Figure 2.14. FESEM image of G2 in water showing unit vesicles with an average diameter ~ 20 nm and conjugate vesicles with an average diameter of ~ 250 nm.

TEM images (Figure 2.15) revealed that the spherical aggregates observed were actually vesicles with a hollow interior and a solid layer, formed through the self-assembly of G1, G2, and G3 copolymer molecules. The self-assembly process resulted in the formation of vesicles with varying size distributions. Examination of G1, G2, and G3 at both normal and high magnifications clearly showed the presence of vesicles with two main dimensions, with average diameters of 10-15 nm and 150-180 nm, respectively. The larger-sized copolymer vesicles exhibited a wall thickness of approximately 20-25 nm.

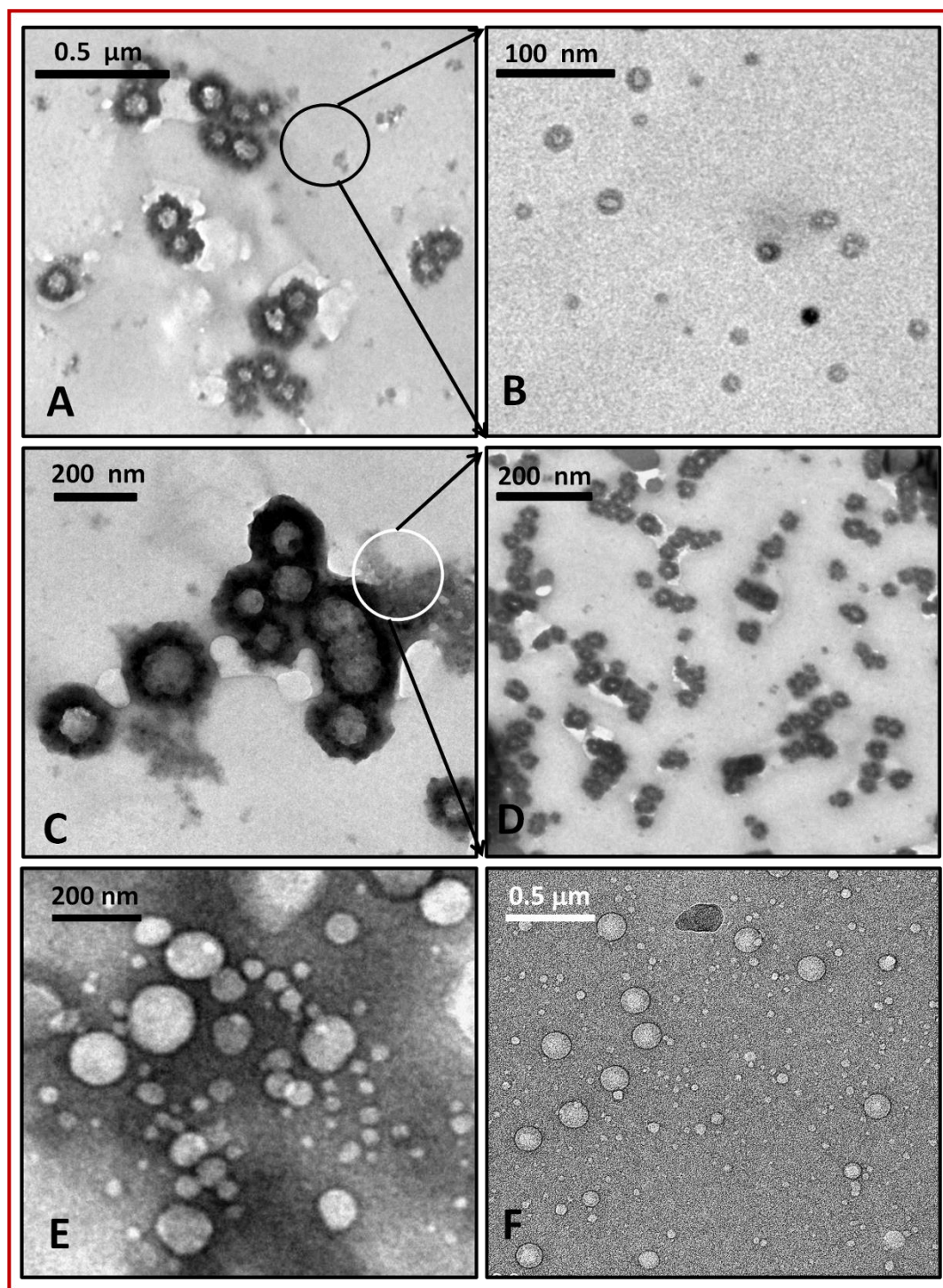


Figure 2.15. TEM images of composite vesicles of G1 (A), high magnification image of a portion of A showing unit vesicles of G1 (B), composite vesicles of G2 (C), and high magnification image of a portion of C showing unit vesicles of G2 in water (D), TEM (E) and cryo-TEM (F) images of G3 solution in water showing unit vesicles and conjugate vesicles.

It was hypothesized that the observed aggregates with small sizes are unit vesicles, which subsequently combine to form composite vesicles with a larger average diameter over a 24-h period. Analysis using DLS, FESEM, and TEM provided data that indicated the presence of copolymer aggregates with two distinct size distributions, even after 24 hours of aging. The DLS results (Figure 2.12) exhibited two separate peaks for all the copolymers, indicating the existence of two distinct vesicular aggregates with different size distributions. One peak corresponded to smaller vesicles with a hydrodynamic diameter (D_h) ranging from 20 to 40 nm, while the other peak represented larger vesicles with a range of 300 to 350 nm. The initial aggregation of copolymer molecules resulted in the formation of smaller particles (unit vesicles), which further coalesced over time to form larger composite vesicular aggregates through secondary aggregation. Importantly, our observations showed that both the small and large aggregates coexisted even after 24 hours, suggesting an equilibrium between these two types of aggregates with different sizes. The data presented in Table 2.2 consistently demonstrated the presence of particles with two distinct size distributions. Additionally, it was noted that the size of the larger composite vesicles increased to some extent over time (Figure 2.12 and Table 2.2). These findings clearly indicate a continuous generation of small unit vesicles, which subsequently transform into larger composite vesicles through secondary aggregation. This mechanism bears resemblance to a phenomenon known as Ostwald ripening, commonly observed in liquid sols, where smaller particles dissolve and redeposit onto larger particles, resulting in their size increase.⁷¹

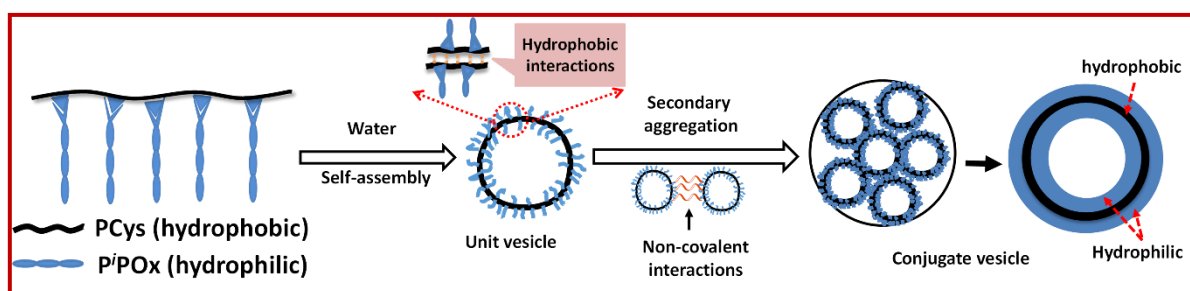
While there is existing literature on the mechanisms of polymeric vesicle formation,^{42, 72-75} none of them directly correlate with our specific system. Therefore, the precise mechanism behind the formation of these graft copolymer vesicles remains unclear. Previous research has demonstrated that self-assembly of polymeric amphiphiles with moderate hydrophobicity can

Table 2.2. Particle size distribution of the graft copolymers (G1, G2 and G3) in water at different time intervals as observed from DLS, showing particles of mainly two different size distributions.

Time interval (h)	Graft Copolymers														
	Particle size distribution (G1)					Particle size distribution (G2)					Particle size distribution (G3)				
	Small (nm)	St dev.	Large (nm)	St dev.	PDI	Small (nm)	St dev.	Large (nm)	St dev.	PDI	Small (nm)	St dev.	Large (nm)	St dev.	PDI
0.0	20.1	9.9	195.0	52.5	0.384	16.0	3.6	237.0	25.9	0.330	40.0	2.8	294.0	56.3	0.303
2.0	21.2	10.8	244.0	83.4	0.345	19.5	6.1	221.0	71.8	0.256	37.8	5.3	294.7	64.3	0.287
6.0	17.6	11.8	246.2	58.3	0.321	22.4	5.9	250.2	74.3	0.282	41.2	8.3	292.0	66.1	0.354
10.0	19.5	8.4	285.0	69.7	0.338	19.7	3.0	293.8	51.1	0.485	37.8	5.3	302.1	78.6	0.351
15.0	21.7	8.3	302.9	45.9	0.379	27.0	2.1	302.4	53.4	0.343	43.18	2.6	302.4	61.1	0.370
20.0	20.8	9.7	309.4	55.3	0.415	25.0	11.7	299.7	61.1	0.370	36.2	5.2	300.9	53.4	0.456
24.0	20.3	7.3	323.1	41.5	0.342	24.2	5.2	334.0	53.4	0.421	31.7	5.9	304.0	50.7	0.434

lead to the formation of polymeric vesicles, while more hydrophilic molecules tend to form polymeric micelles.⁷⁶⁻⁷⁷ In the case of the copolymers described in this study, they possess moderate hydrophobicity due to the hydrophobic PCys backbone and weakly hydrophilic pendent P'POx block. Consequently, the formation of copolymer vesicles aligns with the behaviour reported in similar systems.⁷⁷ Based on these considerations, a possible formation mechanism for the unit vesicles can be proposed as follows: During the initial stage, copolymer molecules undergo self-assembly to form unit vesicles. The vesicle structure consists of an intermediate layer composed of the PCys block, which interacts through hydrophobic interactions. This intermediate layer is sandwiched between the hydrophilic P'POx blocks in the interior and the corona of the vesicle. Non-covalent interactions among the isopropyl groups of the pendent P'POx blocks in the corona may contribute to secondary aggregation, leading to the formation of compound vesicles with a larger diameter (Scheme 2.2). In our previous studies involving self-assembly of peptide-polymer or pseudopeptide-polymer conjugates, we have also observed a similar mechanism for the

formation of primary micelles, followed by their secondary aggregation into conjugate/compound micelles of larger size.^{27, 78}



Scheme 2.2. Schematic representation of probable formation mechanism of unit vesicle and composite vesicle.

To investigate the aggregation behaviour of the copolymer above its LCST, we performed temperature-dependent DLS measurements. The data showed that the D_h of the G2 copolymer aggregates increased from 25 nm to 490 nm as the temperature was raised from 25 °C to 70 °C (Figure 2.16A).

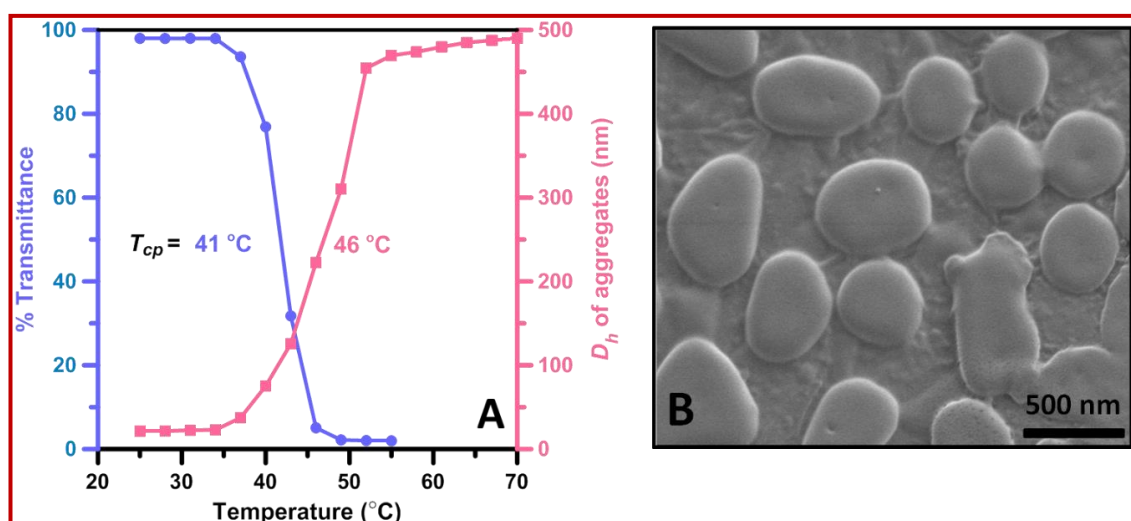


Figure 2.16. (A) Average hydrodynamic diameter of G2 (0.2 wt%, H₂O) vs temperature plot (pink) as measured from DLS. Also, the correlation between D_h (s) (■) and %T (at $\lambda = 500$ nm) (●) of aqueous G2 solution (0.2 wt%) at different temperatures showing prominent cloud point of G2 and (B) FESEM image of aggregated morphology of G2 (0.2 wt %) in water above its T_{cp} (41 °C).

Furthermore, FESEM images revealed the formation of spherical aggregates with a significantly larger size (~ 450 nm) compared to the composite vesicles of G2 observed in water below its LCST (Figure 2.16B). However, the microstructure of these aggregates could not be determined using TEM.

Due to the difference in solubility between the PCys backbone and the pendent P'POx block in nonpolar solvents such as DCM, it was expected that the copolymers would undergo self-aggregation in DCM. We performed DLS of the G2 (0.1 wt%) DCM solution at various time intervals. The DLS data (Figure 2.17A) obtained after clearly demonstrated the presence of both small-sized particles ($D_h \sim 20$ nm) and large-sized particles ($D_h \sim 300$ nm), confirming the

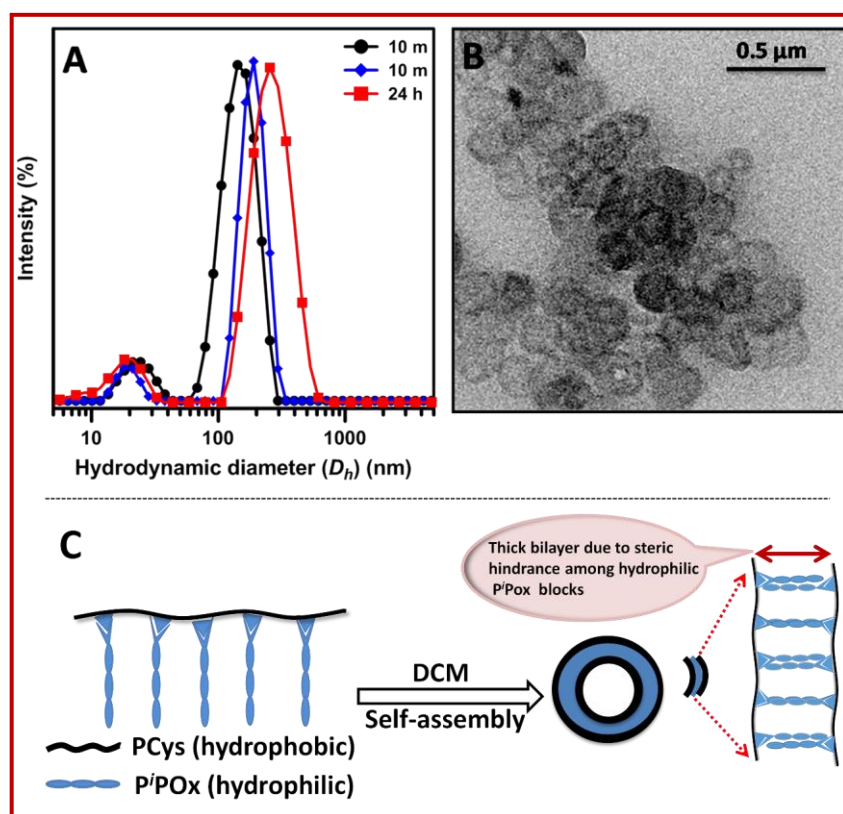


Figure 2.17. DLS curves (A) and TEM image (B) of G2 vesicles in DCM (0.1 wt%). (C) Schematic representation for the formation of vesicles by polypeptide copolymer in DCM.

aggregation of the graft polymer in the DCM solution. TEM imaging (Figure 2.17B) revealed the formation of only large vesicles with an average diameter of approximately 220 nm. The mechanism of vesicle formation in DCM which occurs through a bilayer formation is depicted in Figure 2.13C.

2.4.4. Dye/Drug Encapsulation by Graft Copolymer

Dye encapsulation Block/graft copolymer vesicles, also known as polymersomes, represent highly promising nanostructured systems suitable for encapsulating both hydrophobic and hydrophilic guest molecules in solution.^{58, 79-80} To investigate the encapsulation capability, hydrophobic Nile Red (NR) as a model compound was selected and encapsulated it within representative G2 vesicles in water at a concentration of 0.2 wt%. The results demonstrated a noticeable increase in the emission intensity of NR ($\lambda_{\text{max}} = 630 \text{ nm}$) in the presence of G2 vesicles in water (Figure 2.18A).

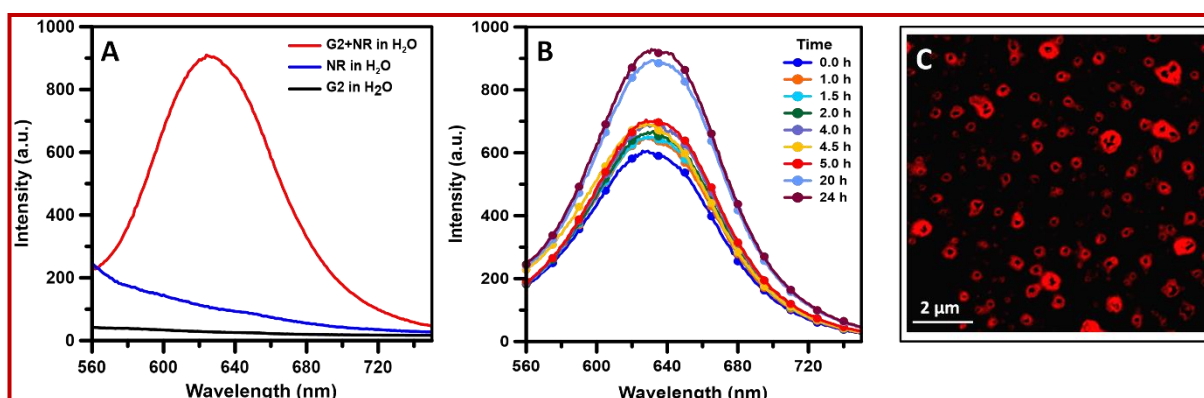
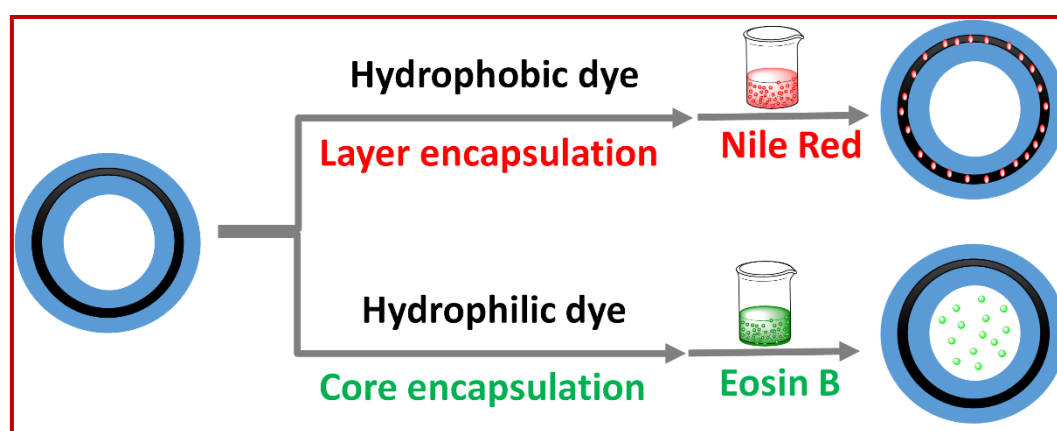


Figure 2.18. (A) fluorescence emission spectra of NR in water in the presence of 0.2 wt% G2 (red line), in the absence of G2 (blue line) and neat G2 molecules in water; (B) Emission spectra of NR in water at different time intervals in the presence of 0.2 wt% of G2.; (C) Fluorescence confocal image of NR-encapsulated G2 vesicles in water showing layer encapsulation.

Conversely, when NR was present without G2 vesicles in water, its solubility was minimal, leading to negligible emission at the same wavelength (Figure 2.18A). Furthermore, the time-dependent uptake of NR by G2 vesicles (0.2 wt%) in water was monitored using fluorescence spectroscopy. The results revealed a gradual increase in the intensity of NR ($\lambda_{\text{max}} = 630 \text{ nm}$) with prolonged incubation time, indicating a slow encapsulation process within the hydrophobic layer of the G2 vesicles (Figure 2.18B). Fluorescence confocal microscopy images of NR-loaded G2 vesicles in water clearly exhibited distinct vesicular structures with black interiors and red coronas, providing visual confirmation of the encapsulation of NR within the vesicular layers (Figure 2.18C). These observations suggested that the NR molecules got encapsulated within the hydrophobic intermediate layer composed of poly(cysteine) (PCys) backbone due to hydrophobic interaction and subsequently dissolved in the aqueous environment (Scheme 2.3).



Scheme 2.3. Schematic representation for the encapsulation behaviors of different dyes by the as-synthesized graft copolymer vesicles in water.

Eosin B (EB), a hydrophilic dye, was selected as a model dye for incubation with G1 for a duration of 24 hours. This incubation aimed to assess the dye's encapsulation within the hydrophilic interior of the G1 vesicles (Scheme 2.3). To achieve this, the aforementioned solution was subjected to

exhaustive dialysis to remove any unencapsulated EB. Analysis of the resultant dialyzed solution through UV spectroscopy (Figure 2.19A), fluorescence emission spectroscopy (Figure 2.19B), and fluorescence confocal microscopy (Figure 2.19C) clearly demonstrated the presence of EB encapsulated within the interior of the vesicles.

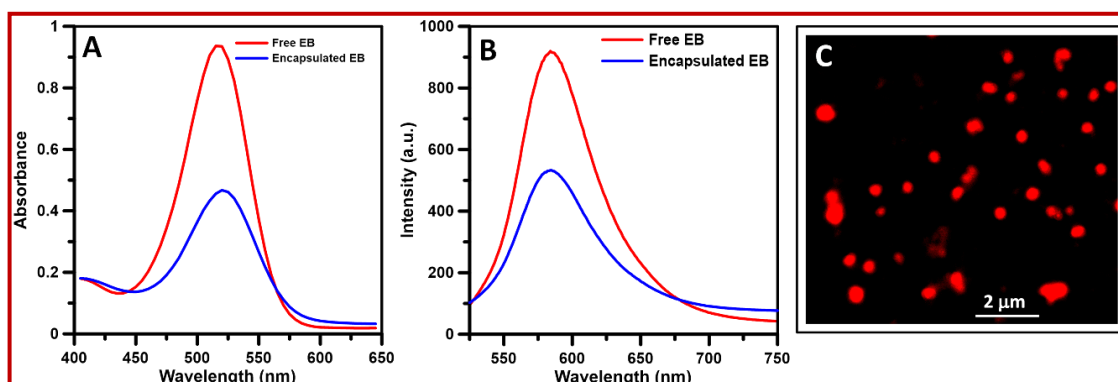


Figure 2.19. (A) Absorption spectra of free EB and EB-encapsulated G1 in water, (B) emission spectra of EB-encapsulated G1 vesicles along with free EB in water and (C) fluorescence confocal microscopic image of EB-loaded G1 vesicles in water.

The UV absorption peak ($\lambda_{\max}= 519$ nm) (Figure 2.19A) and fluorescence emission peak ($\lambda_{\max}= 583$ nm) (Figure 2.19B) of the encapsulated EB within the vesicle's water pool matched those of free EB in water. This outcome suggests that there is no significant interaction between EB and the G1 molecule, and EB molecules are not adsorbed onto the vesicle's surface; instead, they are predominantly localized within the water pool of the vesicles.

To examine the impact of temperature on the release of EB, the emission spectra of EB-loaded G1 vesicles in water was recorded as the solution temperature was incrementally increased (Figure 2.20A). It was observed that the emission intensity of EB exhibited an upward trend with rising temperature, and the rate of increase was particularly pronounced above the T_{cp}

of G1 (45 °C) (Figure 2.20A). This augmentation in emission intensity can be attributed to the disruption of EB-loaded vesicles as temperature increases, leading to the release of the encapsulated EB from the vesicle's interior into the surrounding solution.

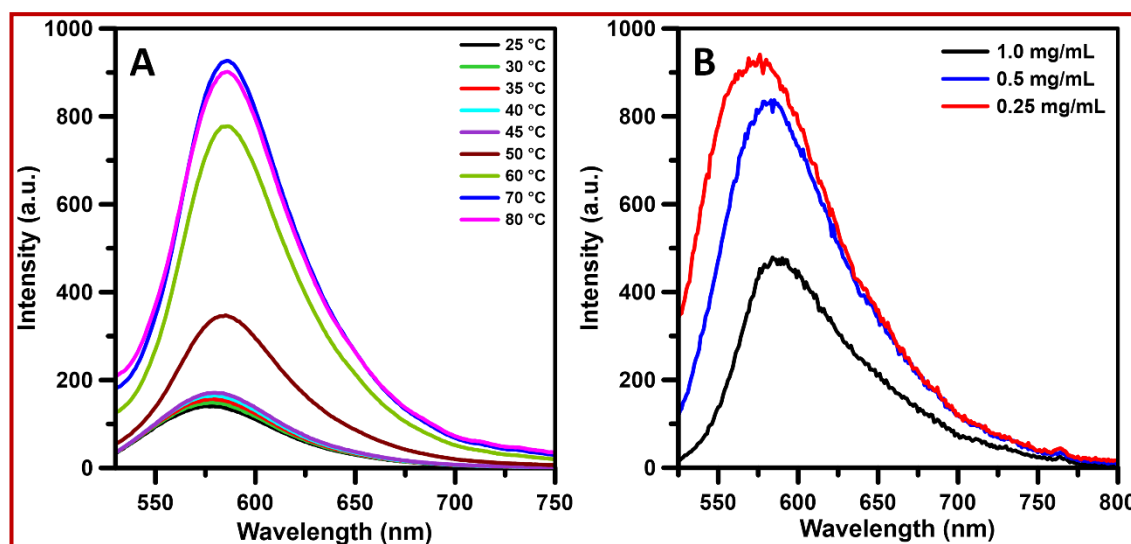


Figure 2.20. (A) Emission spectra of EB-encapsulated G1 vesicle at different temperatures showing increment in intensity with increasing solution temperature; (B) Emission spectra of neat EB in water showing increment in intensity upon dilution.

Above the LCST, the PPOx block of the graft copolymer undergoes a transition to a hydrophobic state due to non-covalent interactions among the isopropyl groups. Consequently, the graft copolymer transforms into a completely hydrophobic polymer at higher temperatures, causing the disruption of the vesicles and facilitating the release of the hydrophilic EB from the vesicle's interior into the external solution. The emission intensity of EB within the vesicle's interior is somewhat quenched due to the higher concentration. However, upon release into the external solution, the concentration of EB decreases, resulting in an increase in emission intensity as the quenching effect diminishes. Moreover, the emission study of EB without

G1 in water clearly indicated an increase in intensity upon dilution (Figure 2.20B).

We investigated the encapsulation of the hydrophilic EB dye within the interior of copolymer vesicles formed in DCM. Initially, EB was insoluble in DCM and did not exhibit any absorbance or emission. However, in the presence of 0.2 wt% of G1 in DCM, the solution's colour transformed into a reddish-pink hue (inset of Figure 2.21A), and an absorption peak at λ_{\max} = 530 nm emerged (Figure 2.21A). The emission spectra of this solution displayed a maximum emission at λ_{\max} = 590 nm (Figure 2.21B) when excited at λ_{ex} =530 nm.

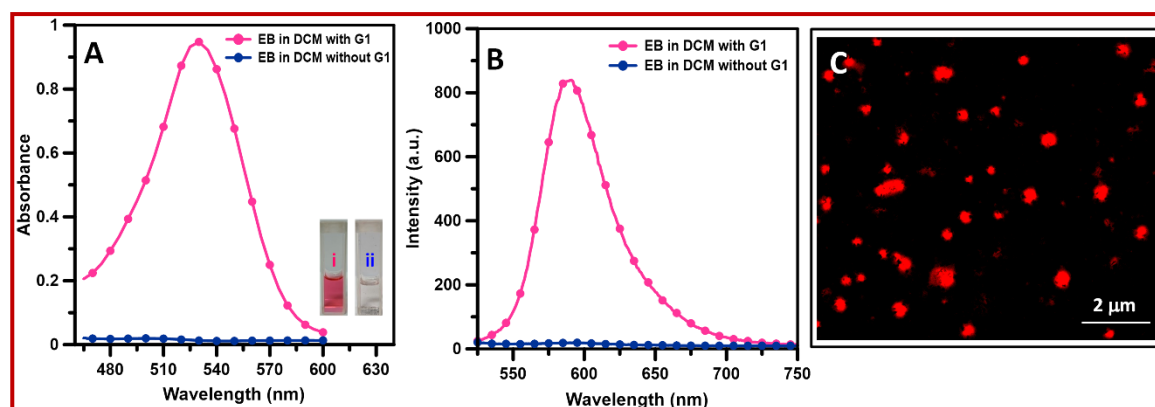


Figure 2.21. (A) UV-vis spectra of free EB and EB-encapsulated G1 in DCM and inset showed difference of color intensity of the EB in DCM with (i) and without (ii) 0.2 wt% of G1 and (B) Emission spectra (λ_{\max} = 590 nm) of free EB and EB-encapsulated G1 in DCM (C) Fluorescence confocal microscopic image of EB-loaded G1 vesicles in DCM.

In DCM, the vesicle's bilayer consists of a hydrophilic P'POx block, which readily facilitates the encapsulation of hydrophilic EB molecules. The thickness of this hydrophilic bilayer is expected to be greater than that of vesicles formed by the copolymer in water (Figure 2.21C). Consequently, in DCM, the G1 vesicles efficiently solubilize the EB dye, resulting in the prominent appearance of absorption and emission peaks. The concentration of dye

adsorbed by this thicker layer is also anticipated to be higher, making it challenging to differentiate between the interior and shell layers of the vesicles based on the confocal image (Figure 2.21C), in contrast to the confocal image of NR-encapsulated vesicles in water (Figure 2.18C).

Drug encapsulation We conducted further investigations to assess the encapsulating behaviour of representative G2 vesicles towards the well-known anticancer drug doxorubicin (Dox). Our observations indicated that the absorption (Figure 2.22A) and emission intensities (Figure 2.22B) of Dox encapsulated within G2 vesicles were lower compared to the freely dissolved Dox molecules in water. The use of fluorescence confocal microscopy confirmed the encapsulation of the drug within the hydrophilic water pool of the G2 vesicles in water (Figure 2.22C).

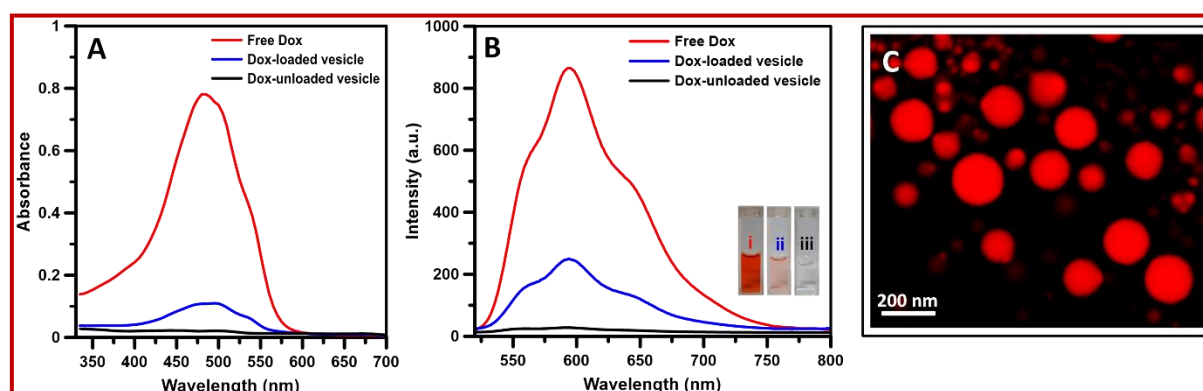


Figure 2.22. (A) UV-vis spectra of free and encapsulated-Dox in water; (B) Emission spectra of free and encapsulated-Dox in water with inset showing photographs of colour changes in free Dox (i), Dox-loaded G2 vesicles (ii) compared to vesicles after Dox release (iii); (C) Fluorescence confocal microscopic image of Dox-loaded G2 vesicle in water.

The drug loading capacity of G2 vesicles was determined by constructing a calibration curve using varying concentrations of free Dox in water and measuring its absorbance (Figure A2.11). The drug loading capacity of G2 was

found to be 0.79 mg per 6 mg of G2 copolymer. The loaded Dox could be easily released from the vesicles by heating, where the Dox molecules were released from the hydrophilic interior water pool of the vesicles into the surrounding bulk water. This was evidenced by the increase in fluorescence emission intensity of Dox with increasing solution temperature (Figure 2.23). In contrast, the emission intensity of Dox molecules without copolymer vesicles remained unchanged between 25 to 85 °C (inset of Figure 2.23) as reported by Wang et al.⁸¹ The lesser quenching of intensity observed for free Dox compared to encapsulated Dox inside the vesicles may explain the increase in emission intensity, as it was noted that the intensity of Dox without any copolymer in water increased upon dilution (Figure A2.13).

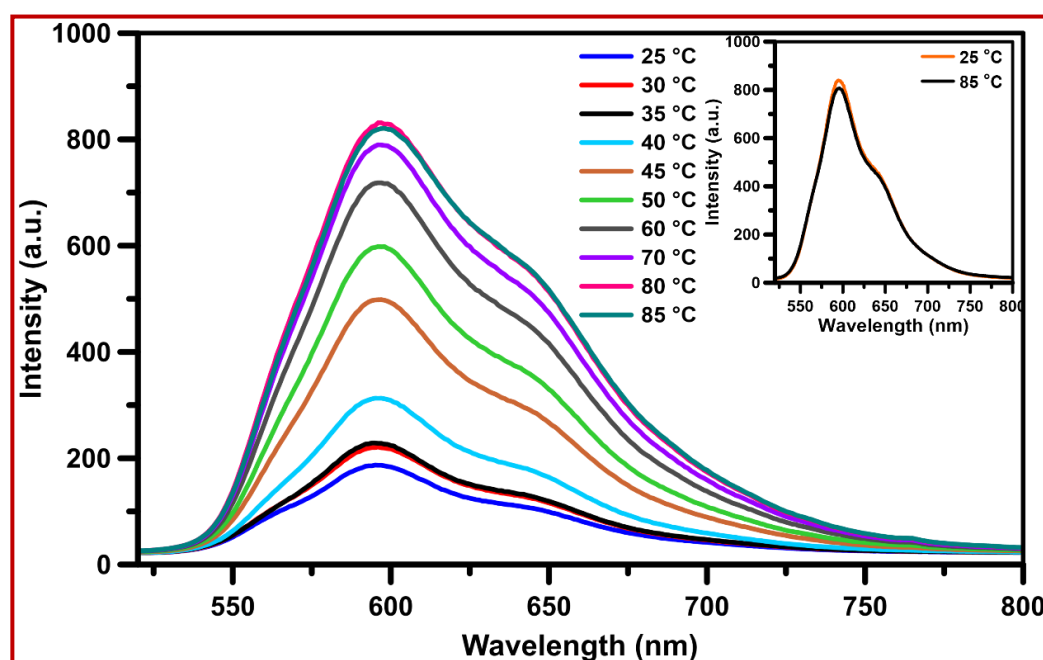


Figure 2.23. Fluorescence emission spectra of Dox-loaded vesicle (G2) as a function of increasing temperature from 25 to 85 °C. Inset showing fluorescence emission spectra of free Dox in water at two extreme temperatures exhibiting no such change in intensity.

We also investigated the release of Dox from G2 vesicles under acidic conditions. Both the polycysteine and poly(2-oxazoline) segments of the graft copolymers are known to respond to external acidic environments. Therefore, it was speculated that the addition of acid might affect the graft copolymers, consequently leading to the release of the encapsulated drug molecule from the interior of the formed graft copolymer vesicles. It was observed that the emission intensity of Dox in the aqueous solution of G2 gradually increased with increasing HCl concentration, and after the addition of 100 μL of concentrated HCl, it became nearly equal to that of free Dox without G2 in water (Figure 2.24).

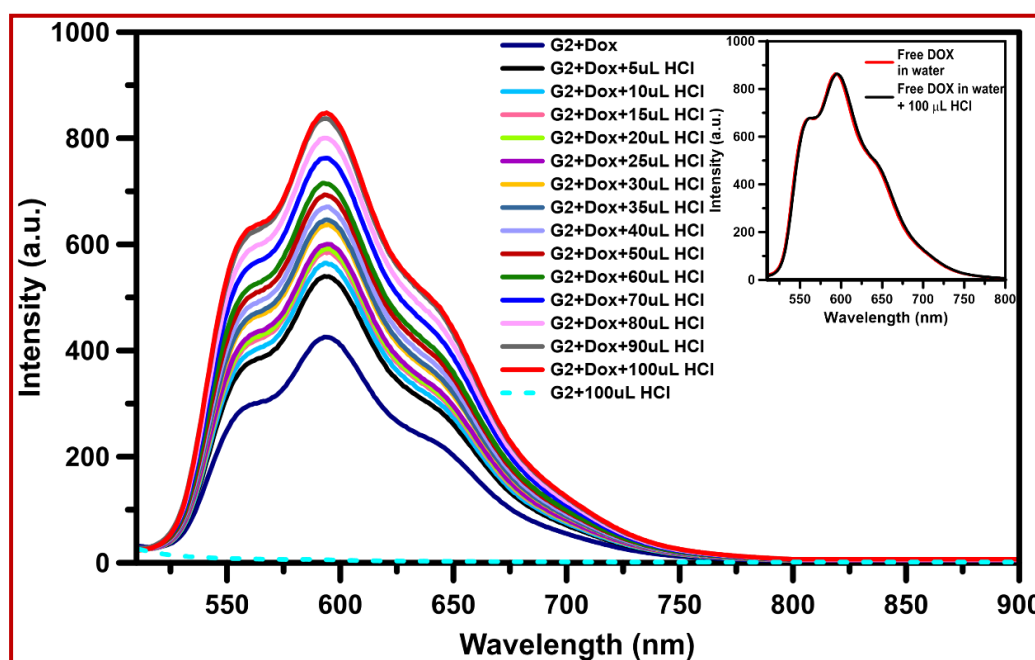


Figure 2.24. Fluorescence emission spectra of Dox-loaded vesicles (G2) suspensions after treated with HCl of varying concentrations and inset showing fluorescence emission spectra of neat Dox in water in the presence of concentrated HCl (12 N) showing no such change in intensity.

However, the control experiment involving the addition of HCl without G2 did not show any change in the intensity of free Dox (inset of Figure 2.24).

Furthermore, dialysis of the acid-treated Dox-encapsulated G2 solution against water and subsequent measurements demonstrated negligible absorbance (Figure 2.22A) and emission intensity of Dox (Figure 2.22B). These findings indicated that Dox was released from the interior of the vesicles upon acid treatment. This release could be attributed to the significant change in the vesicles' size due to swelling caused by the alteration of the copolymer's chemical nature in the presence of concentrated HCl, as evidenced by the dynamic light scattering (DLS) (Figure 2.25A) and transmission electron microscopy (TEM) (Figure 2.25B) results of the Dox-loaded G2 vesicles after treatment with HCl. The size of G2 vesicles changed from 300 to 408 nm and approximately 160 to 300 nm as determined by DLS and TEM experiments, respectively.

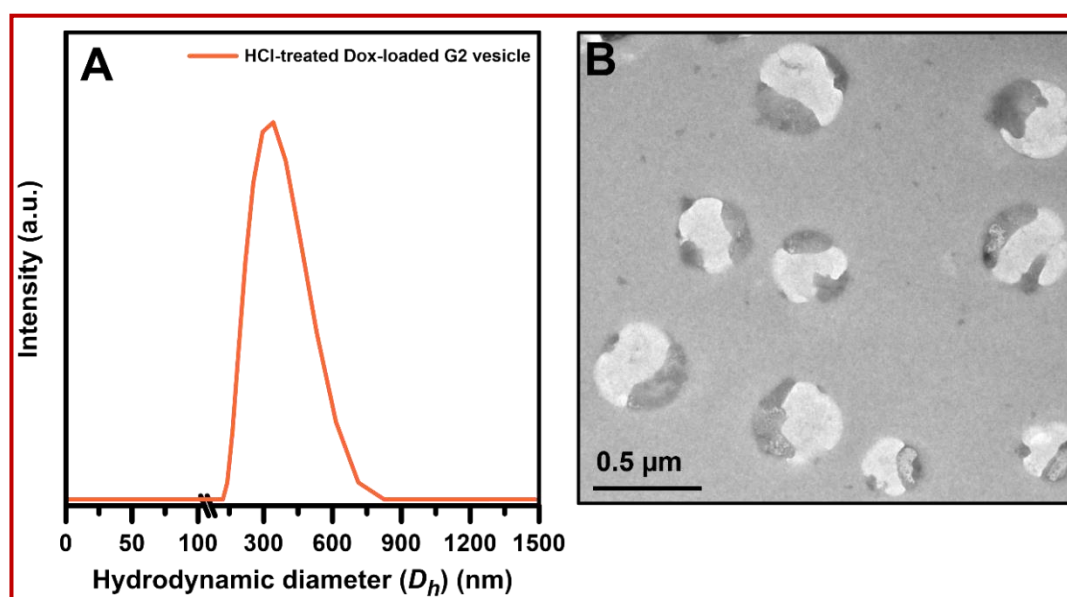


Figure 2.25. Dox-loaded G2 vesicles after treated with HCl: (A) DLS data and (B) TEM image.

It is expected that similar to acid treatment, the chemical nature of the synthetic polypeptide may also undergo changes in the presence of alkali. To investigate this, a Dox-loaded G2 vesicular solution was treated with

concentrated NaOH (12 N). A colour change from light orange to faint blue to colourless was observed (Figure 2.26A). The intensities of the absorption (Figure 2.26A) and emission (Figure 2.26B) peaks of Dox-loaded G2 also decreased sharply and eventually disappeared. The control experiment involving the treatment of free Dox molecules with alkali in water yielded the same results (inset of Figures 2.26A and 2.26B). Consequently, it is challenging to determine whether the release of Dox from G2 vesicles can be modulated by alkali treatment.

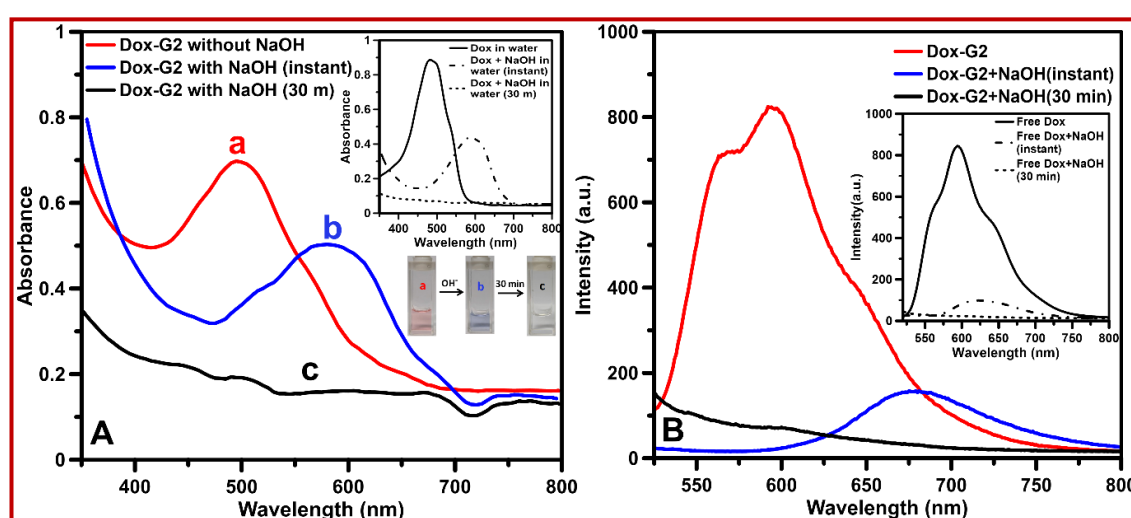


Figure 2.26. (A) Absorption spectra of Dox encapsulated in G2 along with its base (NaOH) treated solution. Inset showed its colour change and the results of control experiment of free Dox in presence of base. (B) Emission spectra of Dox encapsulated in G2 along with its base (NaOH) treated solution. Inset showing results of control experiment of free Dox in presence of base (NaOH).

The release of encapsulated Dox from the interior of G2 vesicles was also investigated using a phosphate buffer solution at two different pH values (4.5 and 7.4) at 37 °C. Upon treating the Dox-loaded vesicles with a buffer solution of pH 4.5 at 37 °C, an increase in the emission intensity of Dox was observed (Figure 2.27). However, no such increase in emission intensity was observed

when the vesicles were treated with a buffer solution at a physiological pH of 7.4 (Figure 2.27).

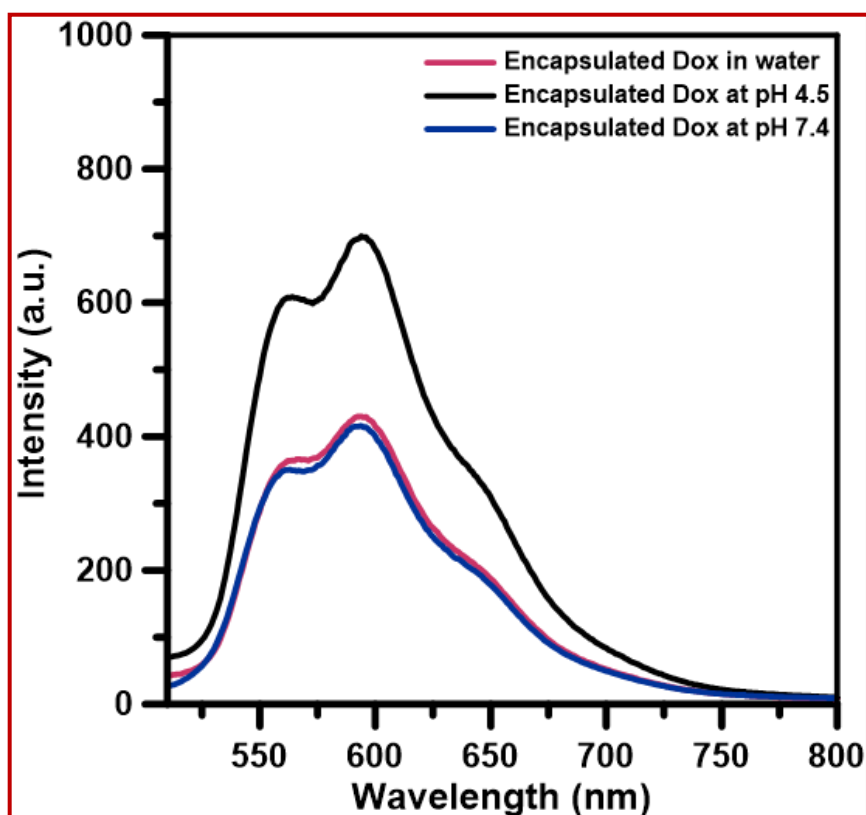


Figure 2.27. Emission spectra of Dox encapsulated in G2 in phosphate buffer solution at two different pHs (4.5 and 7.4) at 37 °C.

These results suggest that Dox is released from the vesicle in an acidic environment while there is no release in a slightly basic environment. Given that Dox is a well-known anticancer drug and cancer cells are known to be highly acidic in nature, these experimental findings support the notion that the synthesized graft copolymer effectively encapsulates Dox for targeted release within cancer cells without interference from other functionalities. We assume that these graft copolymers would be biocompatible as both segments of the graft copolymer, namely polycysteine and poly(2-isopropyl-2-oxazoline), are known to exhibit biocompatible properties.

2.5. Conclusion

In conclusion, we successfully synthesized amphiphilic water-soluble polypeptide copolymers (PCys-*g*-PiPOx)s through the "click" grafting of azide-functionalized poly(2-isopropyl-2-oxazoline) blocks with hydrophobic alkyne-functionalized polycysteine blocks. The synthesis of these polymer blocks involved the ROP and CROP techniques. CD spectral analysis revealed a loss of β -sheet-like secondary structure in PCys due to grafting with the P'POx block. The copolymer exhibited tunable cloud point and thermoresponsive behaviour in aqueous solutions due to the presence of the P'POx block. Instead of forming micelles, this amphiphilic PCys-*g*-P'POx copolymer, with moderate hydrophobicity, self-assembled into vesicles in both aqueous and non-aqueous media. The vesicles efficiently encapsulated hydrophobic and hydrophilic guest molecules within their shell layer and interior, respectively. Furthermore, the anticancer drug doxorubicin (Dox) could be loaded into the interior water pool of these graft copolymer vesicles and released effectively by heating above the copolymer's cloud point or treating with concentrated HCl. Dox release from the copolymer vesicles was also achieved by treating them with a phosphate buffer at an acidic pH of 4.5, while a physiological buffer at pH 7.4 did not affect the release of Dox from the vesicles. Thus, these biocompatible polypeptide graft copolymers hold great promise as vesicular drug delivery agents.

2.6. Appendix: Characterization and Other Experimental Data

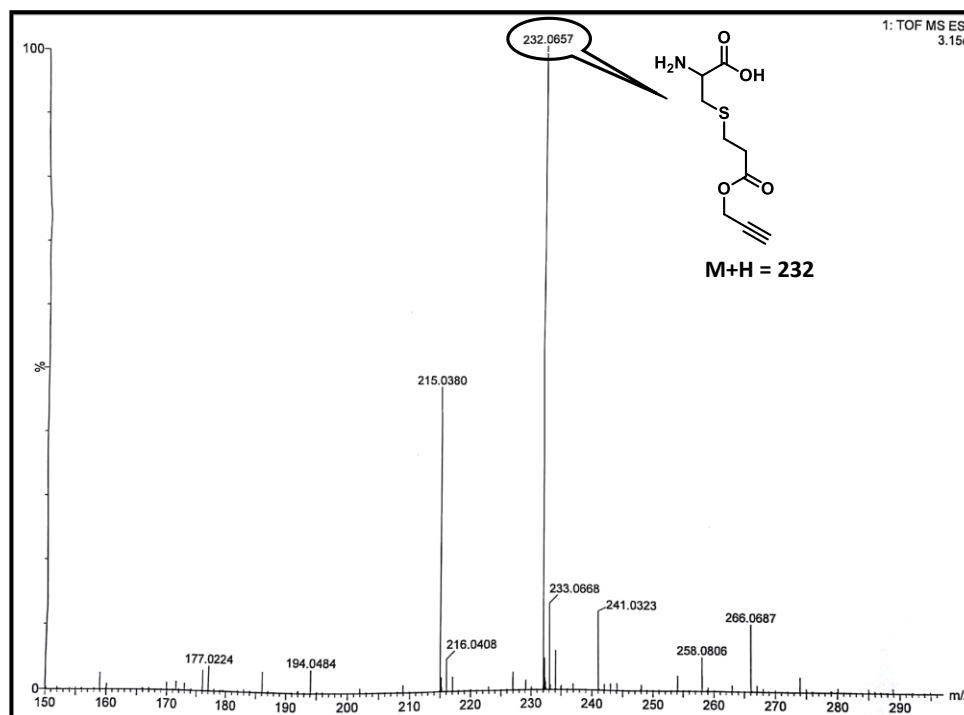


Figure A2.1. ESI-MS spectrum of Cys-S-Pr in mixture of MeOH: H₂O (1:1).

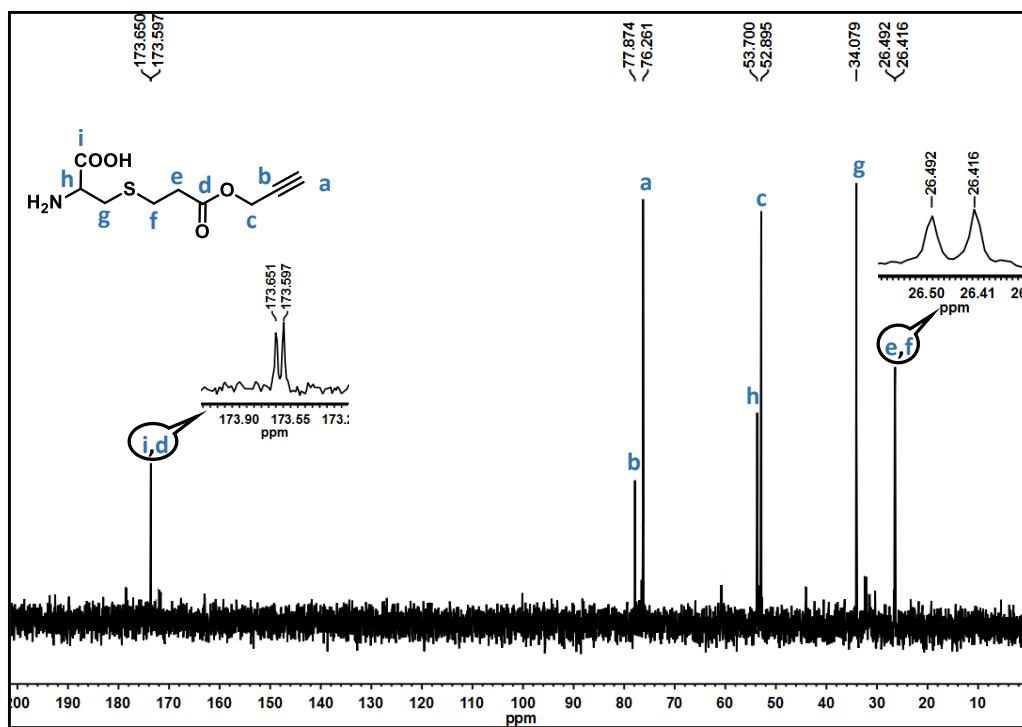


Figure A2.2. ¹³C-NMR spectrum of Cys-S-Pr in D₂O.

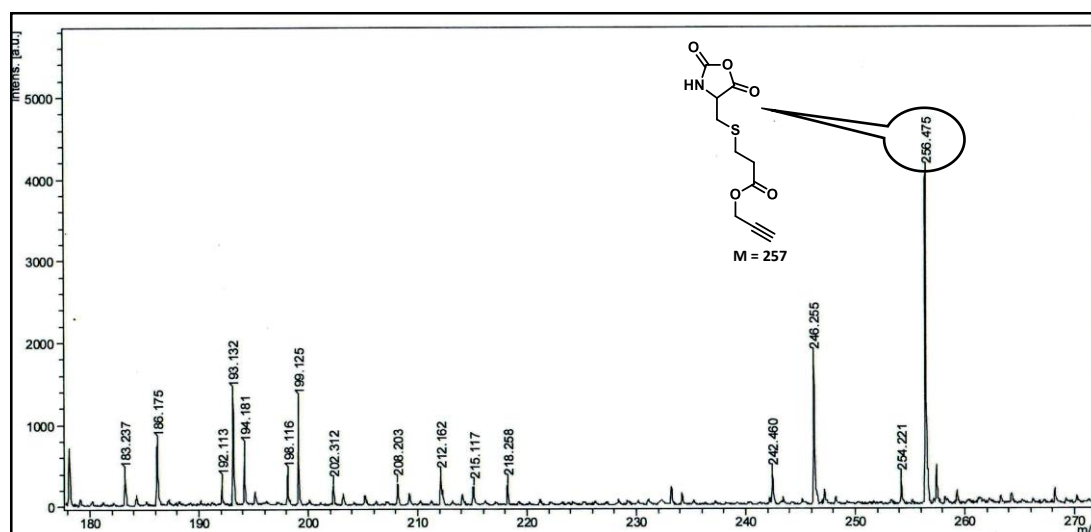


Figure A2.3. MALDI-TOF-MS spectrum of Cys-S-Pr NCA.

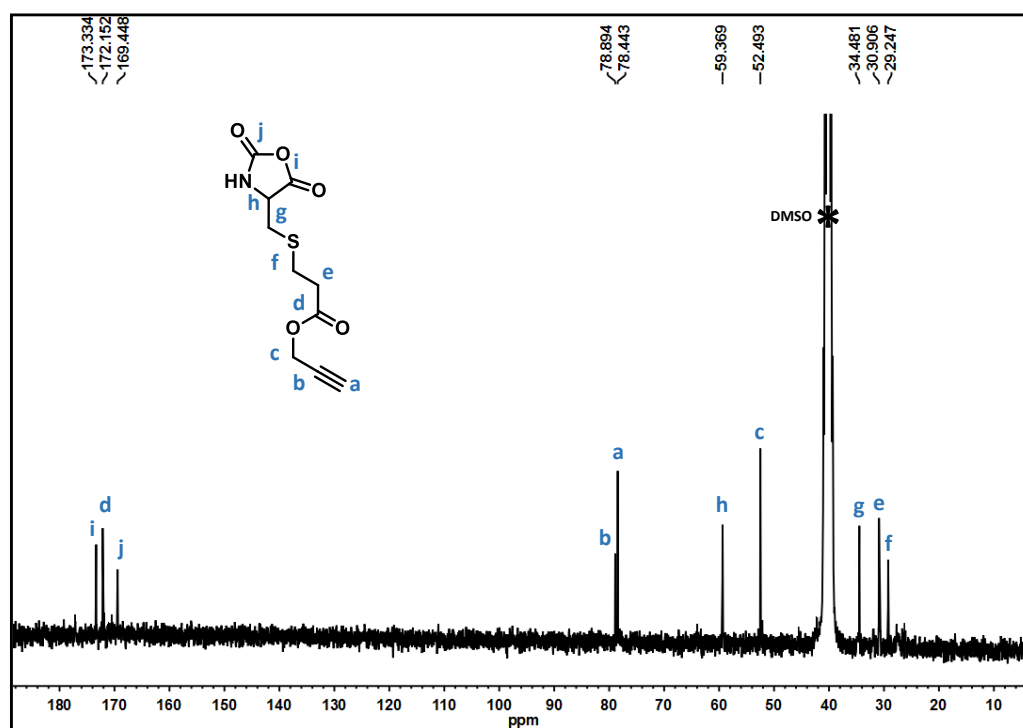


Figure A2.4. ^{13}C -NMR spectrum of Cys-S-Pr NCA in DMSO-d_6 .

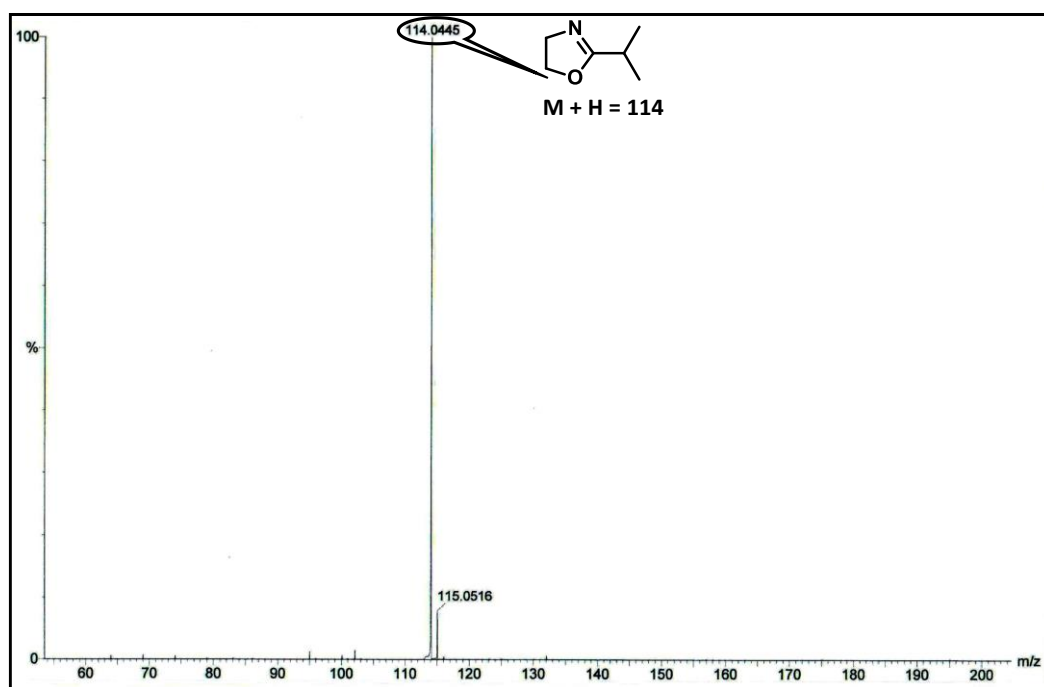


Figure A2.5. ESI-MS spectrum of ¹POx in DCM, m/z (%) = 114.044 (M+1H⁺)

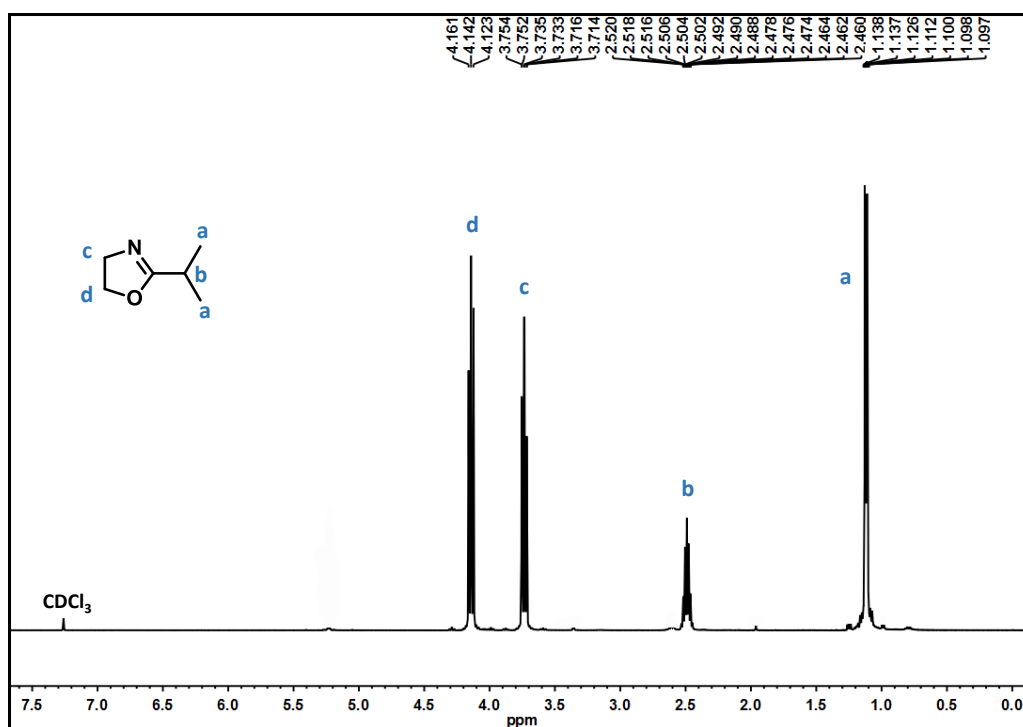


Figure A2.6. ¹H-NMR spectrum of ¹POx in CDCl₃

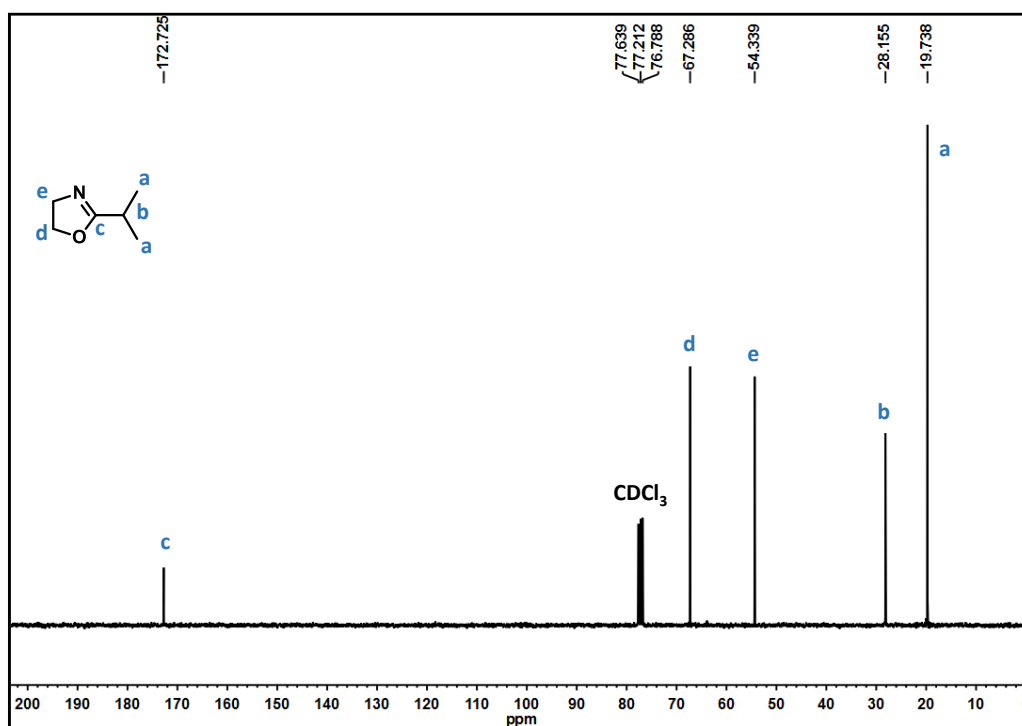


Figure A2.7. ^{13}C -NMR spectrum of POx in CDCl_3

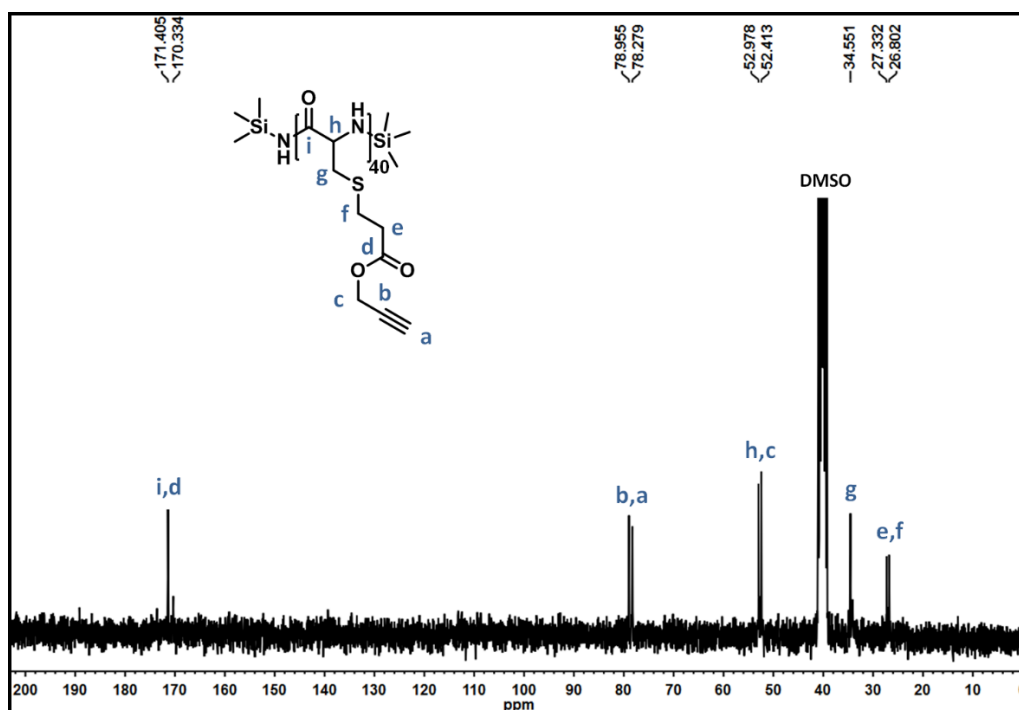


Figure A2.8. ^{13}C -NMR spectrum of PCys-S-Pr (C2) in DMSO-d_6

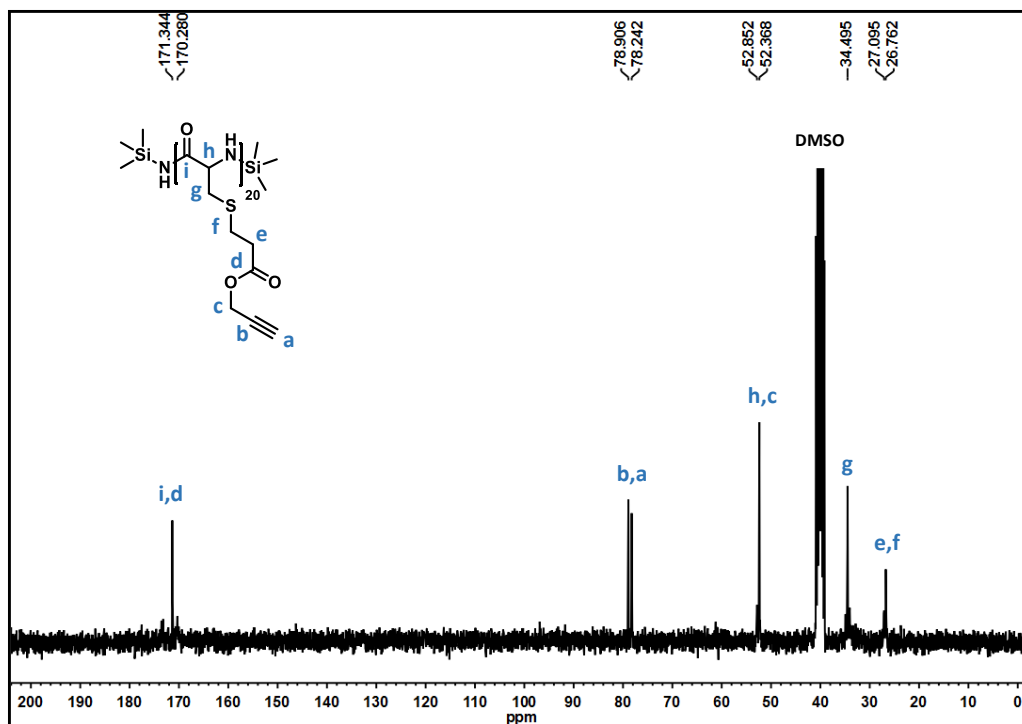


Figure A2.9. ^{13}C -NMR spectrum of PCys-S-Pr (C1) in DMSO-d_6 .

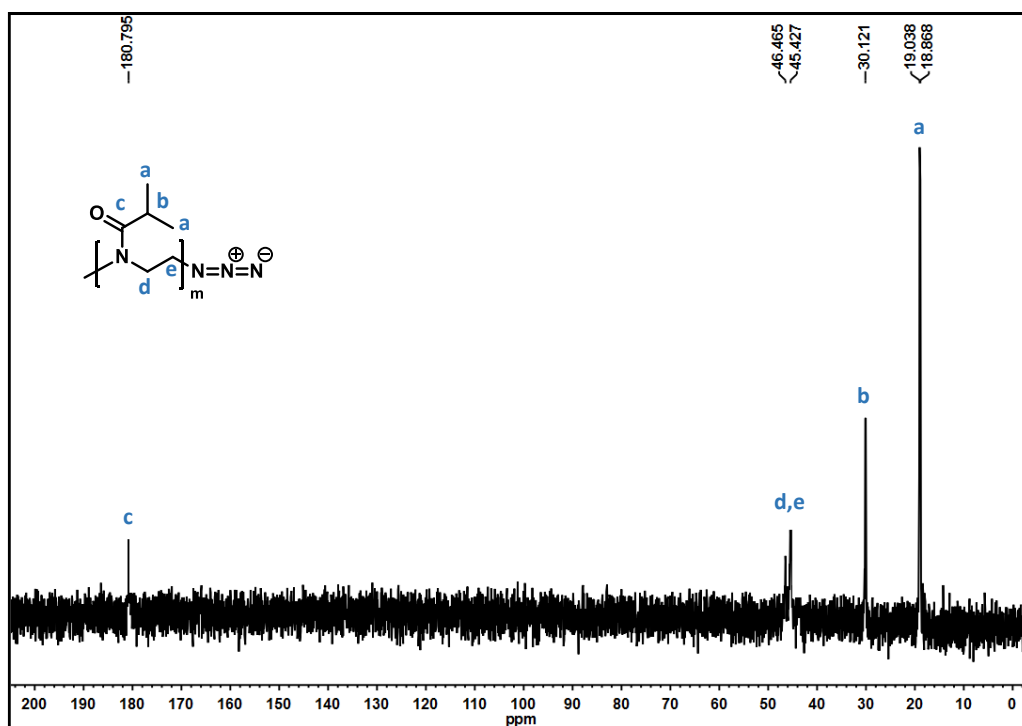


Figure A2.10. ^{13}C -NMR spectrum of P'POx (P1) in D_2O .

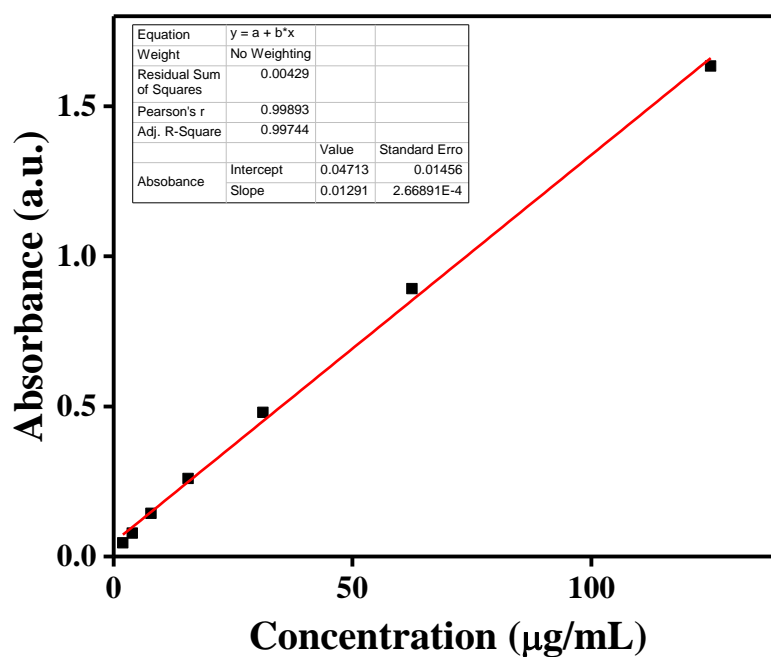


Figure A.2.11. Calibration curve of neat Dox in water.

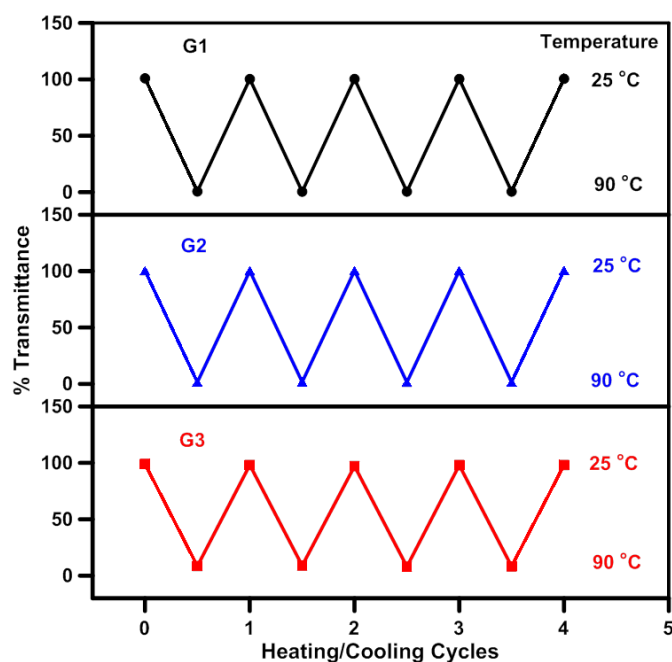


Figure A2.12. Temperature dependent % transmittance of aqueous PCys-*g*-P'POx samples (0.2 wt%) during heating/cooling cycles. Each data point was obtained after equilibrating the sample solution at a particular temperature for 5 min.

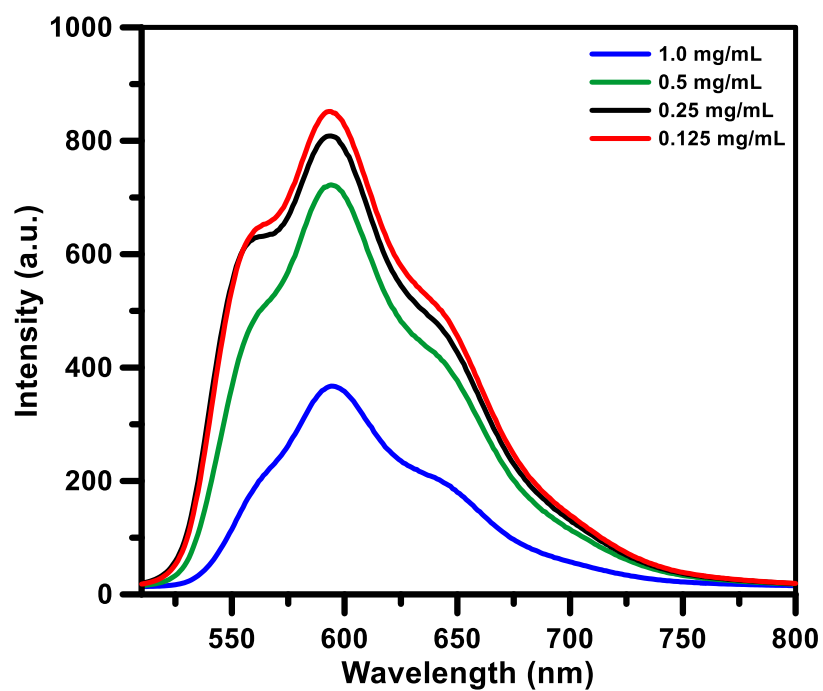


Figure A2.13. Emission spectra of neat Dox in water showing increment in intensity upon dilution.

2.7. References

1. Colson, Y. L.; Grinstaff, M. W., Biologically Responsive Polymeric Nanoparticles for Drug Delivery. *Adv. Mater.* **2012**, *24*, 3878-3886.
2. Deming, T. J., Polypeptide Materials: New Synthetic Methods and Applications. *Adv. Mater.* **1997**, *9*, 299-311.
3. Deming, T. J., Preparation and Development of Block Copolypeptide Vesicles and Hydrogels for Biological and Medical Applications. *Wiley Interdisciplinary Reviews: Nanomedicine and Nanobiotechnology* **2014**, *6*, 283-297.
4. Su, Y.-R.; Yu, S.-H.; Chao, A.-C.; Wu, J.-Y.; Lin, Y.-F.; Lu, K.-Y.; Mi, F.-L., Preparation and Properties of Ph-Responsive, Self-Assembled Colloidal Nanoparticles from Guanidine-Containing Polypeptide and Chitosan for Antibiotic Delivery. *Colloids Surf. A* **2016**, *494*, 9-20.
5. Sun, Y. T.; Wollenberg, A. L.; O'Shea, T. M.; Cui, Y. X.; Zhou, Z. H.; Sofroniew, M. V.; Deming, T. J., Conformation-Directed Formation of Self-Healing Diblock Copolypeptide Hydrogels Via Polyion Complexation. *J. Am. Chem. Soc.* **2017**, *139*, 15114-15121.
6. Wollenberg, A. L.; Perlin, P.; Deming, T. J., Versatile N-Methylaminoxy-Functionalized Polypeptides for Preparation of Neoglycoconjugates. *Biomacromolecules* **2019**, *20*, 1756-1764.
7. Zhang, L.; Lipik, V.; Miserez, A., Complex Coacervates of Oppositely Charged Co-Polypeptides Inspired by the Sandcastle Worm Glue. *J. Mater. Chem. B* **2016**, *4*, 1544-1556.
8. Dai, J.; Lin, S.; Cheng, D.; Zou, S.; Shuai, X., Interlayer-Crosslinked Micelle with Partially Hydrated Core Showing Reduction and Ph Dual Sensitivity for Pinpointed Intracellular Drug Release. *Angew. Chem. Int. Ed.* **2011**, *50*, 9404-9408.

9. Zhang, P.; Wu, H.; Wu, H.; Lu, Z.; Deng, C.; Hong, Z.; Jing, X.; Chen, X., Rgd-Conjugated Copolymer Incorporated into Composite of Poly(Lactide-Co-Glycotide) and Poly(L-Lactide)-Grafted Nanohydroxyapatite for Bone Tissue Engineering. *Biomacromolecules* **2011**, *12*, 2667-2680.
10. Paik, B. A.; Mane, S. R.; Jia, X.; Kiick, K. L., Responsive Hybrid (Poly)Peptide-Polymer Conjugates. *J. Mater. Chem. B* **2017**, *5*, 8274-8288.
11. Sun, H.; Hong, Y.; Xi, Y.; Zou, Y.; Gao, J.; Du, J., Synthesis, Self-Assembly, and Biomedical Applications of Antimicrobial Peptide-Polymer Conjugates. *Biomacromolecules* **2018**, *19*, 1701-1720.
12. Pechar, M.; Kopeckova, P.; Joss, L.; Kopecek, J., Associative Diblock Copolymers of Poly (Ethylene Glycol) and Coiled-Coil Peptides. *Macromol. Biosci.* **2002**, *2*, 199-206.
13. Vandermeulen, G. W. M.; Tziatzios, C.; Duncan, R.; Klok, H.-A., Peg-Based Hybrid Block Copolymers Containing A-Helical Coiled Coil Peptide Sequences: Control of Self-Assembly and Preliminary Biological Evaluation. *Macromolecules* **2005**, *38*, 761-769.
14. Vandermeulen, G. W. M.; Tziatzios, C.; Klok, H.-A., Reversible Self-Organization of Poly (Ethylene Glycol)-Based Hybrid Block Copolymers Mediated by a De Novo Four-Stranded A-Helical Coiled Coil Motif. *Macromolecules* **2003**, *36*, 4107-4114.
15. Huang, J.; Heise, A., Stimuli Responsive Synthetic Polypeptides Derived from N-Carboxyanhydride (Nca) Polymerisation. *Chem. Soc. Rev.* **2013**, *42*, 7373-7390.
16. Meng, F.; Zhong, Z., Polymersomes Spanning from Nano-to-Microscales: Advanced Vehicles for Controlled Drug Delivery and Robust Vesicles for Virus and Cell Mimicking. *J. Phys. Chem. Lett.* **2011**, *2*, 1533-1539.
17. Shen, Y.; Fu, X.; Fu, W.; Li, Z., Biodegradable Stimuli-Responsive Polypeptide Materials Prepared by Ring Opening Polymerization. *Chem. Soc. Rev.* **2015**, *44*, 612-622.

18. Zhang, S.; Li, Z., Stimuli-Responsive Polypeptide Materials Prepared by Ring-Opening Polymerization of L-Amino Acid N-Carboxyanhydrides. *J. Polym. Sci. B: Polym. Phys.* **2013**, *51*, 546-555.
19. Baldwin, S. P.; Saltzman, W. M., Materials for Protein Delivery in Tissue Engineering. *Adv. Drug Deliv. Rev.* **1998**, *33*, 71-86.
20. Shi, F.; Ding, J.; Xiao, C.; Zhuang, X.; He, C.; Chen, L.; Chen, X., Intracellular Microenvironment Responsive Pegylated Polypeptide Nanogels with Ionizable Cores for Efficient Doxorubicin Loading and Triggered Release. *J. Mater. Chem.* **2012**, *22*, 14168-14179.
21. Fu, X.; Shen, Y.; Fu, W.; Li, Z., Thermoresponsive Oligo (Ethylene Glycol) Functionalized Poly-L-Cysteine. *Macromolecules* **2013**, *46*, 3753-3760.
22. Holowka, E. P.; Pochan, D. J.; Deming, T. J., Charged Polypeptide Vesicles with Controllable Diameter. *J. Am. Chem. Soc.* **2005**, *127*, 12423-12428.
23. Murphy, R.; Borase, T.; Payne, C.; O'Dwyer, J.; Cryan, S. A.; Heise, A., Hydrogels from Amphiphilic Star Block Copolypeptides. *RSC Adv.* **2016**, *6*, 23370-23376.
24. Paira, T. K.; Banerjee, S.; Raula, M.; Kotal, A.; Si, S.; Mandal, T. K., Peptide-Polymer Bioconjugates Via Atom Transfer Radical Polymerization and Their Solution Aggregation into Hybrid Micro/Nanospheres for Dye Uptake. *Macromolecules* **2010**, *43*, 4050-4061.
25. Ahrens, C. C.; Welch, M. E.; Griffith, L. G.; Hammond, P. T., Uncharged Helical Modular Polypeptide Hydrogels for Cellular Scaffolds. *Biomacromolecules* **2015**, *16*, 3774-3783.
26. Guo, A.-r.; Yang, W.-x.; Yang, F.; Yu, R.; Wu, Y.-x., Well-Defined Poly (G-Benzyl-L-Glutamate)-G-Polytetrahydrofuran: Synthesis, Characterization and Properties. *Macromolecules* **2014**, *47*, 5450-5461.
27. Bose, A.; Jana, S.; Saha, A.; Mandal, T. K., Amphiphilic Polypeptide-Polyoxazoline Graft Copolymer Conjugate with Tunable Thermoresponsiveness: Synthesis and Self-Assembly into Various

- Micellar Structures in Aqueous and Nonaqueous Media. *Polymer* **2017**, *110*, 12-24.
28. Cai, C.; Wang, L.; Lin, J., Self-Assembly of Polypeptide-Based Copolymers into Diverse Aggregates. *Chem. Commun.* **2011**, *47*, 11189-11203.
 29. Zhang, X.; Li, J.; Li, W.; Zhang, A., Synthesis and Characterization of Thermo-and Ph-Responsive Double-Hydrophilic Diblock Copolypeptides. *Biomacromolecules* **2007**, *8*, 3557-3567.
 30. De, P.; Sumerlin, B. S., Precision Control of Temperature Response by Copolymerization of Di (Ethylene Glycol) Acrylate and an Acrylamide Comonomer. *Macromol. Chem. Phys.* **2013**, *214*, 272-279.
 31. He, X.; Zhou, R.; Ge, C.; Ling, Y.; Luan, S.; Tang, H., Oegylated Polypeptide Bearing Y-Shaped Pendants with a Lcst Close to Body Temperature: Synthesis and Thermoresponsive Properties. *Eur. Polym. J.* **2019**, *112*, 547-554.
 32. Roy, S. G.; Bauri, K.; Pal, S.; Goswami, A.; Madras, G.; De, P., Synthesis, Characterization and Thermal Degradation of Dual Temperature- and Ph-Sensitive Raft-Made Copolymers of N, N-(Dimethylamino)Ethyl Methacrylate and Methyl Methacrylate. *Polym. Int.* **2013**, *62*, 463-473.
 33. Zhao, L.; Wang, X.; Sun, L.; Zhou, R.; Zhang, X.; Zhang, L.; Zheng, Z.; Ling, Y.; Luan, S.; Tang, H., Synthesis and Ucst-Type Thermoresponsive Properties of Polypeptide Based Single-Chain Nanoparticles. *Polym. Chem.* **2019**, *10*, 5206-5214.
 34. Jana, S.; Biswas, Y.; Anas, M.; Saha, A.; Mandal, T. K., Poly [Oligo (2-Ethyl-2-Oxazoline) Acrylate]-Based Poly (Ionic Liquid) Random Copolymers with Coexistent and Tunable Lower Critical Solution Temperature- and Upper Critical Solution Temperature-Type Phase Transitions. *Langmuir* **2018**, *34*, 12653-12663.
 35. Jana, S.; Biswas, Y.; Mandal, T. K., Methionine-Based Cationic Polypeptide/Polypeptide Block Copolymer with Triple-Stimuli

- Responsiveness: DNA Polyplexation and Phototriggered Release. *Polym. Chem.* **2018**, *9*, 1869-1884.
36. Roy, D.; Cambre, J. N.; Sumerlin, B. S., Future Perspectives and Recent Advances in Stimuli-Responsive Materials. *Prog. Polym. Sci.* **2010**, *35*, 278-301.
37. Hocine, S.; Li, M.-H., Thermoresponsive Self-Assembled Polymer Colloids in Water. *Soft Matter* **2013**, *9*, 5839-5861.
38. Deng, Y.; Wang, X.; Yuan, Q.; Zhu, M.; Ling, Y.; Tang, H., Synthesis, Characterization, and Thermoresponsive Properties of Helical Polypeptides Derivatized from Poly (G-4-(3-Chloropropoxycarbonyl)Benzyl-L-Glutamate). *J. Polym. Sci. A: Polym. Chem.* **2015**, *53*, 2469-2480.
39. Motornov, M.; Roiter, Y.; Tokarev, I.; Minko, S., Stimuli-Responsive Nanoparticles, Nanogels and Capsules for Integrated Multifunctional Intelligent Systems. *Prog. Polym. Sci.* **2010**, *35*, 174-211.
40. Ding, A.; Xu, J.; Gu, G.; Lu, G.; Huang, X., Phea-G-Pmma Well-Defined Graft Copolymer: Atrp Synthesis, Self-Assembly and Synchronous Encapsulation of Both Hydrophobic and Hydrophilic Guest Molecules. *Sci. Rep.* **2017**, *7*, 12601.
41. Lee, H. J.; Yang, S. R.; An, E. J.; Kim, J.-D., Biodegradable Polymersomes from Poly (2-Hydroxyethyl Aspartamide) Grafted with Lactic Acid Oligomers in Aqueous Solution. *Macromolecules* **2006**, *39*, 4938-4940.
42. Liu, H.; Zhang, S.; Feng, C.; Li, Y.; Lu, G.; Huang, X., Synthesis and Self-Assembly of a Fluorine-Containing Amphiphilic Graft Copolymer Bearing a Perfluorocyclobutyl Aryl Ether-Based Backbone and Poly(Acrylic Acid) Side Chains. *Polym. Chem.* **2015**, *6*, 4309-4318.
43. Qian, W.; Song, T.; Ye, M.; Xu, P.; Lu, G.; Huang, X., Paa-G-Pla Amphiphilic Graft Copolymer: Synthesis, Self-Assembly and Drug Loading Ability. *Polym. Chem.* **2017**, *8*, 4098-4107.

44. Pechar, M.; Pola, R.; Laga, R.; Braunova, A.; Filippov, S. K.; Bogomolova, A.; Bednarova, L.; Vanek, O.; Ulbrich, K., Coiled Coil Peptides and Polymer–Peptide Conjugates: Synthesis, Self-Assembly, Characterization and Potential in Drug Delivery Systems. *Biomacromolecules* **2014**, *15*, 2590-2599.
45. Kaberov, L. I.; Verbraeken, B.; Riabtseva, A.; Brus, J.; Radulescu, A.; Talmon, Y.; Stepanek, P.; Hoogenboom, R.; Filippov, S. K., Fluorophilic–Lipophilic–Hydrophilic Poly(2-Oxazoline) Block Copolymers as MRI Contrast Agents: From Synthesis to Self-Assembly. *Macromolecules* **2018**, *51*, 6047-6056.
46. Kukula, H.; Schlaad, H.; Antonietti, M.; Forster, S., The Formation of Polymer Vesicles or “Peptosomes” by Polybutadiene-Block-Poly(L-Glutamate)S in Dilute Aqueous Solution. *J. Am. Chem. Soc.* **2002**, *124*, 1658-1663.
47. Sigel, R.; Łosik, M.; Schlaad, H., Ph Responsiveness of Block Copolymer Vesicles with a Polypeptide Corona. *Langmuir* **2007**, *23*, 7196-7199.
48. Zhao, Y.; Gao, H.; Liang, G.; Zhu, F.; Wu, Q., Synthesis of Well-Defined Amphiphilic Branched Polyethylene-Graft-Poly (N-Isopropylacrylamide) Copolymers by Coordination Copolymerization in Tandem with Raft Polymerization and Their Self-Assembled Vesicles. *Polym. Chem.* **2014**, *5*, 962-970.
49. Zhang, Y.; Shen, Z.; Yang, D.; Feng, C.; Hu, J.; Lu, G.; Huang, X., Convenient Synthesis of P^{ba}-G-Pma Well-Defined Graft Copolymer with Tunable Grafting Density. *Macromolecules* **2010**, *43*, 117-125.
50. Kuhnle, H.; Borner, H. G., Biotransformation on Polymer–Peptide Conjugates: A Versatile Tool to Trigger Microstructure Formation. *Angew. Chem. Int. Ed.* **2009**, *48*, 6431-6434.

51. Castelletto, V.; McKendrick, J. E.; Hamley, I. W.; Olsson, U.; Cenker, C., Pegylated Amyloid Peptide Nanocontainer Delivery and Release System. *Langmuir* **2010**, *26*, 11624-11627.
52. Junnila, S.; Houbenov, N.; Karatzas, A.; Hadjichristidis, N.; Hirao, A.; Iatrou, H.; Ikkala, O., Side-Chain-Controlled Self-Assembly of Polystyrene–Polypeptide Miktoarm Star Copolymers. *Macromolecules* **2012**, *45*, 2850-2856.
53. Hoogenboom, R.; Schlaad, H., Bioinspired Poly (2-Oxazoline)S. *Polymers* **2011**, *3*, 467-488.
54. Carlsen, A.; Lecommandoux, S., Self-Assembly of Polypeptide-Based Block Copolymer Amphiphiles. *Current Opinion Colloid Interface Sci.* **2009**, *14*, 329-339.
55. Chang, J. Y.; Park, P. J.; Han, M. J., Synthesis of Poly (4-Methylphenoxyphosphazene)-Graft-Poly (2-Methyl-2-Oxazoline) Copolymers and Their Micelle Formation in Water. *Macromolecules* **2000**, *33*, 321-325.
56. Li, T.; Lin, J.; Chen, T.; Zhang, S., Polymeric Micelles Formed by Polypeptide Graft Copolymer and Its Mixtures with Wolypeptide Block Copolymer. *Polymer* **2006**, *47*, 4485-4489.
57. Liu, H.; Li, C.; Tang, D.; An, X.; Guo, Y.; Zhao, Y., Multi-Responsive Graft Copolymer Micelles Comprising Acetal and Disulfide Linkages for Stimuli-Triggered Drug Delivery. *J. Mater. Chem. B* **2015**, *3*, 3959-3971.
58. Pramod, P. S.; Takamura, K.; Chaphekar, S.; Balasubramanian, N.; Jayakannan, M., Dextran Vesicular Carriers for Dual Encapsulation of Hydrophilic and Hydrophobic Molecules and Delivery into Cells. *Biomacromolecules* **2012**, *13*, 3627-3640.
59. Wang, Y.; Wang, L.; Li, B.; Cheng, Y.; Zhou, D.; Chen, X.; Jing, X.; Huang, Y., Compact Vesicles Self-Assembled from Binary Graft Copolymers with

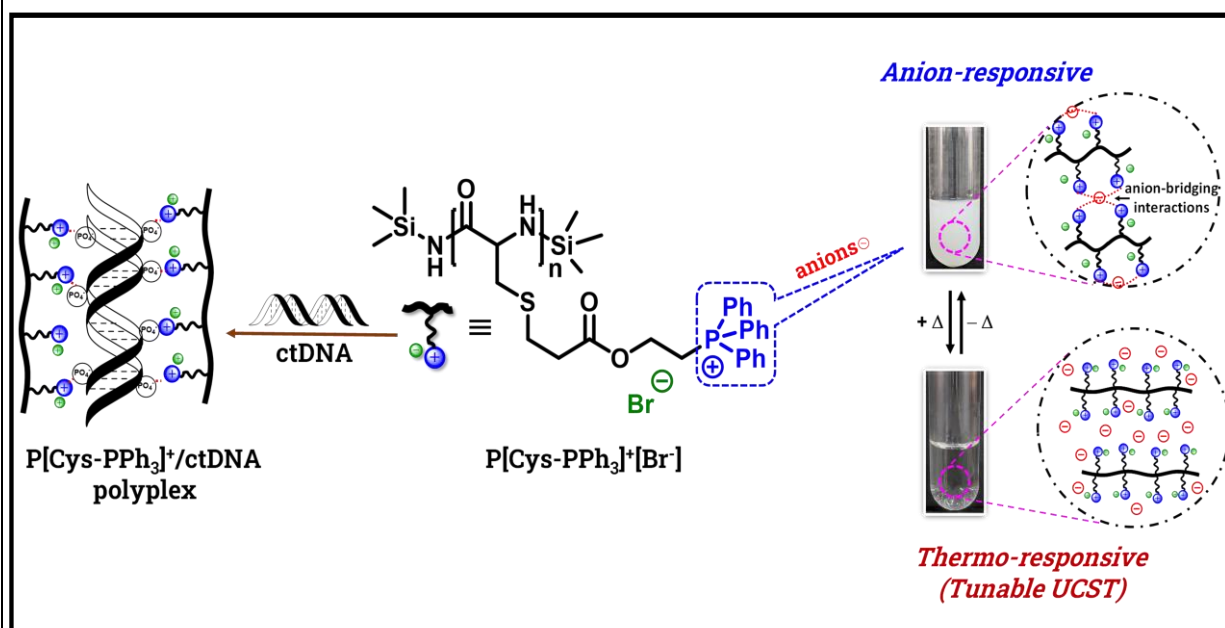
- High Hydrophilic Fraction for Potential Drug/Protein Delivery. *ACS Macro Letters* **2017**, *6*, 1186-1190.
60. Kang, M.; Cho, M.; Kim, S.; Youk, J. H., Microwave-Assisted One-Step Synthesis of Poly(2-Isopropyl-2-Oxazoline) Block Copolymers Using a Dual Initiator for Crop and Raft Polymerization. *Fibers and Polymers* **2017**, *18*, 1215-1220.
61. Bonduelle, C., Secondary Structures of Synthetic Polypeptide Polymers. *Polym. Chem.* **2018**, *9*, 1517-1529.
62. Berger, A.; Noguchi, J.; Katchalski, E., Poly-L-Cysteine. *J. Am. Chem. Soc.* **1956**, *78*, 4483-4488.
63. Blout, E.; de Lozé, C.; Bloom, S.; Fasman, G., The Dependence of the Conformations of Synthetic Polypeptides on Amino Acid Composition^{1, 2}. *J. Am. Chem. Soc.* **1960**, *82*, 3787-3789.
64. Miyazawa, T.; Blout, E., The Infrared Spectra of Polypeptides in Various Conformations: Amide I and II Bands. *J. Am. Chem. Soc.* **1961**, *83*, 712-719.
65. Moore, W. H.; Krimm, S., Vibrational Analysis of Peptides, Polypeptides, and Proteins. I. Polyglycine I. *Biopolymers* **1976**, *15*, 2439-2464.
66. Henkel, B.; Bayer, E., Monitoring of Solid Phase Peptide Synthesis by Ft-Ir Spectroscopy. *J. Pep. Sci.* **1998**, *4*, 461-470.
67. Schlaad, H.; Diehl, C.; Gress, A.; Meyer, M.; Demirel, A. L.; Nur, Y.; Bertin, A., Poly(2-Oxazoline)S as Smart Bioinspired Polymers. *Macromol. Rapid Commun.* **2010**, *31*, 511-525.
68. Jana, S.; Bose, A.; Saha, A.; Mandal, T. K., Photocleavable and Tunable Thermoresponsive Amphiphilic Random Copolymer: Self-Assembly into Micelles, Dye Encapsulation, and Triggered Release. *J. Polym. Sci. Part A: Polym. Chem.* **2017**, *55*, 1714-1729.
69. Deng, Y.; Wang, X.; Yuan, Q.; Zhu, M.; Ling, Y.; Tang, H., Synthesis, Characterization, and Thermoresponsive Properties of Helical Polypeptides Derivatized from Poly(Γ -4-(3-

- Chloropropoxycarbonyl)Benzyl-L-Glutamate). *J. Polym. Sci. A: Polym. Chem.* **2015**, *53*, 2469-2480.
70. Zhang, Q.; Weber, C.; Schubert, U. S.; Hoogenboom, R., Thermoresponsive Polymers with Lower Critical Solution Temperature: From Fundamental Aspects and Measuring Techniques to Recommended Turbidimetry Conditions. *Mater. Horiz.* **2017**, *4*, 109-116.
71. Thompson, K. L.; Derry, M. J.; Hatton, F. L.; Armes, S. P., Long-Term Stability of N-Alkane-in-Water Pickering Nanoemulsions: Effect of Aqueous Solubility of Droplet Phase on Ostwald Ripening. *Langmuir* **2018**, *34*, 9289-9297.
72. Antonietti, M.; Forster, S., Vesicles and Liposomes: A Self Assembly Principle Beyond Lipids. *Adv. Mater.* **2003**, *15*, 1323-1333.
73. Breitenkamp, K.; Emrick, T., Novel Polymer Capsules from Amphiphilic Graft Copolymers and Cross-Metathesis. *J. Am. Chem. Soc.* **2003**, *125*, 12070-12071.
74. Du, J.; O'Reilly, R. K., Advances and Challenges in Smart and Functional Polymer Vesicles. *Soft Matter* **2009**, *5*, 3544-3561.
75. Hou, R. G.; Yi, L. M.; Lin, H. M.; Li, J. W.; Huang, C. X., Formation of Polymer Vesicles by Amphiphilic Fluorosiloxane Graft Copolymers in Solution. *Chinese Chemical Letters* **2011**, *22*, 1119-1122.
76. Filippov, S. K.; Starovoytova, L.; Konak, C.; Hruby, M.; Mackova, H.; Karlsson, G.; Stepanek, P., Ph Sensitive Polymer Nanoparticles: Effect of Hydrophobicity on Self-Assembly. *Langmuir* **2010**, *26*, 14450-14457.
77. Lalatsa, A.; Schatzlein, A. G.; Mazza, M.; Le, T. B. H.; Uchegbu, I. F., Amphiphilic Poly (L-Amino Acids): A New Materials for Drug Delivery. *J. Control. Rel.* **2012**, *161*, 523-536.
78. Saha, A.; Jana, S.; Mandal, T. K., Peptide-Poly(Tert-Butyl Methacrylate) Conjugate into Composite Micelles in Organic Solvents Versus Peptide-Poly(Methacrylic Acid) Conjugate into Spherical and Worm-Llike

- Micelles in Water: Synthesis and Self-Assembly. *J. Polym. Sci. A: Polym. Chem.* **2016**, *54*, 3019-3031.
79. Das, S.; Sharma, D. K.; Chakrabarty, S.; Chowdhury, A.; Sen Gupta, S., Bioactive Polymersomes Self-Assembled from Amphiphilic Ppo-Glycopolypeptides: Synthesis, Characterization, and Dual-Dye Encapsulation. *Langmuir* **2015**, *31*, 3402-3412.
80. Zhao, L.; Li, N.; Wang, K.; Shi, C.; Zhang, L.; Luan, Y., A Review of Polypeptide-Based Polymersomes. *Biomaterials* **2014**, *35*, 1284-1301.
81. Wang, K.; Guo, D.-S.; Wang, X.; Liu, Y., Multistimuli Responsive Supramolecular Vesicles Based on the Recognition of P-Sulfonatocalixarene and Its Controllable Release of Doxorubicin. *ACS Nano* **2011**, *5*, 2880-2894.

Chapter 3: UCST Polypeptide

Synthesis and Anion-Induced Thermoresponsiveness of Cationic Poly(L-Cysteine) and Its Interaction with DNA



3.1. Introduction

Proteins and polypeptides are crucial constituents that play an essential role in biological systems.¹ Hence, numerous research teams have synthesized various types of synthetic polypeptides possessing inherent biocompatibility and biodegradability, making them promising bioinspired materials for several biological applications.¹⁻³ The easy access to the library of natural amino acids and their modified precursors with diverse functional groups and responsive segments allows for the facile synthesis of different functionalized polypeptides and their subsequent customization for distinct properties and functions.⁴ To this end, researchers have developed synthetic polypeptides featuring different functional groups that respond to various stimuli such as temperature,⁵⁻⁶ pH,⁷⁻⁸ light,⁹⁻¹⁰ redox reactions,^{2, 11} enzymes,¹²⁻¹³ and ionic strength,^{9,14} etc. These stimulus-responsive polypeptides are highly sought after due to their wide range of biological applications, particularly in targeted drug/gene delivery, therapeutics, tissue engineering, biosensing, and more.^{1,15-17}

Synthetic polypeptides exhibiting tunable functionality and stimuli-responsiveness can be synthesized using the ROP of NCA derived from chemically modified natural α -amino acids.¹⁸⁻²⁰ Alternatively, the ROP of amino acid NCA, incorporating diverse reactive functional groups such as allyl halide, alkyne, alkene, azide, etc., can be followed by post-modification via various reactions like Michael addition, click reaction, substitution reaction, etc., leading to the development of functionalized polypeptides.^{5, 21-22} Nevertheless, this latter approach may not result in complete functionalization of all reactive groups. Another approach involves employing macroinitiators containing responsive moieties for the ROP of amino acid NCA, yielding end-functional polypeptide conjugates that are sensitive to different stimuli.⁹

Among the various stimuli-responsive systems, thermoresponsive polymers/polypeptides have received the most extensive investigation,

surpassing those responsive to stimuli such as pH, light, redox reactions, etc. These responsive systems exhibit reversible transitions, mainly in aqueous solutions, at critical temperatures known as the lower critical solution temperature (LCST) and upper critical solution temperature (UCST), leading to a transition from a monophasic transparent state to a biphasic cloudy suspension, or vice versa.^{9, 19, 23-24} The underlying mechanism for such transitions in conventional neutral polymers is typically the delicate balance between hydrogen bonding/hydrophobic interactions among the polymer chains and the interactions between the polymer and the solvent.^{5, 25} More recently, it has been reported by several research groups, that ionic polymers also exhibit LCST- and UCST-type phase behaviours in solution due to the presence of Coulombic interactions among the polymer chains.^{9, 26-30}

Several research groups have extensively investigated the physicochemical properties and applications of thermoresponsive polypeptides.^{1, 5-6, 19, 31-32} However, the majority of these functional polypeptides exhibit LCST-type behaviours.^{5-6, 19, 31, 33} In contrast, there has been comparatively less exploration of synthetic polypeptides that display UCST-type phase behaviour in water.^{29, 34-35} For instance, Zhao et al. developed single-chain nanoparticles (SCNPs) based on poly(L-glutamate) that undergo UCST-type transitions near human body temperature, making them promising materials for various biomedical applications.³⁵ Recently, certain research groups have reported tunable UCST-type properties in neutral poly(L-ornithine) copolypeptides.³⁶⁻³⁸ However, there are only a few reports of polypeptides with ionic moieties in their side chains that exhibit UCST-type phase behaviour in aqueous solutions.^{23, 39-40} In a recent study, our group developed photoresponsive cationic polymethionine-based homo- and co-polypeptides with pendant sulfonium cations, which demonstrated tunable UCST-type behaviour in the presence of anions in water.⁹

In contrast, numerous researchers have demonstrated the binding mode and transfection efficiency of various cationic polymers containing phosphonium,⁴¹ sulfonium,⁴² ammonium,⁴³ and pyridinium⁴⁴ cations with DNA. However, despite their inherent biocompatibility and biodegradability, only a limited number of cationic polypeptides have been investigated regarding their binding capabilities with DNA or RNA.^{9, 45-46} Consequently, there is a need to develop new cationic polypeptides and investigate their responsive behaviours in the presence of additional ions, as well as their binding affinity with DNA or RNA. In recent times, our group have made significant advancements by developing a series of poly(ionic liquid)s, amino acids-based polymers, and ionic polymers and have extensively studied their solution properties and elucidated their stimuli-responsive behaviour.^{9, 25-28, 47} For example, we have reported the synthesis of a dual stimuli-responsive phosphonium-based polymer, poly(triphenyl-4-vinylbenzylphosphonium chloride) (P[VBTP][Cl]), by employing reversible addition-fragmentation chain transfer (RAFT) polymerization of an ionic liquid (IL) monomer, [VBTP][Cl].²⁸ The addition of sodium halide anions (Cl⁻, Br⁻, I⁻) to the transparent aqueous solution of P[VBTP][Cl] resulted in cloudiness. However, above a certain temperature (cloud point), the solution became transparent again and vice-versa. This ion-induced UCST-type reversible behaviour could be easily controlled by adjusting factors such as polymer concentration, molecular weight, type of halide salts, and ionic strength of the medium. Alternatively, we also have reported the synthesis of a water-soluble, multistimuli-responsive positively charged functional polypeptide (P[MetNB][Br]) and polypeptide block copolymer (PEtOx-b-P[MetNB][Br]) using ROP and subsequent post-modification technique.⁹ Both the polymers underwent ion-responsive (SCN⁻, ClO₄⁻, I⁻) soluble-to-insoluble transitions (UCST-type) in aqueous solutions. Moreover, these cationic polypeptides could be cleaved into neutral polypeptides through photocleavage, facilitated by the presence of 2-nitrobenzyl moieties as pendent groups. The

cationic polypeptides were capable of interacting with ctDNA and could subsequently release it on photo-irradiation as confirmed by fluorescence spectroscopy and gel electrophoresis.

3.2. Objective and Scope

Cationic polypeptides-based materials exhibit significant potential as smart biomaterials for various biomedical applications, particularly in drug delivery and the binding of biologically active components such as DNA. Furthermore, ionic polypeptides offer distinct advantages over neutral counterparts in terms of their water solubility and intriguing thermoresponsive properties resulting from ionization. However, compared to non-ionic thermoresponsive polymers, there is relatively less research on ionic polymers, particularly ionic polypeptides.^{9, 48} Consequently, there is a significant demand for ionic thermoresponsive polypeptides with excellent water solubility due to their wide range of applications as nanoreactors and controlled delivery agents for drugs/genes.^{1, 15} In spite of having the vital role of polycysteines in protein stabilization, either through disulfide linkages or hydrophobic interactions, they have been relatively less explored compared to other synthetic polypeptides.⁴⁹ These findings motivated us to design and synthesize various novel ionic polypeptides, in particular ionic polycysteins and explore their solution properties and efficiency of DNA binding.

In this study, we describe the synthesis of a water-soluble cationic polypeptide based on L-cysteine. The synthesis involves the ROP of a newly designed L-cysteine NCA monomer functionalized with a bromine group. This ROP process results in the formation of polycysteine with pendant bromine atoms. Subsequent nucleophilic substitution of the bromine atoms with triphenylphosphine leads to the formation of cationic polycysteine (P[Cys-PPh₃]⁺[Br⁻]). The aqueous solution of P[Cys-PPh₃]⁺[Br⁻] exhibits thermoresponsive behavior in the presence of different anions from the

Hoffmeister series (BF_4^- , I^- , ClO_4^- , and SCN^-). This behavior is characterized by a transformation from a transparent state to a cloudy suspension, which is attributed to the formation of water-insoluble aggregates of the polypeptide and the anions. Upon heating, the cloudy suspension becomes transparent, and upon cooling, it reverts to its cloudy state, demonstrating an UCST-type thermoresponsive behavior. The cloud point, at which this transition occurs, can be tuned by changing the concentrations of the cationic polypeptide and the added anions. The effect of other counter-anion (Cl^-) on the UCST-type thermoresponsiveness of the cationic polycysteine $\text{P}[\text{Cys-PPh}_3]^+[\text{Cl}^-]/\text{chaotropes}$ is also investigated. Furthermore, it is expected that the cationic $\text{P}[\text{Cys-PPh}_3]^+[\text{Br}^-]$ will interact with the negatively charged biomolecules, such as nucleic acids. The polyplexation of cationic $\text{P}[\text{Cys-PPh}_3]^+[\text{Br}^-]$ with calf-thymus DNA (ctDNA) is investigated using fluorescence spectroscopy, gel electrophoresis, and circular dichroism spectroscopy. The influence of ionic strength on the polyplexation process is also studied using fluorescence spectroscopy.

Overall, this study provides insights into the synthesis and thermoresponsive behavior of a water-soluble cationic polypeptide derived from L-cysteine, as well as its ability to form polyplexes with ctDNA.

3.3. Experimental

3.3.1. Materials

2-Bromoethanol (98%, Spectrochem), acryloyl chloride (96%, Alfa Aesar), 2-chloroethyl acrylate (97%, Sigma-Aldrich), L-cysteine (SRL), dimethylphenylphosphine (99%, Sigma-Aldrich), triphosgene (>98%, TCI), 1,1,1,3,3,3-hexamethyl disilazane (HMDS; 99.9%, TCI), ethidium bromide (EtBr, 98%, SRL), sodium salt of calf-thymus DNA (ctDNA; Aldrich), agarose (SRL), bromophenol blue (SRL) were used as received. Triethylamine (TEA; $\geq 99\%$, Aldrich) was distilled and was kept over solid KOH before use.

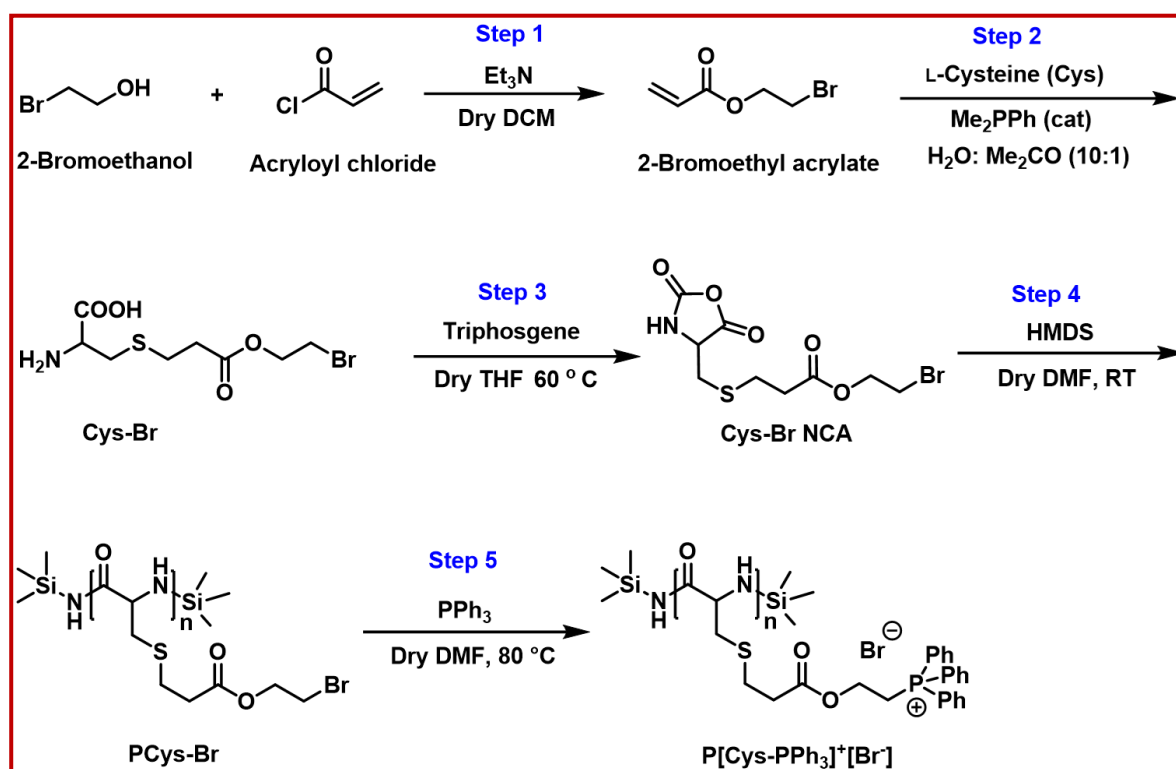
Triphenylphosphine (TPP; TCI) was recrystallized from rectified spirit prior to use. Sodium salts of chaotropic anions (BF_4^- , I^- , ClO_4^- , SCN^-) and sodium dodecyl sulphate (SDS) were purchased from Spectrochem, India and were used as received. Dulbecco's modified eagle medium (DMEM) and streptomycin were purchased from Sigma-Aldrich. Fetal bovine serum (FBS) was purchased from Life technologies. 3-(4,5-Dimethylthiazol-2-yl)-2,5-diphenyltetrazolium bromide (MTT) was purchased from HiMedia. N, N-Dimethylformamide (DMF, Merck) was distilled over calcium hydride under reduced pressure and was further dried with molecular sieve (Linde 4Å) before use. Tetrahydrofuran (THF; Merck) was distilled over metallic sodium prior to use. Dichloromethane (DCM; Merck) was distilled over calcium hydride and further dried with molecular sieve (Linde 4Å) before use. Acetone, ethyl acetate (Rankem), and hexane (Merck) were used after distillation. Milli-Q water was used for the preparation of aqueous solutions.

3.3.2. Synthetic Procedure

3.3.2.1. Synthesis of 2-Bromoethyl Acrylate (2-BrEt-Ac)

The synthesis of the 2-BrEt-Ac monomer was conducted following a previously reported protocol (Step 1, Scheme 3.1).⁵⁰ In a 250 mL round bottom flask equipped with a pressure equalizing stopcock and under N_2 gas atmosphere, a solution of 2-bromoethanol (15 mL; 211.63 mmol) in dichloromethane (DCM) (50 mL) was prepared and cooled in an ice bath at 0 °C. Triethylamine (TEA) (33 mL; 232.8 mmol) was dissolved in 15 mL of dry DCM and added dropwise to the 2-bromoethanol solution over a period of 30 minutes. The reaction mixture was stirred for an additional 30 minutes. Subsequently, a solution of acryloyl chloride (20.5 mL; 253.95 mmol) in dry DCM (35 mL) was slowly added to the reaction mixture over a period of 60 minutes, while maintaining the temperature of the ice bath at 0-5 °C. The resulting reaction mixture was magnetically stirred at the same temperature for 4 hours, followed by overnight stirring at 30 °C. Upon completion of the reaction, the $[\text{Et}_3\text{NH}^+\text{Cl}^-]$ salt was

removed by filtration, and the filtrate was washed with distilled water three times and then with a brine solution. The organic layer containing the desired compound was collected over anhydrous sodium sulfate, filtered, and subsequently evaporated using a rotary evaporator under vacuum. The product, 2-BrEt-Ac, was obtained by vacuum distillation, with a yield of 80%.



Scheme 3.1. Multistep synthetic process for PCys-Br and its cationization to P[Cys-PPh₃]⁺[Br⁻]

Characterization data: FT-IR (Figure 3.1), ESI-MS (*m/z*) = 179.89 (Figure A3.1), ¹H-NMR (400 MHz, CDCl₃, TMS) δ (ppm): 6.46 (dd, 1H), 6.16 (dd, 1H), 5.88 (dd, 1H), 4.47 (t, 2H), 3.55 (t, 2H) (Figure 3.2 and Figure A3.2), ¹³C-NMR (100 MHz, CDCl₃, TMS) δ (ppm): 28.70, 63.99, 127.95, 131.82, 165.74 (Figure 3.3).

3.3.2.2. Synthesis of Bromo- and Chloro-Functionalized L-Cysteine

Bromo-functionalized L-cysteine (Cys-Br) was synthesized through a slight modification of a previously reported protocol involving a Michael addition

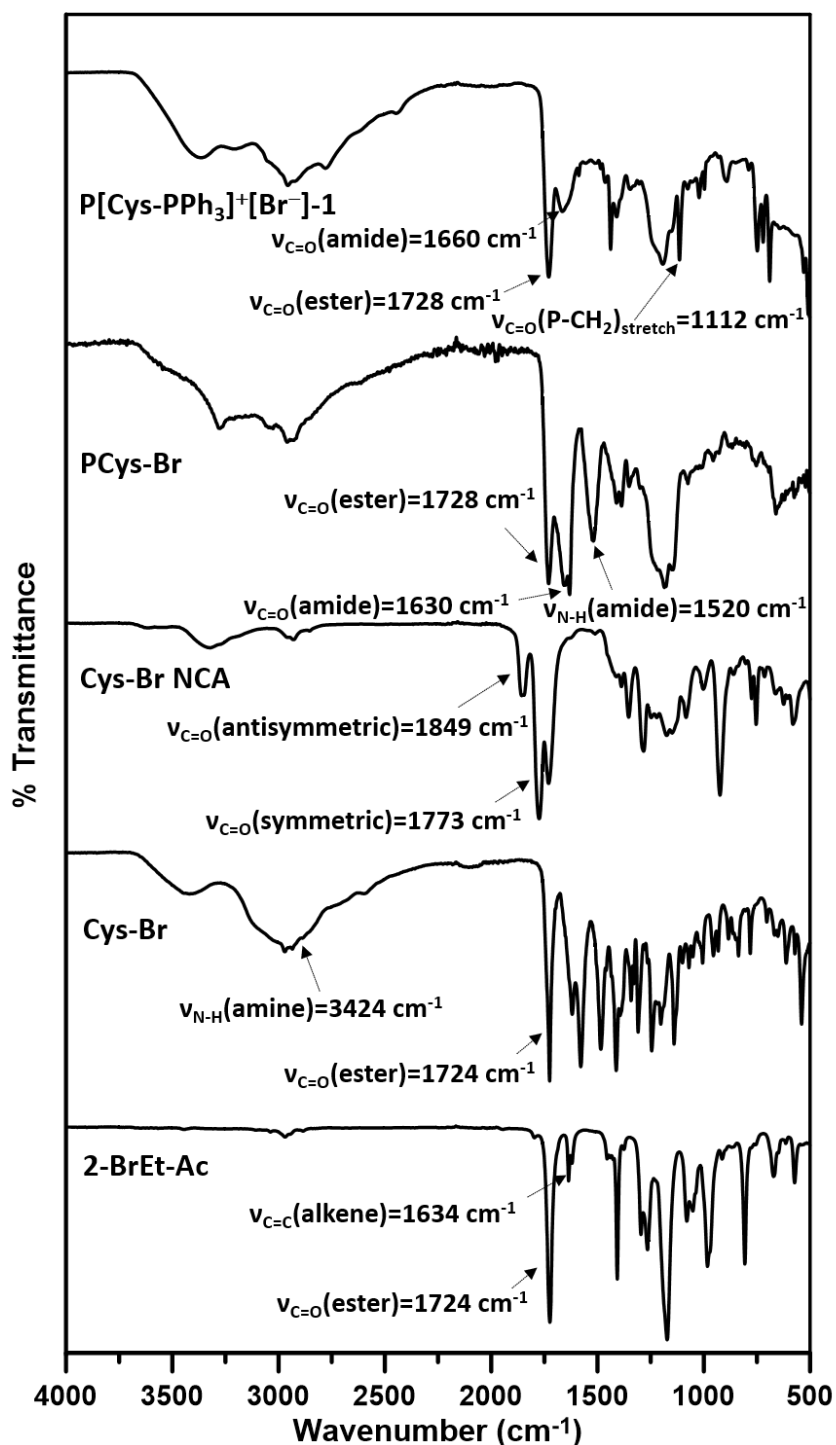


Figure 3.1. FT-IR spectra of all the as-synthesized compounds.

reaction using a phosphine catalyst in water (Step 2, Scheme 1).⁵¹ The procedure was as follows: L-cysteine (5.0 g; 41.27 mmol) was dispersed in 50 mL of water and mixed with a solution of 2-BrEt-Ac (6 mL; 49.52 mmol) in acetone (5 mL).

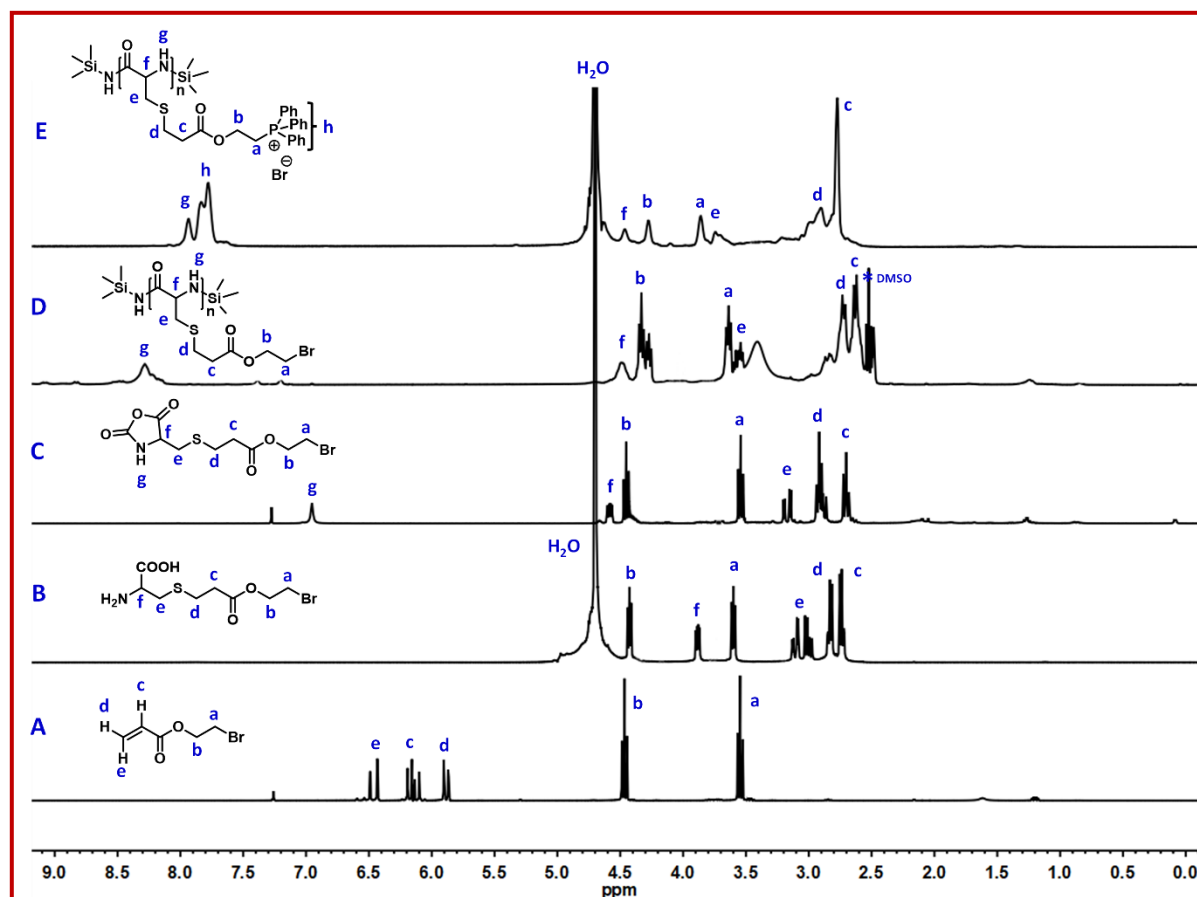


Figure 3.2. $^1\text{H-NMR}$ spectra of 2-BrEt-Ac in CDCl_3 (A), Cys-Br in D_2O (B), Cys-Br NCA in CDCl_3 (C), PCys-Br-1 in DMSO-d_6 (D) and $\text{P}[\text{Cys-PPh}_3]^+[\text{Br}^-]-1$ in D_2O (E).

Dimethylphenylphosphine (15 μL) was then added to the mixture, and the entire solution was stirred magnetically at 20 $^\circ\text{C}$ for 12 hours. After completion of the reaction, the undesired residue was removed by filtration using a Gooch filter (G4 grade), followed by several washes with distilled water. The acetone in the filtrate, containing Cys-Br, was evaporated using a rotary evaporator. The resulting aqueous solution was then washed five times with ethyl acetate to remove excess acrylate monomer and catalyst. The water content was partially reduced by evaporation, and the final white solid product, Cys-Br, was obtained by lyophilizing the concentrated aqueous solution. The yield of the product was 89%.

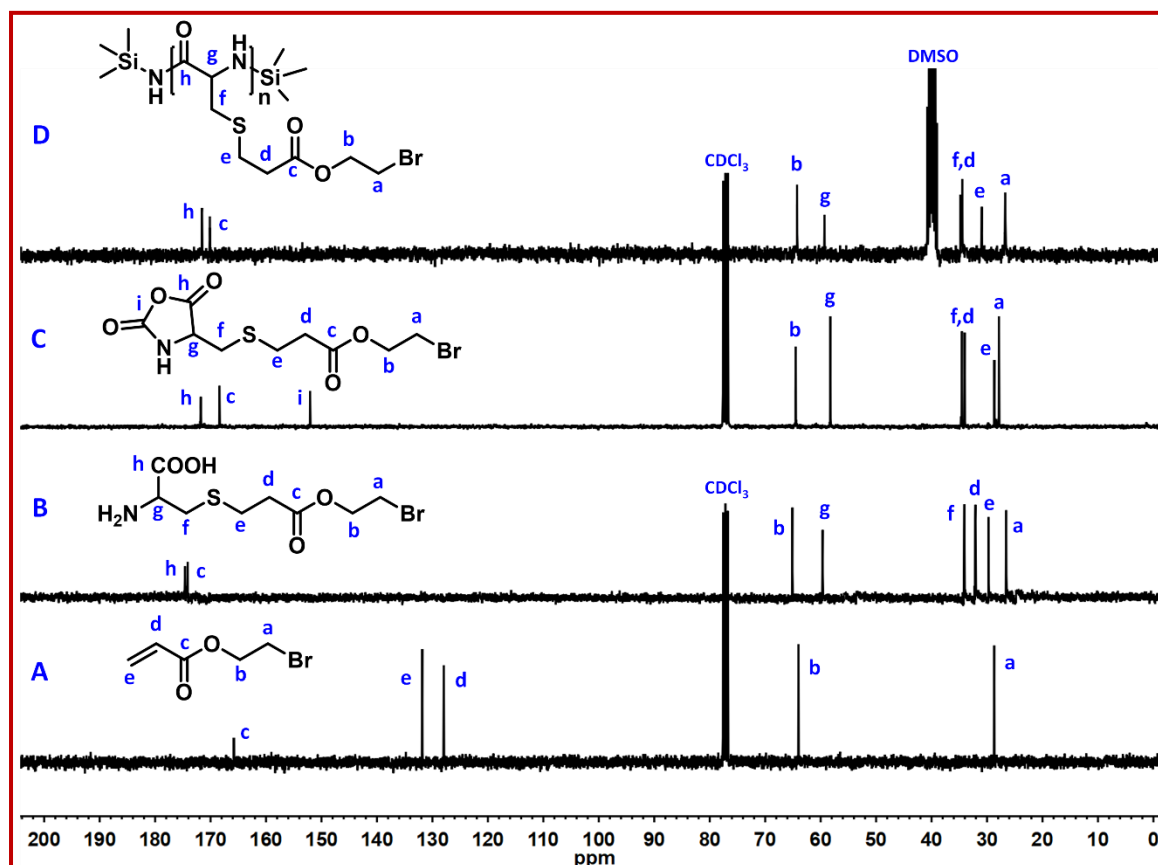
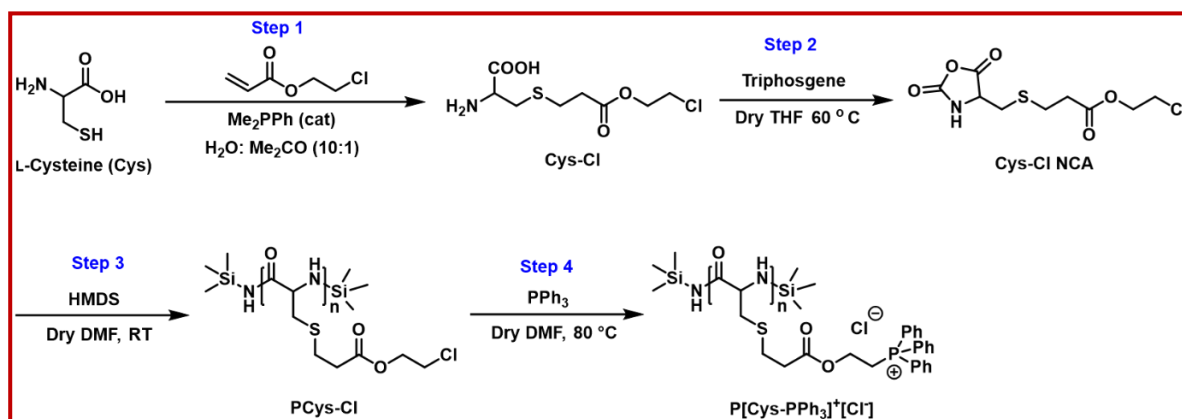


Figure 3.3. ^{13}C -NMR spectra of 2-BrEt-Ac in CDCl_3 (A), Cys-Br in D_2O (B), Cys-Br NCA in CDCl_3 (C) and PCys-Br-1 in DMSO-d_6 (D).

Characterization data: FT-IR (Figure A3.1), ESI-MS (Cys-Br) (m/z) = 301.67 (100) ($M + 1\text{H}^+$) (Figure A3.3), ^1H -NMR (Cys-Br) (400 MHz, D_2O , TMS) δ (ppm): 4.43 (m, 2H), 3.88 (dd, 1H), 3.60 (dd, 2H), 3.06 (m, 2H), 2.83 (m, 2H), 2.74 (m, 2H) (Figure 3.2 and Figure A3.4), ^{13}C -NMR (Cys-Br) (100 MHz, D_2O , TMS) δ (ppm): 26.58, 29.72, 32.13, 34.12, 59.64, 65.09, 174.11, 174.60 (Figure 3.3).

The same methodology described earlier was also used for the synthesis of another monomer, Cys-Cl, instead of 2-BrEt-Ac, L-cysteine was reacted with 2-chloroethyl acrylate (2-ClEt-Ac) to introduce a chlorine atom (Step 1, Scheme 3.2). The reaction conditions and workup procedures were similar to those described before. The yield of Cys-Cl was 91%. The characterization data for Cys-Cl: ESI-MS (Figure A3.5), ^1H -NMR (Figure 3.4).



Scheme 3.2. Synthesis scheme for PCys-Cl and its cationization to $\text{P}[\text{Cys-PPh}_3]^+[\text{Cl}^-]$.

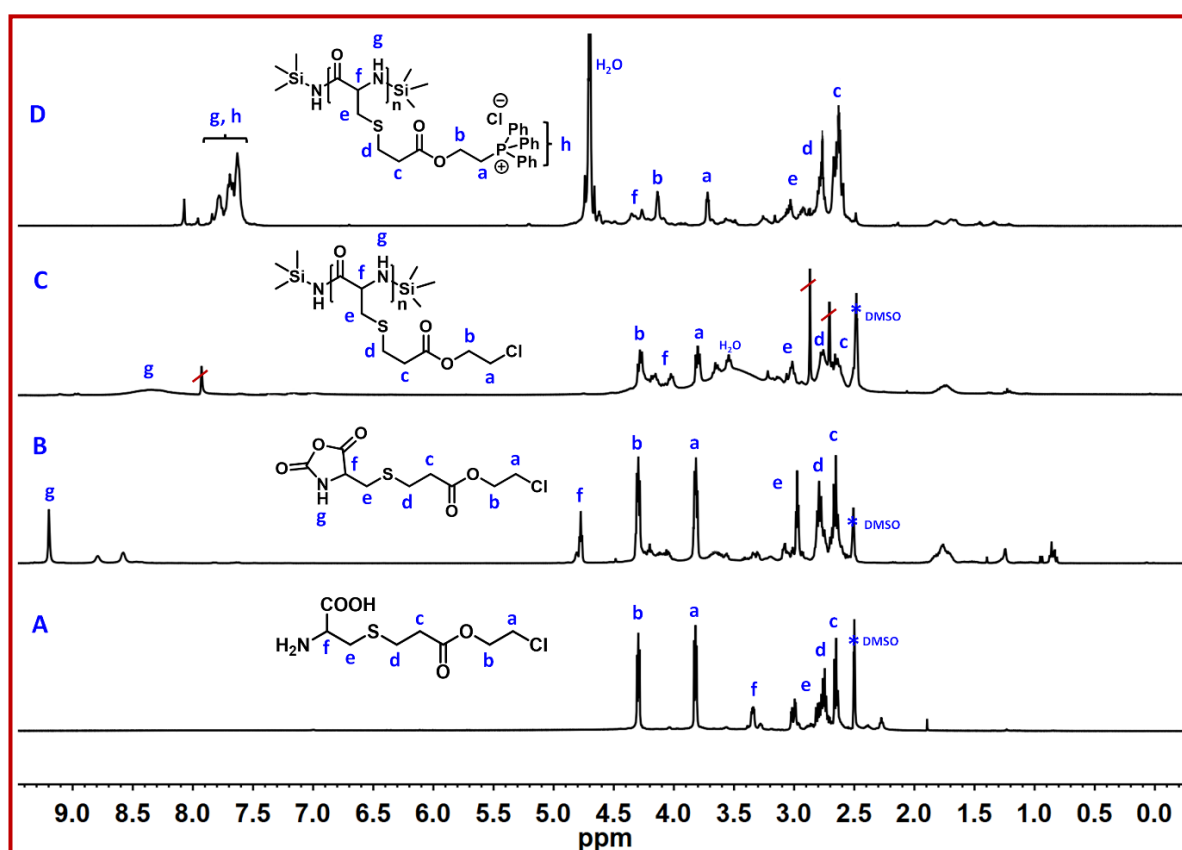


Figure 3.4. $^1\text{H-NMR}$ spectra of Cys-Cl (A), Cys-Cl NCA (B), PCys-Cl (C) in DMSO-d_6 and $\text{P}[\text{Cys-PPh}_3]^+[\text{Cl}^-]$ (D) in D_2O .

3.3.2.3. Synthesis of NCAs

The synthesis of Cys-Br NCA involved the reaction between the previously synthesized Cys-Br and triphosgene in dry THF under an inert atmosphere (Step 3, Scheme 3.1). The procedure was carried out as follows: In a dry round-bottom flask filled with nitrogen gas, Cys-Br (3.0 g; 9.99 mmol) and a pinch of activated charcoal were added. Dry THF (15 mL) was added to the flask, creating a turbid suspension, and the flask was placed in a preheated oil bath at 60 °C. The mixture was stirred for 15 minutes to ensure thorough mixing. A THF solution (5 mL) of triphosgene (1.48 g; 4.99 mmol) was slowly added to the mixture using a syringe. The resulting mixture was refluxed at 60 °C for 7 hours with a condenser fitted. Unreacted reactants and charcoal were removed by centrifugation followed by filtration. The volume of the mixture was reduced to one-third of its initial volume. The product was then precipitated from cold hexane, resulting in a yellow-colored viscous solid. The obtained solid was further purified by column chromatography using silica gel (60-120 mesh) and eluting with a mixture of 90% ethyl acetate and hexane. Finally, Cys-Br NCA was obtained as a pale-yellow colored sticky liquid by drying in a vacuum oven at 50 °C. The yield of Cys-Br NCA was 70%.

Characterization data: FT-IR (Figure 3.1), ESI-MS (Cys-Br NCA) (m/z) = 348.04 ($M + 1Na^+$) (Figure A3.6), 1H -NMR (Cys-Br NCA) (400 MHz, $CDCl_3$, TMS) δ (ppm): 6.95 (s, 1H), 4.58 (dd, 1H), 4.45 (m, 2H), 3.54 (m, 2H), 3.17 (dd, 2H), 2.92 (m, 2H), 2.70 (m, 2H) (Figure 3.2 and Figure A3.7), ^{13}C -NMR (Cys-Br NCA) (100 MHz, $CDCl_3$, TMS) δ (ppm): 27.85, 28.68, 34.02, 34.52, 58.24, 64.49, 152.05, 168.39, 171.87 (Figure 3.3).

Cys-Cl NCA was also prepared by same method from as synthesized Cys-Cl (Step 2, Scheme 3.2). See Figures A3.8 (MALDI-TOF-MS) and 3.4 (1H -NMR) for the characterization data.

3.3.2.4. ROP of Cys-Br/ Cys-Cl NCAs

The ROP of Cys-Br NCA was carried out using HMDS as the initiator in dry DMF at 30 °C (Step 4, Scheme 3.2) keeping the initial molar ratio of monomer/initiator ($[M]_0/[I]_0$) at 30:1. The procedure for the ROP reaction is described as follows: Cys-Br NCA (2.5 g; 7.66 mmol) was dissolved in 4 mL of dry DMF in a flame-dried 25 mL long double-neck round-bottom flask under a nitrogen atmosphere. The flask was sealed with a silicon rubber septum. In a separate test tube fitted with a silicone rubber septum, HMDS (52 μ L; 0.25 mmol) was dissolved in 1 mL dry DMF. The HMDS solution was added dropwise to the flask containing the Cys-Br NCA solution while stirring, and the mixture was stirred further for 96 hours. After the reaction was complete, the brominated polycysteine (PCys-Br) was isolated by precipitation in excess cold anhydrous diethyl ether. The isolated PCys-Br was purified by repeating the precipitation procedure several times. The purified PCys-Br was then vacuum dried at 60 °C. The yield of the PCys-Br was 71%. The polypeptide obtained was designated as PCys-Br-1 (Table 3.1). Another sample, PCys-Br-2, was also prepared by varying the initial feed ratio of monomer to initiator (as mentioned in Table 3.1).

Characterization data: FT-IR spectrum of PCys-Br (Figure A3.1), $^1\text{H-NMR}$ (PCys-Br-1) (400 MHz, DMSO- d_6 , TMS) δ (ppm): 8.25 (s, 1H), 4.54 (m, 1H), 4.34 (m, 2H), 3.65 (q, 2H), 3.56 (m, 2H), 2.73 (m, 2H), 2.62 (m, 2H) (Figure 3.2 and Figure A3.9), $^{13}\text{C-NMR}$ (PCys-Br-1) (100 MHz, DMSO- d_6 , TMS) δ (ppm): 26.72, 30.95, 34.59, 34.70, 59.29, 64.99, 170.13, 171.64 (Figure 3.3).

ROP of as-synthesized Cys-Cl NCA to PCys-Cl (Step 4, Scheme A3.1) was also have been done using same method mentioned above using HMDS as the initiator. $[M]_0/[I]_0$ was kept at 30:1. ($^1\text{H-NMR}$ - Figure 3.4).

Table 3.1. Molecular weight analysis data of as-synthesized polypeptides

Sample name	$[M]_0/[I]_0$	M_n (Theo) (Da)	DP (Theo)	M_n (SEC) (Da)	DP (SEC)	Dispersity (\mathcal{D})
^a PCys-Br-1	30	^b 7000	24	3800	13	1.59
^a PCys-Br-2	50	^b 10500	37	-	-	-
^c P[Cys-PPh ₃] ⁺ [Br ⁻]-1	-	^d 11400	-	5300	-	1.41
^c P[Cys-PPh ₃] ⁺ [Br ⁻]-2	-	^d 17300	-	8700	-	1.62

^a Condition for ROP of Cys-Br NCA: Solvent = Dry DMF, Initiator = HMDS, Temperature = 30 °C

^b Formula of M_n (Theo) = $([M]_0 \times p \times M_{\text{NCA}}) / [I]_0 + M_{\text{HMDS}}$

$[M]_0$ = Initial concentration of NCA, p = % yield, M_{NCA} = Molar mass of NCA, $[I]_0$ = Initial concentration of HMDS, and M_{HMDS} = Molar mass of HMDS

^c Condition for post-polymerization: Solvent = Dry DMF, Nü = PPh₃, Temperature = 80 °C

^d Formula of M_n (Theo) = $\text{DP}(\text{Theo}) \times [(^b M_n + M_{\text{PPh}_3}) - M_{\text{Br}}]$

M_{PPh_3} = Molar mass of PPh₃, M_{Br} = Molar mass of Br

3.3.2.5. Synthesis of Cationic Poly(L-cysteine) (P[Cys-PPh₃]⁺[X⁻]) (X = Br, Cl)

The cationization of PCys-Br-1 was carried out through a post-modification reaction with PPh₃ (Step 5, Scheme 3.1). The procedure for the cationization reaction is as follows: In a long-necked round-bottom flask (25 mL), PCys-Br-1 (1.5 g) and PPh₃ (excess) were added to 5 mL of dry DMF. The mixture was purged with N₂ gas for 30 minutes to remove any oxygen present. The flask was then placed in a preheated oil bath at 80 °C and stirred for 3 days. After the

reaction period, a solid sticky product was formed, which was precipitated out from DMF using cold diethyl ether. The cationic polypeptide was then extracted into water by repeated ultrasonication and vortexing to remove any unreacted compounds. The aqueous mixture was filtered to discard any remaining solid particles or impurities. Finally, the pale-yellow colored sticky solid (P[Cys-PPh₃]⁺[Br⁻]) was collected by lyophilizing the aqueous filtrate. The yield of the cationic polypeptide was 72%. This polypeptide was designated as P[Cys-PPh₃]⁺[Br⁻]-1.

Characterization data: FT-IR spectrum of P[Cys-PPh₃]⁺[Br⁻]-1 (Figure 3.1). ¹H-NMR (P[Cys-PPh₃]⁺[Br⁻]-1) (400 MHz, D₂O, TMS) δ (ppm): 7.94 (s, 1H), 7.90-7.77 (m, aromatic protons), 4.46 (bs, 1H), 4.28 (bs, 2H), 3.86 (bs, 2H), 3.72 (bs, 2H) 2.90 (bs, 2H), 2.78 (bs, 2H) (Figures 3.2 and A3.10), ³¹P-NMR (P[Cys-PPh₃]⁺[Br⁻]-1) (162 MHz, D₂O) δ (ppm): 23.74 (Figure 3.6).

Additional cationic polypeptides, P[Cys-PPh₃]⁺[Br⁻]-2 (Table 3.1) and P[Cys-PPh₃]⁺[Cl⁻], were synthesized using the same methodology by cationizing their respective precursor polypeptides. To obtain P[Cys-PPh₃]⁺[Br⁻]-2, the precursor polypeptide PCys-Br-2 was subjected to post-polymerization modification with PPh₃. Similarly, P[Cys-PPh₃]⁺[Cl⁻] was obtained by cationizing the precursor polypeptide (PCys-Cl) with PPh₃ using an identical procedure.

¹H-NMR spectra of P[Cys-PPh₃]⁺[Br⁻]-2 and P[Cys-PPh₃]⁺[Cl⁻] were given in Figure A3.11 and Figure 3.4.

3.3.3. Experimental Methods

3.3.3.1. Anion-Responsiveness of Aqueous P[Cys-PPh₃]⁺[Br⁻] Solution

To review the anion-responsiveness of the P[Cys-PPh₃]⁺[Br⁻] solution, 1 mL of a 0.5 wt% solution of P[Cys-PPh₃]⁺[Br⁻] was titrated with 1 M solutions of various Hofmeister series anions (BF₄⁻, I⁻, ClO₄⁻, and SCN⁻) as well as a large SDS anion separately. Upon addition of these anions to the P[Cys-PPh₃]⁺[Br⁻] solution, a noticeable change occurred, transitioning the solution from transparent to a cloudy suspension. The degree of cloudiness was quantified by measuring the percent transmittance (%T) of the solution using a UV-Vis spectrophotometer at a wavelength (λ) of 500 nm. By analyzing the titration results, the minimum concentration of each anion ($[\text{anion}]_{\text{min}}$) required to achieve nearly zero percent transmittance was determined. This information provides insights into the sensitivity of the P[Cys-PPh₃]⁺[Br⁻] solution towards different anions.

3.3.3.2. Determination of Cloud Point (T_{cp}) of Aqueous P[CysPPh₃]⁺[Br⁻] solution in the Presence of Added Anions

The cloudy suspension of P[Cys-PPh₃]⁺[Br⁻] in the presence of anion transformed into transparent solution upon heating and became clear again on cooling, revealing the presence of UCST-type phase transition in water. Therefore, T_{cp} of this UCST-type phase transition was determined by measuring the %T of the solutions at a fixed wavelength $\lambda = 500$ nm using Carry UV-Vis Compact Peltier instrument (Agilent) equipped with a temperature sensing probe. The %T of each of the cloudy suspension was measured within a specific temperature window for specific anion containing suspension with a heating/cooling rate of 2 °C/min. Each data point was obtained after equilibrating the suspension/solution at a particular temperature for 2 minutes and at an interval of 2 °C. T_{cp} of the suspension/solution was taken as the temperature at which the %T of the suspension/solution reached half of its original value.

3.3.3.3. ctDNA- P[Cys-PPh₃]⁺[Br⁻] Polyplex Formation: Spectroscopic/ Gel Electrophoresis Study and the Effect of Ionic-Strength

Preparation of ctDNA and Ethidium Bromide Solutions in Tris-HCl Buffer:

To prepare the ctDNA stock solution, 10 mg of solid ctDNA was dissolved in 1 mL of 10 mM Tris-HCl buffer at pH 7.4. From this stock solution, a dilute solution with a concentration of 0.1 mg/mL was prepared. The absorbance of this dilute solution was measured and found to be 1.0901 at 260 nm (Figure 3.5A). Additionally, the absorbance of various diluted ctDNA solutions was recorded at 260 nm to construct a calibration plot (Figure 3.5B). Using the calibration plot and the reported molar extinction coefficient (ϵ_{260}) value of 6600 M⁻¹ cm⁻¹ at 260 nm,⁵² the concentration of the stock ctDNA solution was determined to be 16.3 mM. In a similar manner, a stock solution of ethidium bromide (EtBr) was prepared by dissolving 10 mg of EtBr in 1 mL of water.

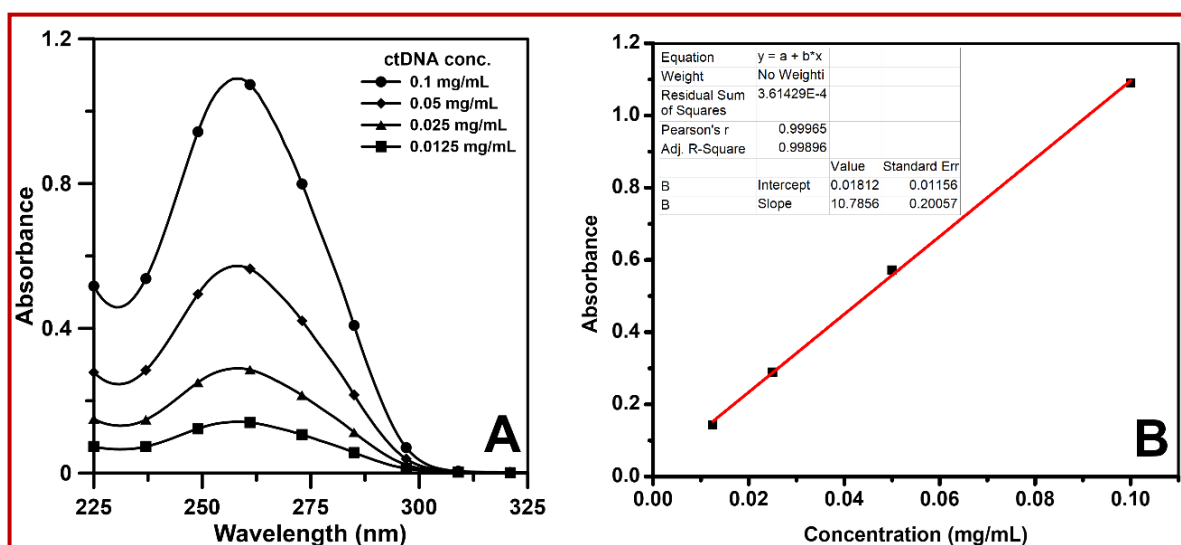


Figure 3.5. UV-Vis absorption spectra of neat ctDNA in Tris-HCl buffer against the variation of its concentration (A). Calibration curve of neat ctDNA in Tris-HCl buffer (B).

Study of Polyplex Formation between P[Cys-PPh₃]⁺Br⁻]-1 and ctDNA via Spectroscopic and Gel Electrophoresis Techniques:

To create the EtBr-ctDNA complex solution, the previously mentioned solution with ctDNA and EtBr concentrations of 508 μM and 50.6 μM , respectively, was used. In a typical experiment, four vials were prepared, each containing an equal volume of the EtBr-ctDNA complex solution. Different volumes of P[Cys-PPh₃]⁺[Br⁻]-1 solution were added to these vials to achieve concentrations of 2, 4, 6, and 8 mg/mL, resulting in final ctDNA and EtBr concentrations of 254 μM and 25.3 μM , respectively, in each solution. The solutions were gently mixed and incubated for 30 minutes at room temperature.

The emission spectra of each solution, along with a control solution, were recorded at room temperature with an excitation wavelength of $\lambda_{\text{ex}} = 517$ nm. The decrease in fluorescence intensities of the mixtures with increasing P[Cys-PPh₃]⁺[Br⁻]-1 concentrations was recorded at $\lambda_{\text{em}} (\text{max}) = 601$ nm.

To determine the electrophoretic mobility of the polypeptide-ctDNA polyplex, gel electrophoresis was performed using a 1% agarose gel in Tris-borate-EDTA buffer with a pH of 8.3, containing 45 mM Tris-borate and 1 mM EDTA. The polyplexes were prepared by mixing the required volume of 16.3 mM ctDNA solution with 2, 4, 6, and 8 mg/mL P[Cys-PPh₃]⁺[Br⁻]-1 solutions in Tris-HCl buffer. The solutions were thoroughly mixed and incubated for 45 minutes at 30 °C. Next, 30 μL of each polyplex solution was mixed with 5 μL of 10X gel-loading dye. These stained polyplex solutions (25 μL) were carefully placed in the wells of the 1% agarose gel. The gel was run at 100V for 2 hours in 1X TBE buffer. Afterward, the polyplex-containing agarose gel was stained with EtBr for 2 hours and visualized under a UV transilluminator. An image of the EtBr-stained polyplex was obtained using a gel documentation instrument (Bio-Rad).

The effect of ionic strength on the fluorescence quenching of the EtBr-ctDNA complex by the addition of P[Cys-PPh₃]⁺[Br⁻]-1 was studied by recording each of their emission spectra in the presence of 0.1 and 0.2 M NaCl solutions.

3.3.4. Characterization

FT-IR spectra of all the compounds were recorded using a Spectrum 2 (PerkinElmer) FT-IR Spectrometer (resolution was kept at 4 cm^{-1}) from their native state.

ESI-MS spectra of 2-BrEt-Ac, Cys-Br and Cys-Br-NCA from their DCM, H₂O: MeOH (1:1) and DCM solutions respectively were recorded using a Waters quadrupole time-of flight (Q-TOF) Micro YA263 mass spectrometer.

¹H-, ¹³C- and ³¹P-NMR spectra of the as-synthesized compounds from their respective solvents were acquired in Bruker DPX 400 MHz spectrometer at 25 °C.

End group analysis of PCys-Br -1 and molecular weight of Cys-Cl NCA were determined by a Bruker MALDI-TOF-MS instrument using 2,5-dihydroxybenzoic acid (DHB) and trans-2-[3-(4-tert-Butylphenyl)-2-methyl-2-propenylidene]malononitrile (DCTB) respectively as matrices. NaI was used to enhance ionization.

Absorption and % transmittance of the solutions/suspensions were recorded by a Carry UV-Vis Compact Peltier instrument (Agilent) equipped with a temperature sensing probe. A quartz cuvette of 1 cm path length was used for each experiment.

Emission spectra were recorded from sample solution using a Cary Eclipse Spectrophotometer from Agilent. Slit width was kept fixed at 5nm for all the measurements.

Number average molecular weight (M_n) and dispersity (\mathcal{D}) were determined by size exclusion chromatography (SEC) using a Waters 1515 isocratic HPLC pump equipped with two Polar Gel-M ($M_n \sim 500\text{ kDa}$) columns at 50 °C and a Waters 2414 refractive index detector at 40 °C. DMF containing 30 mM LiBr was used as the eluent with a flow rate of 1 mL min^{-1} and narrow

PMMA standards were used for calibration. Waters Empower software was used for molecular weight analysis.

Hydrodynamic diameter (D_h) and zeta potential (ξ) were measured in a dynamic light scattering (DLS) instrument, Zetasizer NANO ZS 90, Malvern (Model 3690), equipped with a He-Ne laser ($\lambda = 632.8$ nm). The intensity-weighted distribution data obtained from the DLS instrument were finally plotted to obtain the D_h s at 25 °C. Zeta potential of P[Cys-PPh₃]⁺[Br⁻] was determined from its 0.1 wt% aqueous solution in a glass cuvette equipped with a deep cell (Malvern). Particle size of the P[Cys-PPh₃]⁺[Br⁻]-1/anion aggregates in water was determined by DLS at different temperature intervals also. Intensity average particle size distribution was then measured at different temperature within a temperature window of 10-95 °C. Filtered Mili-Q water was used for preparing sample solution for D_h and ξ measurements.

The morphology of the anion-induced P[Cys-PPh₃]⁺[Br⁻]-1 aggregates in water were studied by field emission scanning electron microscopy (FESEM). Platinum coated samples metal stub were placed under a JEOL JSM-6700F FESEM operated at an accelerating voltage of 2 kV. It was difficult to distinguish the morphologies of the aggregates when samples were prepared by direct drop-casting of aqueous solutions due to their high concentration. To avoid this problem, P[Cys-PPh₃]⁺[Br⁻]-1/anion aggregates were lyophilized from each of different anion containing aqueous sample suspension and the solid residue (frozen aggregates) was dispersed in required volume of diethyl ether. It should be noted that the P[Cys-PPh₃]⁺[Br⁻]-1 and its aggregates are insoluble in diethyl ether. The aggregates' suspension in ether was then drop-casted on a thin Al-plate and dried in air before placing into the sample chamber.

Morphology of the P[Cys-PPh₃]⁺[Br⁻]-1 in was examined by transmission electron microscopy (TEM). Aqueous P[Cys-PPh₃]⁺[Br⁻]-1 solution (1.0 mg/mL) were drop-casted onto carbon-coated copper grid and air-dried for two days.

TEM image was taken by placing the grids under JEOL JEM-1400 Plus electron microscope working at an accelerating voltage of 100 kV.

The circular dichroism (CD) spectra of PCys-Br-1 and P[Cys-PPh₃]⁺[Br⁻]-1 were recorded from their 0.5 wt% solutions in DMF using a JASCO J-1500 CD spectropolarimeter, keeping the path length 1 mm. CD spectra of neat ctDNA (815 μM) and polyplex with varying concentrations of P[Cys-PPh₃]⁺[Br⁻]-1 (2, 4, 6 and 8 mg/mL) were recorded from their 10 mM Tris-HCl buffer solutions. Bandwidth, response time and scanning rate were kept at 1 nm, 1 s and 100 nm/min respectively. A resultant spectrum of three consecutive scans were taken to reduce the signal-to-noise ratio.

Gel electrophoresis of the P[Cys-PPh₃]⁺[Br⁻]-1/ctDNA polyplex solutions were performed using Mini-Sub Cell GT Basic System from Bio-Rad and the image of the EtBr-stained gel was taken using a Bio-Rad Gel Documentation System.

The cytotoxicity of the P[Cys-PPh₃]⁺[Br⁻]-1 was measured by in vitro viability of the KB cells (oral cancer cells) using conventional MTT assay.⁵³ Typically, KB cells were seeded on 24 well plates in DMEM media with 10% fetal bovine serum (FBS) and 1 % streptomycin overnight at 37 °C and 5% CO₂ atmosphere. Then the cells were incubated with P[Cys-PPh₃]⁺[Br⁻]-1 having different final concentration (20-500 μg/mL) for 24 hours. Cells were then washed with PBS buffer solution to remove unbound particles and fresh DMEM media was added followed by incubation with 50 μL of 3-(4,5-dimethylthiazol-2-yl)-2,5-diphenyltetrazolium bromide (MTT, 5 mg/mL in water) for 4 hours. The supernatant was removed to collect the violet formazan and then dissolved by 500 μL of SDS solution in water-DMF (1:1) mixture. The absorbance was measured at 570 nm using microplate reader. The relative cell viability of the P[Cys-PPh₃]⁺[Br⁻]-1 was calculated by assuming 100% cell viability for sample having no polypeptide sample.

3.4. Result and Discussion

3.4.1. Synthesis of PCys-Br and P[PCys-PPh₃]⁺[Br⁻]

Bromo-functionalized poly(L-cysteine) (PCys-Br) was synthesized via a multi-step reaction depicted in Scheme 3.1. Initially, L-cysteine underwent a reaction with 2-BrEt-Ac in the presence of a dimethylphenylphosphine catalyst, resulting in the formation of water-soluble Cys-Br. This was followed by the NCA formation through the ring closing of the cysteine moiety. The synthesis of Br-functionalized poly(L-cysteine) (PCys-Br) involved the ROP of Cys-Br NCA using an HMDS initiator at room temperature.

A nucleophilic substitution reaction of PCys-Br with PPh₃ led to the formation of a water-soluble cationic polypeptide ([PCys-PPh₃]⁺[Br⁻]). The attachment of the 2-BrEt-Ac moiety to cysteine via C-S bond formation was confirmed by the disappearance of a band at 1634 cm⁻¹ in the FT-IR spectrum (Figure 3.1), corresponding to the >C=C< bond. The formation of Cys-Br NCA was indicated by the appearance of characteristic symmetric and antisymmetric stretching bands of >C=O at 1773 cm⁻¹ and 1849 cm⁻¹, respectively, which subsequently vanished after ROP (Figure 3.1). The presence of an amide (O=C-NH) band at 1630 cm⁻¹ further confirmed the formation of the polypeptide backbone in PCys-Br-1. Moreover, in Figure 3.2, the ¹H-NMR signals at δ 6.46, 6.16, and 5.88 ppm, corresponding to the protons of the double bond in 2-BrEt-Ac, disappeared due to the formation of Cys-Br via C-S bond formation. The ¹H-NMR spectrum of [PCys-PPh₃]⁺[Br⁻] (Figure 3.2) exhibited additional aromatic proton signals in the region of δ 7.7-7.9 ppm, which were absent in the case of PCys-Br-1, indicating the attachment of the PPh₃ moiety to PCys-Br-1. The ³¹P-NMR spectrum of [PCys-PPh₃]⁺[Br⁻] displayed a signal at δ 23.74 ppm (Figure 3.6A), corresponding to the phosphorus atom of the PPh₃ group. Furthermore, the zeta potential (ξ) value of +12 mV (Figure 3.6B) for [PCys-PPh₃]⁺[Br⁻] (0.1 mg/mL) in water indicated its positively charged nature.

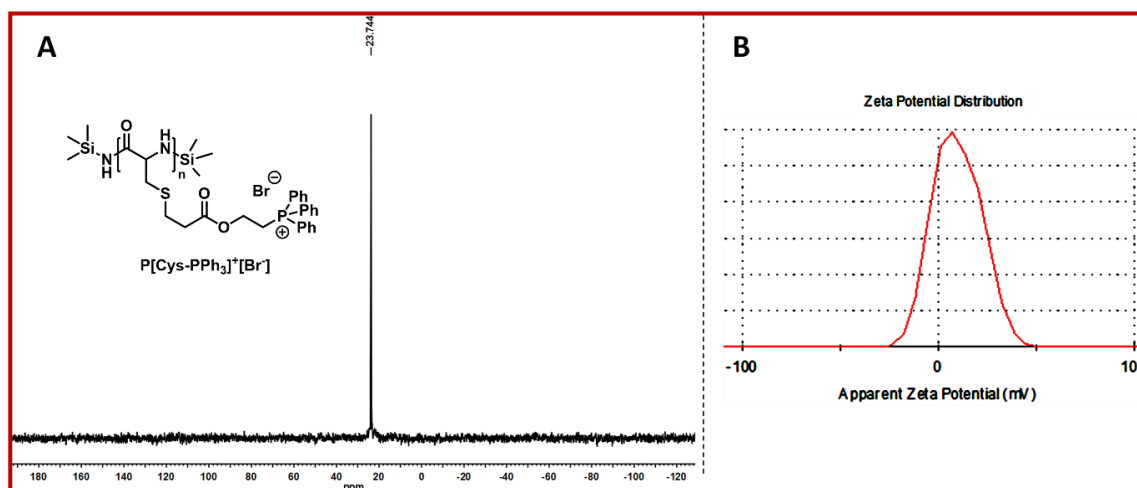


Figure 3.6. ^{31}P -NMR spectrum (A) and zeta potential (ξ) curve (B) of $[PCys-PPh_3]^+[Br]^-$ in D_2O and H_2O respectively.

The MALDI-TOF-MS spectrum of PCys-Br-1 exhibited a series of recurring peaks with a mass difference of $m/z = 282$ Da, precisely corresponding to the molecular weight of the Cys-Br monomeric unit (Figure 3.7). In Figure 3.3, the peak at $m/z = 2495$ was identified as the combined molar masses of two end groups (aminotrimethyl silane and trimethyl silane), 8 units of Cys-Br, and 2 K^+ ions resulting from ionization. The chemical structure of PCys-Br-1, determined through MALDI-TOF analysis and the presence of specific end groups, confirmed the initiation of ROP by the HMDS initiator.

Size exclusion chromatography (SEC) traces of the synthesized polypeptides exhibited a unimodal distribution (Figure 3.8A). The shift in the chromatogram of PCys-Br-1 towards higher molecular weight regions after cationization to form $[PCys-PPh_3]^+[Br]^-$ indicated the substitution of the pendant Br atom with the relatively higher molecular-weight PPh_3 moiety. Figure 3.8A also demonstrated that the elution volume of $[PCys-PPh_3]^+[Br]^-$ was lower than that of PCys-Br-1, clearly indicating that the M_n of $[PCys-PPh_3]^+[Br]^-$ was higher than that of PCys-Br-1. However, reproducible SEC traces for PCys-Br-2 were not observed. Table 3.1 provided

evidence that the M_n of PCys-Br increased from 3800 to 5300 Da for [PCys-PPh₃]⁺[Br⁻]-1. Analysis of the molecular weight data indicated that approximately 80% of the Br atoms in PCys-Br-1 were substituted by PPh₃ moieties through post-functionalization. Although the \bar{D} s of the polypeptides were slightly higher (Table 3.1), suggesting a living nature of the ROP of the Cys-Br NCA molecule.

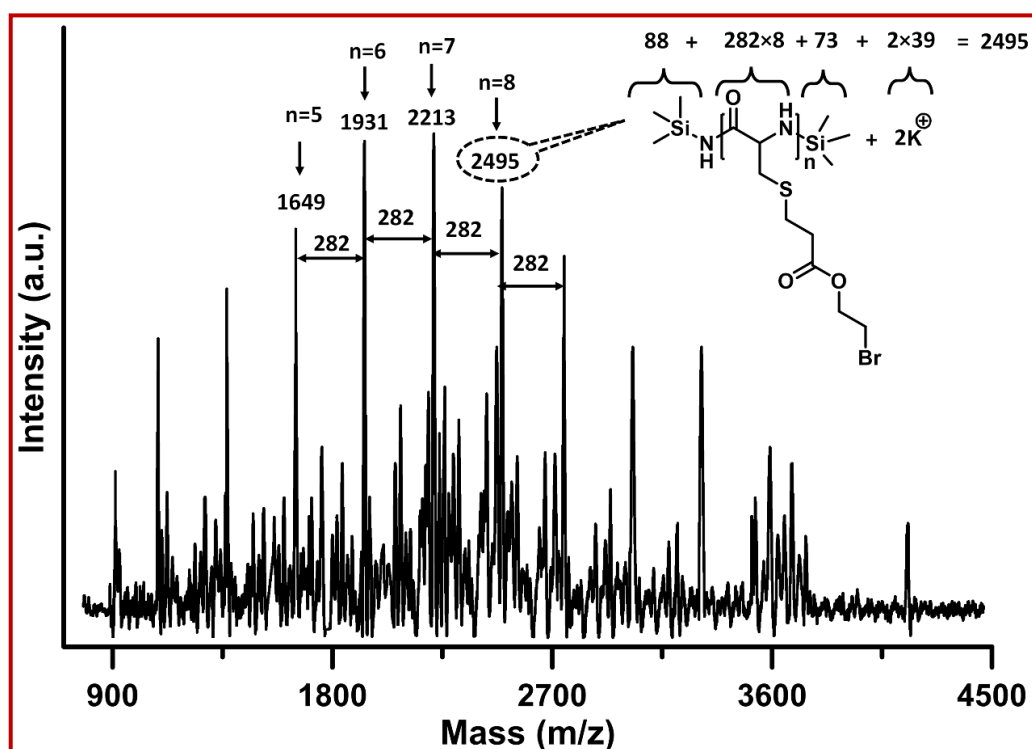


Figure 3.7. MALDI-TOF-MS of PCys-Br-1 in DMF.

The circular CD spectrum of PCys-Br-1 indicated that the polypeptide backbone adopted a β -sheet-like secondary structure in solution (Figure 3.8B). This secondary structure has been reported for polypeptides with similar chemical compositions.^{5,31} However, it is important to note that the negative CD ellipticity at 260 nm for PCys-Br-1 does not exactly match the values reported for polycysteine by other research groups.^{5,31} Nonetheless, the post-modification did not disturb the secondary structure of PCys-Br and [PCys-PPh₃]⁺[Br⁻]-1 in

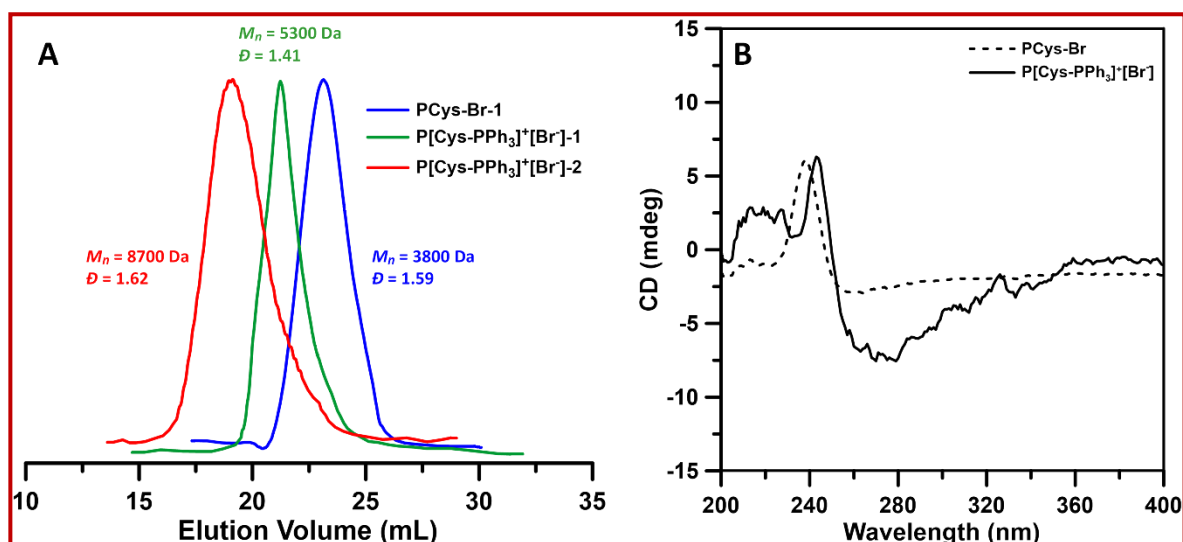


Figure 3.8. (A) SEC chromatograms of PCys-Br-1, [PCys-PPh₃]⁺[Br⁻]-1 and [PCys-PPh₃]⁺[Br⁻]-2, (B) CD spectra of PCys-Br-1 and [PCys-PPh₃]⁺[Br⁻]-1 showing antiparallel β -sheet like secondary structure.

solution (Figure 3.8B), although a shift in the negative CD ellipticity from 260 to 273 nm was observed due to this modification. The exact reason for this peak shift is unknown, but it could be attributed to the substitution of the Br atom by the aromatic PPh₃ moiety in the side chain of the polypeptide. The FT-IR bands observed at 1630/1656 cm^{-1} and 1520 cm^{-1} in the amide-I (1600-1700 cm^{-1}) and amide-II (1500-1600 cm^{-1}) regions, respectively, in the spectrum of PCys-Br-1 (Figure 3.1) were attributed to the stretching vibrations of the C=O bonds and bending vibrations of the N-H bonds present in the polypeptide backbone.⁵ These bands are characteristic of polypeptides adopting a β -sheet-like structure, providing good correlation between the FT-IR and CD spectral analysis data. However, it should be noted that these bands merged to form a broad band at 1660 cm^{-1} for [PCys-PPh₃]⁺[Br⁻]-1, making it difficult to conclusively determine its secondary structure from solid-state FT-IR data. The TEM image of [PCys-Ph₃]⁺[Br⁻]-1 displayed a fibril-like morphology, confirming

the β -sheet conformation of this cationic polypeptide, as reported previously (Figure 3.9).⁵⁴

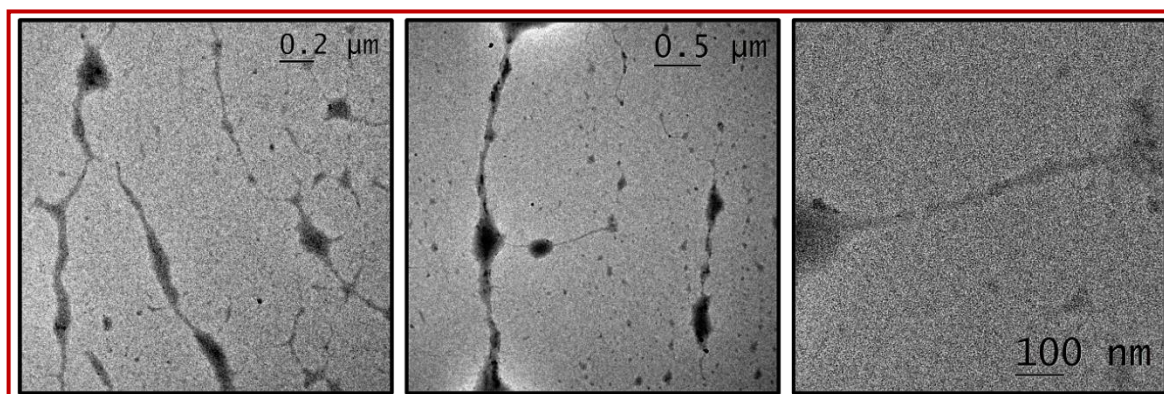


Figure 3.9. TEM images of [PCys-PPh₃]⁺[Br⁻]-1 (1 mg/mL) in water showing sheet-like morphologies.

3.4.2. Anion-responsive Behavior of [PCys-PPh₃]⁺[Br⁻]

The solubility of [PCys-PPh₃]⁺[Br⁻] in water was attributed to the pendant phosphonium cation. Based on previous findings on ionic polymers, it was anticipated that this cationic polypeptide would exhibit anion-responsive behavior.^{9, 25} To investigate this, a 1 mL aqueous solution of [PCys-PPh₃]⁺[Br⁻]-1 (0.5 wt%) was separately titrated against 1M aqueous solutions of various anions from the Hofmeister series such as BF₄⁻, I⁻, ClO₄⁻, SCN⁻, etc. (Figure 3.10). This titration resulted in a visual transition from a transparent solution to a two-phase turbid suspension (see photographs in Scheme 3.2) at a specific anion concentration. This is due to the formation of [PCys-PPh₃]⁺[Br⁻]-1/anion aggregates through anion-bridging interactions. The turbidity curves (Figure 3.6) indicated that the minimum concentration of anions ([anion]_{min}) required to decrease the %T ($\lambda = 500$ nm) of the [PCys-PPh₃]⁺[Br⁻]-1 solution from nearly 100 to almost zero were 115, 65, 35, and 15 mM for BF₄⁻, I⁻, ClO₄⁻, and SCN⁻ respectively. These data revealed that the anions' efficiency in interacting (via anion-bridging, Scheme 3.2) with the phosphonium cation of [PCys-PPh₃]⁺[Br⁻]-1

in water follows the order $\text{SCN}^- > \text{ClO}_4^- > \text{I}^- > \text{BF}_4^-$. These chaotropic anions have been reported to induce salting-out of the polyelectrolyte by screening the electrostatic repulsion between polyelectrolyte chains.^{9, 25, 55}

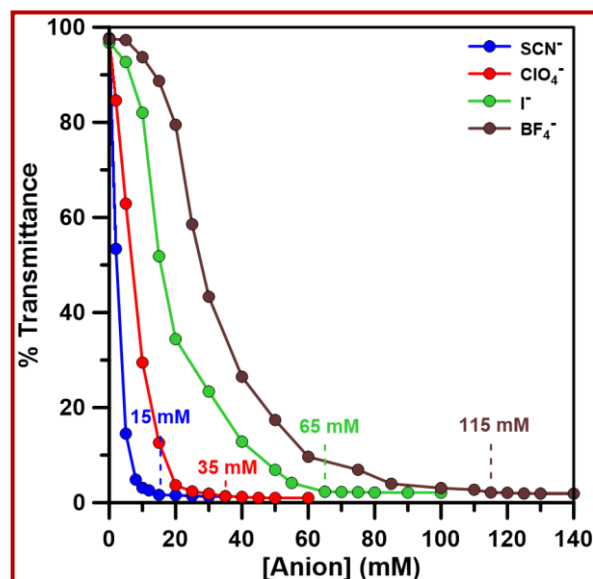
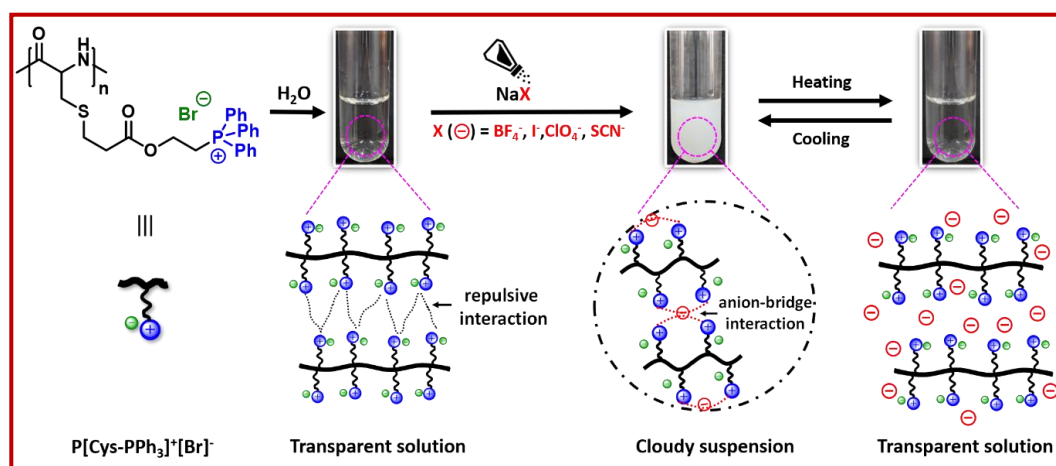


Figure 3.10. Turbidity curves illustrating the change of %T of 0.5 wt% aqueous $\text{P}[\text{Cys-PPh}_3]^+[\text{Br}^-]$ solution (1 mL) in the presence of varying concentration of different chaotropic anions (SCN^- , ClO_4^- , I^- and BF_4^-).



Scheme 3.2. Mechanism of aggregate formation by $\text{P}[\text{Cys-PPh}_3]^+[\text{Br}^-]$ in the presence of added anions in water and its UCST-type thermos-responsive behaviour. These representative photographs were the cloudy suspension and the transparent solution of the 0.5 wt% $\text{P}[\text{Cys-PPh}_3]^+[\text{Br}^-]$ (1 mL) in the presence of 35 mM ClO_4^- anion under different conditions.

The effectiveness order of these anions ($\text{SCN}^- > \text{ClO}_4^- > \text{I}^- > \text{BF}_4^-$) for salting-out matches the observations in this study. The insoluble phase transition in solution upon anion addition is due to the formation of hydrophobic macroscopic aggregates, facilitated by ion-bridging interactions between the phosphonium cations of $[\text{PCys-PPh}_3]^+[\text{Br}^-]$ -1 and the added anion.^{9, 25} It is reported that these anions shield the interaction between the opposite charge present within the cationic macromolecular system by the negative charge of these chaotropic anions, resulting in macromolecular aggregation in the solution.^{9, 25, 55} These ion-bridging interactions are influenced by the anions' polarizabilities. In this case, chains remained soluble in water due to the electrostatic repulsion among the positively charged polypeptide chains, which basically hinder them to form coagulate in solution. But the positive charge of the polypeptide is shielded by the negative charge of the added anions, leading to intra- and/or inter-molecular cross-linking through anion-bridging interactions (Scheme 3.2). Weak anion-bridging electrostatic interactions enhance the effective hydrophobicity of the anionically cross-linked polypeptide chains, causing them to form insoluble aggregates in solution, resulting in a cloudy suspension (Scheme 3.2 photographs). Anions with higher polarizabilities are expected to be more effective in screening a greater number of positive charges within the polypeptide chains. Consistent with our previous report, the polarizabilities of the chaotropic anions followed the order $\text{SCN}^- > \text{ClO}_4^- > \text{I}^- > \text{BF}_4^-$. Thus, the order of the minimum anion concentration required to form $\text{P}[\text{Cys-PPh}_3]^+/\text{anion}$ aggregates in the solution would be as follows: $\text{BF}_4^- > \text{I}^- > \text{ClO}_4^- > \text{SCN}^-$ (Figure 3.10). Similar turbid suspension formation was observed in water for 0.5 wt% $[\text{PCys-PPh}_3]^+[\text{Br}^-]$ -2 in the presence of 22 mM SCN^- , which can be attributed to the higher molecular weight of the polypeptide requiring a larger amount of SCN^- to induce the formation of a cloudy suspension in water via anion-bridging interactions. However, no turbidity formation was observed in a 0.5 wt% aqueous $[\text{PCys-PPh}_3]^+[\text{Br}^-]$ -1 solution in the

presence of kosmotropic anion (SO_4^{2-}) and kosmotropic-chaotropic borderline anions (Cl^- , NO_3^- , Br^- , CH_3COO^- , etc.) even up to their concentration of 500 mM. Above this concentration, $\text{P}[\text{Cys-PPh}_3]^+[\text{Br}^-]-1/\text{anion}$ aggregates precipitated, rather than remaining as a turbid suspension, in the presence of approximately 535 mM SO_4^{2-} ions. These precipitates could not be redissolved upon heating, indicating that the strong electrostatic interaction between the doubly charged SO_4^{2-} ion and the positively charged polypeptide chains is responsible for their precipitation. It should be noted that turbidity formation did occur for cationic polypeptides with different chemical structures in the presence of certain borderline anions such as Br^- in water.⁹

The DLS data of $\text{P}[\text{Cys-PPh}_3]^+[\text{Br}^-]-1$ in the presence of 115, 65, 35, and 15 mM concentrations of BF_4^- , I^- , ClO_4^- , and SCN^- anions (Figure 3.11A/ Table 3.2) clearly indicate the formation of $\text{P}[\text{Cys-PPh}_3]^+[\text{Br}^-]-1/\text{anion}$ aggregates with average hydrodynamic diameters (D_h) of 1700, 1200, 850, and 800 nm, respectively.

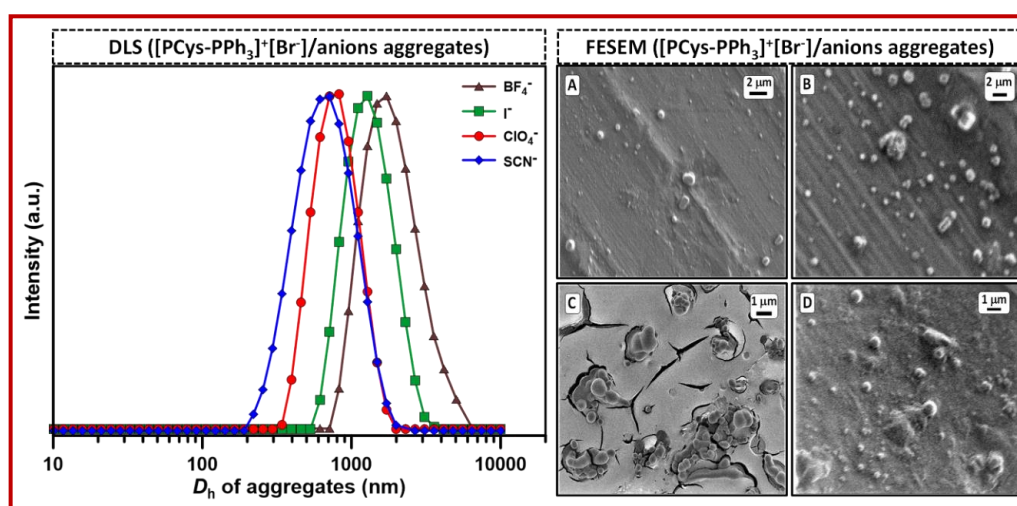


Figure 3.11. (Left) Intensity average particle size distribution of 0.5 wt% aqueous $\text{P}[\text{Cys-PPh}_3]^+[\text{Br}^-]-1$ solution in the presence of different chaotropes (BF_4^- , I^- , ClO_4^- and SCN^-) at their minimum concentration at 25 °C; (Right) FESEM images of $\text{P}[\text{Cys-PPh}_3]^+[\text{Br}^-]-1$ (0.5 wt%) aggregates in water in the

presence of 115 mM BF_4^- (A), 65 mM I^- (B), 35 mM ClO_4^- (C) and 15 mM SCN^- (D), showing spherical morphologies.

It is expected that the extent of anion-bridging interactions is greater for the anion with higher polarizability (SCN^-), leading to the compact globular aggregation of the polypeptide chains. In contrast, the cationic polypeptide chains remain loosely bound to each other through weak anion-bridging interactions with BF_4^- due to its lower polarizability. This difference in anion-bridging strength likely explains the smaller average size of the $\text{P}[\text{Cys-PPh}_3]^+[\text{Br}^-]-1/\text{SCN}^-$ aggregates compared to those of $\text{P}[\text{Cys-PPh}_3]^+[\text{Br}^-]-1/\text{BF}_4^-$. FESEM images of 0.5 wt% turbid suspensions of $\text{P}[\text{Cys-PPh}_3]^+[\text{Br}^-]-1$ in water containing 115, 65, 35, and 15 mM concentrations of BF_4^- , I^- , ClO_4^- , and SCN^- (Figure 3.11B) reveal the formation of spherical aggregates with average diameters of approximately 1400 nm for BF_4^- , 950 nm for I^- , and 600 nm for both ClO_4^- and SCN^- . These results are consistent with the D_h values obtained from DLS measurements (Figure 3.11A, Table 3.2).

Table 3.2. Sizes of aggregates of $\text{P}[\text{Cys-PPh}_3]^+[\text{Br}^-]-1$ (0.5 wt%) in the presence of anions in water obtained from DLS experiment

Polypeptide	Anion	$[\text{Anion}]_{\text{min}}$ (mM)	$^a D_h$ at 25 °C (nm)	$^b T_{cp}$ (°C) (DLS) (Heating)	$^b T_{cp}$ (°C) (Turbidity) (Heating)	$^b T_{cp}$ (°C) (Turbidity) (Cooling)
$\text{P}[\text{Cys-PPh}_3]^+[\text{Br}^-]-1$	BF_4^-	115	1700	36	39	37
	I^-	65	1200	40	45	47
	ClO_4^-	35	850	49	57	57.4
	SCN^-	15	800	58	66	67

^a D_h – Hydrodynamic diameter at 25 °C.

^b T_{cp} – Cloud point (data obtained from the respective experiments which have been discussed later in this section)

3.4.3. Thermoresponsiveness of $[PCys-PPh_3]^+[Br^-]$ in Water with Added Anions

The presence of various chaotropic anions (BF_4^- , I^- , ClO_4^- , SCN^-) caused the aqueous solution of $P[Cys-PPh_3]^+[Br^-]$ -1 to transform from a transparent solution to a turbid suspension. This transformation was attributed to the formation of anion-bridged polypeptide aggregates through weak electrostatic interactions. These aggregates were highly unstable and collapsed into native cationic polypeptide chains upon increasing the solution temperature, a phenomenon previously observed in other cationic macromolecules.^{9, 25, 28} The turbid suspension of $P[Cys-PPh_3]^+[Br^-]$ -1/anion became clear upon heating, indicating the disruption of the anion-bridged aggregates, and returned to a turbid state upon cooling, as shown in the inset of Figure 3.12 for the case of $P[Cys-PPh_3]^+[Br^-]$ -1 (1 mL, 0.5 wt%)/ ClO_4^- (35 mM).

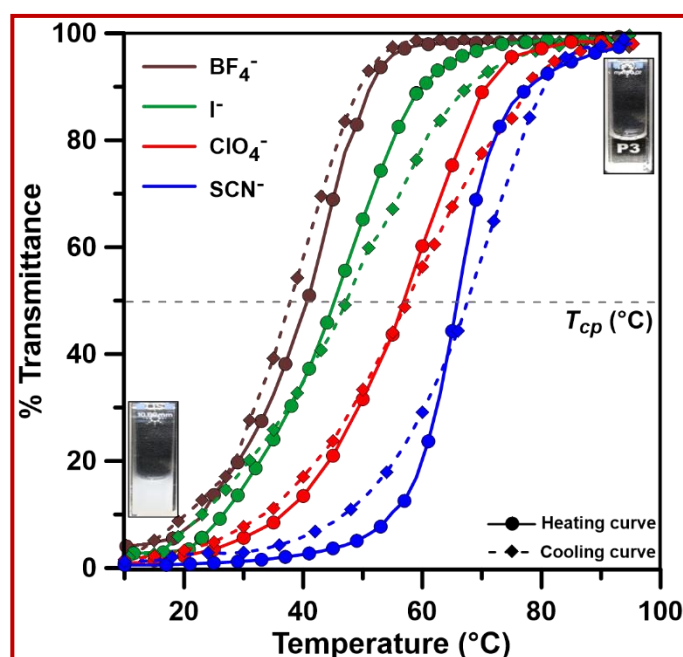


Figure 3.12. Turbidity curves ($\lambda = 500$ nm) of 1 mL aqueous $P[Cys-PPh_3]^+[Br^-]$ -1 solution (0.5 wt%) in the presence of minimum concentration of different chaotropic anions (BF_4^- , I^- , ClO_4^- and SCN^-). Inset showed the photographs of the turbid (bottom left) and transparent (top right) solution of aqueous $P[Cys-PPh_3]^+[Br^-]$ -1 (0.5 wt%) in the presence of 35 mM ClO_4^- at temperatures below and above the cloud point respectively.

This behavior suggested the presence of a reversible upper critical solution temperature (UCST)-type phase transition in water for the P[Cys-PPh₃]⁺[Br⁻]-1 solution in the presence of an anion. Figure 3.12 displayed the turbidity curves of the aqueous P[Cys-PPh₃]⁺[Br⁻]-1 (0.5 wt%) solution in the presence of 115 mM BF₄⁻, 65 mM I⁻, 35 mM ClO₄⁻, and 15 mM SCN⁻, respectively. The cloud points (T_{cp} s) were determined as 39, 45, 57, and 66 °C for BF₄⁻, I⁻, ClO₄⁻, and SCN⁻, respectively, during the heating cycle (Table 3.2). Minimal hysteresis was observed in the heating/cooling cycles of turbidity data P[Cys-PPh₃]⁺[Br⁻]-1 in the presence of each anion (Table 3.2). Notably, the T_{cp} of P[Cys-PPh₃]⁺[Br⁻]-1 was highest for SCN⁻ (66 °C) and lowest for BF₄⁻ (39 °C), indicating that the extent of anion-bridging interactions in the cationic polypeptide is highest for SCN⁻ with high polarizability and lowest for BF₄⁻ with the lowest polarizability. The UCST-type reversible aggregation and disaggregation behavior in response to temperature variations could be repeated for multiple cycles (Figure A3.12), indicating the high thermal stability of P[Cys-PPh₃]⁺[Br⁻]-1 in water.

T_{cp} s of the corresponding anion-containing P[Cys-PPh₃]⁺[Br⁻]-1 solutions (0.5 wt%) were also determined from DLS data (Figure 3.13, Table 3.2). The T_{cp} s obtained from the heating run of the DLS data closely matched those obtained from the turbidity data, supporting the thermal disaggregation of P[Cys-PPh₃]⁺[Br⁻]-1/anion aggregates in water. The cloud point of the heating and cooling runs of P[Cys-PPh₃]⁺[Br⁻]-2 (0.5 wt%)/SCN⁻ (22 mmol) suspension in water was determined to be 71 and 75 °C, respectively (Figure 3.14A). Consistent with previous reports, an increase in the molecular weight of the polypeptide led to an increase in the UCST cloud point of its anion-triggered suspension.⁹ Additionally, to examine the effect of the counter anion of the cationic polypeptide on its cloud point, turbidity measurements were performed using 0.5 wt% aqueous P[Cys-PPh₃]⁺[Cl⁻] in the presence of 115 mM representative BF₄⁻, but no detectable change in the cloud point was observed compared to P[Cys-PPh₃]⁺[Br⁻]-1 (Figure 3.14B).

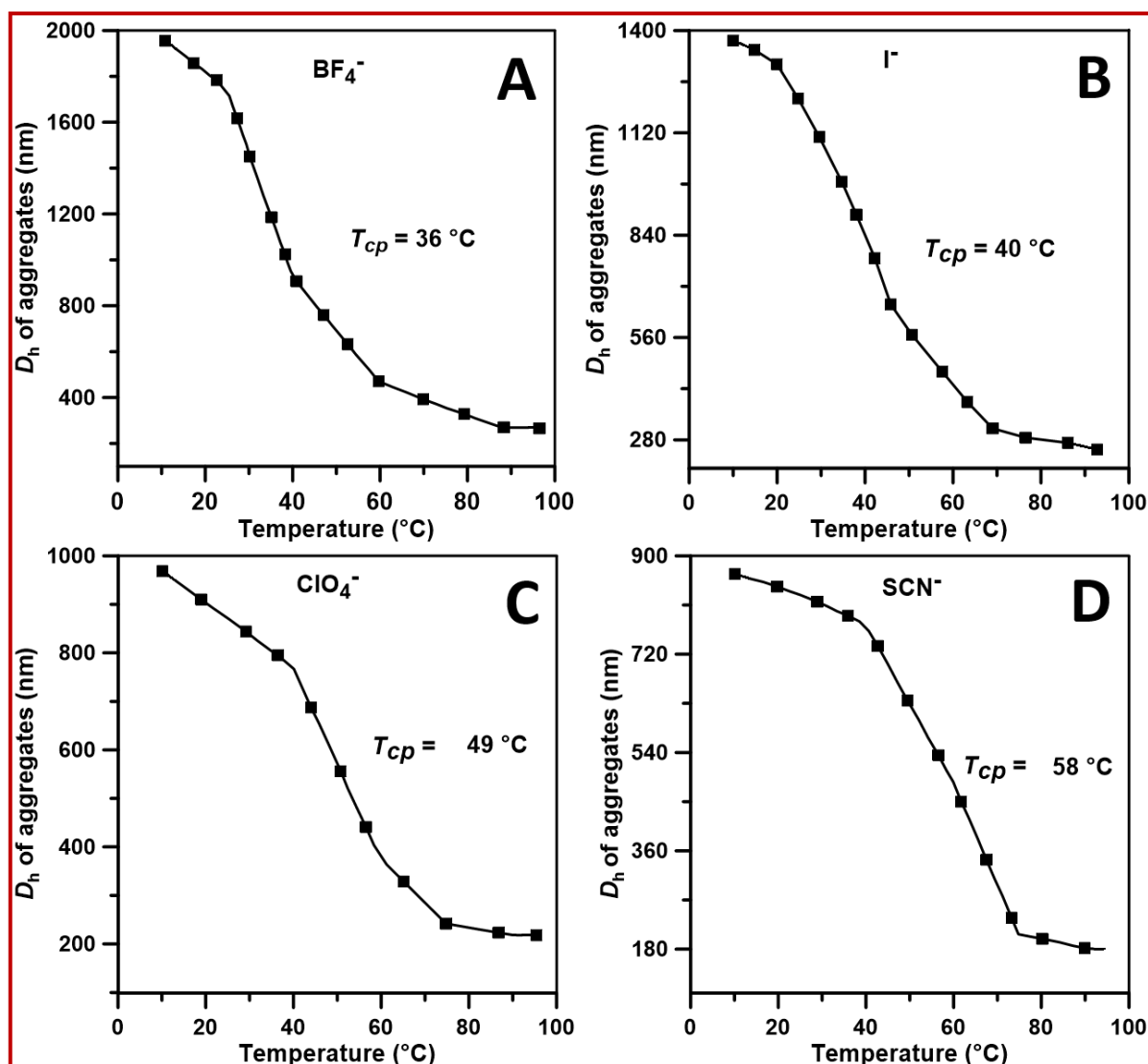


Figure 3.13. Variation of the D_h s of aggregates of P[Cys-PPh₃]⁺[Br⁻]-1 (0.5 wt%) in the presence of 115 mM BF_4^- (A), 65 mM I^- (B), 35 mM ClO_4^- (C) and 15 mM SCN^- (D) at different temperatures.

Further to explicate the effect of large anion on the aggregation behaviour of P[Cys-PPh₃]⁺[Br⁻]-1 in water, 0.5 wt% of its solution was titrated against 0.5 M solution of SDS as a representative anion. It was observed that approximately at 500 μM of SDS concentration, %T of the P[Cys-PPh₃]⁺[Br⁻]-1 solution (0.5 wt%) decreased to almost 1 from 90 indicated the aggregate formation. Figure 3.14C clearly showed the UCST-type phase transition of

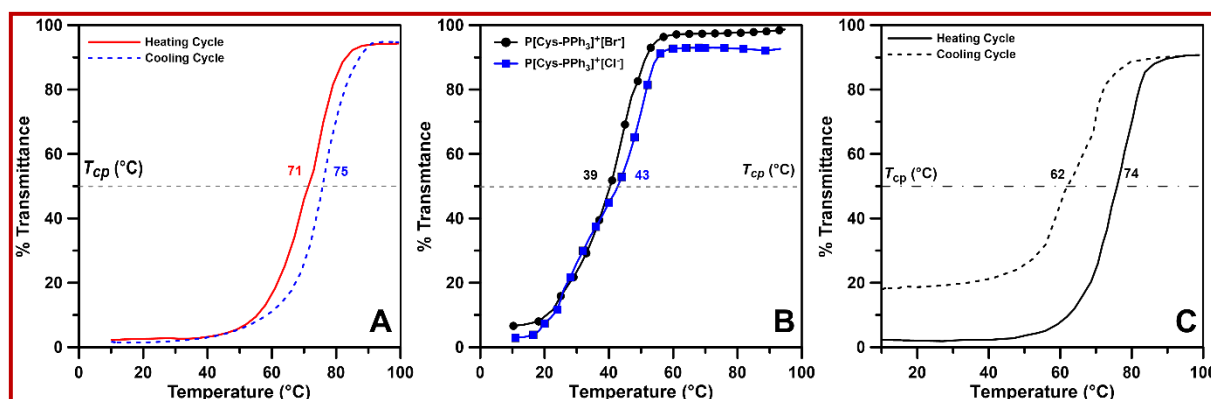


Figure 3.14. (A) Turbidity plot ($\lambda = 500$ nm) of aqueous P[Cys-PPh₃]⁺[Br⁻]-2 (0.5 wt%) solution in the presence of 22 mM SCN⁻, (B) Turbidity plot ($\lambda = 500$ nm) of aqueous P[Cys-PPh₃]⁺[Br⁻] and P[Cys-PPh₃]⁺[Cl⁻] (0.5 wt%) solution in the presence of 115 mM BF₄⁻, (C) UCST-type turbidity curve ($\lambda = 500$ nm) of 0.5 wt% aqueous solution of P[Cys-PPh₃]⁺[Br⁻]-1 in the presence of 500 μ M of SDS; heating and cooling run showed huge hysteresis.

P[Cys-PPh₃]⁺[Br⁻]-1/SDS mixture in water. T_{cp} s for the heating and cooling cycles were found to be 74 and 62 °C respectively (Figure 3.14C), revealing existence of large hysteresis. In the heating cycle, the heat energy required to disintegrate the formed aggregates with high extent of ionic-bridging interactions is usually high resulting in a higher T_{cp} . In the cooling cycle, the dissolved P[Cys-PPh₃]⁺ cation and dodecyl sulphate anion with long hydrophobic chain would not get enough time to interact strongly through anion-bridge interactions resulting in a floppy aggregate, which can easily be disintegrated using lower energy and hence it shows lower cloud point.

Effect of polypeptide concentration on T_{cp}

To study the effect of P[Cys-PPh₃]⁺[Br⁻]-1 concentration on the cloud point of the mixture, a turbidity experiment was conducted using aqueous P[Cys-PPh₃]⁺[Br⁻]-1 solutions of varying concentrations, while keeping the concentration of individual anions (BF₄⁻, I⁻, ClO₄⁻, SCN⁻) constant at their minimum levels for each experiment (Figure 3.15).

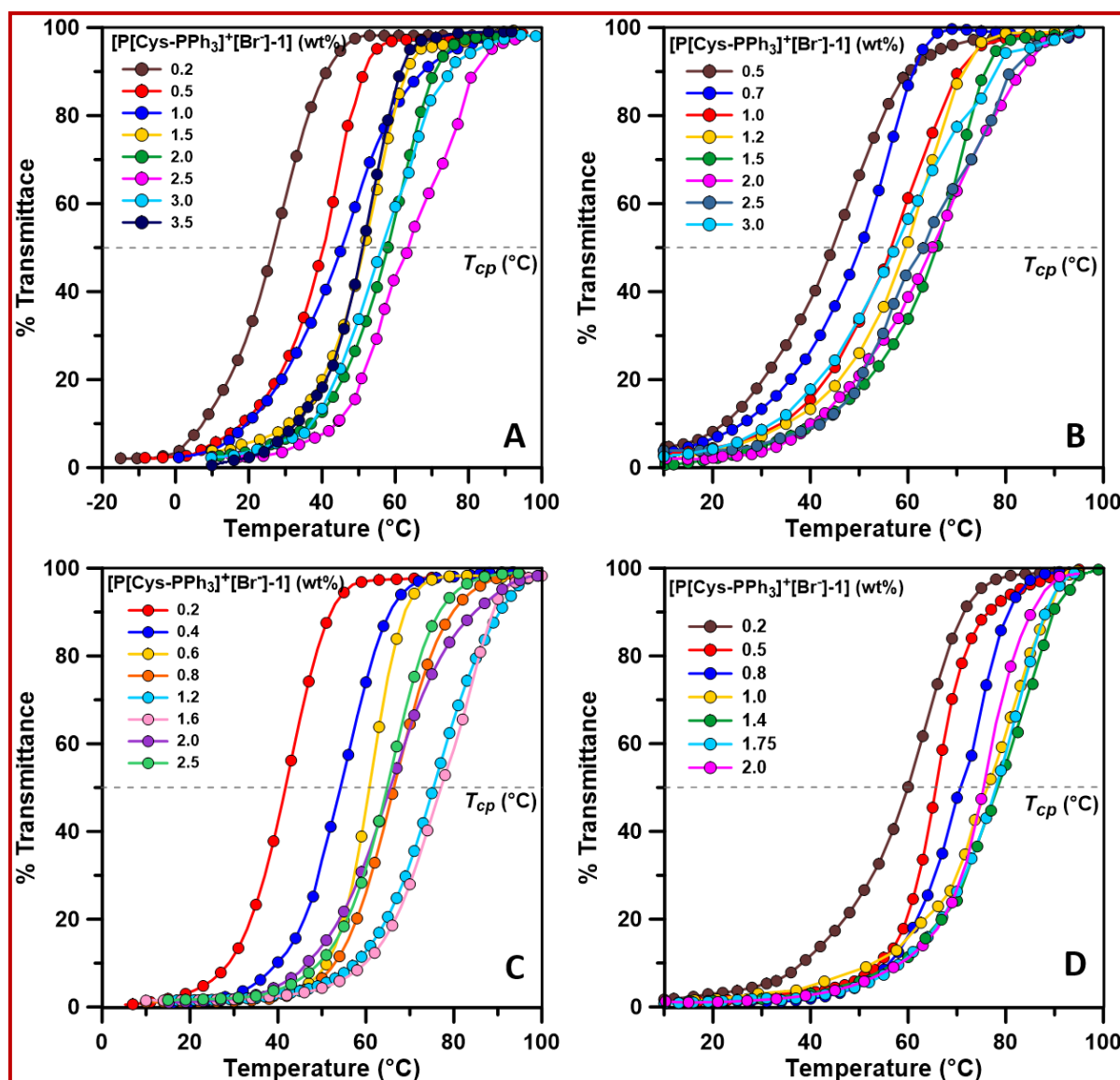


Figure 3.15. Turbidity plots ($\lambda = 500$ nm) of aqueous P[Cys-PPh₃]⁺[Br]⁻1 solutions with varying polypeptide concentration in the presence of 115 mM BF₄⁻ (A), 65 mM I⁻ (B), 35 mM ClO₄⁻ (C) and 15 mM SCN⁻ (D).

The plot of T_{cp} versus [P[Cys-PPh₃]⁺[Br]⁻1] for all the anions (Figure 3.16) demonstrated a concave-type curve with a maximum, similar to a typical UCST-type insoluble to soluble phase diagram. Initially, T_{cp} increased sharply and then decreased with increasing concentration of P[Cys-PPh₃]⁺[Br]⁻1. The maximum of each plot represented the actual UCST values of 60, 66, 75.4, and

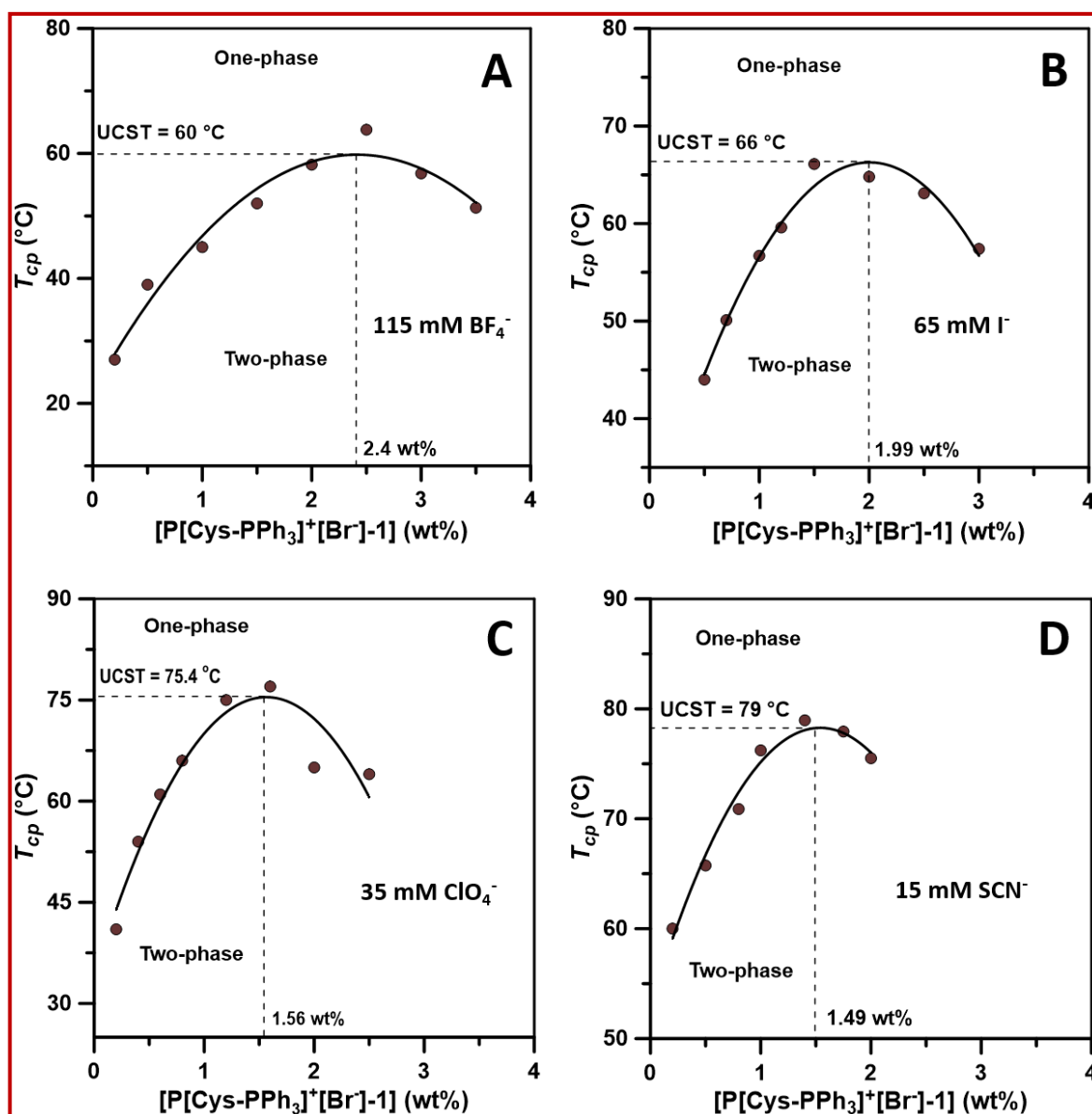


Figure 3.16. UCST-type phase diagram of P[Cys-PPh₃]⁺[Br⁻]-1 of varying concentration in the presence of 115 mM BF₄⁻ (A), 65 mM I⁻ (B), 35 mM ClO₄⁻ (C) and 15 mM SCN⁻ (D) in water.

79 °C for P[Cys-PPh₃]⁺[Br⁻]-1 in the presence of [anion]_{min} of 115 mM BF₄⁻, 65 mM I⁻, 35 mM ClO₄⁻ and 15 mM SCN⁻ respectively, at polypeptide concentrations of 2.4, 1.99, 1.56, and 1.49 wt%, respectively (Figure 3.16). The increase in T_{cp} with increasing polypeptide concentration can be attributed to the dominant ion-bridging interactions over the electrostatic repulsive interactions between

positively charged polypeptide chains. However, after a certain polypeptide concentration (which varies for different anions), the electrostatic repulsion becomes influential, resulting in a decrease in the cloud point with increasing P[Cys-PPh₃]⁺[Br⁻]-1 concentration. These findings align with previous observations for other ionic polymers.^{9, 25} Importantly, the concentration of P[Cys-PPh₃]⁺[Br⁻]-1 required to reach the maximum T_{cp} (= 60 °C) for the 115 mM BF₄⁻ ion was the highest, while it was the lowest for achieving a maximum T_{cp} (= 79 °C) for the 15 mM SCN⁻. As discussed earlier, this observation is expected as the polarizability of the chaotropic anions follows the order SCN⁻ > ClO₄⁻ > I⁻ > BF₄⁻.

Effect of anion concentration on T_{cp}

Also, to explore the impact of anion concentration on the cloud point, the temperature-dependent transmittance of 0.5 wt% P[Cys-PPh₃]⁺[Br⁻]-1 solution in the presence of varying concentrations of different chaotropic anions (BF₄⁻, I⁻, ClO₄⁻, SCN⁻) was checked (Figure 3.17). The T_{cp} values were plotted against the concentration of each individual anion, revealing a concave curve with a distinct maximum (Figure 3.18). This behavior is characteristic of a typical UCST-type phase transition.

When the polypeptide concentration was maintained at 0.5 wt%, it was observed that the highest amount of anions required to reach the peak T_{cp} differed for each anion. Specifically, it was found to be 229 mM for BF₄⁻, 168 mM for I⁻, 79 mM for ClO₄⁻, and 60 mM for SCN⁻. Correspondingly, the T_{cp} values at these specific anion concentrations followed the expected order: 82 °C (for 60 mM SCN⁻) > 69.5 °C (for 79 mM ClO₄⁻) > 65.3 °C (for 168 mM I⁻) > 58.5 °C (for 229 mM BF₄⁻). The observed anion concentration-dependent cloud point of P[Cys-PPh₃]⁺[Br⁻]-1 can be rationalized as follows: initially, as the concentration of anions increases, the extent of anion-bridging interactions between the anions and the pendant cations of the polypeptide chains strengthens. As a result,

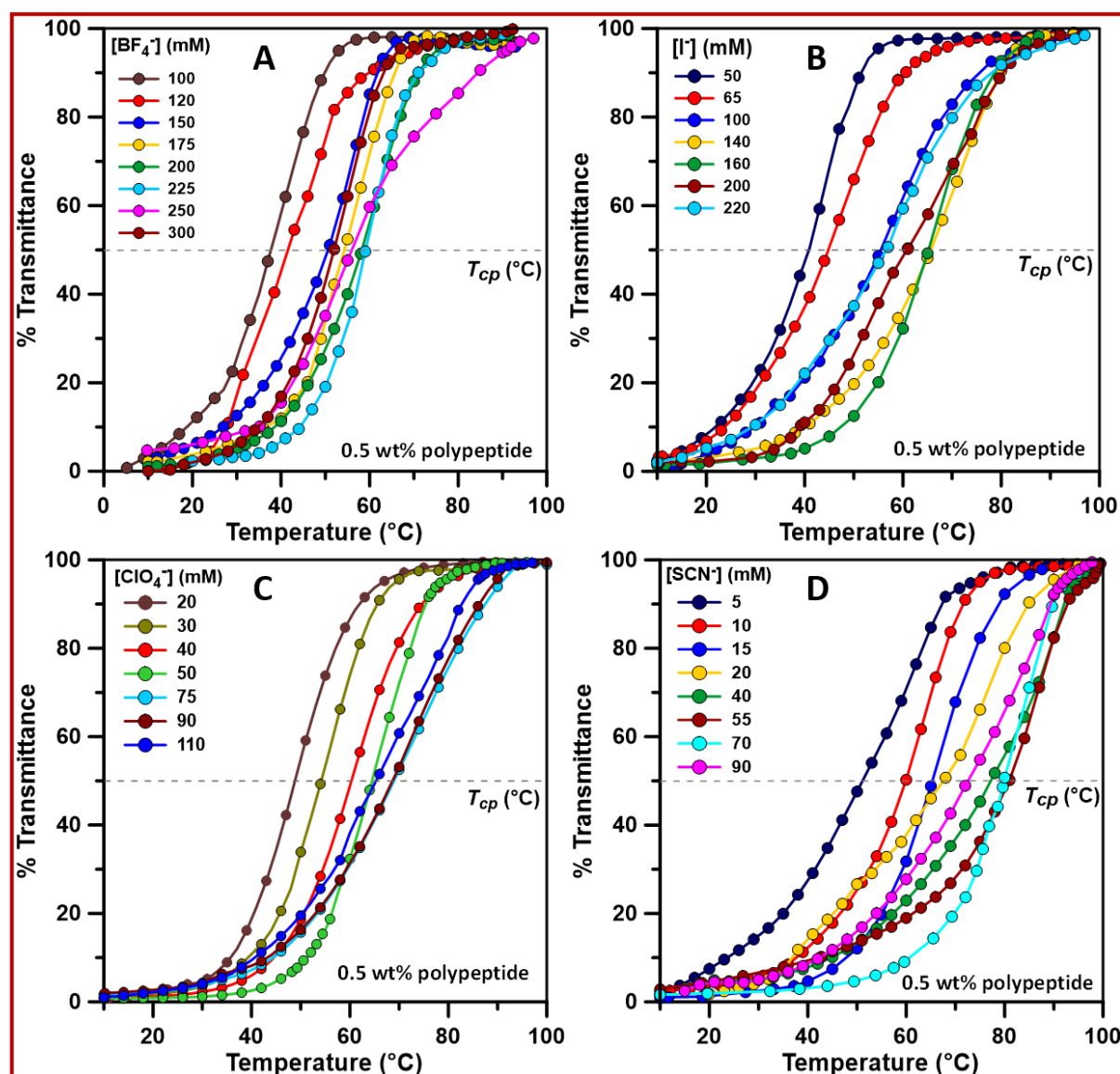


Figure 3.17. Turbidity plots ($\lambda = 500$ nm) of 0.5 wt% aqueous P[Cys-PPh₃]⁺[Br⁻]-1 solutions with varying concentration of BF₄⁻ (A), I⁻ (B), ClO₄⁻ (C) and SCN⁻ (D).

more energy is required to break these stronger anion-bridge interactions resulting in an elevation of T_{cp} . However, there is a saturation point beyond which further addition of anions leads to their adsorption onto the surface of the polypeptide aggregates. This adsorption increases the hydrophilicity of the aggregates, causing their solubility to rise at lower temperatures due to disruption, consequently lowering the cloud point. So, the concentration of anions also plays a crucial role in tuning the cloud point behavior of

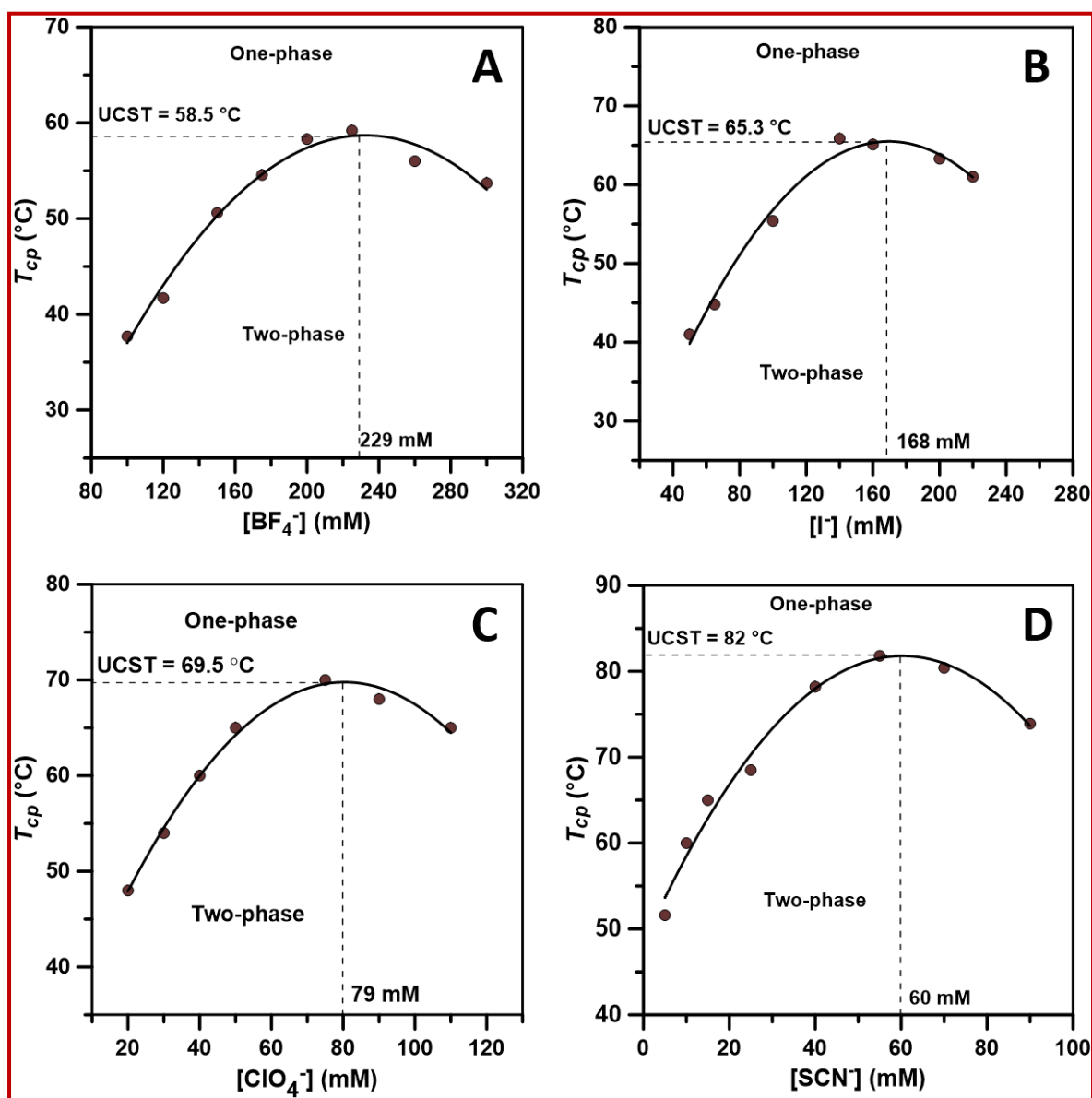


Figure 3.18. UCST-type phase diagram of P[Cys-PPh₃]⁺[Br]⁻-1 (0.5 wt%) in the presence of anions, BF_4^- (A), I^- (B), ClO_4^- (C) and SCN^- (D) of varying concentrations in water.

P[Cys-PPh₃]⁺[Br]⁻-1. The optimal anion concentration necessary to achieve the maximum T_{cp} varies among the anions studied, and this phenomenon arises from the interplay between anion-bridging interactions and surface adsorption on the polypeptide aggregates at a threshold anion concentration.

3.4.4. Intercalation of $[PCys-PPh_3]^+[Br^-]$ with DNA

It is anticipated that the cationic $P[Cys-PPh_3]^+[Br^-]$ would bind to the negatively charged oxygen atoms of the phosphate groups present in the periphery of the ctDNA double helix strand. To investigate the binding capability of $P[Cys-PPh_3]^+[Br^-]$ -1 with ctDNA, a 0.5 wt% aqueous solution of $P[Cys-PPh_3]^+[Br^-]$ was titrated against a ctDNA solution. The addition of ctDNA led to the formation of a cloudy solution, accompanied by a decrease in the transmittance (%T) of the binary solution from 90% to approximately 10% (Figure 3.19A). This observation suggested that $P[Cys-PPh_3]^+$ was capable of interacting with the negatively charged ctDNA.

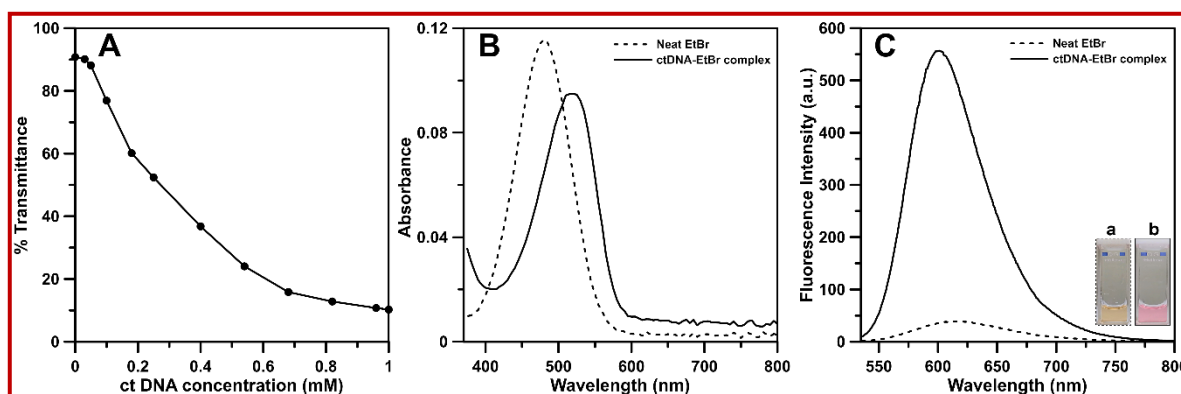
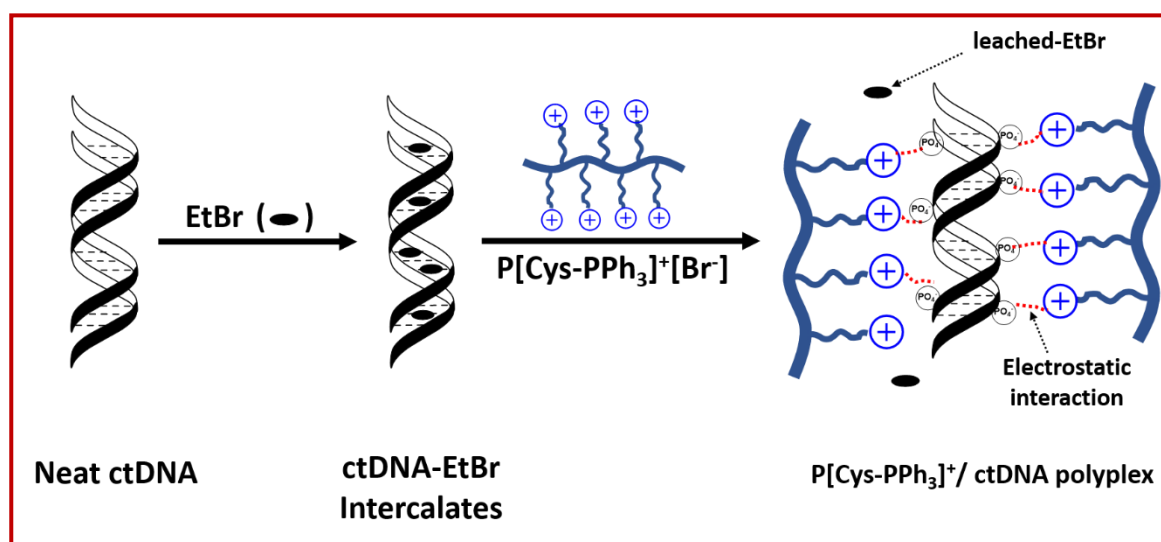


Figure 3.19. (A) Titration plot, showing the % transmittance of 0.5 wt% aqueous $P[Cys-PPh_3]^+[Br^-]$ -1 solution in the presence of different concentration of ctDNA; absorption (B) and emission (C) spectra of neat EtBr in water and EtBr-ctDNA complex in Tris-HCl buffer. Inset of the Figure C showed the change in colour of EtBr solution before (a) and after (b) the intercalation with ctDNA.

To further investigate the formation of polyplexes between ctDNA and $P[Cys-PPh_3]^+[Br^-]$ -1, ethidium bromide (EtBr) was used as a fluorescence probe. EtBr is known to intercalate between adjacent DNA base pairs, resulting in a red shift in the absorption maximum (λ_{max}) (from 480 to 517 nm) and an enhancement in fluorescence emission (Figures 3.19B and 3.19C).^{9,52}

In the presence of ctDNA, intercalated EtBr exhibited an emission peak at $\lambda_{\max} \approx 601$ nm, accompanied by a change in solution color from orange to pink (Figure 3.19C, inset of Figure 3.19C). The fluorescence intensity of the EtBr-ctDNA complex decreased upon the addition of other competing cations, indicating the displacement of ethidium cations from the EtBr-ctDNA intercalated complex due to stronger interactions between ctDNA and the competing cations. The extent of this fluorescence quenching of EtBr, bound to ctDNA, can be used to determine the binding efficiency of cationic molecule with negatively charged ctDNA.⁵² In this case also, the emission intensity of the EtBr-ctDNA complex at 601 nm in 10 mM Tris-HCl buffer showed a sharp decrease with increasing concentration of P[Cys-PPh₃]⁺[Br⁻]-1 from 2 to 8 mg/mL, confirming the leaching out of EtBr from its intercalated state into the bulk solvent due to polyplex formation (Scheme 3.3 and Figure 3.20).



Scheme 3.3. Schematics of polyplex formation of P[Cys-PPh₃]⁺[Br⁻] with ctDNA in aqueous solution.

This decrease in the fluorescence intensity of the EtBr-ctDNA complex was also supplemented by the change in the colour intensity of the EtBr-ctDNA complex upon gradual addition of P[Cys-PPh₃]⁺[Br⁻]-1 (Figure 3.20B).

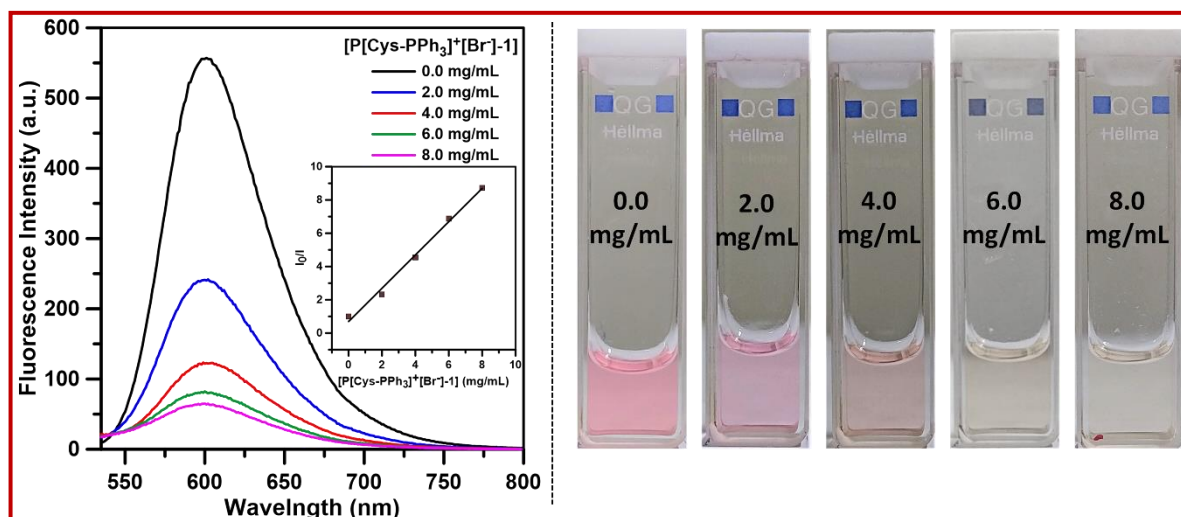


Figure 3.20. (Left) Emission spectra of EtBr-ctDNA intercalated complex in the presence of different concentration of P[Cys-PPh₃]⁺[Br⁻]-1 showing the quenching of fluorescence with increase its concentration. Inset showed the plot of the ratio of intensity (I_0/I) against the P[Cys-PPh₃]⁺[Br⁻]-1 concentration; (Right) Photographs showing the decrease in colour intensity of the ctDNA-EtBr complex with increase in P[Cys-PPh₃]⁺[Br⁻]-1 concentration in Tris-HCl buffer, indicating the leaching out of EtBr from its intercalated state into the bulk solvent.

The intensity ratio (I_0/I), where I_0 is the intensity of the EtBr-ctDNA intercalated complex at 601 nm and I is the intensity of the complex in the presence of varying concentrations of P[Cys-PPh₃]⁺[Br⁻]-1, was plotted against the concentration of the polypeptide (inset of Figure 3.20). The fluorescence quenching constant (K_{sv}) of P[Cys-PPh₃]⁺[Br⁻]-1 was then determined using the following Stern-Volmer equation,

$$\frac{I_0}{I} = 1 + K_{sv} \times (X)$$

where X is the concentration of the polypeptide. The plot of I_0/I versus X yielded a linear relationship, and the slope of this plot provided the value of the quenching constant K_{sv} . The quenching constant of P[Cys-PPh₃]⁺[Br⁻]-1 was

calculated to be $1.0004 \text{ mg}^{-1} \text{ mL}$ from the plot shown in the inset of Figure 3.20. This quenching constant indicates the extent of fluorescence quenching of the EtBr-ctDNA complex in the presence of $\text{P}[\text{Cys-PPH}_3]^+[\text{Br}^-]$ -1 and reflects the binding affinity of the cationic polypeptide to the negatively charged ctDNA.

The binding mechanism between negatively charged ctDNA and cationic polypeptide can be better understood by considering the influence of varying ionic strength. When NaCl is introduced to the mixture, the presence of sodium ions reduces the electrostatic interactions between the negatively charged phosphate groups of ctDNA and $\text{P}[\text{Cys-PPH}_3]^+$. To investigate this effect, the emission spectra of the EtBr-ctDNA complex were monitored in the presence of different amounts of polypeptide and NaCl. It was observed that the extent of fluorescence quenching of the EtBr-ctDNA complex by the polypeptide significantly decreased in the presence of NaCl (Figure 3.21).

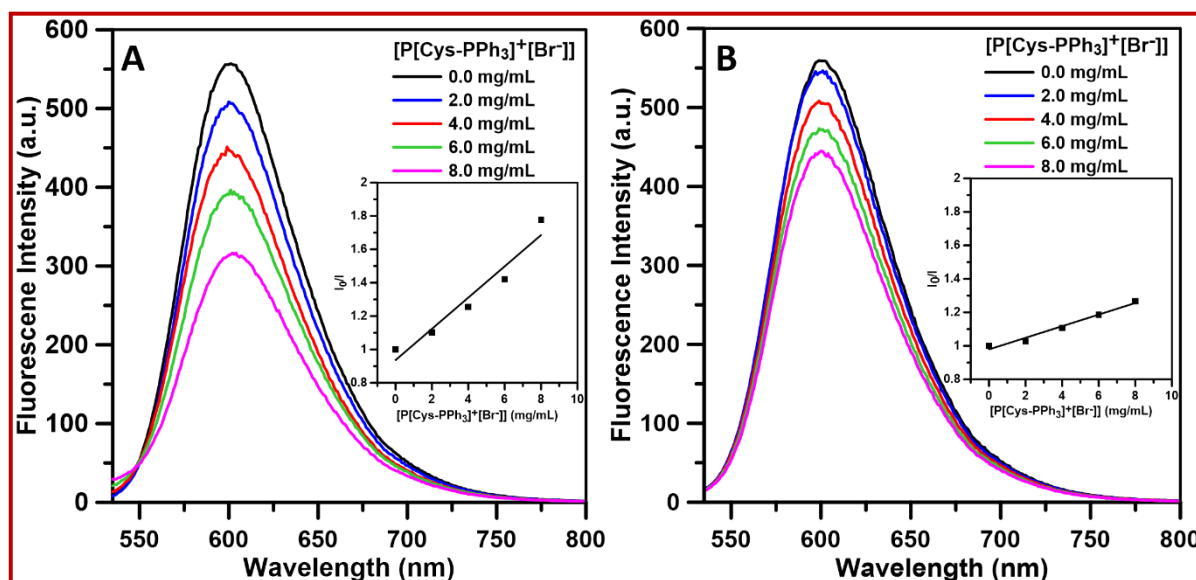


Figure 3.21. Emission spectra of EtBr-ctDNA complex with different amount of $\text{P}[\text{Cys-PPH}_3]^+[\text{Br}^-]$ -1 and 0.1 M NaCl (A) and 0.2 M NaCl (B). The insets of the both figures showed the plot of I_0/I vs respective $[\text{P}[\text{Cys-PPH}_3]^+[\text{Br}^-]$ -1], revealing the decrease in fluorescence quenching of EtBr-ctDNA complex.

Furthermore, as the ionic strength was increased from 0.1 to 0.2 M, the degree of fluorescence quenching was further diminished. The quenching constants of $P[\text{Cys-PPh}_3]^+[\text{Br}^-]-1$ in the presence of 0.1 M and 0.2 M NaCl were determined to be 0.0936 and 0.0346 $\text{mg}^{-1} \text{mL}$, respectively, based on their respective plots (Insets of Figures 3.21A-3.21B). These values are much lower than the quenching constant obtained without the addition of NaCl. The decrease in the quenching constant with increasing ionic strength indicates the electrostatic nature of the interaction between $P[\text{Cys-PPh}_3]^+$ and ctDNA.

Additionally, the formation of ctDNA- $P[\text{Cys-PPh}_3]^+$ polyplexes was assessed using agarose gel electrophoresis to determine their extent. In general, during electrophoresis, negatively charged ctDNA moves towards the anode when it remains unbound. However, any interaction hinders its electrophoretic mobility towards the anode. Hence, it was anticipated that the migration of ctDNA would be impeded in the presence of the polycation $P[\text{Cys-PPh}_3]^+$. Figure 3.22A depicts the representative gel image of the ctDNA- $P[\text{Cys-PPh}_3]^+[\text{Br}^-]-1$ polyplex at various polypeptide concentrations. Lane 1 corresponds to the control, where ctDNA was illuminated without the presence of a polypeptide molecule. Lanes 2-5 correspond to illuminated ctDNA with 2, 4, 6, and 8 mg/mL of $P[\text{Cys-PPh}_3]^+[\text{Br}^-]-1$, respectively. It was evident that in lane 1, ethidium bromide (EtBr)-stained ctDNA migrated freely towards the anode under a potential gradient of 100V. However, no migration occurred for the mixtures in lanes 2-5. The intensity of EtBr-stained ctDNA illumination decreased in lanes 2-5, indicating a higher degree of neutralization of the negatively charged phosphate groups of the ctDNA molecule by the positive phosphonium ion of $P[\text{Cys-PPh}_3]^+[\text{Br}^-]-1$, as its concentration increased. This result also confirmed the stronger electrostatic interactions between ctDNA and $P[\text{Cys-PPh}_3]^+$.

To further investigate the impact of increasing $P[\text{Cys-PPh}_3]^+$ concentration on the secondary structure of ctDNA, CD spectropolarimetry was employed. The CD spectra (Figure 3.22B) of free ctDNA and ctDNA in the

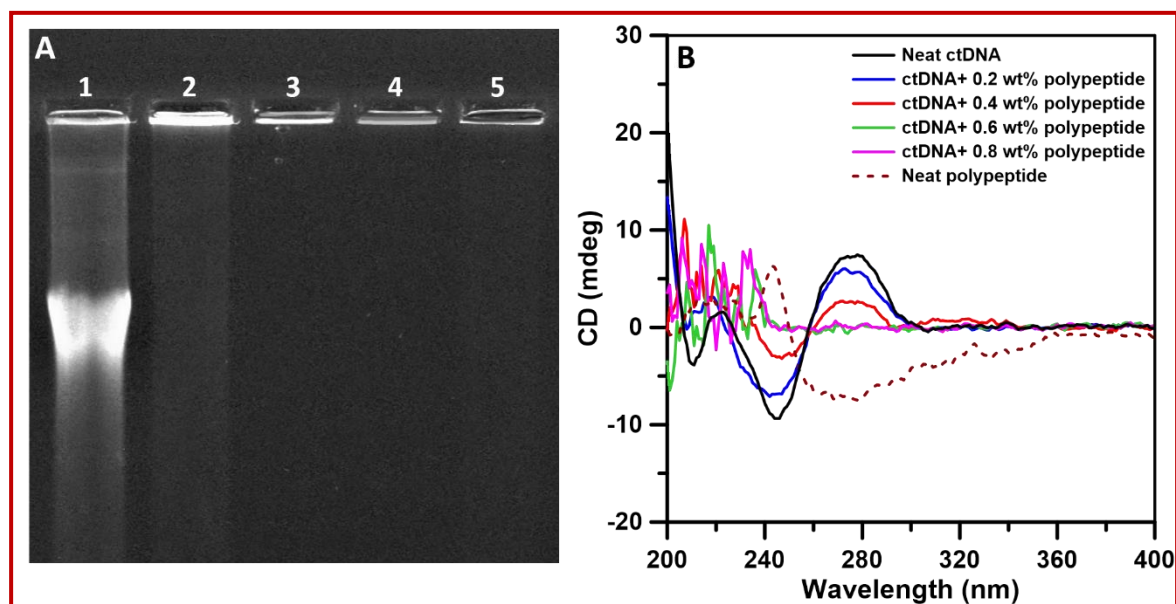


Figure 3.22. (A) Image of the 1% agarose gel used under a potential gradient of 100V showing the electrophoretic mobility of ctDNA in the presence of different amount of $P[Cys-PPh_3]^+[Br^-]$ -1 lane 1 contains free ctDNA while lane 2-5 contain ctDNA with 2, 4, 6 and 8 mg/mL $P[Cys-PPh_3]^+[Br^-]$ -1 respectively. (B) CD spectra of ctDNA in the absence and in the presence of different amount of $P[Cys-PPh_3]^+[Br^-]$ -1 in 10 mM Tris-HCl buffer.

presence of varying concentrations of $P[Cys-PPh_3]^+[Br^-]$ -1 showed characteristic ellipticity changes at 245 nm (negative) and 276 nm (positive), which correspond to the π - π base stacking and helicity of ctDNA, respectively. The CD spectra demonstrated that the ellipticity of ctDNA decreased at both negative (245 nm) and positive (276 nm) bands as the concentration of $P[Cys-PPh_3]^+[Br^-]$ -1 increased from 0-4 mg/mL. Moreover, when the polypeptide concentration was further increased from 6-8 mg/mL, the CD plot did not exhibit the characteristic spectra with ellipticity at 245 and 276 nm. The decrease in CD signal intensity and subsequent loss of characteristic peaks with increasing polypeptide concentration can be attributed to the aggregation of ctDNA induced by the cationic polypeptide.

The optical activity of the cationic polypeptide was probably disrupted after the intercalation with the ctDNA as confirmed from the Figure 3.22B. The ctDNA-polypeptide polyplex exists without displaying the characteristic features of either ctDNA or the polypeptide.

MTT assay (Figure 3.23) showed that the cell viability of the KB cells was greater than 90% at the concentration level of $\text{P}[\text{Cys-PPh}_3]^+[\text{Br}^-]-1 \leq 150 \mu\text{g/mL}$ and even at highest test dose of $\text{P}[\text{Cys-PPh}_3]^+[\text{Br}^-]-1$ (500 $\mu\text{g/mL}$) good cell viability was observed. Thus, it can be said that cationic polypeptide ($\text{P}[\text{Cys-PPh}_3]^+[\text{Br}^-]$) is biocompatible in nature.

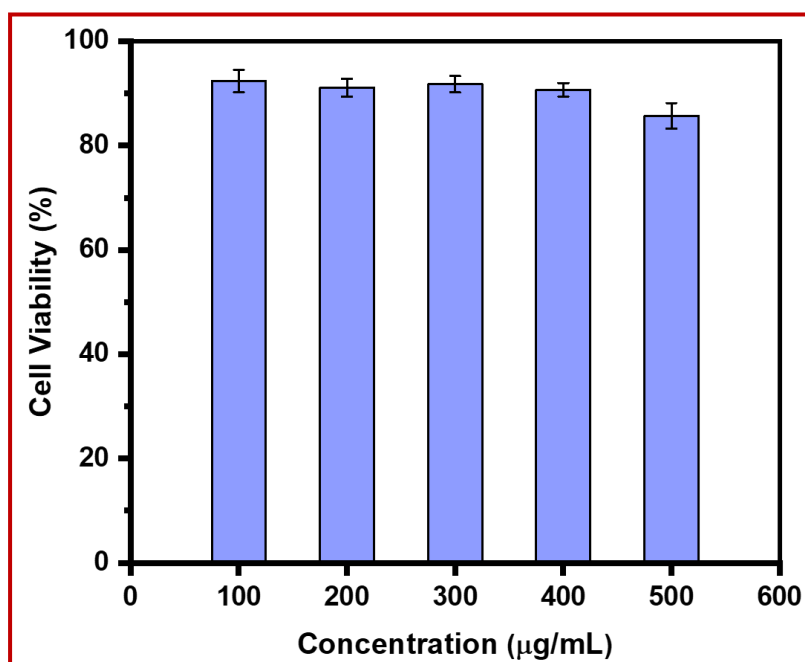


Figure 3.23. The cell viability of KB cells with different concentrations of $\text{P}[\text{Cys-PPh}_3]^+[\text{Br}^-]-1$ after 24 h of incubation.

3.5. Conclusion

In summary, we have successfully synthesized a novel water-soluble polypeptide, $[\text{PCys-PPh}_3]^+[\text{Br}^-]$ with cationic triphenylphosphonium ions attached to the sidechain of the polycysteine. The synthesis process involved the ROP of a specifically designed bromo-functionalized L-cysteine NCA to form bromo-functional polycysteine (PCys-Br) and subsequent nucleophilic substitution of the bromine atom with triphenylphosphine resulting in a cationic polycysteine with pendant triphenylphosphonium groups $[\text{PCys-PPh}_3]^+[\text{Br}^-]$. PCys-Br exhibited insolubility in water, but upon cationization, positive charges were introduced to the side chains, resulting in water solubility of the final $[\text{PCys-PPh}_3]^+[\text{Br}^-]$ polypeptide.

The presence of positive charges enabled electrostatic interactions between the $[\text{PCys-PPh}_3]^+[\text{Br}^-]$ chains and various anions from the Hoffmeister series (BF_4^- , I^- , ClO_4^- , SCN^-) through anion-bridge, leading to the formation of water-insoluble spherical aggregates, resulting in a turbid suspension in water. On increasing the solution temperature, these electrostatic interactions were disrupted, causing the dissolution of the aggregates, and making the cloudy binary solution transparent again. The reverse phenomenon occurred on cooling the binary mixture. This behavior demonstrated the thermoresponsive nature of $[\text{PCys-PPh}_3]^+[\text{Br}^-]$, exhibiting an upper critical solution temperature (UCST) in water. The cloud point, of the anion-induced UCST-type phase transition was significantly influenced by the molecular weight and concentration of $[\text{PCys-PPh}_3]^+[\text{Br}^-]$. Additionally, the cloud point was also dependent on the type and concentration of the added anions.

Moreover, the cationic $[\text{PCys-PPh}_3]^+[\text{Br}^-]$ readily formed polyplexes with ctDNA in Tris-HCl buffer due to the interaction between the positively charged triphenylphosphonium ions of $[\text{PCys-PPh}_3]^+[\text{Br}^-]$ and the negatively charged phosphate ions of ctDNA. The extent of polyplexation was affected by the ionic

strength of the solution, indicating the electrostatic nature of this interaction. Hence, this biocompatible cationic polypeptide holds promise for various biological applications, such as gene delivery.

3.6. Appendix: Characterization and Other Experimental Data

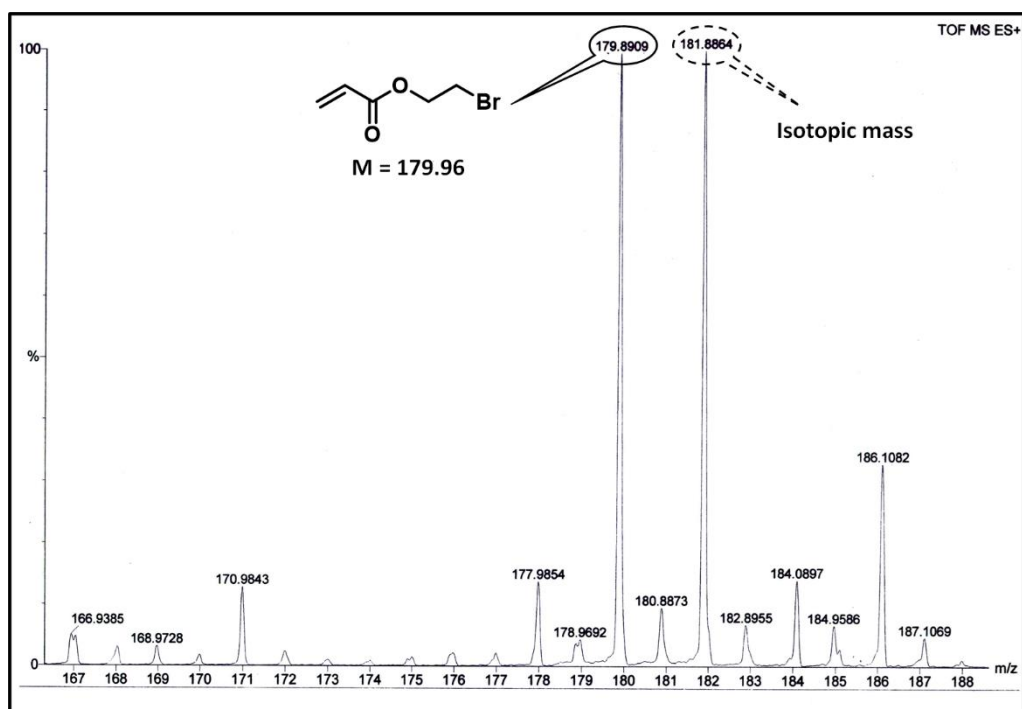


Figure A3.1. ESI-MS spectrum of 2-BrEt-Ac in DCM.

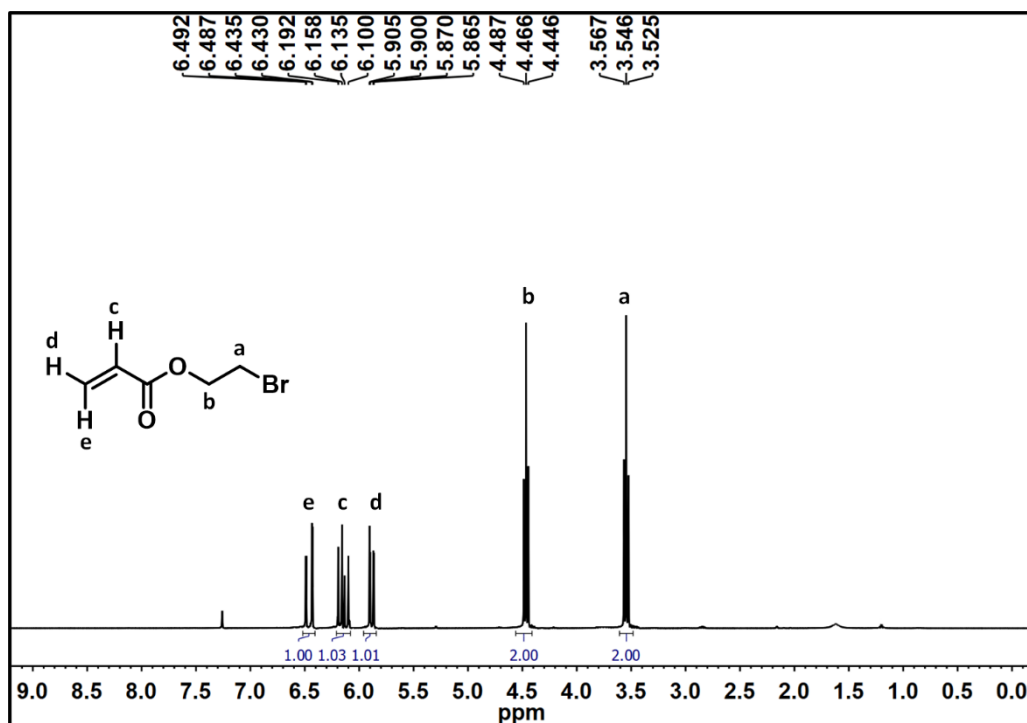


Figure A3.2. ^1H -NMR spectrum of 2-BrEt-Ac in CDCl_3 .

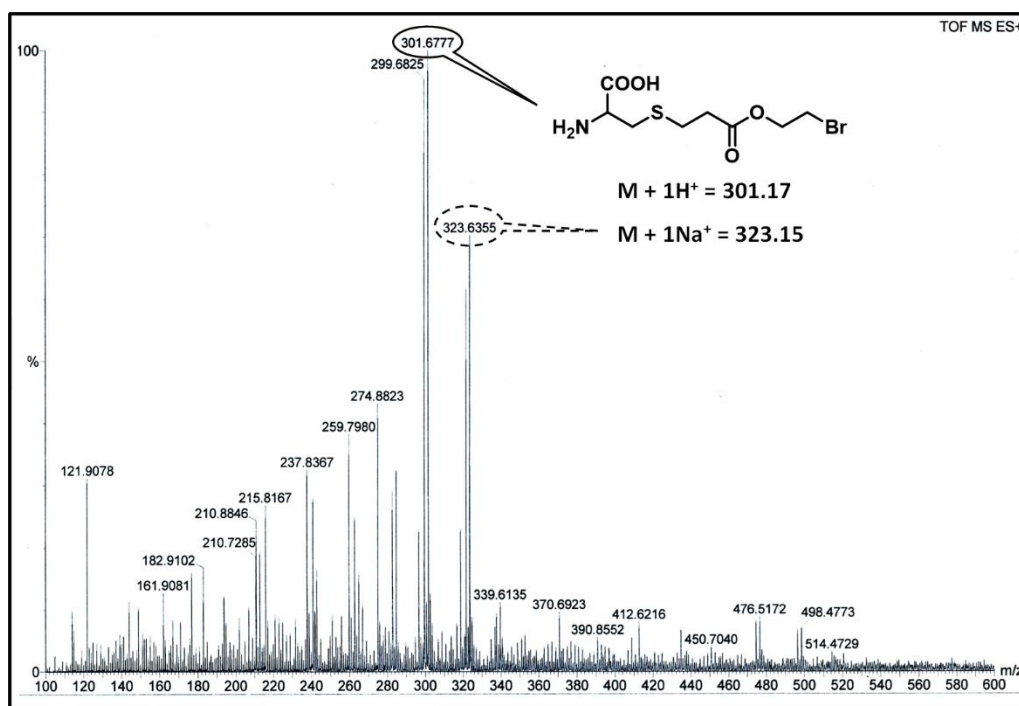


Figure A3.3. ESI-MS spectrum of Cys-Br in H₂O: MeOH (1:1) mixture.

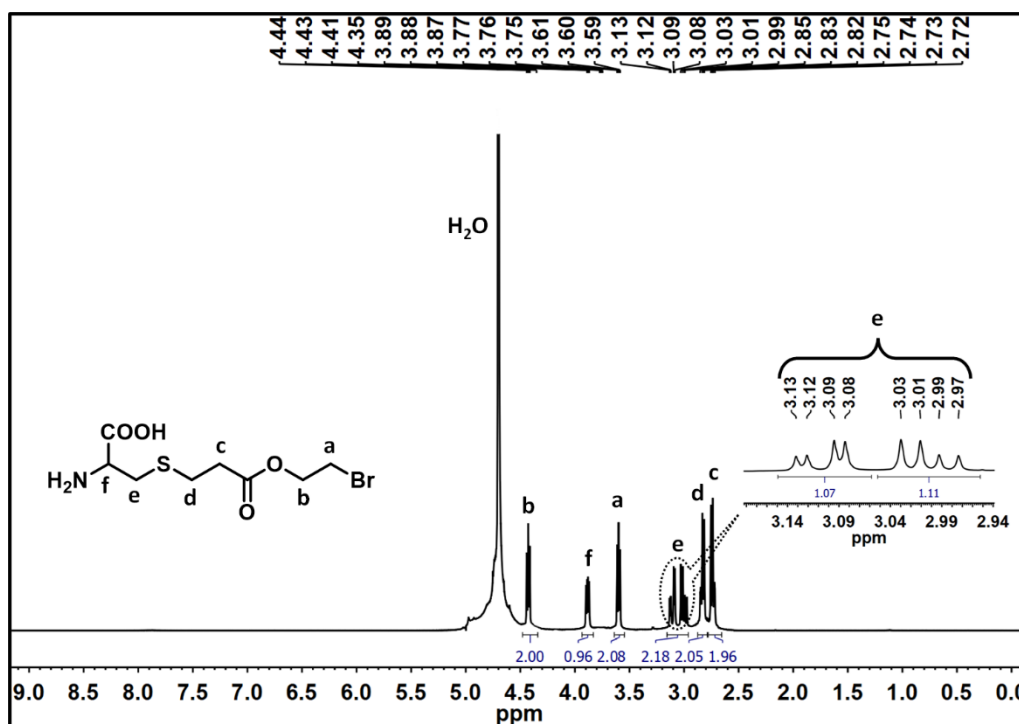


Figure A3.4. ¹H-NMR spectrum of Cys-Br in D₂O.

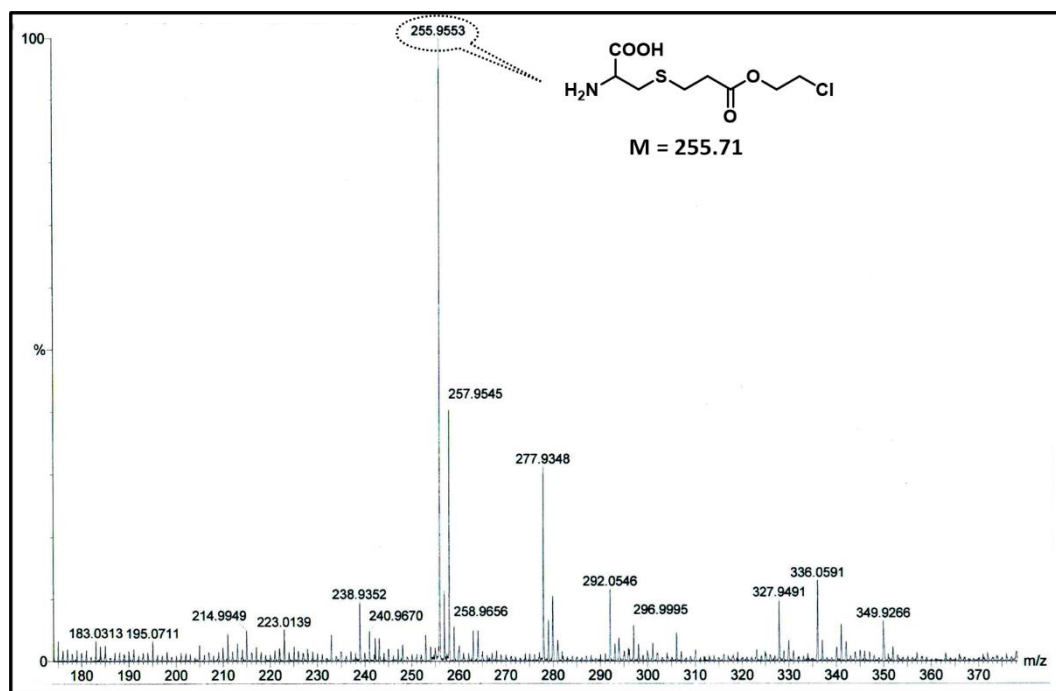


Figure A3.5. ESI-MS spectrum of Cys-Cl in H₂O: MeOH (1:1) mixture.

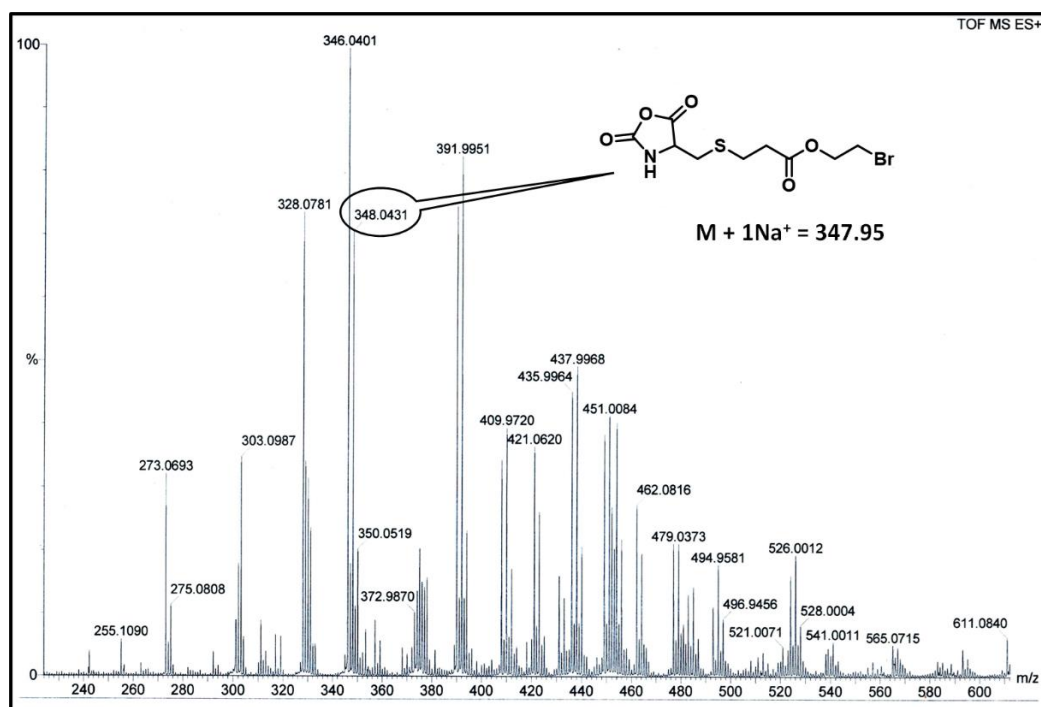


Figure A3.6. ESI-MS spectrum of Cys-Br NCA in DCM.

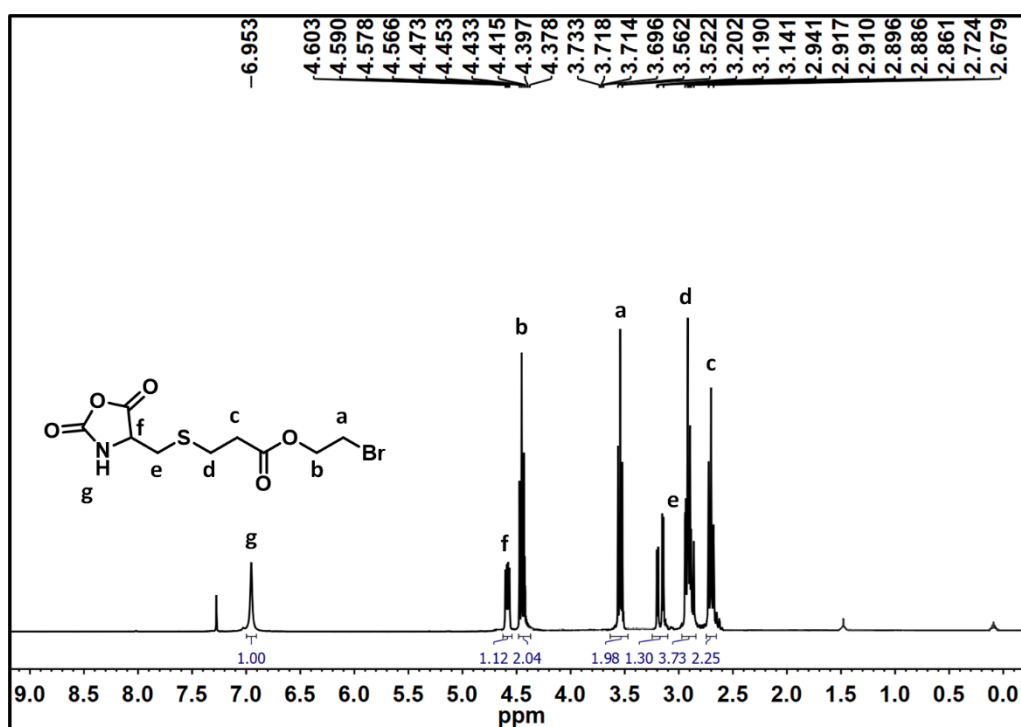


Figure A3.7. ¹H-NMR spectrum of Cys-Br NCA in CDCl₃.

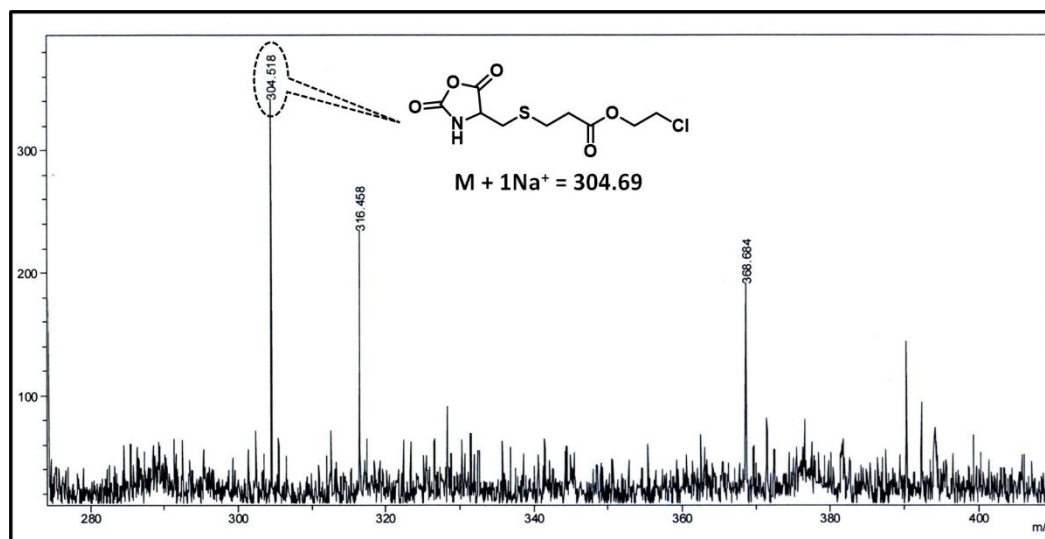


Figure A3.8. MALDI-TOF-MS of Cys-Cl NCA in THF using DCTB matrix and NaI.

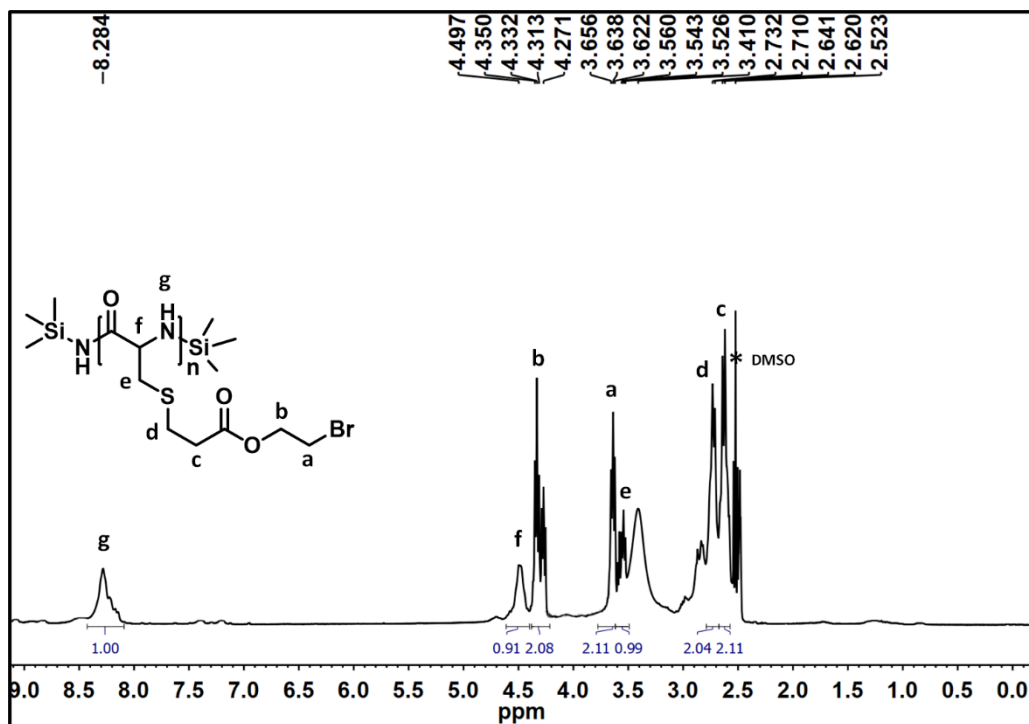


Figure A3.9. $^1\text{H-NMR}$ spectrum of PCys-Br-1 in DMSO-d_6 .

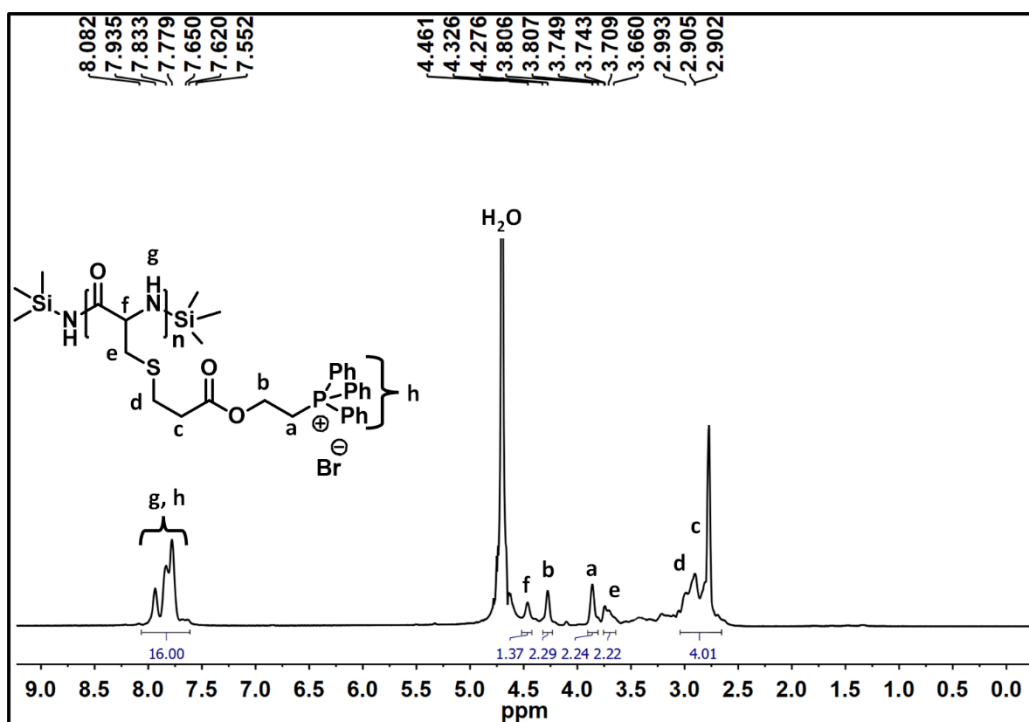


Figure A3.10. $^1\text{H-NMR}$ spectrum of $\text{P}[\text{Cys-PPh}_3]^+[\text{Br}^-]-1$ in D_2O .

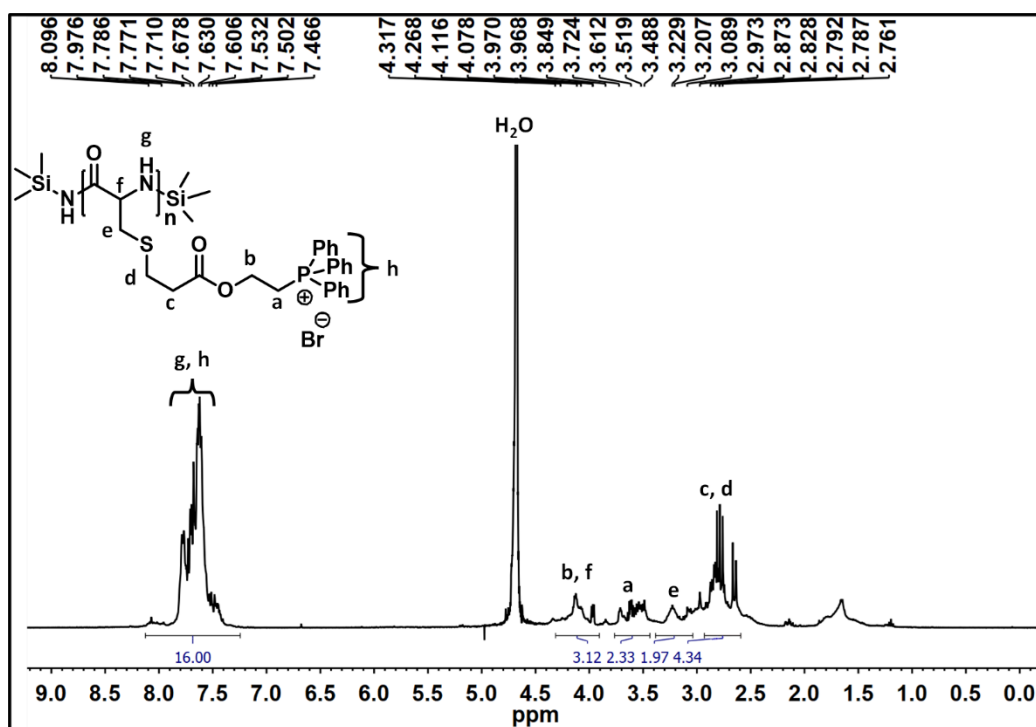


Figure A3.11. ^1H -NMR spectrum of $\text{P}[\text{Cys-PPh}_3]^+[\text{Br}^-]\text{-2}$ in D_2O .

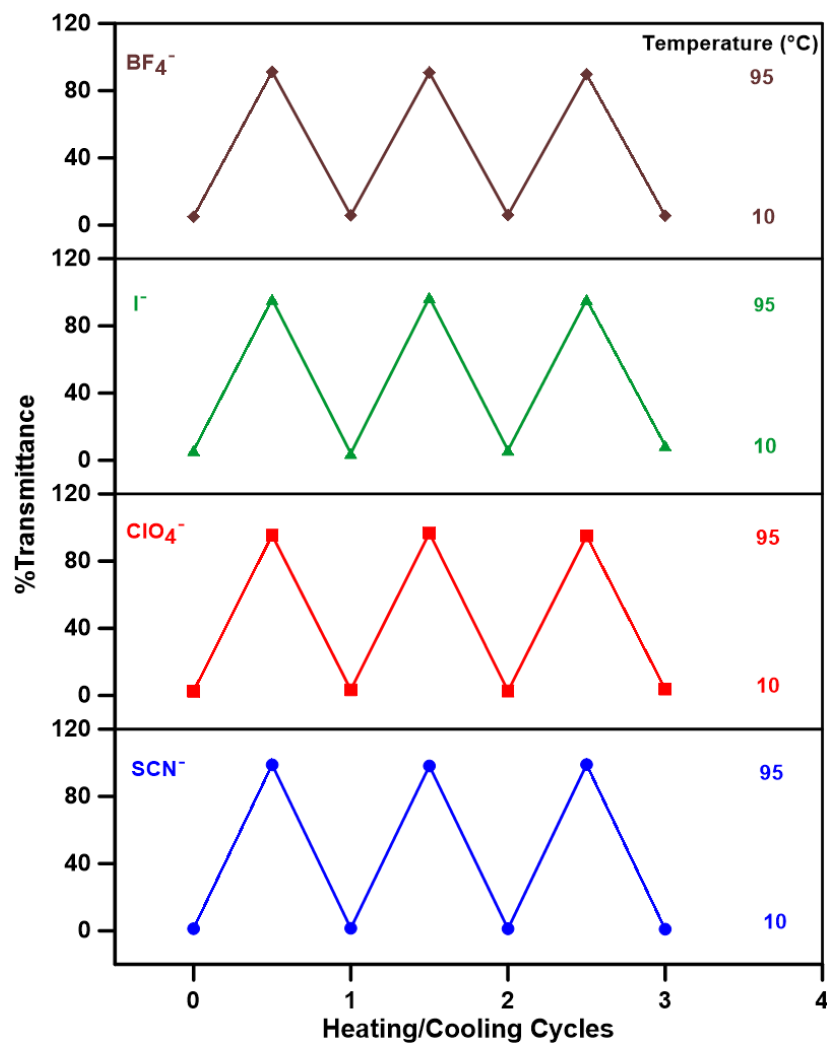


Figure A3.12. Temperature-dependent % transmittance of 0.5 wt% aqueous P[Cys-PPh₃]⁺[Br⁻]-1 solutions in the presence of different chaotropic anions. Each data point was obtained after equilibrating the corresponding sample solution at the particular temperature for 5 min.

3.7. References

1. Deming, T. J., Synthetic Polypeptides for Biomedical Applications. *Prog. Polym. Sci.* **2007**, *32*, 858-875.
2. Fu, X.; Ma, Y.; Shen, Y.; Fu, W.; Li, Z., Oxidation-Responsive Oegylated Poly-L-Cysteine and Solution Properties Studies. *Biomacromolecules* **2014**, *15*, 1055-1061.
3. Rad-Malekshahi, M.; Lempsink, L.; Amidi, M.; Hennink, W. E.; Mastrobattista, E., Biomedical Applications of Self-Assembling Peptides. *Bioconjugate Chem.* **2016**, *27*, 3-18.
4. Deming, T. J., Synthesis of Side-Chain Modified Polypeptides. *Chem. Rev.* **2016**, *116*, 786-808.
5. Anas, M.; Jana, S.; Mandal, T. K., Vesicular Assemblies of Thermoresponsive Amphiphilic Polypeptide Copolymers for Guest Encapsulation and Release. *Polym. Chem.* **2020**, *11*, 2889-2903.
6. Bose, A.; Jana, S.; Saha, A.; Mandal, T. K., Amphiphilic Polypeptide-Polyoxazoline Graft Copolymer Conjugate with Tunable Thermoresponsiveness: Synthesis and Self-Assembly into Various Micellar Structures in Aqueous and Nonaqueous Media. *Polymer* **2017**, *110*, 12-24.
7. Chen, L.; Chen, T.; Fang, W.; Wen, Y.; Lin, S.; Lin, J.; Cai, C., Synthesis and Ph-Responsive "Schizophrenic" Aggregation of a Linear-Dendron-Like Polyampholyte Based on Oppositely Charged Polypeptides. *Biomacromolecules* **2013**, *14*, 4320-4330.
8. Yin, L.; Tang, H.; Kim, K. H.; Zheng, N.; Song, Z.; Gabrielson, N. P.; Lu, H.; Cheng, J., Light-Responsive Helical Polypeptides Capable of Reducing Toxicity and Unpacking DNA: Toward Nonviral Gene Delivery. *Angew. Chem. Int. Ed.* **2013**, *52*, 9182-9186.

9. Jana, S.; Biswas, Y.; Mandal, T. K., Methionine-Based Cationic Polypeptide/Polypeptide Block Copolymer with Triple-Stimuli Responsiveness: DNA Polyplexation and Phototriggered Release. *Polym. Chem.* **2018**, *9*, 1869-1884.
10. Liu, G.; Dong, C.-M., Photoresponsive Poly(S-(O-Nitrobenzyl)-L-Cysteine)-B-Peo from a L-Cysteine N-Carboxyanhydride Monomer: Synthesis, Self-Assembly, and Phototriggered Drug Release. *Biomacromolecules* **2012**, *13*, 1573-1583.
11. Kramer, J. R.; Deming, T. J., Multimodal Switching of Conformation and Solubility in Homocysteine Derived Polypeptides. *J. Am. Chem. Soc.* **2014**, *136*, 5547-5550.
12. Carlini, A. S.; Gaetani, R.; Braden, R. L.; Luo, C.; Christman, K. L.; Gianneschi, N. C., Enzyme-Responsive Progelator Cyclic Peptides for Minimally Invasive Delivery to the Heart Post-Myocardial Infarction. *Nat. Commun.* **2019**, *10*, 1735.
13. Fan, J.; Li, R.; Wang, H.; He, X.; Nguyen, T. P.; Letteri, R. A.; Zou, J.; Wooley, K. L., Multi-Responsive Polypeptide Hydrogels Derived from N-Carboxyanhydride Terpolymerizations for Delivery of Nonsteroidal Anti-Inflammatory Drugs. *Org. Biomol. Chem.* **2017**, *15*, 5145-5154.
14. Ma, G.; Lin, W.; Yuan, Z.; Wu, J.; Qian, H.; Xu, L.; Chen, S., Development of Ionic Strength/Ph/Enzyme Triple-Responsive Zwitterionic Hydrogel of the Mixed L-Glutamic Acid and L-Lysine Polypeptide for Site-Specific Drug Delivery. *J. Mater. Chem. B* **2017**, *5*, 935-943.
15. Lee, D.; Rejinold, N. S.; Jeong, S. D.; Kim, Y.-C., Stimuli-Responsive Polypeptides for Biomedical Applications. *Polymers* **2018**, *10*, 830.
16. Song, Z.; Han, Z.; Lv, S.; Chen, C.; Chen, L.; Yin, L.; Cheng, J., Synthetic Polypeptides: From Polymer Design to Supramolecular Assembly and Biomedical Application. *Chem. Soc. Rev.* **2017**, *46*, 6570-6599.

17. Nath, N.; Chilkoti, A., Creating “Smart” Surfaces Using Stimuli Responsive Polymers. *Adv. Mater.* **2002**, *14*, 1243-1247.
18. Kramer, J. R.; Deming, T. J., Glycopolypeptides with a Redox-Triggered Helix-to-Coil Transition. *J. Am. Chem. Soc.* **2012**, *134*, 4112-4115.
19. Chen, C.; Wang, Z.; Li, Z., Thermoresponsive Polypeptides from Pegylated Poly-L-Glutamates. *Biomacromolecules* **2011**, *12*, 2859-2863.
20. Das, S.; Kar, M.; Gupta, S. S., Synthesis of End-Functionalized Phosphate and Phosphonate-Polypeptides by Ring-Opening Polymerization of Their Corresponding N-Carboxyanhydride. *Polym. Chem.* **2013**, *4*, 4087-4091.
21. Rhodes, A. J.; Deming, T. J., Soluble, Clickable Polypeptides from Azide-Containing N-Carboxyanhydride Monomers. *ACS Macro Lett.* **2013**, *2*, 351-354.
22. Zhou, J.; Chen, P.; Deng, C.; Meng, F.; Cheng, R.; Zhong, Z., A Simple and Versatile Synthetic Strategy to Functional Polypeptides Via Vinyl Sulfone-Substituted L-Cysteine N-Carboxyanhydride. *Macromolecules* **2013**, *46*, 6723-6730.
23. Agut, W.; Brûlet, A.; Schatz, C.; Taton, D.; Lecommandoux, S., Ph and Temperature Responsive Polymeric Micelles and Polymersomes by Self-Assembly of Poly[2-(Dimethylamino)Ethyl Methacrylate]-B-Poly(Glutamic Acid) Double Hydrophilic Block Copolymers. *Langmuir* **2010**, *26*, 10546-10554.
24. Ajiro, H.; Takahashi, Y.; Akashi, M., Thermosensitive Biodegradable Homopolymer of Trimethylene Carbonate Derivative at Body Temperature. *Macromolecules* **2012**, *45*, 2668-2674.
25. Biswas, Y.; Mandal, T. K., Structural Variation in Homopolymers Bearing Zwitterionic and Ionic Liquid Pendants for Achieving Tunable Multi-Stimuli Responsiveness and Hierarchical Nanoaggregates. *Macromolecules* **2017**, *50*, 9807-9820.

26. Banerjee, P.; Jana, S.; Mandal, T. K., Coulomb Interaction-Driven Ucst in Poly(Ionic Liquid) Random Copolymers. *Eur. Polym. J.* **2020**, *133*, 109747.
27. Jana, S.; Anas, M.; Maji, T.; Banerjee, S.; Mandal, T. K., Tryptophan-Based Styryl Homopolymer and Polyzwitterions with Solvent-Induced Ucst, Ion-Induced Lcst and Ph-Induced Ucst. *Polym. Chem.* **2019**, *10*, 526-538.
28. Biswas, Y.; Maji, T.; Dule, M.; Mandal, T. K., Tunable Doubly Responsive Ucst-Type Phosphonium Poly(Ionic Liquid): A Thermosensitive Dispersant for Carbon Nanotubes. *Polym. Chem.* **2016**, *7*, 867-877.
29. Li, M.; He, X.; Ling, Y.; Tang, H., Dual Thermoresponsive Homopolypeptide with Lcst-Type Linkages and Ucst-Type Pendants: Synthesis, Characterization, and Thermoresponsive Properties. *Polymer* **2017**, *132*, 264-272.
30. Men, Y.; Schlaad, H.; Yuan, J., Cationic Poly(Ionic Liquid) with Tunable Lower Critical Solution Temperature-Type Phase Transition. *ACS Macro Lett.* **2013**, *2*, 456-459.
31. Fu, X.; Shen, Y.; Fu, W.; Li, Z., Thermoresponsive Oligo(Ethylene Glycol) Functionalized Poly-L-Cysteine. *Macromolecules* **2013**, *46*, 3753-3760.
32. Kramer, J. R.; Deming, T. J., Preparation of Multifunctional and Multireactive Polypeptides Via Methionine Alkylation. *Biomacromolecules* **2012**, *13*, 1719-1723.
33. Petitdemange, R.; Garanger, E.; Bataille, L.; Bathany, K.; Garbay, B.; Deming, T. J.; Lecommandoux, S., Tuning Thermoresponsive Properties of Cationic Elastin-Like Polypeptides by Varying Counterions and Side-Chains. *Bioconjugate Chem.* **2017**, *28*, 1403-1412.
34. Xue, X.; Thiagarajan, L.; Dixon, J. E.; Saunders, B. R.; Shakesheff, K. M.; Alexander, C., Post-Modified Polypeptides with Ucst-Type Behavior for Control of Cell Attachment in Physiological Conditions. *Materials* **2018**, *11*, 95.

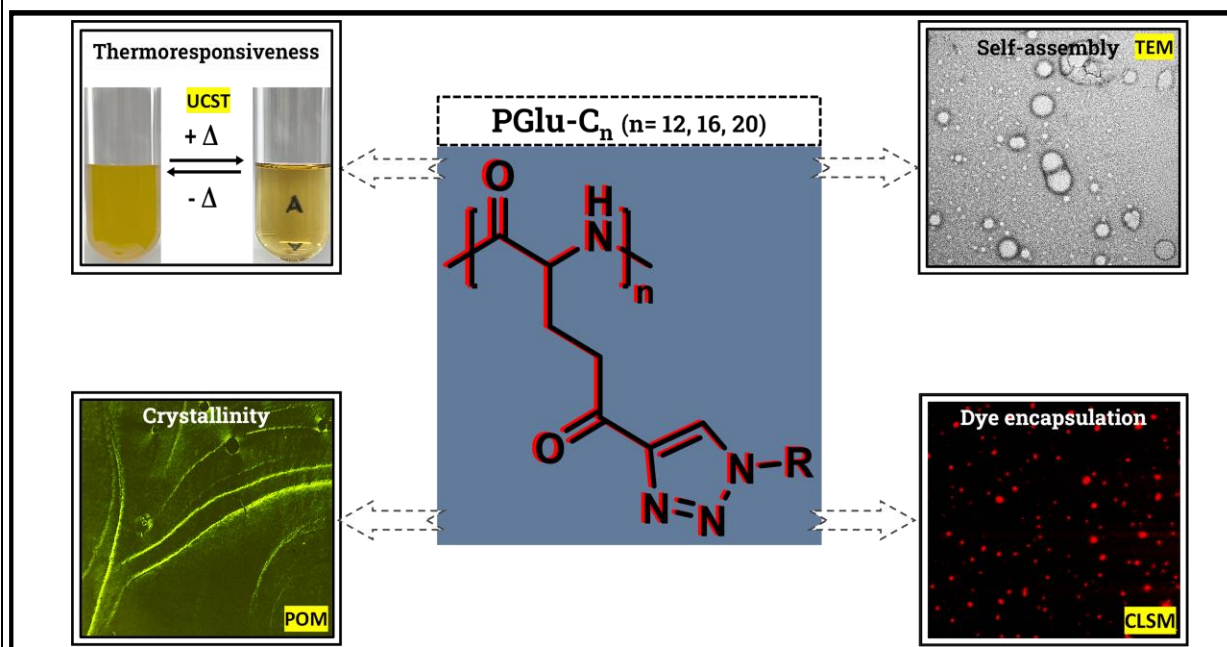
35. Zhao, L.; Wang, X.; Sun, L.; Zhou, R.; Zhang, X.; Zhang, L.; Zheng, Z.; Ling, Y.; Luan, S.; Tang, H., Synthesis and Ucst-Type Thermoresponsive Properties of Polypeptide Based Single-Chain Nanoparticles. *Polym. Chem.* **2019**, *10*, 5206-5214.
36. Zhou, Q.; Palanisamy, A.; Albright, V.; Sukhishvili, S. A., Enzymatically Degradable Star Polypeptides with Tunable Ucst Transitions in Solution and within Layer-by-Layer Films. *Polym. Chem.* **2018**, *9*, 4979-4983.
37. Shimada, N.; Ino, H.; Maie, K.; Nakayama, M.; Kano, A.; Maruyama, A., Ureido-Derivatized Polymers Based on Both Poly(Allylurea) and Poly(L-Citrulline) Exhibit Ucst-Type Phase Transition Behavior under Physiologically Relevant Conditions. *Biomacromolecules* **2011**, *12*, 3418-3422.
38. Kuroyanagi, S.; Shimada, N.; Fujii, S.; Furuta, T.; Harada, A.; Sakurai, K.; Maruyama, A., Highly Ordered Polypeptide with Ucst Phase Separation Behavior. *J. Am. Chem. Soc.* **2019**, *141*, 1261-1268.
39. Ge, C.; Zhao, L.; Ling, Y.; Tang, H., Thermo and Ph Dual Responsive Polypeptides Derived from "Clickable" Poly(Γ -3-Methylthiopropyl-L-Glutamate). *Polym. Chem.* **2017**, *8*, 1895-1905.
40. Deng, Y.; Xu, Y.; Wang, X.; Yuan, Q.; Ling, Y.; Tang, H., Water-Soluble Thermoresponsive α -Helical Polypeptide with an Upper Critical Solution Temperature: Synthesis, Characterization, and Thermoresponsive Phase Transition Behaviors. *Macromol. Rapid. Commun.* **2015**, *36*, 453-458.
41. Hemp, S. T.; Allen, M. H.; Green, M. D.; Long, T. E., Phosphonium-Containing Polyelectrolytes for Nonviral Gene Delivery. *Biomacromolecules* **2012**, *13*, 231-238.
42. Hemp, S. T.; Allen, M. H.; Smith, A. E.; Long, T. E., Synthesis and Properties of Sulfonium Polyelectrolytes for Biological Applications. *ACS Macro Lett.* **2013**, *2*, 731-735.

43. Davies, M. L.; Burrows, H. D.; Cheng, S.; Morán, M. C.; Miguel, M. d. G.; Douglas, P., Cationic Fluorene-Based Conjugated Polyelectrolytes Induce Compaction and Bridging in DNA. *Biomacromolecules* **2009**, *10*, 2987-2997.
44. Han, F.; Lu, Y.; Zhang, Q.; Sun, J.; Zeng, X.; Li, C., Homogeneous and Sensitive DNA Detection Based on Polyelectrolyte Complexes of Cationic Conjugated Poly(Pyridinium Salt)S and DNA. *J. Mater. Chem.* **2012**, *22*, 4106-4112.
45. Gabrielson, N. P.; Lu, H.; Yin, L.; Li, D.; Wang, F.; Cheng, J., Reactive and Bioactive Cationic α -Helical Polypeptide Template for Nonviral Gene Delivery. *Angew. Chem. Int. Ed.* **2012**, *51*, 1143-1147.
46. Takemoto, H.; Ishii, A.; Miyata, K.; Nakanishi, M.; Oba, M.; Ishii, T.; Yamasaki, Y.; Nishiyama, N.; Kataoka, K., Polyion Complex Stability and Gene Silencing Efficiency with a Sirna-Grafted Polymer Delivery System. *Biomaterials* **2010**, *31*, 8097-8105.
47. Maji, T.; Banerjee, S.; Biswas, Y.; Mandal, T. K., Dual-Stimuli-Responsive L-Serine-Based Zwitterionic Ucst-Type Polymer with Tunable Thermosensitivity. *Macromolecules* **2015**, *48*, 4957-4966.
48. Ge, C.; Liu, S.; Liang, C.; Ling, Y.; Tang, H., Synthesis and Ucst-Type Phase Behavior of α -Helical Polypeptides with Y-Shaped and Imidazolium Pendants. *Polym. Chem.* **2016**, *7*, 5978-5987.
49. Ulkoski, D.; Scholz, C., Synthesis and Application of Auophilic Poly(Cysteine) and Poly(Cysteine)-Containing Copolymers. *Polymers* **2017**, *9*, 500.
50. Barlow, T. R.; Brendel, J. C.; Perrier, S., Poly(Bromoethyl Acrylate): A Reactive Precursor for the Synthesis of Functional Raft Materials. *Macromolecules* **2016**, *49*, 6203-6212.
51. Li, G.-Z.; Randev, R. K.; Soeriyadi, A. H.; Rees, G.; Boyer, C.; Tong, Z.; Davis, T. P.; Becer, C. R.; Haddleton, D. M., Investigation into Thiol-

- (Meth)Acrylate Michael Addition Reactions Using Amine and Phosphine Catalysts. *Polym. Chem.* **2010**, *1*, 1196-1204.
52. Manojkumar, K.; Prabhu Charan, K. T.; Sivaramakrishna, A.; Jha, P. C.; Khedkar, V. M.; Siva, R.; Jayaraman, G.; Vijayakrishna, K., Biophysical Characterization and Molecular Docking Studies of Imidazolium Based Polyelectrolytes–DNA Complexes: Role of Hydrophobicity. *Biomacromolecules* **2015**, *16*, 894-903.
53. Paira, T. K.; Saha, A.; Banerjee, S.; Das, T.; Das, P.; Jana, N. R.; Mandal, T. K., Fluorescent Amphiphilic Peg-Peptide-Peg Triblock Conjugate Micelles for Cell Imaging. *Macromol. Biosci.* **2014**, *14*, 929-935.
54. Ivnitski, D.; Amit, M.; Rubinov, B.; Cohen-Luria, R.; Ashkenasy, N.; Ashkenasy, G., Introducing Charge Transfer Functionality into Prebiotically Relevant B-Sheet Peptide Fibrils. *Chem. Commun.* **2014**, *50*, 6733-6736.
55. Karjalainen, E.; Suvarli, N.; Tenhu, H., Thermoresponsive Behavior of Poly[Trialkyl-(4-Vinylbenzyl)Ammonium] Based Polyelectrolytes in Aqueous Salt Solutions. *Polym. Chem.* **2020**, *11*, 5870-5883.

Chapter 4: Crystalline Polypeptide

Alkyl Functionalized Thermoresponsive Semicrystalline Poly(L-Glutamate)s and Their Self-Assembly



4.1. Introduction

There has been significant interest in the functionalization of synthetic polypeptides through the incorporation of specifically designed moieties in the last couple of years. This approach aims to introduce enhanced functionality and adjustable physico-chemical properties such as amphiphilicity and stimuli-responsiveness in the polypeptide-based materials. By mimicking natural proteins, these functional polypeptides can adopt various secondary structures, such as α -helix, β -sheet, and random coil etc.¹⁻² Consequently, numerous research groups have dedicated considerable efforts to the design and synthesis of these functionalized polypeptides for several decades. This is primarily due to their favorable solubility in a wide range of solvents, their ability to respond to stimuli and self-assemble, and, most importantly, their excellent biocompatibility and biodegradability.³⁻⁶ These inherent properties make functionalized polypeptides promising candidates for diverse biomedical applications, such as drug/gene delivery and tissue engineering.⁷⁻¹⁰

Among the various types of stimuli-responsive polypeptides, thermoresponsive systems have garnered significant attention due to their intriguing solution properties.^{7-8,11-13} In particular, the solubility of thermoresponsive polymeric materials, especially in water, can be easily manipulated by altering their architecture and the surrounding solution conditions.¹⁴⁻¹⁷ This manipulation also results in a phase transition from a transparent, single-phase solution to a hazy, biphasic suspension or vice versa, upon heating or cooling above or below a specific temperature (cloud point, T_{cp}), known as the lower critical solution temperature (LCST)⁸ or upper critical solution temperature (UCST)¹⁸ respectively.⁷⁻⁸ The formation of physically crosslinked aggregates, facilitated by interactions such as hydrophobicity and hydrogen bonding, is responsible for the observed hazy suspension or gelation above or below the critical temperature.¹⁹⁻²⁰ Extensive research has been

conducted on the synthesis of polymers and polypeptides, as well as the investigation of their thermoresponsive properties in aqueous solutions.^{7-8,17-18} However, the thermoresponsive behavior of polymers in nonaqueous solvents has been explored only for a limited number of systems.²¹⁻²³

Poly(L-glutamate)s (PGLus) have been extensively investigated due to their favourable characteristics for functionalization in their side chains. Consequently, several research groups have successfully developed functionalized PGLus through either pre- or post-polymerization modifications.^{10-11,19,24-25} These modifications have been utilized to incorporate diverse functional groups in the PGLu side chain, leading to the development of "smart materials" or biomaterials with versatile applications. Notably, post-polymerization modification using "click chemistry" has been widely employed due to its ability to incorporate a wide range of functional groups into the polypeptide backbone with high specificity.^{8,26-28} This approach offers flexibility and control in functionalization. For instance, Hammond et al. employed a combination of ROP of γ -propargyl-L-glutamate NCA and Cu-AAC reaction to synthesize functionally diverse PGLus.²⁷⁻²⁹ Similarly, Li research group achieved the synthesis of oligo(ethylene glycol) side chain-functionalized stimuli-responsive PGLus by ROP of the same NCA, followed by thiol-yne "click" photochemistry.³⁰ Other studies have also reported the synthesis of functionalized PGLus with varying physicochemical properties by combining ROP of functionalized amino acid NCA with "click" or other reactions.³¹⁻³³

Many polymeric and liquid crystalline materials have been extensively investigated to explore their crystalline nature and their applications due to their high thermal stability and excellent mechanical properties.^{21,34-35} Nonionic semicrystalline polymers like aromatic or aliphatic polyesters and polycaprolactones exhibit main-chain crystallinity owing to their inherent polarity.³⁶⁻³⁹ On the other hand, polyolefins, and polystyrene display

crystallinity due to the stereoregularity among the functional groups.³⁶⁻³⁹ Furthermore, the inclusion of long alkyl chains in the macromolecular architecture gives rise to side-chain crystallinity.^{21,40} In this regard, various efforts have been made to incorporate long alkyl side chains into the polymer backbone to achieve polymeric systems with desirable properties such as crystallinity, tunable melting temperature, and self-aggregation.⁴¹⁻⁴³ The covalent attachment of flexible long alkyl chains to the polymer backbone restricts the mobility of the side chains, thereby promoting their ordered arrangement in the bulk, resulting in crystalline behaviour. Recently, our research group have reported the synthesis of a series of long chain alkylvinylimidazolium ionic liquid monomers (ILMs) accompanied by bromide (Br^-) and bis(trifluoromethylsulfonyl)imide (NTf_2^-) counter anions and their corresponding poly(ionic liquid)s (PILs).²¹ The purpose of this study was to conduct a detailed investigation into the thermal behaviour and crystallinity of these materials, specifically focusing on the influence of chain length of the pendant alkyl groups. For both ILMs and PILs, they have observed a significant enhancement in both the melting points and enthalpy of fusions as the length of the associated alkyl chains increased. Interestingly, they found that the side-chain crystallinity of the PILs, which arose due to the ordered arrangement of the attached alkyl groups, was considerably lower when compared to their corresponding ILMs. As observed, all the ILMs exhibited a liquid crystalline phase alongside their crystalline solid phase. In contrast, the PILs exclusively displayed a solid crystal phase without any liquid crystalline properties. This correlation emphasized the direct influence of the chain length of the alkyl groups on the thermal properties of a polymeric materials. These finding paved the way for further exploration and utilization of polymeric materials having different backbone and with pendant long alkyl chains. Several research groups have reported the crystallinity of side-chain alkylated polymers with effectively rigid backbones, such as polyamides/polypeptides.⁴⁴⁻⁴⁶ Poly(γ -benzyl

L-glutamate)s, in particular, are known for their liquid-crystalline phase behaviour under specific conditions. Consequently, researchers have directed their attention towards synthesizing differently functionalized poly(L-glutamate) and studying their liquid crystalline properties.⁴⁷⁻⁵⁰

Polypeptides containing specifically designed functional groups exhibit self-assembly behaviour, leading to the formation of diverse nanostructures in different solvents.⁵¹⁻⁵³ These nanostructures hold significant importance for biomedical applications, particularly in the field of therapeutics, owing to their inherent biocompatibility.⁵⁴⁻⁵⁶ The presence of functional groups, such as carboxyl, hydroxyl, amino, and thiol, in the side chains of α -amino acid units enables the attachment of responsive moieties/polymers through suitable chemical reactions. These chemical modifications allow for the fine-tuning of polypeptide properties, including solubility, hydrophilic-hydrophobic balance, and self-assembly etc.⁵⁷⁻⁵⁸ Thermoresponsive polypeptide vesicles offer advantages over those composed of conventional polymers, making them attractive for bioinspired materials in therapeutics. For instance, Hammond's group has successfully post-functionalized poly(γ -propargyl L-glutamate) with various azide end-functional moieties using click chemistry, resulting in the formation of block copolypeptides that undergo micellar aggregation in aqueous media.²⁸ They further demonstrated the introduction of responsiveness in the micellar core through various functionalization of these block copolypeptides.^{27,53} The micellization of these responsive copolypeptides has predominantly been carried out in aqueous media or mixed solvents. However, the generation of such assemblies in a single organic solvent is rarely reported.⁸ Therefore, investigating the self-assembly behaviour of hydrophobic polypeptides in organic media would be an interesting area of study.

4.2. Objective and Scope

In comparison to conventional polymers, the number of reported functionalized polypeptides exhibiting thermoresponsiveness in water is relatively small.^{7-8,11,26} Moreover, the occurrence of thermoresponsive behavior in functionalized polypeptides in nonaqueous solvents is exceedingly rare.⁵⁹⁻⁶⁰ The solid-state crystalline behaviour of side-chain functionalized polyglutamates has not been thoroughly investigated in comparison to their corresponding monomeric segments. Therefore, it would be intriguing to explore the crystalline phase behaviour of poly(γ -alkyl L-glutamate) in comparison to the constituent monomeric units containing same long alkyl chains.

Furthermore, the precise functionalization of synthetic polypeptides plays a crucial role in introducing stimuli-responsiveness and amphiphilicity, enabling the formation of self-assembled nanostructures such as micelles and vesicles. These nanostructures have significant potential in various applications including drug/gene delivery and tissue engineering. This chapter focuses on the functionalization of poly(L-glutamate)s with long-chain alkyl groups and investigates their semi-crystalline and solution-phase behavior, including thermoresponsiveness and self-aggregation to nanostructures.

Propargyl functionalized poly(L-glutamate) (PGlu-Pr) is synthesized through the ROP of γ -propargyl-L-glutamate NCA, resulting in a PGlu with pendant propargyl groups. Subsequently, the propargyl-functionalized PGlu-Pr is subjected to a Cu-catalyzed alkyne-azide-cycloaddition (Cu-AAC) reaction with long-chain alkyl azides, yielding alkyl-grafted poly(L-glutamate)s [PGlu-C_n(s), n = 10, 12, 16, 20]. Both in the solution phase and solid state, PGlu-Pr and PGlu-C_n(s) exhibit a predominant helical secondary conformation, with the extent of helicity decreasing as the length of the alkyl chains increases. The corresponding monomeric analogs, alkyl-grafted L-glutamates (Glu-C_n)s, form birefringent crystals due to the presence of the long alkyl chains, as confirmed

by DSC and POM studies. In contrast, PGlu-C_n(s) with $n \geq 12$ display minimal crystallinity in the solid state. Interestingly, solutions of PGlu-C_n(s) in CHCl₃ and THF exhibit an UCST-type thermoresponsive behavior, with a tunable cloud point. In contrast, Glu-C_n(s) does not display such thermoresponsive properties. Self-assembly of PGlu-C_n(s) in these solvents leads to the formation of vesicular nanoaggregates, as confirmed by DLS and TEM. Furthermore, these nanoaggregates can encapsulate an organic dye (Eosin B), as demonstrated by fluorescence and confocal microscopy analysis.

Overall, all the findings demonstrate the synthesis and characterization of thermoresponsive functionalized poly(L-glutamate)s with side-chain alkyl groups, which exhibit semi-crystallinity and self-assembly into vesicular nanoaggregates capable of dye encapsulation.

4.3. Experimental

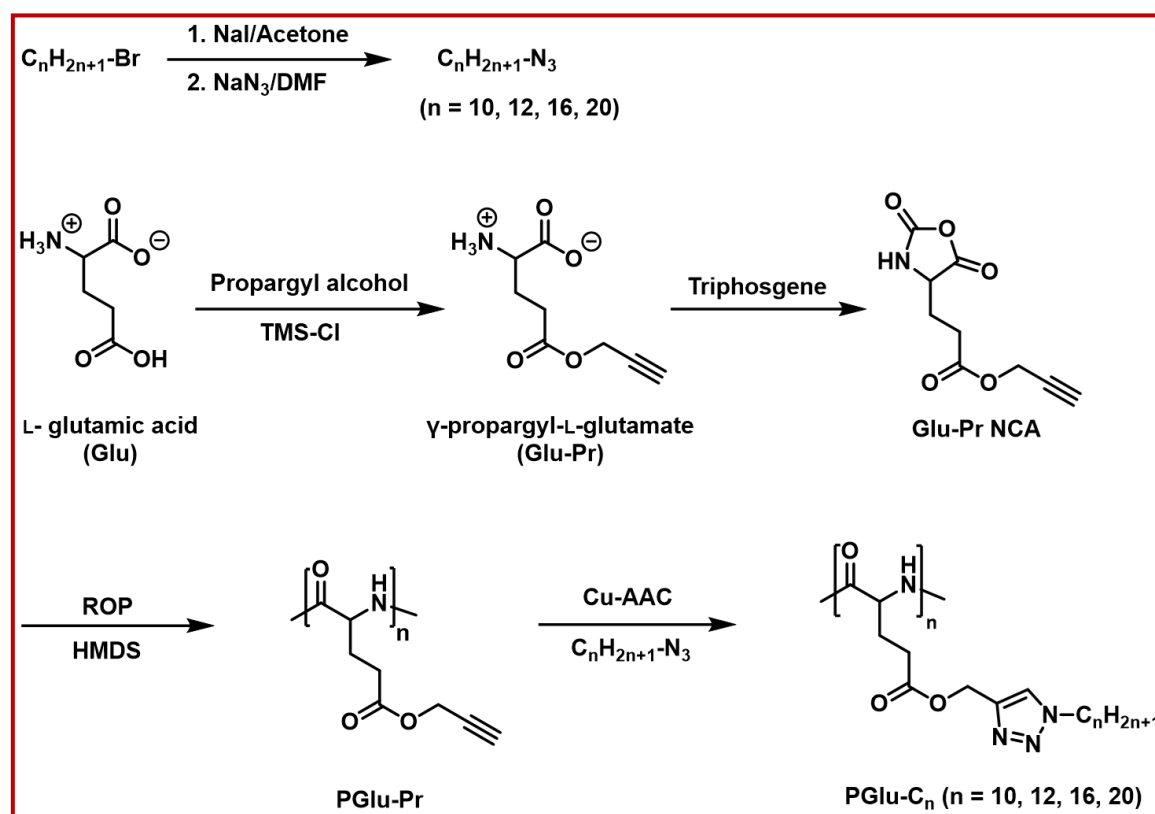
4.3.1. Materials

1-Bromodecane (C₁₀-Br; 98%), 1-bromododecane (C₁₂-Br; >98%), 1-bromohexadecane (C₁₆-Br; >96%), 1-bromoeicosane (C₂₀-Br; >95%) and triphosgene (>98%) were used as received from TCI Chemicals. L-glutamic acid, trimethylchlorosilane (TMSCl; >98%), sodium iodide (>98%) and acetone (99%) were purchased from Spectrochem. Propargyl alcohol and (+)- α -pinene (98%) were purchased from Aldrich. Propargyl alcohol and sodium azide were purified by distillation and recrystallization from hot water respectively prior use. 1,1,1,3,3,3-Hexamethyl disilazane (HMDS; >98%) was obtained from Alfa Aesar. N, N-dimethylformamide (DMF), ethyl acetate (EtOAc), hexane, tetrahydrofuran (THF), chloroform (CHCl₃), sodium ascorbate and copper sulphate (pentahydrate) were obtained from Merck. DMF and EtOAc and were distilled over calcium hydride under reduced and normal pressure respectively and kept over a molecular sieve (Linde, 4 Å) before use. THF was distilled over metallic sodium prior use. CHCl₃ and hexane were also used after distillation.

4.3.2. Synthetic Procedure

4.3.2.1. Azidation of Alkyl Bromide (C_n -Br) ($n = 10, 12, 16, 20$)

Long-chain alkyl azides (C_{10} -N₃, C_{12} -N₃, C_{16} -N₃, C_{20} -N₃) were synthesized by azidation of the corresponding alkyl bromides. In a typical procedure, $C_{20}H_{41}Br$ (C_{20} -Br) (2.0 g, 5.52 mmol), sodium iodide (1.65 g, 11.04 mmol), and 50 mL of dry acetone were combined in a 100 mL round-bottom flask. The mixture was refluxed at 60°C for 24 hours under an argon atmosphere (Scheme 4.1).



Scheme 4.1. Synthesis of alkyl-grafted poly(L-glutamate)s (PGlu-C_n(s))

After refluxing, the mixture was filtered using a G-4 sintered funnel to remove residual NaBr. The filtrate was then evaporated to dryness using a rotary evaporator. Next, NaN_3 (2.0 g, 31.14 mmol) and 20 mL of dry DMF were added to the evaporated residue. The resulting mixture was transferred to a pre-heated oil bath at 90°C and stirred for 48 hours under an argon atmosphere. The reaction solution was filtered to remove any precipitate. The brown-colored

filtrate was mixed with small ice cubes in a separating funnel to create a suspension. Finally, the product from this aqueous-DMF suspension was extracted using an appropriate volume of diethyl ether. The whole process was repeated 4 times to ensure complete extraction of the product. The ether layer so obtained was accumulated and washed with fresh milli-Q water followed by brine solution and finally collected over anhydrous sodium sulphate. The reaction solution was filtered and evaporated in a rotary evaporator followed by vacuum drying to give a white waxy solid product, C₂₀-N₃ with a yield of 77 %. A similar protocol was used to synthesize C₁₆-N₃ (yield 72%), C₁₂-N₃ (yield 81%) and C₁₀-N₃ (yield 80%).

Characterization data: FT-IR (C₂₀-N₃)- Figure 4.1, ESI-MS (C₂₀-N₃, C₁₆-N₃, C₁₂-N₃ and C₁₀-N₃)- Figures A4.1, A4.2, A4.3, and A4.4 respectively.

¹H-NMR, 400 MHz, CDCl₃, TMS, δ (ppm) (Figure 4.2): C₂₀-N₃ - 0.88 (t, 3H), 1.25 (s, 34H), 1.58 (m, 2H), 3.25 (t, 2H); C₁₆-N₃ - 0.87 (t, 3H), 1.26 (s, 25H), 1.61 (m, 2H), 3.25 (t, 2H); C₁₂-N₃ - 0.92 (t, 3H), 1.33 (s, 18H), 1.70 (m, 2H), 3.16 (t, 2H); C₁₀-N₃ - 0.87 (t, 3H), 1.28 (s, 18H), 1.59 (m, 2H), 3.25 (t, 2H).

¹³C-NMR, 75 MHz, CDCl₃, δ (ppm) (Figure 4.3): C₂₀-N₃ - 14.24 (1C), 22.82 (1C), 26.85 (1C), 28.98 – 29.75 (15C), 32.04 (1C), 51.64 (1C); C₁₆-N₃ - 14.23 (1C), 22.82 (1C), 26.86 (1C), 28.98 – 29.75 (11C), 32.06 (1C), 51.64 (1C); C₁₂-N₃ - 14.24 (1C), 22.82 (1C), 26.86 (1C), 28.98 – 29.75 (7C), 32.05 (1C), 51.64 (1C); C₁₀-N₃ - 15.64, 24.23, 28.28, 30.40, 30.71, 30.84, 31.04, 31.06, 33.43, 53.06.

4.3.2.2. Synthesis of γ -Propargyl-L-Glutamate (Glu-Pr)

The synthesis of Glu-Pr, as depicted in Scheme 4.1, was conducted following a previously reported procedure.²⁷ In a 250 mL double-neck round-bottom flask, L-glutamic acid (5 g, 34 mmol) was suspended in propargyl alcohol (150 mL) under an argon atmosphere. Trimethylsilyl chloride (TMSCl) (8.6 mL, 68 mmol) was added dropwise to the mixture at 10°C. Upon stirring at room temperature, the initially heterogeneous solution became homogeneous. The volume of the

solution was reduced to some extent, and the resulting mixture was precipitated by the addition of cold diethyl ether. The white solid product was filtered, washed with diethyl ether, and dried under vacuum at 65°C overnight, yielding a product with 80% yield.

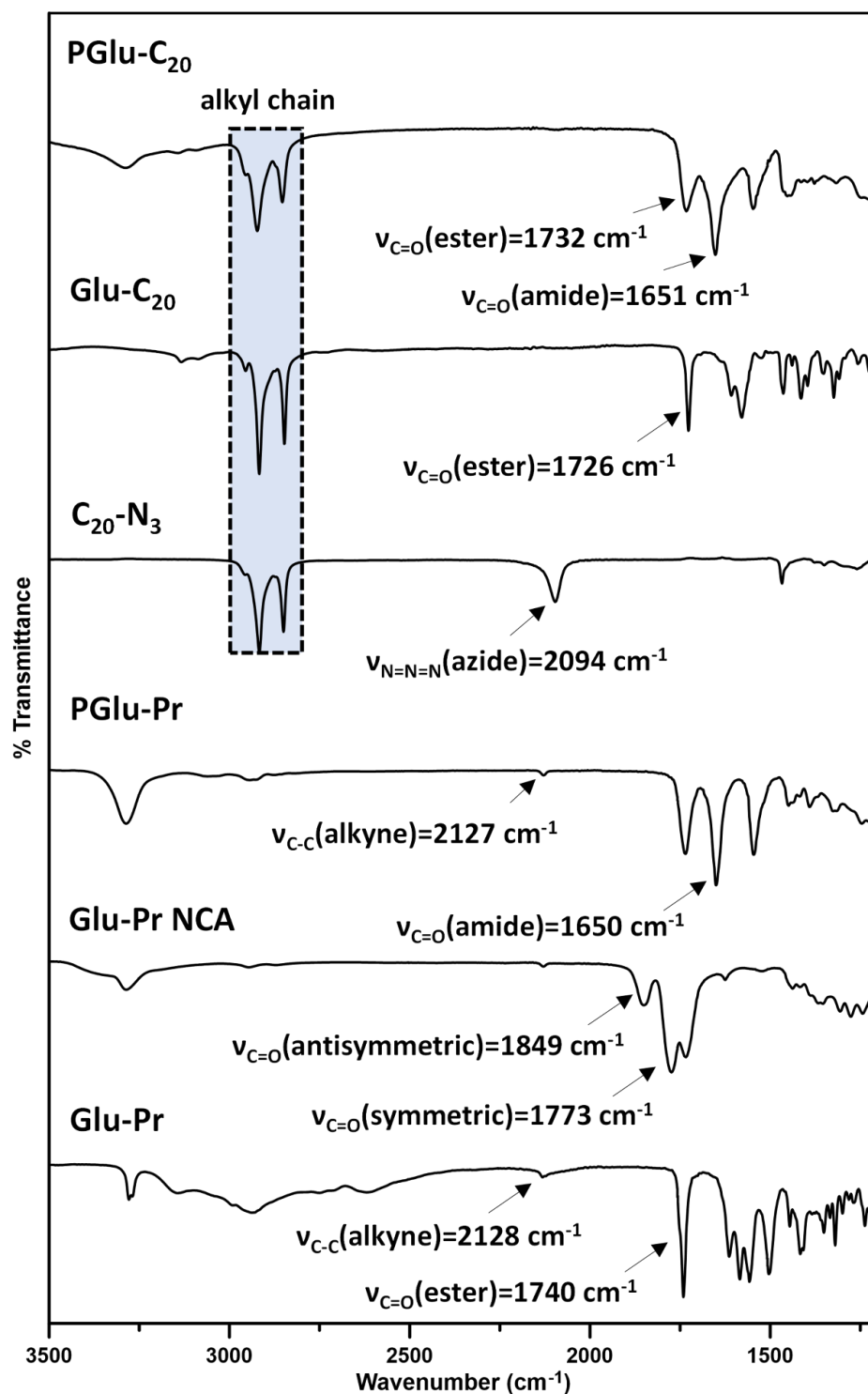


Figure 4.1. FT-IR spectra of all the synthesized compounds.

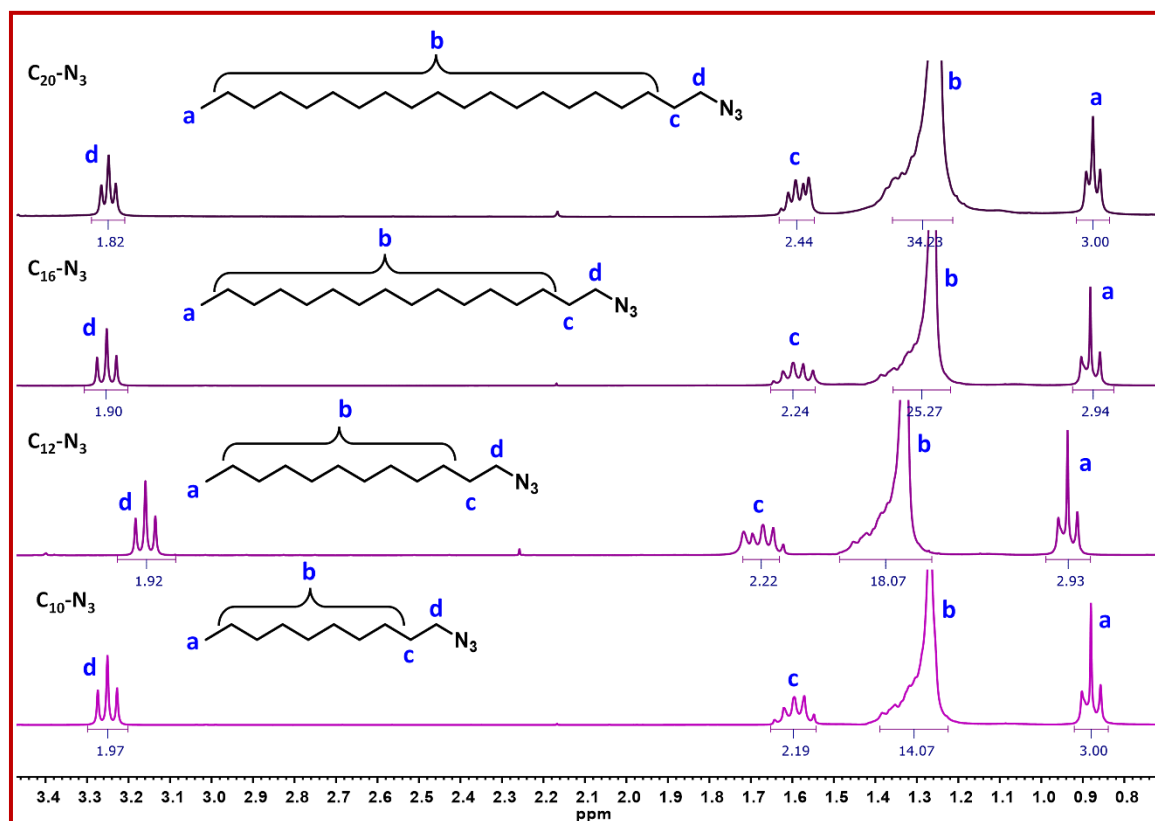


Figure 4.2. $^1\text{H-NMR}$ spectra of $\text{C}_{10}\text{-N}_3$, $\text{C}_{12}\text{-N}_3$, $\text{C}_{16}\text{-N}_3$ and $\text{C}_{20}\text{-N}_3$ in CDCl_3 .

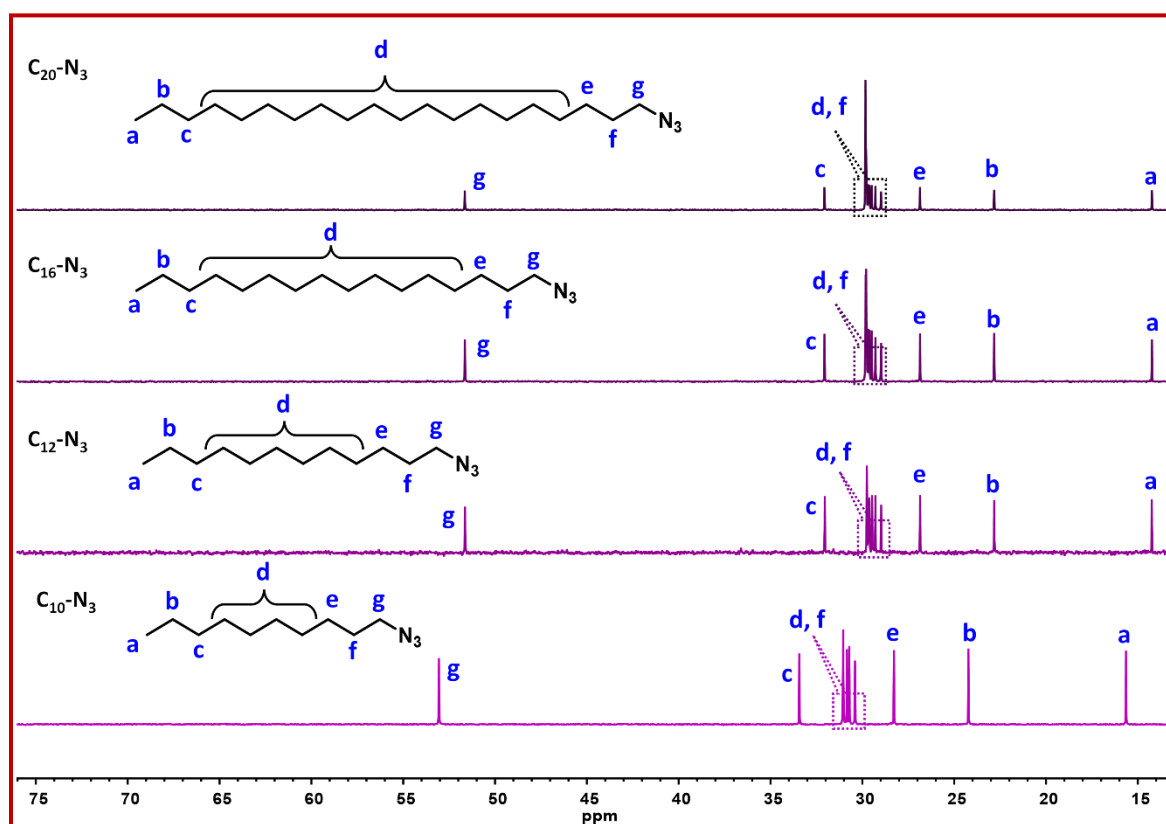


Figure 4.3. $^{13}\text{C-NMR}$ spectra of $\text{C}_{10}\text{-N}_3$, $\text{C}_{12}\text{-N}_3$, $\text{C}_{16}\text{-N}_3$ and $\text{C}_{20}\text{-N}_3$ in CDCl_3 .

Characterization data: FT-IR (Glu-Pr)- Figure 4.1, ESI-MS (Glu-Pr)- Figure A4.5, $^1\text{H-NMR}$, 400 MHz, D_2O , TMS, δ (ppm) (Figure 4.4): 2.15(m, 2H), 2.58 (m, 2H), 2.81 (t, 1H), 3.98 (t, 1H), 4.65 (d, 2H). $^{13}\text{C-NMR}$, 75 MHz, D_2O , δ (ppm) (Figure 4.5): 24.92, 29.56, 52.42, 52.89, 76.18, 77.72, 172.0, 173.59.

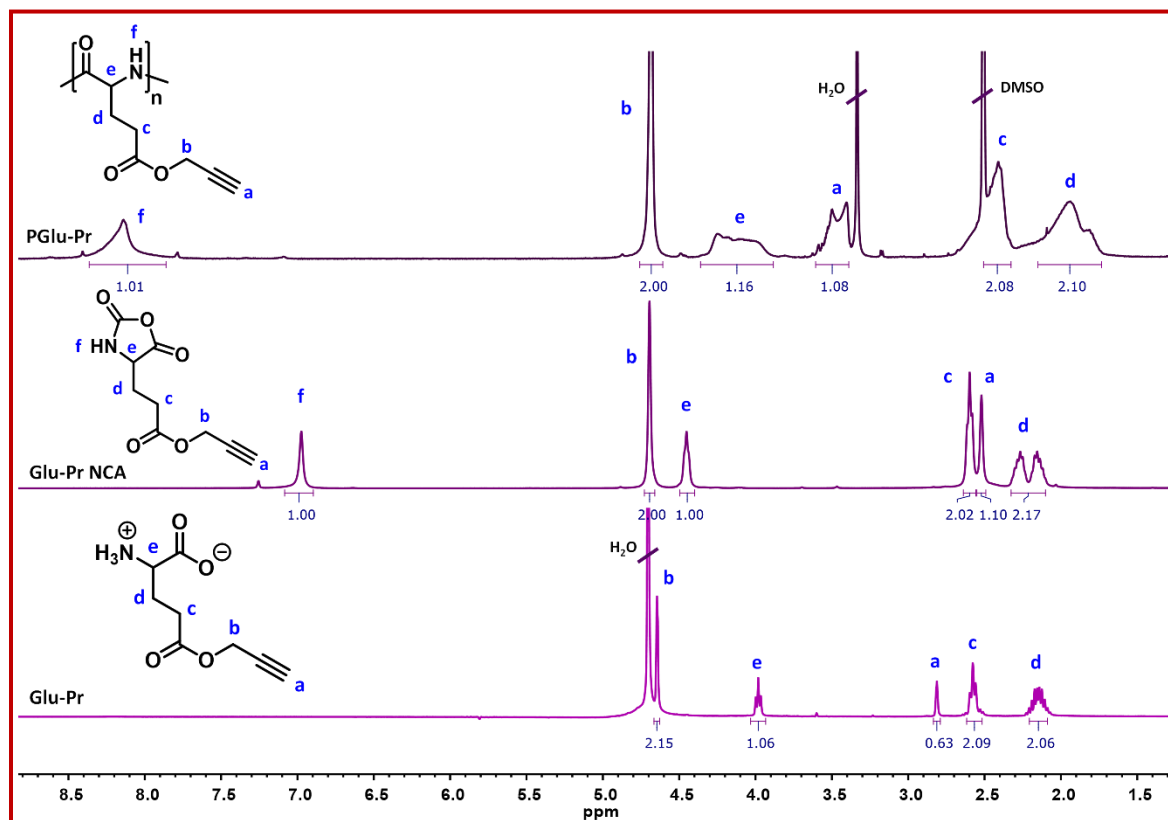


Figure 4.4. $^1\text{H-NMR}$ spectra of Glu-Pr (in D_2O), Glu-Pr NCA (in CDCl_3) and PGlu-Pr (in DMSO-d_6).

4.3.2.3. Synthesis of N-Carboxyanhydride of Glu-Pr (Glu-Pr NCA)

Glu-Pr NCA was synthesized by the reaction between Glu-Pr and triphosgene, as shown in Scheme 4.1, following a procedure reported by the Zelzer group.⁶¹ In a dried 250 mL double-neck round-bottom flask, 2 g of Glu-Pr and 100 mL of dry ethyl acetate were charged with α -pinene (6 mL, 37.8 mmol) under an argon atmosphere. The entire system was then transferred to a pre-heated oil bath at 90°C and refluxed for 15 minutes. Triphosgene (1.6 g, 5.4 mmol), dissolved in 5 mL of dry ethyl acetate, was added dropwise to the reaction mixture. After 5

hours, the resulting solution was cooled to room temperature, and any unreacted reactant was removed through centrifugation followed by filtration. Glu-Pr NCA was isolated by precipitating the concentrated reaction mixture in cold hexane. The resulting viscous yellow solid (yield: 75%) was collected by centrifugation and dried under vacuum at 50°C.

Characterization data: FT-IR (Glu-Pr NCA)- Figure 4.1, ESI-MS (Glu-Pr NCA)- Figure A4.6; $^1\text{H-NMR}$, 400 MHz, D_2O , TMS, δ (ppm) (Figure 4.4): 2.21 (dm, 2H), 2.52 (s, 1H), 2.60 (t, 2H), 4.45 (t, 1H), 4.69 (d, 2H), 6.98 (s, 1H); $^{13}\text{C-NMR}$, 75 MHz, CDCl_3 , δ (ppm) (Figure 4.5): 26.79, 29.44, 52.73, 56.87, 75.64, 77.2, 152.4, 169.60, 171.86.

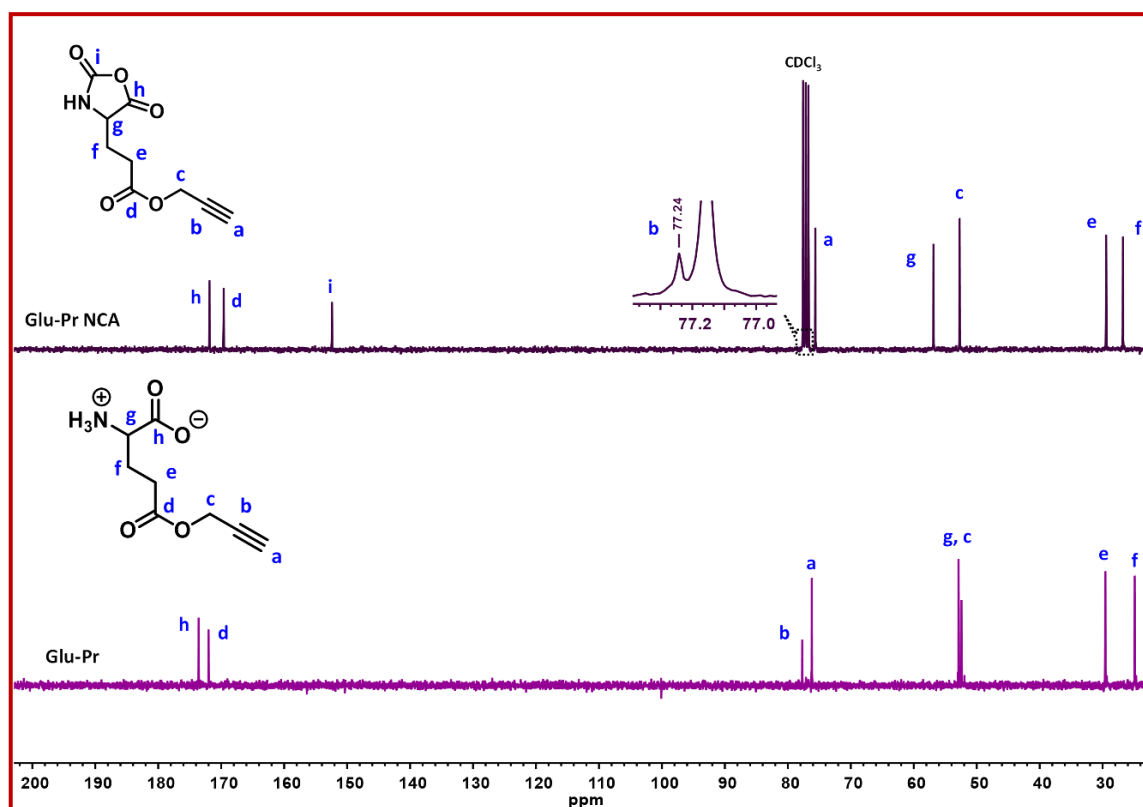


Figure 4.5. $^{13}\text{C-NMR}$ spectra of Glu-Pr (in D_2O) and Glu-Pr NCA (in CDCl_3).

4.3.2.4. Synthesis of Poly(γ -propargyl-L-glutamate) (PGlu-Pr)

The ROP of Glu-Pr NCA was performed to obtain PGlu-Pr using HMDS as the initiator in dry DMF under inert conditions, as shown in Scheme 4.1. The

synthetic protocol followed was similar to the previously reported procedure, with an initial molar ratio of monomer/initiator ($[M]_0/[I]_0$) of 50:1.⁷⁻⁸ In a 25 mL round-bottom flask, a DMF solution (5 mL) of Glu-Pr NCA (1.5 g, 7.1 mmol) was prepared, and the solution was purged with argon gas. The flask was then subjected to four consecutive freeze-pump-thaw cycles before being transferred into a glove box. HMDS (30 μ L, 0.14 mmol) was added to the solution, and the mixture was stirred for 48 hours. Subsequently, the mixture was removed from the glove box and precipitated in cold anhydrous diethyl ether to obtain solid PGlu-Pr. The product was further purified by dissolving it in a minimum volume of DMF, followed by reprecipitation, washing with diethyl ether, and vacuum drying at 60°C (yield: 72%).

Characterization data: FT-IR (PGlu-Pr)- Figure 4.1; ¹H-NMR, 400 MHz, DMSO-d₆, TMS, δ (ppm) (Figure 4.4): 1.93 (m, 2H), 2.40 (m, 2H), 3.46 (m, 1H), 4.11 (m, 1H), 4.68 (s, 2H), 8.14 (s, 1H).

4.3.2.5. Click Reaction Between the PGlu-Pr and Long-Chain-Alkyl Azides

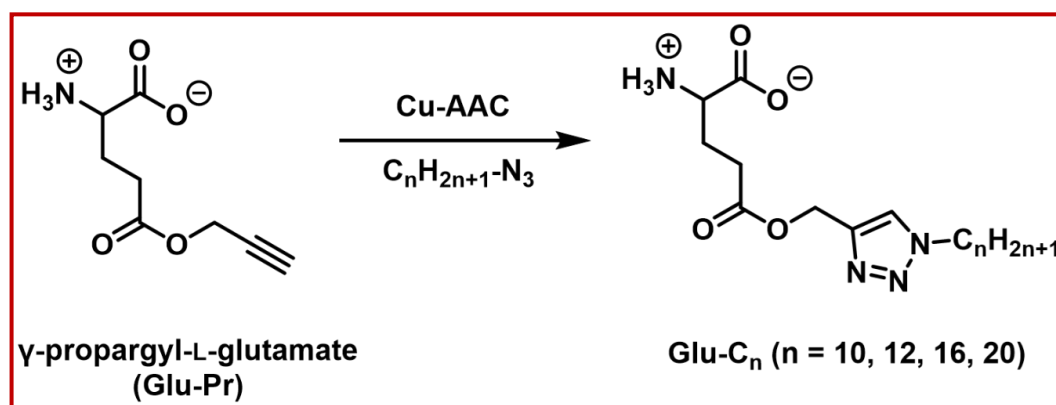
The click reaction between PGlu-Pr and C_n-N₃(s) was carried out using a procedure previously reported (Scheme 4.1). In a typical procedure, 500 mg of PGlu-Pr and an excess of C₂₀-N₃ (2.0 g) were dissolved in 5 mL of dry tetrahydrofuran (THF) in a 25 mL long-neck round-bottom flask. The solution was purged with argon for 30 minutes. Separately, CuSO₄·5H₂O (75 mg, 0.3 mmol) and sodium ascorbate (88.3 mg, 0.44 mmol) were dissolved in 100 μ L of milli-Q water. The aqueous solution was then added to the reaction mixture under continuous argon purging. The flask was sealed with a rubber septum and transferred to a pre-heated oil bath at 65°C for 3 days. After completion of the reaction, the heterogeneous mixture was cooled to room temperature and precipitated in excess diethyl ether. The resulting product was suspended in THF and subjected to dialysis (Thermo Scientific, MWCO 3500 D) against water for purification. The water-insoluble product was collected by filtration and

washed with methanol and acetone. Finally, it was dried under vacuum at 60°C. This compound was designated as P Glu-C_{20} . P Glu-C_{16} , P Glu-C_{12} , and P Glu-C_{10} were synthesized following the same protocol (Table 4.1).

Characterization data: FT-IR (P Glu-C_{20})- Figure 4.1; $^1\text{H-NMR}$ - 400 MHz, TMS, δ (ppm) (Figure 4.6): **P Glu-C_{20}** (CDCl_3) - 0.87 (s, 3H), 1.24 (bs, 34H), 1.86 (s, 1H), 2.03 (s, 2H), 2.46 (m, 3H), 3.98 (d, 1H), 4.38 (d, 2H), 4.67 (m, 1H), 5.15 (m, 1H), 7.75 (s, 1H), 8.34 (s, 1H), **P Glu-C_{16}** (CDCl_3) - 0.86 (d, 3H), 1.26 (bs, 25H), 1.88 (s, 2H), 2.35 (m, 4H), 3.94 (s, 1H), 4.31 (s, 2H), 5.14 (m, 2H), 7.79 (s, 1H), 8.30 (s, 1H), **P Glu-C_{12}** (CDCl_3) - 0.85 (s, 3H), 1.25 (bs, 18H), 1.87 (s, 2H), 2.08 (s, 2H), 2.31 (d, 2H), 2.62 (s, 1H), 3.91 (s, 1H), 4.32 (s, 2H), 5.22 (m, 2H), 7.81 (s, 1H), 8.28 (s, 1H), **P Glu-C_{10}** (DMSO-d_6) - 0.85 (s, 3H), 1.24 (bs, 14H), 1.78- 2.52 (m, 6H), 4.26-4.36 (m, 4H), 5.12 (s, 2H), 8.07 (s, 1H), 8.14 (s, 1H).

4.3.2.6. Synthesis of Alkyl-L-Glutamates (Glu-C_n , $n = 10, 12, 16, 20$)

The synthesis involved the click reaction of Glu-Pr with alkyl azides using a procedure previously described (Scheme 4.2).⁸ In a typical procedure, Glu-Pr (500 mg, 2.7 mmol) was suspended in a mixture of 5 mL of THF and H_2O (10:1 v/v). $\text{C}_{20}\text{-N}_3$ (1.3 g, 4.05 mmol) was dissolved in 2 mL of THF and added to the above suspension with continuous argon gas purging. Separately, an aqueous solution of $\text{CuSO}_4 \cdot 5\text{H}_2\text{O}$ (68 mg, 0.27 mmol) and sodium ascorbate (80 mg, 0.4 mmol) was



Scheme 4.2. Synthesis of Glu-C_n .

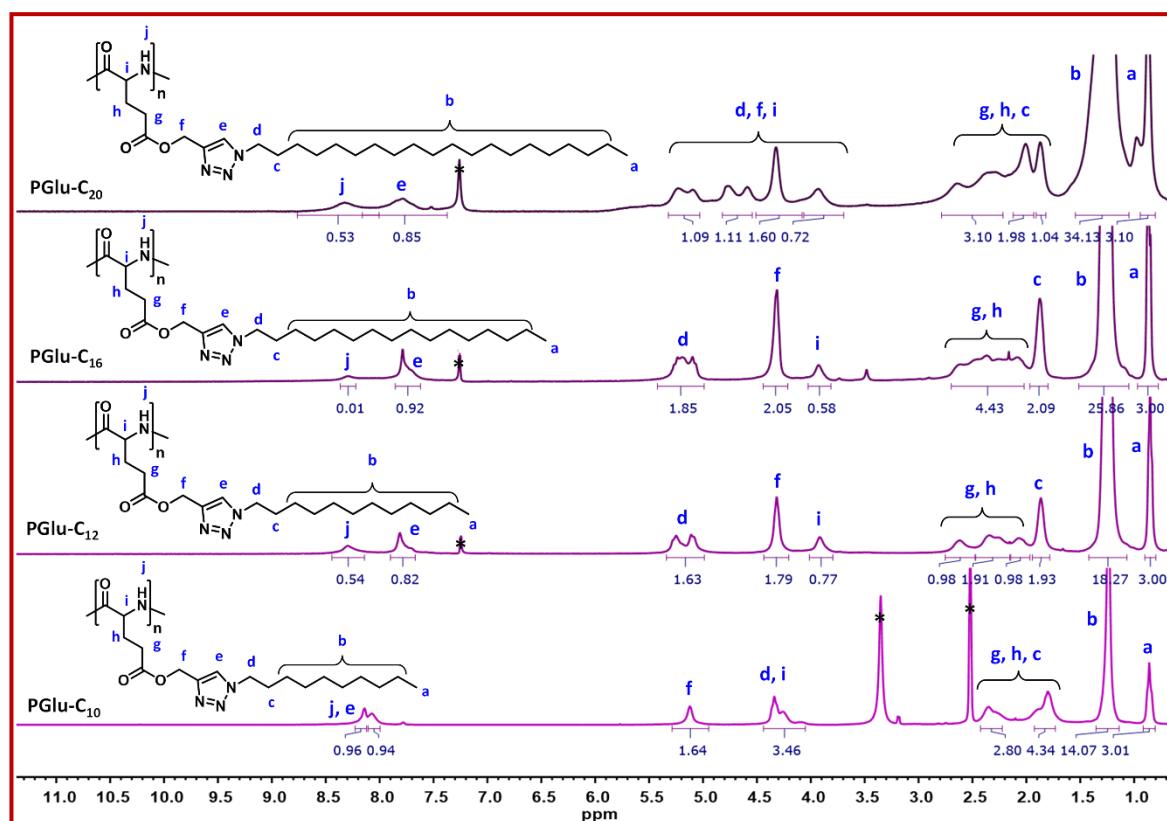


Figure 4.6. $^1\text{H-NMR}$ spectra of PGlu-C₁₀ (in DMSO- d_6) and PGlu-C₁₂, PGlu-C₁₆, PGlu-C₂₀ (in CDCl_3).

*- signal from solvent impurities.

added, followed by 45 minutes of argon gas purging. The entire reaction mixture was transferred to an oil bath and stirred at 65°C for 24 hours. After completion of the reaction, the mixture was evaporated using a rotary evaporator and the residue was dissolved in THF. The product was then collected by precipitation in excess diethyl ether. The solid product was washed multiple times with water to remove the catalyst and unreacted chemicals, and finally collected by filtration. It was then vacuum dried overnight at 60°C , yielding a product with a 51% yield. Similar procedures were used to synthesize Glu-C₁₆, Glu-C₁₂, and Glu-C₁₀, which served as control samples to compare their crystalline properties with their respective polymers.

Characterization data: FT-IR (Glu-C₂₀) - Figure 4.1; MALDI-TOF-MS (Glu-C₂₀) - Figure A4.7; ESI-MS (Glu-C₁₆, Glu-C₁₂ and Glu-C₁₀) - Figures A4.8, A4.9, and A4.10.

¹H-NMR, 400 MHz, TMS, δ (ppm) (Figure 4.7): **Glu-C₂₀** (CDCl₃) - 0.87 (m), 1.24 (s), 1.89 (m), 2.64 (m), 2.80 (m), 4.33 (t), 4.79 (s), 5.23 (s), 7.55 (d), **Glu-C₁₆** (CD₃OD) - 0.85 (m), 1.25 (s), 1.62 (m), 2.30 (m), 2.52 (m), 2.88 (t), 3.30(d), 4.30 (s), 7.49 (s), **Glu-C₁₂** (CD₃OD) - 0.88 (t), 1.29 (s), 1.62 (m), 2.32 (m), 2.49 (m), 2.91 (t), 3.30(d), 4.26 (s), 7.44 (s), **Glu-C₁₀** (CD₃OD) - 0.86 (t), 1.29 (s), 1.62 (m), 2.20 (m), 2.59 (m), 2.89 (t), 3.30 (d), 4.27 (s), 7.48 (s).

¹³C-NMR, 75 MHz, CDCl₃, δ (ppm) (Glu-C₂₀) (Figure A4.11): 14.25 (1C), 22.83 (1C), 26.64 – 32.06 (19 C), 50.60 (1C), 57.50 (1C), 58.28 (1C), 123.59 (1C), 152.27 (1C), 186.08 (1C), 199.89 (1C)

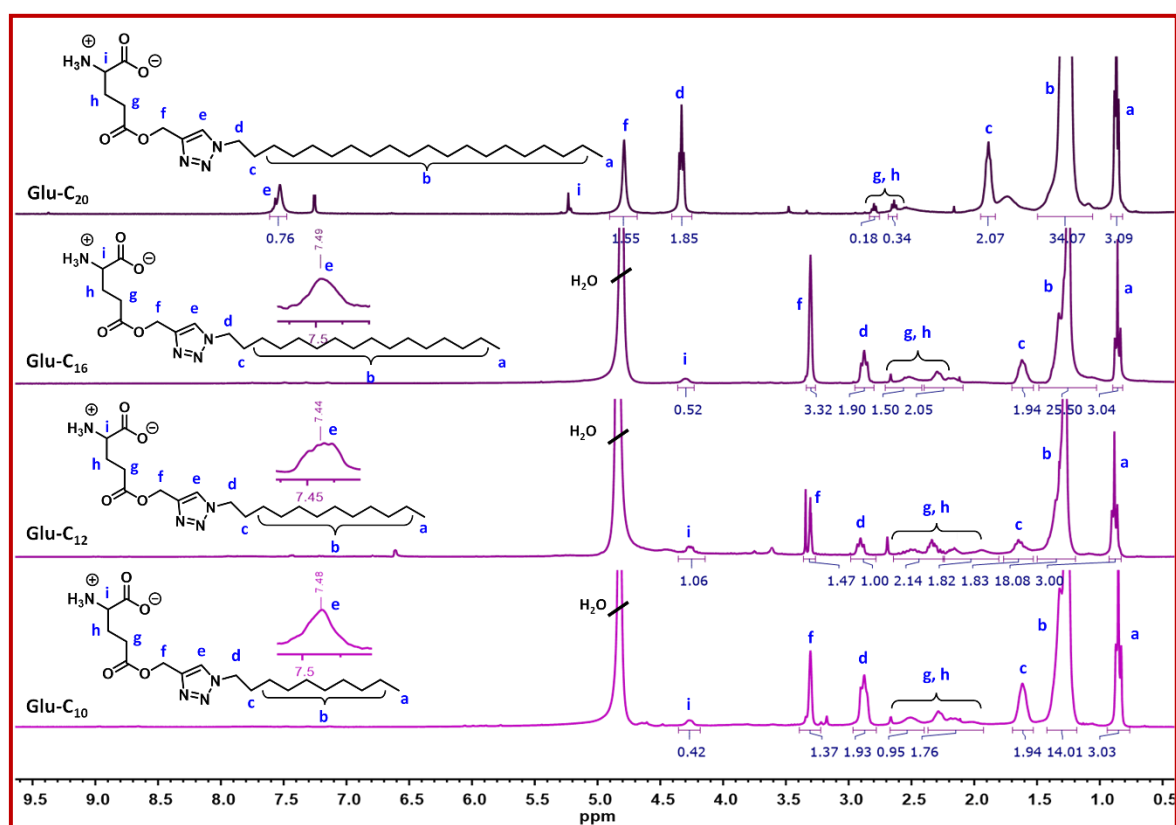


Figure 4.7. ¹H-NMR spectra of Glu-C₁₀, Glu-C₁₂, Glu-C₁₆ (in CD₃OD) and Glu-C₂₀ (in CDCl₃).

4.3.3. Experimental Methods

4.3.3.1. Cloud point (T_{cp}) Measurement of PGlu-C_n(s) in Non-Aqueous Solvents

The cloud points (T_{cp}) of PGlu-C_n(s) in CHCl₃ and THF solution (2 wt%) were determined using a UV-vis spectrophotometer equipped with a fiber-optic probe and a low-temperature thermostatic alcohol bath. In a procedure, solutions of PGlu-C_n(s) in CHCl₃/THF were filtered through a membrane filter with a diameter of approximately 0.45 μ m. Subsequently, the filtered solutions were transferred into test tubes, and the optical probe was immersed into the solution. The entire setup was then placed in a low-temperature alcohol bath. T_{cp} values were measured by monitoring the percentage transmittance (at $\lambda = 500$ nm) within a temperature range of 30 to – 65 °C, using a heating/cooling rate of 3 °C/ min. The system was allowed to equilibrate for 5 minutes at each experimental temperature before taking the reading. Additionally, the phase transition temperatures were determined through calorimetric measurements using a micro-DSC instrument, analyzing the samples obtained from their respective solvents. Notably, the turbidity experiment was not conducted for PGlu-C₁₀ due to its insolubility in CHCl₃ and THF.

4.3.3.2. Self-Aggregation Study of PGlu-C_n(s) (n = 12, 16, 20)

Hydrophobic PGlu-C_n(s) (n= 12, 16, 20) were found to be soluble in few organic solvents like CHCl₃, THF etc. Hence, the self-aggregation of copolypeptides was studied by dynamic light scattering (DLS), field-emission scanning electron microscopy (FESEM), and field emission gun- transmittance electron microscopy (FEG-TEM) in CHCl₃ and THF. Typically, 0.5 wt% solution of the as synthesized PGlu-C_n(s) were prepared in both the CHCl₃ and THF. All the solutions were vortexed, centrifuge and finally filtered through membrane filter (0.45 μ m pore size). The filtered solutions were kept undisturbed for 2 h and were examined by DLS at 25 °C. The above prepared solutions were also taken for morphological study using FESEM and FEG-TEM. Note that, self-

aggregation of the P_{Glu}-C_n(s) below their UCST in respective solvents was also investigated by FESEM.

4.3.3.3. Dye Encapsulation Study

For dye uptake study Eosin B (EB) was chosen as model dye and P_{Glu}-C₁₆ as a representative sample. At first, 300 μ L of 1.0×10^{-3} M of EB solution in MeOH was taken into a glass vial and was evaporated to dryness. A 2 mL 5 mg/mL CHCl₃ solution of P_{Glu}-C₁₆ was added into it to make the final concentration of EB 1.5×10^{-4} M. This solution and a control solution without any copolypeptide were sonicated for 15 min and stirred for 2 days at room temperature. Both the solutions were then centrifuged and filtered through 0.45 μ m pore size filter membrane to discard the free dye molecules. EB loaded CHCl₃ solution of P_{Glu}-C₁₆ was then added to excess diethyl ether and dye loaded P_{Glu}-C₁₆ was separated by centrifugation. The product so obtained was washed with fresh water to remove any surface-adsorbed EB molecules. Finally, it was dried in vacuum oven to dryness and re-dispersed in CHCl₃ and were examined via absorption and fluorescence spectroscopy.

4.3.4. Characterization

FT-IR spectra of all the samples were recorded from their native state using Spectrum 2 (PerkinElmer) Spectrometer.

Waters quadrupole time-of flight (Q-TOF) Micro YA263 mass spectrometer was used to record the ESI-MS spectra of Glu-Pr, Glu-C₁₆, Glu-C₁₂, Glu-Pr NCA and all three alkyl azides. A H₂O: MeOH (1:1 v/v) solution was used to record the spectra of Glu-Pr and MeOH solution was used for rest of them.

Bruker 400 and 300 MHz spectrometer were respectively used to acquire the ¹H- and ¹³C-NMR spectra of all the as synthesized compounds from their respective solvents.

The circular dichroism (CD) spectra of P_{Glu}-Pr and P_{Glu}-C_n(s) were recorded from their 0.1 wt% solutions in THF using a JASCO J-1500 CD

spectropolarimeter, keeping the path length 1 mm. Bandwidth, response time and scanning rate were kept at 1 nm, 1 s and 100 nm/min respectively. A resultant spectrum of three consecutive scans were taken to reduce the signal-to-noise ratio.

Molecular weight of Glu-C₂₀ and end group analysis of PGlu-Pr were performed by a Bruker MALDI-TOF-MS instrument using 2,5-dihydroxybenzoic acid (DHB) as matrix and NaI salt to enhance their ionization.

Size exclusion chromatography (SEC) was used to determine the number average molecular weight (M_n) and dispersity (\mathcal{D}) of the as synthesized polypeptide/copolypeptides using a Waters 1515 isocratic HPLC pump and a Waters 2414 refractive index detector at 35 °C. Four styragel columns of different size-exclusion limits were connected in a series at 40 °C and THF containing 25 mM LiBr was used as the eluent with 1 mL/min flow rate. PMMA standards were used to calibrate the column. Waters Empower software was used for molecular weight analysis.

Thermogravimetric analysis (TGA) of all the as synthesized control samples Glu-C_n(s) and polymers PGlu-C_n(s) were recorded using a TGA 4000 instrument from Perkin Elmer under N₂ atmosphere and at a heating rate of 10 °C/min. All the samples were dried well in vacuum oven (60 °C) before analysis.

Differential scanning calorimetry (DSC) technique was adopted to measure the melting points (T_m s), glass transition temperatures (T_g s) or crystallization temperature (T_c s) of all the as synthesized compounds using PerkinElmer DSC 8000 instrument equipped with an intracooler. All the samples were dried at 60 °C in vacuum oven before the analysis. In a process, sample pan was first annealed at 150 °C for 5 minutes to remove any previous thermal history. It was then cooled to – 60 °C at a rate of 5 °C/min inside the DSC cell and held for 5 min. All the experiments were carried out under a nitrogen flow of 40 mL/min. The exothermic peak in this cooling thermogram was considered as the crystallization temperature (T_c) and the enthalpy of

crystallization (ΔH_c) was calculated integrating the exothermic peak. The sample pan was then heated to 150 °C at a rate of 10 °C/min and the endothermic peak in this second heating was considered as the melting temperature (T_m). The melting enthalpy of melting (ΔH_m) was obtained from the integration value of the endothermic peak at T_m .

The crystal morphology of Glu- C_n (s) and PGlu- C_n (s) were examined through polarized optical microscope (POM) (Model BX51), equipped with a heating stage. 2.5 wt% chloroform/MeOH solutions of the samples were drop-casted individually on a clean microscopic coverslip and dried in air to develop a thin film of the samples. The dried films were then sandwiched by putting another coverslip on it and placed on a microscopic heating stage (Linkam THMS 600 equipped with a T-95 temperature programmer) and subjected to heating at 100- 150 °C (at a rate of 10 °C/min for 5 min) to melt completely. It was then cooled below the T_c of the respective samples at a rate of 5 °C/min and allowed to recrystallize for 2 h. The recrystallized sample films were then placed under the POM to investigate their crystal morphology. All the images have been captured using a 10X/0.25 P and 20X/0.40 objective lens and ProgRes Capture Pro 2.7 software was used for the analysis.

The crystallinity of the as synthesized control samples and the copolypeptides were also studied by powder X-ray diffractometry (PXRD) using a Bruker D8 X-ray diffractometer operated at an accelerating voltage of 40 kV using Cu $K\alpha$ ($\lambda = 1.5405 \text{ \AA}$) as the X-ray radiation source with a current intensity of 40 mA. All the samples were dried well before experiment and used in the form of finely grinded powder on a glass slide. Degree of crystallinity of the samples were also calculated from their corresponding PXRD plots.

Micro-differential scanning calorimetry (Micro-DSC) (TA Instrument) experiment of PGlu- C_n (s) ($n = 16, 20$) (2 wt% CHCl_3 /THF solution) was performed between - 30 to 25 °C to measure the solution phase transition temperature (T_{cp} s) and ΔH s of the transition. Scanning rate was kept at 1 °C/min. Standard

sample holders were used with an average sample volume of 600 μL . Almost same mass of the sample and the reference were weighted to reduce the differences in heat capacities between them. The samples were equilibrated at 25 $^{\circ}\text{C}$ for h before each scan.

Emission spectra of dye/dye-loaded copolypeptide particles were recorded using a Cary Eclipse (Agilent) Spectrophotometer with a slit width of 5 nm.

Dynamic light scattering (DLS) experiment to measure the hydrodynamic diameters (D_{hs}) were carried out using a Malvern Zetasizer NANO ZS 90 (Model: 3690) instrument. CHCl_3 and THF solution (0.5 wt%) of PGlu- $\text{C}_n(\text{s})$ were filtered through membrane filter (0.45 μm pore size) and subjected to analysis. Each data point was obtained by scanning the sample solution for 15 times in a single run at a certain time. The intensity-weighted distribution data obtained from the DLS instrument was finally plotted to obtain D_h .

Sample solution of PGlu- C_{20} (representative sample) (0.5 wt%) in CHCl_3 and THF were casted on a clean glass slide and dried for morphological analysis using a JEOL JSM-6700F FESEM operated at an accelerating voltage of 2 kV. Aggregates of the PGlu- $\text{C}_n(\text{s})$ ($n = 16, 20$) below their UCST in the respective solvents were also imaged from their drop-casted samples. Respective solutions were first brought to the desired temperature to from the hazy suspension and 10 μL of that suspension was then added to 500 μL of diethyl ether kept at the temperature below the UCST of the corresponding sample. The frozen aggregates immediately casted from that ether solution on a glass slide and dried very quickly by blowing air followed by drying in vacuum. It is to be noted that PGlu- $\text{C}_n(\text{s})$ are insoluble in diethyl ether.

The morphology of aggregated PGlu- $\text{C}_n(\text{s})$ in CHCl_3 and THF (0.5 wt%) was studied by acquiring the images from the cast samples using a JEOL JEM-2100F Field Emission Gun-Transmission Electron Microscope (FEG-TEM)

working at an accelerating voltage of 200 kV. Sample solution was drop-casted onto a carbon-coated copper grid and air-dried for two days before analysis.

Confocal microscopic images of dye-encapsulated PGlu-C₁₆ particles were obtained by using LSM 880 (Carl Zeiss) instrument from drop-casted and dried samples.

UV-vis absorption spectra of free and encapsulated dye were acquired using a Cary 60 spectrophotometer (Agilent). For turbidity experiment, the upper critical solution temperature (UCST)-type cloud points (T_{cp})s of the PGlu-C_n(s) in respective solvents were determined by measuring the % transmittance at different temperatures at a fixed wavelength ($\lambda = 500$ nm) using the same spectrophotometer along with a fiber-optic probe (Agilent) and a low temperature thermostat alcohol bath. The probe was dipped into the sample solution taken in a test tube and the % transmittance was recorded with a heating/cooling rate of 3 °C/min.

4.4. Results and Discussion

4.4.1. Synthesis of PGlu-C_n(s) (n = 10, 12, 16, 20)

Synthesis of long-chain-alkyl grafted poly(L-glutamate)s, PGlu-C_n (n = 10, 12, 16, 20), involved the click reaction between the as synthesized PGlu-Pr and long-chain-alkyl azides (Scheme 4.1). Firstly, PGlu-Pr was synthesized by the ROP of Glu-Pr NCA using HMDS as the initiator. The formation of Glu-Pr NCA can be ascertained from the appearance of characteristic symmetric and antisymmetric stretching bands of >C=O of anhydride in 1773 and 1849 cm⁻¹ respectively in the FT-IR spectrum (Figure 4.1). ROP of Glu-Pr NCA resulted in the poly(L-glutamate) with pendant propargyl group (PGlu-Pr) which was subjected to click reaction with the as synthesized alkyl azides [C_n-N₃ (n = 10, 12, 16, 20)] to form the long-chain-alkyl grafted poly(L-glutamate)s [PGlu-C_n (n = 10, 12, 16, 20)] as confirmed by the FT-IR (Figure 4.1) and ¹H-NMR (Figure 4.6) spectra. FT-IR spectrum (Figure 4.1) of PGlu-Pr showed strong bands at 1650

and 1734 cm^{-1} and a relatively weak band at 2127 cm^{-1} due the presence of amide, ester, and terminal alkyne groups respectively, whereas $\text{C}_{20}\text{-N}_3$ (representative sample) showed a sharp band at 2094 cm^{-1} in the FT-IR spectrum for the azide group. But, for PGlu-C_{20} , absence of any IR bands for terminal alkyne or azide and presence of sharp bands for amide (1654 cm^{-1}) as well as long alkyl backbone ($2852/2922\text{ cm}^{-1}$) confirmed the successful click reaction between them. $^1\text{H-NMR}$ spectra of PGlu-C_{20} showed signals of the different protons present along with a sharp broad singlet peak at $\delta\ 1.24\text{ ppm}$ and relatively small peak at $\delta\ 7.75\text{ ppm}$ due the protons of alkyl chain and the triazole ring formed due to the click reaction between PGlu-Pr and $\text{C}_{20}\text{-N}_3$ respectively (Figure 4.6). These peaks were absent in the $^1\text{H-NMR}$ spectrum of PGlu-Pr as can be seen in Figure 4.4, which basically proved the grafting of alkyl chain (C_{20}) with PGlu-Pr through click reaction. This result as obtained from the $^1\text{H-NMR}$ spectrum were also be found same but with slightly different chemical shift (ppm) for PGlu-C_{16} , PGlu-C_{12} and PGlu-C_{10} (Figure 4.6).

Synthesis of Glu-C_{20} through the Cu-AAC click reaction between the as synthesized Glu-Pr and $\text{C}_{20}\text{-N}_3$ molecules (Scheme 4.2) was confirmed by the disappearance of the characteristics FT-IR band of the propargyl group (2128 cm^{-1}) of Glu-Pr and azide (2094 cm^{-1}) of $\text{C}_{20}\text{-N}_3$ respectively in Glu-C_{20} (Figure 4.1). $^1\text{H-NMR}$ spectrum of Glu-C_{20} (Figure 4.7) also showed the peaks for the signal of the protons of the alkyl groups at $\delta\ 0.87\text{ (t)}$, 1.24 (bs) , 1.89 (m) and 4.33 (t) and for the triazole ring proton at $\delta\ 7.55\text{ (d)}$ ppm which were absent in the $^1\text{H-NMR}$ spectrum of Glu-Pr (Figure 4.4). $^{13}\text{C-NMR}$ (Figure A4.11) of the Glu-C_{20} also showed the additional signal from the carbon atoms of the alkyl chain along with that of the Glu-Pr . Moreover, shifting of the signal of the propargylic carbons ($\delta\ 76.18$ and 77.72 ppm) of Glu-Pr (Figure 4.5) towards downfield ($\delta\ 123.59$ and 152.27 ppm) (Figure A4.11) in case of Glu-C_{20} due to the triazole ring formation also confirm the successful synthesis of Glu-C_{20} .

MALDI-TOF-MS spectrum of PGlu-Pr (Figure 4.8) contained equidistant peaks separated by a m/z of 167 Da, which exactly matched with the molecular weight of the Glu-Pr unit. One such peak, at $m/z = 5528$, can be attributed to the sum of molar masses of two end groups (amido and amino) and 33 units of Glu-Pr (see calculation in Figure 4.8). Such end groups were formed due to the hydrolysis of the *N*-(trimethylsilyl)-amido end groups, as reported elsewhere (Scheme 4.3).⁶²⁻⁶³

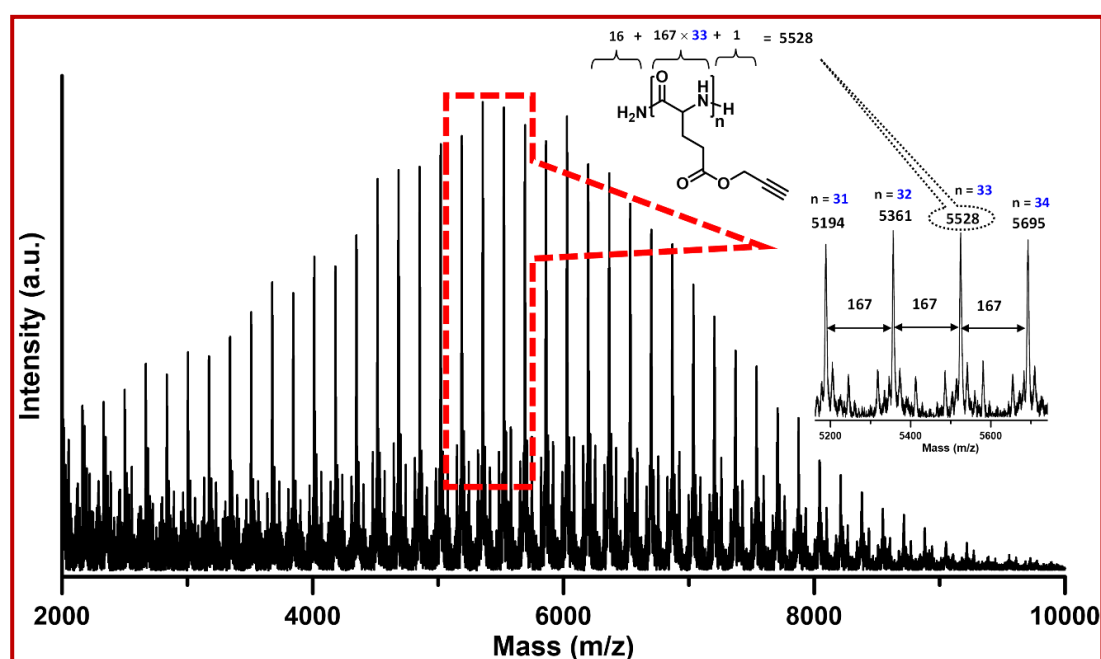
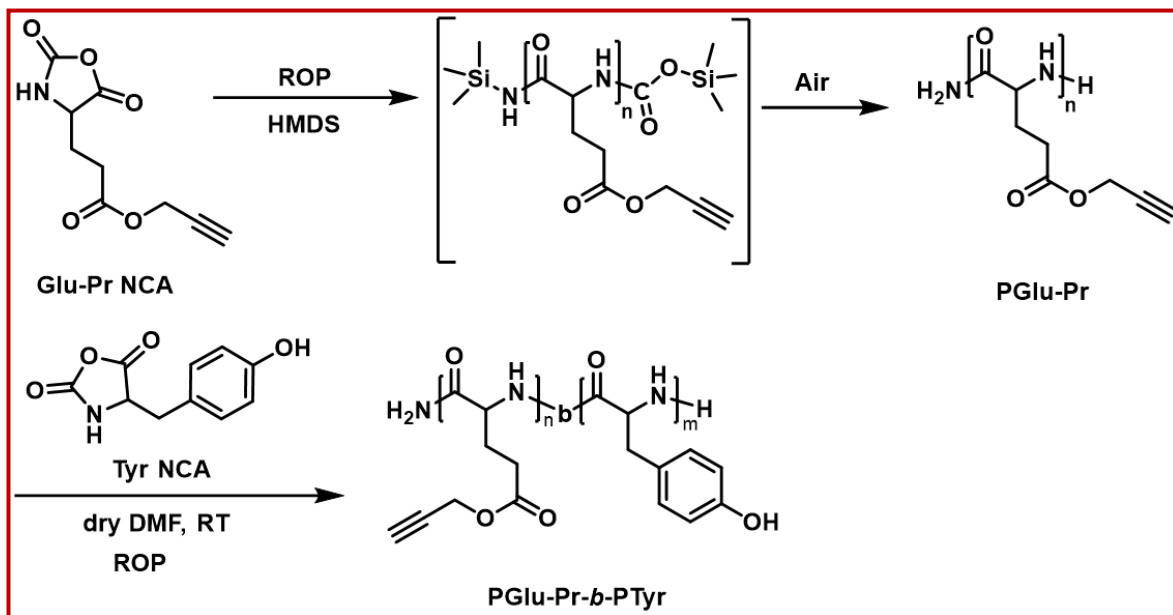


Figure 4.8. MALDI-TOF-MS spectrum of PGlu-Pr.

To demonstrate the presence of an amino-end group in the PGlu-Pr, it was further used as the macroinitiator in a chain extension experiment via ROP of L-tyrosine NCA (Tyr-NCA) (Scheme 4.3). Tyr-NCA was synthesized by following an earlier reported procedure.²⁶ This ROP of Tyr-NCA produced PGlu-Pr-*b*-PTyr copolypeptide, which was confirmed from the disappearance of the symmetric (1756 cm^{-1}) and antisymmetric (1830 cm^{-1}) stretching bands of Tyr-NCA (Figure 4.9A). PGlu-Pr-*b*-PTyr also contained bands at 2160 and 1513 cm^{-1} respectively for the propargyl and C=C (aromatic) groups present in the two blocks. $^1\text{H-NMR}$ signals (Figure 4.9B) at 9.13, 6.97, 6.63, 2.85, 2.65 for the protons

of the PTyr block also confirmed the successful synthesis of the PGlu-Pr-*b*-PTyr.



Scheme 4.3. Synthesis of PGlu-Pr-*b*-PTyr copolypeptide.

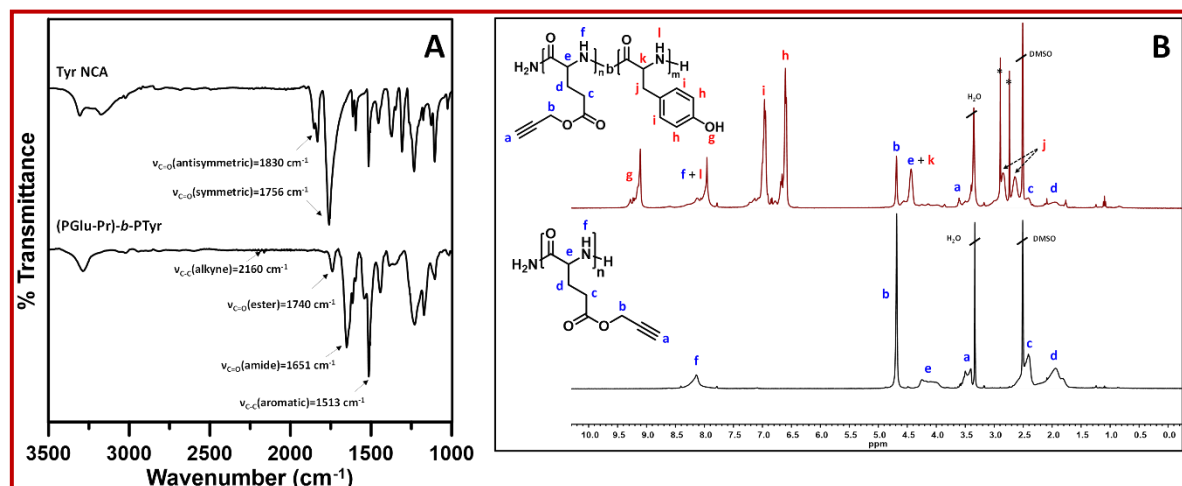


Figure 4.9. (A) FT-IR spectra of Tyr NCA and PGlu-Pr-*b*-PTyr, (B) $^1\text{H-NMR}$ spectra of PGlu-Pr-*b*-PTyr (top) and PGlu-Pr (bottom) in DMSO-d_6 .

SEC chromatogram of PGLu-Pr showed narrow and unimodal peak with very low D (Table 4.1) indicating a good control over its molecular weight during ROP (Figure 4.10A). The theoretical M_n was also very close to the M_n (GPC) indicating good control over ROP. It was observed that the grafting of alkyl groups of different lengths onto the PGLu-Pr resulted in the shifting of its chromatographic peak position towards high molecular weight region according to the molar mass of alkyl chain (Figure 4.10A). However, the experimental M_n s (SEC) of PGLu- C_n (s) were a little higher than those of calculated M_n s (Table 4.1). At this point, the exact reason is unknown, but it can be assumed that this difference might be due to improper calibration using PMMA standards, which is structurally quite different from the PGLu- C_n (s).

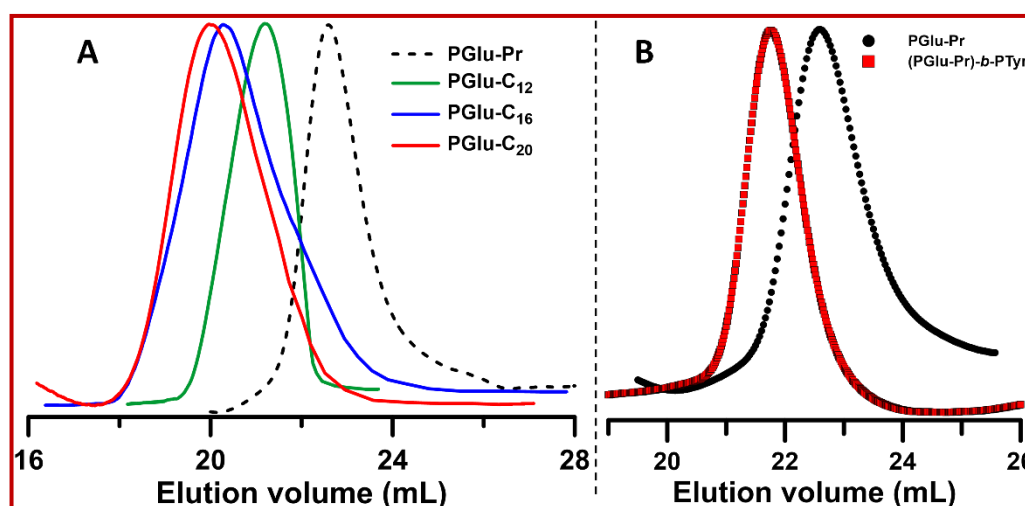


Figure 4.10. (A) SEC chromatograms of the as-synthesized polypeptides, (B) SEC chromatograms of PGLu-Pr and PGLu-Pr- b -PTyr.

Furthermore, a lateral shifting of SEC chromatogram of the PGLu-Pr- b -PTyr was observed compared to that of macroinitiator, H_2N -PGLu-Pr towards the high molecular weight region also confirmed chain extension with PTyr block (Figure 4.10B). The M_n of PGLu-Pr- b -PTyr was measured to be 9600 Da, which was higher than that of H_2N -PGLu-Pr (5600 Da).

The secondary structure of protein/polypeptide plays a vital role in their reactivity, stability as well as aggregation behaviour in solution phase.⁶⁴ In the case of PGlu-Pr, a CD spectrum analysis in THF (0.1 wt%) revealed two negative

Table 4.1. Molecular characterization data

Sample name	$[M]_0/[I]_0$	M_n (Theo) (Da)	DP (Theo)	M_n (SEC) (Da)	DP (SEC)	Dispersity (\mathcal{D})
^a PGlu-Pr	50	^b 6100	36	5600	33	1.13
^c PGlu-C ₁₂	-	^d 13600	-	17400	-	1.28
^c PGlu-C ₁₆	-	^d 15600	-	19500	-	1.52
^c PGlu-C ₂₀	-	^d 17600	-	21100	-	1.36

^a Condition for ROP of Glu-Pr NCA: Solvent = Dry DMF, Initiator = HMDS, Temperature = 30 °C

^b Formula of M_n (Theo) = $([M]_0/[I]_0 \times p \times M_{ru}) + M_{HMDS}$

$[M]_0/[I]_0$ = Initial concentration of NCA/ Initial concentration of HMDS, p = % yield, M_{ru} = Molar mass of repeating unit of the polypeptide (~ 167 Da), and M_{HMDS} = Molar mass of HMDS

^c Condition for click reaction: Solvent = THF: H₂O (10:1) and Temperature = 65 °C

^d Formula of M_n (Theo) = ^b $M_n + DP_{theo} \times M_{Cn-N3}$ ($n = 12, 16, 20$)

M_{Cn-N3} = Molar mass of the long-chain alkyl azide

bands at 210 and 222 nm, indicating the presence of an α -helical structure (Figure 4.11A), consistent with previous reports.²⁷ Similarly, PGlu-C_n(s) ($n = 12, 16, 20$) also exhibited a helical conformation in THF, as evident by the characteristic negative ellipticities at 210 and 222 nm (Figure 4.11B). However, for PGlu-C_n(s), the intensities of minima at both 210 and 222 nm were lower indicating a lower fraction of helicities (f_{HS}) than that of pristine PGlu-Pr. The grafting of the longer flexible alkyl groups into the side chain of the PGlu is likely to restrict the PGlu backbone to adopt α -helical structure through

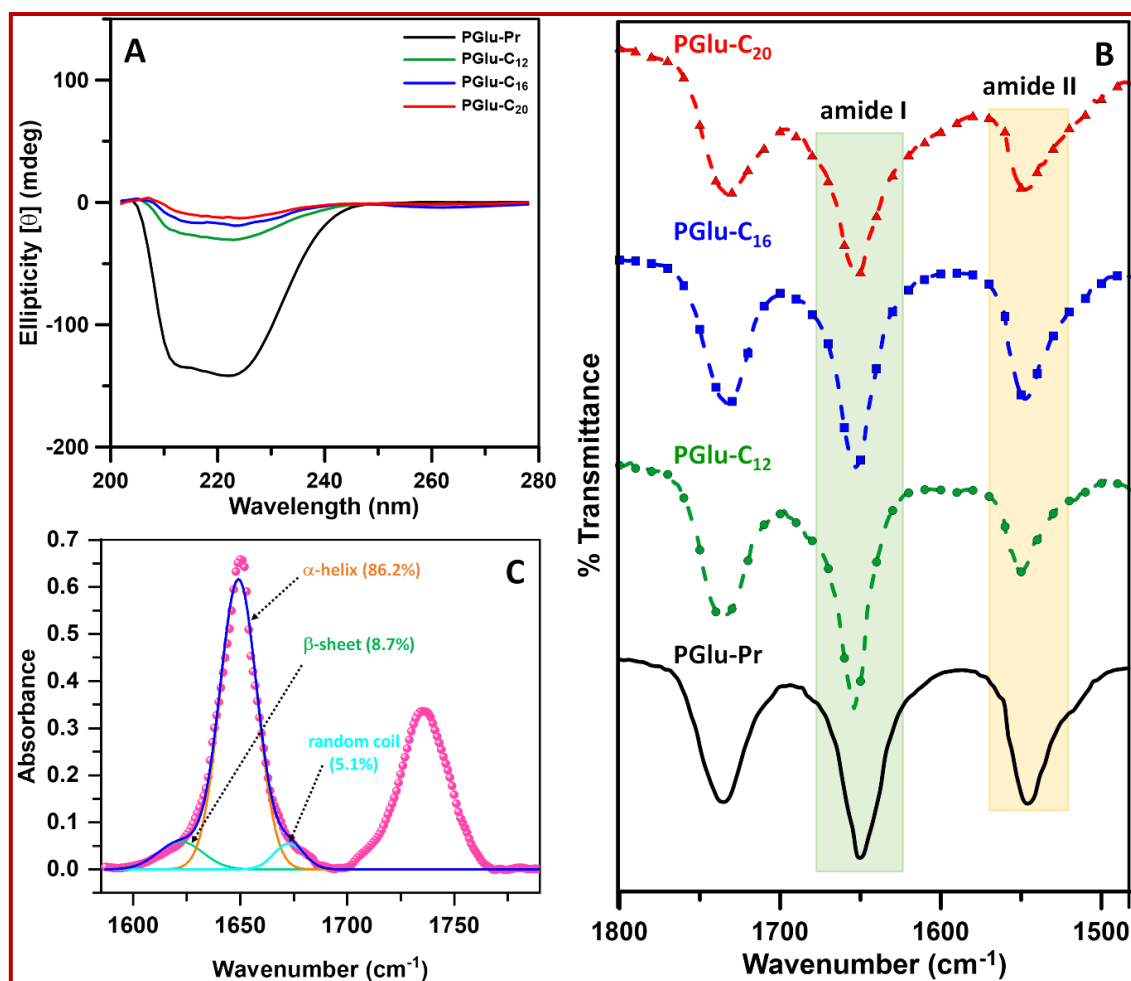


Figure 4.11. (A) CD spectra of PGLu-Pr and PGLu-C_n(s) ($n = 12, 16, 20$) recorded from their THF solution (0.1 wt%), (B) FT-IR spectra of the as-synthesized compounds showing the vibration bands related to their secondary structure, (C) Curve fitting plot of the amide-I region of the PGLu-Pr in FT-IR spectra, showing different fraction of secondary conformation adopted by PGLu backbone.

hydrogen-bonding properly. The intensity of the ellipticity of PGLu-C_n(s) further decreased with the increase of the chain length of the grafted alkyl groups (Figure 4.11A). This observation also supported that the strength of the interstrand hydrogen bonding between the PGLu backbone decreases with

increasing chain length of the side chains. Fraction of helicity (f_H) for each of the samples was calculated using an equation reported elsewhere⁶⁵:

Equation for calculating the fractional helicity (f_H) of the samples:

$$f_H = ([\theta]_{222} + 3000) / 39000$$

$[\theta]_{222}$ is the mean residue ellipticity at 222 nm

$$[\theta]_{222} = MRW \times \theta_{222} / 10 \times d \times c$$

where θ_{222} is the observed ellipticity (degrees) at 222 nm, d is the pathlength (cm), and c is the concentration (g/mL). Mean Residue Weight (MRW) for the peptide bond is calculated from $MRW = M_w / (N-1)$, where M_w is the molecular weight of the polypeptide in Da (M_n , Table 4.1), and N is the number of amino acids in the chain that is DP of the polypeptide. To be noted, we have used the theoretical values of the M_n and DP for the calculation.

It was found that fractional helicity decreased abruptly from 85.5% (PGlu-Pr) to 46.2%, 35.3% and 27.9% for PGlu-C₁₂, PGlu-C₁₆ and PGlu-C₂₀ respectively. It is also reported that polypeptides with α -helix type secondary structure usually show strong vibrational band at $\sim 1650 \text{ cm}^{-1}$ in the amide-I region.⁶⁶ Whereas polypeptide with β -sheet or random coil conformations show IR band near 1620 and 1690 cm^{-1} respectively in amide-I region. In our case, PGlu-Pr showed a strong band at 1650 cm^{-1} (Figure 4.11B), which was certainly intrinsic to the α -helix conformation. However, the peak deconvolution result (Figure 4.11C) showed that PGlu-Pr mostly adopted helical (86.2%) conformation with very minute fraction of sheet- (8.7%) and coil-type (5.1%) conformation.³³ In the cases of PGlu-C_n(s), amide-I region also exhibited a sharp band at 1654 cm^{-1} , indicating their helical conformations. Quantitative analysis of the FTIR spectra (Figure 4.11B) clearly showed that the intensity of the vibrational band at 1654 cm^{-1} decreased with the increase of the chain length of the grafted alkyl group, which again support the conclusion drawn from CD analysis.

4.4.2. Thermoresponsive Property of PGlu-C_n(s) (n = 12, 16, 20)

Thermoresponsive polymers/polypeptides are of high interest due to their easy tuning of the solution properties upon changing the temperature. In comparison to There are quite a few reports of the thermoresponsiveness of the synthetic polymers in nonaqueous solvent.²¹⁻²³ However, synthetic polypeptides exhibiting thermoresponsiveness in nonaqueous solvent are hardly reported.⁵⁹⁻⁶⁰ Thus synthesis of functionalized polypeptides and investigating their thermoresponsive properties in nonaqueous solvent would worthy of interest to the scientific community. Poly(L-glutamate) based thermoresponsive polypeptides are widely investigated by various research groups but most of them are in aqueous medium.^{11,30} In this case, PGlu-C_n(s) were found to be water insoluble but were soluble in CHCl₃ and THF, which remained transparent for a longer period at ambient temperature. A 2 wt% CHCl₃ solution of PGlu-C₁₂ also remained clear within a temperature range of – 65 to 50 °C, indicating the absence of any thermoresponsiveness within that temperature range. However, corresponding solution of PGlu-C₁₆ and PGlu-C₂₀ stayed clear at ambient or even high temperature (50 °C) but interestingly they became turbid when the solution temperature was dropped to – 35 °C (Figure 4.12). The turbid suspension became clear again upon heating and vice versa, exhibiting the reversible UCST-type thermoresponsiveness in CHCl₃. Figure 4.13A showed the gradual change of % transmittance of PGlu-C₁₆/PGlu-C₂₀ in CHCl₃ (2 wt%) from 98 to 10/~0 respectively on decreasing the temperature and vice-versa on increasing. The T_{cpS} (measured from the heating curve) were found to be – 9.1 and 3.6 °C for PGlu-C₁₆ and PGlu-C₂₀ respectively with a low hysteresis between the heating and cooling curves (see Table 4.2).

Similar phenomenon of UCST-type phase transitions was also observed in the THF solution (2 wt%) of copolypeptides also (Figure 4.13B). But unlike the CHCl₃ solution, 2 wt% THF solution of PGlu-C₁₂ showed turbid suspension

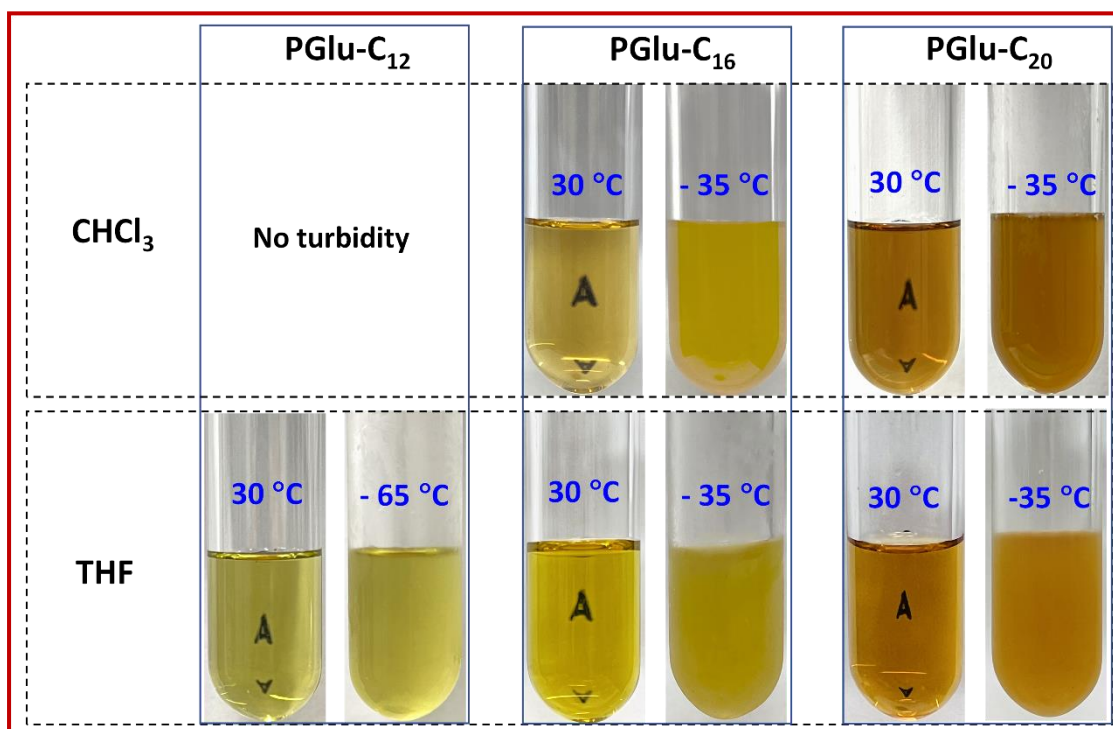


Figure 4.12. Photographs of the solutions (2 wt%) of the PGLu-C_n(s) in CHCl₃ and THF respectively, at different solution temperature, showing clear to turbid suspension formation upon decreasing the temperature.

formation on lowering the temperature to – 65 °C which again became clear on heating (Figure 4.12). T_{cp} of that 2 wt% PGLu-C₁₂, PGLu-C₁₆ and PGLu-C₂₀ solutions in THF was found to be – 32, – 5.8 and 22.5 °C respectively (Table 4.2). The UCST-type phase transition of all the copolypeptides in their respective solutions was reversible and could be repeated for at least 4 cycles (Figure A4.12). It is worth mentioning that Glu-C_n(s) didn't show any thermoresponsiveness neither in CHCl₃ nor in THF within the temperature range – 65 to 50 °C.

The UCST-type phase behaviour of the PGLu-C_n(s) in CHCl₃ and THF can be elucidated according to a previously reported explanation for the long chain alkyl substituted poly(vinyl imidazole).²¹ As described, above the UCST point all the PGLu-C_n(s) remained soluble in CHCl₃/THF due to greater extent of polymer-

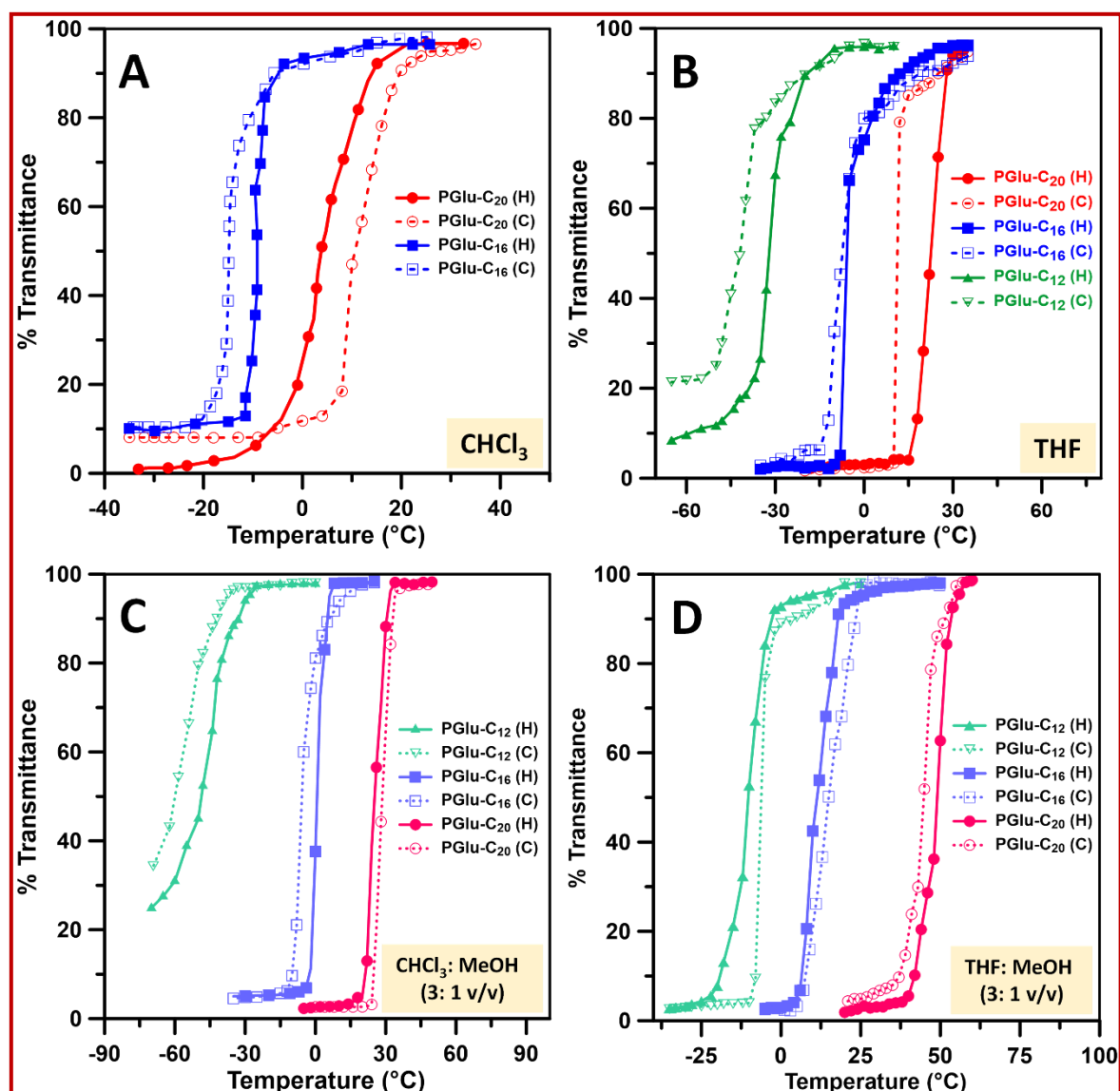


Figure 4.13. Turbidity plots of PGLu-C₁₆ and PGLu-C₂₀ solutions in CHCl₃ (2 wt%) (A) and of PGLu-C₁₂, PGLu-C₁₆ and PGLu-C₂₀ solutions in THF (2 wt%) (B). Turbidity plots of PGLu-C_n (n = 12, 16, 20) (2 wt%) in CHCl₃-MeOH mixture (3:1 v/v) (C) and in THF-MeOH mixture (3:1 v/v) (D). Solid and dashed lines represent heating and cooling curve respectively.

solvent interaction. But when the solution temperature was decreased to a certain level, intermolecular chain-chain interaction between the alkyl groups of the adjacent polypeptide molecules predominated over the polymer-solvent interaction restricting their free movement in the solution. This resulted in the

Table 4.2. Cloud points of PGlu-C₁₂, PGlu-C₁₆ and PGlu-C₂₀ obtained by the turbidimetric and calorimetric study in different solvents.

Sample name	Solvent	Phase transitions measured in UV-Vis spectrophotometer		Phase transitions measured in Micro-DSC	
		T_{cp} (°C) heating	T_{cp} (°C) cooling	T_{cp} (°C) heating	ΔH (J/g)
PGlu-C ₁₂	CHCl ₃	–	–	–	–
PGlu-C ₁₆		– 9.1	– 14.6	– 4.7	0.081
PGlu-C ₂₀		3.6	10.3	8.58	0.163
PGlu-C ₁₂	THF	– 32	– 40.0	–	–
PGlu-C ₁₆		– 5.5	– 7.2	9.3	0.208
PGlu-C ₂₀		22.5	11.8	24.8	0.343
PGlu-C ₁₂	CHCl ₃ -MeOH (3:1 v/v)	– 48.5	– 60		
PGlu-C ₁₆		0.5	– 5.2		
PGlu-C ₂₀		25.4	28.8		
PGlu-C ₁₂	THF-MeOH (3:1 v/v)	–10.1	–6.1		
PGlu-C ₁₆		11.3	15.1		
PGlu-C ₂₀		49.3	44.7		

aggregation of the copolypeptides into the nanogel making the solution turbid. The intermolecular hydrophobic interaction between the alkyl chains disappeared on heating and the solution became transparent again due to solvation. It could be assumed that grafting of the long alkyl groups on to the amphiphilic PGlu-Pr side chain reinforce the hydrophobicity of the overall polypeptide and the extent of hydrophobicity increases with increase in the alkyl chain length. This increase in the hydrophobicity also enhanced the extent of intermolecular hydrophobic interaction between the adjacent alkyl chains on cooling the solution temperature. Increase in the T_{cp} (Table 4.2) with increase in the alkyl chain length clearly supported our assumptions that interchain hydrophobic interactions are responsible for such UCST-type phase transition.

In case of THF solution, higher T_{cp} than in CHCl_3 (Table 4.2) can be attributed to the higher polarity of the THF than CHCl_3 . Here solvent polarity also plays an important role along with the intermolecular hydrophobic interaction in the T_{cp} of the PGlu- $\text{C}_n(\text{s})$. The polymer-solvent interaction between the hydrophobic copolypeptides and relatively more polar THF is quite low than in CHCl_3 . Thus, in THF intermolecular hydrophobic interactions between the alkyl chains got favoured easily over the polymer-solvent interactions and hence more energy is required to break this intermolecular hydrophobic interaction, resulting in the increase in the T_{cp} . To support this assumption, we have performed the turbidity experiment of the PGlu- $\text{C}_n(\text{s})$ in mixed solvents like CHCl_3 -MeOH (3:1 v/v) or THF-MeOH (3:1 v/v). It is to be noted that PGlu- $\text{C}_n(\text{s})$ are insoluble in MeOH and addition of excess MeOH caused a complete phase separation to a solid (polymer) and a liquid (solvent). Figure 4.13 showed the turbidity plots of PGlu- $\text{C}_n(\text{s})$ in CHCl_3 -MeOH (Figure 4.13C) and THF-MeOH (Figure 4.13D) mixture. It is clear from the plots and Table 4.2 that T_{cp} of 2 wt% PGlu- $\text{C}_n(\text{s})$ in those mixed solvents are higher than that of in CHCl_3 and THF respectively (Table 4.2). Again, it is worth mentioning

that PGlu-C₁₂ exhibit observable thermoresponsiveness in CHCl₃-MeOH mixture (Figure 4.13C) unlike in CHCl₃ only. These results were evident that T_{cp} of the PGlu-C_n(s) could be regulated by changing the polarity of the solvent.

The enthalpy of phase transition of the PGlu-C_n(s) also increased with the increase in the chain length of the alkyl groups, and it is higher in THF than CHCl₃ as obtained from the micro-DSC (Figures 4.14A and 4.14B and Table 4.2).

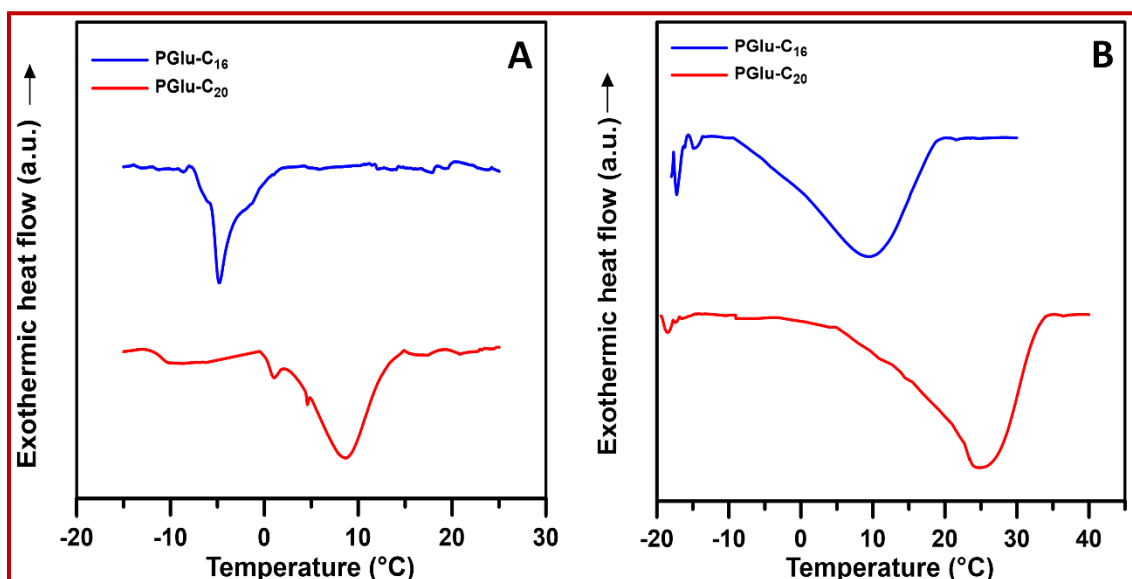


Figure 4.14. Micro-DSC thermograms of PGlu-C₁₆ and PGlu-C₂₀ in CHCl₃ (A) and in THF (B).

Calorimetric measurements of 2 wt% PGlu-C₁₆ and PGlu-C₂₀ in CHCl₃ (Figure 4.14A) showed exothermic peaks at -4.77 and 8.58 °C respectively and at 9.3 and 24.8 °C in THF respectively (Figure 4.14B). These values are almost close to the corresponding T_{cp} of the PGlu-C₁₆ and PGlu-C₂₀ in the respective solvents as obtained by turbidimetry (Table 4.2). These results also suggested that T_{cp} can be tuned by changing the chain length of the alkyl groups as well as solvent polarity. However, we didn't observe any calorimetric phase transition of PGlu-C₁₂ in CHCl₃ and THF within the temperature range -30 to 50 °C.

The nanogel aggregates of P_{Glu}-C₂₀ and P_{Glu}-C₁₆ formed below their cloud points in CHCl₃ and THF were also examined by FESEM. FESEM images (Figure 4.15) showed the formation of aggregates of somewhat dendritic morphology of P_{Glu}-C₂₀ in CHCl₃ (Figure 4.15A). But we observed a kind of fibrillar morphology for the P_{Glu}-C₂₀ aggregates in THF (Figure 4.15B). Whereas P_{Glu}-C₁₆ formed globular aggregates, which seemed to be agglomerated during sample preparation in both solvents below UCST (Figures 4.15C-4.15D).

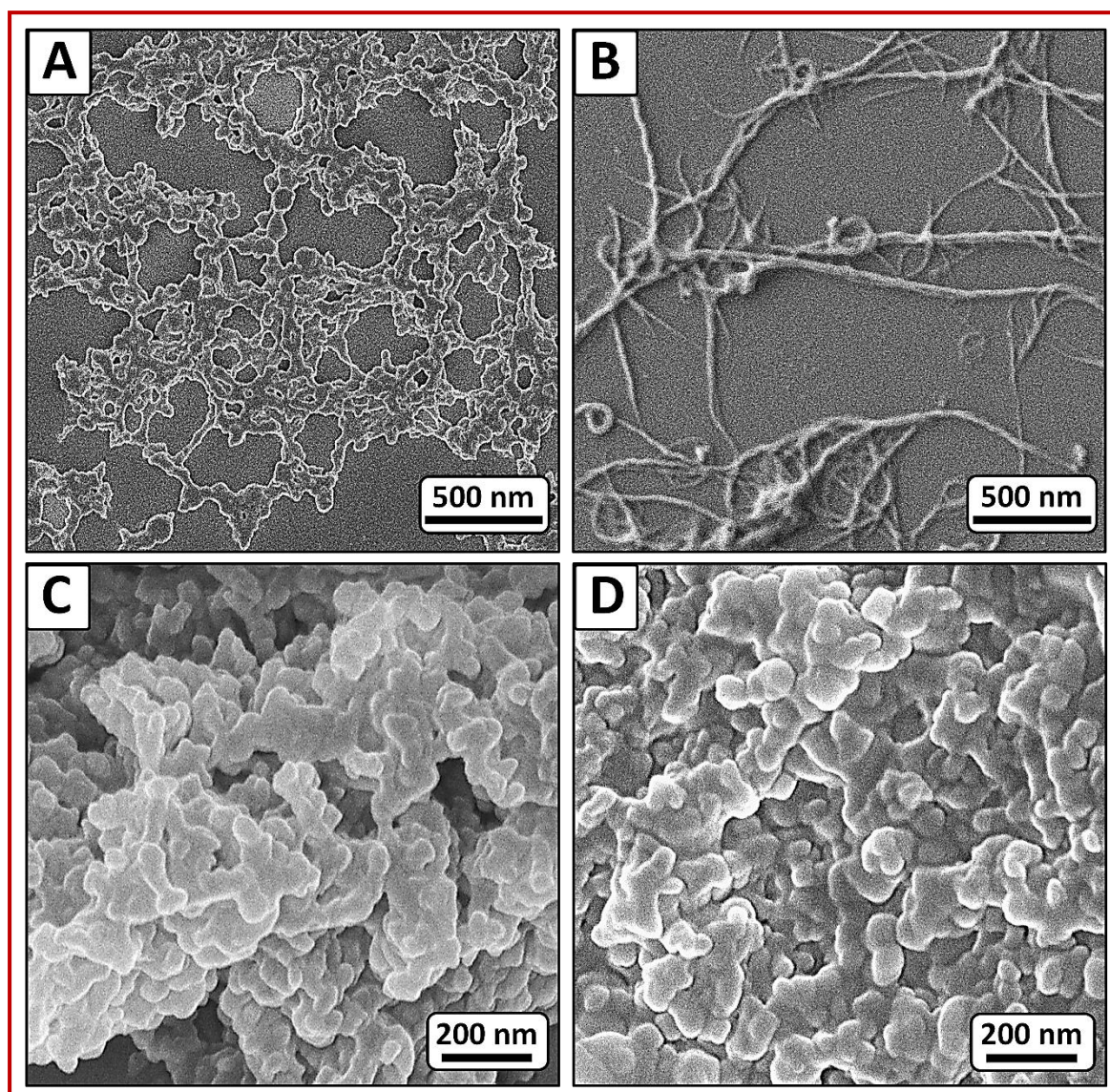


Figure 4.15. FESEM images showing formation of nanogel aggregates by P_{Glu}-C₂₀ in CHCl₃ (A) and in THF (B) below the UCST cloud point. Image C and D show the globular aggregates formation by P_{Glu}-C₁₆ in CHCl₃ and THF below the UCST respectively.

It is also likely that the extent of the hydrophobic interaction between the alkyl chains would be greater in P Glu-C_{20} than in P Glu-C_{16} . Thus, the physical crosslinking among polypeptide chains would also be higher in P Glu-C_{20} than P Glu-C_{16} . However, we couldn't be able to examine the morphology of the P Glu-C_{12} below the UCST because of its very low cloud point (Table 4.2).

4.4.3. Crystalline Properties of The $\text{Glu-C}_n(\text{s})$ and $\text{P}\text{Glu-C}_n(\text{s})$

TGA and DSC study

To assess the thermal stability of $\text{Glu-C}_n(\text{s})$ and $\text{P}\text{Glu-C}_n(\text{s})$, TGA was performed under a nitrogen atmosphere. The analysis of their respective thermograms (Figure 4.16) indicated that the majority of the samples exhibited no noticeable weight loss within the temperature range of 30-200°C. All samples demonstrated significant thermal stability up to 260°C, with weight loss becoming apparent beyond this temperature. The decomposition process was observed to occur in a single step, reaching completion near 600°C. Notably, after the experiment, it was observed that the residual mass (%) of all $\text{P}\text{Glu-C}_n(\text{s})$ samples were higher compared to that of $\text{Glu-C}_n(\text{s})$ samples, indicating their higher thermal stability.

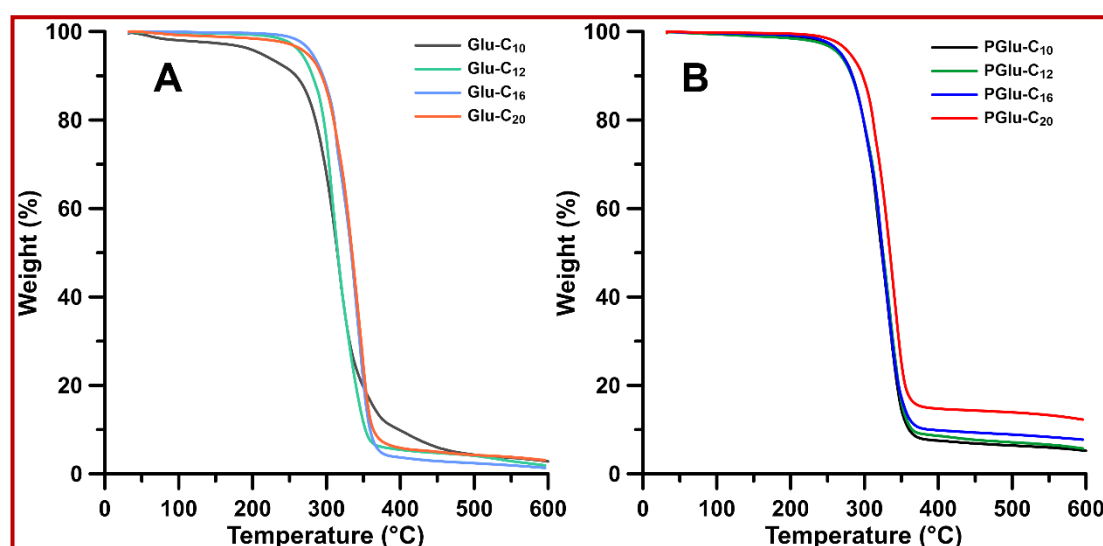


Figure 4.16. TGA thermograms of the $\text{Glu-C}_n(\text{s})$ (A) and $\text{P}\text{Glu-C}_n(\text{s})$ (B) ($n = 10, 12, 16, 20$).

P_{Glu}-C_n(s) and the control Glu-C_n(s) samples would expect to exhibit semicrystalline behaviour in the bulk state due to the presence of long alkyl chains. DSC study of the P_{Glu}-C_n (n = 10, 12, 16, 20) as well as Glu-C_n (n = 10, 12, 16, 20) were carried out to investigate their thermodynamic properties such as melting temperature (T_m), crystallization temperature (T_c) and their corresponding change in enthalpy i.e., enthalpy of melting (ΔH_m) and enthalpy of crystallization (ΔH_c) respectively.

Figure 4.17A displays the DSC thermograms of Glu-C_n(s) (n = 10, 12, 16, 20), revealing the presence of both exothermic and endothermic peaks attributed to the crystallization (T_c) of Glu-C_n(s) molecules and the melting (T_m) of the formed Glu-C_n(s) crystals.

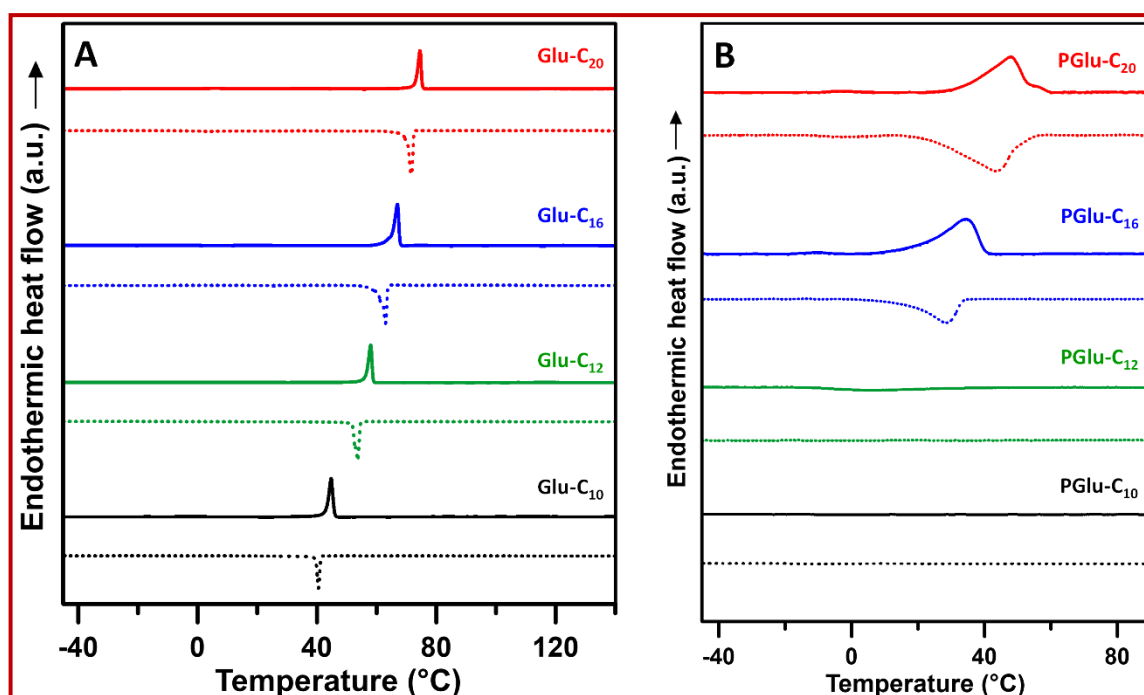
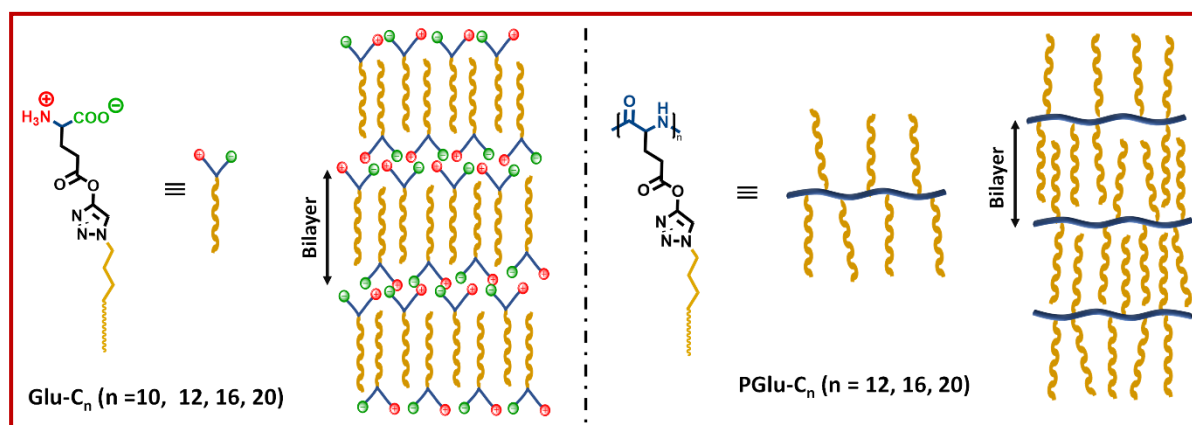


Figure 4.17. DSC thermograms of the Glu-C_n(s) (A) and P_{Glu}-C_n(s) (B) showing crystallization (dashed line) and melting (solid line) peaks.

Upon cooling from the melt, Glu-C_n(s) molecules organized themselves into crystal phases with a bilayer structure, facilitated by hydrophobic interactions among the long hydrocarbon chains (Scheme 4.4). Table 4.3 demonstrates an



Scheme 4.4. Schematic representation for the possible packing of the Glu-C_n(s) (left) and PGLu-C_n(s) (right) molecules in the crystalline phase.

Table 4.3. Thermodynamic data of Glu-C_n(s) and PGLu-C_n(s) as obtained from the DSC.

Sample name	Melting temperature (T_m) (° C) ^a	ΔH_m (J/g)	Crystallization temperature (T_c) (° C) ^b	ΔH_c (J/g)
Glu-C ₁₀	44.8	38.1	40.5	25.6
Glu-C ₁₂	58	48.3	53.7	48.2
Glu-C ₁₆	67	55.6	63	52.1
Glu-C ₂₀	75	67.4	72	64.6
PGLu-C ₁₀	-	-	-	-
PGLu-C ₁₂	-	-	-	-
PGLu-C ₁₆	34.5	20.8	28.5	19.2
PGLu-C ₂₀	47.9	45.6	43.4	43.6

^a Measured from the second heating run.

^b Measured from the first cooling run.

increasing trend in T_c and ΔH_c as the length of the alkyl groups increases. This can be attributed to the enhanced hydrophobic interactions among the alkyl chains, resulting in more efficient packing of molecules into bilayer structures from Glu-C₁₀ to Glu-C₂₀. During the heating scan, all compounds exhibited a distinct endothermic peak (Figure 4.17A) corresponding to the melting of crystals formed in the solid state during slow cooling. T_m and the enthalpy of melting (ΔH_m) were found to increase with the length of the alkyl chain in Glu-C_n(s) (Table 4.3). The increase in hydrophobic chain-chain interactions, attributed to the longer alkyl chains, facilitated the formation of more compact crystals through dense packing of Glu-C_n(s) molecules. Consequently, such compact crystals required higher temperatures and exhibited higher ΔH_m during melting. It is worth noting that beyond the melting of Glu-C_n(s), no other mesomorphic transitions were detected. Similar bilayer arrangements of molecules with pendant long alkyl chains have been reported to form such types of crystals in previous studies.^{21,40-41}

Since PGlu-C_n(s) also bears the same alkyl groups in their side chains, thus it was expected that those polymers also can arrange themselves into bilayer fashion (Scheme 4.4). DSC thermograms of PGlu-C₁₆ and PGlu-C₂₀ in Figure 4.17B indeed showed exothermic peaks at 28.5/43.4 °C and endothermic peaks at 34.5/47.9 °C respectively due to the crystallization and melting. The reason for such crystalline behaviour is some sort of regular arrangements of polypeptide molecules driven by the hydrophobic interactions among the pendent long alkyl chains. However, PGlu-C₁₀ and PGlu-C₁₂ didn't show any such peaks in their respective DSC thermograms, which is ascribed to the absence of any measurable crystallinity. This is quite obvious as the weak hydrophobic interactions among the relatively short C10 and C12 chains of PGlu-C₁₀ and PGlu-C₁₂ molecules respectively in melt would not be able to organizes themselves into crystal lattice during slow cooling. It is to be noted again that both T_c and T_m of PGlu-C₁₆ and PGlu-C₂₀ were low compared to their

monomeric moieties (i.e., Glu-C₁₆ and Glu-C₂₀) (Table 4.3). Enthalpy of crystallization and melting were also found to be significantly low in case of PGlu-C₁₆ and PGlu-C₂₀ compared to Glu-C₁₆ and Glu-C₂₀, suggesting that their lower crystallization after polymerization. It is reported that freedom of long alkyl chains to form tight packing through noncovalent hydrophobic interaction would be limited in polymers than in their monomeric form.⁴² This resulted in the loose packing of the alkyl chains in the polymers, imparting low crystallinity as shown in Scheme 4.4. It has been reported that arrangement of the pendant alkyl chains into bilayer structures imparts crystallinity into some polymers forming lamellar morphology.²¹ In our case also the crystallinity of the PGlu-C₁₆ and PGlu-C₂₀ arose due to the partial arrangement of the alkyl chains into bilayer structures through noncovalent hydrophobic interactions (Scheme 4.4). As the extent of crystallization also increases with increase in the length of the alkyl groups, thus it is expected that crystallization and melting temperature of the PGlu-C₁₆ and PGlu-C₂₀ would also increase accordingly. Table 4.3 clearly showed that T_c , T_m , and enthalpy change (ΔH_c , ΔH_m) for the PGlu-C₁₆ and PGlu-C₂₀ increased with the increase in the length of the pendant alkyl groups, which is ascribed to the higher extent of the inter chain hydrophobic interactions as described earlier. It is worth mentioning that PGlu-Pr didn't show any crystalline arrangements as confirmed by the DSC experiment (Figure A4.13).

POM study

The crystal morphologies of the Glu-C_n(s) and PGlu-C_n(s) were determined by the POM study. All the Glu-C_n(s) (n = 10, 12, 16, 20) showed a dark image (Figure 4.18) in POM at a temperature much above their respective melting temperature. The dark images were due to the formation of isotropic molten phase. When they were cooled down to a particular temperature, POM images showed the formation of crystals with plumose type morphologies (Figures 4.19A-4.19D). The crystals of Glu-C₂₀ and Glu-C₁₆ were found to be denser and

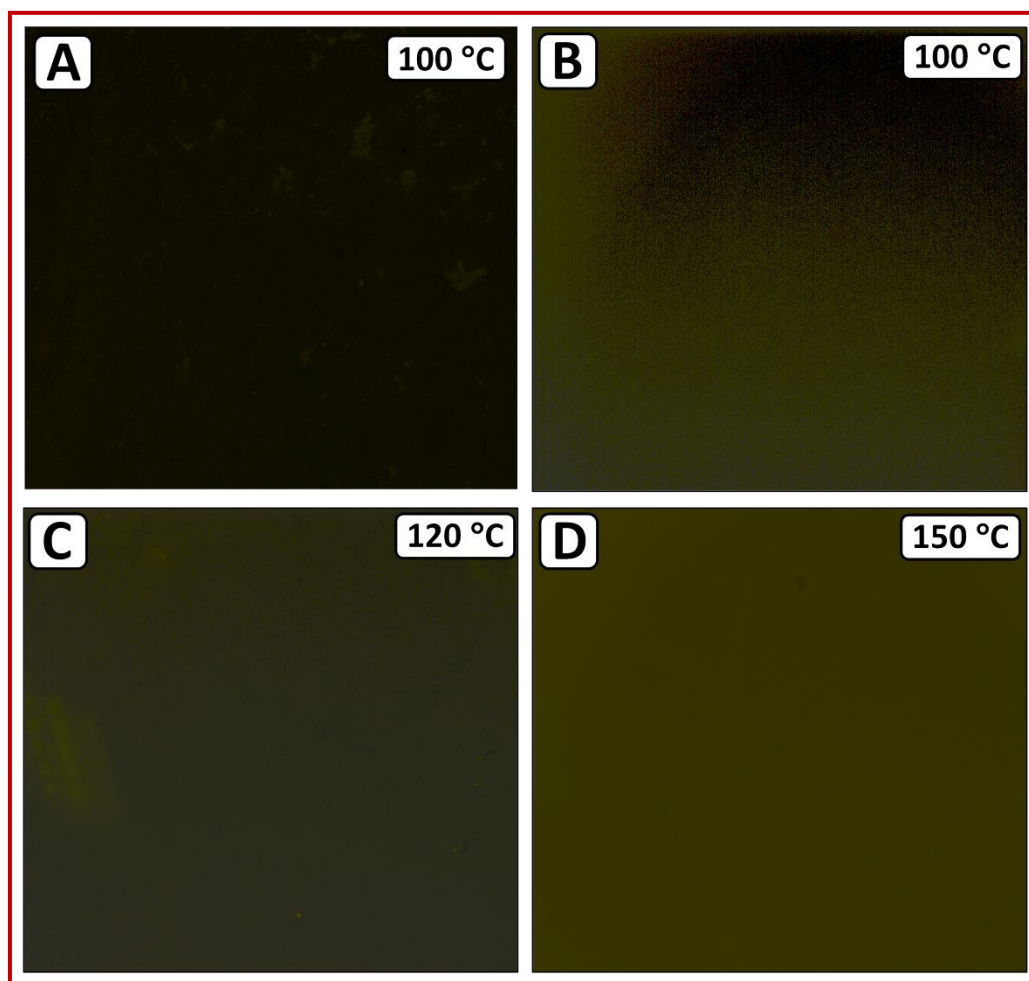


Figure 4.18. POM images of Glu-C₁₀ (A), Glu-C₁₂ (B), Glu-C₁₆ (C) and Glu-C₂₀ (D) much above their respective melting temperature.

more compact compared to those of Glu-C₁₀ and Glu-C₁₂. This suggests that the longer alkyl chains (C₁₆ and C₂₀) packed more tightly in the bilayer structure, resulting in denser crystals. However, PGlu-C_n(s) (n = 10, 12, 16, 20) samples exhibited the formation of birefringent crystals with a fibrillar texture (Figures 4.19E-4.19H). Similar fibrillar crystals were observed in previous studies involving imidazolium-based poly(ionic liquid)s with long alkyl chains.²¹ The fibrillar texture was less pronounced for PGlu-C₁₂ but became more clearly visible for PGlu-C₁₆ and PGlu-C₂₀. This is attributed to the relatively dense packing of C₂₀ chains in the bilayer structure of PGlu-C₂₀, leading to the formation of prominent crystals with a fibrillar texture. Interestingly, PGlu-C₁₂

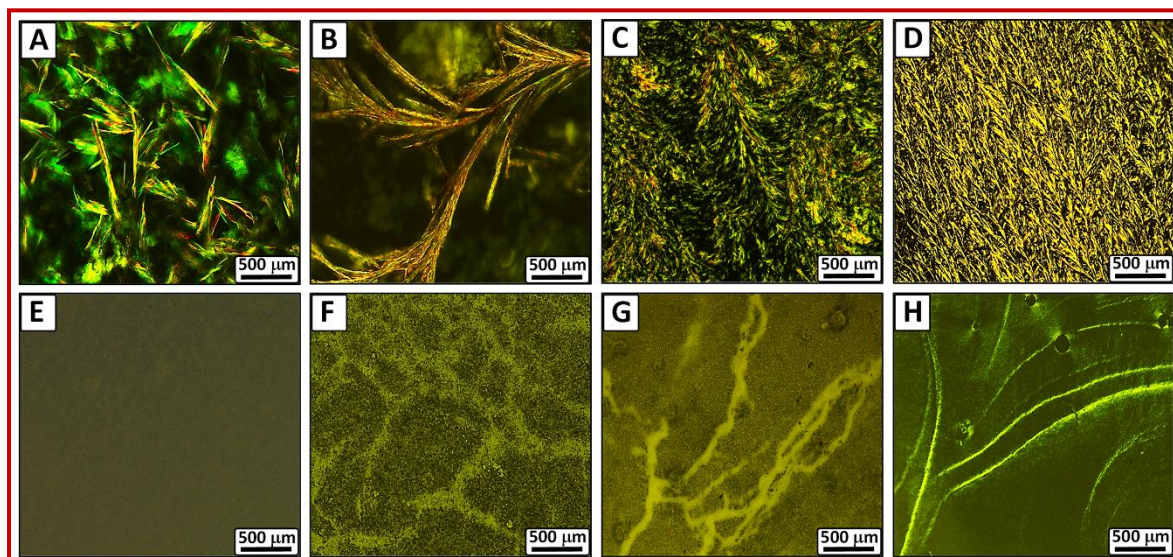


Figure 4.19. POM images of crystallized Glu-C_n(s) (A-D) and PGLu-C_n(s) (E-H) captured using a 20X and 10X objective lens respectively. Glu-C₁₀ (A), Glu-C₁₂ (B), Glu-C₁₆ (C), Glu-C₂₀ (D), PGLu-C₁₀ (E), PGLu-C₁₂ (F), PGLu-C₁₆ (G) and PGLu-C₂₀ (H).

did not exhibit any peaks in the DSC thermogram (Figure 4.17B), indicating the absence of a clear crystalline transition. However, it did show a weak birefringent crystalline phase when observed under POM (Figure 4.19F), suggesting the presence of some feeble crystalline arrangements. On the other hand, PGLu-C₁₀ did not show any peaks in the DSC thermogram (Figure 4.17B) and did not exhibit a birefringent fibrillar crystal structure under POM (Figure 4.19E). This implied that a minimum alkyl chain length of C12 is required to observe any organized crystalline arrangements of the PGLu-C_n chains.

PXRD study

In order to gain further understanding of the crystallinity, low and wide angle PXRD analysis of the control Glu-C_n(s) samples were conducted (Figure 4.20). The low angle pattern revealed two prominent peaks: one at around $2\theta = 2.9\text{-}3.5$ degree with relatively high intensity, indicating the presence of ordered lamellar structures in the crystals, and another weaker peak in the range of 2θ

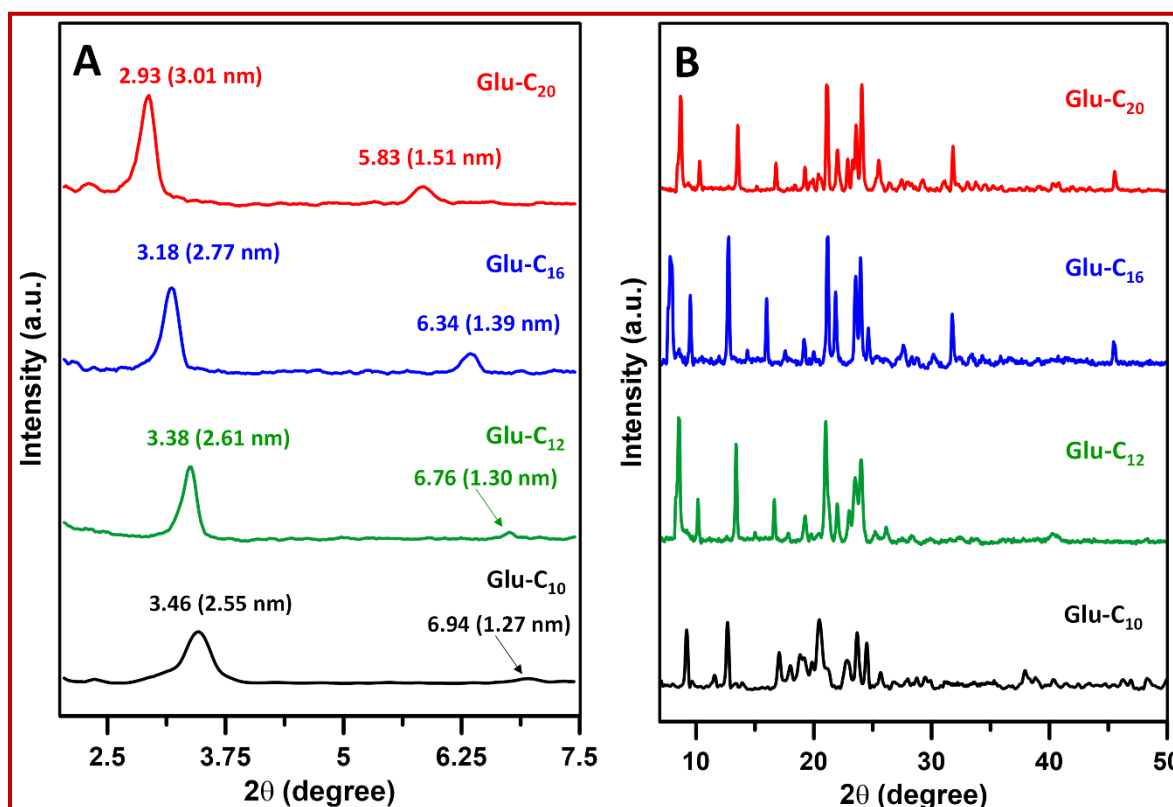


Figure 4.20. Low (A) and wide angle (B) XRD plots of Glu-C₁₀, Glu-C₁₂, Glu-C₁₆ and Glu-C₂₀.

= 5.8-7.0 degree (Figure 4.20A). As progressed from Glu-C₁₀ to Glu-C₂₀ these peaks gradually shifted towards lower angles (Figure 4.20A and Table 4.4). The corresponding *d*-spacing values, summarized in Table 4.4, showed a nearly linear increase with the length of the alkyl chain attached to the glutamate molecule. Notably, the *d*-spacing for the first peak in the low angle region was found to be approximately twice that of the second peak. These findings suggested the formation of similar ordered arrangements in the Glu-C_n(s) crystal lattice, with variations in alkyl chain length.

The wide angle PXRD patterns of Glu-C_n(s) exhibited multiple sharp peaks (Figure 4.20B), although their interpretation was challenging due to their complex nature. The degree of crystallinity was observed to increase as the alkyl chain length increased from Glu-C₁₀ to Glu-C₂₀, primarily attributed to

higher molecular packing density in the bilayer structured crystals (Table 4.4). In contrast, the PGlu-C_n(s) samples displayed a broad peak in the wide angle range of 2θ = 19-22 degrees, instead of distinct sharp peaks. Specifically, PGlu-C₁₀, PGlu-C₁₂, PGlu-C₁₆, and PGlu-C₂₀ exhibited broad peaks at 2θ = 19.6, 20.5, and 20.9 degrees, respectively, and the broadness decreased with longer alkyl chains (Figure 4.21).

Table 4.4. PXRD analysis data of the Glu-C_n(s) and PGlu-C_n(s) (n = 12, 16, 20) at room temperature.

Sample name	2θ (degree) (small angle)		<i>d</i> -spacing (nm)		Degree of crystallinity (<i>X_c</i>) (%) (PXRD) ^a
	1 st peak	2 nd peak	1 st peak	2 nd peak	
Glu-C ₁₂	3.46	6.94	2.55	1.27	55.6
Glu-C ₁₂	3.38	6.76	2.61	1.30	61
Glu-C ₁₆	3.18	6.34	2.77	1.39	71.4
Glu-C ₂₀	2.93	5.83	3.01	1.51	78.8
PGlu-C ₁₀	-	-	-	-	15.5
PGlu-C ₁₂	-	-	-	-	23.1
PGlu-C ₁₆	-	-	-	-	34
PGlu-C ₂₀	-	-	-	-	37.9

^a Degree of crystallinity (*X_c*) (%) = $[A_c / (A_c + A_a)] \times 100$

A_c = Area of all the crystalline peaks, *A_a* = Area of the amorphous peaks and (*A_c* + *A_a*) is the total area of the plot as obtained from the PXRD.

This broad peak suggests a predominantly amorphous nature of the PGlu-C_n(s) samples, with very low crystallinity, as supported by the corresponding DSC results (Figure 4.17B and Table 4.3). Table 4.4 also illustrates the significantly lower degree of crystallinity in the PGlu-C_n(s) samples compared to their control counterparts, with an increase observed as the length of the pendant alkyl groups increased, mirroring the trend observed in the control samples.

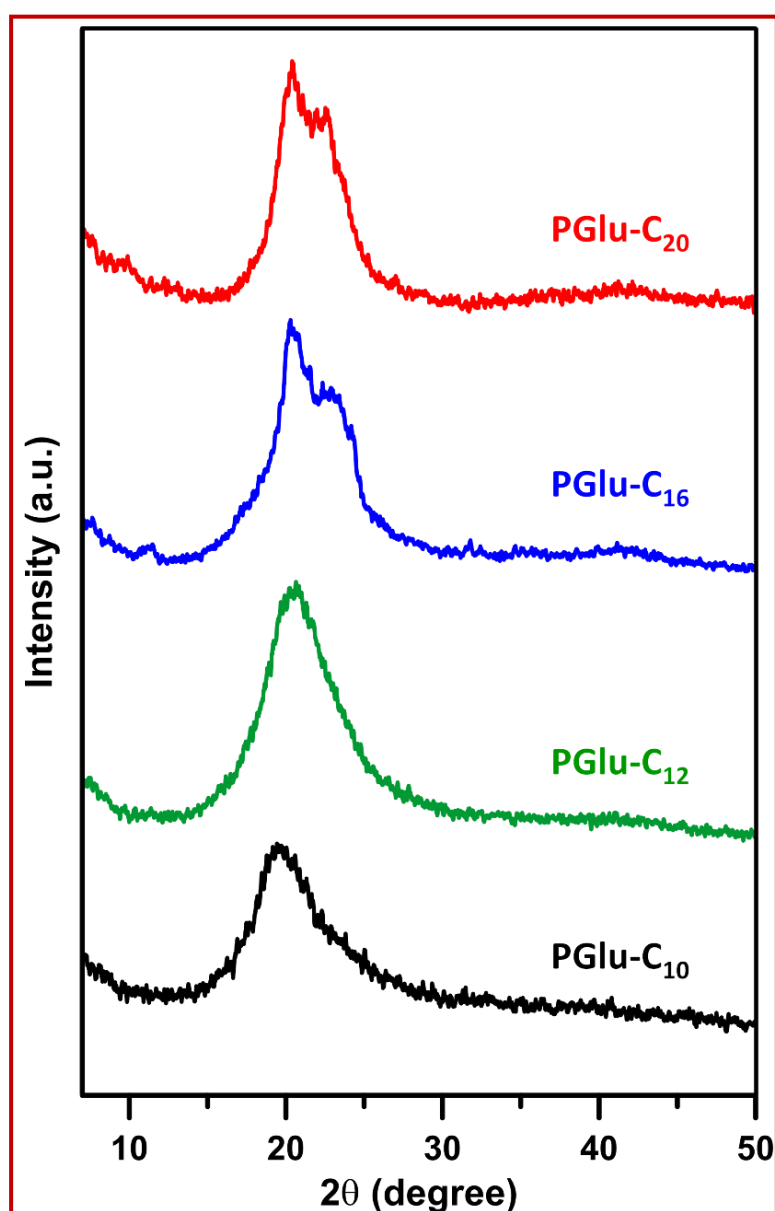


Figure 4.21. Wide-angle XRD patterns of the PGlu-C_n(s) at room temperature.

4.4.4. Self-Assembly of The PGlu-C_n(s) (n= 12, 16, 20)

Synthetically prepared functionalized polypeptides consisting of a polar amide backbone can be hydrophilic, hydrophobic, or amphiphilic depending on the nature of their side chains. They can undergo self-assembly in solution through well-defined interaction (H-bonding, hydrophobic interaction, electrostatic interaction etc.) to form different self-assembled nanostructures (micelle, vesicle etc.) which can further organize themselves into hierarchical structures.⁵¹⁻⁵² In this case, PGlu-C_n(s) (n = 12, 16, 20) were found to be hydrophobic in nature due to having long alkyl side chains. Their self-assembly was studied in nonaqueous media like CHCl₃ and THF.

DLS analysis of 0.5 wt% solutions of PGlu-C_n(s) (n = 12, 16, 20) in both CHCl₃ (Figure 4.22A) and THF (Figure 4.22B) showed the presence of small- and large-sized aggregates with varying D_h s, as summarized in Table 4.5.

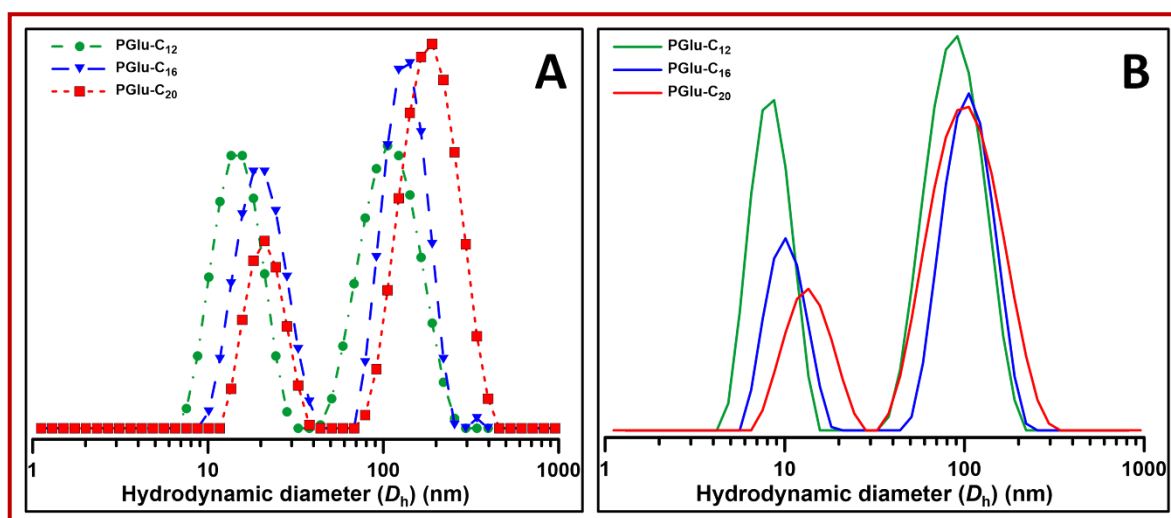


Figure 4.22. Intensity average particle size distribution of the PGlu-C_n(s) (n = 12, 16, 20) in CHCl₃ (A) and in THF (B) as observed from DLS.

Notably, the D_h s of PGlu-C_n(s) aggregates in both solvents increased with the length of the associated alkyl groups. However, the D_h s of both small and large particles in THF were lower compared to those formed in CHCl₃. This

observation can be attributed to the hydrophobic nature of PGlu-C_n(s), which results in better solvation in the nonpolar CHCl₃ compared to the polar THF. Consequently, the solvated PGlu-C_n(s) aggregates exhibited higher D_h s in CHCl₃ than in THF. As expected, the scattering intensity of the large aggregates was higher than that of the smaller ones.

Table 4.5. Particle size distribution of PGlu-C_n(s) (n = 12, 16, 20) in different solvents as observed from DLS and TEM study

Sample	Solvent	D_h (DLS) (nm)		D_h (TEM) (nm)	
		Small	Large	Small	Large
PGlu-C ₁₂	CHCl ₃	14.6	111.0	~9	~100
PGlu-C ₁₆		19.8	137.6	~10	~107
PGlu-C ₂₀		20.9	189.7	~10	~120
PGlu-C ₁₂	THF	8.6	91.9	~7	~90
PGlu-C ₁₆		10.1	104.2	~8	~100
PGlu-C ₂₀		13.5	109.8	~8	~100

It was postulated that the small particles represent the primary units of aggregation for PGlu-C_n(s) molecules in CHCl₃. These unit-aggregates further underwent secondary aggregation to form composite aggregates with larger D_h (s). The secondary aggregation process is driven by intermolecular hydrophobic interactions between the alkyl groups of functionalized polyglutamate. This secondary aggregation occurs rapidly and incessantly, potentially reaching an equilibrium state as the particle sizes of the PGlu-C_n(s) aggregates didn't change over time. Similar types of secondary aggregation in the self-assembly of amphiphilic polypeptides forming various nanoaggregates have been previously reported elsewhere.^{8,26,67}

FESEM images of a representative alkyl-polyglutamate, PGlu-C₁₆, in both CHCl₃ and THF solutions (0.5 wt%), confirmed the formation of spherical aggregates with diameters of approximately 10-20 nm and 100-150 nm, respectively, in line with the DLS results (Figure 4.23).

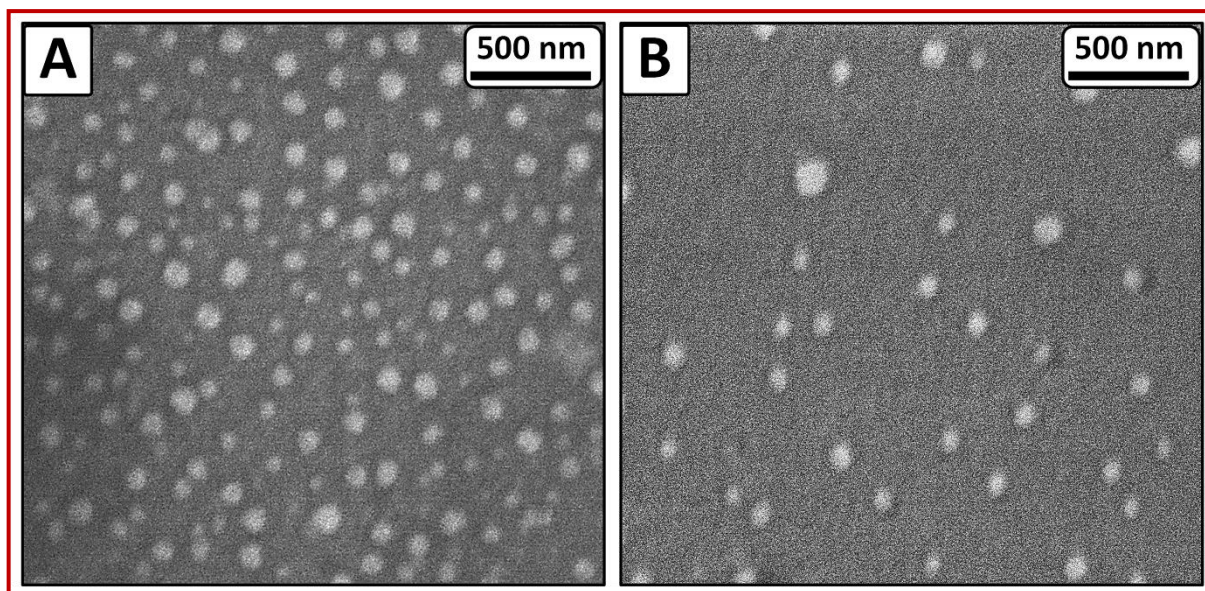


Figure 4.23. FESEM images of the PGlu-C₂₀ aggregates in CHCl₃ (A) and in THF (B).

TEM images clearly revealed that these spherical entities were vesicular aggregates of PGlu-C_n(s) molecules formed through self-assembly in CHCl₃ and THF, respectively (Figure 4.24). Figure 4.24 exhibited the presence of both smaller-sized unit vehicles and large vesicles formed through their secondary aggregation, with diameters ranging from approximately 7-10 nm and 90-120 nm for PGlu-C_n(s) in CHCl₃ (Figures 4.24A-4.24C) and THF (Figures 4.24D-4.24F), respectively. These findings aligned well with the DLS results (Figure 4.22). While there have been reports on vesicle formation by different amphiphilic polypeptides, most of them have been observed in aqueous media. Limited reports exist on the vesicular self-assembly of functionalized polypeptides in non-aqueous media.⁸

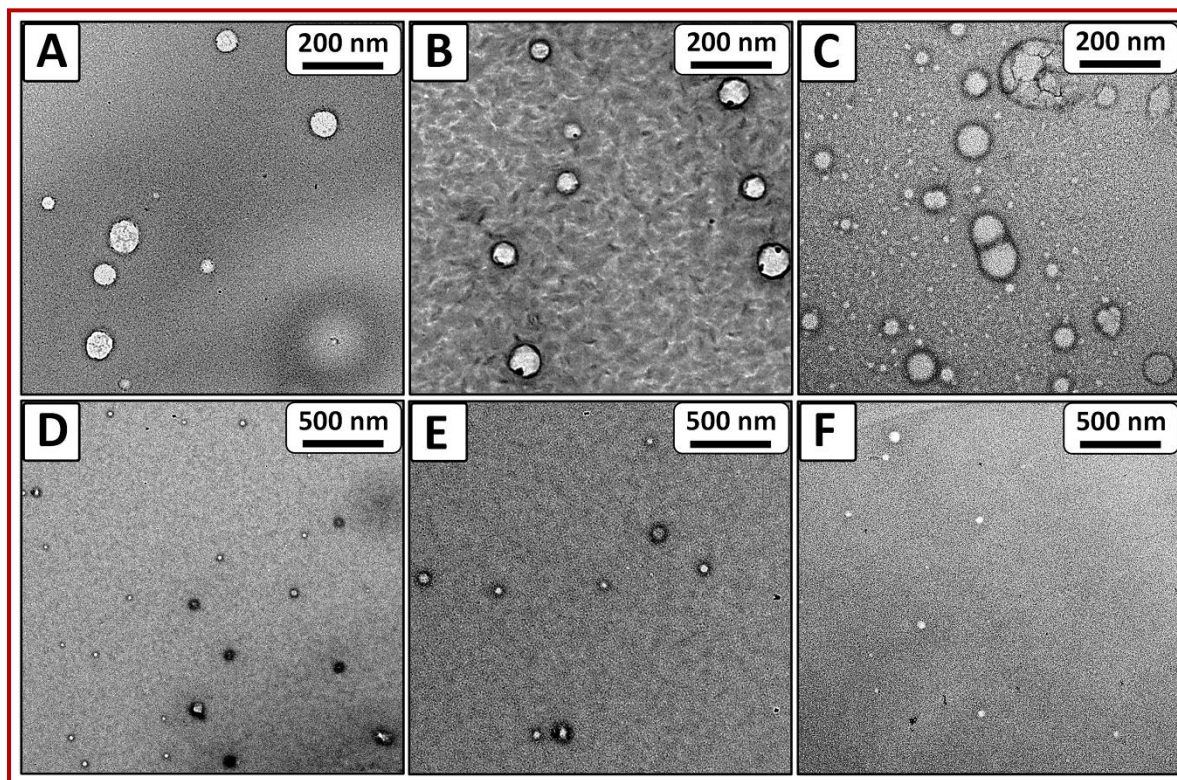
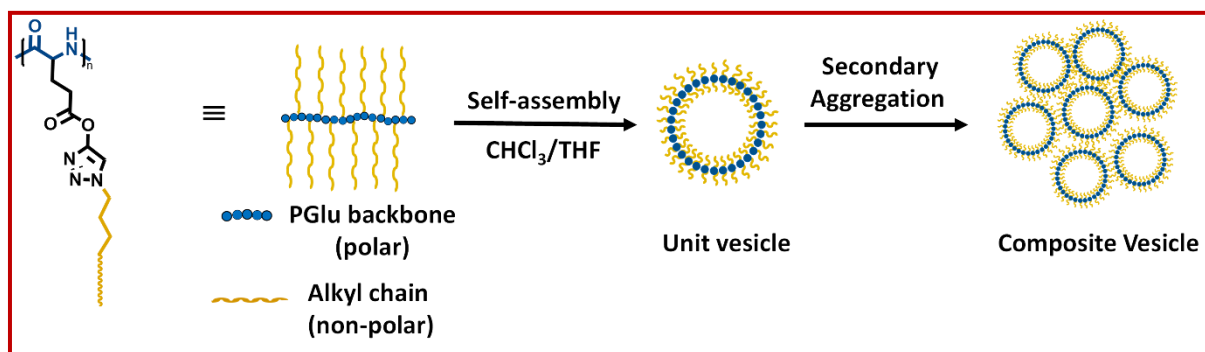


Figure 4.24. Vesicular aggregates formed by the self-assembly of PGLu-C_n(s) ($n = 12, 16, 20$) in CHCl₃ (A-C) and THF (D-F) as observed by TEM study. Images from CHCl₃: PGLu-C₁₂ (A), PGLu-C₁₆ (B) and PGLu-C₂₀ (C); Images from THF: PGLu-C₁₂ (D), PGLu-C₁₆ (E) and PGLu-C₂₀ (F).

However, none of them involve structurally hydrophobic functionalized polypeptides with pendant long alkyl groups. Nonetheless, a few reports have demonstrated that polymeric amphiphiles with relatively high hydrophobicity tend to aggregate into vesicles through self-assembly in solution.⁶⁸ Based on these reports, a possible mechanism for the formation of these vesicles of PGLu-C_n(s) in non-aqueous media was proposed (Scheme 4.5). As mentioned earlier, the primary aggregation of PGLu-C_n(s) molecules in CHCl₃ and THF initially leads to the formation of small-sized unit vesicles. These unit vesicles then undergo hydrophobic-interaction-driven secondary aggregation, resulting in the formation of relatively large composite vesicles.



Scheme 4.5. Probable mechanism of formation of unit and composite vesicles of PGLu-C_n(s) ($n = 12, 16, 20$) in solution.

4.4.5. Dye Encapsulation by PGLu-C_n vesicles

PGLu-C_n(s) molecules underwent self-assembly in different solvents such as CHCl₃ and THF, forming vesicular nanoaggregates. These nanoaggregates were capable of encapsulating organic dye from a solution. For the dye uptake study, EB was selected as a model dye and tested with PGLu-C₁₆ aggregates in CHCl₃. EB, being hydrophilic and sparingly soluble in nonpolar solvents like CHCl₃, exhibited negligible absorption (Figure 4.25A).

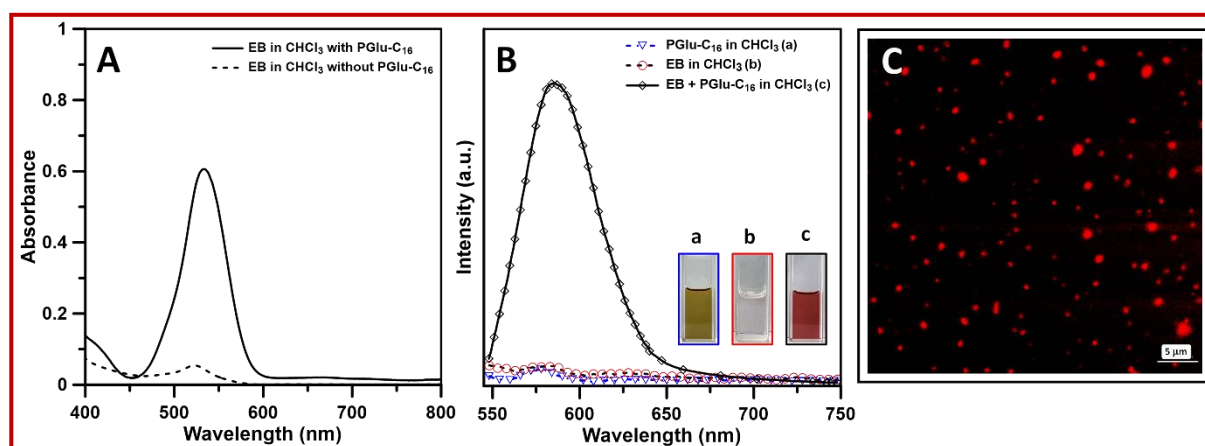


Figure 4.25. Absorption (A) and emission (B) spectra of EB with and without the presence of PGLu-C₁₆ in CHCl₃. Fluorescence confocal microscopic image of the EB-loaded PGLu-C₁₆ vesicular nanoaggregates (C).

But in the presence of PGlu-C₁₆, displayed an enhanced absorption peak at $\lambda_{\max} = 532$ nm (Figure 4.25A). Furthermore, the emission spectra of EB in CHCl₃ demonstrated a distinct, intense peak at $\lambda_{\max} = 585$ nm when PGlu-C₁₆ was present (Figure 4.25B). However, the solution of PGlu-C₁₆ alone in CHCl₃ did not exhibit any emission peak. Additionally, the colour of PGlu-C₁₆ solution in CHCl₃ changed from olive green to brick red, as depicted in the inset of Figure 4.25B. Fluorescence confocal microscopic imaging (Figure 4.25C) confirmed the encapsulation of EB molecules within the PGlu-C₁₆ vesicles. It is assumed that the hydrophilic EB was encapsulated within the bilayered-wall of the PGlu-C₁₆ vesicles, which is expected to consist of a relatively polar PGlu backbone (Scheme 4.5).

4.5. Conclusion

Poly(L-glutamate)s functionalized with alkyl side chains of different lengths [PGlu-C_n(s), n = 10, 12, 16, 20] were successfully synthesized through the ring-opening polymerization of as-synthesized γ -propargyl L-glutamate NCA, followed by post-polymerization modification using 'click reaction' with corresponding as-synthesized alkyl azides. CD and FT-IR studies confirmed that PGlu-C_n(s) adopted an α -helical conformation and fraction of helicity decreased with increase in the length of the alkyl chains. The introduction of alkyl groups endowed PGlu-C_n(s) with UCST-type thermoresponsive behaviour in CHCl₃ and THF solutions, with tunable cloud points with respect to the pendant alkyl chain length and solvent polarity. In contrast, their monomeric analogues, Glu-C_n(s), did not exhibit such thermoresponsiveness in CHCl₃ and THF. The presence of long alkyl chains in Glu-C_n(s) led to the formation of highly birefringent plumose-type crystals, suggesting an ordered bilayer arrangement of the molecules. However, PGlu-C_n(s) formed low birefringent fibrillar texture-type crystals (for PGlu-C₂₀, PGlu-C₁₆, and PGlu-C₁₂) due to the bilayer arrangement of the side alkyl chains. Only PGlu-C₂₀ and PGlu-C₁₆ exhibited distinct crystallization and melting peaks, whereas PGlu-C₁₂ and PGlu-C₁₀ formed loosely packed crystals without observable peaks. The Glu-C_n(s) samples displayed well-defined T_c and T_m values, which increased with longer alkyl chain lengths. PGlu-C_n(s) molecules formed small primary nanostructures that further aggregated into large composite particles in CHCl₃ and THF. TEM studies confirmed the vesicular nanostructure formation of PGlu-C_n(s) in both solvents. A proof of concept was successfully demonstrated for the encapsulation of an organic dye (Eosin B) within PGlu-C_n(s) vesicles, as confirmed by fluorescence and confocal microscopic studies.

4.6. Appendix: Characterization and Other Experimental Data

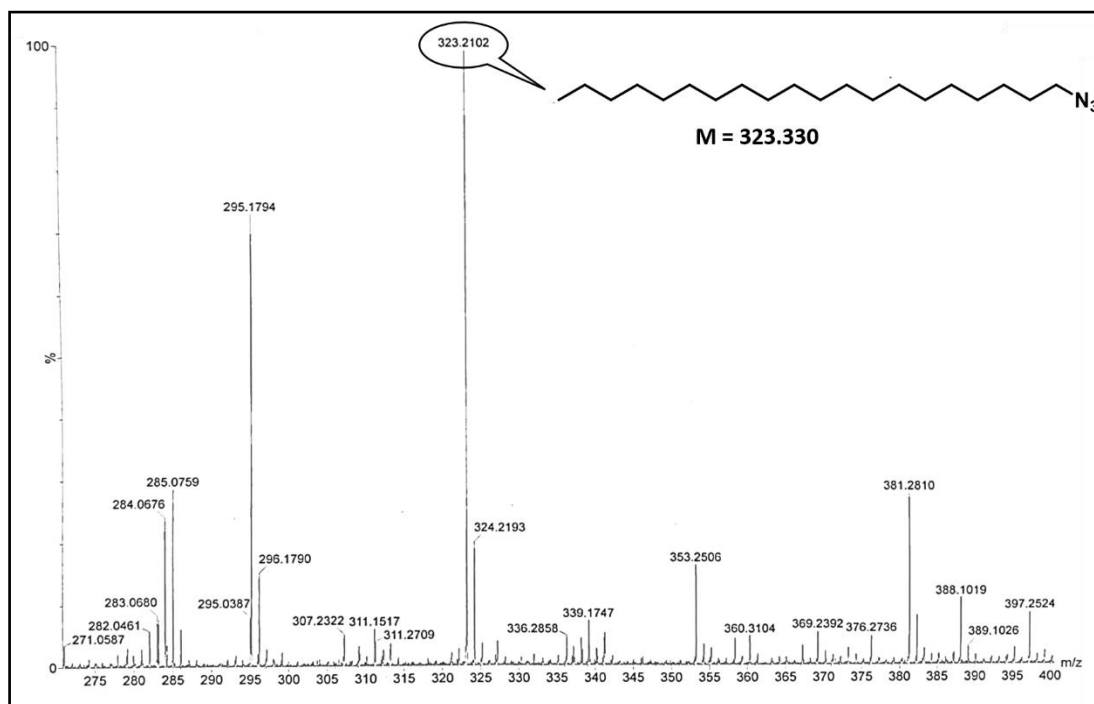


Figure A4.1. ESI-MS spectrum of $C_{20}-N_3$ in MeOH. ESI-MS: m/z (%): 323.21

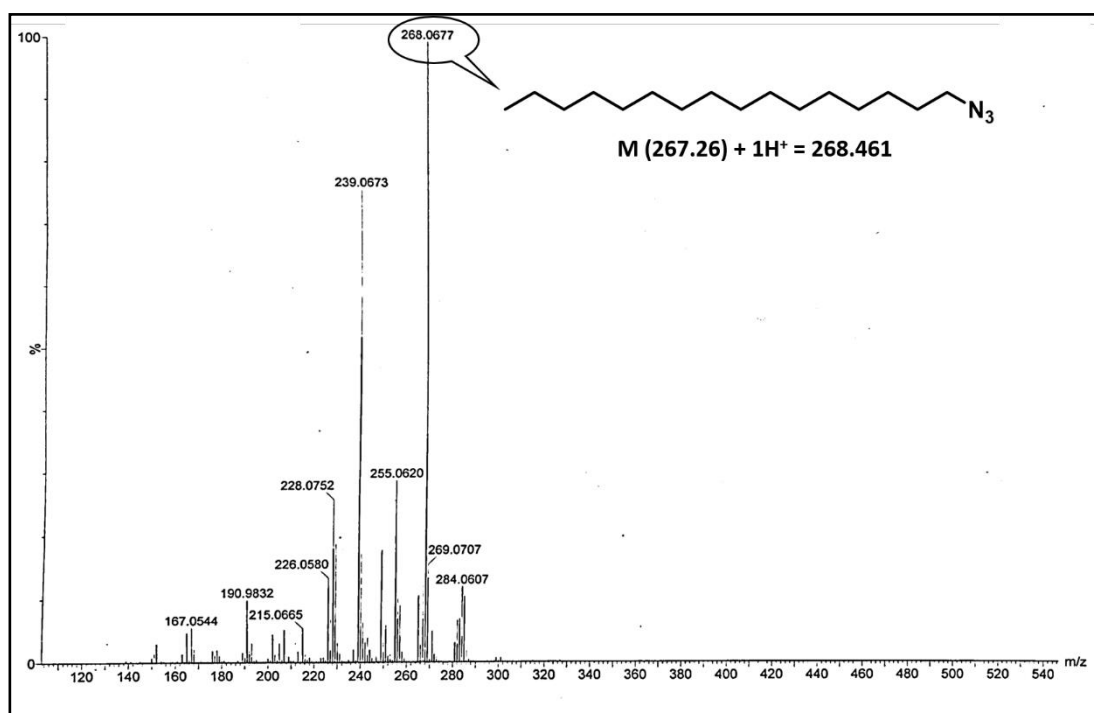


Figure A4.2. ESI-MS spectrum of $C_{16}-N_3$ in MeOH. ESI-MS: $[M + 1H^+]$ m/z (%): 268.06

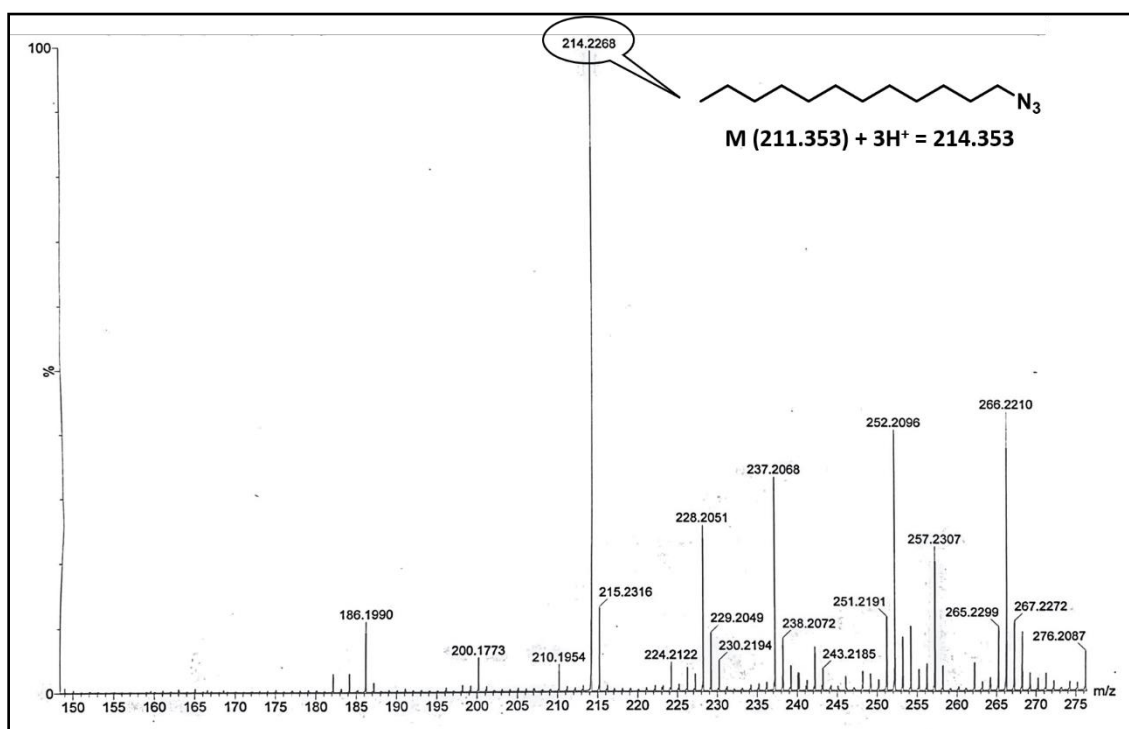


Figure A4.3. ESI-MS spectrum of $C_{12}-N_3$ in MeOH. ESI-MS: $[M + 3H^+]$ m/z (%): 214.22

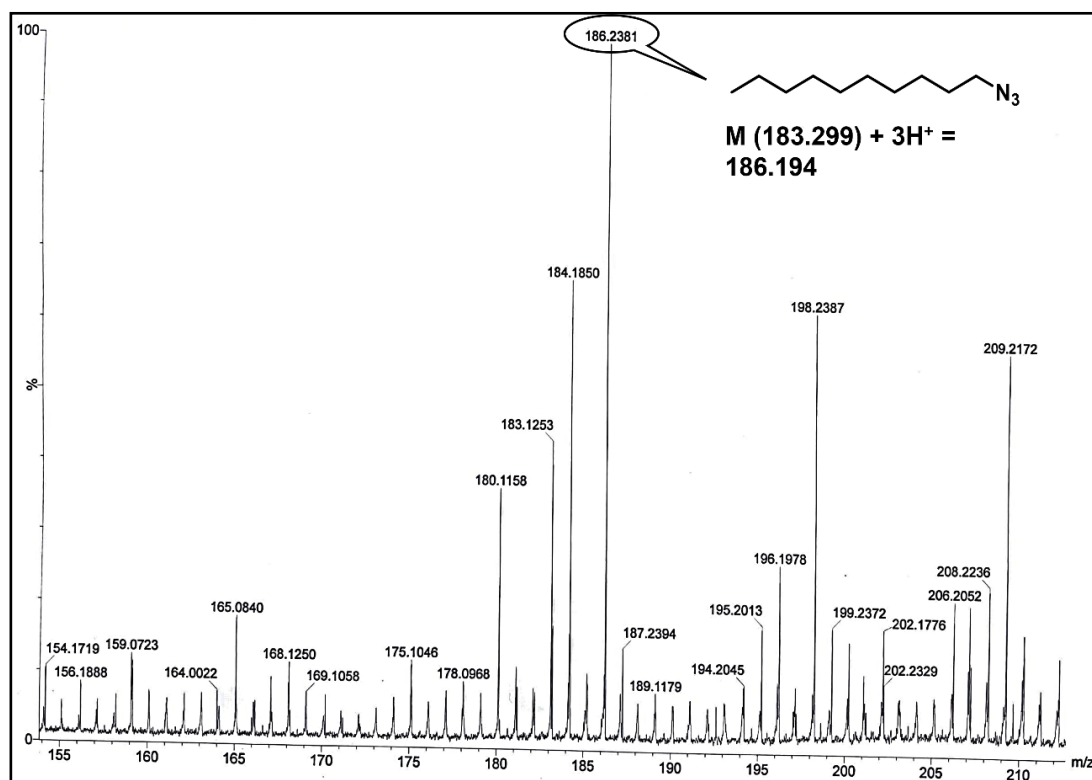


Figure A4.4. ESI-MS spectrum of $C_{10}-N_3$ in MeOH. ESI-MS: $[M + 3H^+]$ m/z (%): 186.23

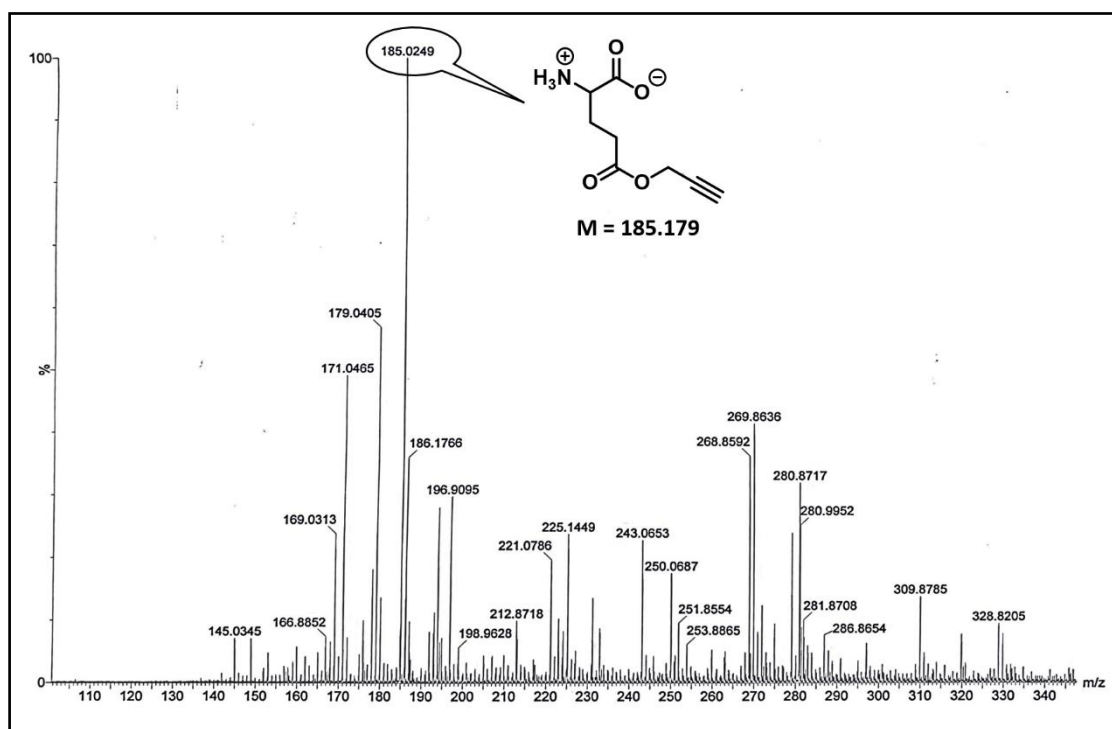


Figure A4.5. ESI-MS spectrum of Glu-Pr in MeOH: H₂O (1: 1) mixture. ESI-MS: [M]
m/z (%): 185.02

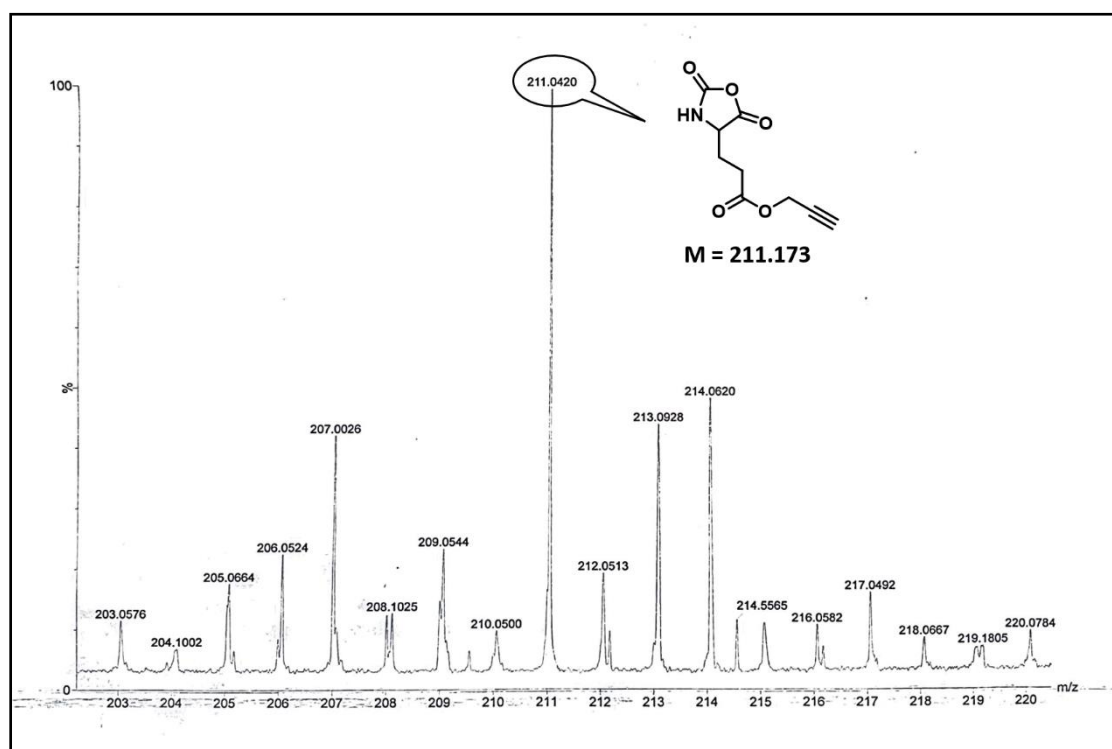


Figure A4.6. ESI-MS spectrum of Glu-Pr NCA in MeOH. ESI-MS: [M] m/z (%):
211.04

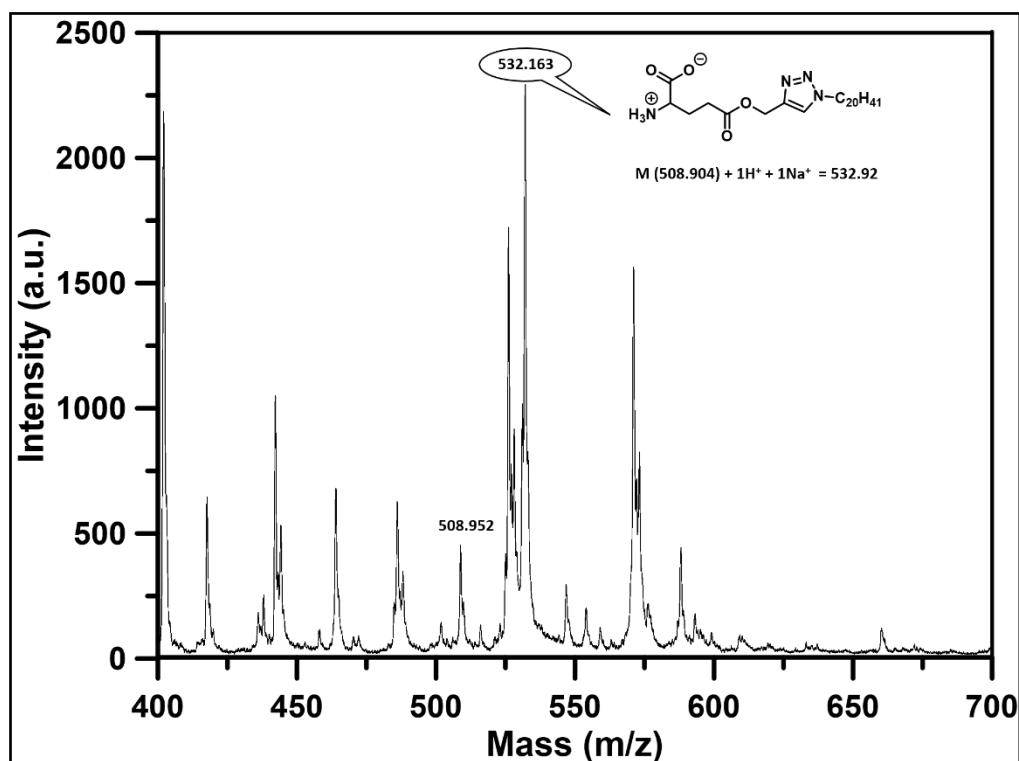


Figure A4.7. MALDI-TOF-MS spectra of Glu-C₂₀ using DHB as matrix.

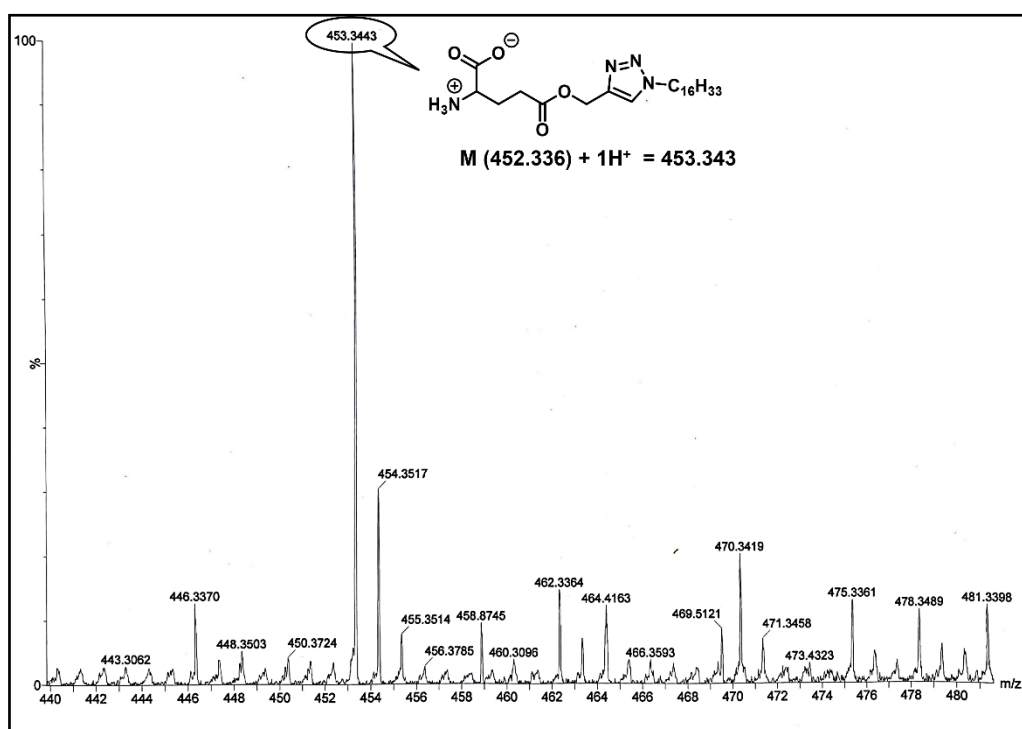


Figure A4.8. ESI-MS spectrum of Glu-C₁₆ in MeOH. ESI-MS: $[M + 1H]^+$ m/z (%), Glu-C₁₆: 453.34

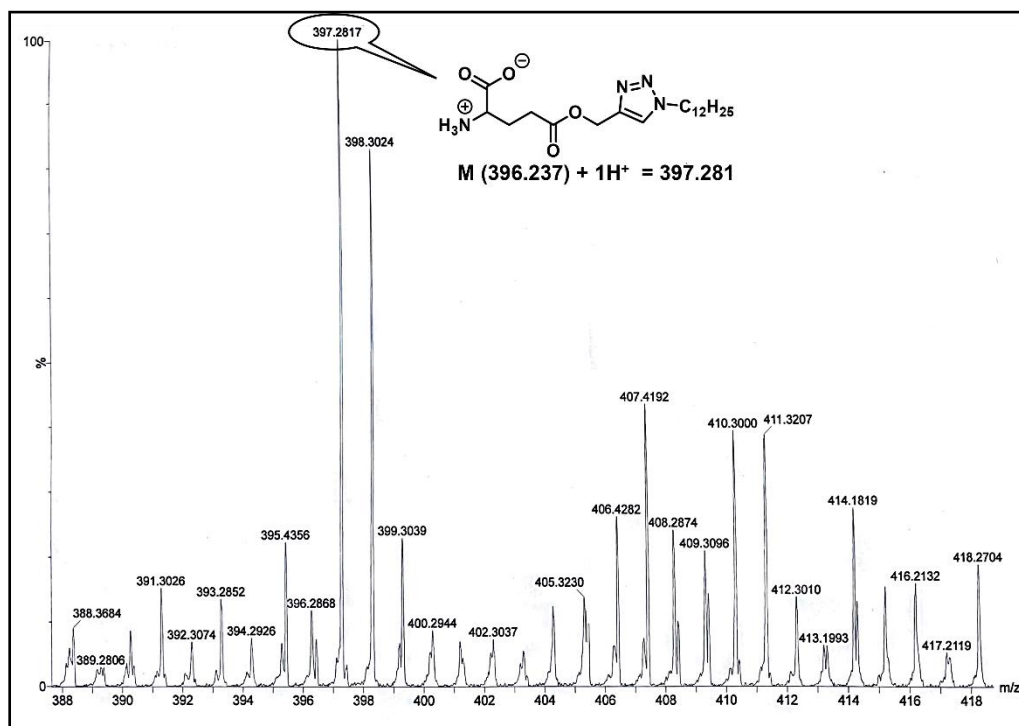


Figure A4.9. ESI-MS spectrum of Glu-C₁₂ in MeOH. ESI-MS: $[M + 1H^+]$ m/z (%),
Glu-C₁₂: 397.28

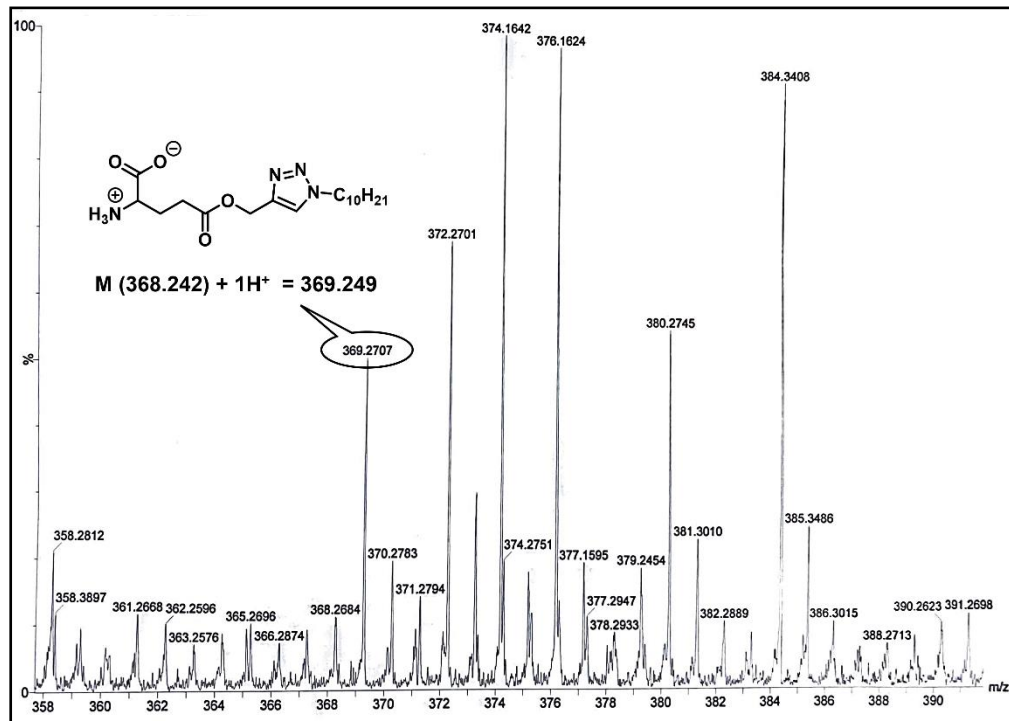


Figure A4.10. ESI-MS spectrum of Glu-C₁₀ in MeOH. ESI-MS: $[M + 1H^+]$ m/z (%),
Glu-C₁₀: 369.27

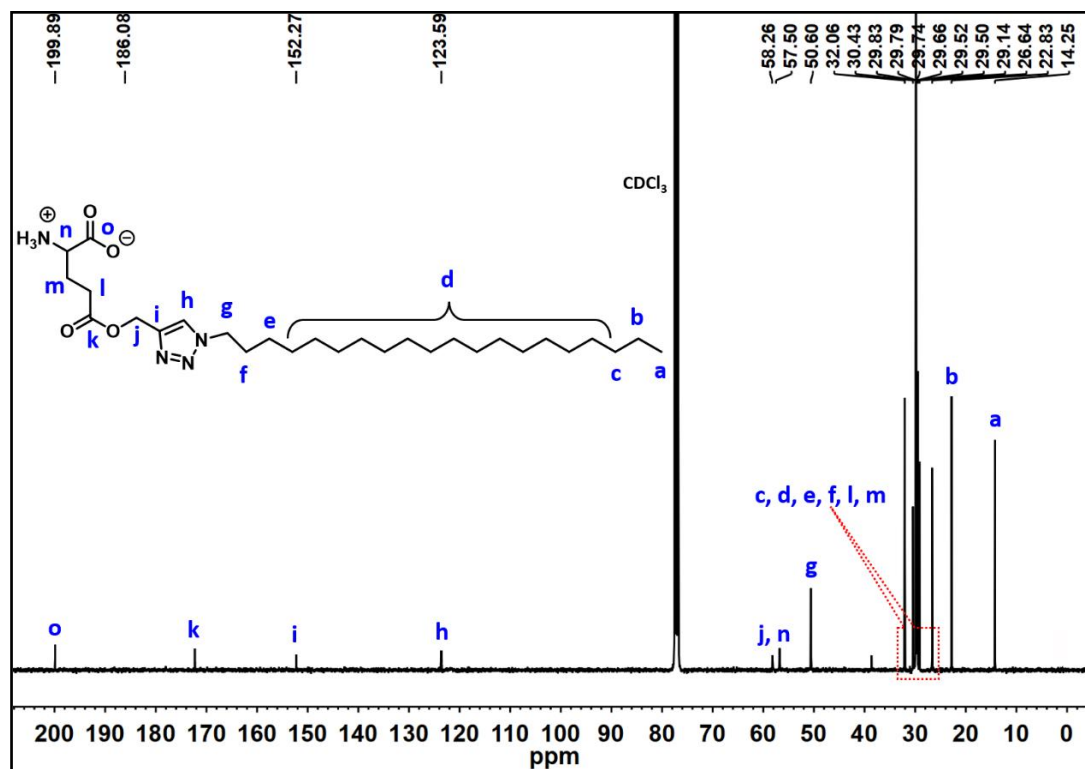


Figure A4.11. ^{13}C -NMR spectrum of Glu-C₂₀ in CDCl_3 .

75 MHz, CDCl_3 , δ (ppm): 14.25 (1C), 22.83 (1C), 26.64 – 32.06 (19 C), 50.60 (1C), 57.50 (1C), 58.28 (1C), 123.59 (1C), 152.27 (1C), 186.08 (1C), 199.89 (1C)

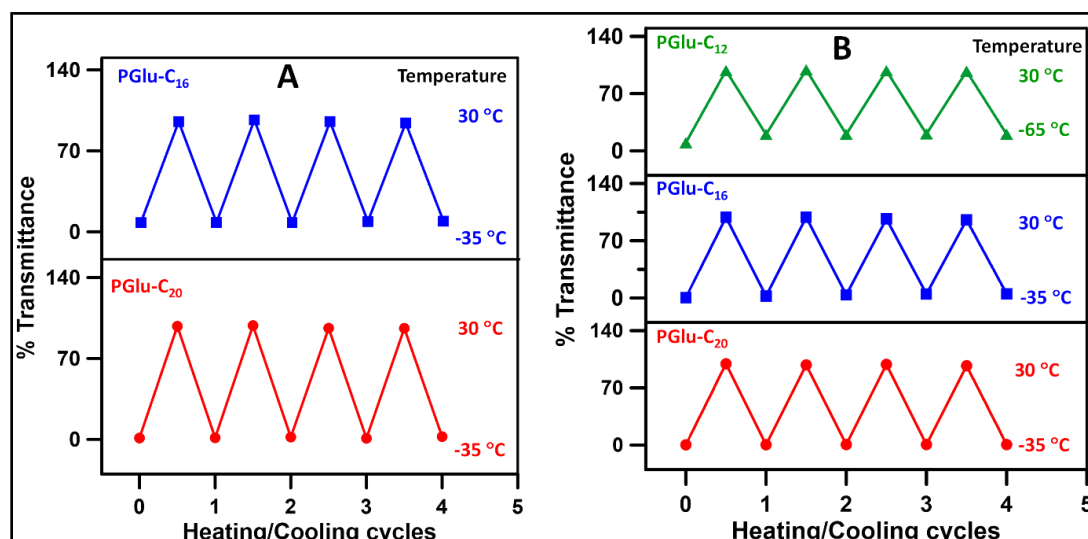


Figure A4.12. Temperature dependent % transmittance of PGLu-C₁₆ and PGLu-C₂₀ in CHCl₃ (A) and PGLu-C₁₂, PGLu-C₁₆ and PGLu-20 in THF (B) during the heating/cooling cycles. Each data point was obtained after equilibrating the sample solutions for 5 min at each temperature.

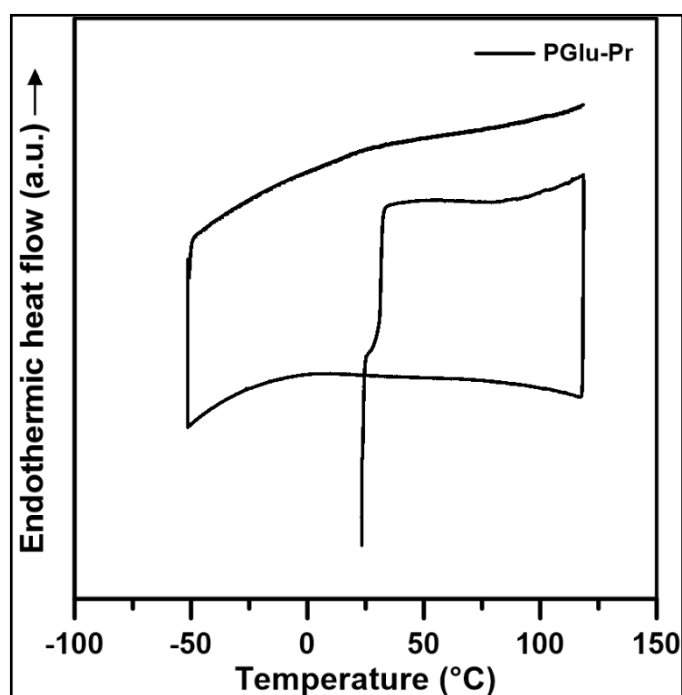


Figure A4.13. DSC thermograms of PGLu-Pr showing no signs of crystallization or melting peaks.

4.7. References

1. Lu, H.; Wang, J.; Bai, Y.; Lang, J. W.; Liu, S.; Lin, Y.; Cheng, J., Ionic Polypeptides with Unusual Helical Stability. *Nat. Commun.* **2011**, *2*, 206.
2. Nisal, R.; Jayakannan, M., Tertiary-Butylbenzene Functionalization as a Strategy for B-Sheet Polypeptides. *Biomacromolecules* **2022**, *23*, 2667-2684.
3. Song, Z.; Han, Z.; Lv, S.; Chen, C.; Chen, L.; Yin, L.; Cheng, J., Synthetic Polypeptides: From Polymer Design to Supramolecular Assembly and Biomedical Application. *Chem. Soc. Rev.* **2017**, *46*, 6570-6599.
4. Song, Z.; Tan, Z.; Cheng, J., Recent Advances and Future Perspectives of Synthetic Polypeptides from N-Carboxyanhydrides. *Macromolecules* **2019**, *52*, 8521-8539.
5. V, D.; P. J, S.; Rajeev, N.; S, A. L.; Chandran, A.; G. B, G.; Sadanandan, S., Recent Advances in Peptides-Based Stimuli-Responsive Materials for Biomedical and Therapeutic Applications: A Review. *Mol. Pharmaceutics* **2022**, *19*, 1999-2021.
6. Schlaad, H., Solution Properties of Polypeptide-Based Copolymers. In *Peptide Hybrid Polymers*, Klok, H.-A.; Schlaad, H., Eds. Springer Berlin Heidelberg: Berlin, Heidelberg, 2006; pp 53-73.
7. Anas, M.; Dinda, P.; Kar, M.; Mandal, T. K., Anion-Induced Thermoresponsiveness in Cationic Polycysteine and DNA Binding. *Polym. Chem.* **2021**, *12*, 6329-6343.
8. Anas, M.; Jana, S.; Mandal, T. K., Vesicular Assemblies of Thermoresponsive Amphiphilic Polypeptide Copolymers for Guest Encapsulation and Release. *Polym. Chem.* **2020**, *11*, 2889-2903.
9. Cui, N.; Qian, J.; Wang, J.; Ji, C.; Xu, W.; Wang, H., Preparation and Characterization of Foamy Poly(Γ -Benzyl-L-Glutamate-Co-L-Phenylalanine)/Bioglass Composite Scaffolds for Bone Tissue Engineering. *RSC Adv.* **2016**, *6*, 73699-73708.

10. Qian, J.; Yong, X.; Xu, W.; Jin, X., Preparation and Characterization of Bimodal Porous Poly(Γ -Benzyl-L-Glutamate) Scaffolds for Bone Tissue Engineering. *Mater. Sci. Eng. C* **2013**, *33*, 4587-4593.
11. Chen, C.; Wang, Z.; Li, Z., Thermoresponsive Polypeptides from Pegylated Poly-L-Glutamates. *Biomacromolecules* **2011**, *12*, 2859-2863.
12. Jana, S.; Biswas, Y.; Mandal, T. K., Methionine-Based Cationic Polypeptide/Polypeptide Block Copolymer with Triple-Stimuli Responsiveness: DNA Polyplexation and Phototriggered Release. *Polym. Chem.* **2018**, *9*, 1869-1884.
13. Petitdemange, R.; Garanger, E.; Bataille, L.; Bathany, K.; Garbay, B.; Deming, T. J.; Lecommandoux, S., Tuning Thermoresponsive Properties of Cationic Elastin-Like Polypeptides by Varying Counterions and Side-Chains. *Bioconjugate Chem.* **2017**, *28*, 1403-1412.
14. Gharakhanian, E. G.; Deming, T. J., Role of Side-Chain Molecular Features in Tuning Lower Critical Solution Temperatures (Lcsts) of Oligoethylene Glycol Modified Polypeptides. *J. Phy. Chem. B* **2016**, *120*, 6096-6101.
15. Jana, S.; Anas, M.; Maji, T.; Banerjee, S.; Mandal, T. K., Tryptophan-Based Styryl Homopolymer and Polyzwitterions with Solvent-Induced Ucst, Ion-Induced Lcst and Ph-Induced Ucst. *Polym. Chem.* **2019**, *10*, 526-538.
16. Jana, S.; Biswas, Y.; Anas, M.; Saha, A.; Mandal, T. K., Poly[Oligo(2-Ethyl-2-Oxazoline)Acrylate]-Based Poly(Ionic Liquid) Random Copolymers with Coexistent and Tunable Lower Critical Solution Temperature- and Upper Critical Solution Temperature-Type Phase Transitions. *Langmuir* **2018**, *34*, 12653-12663.
17. Dinda, P.; Anas, M.; Banerjee, P.; Mandal, T. K., Dual Thermoresponsive Boc-Lysine-Based Acryl Polymer: Raft Kinetics and Anti-Protein-Fouling of Its Zwitterionic Form. *Macromolecules* **2022**, *55*, 4011-4024.
18. Kar, M.; Anas, M.; Singh, A.; Basak, A.; Sen, P.; Mandal, T. K., Ion-/Thermo-Responsive Fluorescent Perylene-Poly(Ionic Liquid) Conjugates: One-Pot

- Microwave Synthesis, Self-Aggregation and Biological Applications. *Eur. Polym. J.* **2022**, *179*, 111561.
19. Cheng, Y.; He, C.; Xiao, C.; Ding, J.; Zhuang, X.; Huang, Y.; Chen, X., Decisive Role of Hydrophobic Side Groups of Polypeptides in Thermosensitive Gelation. *Biomacromolecules* **2012**, *13*, 2053-2059.
 20. Xiong, Y.; Liu, J.; Wang, Y.; Wang, H.; Wang, R., One-Step Synthesis of Thermosensitive Nanogels Based on Highly Cross-Linked Poly(Ionic Liquid)S. *Angew. Chem. Int. Ed.* **2012**, *51*, 9114-9118.
 21. Biswas, Y.; Banerjee, P.; Mandal, T. K., From Polymerizable Ionic Liquids to Poly(Ionic Liquid)S: Structure-Dependent Thermal, Crystalline, Conductivity, and Solution Thermoresponsive Behaviors. *Macromolecules* **2019**, *52*, 945-958.
 22. Zhang, Q.; Hoogenboom, R., Polymers with Upper Critical Solution Temperature Behavior in Alcohol/Water Solvent Mixtures. *Prog. Polym. Sci.* **2015**, *48*, 122-142.
 23. Concilio, M.; Beyer, V. P.; Becer, C. R., Thermoresponsive Polymers in Non-Aqueous Solutions. *Polym. Chem.* **2022**, *13*, 6423-6474.
 24. Engler, A. C.; Bonner, D. K.; Buss, H. G.; Cheung, E. Y.; Hammond, P. T., The Synthetic Tuning of Clickable Ph Responsive Cationic Polypeptides and Block Copolypeptides. *Soft Matter* **2011**, *7*, 5627-5637.
 25. Jahanshahi, K.; Botiz, I.; Reiter, R.; Thomann, R.; Heck, B.; Shokri, R.; Stille, W.; Reiter, G., Crystallization of Poly(Γ -Benzyl L-Glutamate) in Thin Film Solutions: Structure and Pattern Formation. *Macromolecules* **2013**, *46*, 1470-1476.
 26. Bose, A.; Jana, S.; Saha, A.; Mandal, T. K., Amphiphilic Polypeptide-Polyoxazoline Graft Copolymer Conjugate with Tunable Thermoresponsiveness: Synthesis and Self-Assembly into Various Micellar Structures in Aqueous and Nonaqueous Media. *Polymer* **2017**, *110*, 12-24.

27. Engler, A. C.; Lee, H.-i.; Hammond, P. T., Highly Efficient "Grafting onto" a Polypeptide Backbone Using Click Chemistry. *Angew. Chem.* **2009**, *48*, 9334-9338.
28. Zhao, X.; Poon, Z.; Engler, A. C.; Bonner, D. K.; Hammond, P. T., Enhanced Stability of Polymeric Micelles Based on Postfunctionalized Poly(Ethylene Glycol)-B-Poly(Γ -Propargyl L-Glutamate): The Substituent Effect. *Biomacromolecules* **2012**, *13*, 1315-1322.
29. He, H.; Sofman, M.; Wang, A. J. S.; Ahrens, C. C.; Wang, W.; Griffith, L. G.; Hammond, P. T., Engineering Helical Modular Polypeptide-Based Hydrogels as Synthetic Extracellular Matrices for Cell Culture. *Biomacromolecules* **2020**, *21*, 566-580.
30. Fu, X.; Ma, Y.; Sun, J.; Li, Z., Biodegradable Thermal- and Redox-Responsive Poly(L-Glutamate) with Y-Shaped Oligo(Ethylene Glycol) Side-Chain and Tunable Phase Transition Temperature. *RSC Adv.* **2016**, *6*, 70243-70250.
31. O'Brien, S.; Brannigan, R. P.; Ibanez, R.; Wu, B.; O'Dwyer, J.; O'Brien, F. J.; Cryan, S.-A.; Heise, A., Biocompatible Polypeptide-Based Interpenetrating Network (Ipn) Hydrogels with Enhanced Mechanical Properties. *J. Mater. Chem. B* **2020**, *8*, 7785-7791.
32. Oelker, A. M.; Morey, S. M.; Griffith, L. G.; Hammond, P. T., Helix Versus Coil Polypeptide Macromers: Gel Networks with Decoupled Stiffness and Permeability. *Soft Matter* **2012**, *8*, 10887-10895.
33. Lin, Y.-C.; Kuo, S.-W., Hierarchical Self-Assembly and Secondary Structures of Linear Polypeptides Graft onto Pss in the Side Chain through Click Chemistry. *Polym. Chem.* **2012**, *3*, 162-171.
34. Murmu, U. K.; Adhikari, J.; Naskar, A.; Dey, D.; Roy, A.; Ghosh, A.; Ghosh, M., Mechanical Properties of Crystalline and Semicrystalline Polymer Systems. In *Encyclopedia of Materials: Plastics and Polymers*, Hashmi, M. S. J., Ed. Elsevier: Oxford, 2022; pp 917-927.

35. Ezhov, A. A.; Shandryuk, G. A.; Bondarenko, G. N.; Merekalov, A. S.; Abramchuk, S. S.; Shatalova, A. M.; Manna, P.; Zubarev, E. R.; Talroze, R. V., Liquid-Crystalline Polymer Composites with Cds Nanorods: Structure and Optical Properties. *Langmuir* **2011**, *27*, 13353-13360.
36. Woo, E. M.; Wu, P. L.; Wu, M. C.; Yan, K. C., Thermal Behavior of Ring-Band Versus Maltese-Cross Spherulites: Case of Monomorphic Poly(Ethylene Adipate). *Macromol. Chem. Phys.* **2006**, *207*, 2232-2243.
37. López-Barrón, C. R.; Tsou, A. H.; Younker, J. M.; Norman, A. I.; Schaefer, J. J.; Hagadorn, J. R.; Throckmorton, J. A., Microstructure of Crystallizable A-Olefin Molecular Bottlebrushes: Isotactic and Atactic Poly(1-Octadecene). *Macromolecules* **2018**, *51*, 872-883.
38. Lugito, G.; Woo, E. M.; Hsieh, Y.-T., Transitional Ring Bands Constructed by Discrete Positive- and Negative-Birefringence Lamellae Packed in Poly(1,6-Hexamethylene Adipate) Spherulites. *Macromolecules* **2015**, *48*, 7953-7967.
39. Paira, T. K.; Banerjee, S.; Mandal, T. K., Peptide-Poly(E-Caprolactone) Biohybrids by Grafting-from Ring-Opening Polymerization: Synthesis, Aggregation, and Crystalline Properties. *J. Polym. Sci. A Polym. Chem.* **2012**, *50*, 2130-2141.
40. Wang, Q., et al., Multiscale Crystalline Structure of Confined Polypeptoid Films: The Effect of Alkyl Side Chain Branching. *ACS Macro Lett.* **2022**, *11*, 1060-1066.
41. Zhang, Z.-K.; Guo, X.-S.; Zhang, T.-Y.; Wang, R.-Y.; Du, B.-Y.; Xu, J.-T., Hierarchical Structures with Double Lower Disorder-to-Order Transition and Closed-Loop Phase Behaviors in Charged Block Copolymers Bearing Long Alkyl Side Groups. *Macromolecules* **2020**, *53*, 8714-8724.
42. Chakraborty, S.; Ramkumar, S. G.; Ramakrishnan, S., Amphiphilic Double-Brush Polymers Based on Itaconate Diesters. *Macromolecules* **2017**, *50*, 5004-5013.

43. Lee, C.-U.; Li, A.; Ghale, K.; Zhang, D., Crystallization and Melting Behaviors of Cyclic and Linear Polypeptoids with Alkyl Side Chains. *Macromolecules* **2013**, *46*, 8213-8223.
44. Ballauff, M.; Schmidt, G. F., Rigid Rod Polymers with Flexible Side Chains, 2. Observation of a Novel Type of Layered Mesophase. *Makromol. Chem. Rapid. Commun.* **1987**, *8*, 93-97.
45. Kricheldorf, H. R.; Domschke, A. J. M., Layer Structure. 1. Poly (Phenylene-Terephthalamide)S Derived from Mono-, Di-, and Tetrakis(Alkylthio) Terephthalic Acids. *Macromolecules* **1994**, *27*, 1509-1516.
46. Watanabe, J.; Harkness, B. R.; Sone, M.; Ichimura, H. J. M., Rigid-Rod Polyesters with Flexible Side Chains. 4. Thermotropic Behavior and Phase Structures in Polyesters Based on 1, 4-Dialkyl Esters of Pyromellitic Acid and 4, 4'-Biphenol. *Macromolecules* **1994**, *27*, 507-512.
47. Watanabe, J.; Fukuda, Y.; Gehani, R.; Uematsu, I., Thermotropic Polypeptides. 1. Investigation of Cholesteric Mesophase Properties of Poly (Γ -Methyl-D-Glutamate-Co- Γ -Hexyl-D-Glutamate)S. *Macromolecules* **1984**, *17*, 1004-1009.
48. Gehani, R.; Watanabe, J.; Kasuya, S.; Uematsu, I., Different Packing Structures Observed in Copoly(Γ -Methyl, Benzyl L-Glutamate) Films. *Polymer J.* **1980**, *12*, 871-882.
49. Watanabe, J.; Uematsu, I., Dielectric Properties of Poly(Γ -Methyl D-Glutamate) and Copoly(Γ -Methyl D,L-Glutamate) Films. *Polymer J.* **1977**, *9*, 195-200.
50. Watanabe, J.; Tominaga, T., Thermotropic Liquid Crystals in Polypeptides with Mesogenic Side Chains. 1. *Macromolecules* **1993**, *26*, 4032-4036.
51. Lu, H.; Wang, J.; Song, Z.; Yin, L.; Zhang, Y.; Tang, H.; Tu, C.; Lin, Y.; Cheng, J., Recent Advances in Amino Acid N-Carboxyanhydrides and Synthetic Polypeptides: Chemistry, Self-Assembly and Biological Applications. *Chem. Commun.* **2014**, *50*, 139-155.

52. Cai, C.; Lin, J.; Lu, Y.; Zhang, Q.; Wang, L., Polypeptide Self-Assemblies: Nanostructures and Bioapplications. *Chem. Soc. Rev.* **2016**, *45*, 5985-6012.
53. Engler, A. C.; Shukla, A.; Puranam, S.; Buss, H. G.; Jreige, N.; Hammond, P. T., Effects of Side Group Functionality and Molecular Weight on the Activity of Synthetic Antimicrobial Polypeptides. *Biomacromolecules* **2011**, *12*, 1666-1674.
54. Wei, C.; Li, P.; Liu, L.; Zhang, H.; Zhao, T.; Chen, Y., Degradable Poly(Amino Acid) Vesicles Modulate DNA-Induced Inflammation after Traumatic Brain Injury. *Biomacromolecules* **2022**, *24*, 909-920.
55. Bu, S.; Yan, S.; Wang, R.; Xia, P.; Zhang, K.; Li, G.; Yin, J., In Situ Precipitation of Cluster and Acicular Hydroxyapatite onto Porous Poly(Γ -Benzyl-L-Glutamate) Microcarriers for Bone Tissue Engineering. *ACS Appl. Mater. Interfaces* **2020**, *12*, 12468-12477.
56. Shi, Z.; Zhang, X.; Yu, Z.; Yang, F.; Liu, H.; Xue, R.; Luan, S.; Tang, H., Facile Synthesis of Imidazolium-Based Block Copolypeptides with Excellent Antimicrobial Activity. *Biomacromolecules* **2021**, *22*, 2373-2381.
57. Cai, C.; Wang, L.; Lin, J., Self-Assembly of Polypeptide-Based Copolymers into Diverse Aggregates. *Chem. Commun.* **2011**, *47*, 11189-11203.
58. Carlsen, A.; Lecommandoux, S., Self-Assembly of Polypeptide-Based Block Copolymer Amphiphiles. *Curr. Opin. Colloid Interface Sci.* **2009**, *14*, 329-339.
59. Li, M.; Xu, Y.; Liu, T.; Li, Y.; Ling, Y.; Tang, H., Preparation and Thermoresponsive Properties of Ucst-Type Polypeptide Bearing P-Tolyl Pendants and 3-Methyl-1,2,3-Triazolium Linkages in Methanol or Ethanol/Water Solvent Mixtures. *Macromol. Chem. Phys.* **2017**, *218*, 1700006.
60. Zhu, M.; Xu, Y.; Ge, C.; Ling, Y.; Tang, H., Synthesis and Ucst-Type Phase Behavior of Oegylated Poly(Γ -Benzyl-L-Glutamate) in Organic Media. *J. Polym. Sci. Part A: Polym. Chem.* **2016**, *54*, 1348-1356.

61. Canning, A.; Pasquazi, A.; Fijten, M.; Rajput, S.; Buttery, L.; Aylott, J. W.; Zelzer, M., Tuning the Conformation of Synthetic Co-Polypeptides of Serine and Glutamic Acid through Control over Polymer Composition. *J. Polym. Sci. A Polym. Chem.* **2016**, *54*, 2331-2336.
62. Lu, H.; Cheng, J., Hexamethyldisilazane-Mediated Controlled Polymerization of α -Amino Acid N-Carboxyanhydrides. *J. Am. Chem. Soc.* **2007**, *129*, 14114-14115.
63. Lu, H.; Cheng, J., N-Trimethylsilyl Amines for Controlled Ring-Opening Polymerization of Amino Acid N-Carboxyanhydrides and Facile End Group Functionalization of Polypeptides. *J. Am. Chem. Soc.* **2008**, *130*, 12562-12563.
64. Bauer, T. A.; Imschweiler, J.; Muhl, C.; Weber, B.; Barz, M., Secondary Structure-Driven Self-Assembly of Thiol-Reactive Polypept(O)ides. *Biomacromolecules* **2021**, *22*, 2171-2180.
65. Wu, Y.; Deng, Y.; Yuan, Q.; Ling, Y.; Tang, H., Thermoresponsive Poly(Γ -Propyl-L-Glutamate)-Graft-(Oligo Ethylene Glycol)S: Synthesis, Characterization, and Properties. *J. Appl. Polym. Sci.* **2014**, *131*.
66. DeFlores, L. P.; Ganim, Z.; Nicodemus, R. A.; Tokmakoff, A., Amide I'-II' 2d IR Spectroscopy Provides Enhanced Protein Secondary Structural Sensitivity. *J. Am. Chem. Soc.* **2009**, *131*, 3385-3391.
67. Paira, T. K.; Banerjee, S.; Raula, M.; Kotal, A.; Si, S.; Mandal, T. K., Peptide-Polymer Bioconjugates Via Atom Transfer Radical Polymerization and Their Solution Aggregation into Hybrid Micro/Nanospheres for Dye Uptake. *Macromolecules* **2010**, *43*, 4050-4061.
68. Lalatsa, A.; Schätzlein, A. G.; Mazza, M.; Le, T. B. H.; Uchegbu, I. F., Amphiphilic Poly(L-Amino Acids) – New Materials for Drug Delivery. *J. Controlled Release* **2012**, *161*, 523-536.

Summary

In summary, this thesis covered the synthesis, exploration, and study of the solution properties of differently functionalized polypeptides exhibiting diverse functionalities such as responsiveness and self-assembly etc. The focus was on investigating the potential of these functionalized polypeptides to enhance therapeutic effectiveness, biocompatibility, and materialistic applications. In particular, a library of functionalized polypeptide based on different α - amino acids (L-cysteine, L-glutamic acid) were synthesized. To achieve this, at first α - amino acids were first coupled with different chemical moieties having different functional groups (acrylate, hydroxyl etc), followed by NCA formation. ROP of these NCAs, resulted in functional polypeptides with different pendant reactive groups. Post-polymerization modification of these functional polypeptides via different chemical reaction (click, substitution etc.) finally gave rise to the functionalized polypeptides. Furthermore, responsiveness and self-assembly of these functionalized polypeptides were thoroughly investigated and demonstrated. The potential application of these functionalized polypeptides towards different biomedical areas such as drug or gene delivery had also been explored meticulously.

The introduction section provided a brief overview on the advancements in functionalized polypeptides synthesized through ROP of NCA, along with their applications as biomaterials. The review delved into various methods of ROP using different initiators, highlighting the synthesis of functional polypeptides exhibiting stimuli-responsive properties. The chapter also focused on the systematic self-assembly behaviours of these functionalized polypeptides, elucidating their ability to form micro-/nano-structured aggregates in different solvents. Finally, the potential applications of these functionalized responsive polypeptides as biomaterials were discussed.

Chapter 2 summarised the synthesis, thermoresponsiveness and self-assembly behaviour of a novel amphiphilic graft copolypeptides (PCys-*g*-P'POx) with hydrophobic polycysteine backbone and hydrophilic pendant poly(2-isopropyl-2-oxazoline) side chain. A series of PCys-*g*-P'POx copolypeptides were synthesized with the help of different techniques such as ROP, CROP, click grafting etc. For this at first L-cysteine was reacted with propargyl acrylate via Michael reaction to produce propargyl functionalized L-cysteine (Cys-S-Pr), followed by NCA formation. ROP of Cys-S-Pr gave poly(L-cysteine) with pendant propargyl groups. Another polymer, poly(2-isopropyl-2-oxazoline) (P'POX), was synthesized via CROP of the as synthesized 2-isopropyl-2-oxazoline (P'Pox) monomer and subsequently end-terminated with azide group to produce azide end-capped P'Pox (P'POx-N₃). Finally, these two polymers were then coupled via click reaction (CuAAC) to obtain the final graft copolypeptides. PCys-*g*-P'Pox(s) showed LCST type thermoresponsive behaviour in water due to the presence of P'POx unit in their side chains. The T_{cp} of the LCST-transition of the PCys-*g*-P'Pox(s) were tuned by varying the chain length of the PCys backbone as well the P'POx side chains. Self-assembly of these amphiphilic copolypeptides in aqueous and nonaqueous media, resulted in vesicular morphologies with different size distribution. The smaller vesicles were termed as unit vesicle which underwent secondary aggregation in the solution due to the hydrophobic interaction between the isopropyl groups present in the periphery of the vesicles, which led to the composite vesicles with larger diameter. These vesicles showed dual encapsulation behaviour towards different types of dyes in both aqueous and non-aqueous solvents. Hydrophobic dye (NR) molecule could easily be encapsulated into the hydrophobic layer of the vesicles in water. Whereas hydrophilic dye (EB) got encapsulated efficiently into the interior pool of the vesicles. Similarly, Dox was encapsulated into the interior of the vesicles and subsequently released from it by treatment of acid

as well as by increasing the solution temperature. These findings helped to conclude that PCys-*g*-P'Pox can be used as potential drug carrier.

Chapter 3 presented the synthesis of a dual stimuli-responsive polypeptide achieved through the ROP of a bromo-functionalized L-cysteine NCA monomer and subsequent post-polymerization modification. Michael reaction between the as synthesized 2-bromoethyl acrylate and L-cysteine in water gave Cys-Br. NCA formation and successive ROP resulted in PCys-Br with pendant Br atoms. The resulting functional polypeptide was then subjected to nucleophilic substitution, using triphenyl phosphine, to replace the pendant Br atom and produce cationic homopolypeptides ([PCys-PPh₃]⁺[Br⁻]). Another homopolypeptides with different counter-anion ([PCys-PPh₃]⁺[Cl⁻]) was also synthesized following similar schematic pathways. These ionic polypeptides exhibited water solubility, but the transparent aqueous solution transformed into a hazy suspension when different chaotropic anions (BF₄⁻, I⁻, ClO₄⁻, SCN⁻) were added into the solution at a specific concentration due to the formation of anion-bridge interaction among the adjacent polypeptide chains. The hazy suspension turned clear again on increasing the solution temperature and *vice-versa*, demonstrating UCST-type thermoresponsiveness in water. The T_{cp} of the UCST-type phase behaviour could be tuned by varying the molecular weight and concentration of the polypeptides, as well as the concentration and polarizability of the added anions. The anion-induced UCST-type phase transition of the cationic polypeptide was also tested positive for large anion but negative for kosmotropic/ kosmotropic-chaotropic border line anions. The ionic nature of the [PCys-PPh₃]⁺[Br⁻] polypeptide made it a promising candidate for DNA intercalation, as confirmed by fluorescence spectroscopy and gel electrophoresis studies. The binding mode between the cationic polypeptide and DNA was purely electrostatic, which depends on the ionic strength of the solution.

Chapter 4 demonstrated the synthesis of poly(L-glutamate) based functionalized polypeptides with pendant long alkyl groups of varying chain length, PGlu-C_n (n = 10, 12, 16, 20). The synthesis involved the combination of ROP of as synthesized γ -propargyl L-glutamate NCA and successive click reactions with long chain alkyl azides, prepared from their alkyl bromide precursors. Similarly, long chain alkyl functionalized glutamates, Glu-C_n(s), were also prepared for comparison. The resulting polypeptides adopted helical conformation in both solid and solution phase and the fraction of helicity decreased with increase in the length of the alkyl groups as confirmed by CD and FT-IR analyses. Hydrophobic PGlu-C_n(s) were soluble in organic solvents such as CHCl₃, THF etc. and exhibited UCST-type thermoresponsiveness in those solvents. The T_{cp} and the enthalpy of phase transition were greatly affected by the pendant alkyl chain length as well the polarity of the solvents. However, Glu-C_n(s) didn't show such thermoresponsiveness in any of these solvents. Glu-C_n(s) exhibited highly birefringent plumose-type crystalline phase in bulk due to the compact bilayered arrangements of the attached alkyl chains through hydrophobic interaction. Comparing the functionalized polypeptides (PGlu-C_n) with their monomeric analogues (Glu-C_n), it was observed that some of the PGlu-C_n exhibited reduced crystallinity forming low birefringent fibrillar texture-type crystals due to the loosely packed bilayer arrangement of the side alkyl chains. T_c , T_m , and the corresponding enthalpy change (ΔH_c , ΔH_m) were found to be increased with increase in the length of the alkyl groups for both Glu-C_n(s) and PGlu-C_n(s). XRD analysis also confirmed that the degree of crystallinity increased with longer alkyl chain length for both of the Glu-C_n(s) and PGlu-C_n(s). Additionally, the PGlu-C_n(s) self-assembled into vesicular aggregates in both CHCl₃ and THF. DLS study confirmed the formation of both small (unit) vesicles and large (composite) vesicles at a time. These vesicles were capable of encapsulating dye molecules, indicating their potential application as nano-sized delivery systems.

List of Publications

Publications Included in this Thesis

- 1) "Anion-Induced Thermoresponsiveness in Cationic Polycysteine and DNA Binding."
Mahammad Anas, Priyanka Dinda, Mahuya Kar and Tarun K Mandal.
Polym. Chem., **2021**, 12 (43), 6329-6343
- 2) "Vesicular Assemblies of Thermoresponsive Amphiphilic Polypeptide Copolymers for Guest Encapsulation and Release."
Mahammad Anas, Somdeb Jana and Tarun K Mandal.
Polym. Chem., **2020**, 11 (16), 2889-2903
- 3) "Side-chain Functionality Driven Thermoresponsive and Semicrystalline Poly(L-glutamate)s and Self-assembly."
Mahammad Anas and Tarun K Mandal. (*Manuscript submitted*) **2023**.

Other Co-authored Publications

- 4) "Ion-/Thermo-Responsive Fluorescent Perylene-Poly(ionic liquid) Conjugates: One-Pot Microwave Synthesis, Self-aggregation and Biological Applications."
Mahuya Kar, **Md. Anas**, Arpana Singh, Ambuz Basak, Prosenjit Sen and Tarun K. Mandal.
Eur. Polym. J., **2022**, 179, 111561
- 5) "Dual Thermoresponsive Boc-Lysine-Based Acryl Polymer: RAFT Kinetics and Anti-Protein Fouling of Its Zwitterionic Form."
Priyanka Dinda, **Mahammad Anas**, Palash Banerjee and Tarun K Mandal.
Macromolecules, **2022**, 55, 10, 4011–4024
- 6) "Amphiphilic Perylene Bisimide–Polymer Conjugates by Cysteine-Based Orthogonal Strategy: Vesicular Aggregation, DNA Binding, and Cell Imaging".

Mahuya Kar, **Md. Anas**, Palash Banerjee, Arpana Singh, Prosenjit Sen and Tarun K Mandal

ACS Appl. Polym. Mater., **2022**, 4 (5), 3697-3710

- 7) "Carbon Dot Cross-Linked Gelatin Nanocomposite Hydrogel for pH-Sensing and pH Responsive Drug Delivery".

Swarup Krishna Bhattacharyya, Madhab Dule, Raj Paul, Jyotirmayee Dash, **Md. Anas**, Tarun Kumar Mandal, Poushali Das, Narayan Chandra Das, Susanta Banerjee.

ACS Biomater. Sci. Eng., **2020**, 6 (10), 5662-5674

- 8) "Recent Developments in Stimuli-Responsive Poly(Ionic Liquid)s."

Palash Banerjee*, **Md. Anas***, Somdeb Jana, Tarun K Mandal (* **equal 1st authorship**)

J. Polym. Res., **2020**, 27 (7), 177

- 9) "Tryptophan-Based Styryl Homopolymer and Polyzwitterions With Solvent-Induced UCST, Ion-Induced LCST and pH-Induced UCST."

Somdeb Jana*, **Mahammad Anas***, Tanmoy Maji, Sanjib Banerjee, Tarun K Mandal. (* **equal 1st authorship**)

Polym. Chem., **2019**, 10 (4), 526-538

- 10) "Poly[Oligo(2-Ethyl-2-Oxazoline)Acrylate]-Based Poly(Ionic Liquid) Random Copolymers with Coexistent and Tunable Lower Critical Solution Temperature- and Upper Critical Solution Temperature-type Phase Transitions."

Somdeb Jana, Yajnaseni Biswas, **Md. Anas**, Anupam Saha, Tarun K Mandal

Langmuir **2018**, 34 (42), 12653

- 11) "Functional Diversification of Poly(acryloyl-L-serine) to introduce Stimuli-Responsiveness, Amphiphilicity and Gelation."

Priyanka Dinda, **Mahammad Anas**, Mahuya Kar, Joy Das, Tarun K Mandal
(*Manuscript submitted*), **2023**.

Papers Presented in Conferences

- 1) *"Self-assembly and Thermoresponsive Behaviours of Polypeptide-Polyoxazoline Graft Copolymers."*
Md. Anas, Somdeb Jana and Tarun K Mandal.
 Poster presentation in *SPSI- MACRO 2018 (15th International Conference on Polymer Science and Technology)*, Indian Institutes of Science Education and Research (IISER)-Pune, Pune, India.
- 2) *"Thermoresponsive Polypeptide Copolymer: Synthesis and Vesicular Self-assembly."*
Md. Anas, Somdeb Jana and Tarun K Mandal.
 Oral presentation in *InAdvanCS, SCS Annual Symposium 2019*, Indian Association for the Cultivation of Science (IACS), Kolkata, India
- 3) *"Development of Surface-Immobilized Polypeptides for Capture and Release of Phosphate from Contaminated Water."*
Mahammad Anas, Henry Wallace, Tarun Mandal and Mischa Zelzer.
 Poster presentation (online) in *RSC Biomaterials Chemistry Special Interest Group Annual Meeting 2022*, King's College, London, UK.
- 4) *"Synthesis of Cationic Polycysteine for Stimuli-responsiveness and DNA Polyplexation."*
Mahammad Anas, Priyanka Dinda, Mahuya Kar, and Tarun K. Mandal.
 Poster presentation in *14th International Symposium on Ionic Polymerization (IP 2022)*, University of Ghent, Ghent, Belgium. (* best poster award)
- 5) *"Long-Chain-Alkyl-Functionalized Thermoresponsive Semicrystalline Poly(γ -propargyl-L-glutamate): Synthesis, Self-assembly and Dye Encapsulation."*
Mahammad Anas and Tarun K Mandal.
 Poster Presentation in *InAdvanCS, SCS Annual Symposium, 2023*, Indian Association for the Cultivation of Science (IACS), Kolkata, India.

Reprints of the First Page of the Published Papers



Cite this: *Polym. Chem.*, 2020, **11**, 2889

Vesicular assemblies of thermoresponsive amphiphilic polypeptide copolymers for guest encapsulation and release†

Mahammad Anas, Somdeb Jana and Tarun K. Mandal *

Synthetic polypeptides are bio-inspired materials with good self-assembling capabilities. However, their hydrophobic nature restricts their use in biomedical applications. Pseudopeptidic poly(2-oxazoline)s are also bio-inspired and water-soluble polymers. Thus, the motivation for this research work is to integrate these two units to produce amphiphilic copolymers with a high propensity to self-assemble into vesicular nanostructures that are useful for various potential applications. To achieve this, a convenient “click” grafting technique is utilized to prepare water-soluble amphiphilic poly(cysteine)-graft-poly(2-isopropyl-2-oxazoline) (PCys-*g*-PⁱPOx) copolymers. This involves synthesis of propargylated polycysteine (PCys-S-Pr) and azide-functionalized poly(2-isopropyl-2-oxazoline) (PⁱPOx-N₃) blocks *via* ring-opening polymerization (ROP) of the corresponding *N*-carboxyanhydride (NCA) and cationic ring-opening polymerization (CROP) techniques, respectively, followed by their grafting. The grafting of the PⁱPOx block introduces thermoresponsiveness in the copolymer, exhibiting LCST phase behaviour in water, whose cloud point can be tuned by varying the copolymer’s composition and concentration. The amphiphilic nature of PCys-*g*-PⁱPOx molecules drives them to self-assemble into nanostructures with vesicular morphology in aqueous and nonaqueous media, as clearly evident from the transmission electron microscopic images. These polypeptide copolymer vesicles are capable of encapsulating both hydrophobic and hydrophilic dyes present in different environments and confirmed through fluorescence and confocal microscopy. These copolymer vesicles can also be highly efficiently used for encapsulating the drug doxorubicin and their subsequent triggered release was also studied by absorption and emission spectroscopy.

Received 26th January 2020.

Accepted 18th March 2020

DOI: 10.1039/d0py00135j

rsc.li/polymers

Introduction

Polypeptides containing the same or different amino acid sequences play roles in a multitude of biological functionalities.^{1–4} However, owing to the poor solubility of synthetic polypeptides in different solvents, particularly in water, several research groups are focusing on increasing their solubility. Functionalization with hydrophilic polymers is one of the simplest methods for solubilisation of polypeptides in water. Owing to their inherent biodegradability and biocompatibility, these functionalized polypeptides play pivotal roles in biomedical applications, such as tissue engineering, bio-inspired materials and controlled release systems.^{5–8} A synthetic poly-

peptide made from only one amino acid may not be good enough to meet the demands of various biomedical applications.^{9,10} Thus, polypeptide–polymer conjugates and copolypeptides are in great demand in biomedical areas.^{11,12} These conjugates have enhanced mechanical properties owing to the presence of a synthetic polymeric component.^{13–15} Furthermore, amphiphilic polypeptide-based conjugates with a responsive polymeric component can easily form nanoaggregates (micelles, vesicles, *etc.*), which are very useful for making sustainable drug/gene carriers in solution because of their responsiveness towards pH, light, ionic strength or redox systems.^{16–19} The functionalization of polypeptides with poly(ethylene glycol) (PEG) or other polymers enhances their enzymatic/chemical stability, which is one of the key requirements in many applications, including tissue engineering and as delivery vehicles.^{20,21}

Until now, different pathways, typically based on different controlled polymerization techniques, have been utilized to synthesize many such conjugates or block/graft copolypeptides.^{22–25} For example, Ahrens *et al.* synthesized a poly(L-glutamic acid)-based hydrogel *via* a ‘click’ reaction to be

School of Chemical Sciences, Indian Association for the Cultivation of Science, Jadavpur, Kolkata 700032, India. E-mail: psutkm@iacs.res.in; Fax: +91-33-2473 2805

† Electronic supplementary information (ESI) available: Synthesis of ⁱPOx, FTIR, ESI-MS, MALDI-TOF-MS and NMR spectroscopic data, CAC measurement, DLS and FESEM images, absorption and emission spectroscopic data for encapsulation and release. See DOI: 10.1039/d0py00135j



Cite this: *Polym. Chem.*, 2021, **12**, 6329

Anion-induced thermoresponsiveness in cationic polycysteine and DNA binding†

Mahammad Anas, Priyanka Dinda, Mahuya Kar and Tarun K. Mandal *

Cationic polypeptide based smart biomaterials offer immense potential for biomedical applications including the field of drug delivery and the capability of spontaneously binding to biologically active components such as DNA. This study unfolds the synthesis of an L-cysteine-based water-soluble cationic polypeptide, an investigation of its thermoresponsive behaviour in the presence of added anions and its binding ability with DNA. Ring opening polymerization (ROP) of the newly designed bromo-functionalized L-cysteine N-carboxyanhydride (NCA) monomer results in the formation of polycysteine with a pendant Br atom. Subsequent nucleophilic substitution of the Br atom with triphenylphosphine gives cationic polycysteine (P[Cys-PPh₃]⁺[Br⁻]). An aqueous solution of P[Cys-PPh₃]⁺[Br⁻] is responsive to different Hofmeister series anions (BF₄⁻, I⁻, ClO₄⁻ and SCN⁻) showing a clear transformation from transparent to a cloudy suspension due to the formation of water-insoluble polypeptide/anion aggregates. The cloudy suspension of P[Cys-PPh₃]⁺[Br⁻]/anion aggregates in water becomes transparent upon heating and reappears on cooling, revealing an upper critical solution temperature (UCST)-type thermoresponsivity with a tunable cloud point with respect to the concentrations of both the cationic polypeptide and the added anions. The MTT assay result shows low cytotoxicity of the cationic polypeptide against human cells indicating its biocompatible nature. The polyplexation of cationic P[Cys-PPh₃]⁺[Br⁻] with calf-thymus DNA (ctDNA) was monitored by fluorescence spectroscopy, gel electrophoresis and circular dichroism spectroscopy. The effect of ionic strength on the polyplexation was also monitored by fluorescence spectroscopy.

Received 2nd September 2021.
Accepted 9th October 2021

DOI: 10.1039/d1py01187a

rs.c.li/polymers

Introduction

Proteins and polypeptides are important components and play a pivotal role in biological systems.¹ Therefore, several research groups have developed varieties of different synthetic polypeptides with inherent biocompatibility and biodegradability as promising bioinspired materials for biological applications.^{1–4} With the easy availability of natural amino acids and their artificial precursors functionalized with different moieties and responsive segments, synthetic polypeptides with different properties and functions can be customized simply by chemically combining these different sequences.⁵ In this direction, synthetic polypeptides with different functional groups, responsive towards different stimuli such as temperature,^{6,7} pH,^{8,9} light,^{10,11} redox reaction,^{2,12} enzyme,^{13,14} ionic strength,^{10,15}

etc. have been developed by many groups. These stimuli-responsive polypeptides are in great demand because of their wide range of biological applications, especially in targeted drug/gene delivery, therapeutics, tissue engineering, biosensing *etc.*^{1,16–18}

Synthetic polypeptides with tunable functionality and stimuli-responsiveness can be achieved through the ring-opening polymerization (ROP) of N-carboxyanhydride (NCA) from chemically modified natural α-amino acids.^{19–21} Alternatively, the ROP of amino acid NCA, containing different reactive functional groups such as allyl halide, alkyne, alkene, azide, *etc.* followed by their post-modification *via* different reactions such as Michael addition, click reaction, substitution reaction *etc.* can give rise to such functionalized polypeptides.^{6,22,23} However, the latter strategy lacks complete functionalization of all of its reactive groups. Macroinitiators with responsive moieties can also be utilized for the ROP of amino acid NCA to obtain end-functionalized polypeptide conjugates sensitive to different stimuli.¹⁰

Thermoresponsive polymers/polypeptides are the most widely investigated system in comparison to those responsive to other stimuli such as pH, light, or redox. These responsive systems undergo a reversible transition from a monophasic

School of Chemical Sciences, Indian Association for the Cultivation of Science, Jadavpur, Kolkata 700032, India. E-mail: psutkm@iacs.res.in; Fax: +91-33-2473 2805

† Electronic supplementary information (ESI) available: FTIR, ESI-MS, and NMR spectroscopic data, zeta potential, FESEM and temperature dependent DLS data, CD plot, turbidity curves, cell viability study, absorption and emission spectroscopic data for ctDNA intercalation. See DOI: 10.1039/d1py01187a



Recent developments in stimuli-responsive poly(ionic liquid)s

Palash Banerjee¹ · Md. Anas¹ · Somdeb Jana¹ · Tarun K. Mandal¹

Received: 23 September 2019 / Accepted: 25 March 2020
© The Polymer Society, Taipei 2020

Abstract

The current challenge is to focus on the fundamental understanding of ion-containing polymers. Poly(ionic liquid)s (PILs) belong to an important subclass of ionic polyelectrolyte with broad range of structural and functional properties. This review outlines the different kinds of stimuli-responsive PILs those are recently developed, specifically highlighting our own work and their materialistic applications. A brief introduction is also been provided to describe the advancement of PILs over their monomeric ionic liquids' (ILs) moiety and their smart responsive behaviour towards different chemical, physical and biochemical stimuli such as pH, redox, CO₂, temperature, light, enzyme etc. The thermoresponsive PILs with lower critical solution temperature (LCST)- or upper critical solution temperature (UCST)-type phase transition behaviours are discussed in a generalized way. The pH-responsive PILs also prove themselves as a potent candidate for potential applications in the biomedical area including therapy, drug delivery, diagnostics, etc. and the synthetic developments of those are also described here briefly. The rise of atmospheric CO₂ level is now a matter of worldwide concern. Thus, in particular, CO₂ responsive materials have attracted much attention and in this regards, PILs are much familiar and are found to be sorptive in nature both physically and chemically. Therefore, it is indeed important to describe the role and potential applications of PILs those are responsive to CO₂. Polymerized ionic liquids (PILs), those are responsive to other different stimuli such as photo, redox etc., are also described in this review.

Keywords Ionic liquid · Poly(ionic liquid)s · Stimuli-responsive · Thermoresponsive · pH-responsive · Photoresponsive · CO₂-responsive · Redox-responsive

Introduction

Ionic liquids (ILs) are known as a particular class of organic salts, comprising of poorly interacted ionic counterparts in which either, at least the cationic or the anionic part should be a relatively large organic moiety. [1] The large size of the ionic counterpart and their delocalized charge distribution hinder close packing of the IL molecules to form a crystal lattice. This results them in being liquid below 100 °C. ILs those are liquid at ambient temperature are known as room temperature ionic liquids (RTILs). [2] On the other hand, poly(ionic liquid)s (PILs), also called polymerized ionic liquids are basically a class of ionic polymer with monomer repeating units containing IL species in the side chain or in the backbone

(Fig. 1). [3–7] The later types of PILs are usually prepared by step-growth polymerization and they usually contain cationic charges located within the polymer main-chain, are also known as “ionenes” (Fig. 1). [4, 6] Thus, PILs fall under the subclass of polyelectrolytes bearing many additional properties of IL moiety including thermal stability, negligible vapor pressure, non-flammability, high ionic conductivity and a wide window of electrochemical stability while converting from monomer molecules to its macromolecular architecture. [7] PILs also possess some other properties of polymer such as enhanced thermal stability, improved processability, flexibility and durability, which actually make them good candidates with high performance that could not be readily delivered by ILs. Unlike ILs, which is generally liquid with weak intermolecular interaction among small molecules, the strong intermolecular forces between the macromolecular chains make PILs solid. In the last decade, PILs are attracting increasing interest as an emerging interdisciplinary topic of research in the areas of polymer science, materials science, [8] catalysis, [9] separation, [10] analytical chemistry, cell biology [11] and electrochemistry. [12] The researchers in these areas used different PILs with different structures and properties in several

Palash Banerjee and Md. Anas contributed equally to this work.



✉ Tarun K. Mandal
psutkm@iacs.res.in

¹ School of Chemical Sciences, Indian Association for the Cultivation of Science, Jadavpur, Kolkata 700032, India



Cite this: *Polym. Chem.*, 2019, **10**, 526

Tryptophan-based styryl homopolymer and polyzwitterions with solvent-induced UCST, ion-induced LCST and pH-induced UCST†

Somdeb Jana,‡ Mahammad Anas,‡ Tanmoy Maji, Sanjib Banerjee  § and Tarun K. Mandal  *

A new multi-stimuli responsive tryptophan-based styryl homopolymer exhibiting dual upper critical solution temperature (UCST)- and lower critical solution temperature (LCST)-type thermosensitivities under different conditions is presented. The monomer 4-vinylbenzyl *N*-[(*tert*-butoxy)carbonyl]-*L*-tryptophan (Boc-TrpVBz) is prepared by a simple substitution reaction followed by its subsequent RAFT polymerization to produce the poly(Boc-TrpVBz) homopolymer. Poly(Boc-TrpVBz) is not soluble in water, but is soluble in different organic solvents (such as DMSO, DMF and MeOH). An interesting upper critical solution temperature (UCST)-type turbid-to-transparent phase transition is detected for poly(Boc-TrpVBz) in mixed solvents containing any of these three solvents and a minimum percentage of water. The UCST-type cloud point is found to increase upon increasing the percentage of added water and the molecular weight of poly(Boc-TrpVBz). Furthermore, poly(Boc-TrpVBz) is soluble in water at above pH 7.5 and exhibits a lower critical solution temperature (LCST)-type transparent-to-turbid transition upon addition of tetrabutylammonium halide salts with a large organic cation. The LCST-type cloud point is variable with respect to the salt concentration and the nature of the halide ion. The deprotection of the Boc moiety of poly(Boc-TrpVBz) produces zwitterionic poly(TrpVBz) containing $-NH_2$ and $-COOH$ groups, which exhibits dual pH- and thermo-responsiveness in aqueous solution below pH 2. In the cases of UCST- and LCST-type transitions, the turbidity is caused by the formation of spherical polymer aggregates as observed *via* TEM and FESEM.

Received 23rd October 2018,
Accepted 7th December 2018

DOI: 10.1039/c8py01512k

rsc.li/polymers

Introduction

Bioinspired polymers have attracted considerable interest because of their potential applications in tissue engineering,¹ drug delivery,² and therapeutics³ as they possess several interesting properties, such as biocompatibility, biodegradability and stimuli-responsiveness.⁴ Thus, in this area, researches focuses on the development of new biofriendly responsive polymeric materials to mimic the functions of organisms in living systems.^{5–7} The incorporation of amino acid residues by coupling with reactive vinyl monomers and their subsequent

polymerization is one of the smart ways to prepare bioactive polymers with diverse functionalities.^{8–10} For example, the side chain amino acid-based poly(meth)acryloyls were synthesized by polymerizing the corresponding functionalized monomers and their biocompatibility and bioactivity were investigated.¹¹ To make such type of material, the post-polymerization technique is also equally applied to modify aldehyde-containing vinyl polymers with the amine group of an amino acid.¹² To date, the amino acid-based polymers reported so far are acryloyl-(meth)acryloyl-type polymers, whereas very limited examples of amino acid-based styryl polymers have been reported,^{13,14} even though the presence of the styrene unit in the polymer backbone could improve its physicochemical properties.¹⁵

Recently, there has been significant research on the development of multi-stimuli responsive polymers to enlarge the switching window for a wide range of important applications.¹⁶ However, most of them are copolymers containing different functional groups, responsive to different stimuli.^{17–19} The syntheses of such copolymers mostly require multi-step processes and sometimes complex chemistries.^{20,21}

Polymer Science Unit, School of Chemical Sciences, Indian Association for the Cultivation of Science, Jadavpur, Kolkata 700 032, India. E-mail: psutkm@iacs.res.in; Fax: +91-33-2473 2805

† Electronic supplementary information (ESI) available: Synthesis scheme for Boc-poly(TrpVBz), cloud points and MWP data, NMR/ESI-MS/FTIR/MALDI-TOF-MS spectra, DLS data, turbidity curves of polymers under different conditions, and TEM and FESEM images. See DOI: 10.1039/c8py01512k

‡ These authors contributed equally to this manuscript.

§ Present address: Department of Chemistry, Indian Institute of Technology, Bhubaneswar, India.

Dual Thermoresponsive Boc-Lysine-Based Acryl Polymer: RAFT Kinetics and Anti-Protein-Fouling of Its Zwitterionic Form

Priyanka Dinda, Mahammad Anas, Palash Banerjee, and Tarun K. Mandal*



Cite This: <https://doi.org/10.1021/acs.macromol.2c00633>



Read Online

ACCESS |



Metrics & More

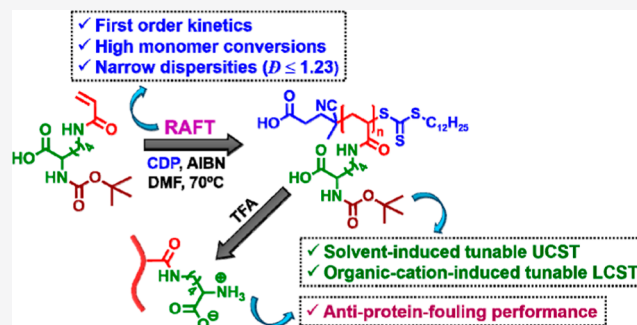


Article Recommendations



Supporting Information

ABSTRACT: There are significant developments on the responsive polymers that are programmed for various stimuli such as temperature, pH, light, and so forth. Such focus and progress remain mainly centered around conventional polymers compared to amino acid-based polymers offering a diverse range of applications in biomedical area. Thus, this study focuses on designing of a Boc-lysine-based monomer and its reversible addition-fragmentation chain transfer (RAFT) polymerization to poly(Boc-L-lysinylacrylamide)s [P(Boc-lysA)s] of controllable molecular weights (M_n s) and low dispersities ($D_s \leq 1.23$). This RAFT polymerization follows a first order rate kinetics up to very high monomer conversions (ca. 91.4%) with a good control over M_n and excellent agreement with the theoretical value. P(Boc-lysA) exhibits an interesting reversible upper critical solution temperature (UCST)-type phase behavior in mixed solvents comprising water and different polar organics (e.g., *N,N*-dimethylformamide, dimethyl sulfoxide, and methanol). The UCST-type cloud point (T_{cU}) increases linearly with increase of molecular weight of P(Boc-lysA) and percentage of water content in the mixed solvent. The addition of large organic cations in the aqueous solution of P(Boc-lysA) at pH 8.5 induces a lower critical solution temperature (LCST)-type phase transition with a tunable cloud point (T_{cL}) with respect to polymer concentration and its M_n as well as nature of added ion and its concentration. Furthermore, the Boc-deprotection of P(Boc-lysA) produces zwitterionic PlysA, which shows excellent anti-protein-fouling property compared to those of conventional antifouling polymers when tested with bovine serum albumin and monitored by dynamic light scattering.



INTRODUCTION

Amino acid-based polymers are one of the most important classes of bio-inspired materials not only for their biocompatibility and/or biodegradability but also for their inherent responsive properties toward different environmental stimuli such as pH,¹ temperature,² light,³ redox,⁴ ions,⁵ enzymes,⁶ nucleic acids,⁷ and proteins.⁸ Thus, designing and development of such stimuli-responsive polymers have drawn attention to the polymer scientists because of their ability to mimic biological systems and potential applications in biomedical and biotechnological areas such as drug delivery,^{9–11} gene delivery,¹² tissue engineering,¹³ therapeutics,¹⁴ as well as materials for making bio-fouling surfaces.¹⁵ The best way to synthesize these amino acid-based polymers with controlled molecular weights (M_n s) is to incorporate specific amino acids to polymerizable moieties (e.g., acryloyl, styryl, and so forth), followed by their polymerization via reversible addition-fragmentation chain transfer (RAFT), atom transfer radical polymerization, and so forth.^{16–18} Postmodification of the presynthesized polymers also offers greater prospects in developing such responsive polymers.^{19–21} It is worth mentioning that the nature of stimuli-responsiveness of these polymers is mainly governed by the side chain functionality of

their constituent amino acids. Also, there are only very few reports of development of multistimuli-responsive amino acid-based homo- and co-polymers.^{22,23} For example, Mori et al. have synthesized a multistimuli-responsive amino acid-based block copolymer nanoparticle by RAFT polymerization of a threonine containing monomer.²⁴

Thermoresponsive polymers are the well-studied systems from the category of responsive polymers due to their diverse range of applications starting from sensory materials to biocompatible materials for biology and medicine.^{25–27} By far, there have been some developments of amino acid-based polymers exhibiting thermoresponsive behaviors in solution.^{28,29} For example, Zhang et al. have synthesized lower critical solution temperature (LCST)-type poly(*N*-acryloyl-L-valine-*N'*-methylamide) by RAFT polymerization.³⁰ LCST-

Received: March 28, 2022

Revised: April 21, 2022



Ion-/Thermo-Responsive fluorescent perylene-poly(ionic liquid) conjugates: One-pot microwave synthesis, self-aggregation and biological applications

Mahuya Kar^a, Mohammad Anas^a, Arpana Singh^b, Ambuz Basak^a, Prosenjit Sen^b, Tarun K. Mandal^{a,*},¹

^a School of Chemical Sciences, Indian Association for the Cultivation of Science, Jadavpur, Kolkata 700032, India

^b School of Biological Sciences, Indian Association for the Cultivation of Science, Jadavpur, Kolkata 700032, India

ARTICLE INFO

Keywords:

Perylene bisimide
Poly(ionic liquid)
Fluorescent conjugate
Ion-/thermo-responsive
UCST
Self-aggregation
Vesicles
DNA binding
Bioimaging

ABSTRACT

This manuscript describes the attachment of alkylvinylimidazolium-based poly(ionic liquid) (PIL) to the imide positions of perylene bisimide (PBI) to introduce stimuli-responsiveness and to make the conjugate soluble in water and water-based mixed solvents with the possibilities of using them as a probe for imaging and diagnostics in biomedical domain. The alkylvinylimidazolium ionic liquid monomers (ILMs) are tailor-made and a one-step microwave-assisted method is employed for synthesizing the PBI-(Cys-PIL)₂ conjugates by thiol-mediated radical polymerization of the ILMs using L-cysteine (Cys) with AIBN as initiator and in the presence of perylene-3,4,9,10-tetracarboxylic dianhydride (PDA). The introduction of PIL segment induces amphiphilicity to the conjugate, and it undergoes self-aggregation into vesicles in water and methanol/water mixture. Owing to the presence of PIL segments, the conjugates are responsive to anions forming insoluble spherical aggregates through the multipoint ionic crosslinking between the cationic PIL segments of neighbouring conjugate molecules in water and methanol/water mixture. The turbid color dispersion, containing spherical conjugate's aggregates, shows upper critical solution temperature (UCST)-type phase transition to transparent solution upon heating. The variation of cloud point of conjugate could be done by changing different parameters such as molecular weight, nature of anions, and the length of the alkyl chain present in the PIL segment of the conjugate. The UV-vis and fluorescence spectra of the conjugate's aggregates in solution change upon addition of anions. The monitoring of the spectral change upon heating due to disruption of aggregates allows us to determine the cloud point, which exactly matches with that obtain from turbidimetry. The water-soluble fluorescent PBI-(Cys-PIL)₂ conjugate having cationic PIL segments shows low cytotoxicity and can be used in binding with ctDNA/plasmid DNA and imaging HeLa cells.

1. Introduction

Recently, stimuli-responsive fluorescent polymers/polymeric conjugates are gaining lots of attention among researchers because they can be used as potential materials for sensing, including specific applications in the biomedical domain.[1–7] On one hand, the development of stimuli-responsive polymers, particularly those responsive to temperature, has increased rapidly due to the availability of well-controlled polymerization techniques.[8–17] These thermoresponsive polymers with either lower critical solution temperature (LCST)- [18] or upper

critical solution temperature (UCST)-type behaviours,[19,20] have found promising applications in many areas such as smart coatings, diagnostics, sensing, tissue engineering and the delivery of drugs/genes. [6,21–23] Note that the reported UCST polymers are mostly ionic in nature, containing either zwitterionic or ionic liquid (IL) pendant groups.[9–11,14–16,24–27] Especially, thermoresponsive poly(ionic liquid)s (PILs) are widely used as interesting materials for various applications, including energy storage and making porous materials. [7,28,29] Thus, in this direction, we and other research groups have developed several different phosphonium- and imidazolium-based PILs,

* Corresponding author.

E-mail address: psutkm@iacs.res.in (T.K. Mandal).

¹ The manuscript is dedicated to Dr. Swaminathan Sivaram on the occasion of his 75th birthday.

Amphiphilic Perylene Bisimide–Polymer Conjugates by Cysteine-Based Orthogonal Strategy: Vesicular Aggregation, DNA Binding, and Cell Imaging

Mahuya Kar, Md. Anas,[#] Palash Banerjee,[#] Arpana Singh, Prosenjit Sen, and Tarun K. Mandal*Cite This: <https://doi.org/10.1021/acscapm.2c00227>

Read Online

ACCESS |



Metrics & More



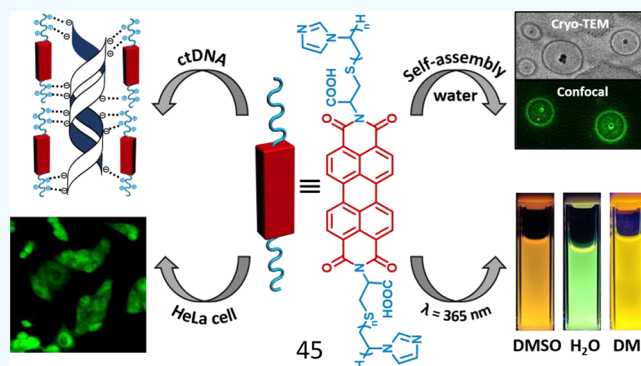
Article Recommendations



Supporting Information

ABSTRACT: Perylene bisimides (PBIs) with high quantum yields and high chemical and photophysical stabilities are usually suffering from poor solubility in various solvents, including water, which restricts their use in biomedical and other applications. Thus, in this study, as-synthesized hydrophilic poly(1-vinylimidazole) (PVim) is introduced at both the imide positions of the hydrophobic PBI unit by using L-cysteine (Cys) bearing two orthogonally reactive groups to produce a water- and organic-soluble PBI-based polymer conjugate. To do so, first, L-cysteine is used for thiol-mediated radical polymerization of 1-vinylimidazole (Vim). In the next step, the cysteine-end-capped poly(1-vinylimidazole) (Cys–PVim) with free –NH₂ is coupled with perylene-3,4,9,10-tetracarboxylic dianhydride (PDA) by employing a one-step microwave-assisted reaction to produce PBI–(Cys–PVim)₂ conjugate. The solution optical properties of this conjugate are thoroughly investigated to ascertain the extent of aggregation among PBIs units in both aqueous and organic media. The aqueous PBI–(Cys–PVim)₂ solution emits characteristic green fluorescence of PBI under UV irradiation of 365 nm wavelength. Owing to the presence of a protonable imidazole moiety, the PBI–(Cys–PVim)₂ conjugate shows pH-dependent optical properties. The amphiphilic PBI–(Cys–PVim)₂ molecules undergo self-assembly into vesicular nanostructures in water as confirmed from cryo- and high-resolution-transmission electron microscopy. The conjugate binds with ctDNA and plasmid DNA in water to form polyplexes. The fluorescent PBI–(Cys–PVim)₂ conjugate with low cytotoxicity and high quantum yield is efficiently used for the imaging of HeLa cells. The cellular uptake of the conjugate is studied at different time intervals and at different pHs using fluorescence microscopy.

KEYWORDS: perylene bisimide, fluorescent polymer conjugate, pH-responsive, self-assembly, vesicles, DNA polyplex, biocompatible, cell imaging



INTRODUCTION

Perylene-3,4,9,10-bis(dicarboximide)s (perylene bisimides, PBIs) are a significant class of dye exhibiting strong absorption and high fluorescence quantum yield as well as excellent thermal to photochemical stabilities.^{1–3} Therefore, PBI-based compounds are considered as promising functional materials for applications in diverse areas ranging from fluorescent probes for imaging,^{4,5} biosensors,⁶ and organic solar cells^{7,8} to organic semiconductors.^{9,10} However, owing to the presence of exceptionally strong π – π stacking interaction among the large aromatic perylene moieties, PBIs are very difficult to solubilize in organic solvents, particularly in water.^{11,12} All these cause a major concern for applying PBIs in bioimaging and also in various important research fields. Therefore, research is being carried out to attach different small organic moieties to their bay or imide positions to increase their solubility in organic solvents and in water.^{13–16} For example, the Wurthner group developed PBIs containing one bulky alkyl and one

dialkoxybenzyl substituent with good solubility in organic solvents.¹⁵ Also, the functionalization of PBI with different amino acids in the imide position enables them to solubilize in both aqueous and organic media because of the amphiphilic nature of the resultant molecule.¹³

In this context, one of the easiest and smartest ways to increase the solubility of PBIs in water for biological applications is the anchoring of a hydrophilic polymer instead of a small organic molecule. Such amphiphilic PBI–polymer conjugates can be synthesized either by growing polymers from

Received: February 4, 2022

Accepted: March 18, 2022

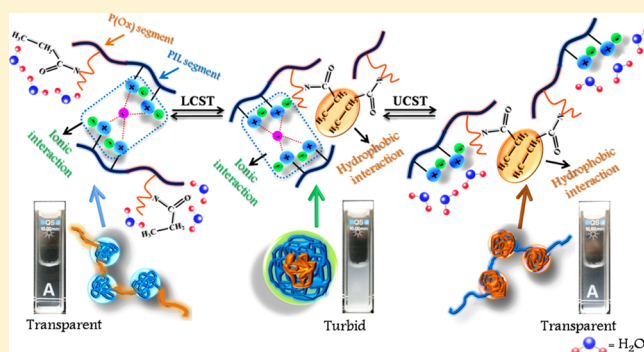
Poly[oligo(2-ethyl-2-oxazoline)acrylate]-Based Poly(ionic liquid) Random Copolymers with Coexistent and Tunable Lower Critical Solution Temperature- and Upper Critical Solution Temperature-Type Phase Transitions

Somdeb Jana, Yajnaseni Biswas, Md. Anas, Anupam Saha, and Tarun K. Mandal*[✉]

Polymer Science Unit, Indian Association for the Cultivation of Science, Jadavpur, Kolkata 700032, India

S Supporting Information

ABSTRACT: The synthesis of a series of dual thermosensitive nonionic–ionic random copolymers with varying compositions by reversible addition–fragmentation chain transfer polymerization is described. These copolymers contain oligo(2-ethyl-2-oxazoline)acrylate (OEtOxA) and either triphenyl-4-vinylbenzylphosphonium chloride ([VBTP][Cl]) or 3-*n*-butyl-1-vinylimidazolium bromide ([VBuIm][Br]) ionic liquid (IL) units. The copolymers having low content of ionic poly(ionic liquid) (PIL) (P[VBTP][Cl]/P[VBuIm][Br]) segments show only lower critical solution temperature (LCST)-type phase transition with almost linear increase of their cloud points with increasing percentage of ionic PIL segments. Furthermore, LCST-type cloud points (T_{cL} s) are found very sensitive and tunable with respect to the nature and concentration of halide ions ($X^- = Cl^-, Br^-, \text{ and } I^-$) and copolymer compositions. However, copolymers with high content of ionic PIL segments show both LCST-type followed by upper critical solution temperature (UCST)-type phase transitions in the presence of halide ions. Dual LCST- and UCST-type phase behaviors are prominent and repeatable for many heating/cooling cycles. Both types of cloud points are found to be sensitive to copolymer compositions, concentration, and nature and concentration of the halide ions. The phase behaviors of both types of copolymers with a very high ionic content (>90%) are exactly similar to that of P[VBTP][Cl] or P[VBuIm][Br] homopolymers showing only UCST-type phase transition in the presence of halide ions. The inherent biocompatibility of the P(OEtOxA) segment along with the interesting dual thermoresponsiveness makes these copolymers highly suitable candidates for biomedical applications including drug delivery.



INTRODUCTION

The stimuli-responsive polymers, showing sharp responses to external stimuli such as temperature,^{1–7} light,^{2,3,8,9} pH,^{10,11} ionic strength,^{12,13} CO₂,¹⁴ and so forth have recently gained immense attention among the polymer scientists in the context of their basic research and various applications.^{15–18} Of them, the thermoresponsive polymers are certainly very much versatile, widely studied,^{1–7} and promising candidates for various potential applications including membrane fabrication, delivery agents, tissue engineering, enzyme recycling, and so forth.^{19–23}

The lower critical solution temperature (LCST)-type polymers are the most studied systems because of their certain similarities with the denaturation of proteins.^{1,4,24–26} One such widely investigated systems is the bioinspired poly(2-oxazoline) (POx)-based LCST polymers with potential for several biomedical applications.^{23,27–30} Recently, we reported various POx-based nonionic LCST-type copolymers.^{2,31} However, the development of new POx-based copolymers with tunable cloud points in wide temperature ranges still remains a

challenge. In this context, the design of a copolymer by the incorporation of ionic segments into LCST-type polymer segments is one of the ways to tune the cloud point.^{32–35} Thus, the introduction of the ionic segment in the POx-based copolymer would certainly be interesting in terms of tuning of their thermoresponsive properties.

There is also handful of reports that describes polymers/copolymers with upper critical solution temperature (UCST)-type behaviors in water because of ionic and/or H-bonding interactions.^{36–40} Poly(dimethylaminoethyl methacrylate) (PDMAEMA) is an interesting dual responsive polymer showing soluble-to-insoluble (S–I) transition in the presence of counterions at a low temperature followed by an UCST-type transition upon heating.⁴¹ Besides nonionic polymers, ionic polymers such as poly(ionic liquid)s (PIL),⁴² poly(zwitterions),^{43–46} and poly(zwitterions) block copoly-

Received: September 5, 2018

Revised: September 28, 2018

Published: September 28, 2018

Carbon Dot Cross-Linked Gelatin Nanocomposite Hydrogel for pH-Sensing and pH-Responsive Drug Delivery

Swarup Krishna Bhattacharyya, Madhab Dule, Raj Paul, Jyotirmayee Dash, Md Anas, Tarun Kumar Mandal, Poushali Das, Narayan Chandra Das,* and Susanta Banerjee*

Cite This: <https://dx.doi.org/10.1021/acsbiomaterials.0c00982>

Read Online

ACCESS |

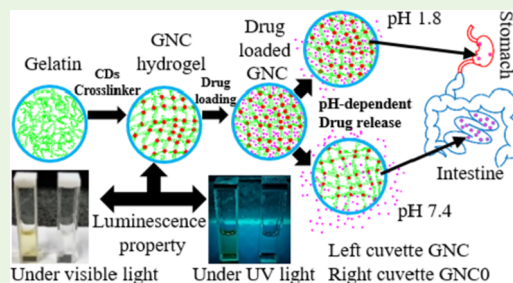
Metrics & More

Article Recommendations

Supporting Information

ABSTRACT: Delivery of therapeutics to the intestinal region bypassing the harsh acidic environment of the stomach has long been a research focus. On the other hand, monitoring a system's pH during drug delivery is a crucial diagnosis factor as the activity and release rate of many therapeutics depend on it. This study answered both of these issues by fabricating a novel nanocomposite hydrogel for intestinal drug delivery and near-neutral pH sensing at the same time. Gelatin nanocomposites (GNCs) with varying concentrations of carbon dots (CDs) were fabricated through simple solvent casting methods. Here, CDs served a dual role and simultaneously acted as a cross-linker and chromophore, which reduced the usage of toxic cross-linkers. The proposed GNC hydrogel sample acted as an excellent pH sensor in the near-neutral pH range and could be useful for quantitative pH measurement. A model antibacterial drug (cefadroxil) was used for the *in vitro* drug release study at gastric pH (1.2) and intestinal pH (7.4) conditions. A moderate and sustained drug release profile was noticed at pH 7.4 in comparison to the acidic medium over a 24 h study. The drug release profile revealed that the pH of the release medium and the percentage of CDs cross-linking influenced the drug release rate. Release data were compared with different empirical equations for the evaluation of drug release kinetics and found good agreement with the Higuchi model. The antibacterial activity of cefadroxil was assessed by the broth microdilution method and found to be retained and not hindered by the drug entrapment procedure. The cell viability assay showed that all of the hydrogel samples, including the drug-loaded GNC hydrogel, offered acceptable cytocompatibility and nontoxicity. All of these observations illustrated that GNC hydrogel could act as an ideal pH-monitoring and oral drug delivery system in near-neutral pH at the same time.

KEYWORDS: nanocomposite, gelatin hydrogel, drug delivery, pH sensing, cytocompatibility



1. INTRODUCTION

Approximately 90% of all of the therapeutics are orally administrated as it is less painful, noninvasive, and produces a maximum patient response. However, successful oral deliveries of some therapeutics (protein drugs, insulin, anticancer drugs) for the treatment of local maladies such as ulcerative colitis, inflammation, Crohn's diseases, infections, and colon carcinoma remain a challenge.¹ During passage through the GI (gastrointestinal) tract, drug molecules encounter numerous challenges, like rapid enzymatic degradation, a harsh acidic environment, poor intestinal absorption, and low residence time, which limit the therapeutic efficiency.² All of these issues can be addressed by conjugating the therapeutics with some specially designed drug carriers. Together, they can successfully bypass the harsh acidic environment of the stomach and release the drugs in the targeted location. In real practice, some specific types of hydrogel (gelatin, chitosan, pectin, alginate) serve as drug carriers.² These hydrogels show a pH-responsive behavior due to the presence of large numbers of carboxylated groups in the main chains. At low pH values, these hydrogels swell less, but at higher pH, they swell more and release the

entrapped drug molecules to the target. On the other hand, monitoring a system's pH during drug delivery is also very important. As we know, pH plays a crucial role in many biological and chemical systems. For many pathological and physiological events, precise monitoring of a system's pH is highly recommended. A slight deviation in pH may lead to serious health problems, such as neurological disorder, cardiopulmonary disease, and cancer.³ To date, different techniques have been reported for pH measurement, including colorimetric, electrochemical, and electromechanical-based methods.⁴ However, these techniques are sophisticated, nonuser friendly, and come at a high cost,⁴ which reduce their direct application in pH sensing. In this scenario,

Received: July 2, 2020

Accepted: September 17, 2020

Published: September 17, 2020

